The Direct Torque Control of Induction Motors

by

Ingo Lüdtke, Dipl.-Ing.

A thesis submitted in partial fulfilment of the requirements of the University of Glamorgan for the degree of

Doctor of Philosophy in Electrical Engineering

Department of Electronics and Information Technology
University of Glamorgan

May 1998

Abstract

This thesis is mainly devoted to the investigation of speed control methods of three phase, cage rotor induction motors with particular emphasis being given to vector control and direct torque control techniques. Modern control strategies such as vector control and direct torque control are investigated as well as the conventional methods such as open loop (constant V/f) operation. A number of different pulse width modulation (p.w.m.) waveform generation strategies are simulated and discussed and their application to the above speed control systems fully investigated. A 3kW, three phase induction motor drive has been designed and experimental data obtained from it in order to verify the results achieved by simulation. It is shown that direct torque control achieves decoupling of the motor torque and the motor flux without the use of a co-ordinate transform. A variation of the direct torque control algorithm has also been developed and implemented. It is shown, that by using different switching tables for the selection of voltage vectors, the performance of direct torque control can be further improved. Further insight into the nature of direct torque control has been gained from the study of the effect of the application of inverter switch settings, or the application of corresponding voltage vectors, on the motor flux and torque. It has been found that the range of torque variation of the motor drive system depends strongly on both the motor load torque and the motor speed.

The results of the work reported indicate that the range of torque variation for a drive system which strongly depends on motor load torque and motor speed is considerably reduced by the novel direct torque control system resulting from the research.

The control algorithms have been implemented on 32 bit micro processors which facilitate the use of parallelism in both the hardware and the software design. The resulting system is capable of controlling a three phase induction motor with variable voltage and variable frequency with control strategies such as six step operation, symmetric and asymmetric regular and natural sampled p.w.m. waveforms, sigma delta modulation methods, space vector modulation techniques, flux vector control and direct torque control.

Table of Contents

List of Figures

List of Tables

Acknowledgements

I am most grateful to my Director of Studies Dr. Marcel Jayne for his continuous help, support and advice throughout the period of research to which this thesis relates.

I also like to thank my second supervisors Dr. David Rees and Dr. Robert Payne for their support.

I am most appreciative to Prof. L. Hobson for providing much of the facilities used in the former Power Electronics Research Laboratory at the University of Glamorgan.

I am also thankful to the industrial collaboration of Black Clawson International of Newport, Gwent.

May I also thank Prof. Dr. rer.nat. Klaus Harbusch and Prof. Dr.-Ing. Walter Heinecke from the Fachhochschule Braunschweig / Wolfenbüttel who have made my stay in South Wales possible.

I am most indebted to the late Dr. Stefan Hadjivassilev, for his advice regarding the design of the inverter. Thanks must also go to my friends and fellow students at the University of Glamorgan, especially Michael Weiss, for many useful discussions.

Last but not least, I like to thank my parents for their patience and support and also thank Andrea for her encouragement.

Declaration

This work is submitted for the award of the degree of Doctor of Philosophy of the University of Glamorgan.

The data presented and the conclusions drawn are the result of the candidate's own efforts, except where otherwise stated.

This thesis has not been, nor is being currently submitted for the award of any other degree or similar qualification.

Candidate : _____

Director of Studies: _____

Nomenclature

a_k	Fourier coefficient	p.u.
b_k	Fourier coefficient	p.u.
C	Cost function	p.u.
f_c	Carrier frequency	Hz
$f_n(x)$	Waveform described by Fourier coefficients	p.u.
f_{sN}	Nominal supply frequency of induction motor	Hz
I_A	Instantaneous stator winding current of phase 'A'	A
$\vec{I}_M$	Magnetising current space vector	A
$\vec{I}_r$	Rotor current space vector	A
$\vec{i}_r$	Rotor current space vector	A
$\vec{i}_s$	Stator current space vector	A
$\vec{I}_s$	Stator current space vector	A
J	Moment of Inertia	kgm^2
$L_{\sigma A}$	Leakage inductance of stator winding 'A'	H
L_A	Self Inductance of Phase 'A'	H
L_M	Mutual inductance	H
L_r	Rotor winding self inductance	H
L_s	Stator winding self inductance	H
M	Fraction of the fundamental for six step voltage waveform	H
M	Mutual inductance	H
M_{Aa}	Mutual inductance of stator phase 'A' and rotor phase 'a'	H
n_a	Number of turns in rotor winding 'a'	-
n_A	Number of turns of stator winding 'A'	-
$P(t)$	Instantaneous power	W
p_b	number of pole pairs	-
P_{in}	Induction motor input power	p.u.
P_{loss}	Induction motor power losses	p.u.
P_{out}	Shaft output power of induction motor	p.u.
Q	Induction motor reactive power	p.u.
R	Number of sub-cycles per period	-

R_A	Resistance of stator winding 'A'	Ω
R_r	Rotor resistance	Ω
R_s	Stator resistance	Ω
r_r	Rotor resistance	p.u.
r_s	Resistance of stator winding	p.u.
r_s	Stator resistance	p.u.
S	Apparent power	p.u.
s	Derivative operator, complex Laplace variable	-
s	Motor slip	p.u.
T	Duration of sub-cycle in space vector modulation	s
T	Electromagnetic torque	p.u.
t	Time	s
T_d	Dynamic torque (acceleration or deceleration)	p.u.
T_L	Load torque	p.u.
T_M	Inertia time constant of the induction motor	s
T_N	Nominal time constant	s
V_A	Instantaneous stator phase voltage (phase 'A' to neutral of load)	V
v_{ab}	Phase to phase voltage	p.u.
v_{an}	Phase to neutral of load voltage	p.u.
v_{ao}	Phase to neutral of the d.c. supply voltage	p.u.
V_{dc}	Voltage across the inverter d.c. link	p.u.
V_{out}	Output voltage	V
V_{ref}	Reference voltage	V
$\vec{v}_s$	Stator voltage space vector	p.u.
$\vec{V}_s$	Stator voltage space vector	V
x_{lr}	Rotor leakage reactance	p.u.
x_{ls}	Magnetising reactance	p.u.
x_{ls}	Stator leakage reactance	p.u.
x_r	Rotor self reactance	p.u.
x_s	Stator inductance	p.u.
x_s	Stator self reactance	p.u.
z	Discrete time operator	-
Z	Induction motor impedance	p.u.

List of Symbols

α	Switching angle	rad
γ_k	Angle of arbitrary co-ordinate system referred to stator axis	rad
γ_m	Rotor position angle	rad
γ_s	Angle of synchron. rotating co-ordinate system referred to stator axis	rad
ϕ_{AA}	Flux in stator winding 'A' due to the current in phase 'A'	Wb
φ	power angle	rad
η	Induction motor efficiency	Wb
$\vec{\Psi}_r$	Rotor flux linkage space vector	Wb
$\vec{\Psi}_{r\sigma}$	Rotor leakage flux linkage space vector	Wb
$\vec{\Psi}_s$	Stator flux linkage space vector	Wb
$\vec{\Psi}_{s\sigma}$	Stator leakage flux linkage space vector	Wb
$\vec{\psi}_m$	Magnetising flux linkage space vector	p.u.
$\vec{\psi}_r$	Rotor flux linkage space vector	p.u.
$\vec{\psi}_s$	Stator flux linkage space vector	p.u.
ψ_a	Flux linkage of rotor phase 'a'	p.u.
Ψ_A	Flux linkage of stator winding 'A'	Wb
ψ_{BA}	Flux linkage of phase 'B' generated by current in phase 'A'	p.u.
σ_r	Rotor leakage factor	-
σ_s	Stator leakage factor	-
Ω_k	Angular velocity of arbitrary co-ordinate system	rad/s
Ω_m	Angular velocity of rotor	rad/s
ω_m	Motor speed	p.u.
ω_r	Rotor slip speed of induction motor	p.u.
ω_s	Supply frequency of induction motor	p.u.

Subscripts

A-B-C	Stator Phases
a-b-c	Rotor phases
α-β	Space vector components in stationary co-ordinates
b	Base unit
c	Motor parameter used by controller
d-q	Co-ordinate system fixed to the rotor axis
err	Error
est	Estimated quantity
H	Hysteresis
k	Arbitrary co-ordinate system
ref	Reference quantity
x-y	Synchronously rotating co-ordinates

Superscripts

*	Complex conjugate
*	Rotor quantity referred to stator side
s	Co-ordinate system referred to stator side

Chapter 1: Introduction

This chapter serves to identify the induction motor as an ideal motor for industry. The basic principles of speed regulation of induction motor drives are outlined. Advanced control strategies including the latest developments are then discussed in more detail. The remainder of this chapter outlines the structure of the thesis.

1.0 Historical Review

The history of electrical motors goes back as far as 1820, when Hans Christian Oersted discovered the magnetic effect of an electric current. One year later, Michael Faraday discovered electromagnetic rotation and built the first primitive d.c. motor. Faraday went on to discover electromagnetic induction in 1831, but it took until 1883 when Nikola Tesla invented the a.c. asynchronous motor. Presently, over one hundred years after its invention, the main types of electric motor are still the d.c. motor, the a.c. synchronous motor and the a.c. asynchronous motor which are all based on the theories developed by Oersted and Faraday.

Since its invention, the a.c. asynchronous motor, also termed induction motor, has evolved into the standard industrial motor of today. At present, 60% of all the electrical energy generated in the UK is converted to mechanical energy by induction motors. This development is not by chance as induction motors have some considerable advantages over other types of motors. The main advantage is that induction motors do not require an electrical connection between stationary and rotating parts of the motor. Therefore, they do not need a mechanical commutator and brushes which in turn results in a virtually maintenance-free motor. Induction motors also have low weight and inertia, high efficiency and a high overload capability. Because of this, induction motors are cheap to buy and to operate and are not prone to catastrophic failure at high speeds as is the separately exited d.c. motor. Furthermore, the motor can also work in explosive environments because no sparks are produced. Induction motors have fewer moving parts and are routinely supplied to IP55 (hose proof) instead of the normal IP23 (drip proof) protection, to which most d.c. motors are applied.

With the advantages outlined above, the induction motor should be the ideal electrical to mechanical energy converter. However, mechanical energy is often required at variable speeds and the speed control of an induction motor is not a trivial matter.

1.1 Speed Control of Induction Motors

The only effective way of producing an infinitely variable induction motor speed drive is to supply the induction motor with three phase voltages of variable frequency and variable amplitude. A variable frequency is required because the rotor speed depends on the speed of the rotating magnetic field provided by the stator. A variable voltage is required because the motor impedance reduces at low frequencies and therefore, the current has to be limited by means of reduced supply voltages.

Before the days of power electronics, a limited speed control of induction motors was achieved by switching the three stator windings from delta connection into star connection. This allows voltage at the motor windings to be reduced without introducing losses outside the motor. Induction motors are also available with more than three stator windings to allow a change of the number of pole pairs. However, a motor with several windings is more expensive because more than three connections to the motor are needed and only certain discrete speeds are available. An alternative method of speed control can be realised by means of a wound rotor induction motor, where the rotor winding ends are brought out to slip-rings. This of course, removes many of the advantages of the cage rotor induction motor and introduces additional losses. By connecting resistors or reactances in series with the stator windings of the induction motor, poor performance is realised at low speed operation because of the resulting high slip operation.

When, during the last century, an electrical infinitely variable speed drive with good control characteristics was specified, the natural choice was a d.c. motor supplied from either a constant speed d.c. generator, mercury-arc rectifier or, more recently, a solid state switched power converter. These drives, which were built over a wide power range, permitted operation in the four quadrants of the torque-speed plane including temporary standstill. They had good efficiency, and with suitable control, excellent dynamic response. Their main limitation, however, was the requirement of a commutator and brushes, which in turn limited speed.

Prior to the advent of solid state variable voltage, variable frequency converters induction motors were mainly used in applications for which, essentially, constant speed was acceptable. For variable speed applications, however, the induction motor was not ideally suited. With the decreasing cost and improved performance in power electronic devices it has become both possible and economical to produce converters which provide variable frequency and variable voltage supplies. These converters can be used with induction motors to produce drives that can compete with d.c. motor drives in both performance and cost. Therefore, many applications that have conventionally used constant speed induction motors are now being converted to adjustable speed drives so that the optimum speed can be chosen for each operating condition, thus achieving higher system efficiency and energy conservation. Induction motors with semiconductor converters are being used extensively for applications requiring precise, rapid speed and position control.

For such applications however, two main preconditions have to be met:

1. The availability of efficient, fast switching and not too costly power converters so that the fixed frequency line voltages can be transformed to variable voltage, variable frequency supplies.
2. The development of suitable methods to control the speed of a.c. machines because the relative simplicity of their mechanical design is contrasted by a complex dynamic structure (multivariable and non-linear).

With the enormous advances made in semiconductor technology during the last 20 years, both these obstacles can now be overcome. The first obstacle is removed by the availability of power electronics which offers ever more efficient and compact switching devices, whilst the second obstacle is overcome by micro electronics, providing effective means for solving any control problem using hardware or software techniques.

The speed of an induction motor is determined by its synchronous speed and the slip of the rotor. The synchronous speed, is related to the supply frequency, whilst the slip is dependent upon the load. The slip can be controlled by regulation of the amplitude of the voltage supplied to the motor. As the impedance of an induction motor decreases with decreasing frequency the voltage to the motor has to be reduced if the current and flux are to be constant. This, therefore, leads to the requirement of variable voltage, variable frequency supplies. However, since the frequency of the mains supply is

constant at 50 or 60 Hz, a variable frequency converter is required. For many applications the drive should be able to operate in all four quadrants of the torque-speed plane and have a soft-start and flying-start capability with provision for electrical braking. It is only with the advent of power electronics that these requirements can be adequately met.

The generation of the three phase supply at variable voltage and variable frequency makes the infinitely variable speed control of induction motors such a challenging and interesting subject. A number of different topologies, which have been applied in the past, depending on motor size, available technology and control strategy, are outlined below:

1. Cycloconverters have the capability of converting the power from a constant voltage, constant frequency source to a variable voltage, variable frequency source directly. However, these converters are useful for producing output power at low frequencies only. The maximum useful range of output frequency is about one third of the supply frequency for a three phase system. Typically, eighteen switching devices are needed because two three phase rectifiers for each phase are required. Cycloconverter operation is mainly used for high power electrical drive systems.
2. Six step inverters have a controlled rectifier at the mains side, a d.c. voltage link and a three phase inverter at the load side. The voltage level is controlled by the rectifier and the frequency by the inverter. For low output voltages, however, a controlled rectifier leads to a poor power factor for the drive and, due to the six-step operation, the voltages and current waveforms have a high harmonic content. In addition, low speed torque pulsations can present a problem.
3. Pulse width modulated inverters with a d.c. current fed link have the advantage that four-quadrant operation is simple to achieve. Nevertheless, due to the phase control of the mains rectifier, a poor power factor is apparent in this scheme. The drive cannot be operated in open loop and voltage spikes may present a problem.
4. Pulse width modulated converters with a d.c. voltage link consist of a diode rectifier and an inverter. The voltage amplitude and the frequency are controlled by the pulse pattern applied to the inverter switches. This type of operation is associated with high power factor and good efficiency. A disadvantage is the trade-off between the reduction in harmonic content of output voltage and the reduction of switching frequency to limit the switching losses.

5. Pulse width modulated inverters with resonant d.c. links overcome the problem of high switching losses. The link voltage is oscillating and periodically clamped to zero. This is synchronised with the switching instants of the inverter switches, thereby providing so called soft switching, as opposed to hard switching which occurs with a constant d.c. link voltage. Device stresses and electromagnetic emission are therefore very much reduced, and with switching frequencies in the ultrasonic range, audible noise is also reduced.

The inverter topologies, described above, allow an induction motor to operate with any load at any speed within its maximum ratings. However, it has become equally important to provide a rapid but smooth transition from one speed to another. In fact, the uncontrolled variation of the supply frequency can produce undesirable current and torque transients which do not occur with constant supply frequency operation.

A great number of different strategies have been devised in order to allow rapid and controlled variation of the operating speed of the induction motor. These strategies may be grouped into what is known as scalar and vector control techniques.

1.2 Scalar Control Schemes

Scalar control schemes mainly entail the control of scalar quantities such as frequency, slip frequency and the amplitudes of voltage and current. The scalar techniques include a modulator which converts frequency and amplitude signals into balanced three phase pulse-width-modulated waveforms. Appropriate frequency and amplitude signals are derived from the measured rotor speed and an input reference speed. The frequency and amplitude signals can either be related as in constant V/f control or can be momentarily independent as, for example, in slip control, which results in a more desirable transient response. However, in terms of transient response, it is fair to say that the scalar methods are inferior when compared to vector control.

1.3 Vector Control Schemes

Vector control techniques involve the control of space vector quantities namely current space vectors, voltage space vectors and flux space vectors, by which independent control of motor torque and motor flux can be achieved.

Vector control was first introduced by Hasse in 1969 (Hasse, 1969). Pioneering work was also carried out by Leonhard (1970) and Blaschke (1970). The main idea is that the three stator currents are resolved into two components in a co-ordinate system rotating with the supply frequency. It is possible to identify one component proportional to the motor flux and the other proportional to the motor torque. Thereby, the control task is greatly simplified as d.c. quantities are controlled, as is the case with a separately exited d.c. motor. In the past, one drawback of the vector control strategy was that the complexity of the control algorithm required fast micro-controllers which were not available when vector control was invented. However, fast and cheap micro-controllers have become available since and today, a great variety of commercially available high performance induction motor drive controllers incorporate vector control.

A great deal of research has been carried out into numerous variants of vector control. The sensitivity of vector control decoupling to motor parameter changes with temperature and magnetic saturation has led to the application of adaptive control methods (Kao, Luo and Liu, 1992). The co-ordinate system can be made to rotate with either the stator, air-gap or rotor flux vector (Boldea and Nasar, 1992). The modulator used can be either voltage (Atkinson and France, 1995) or current (Ohtani, Takada and Tanaka, 1992) controlled. Sliding mode control as opposed to PID control for the speed and position controller has also been applied (Ho and Sen, 1989). The slip angle may be determined by using either the rotor position (Lorenz and Yang, 1992), the rotor speed (Honderd *et al*, 1991) or currents and voltages only, as in 'sensor-less' systems (Ohtani, Takada and Tanaka, 1992). Modulators have evolved from triangular carrier wave based sampling (Jayne *et al*, 1990) to harmonic elimination (Bowes and Clark, 1992), sigma-delta modulation (Mertens, 1992), random pulse width modulation (Bourgeois, 1993) and space vector modulation techniques (Handley and Boys, 1992). Although there can be virtually hundreds of different combinations of the above mentioned components in vector control, the main principle always remains the same: the stator current is resolved into a flux and a torque producing component which allow rapid, precise and most of all independent control of flux and torque.

1.4 Direct Torque Control

Until recently, it looked as if the co-ordinate transform method was going to become the standard technique for controlling induction motors. However, in 1985, Takahashi (1985) and Depenbrock (1985) introduced methods for decoupling the motor flux and the motor torque without the use of a co-ordinate transform. In fact, their systems did not require voltage nor current modulators, decoupling networks, controllers for flux and torque, and two to three axis transformation of reference quantities. They called their technique quite rightly 'direct torque control', 'torque vector control', or 'direct self control'.

Although claimed to be superior to flux vector control (Takahashi, 1990), few research activities have been carried out into this technique. The first direct torque control drive became commercially available in 1996 (Schofield and Taylor, 1996) and publications were made in Poland (Kazmierkowski, 1994), USA (Habletler *et al*, 1992), Romania (Boldea and Trica, 1990), as well as in Japan (Takahashi, 1986) and Germany (Baader, 1990).

1.5 Present Converter Technology

The requirements of an inverter in addition to the provision of a variable voltage and variable frequency output have changed with the advances made in microelectronics. State of the art inverters now have Fieldbus interfaces (Profibus, Interbus, DeviceNet, CAN, ...) to integrate the frequency inverter into factory automation applications. Many manufacturers offer these communication protocols as modules which plug into the inverter. For high speed, high noise immunity, some manufacturers also offer optical fibre communications. In most cases, these communication options are offered in addition to the traditional interfaces (RS 232, RS 485, PLC interface, analogue and digital inputs and outputs).

Another trend in a.c. inverter operation is the application of commissioning, maintenance, diagnostics, service, fault finding and control software. With serial communication, many frequency inverters can be connected to a single PC or PLC. All parameter settings and the control can be carried out via the central controller. Much of the diagnostics, which normally would be carried out by 'customer care technicians', can now be carried out by the customer directly, which reduces downtime and cuts service costs.

Standardised software modules can be bought off the shelf to suit special applications. This may allow several drives to run in speed or position synchronisation. Furthermore, shaft positions can be offset or an adjustable speed ratio can be introduced to compensate for elongation or shrinkage in applications such as plastics extrusion, wire drawing and textile manufacture. 'S'-Ramp acceleration and deceleration curves provide greater smoothness and progressive speed transitions for lifts, hoists, cranes and conveyors. CNC machine spindle orientation software modules are also available for tool changing or other automated applications. The final position of the motor shaft relative to an electronic feedback datum can be specified by the user with a different module. A software module, which maintains a constant 'web' tension in coiling and uncoiling applications for the paper, wire, plastics and metal industries, allows the drive torque to be continuously adjusted to compensate for coil diameter, machine losses and coil inertia. Software modules can also provide accurate indication of physical power consumption in applications like mixers, extruders and calendars.

At present, the most commonly used variable speed induction motor drives incorporate a pulse width modulated inverter, where the implemented control strategies have evolved from open loop to closed loop schemes. Since the introduction of vector control in 1969 by Hasse, induction motor drives have achieved the same dynamic performance as d.c. drives. However, one of the problems with vector control is its sensitivity to parameter variations in the induction motor, for example, the change in rotor resistance with temperature presented a considerable design problem. The introduction of direct torque control improved the situation because direct torque control does not rely on a co-ordinate transform. It has the following advantages compared to flux vector control (Takahashi, 1990):

a) less sensitive to changes in resistance with temperature.
b) dynamic performance superior to vector control,
c) produces fewer torque ripples,
d) less complex than vector control.

The co-ordinate transform from stationary orientation to rotor flux vector orientation, as well as sinusoidal reference waves are not required. With given stator flux and torque error, the scheme directly selects appropriate inverter switch settings.

1.6 Structure of the Thesis

The work reported in this thesis shows that with an expansion of the voltage vector selection table used in direct torque control, the stator flux and torque ripples can be reduced further which is of considerable importance to the fiber optics and paper industries, where precise torque control is required.

The microprocessors used in this investigation are Transputers, which provide the means of handling parallelism in a straightforward manner. Together with the associated programming language Occam this provided a very flexible design, which can be modified to a wide range of pulse width modulation techniques in a short programming time.

The following ten chapters of this thesis are organised as follows:

Chapter 2 introduces a mathematical model of cage rotor induction motors. The elements of space vector notation are also introduced in this chapter and are used to develop a compact and convenient means of representing magnetic fields. Different models are presented and the relationship between current and torque is established.

Chapter 3 is devoted to the steady state operation of induction motors. The analysis is thereby organised by the capabilities of the power converter connected to the induction motor. The investigated operating modes are constant voltage, constant frequency operation (CVCF), constant voltage, variable frequency operation (CVVF), variable voltage, constant frequency operation (VVCF) and variable voltage, variable frequency operation (VVVF). As VVVF operation introduces a second degree of freedom for setting up a particular operating condition of the motor, an optimisation is carried out to find desirable voltage and frequency combinations in order to satisfy different optimisation criteria.

In chapter 4 the well known six step mode of inverter operation is reviewed.

Cnapter 5 covers a number of different pulse width modulation strategies. P.w.m. methods such as natural sampling, symmetrical and asymmetrical sampling, space

vector modulation, harmonic elimination and optimised p.w.m methods are analysed and compared.

Chapter 6 is mainly devoted to the discussion and analysis of flux vector control strategies. Direct and indirect control, as well different modes of flux orientation of the co-ordinate system such as orientation with the stator flux space vector, the magnetising flux space vector and rotor flux space vector are analysed. The chapter concludes with a discussion on the sensitivity of flux vector control on changes of the motor parameters.

In chapter 7 a number of different direct torque control strategies are discussed. The system first published by Takahashi in 1985 as well as variants are discussed. Also included is a study on the effect of the application of a voltage vector on motor flux and motor torque.

In chapter 8 the development of the experimental inverter system is described. The design of the circuitry including insulated gate bipolar transistors (IGBT's) with associated driver interface are fully described. The design procedure for the Transputer interfaces to driver circuitry, analogue to digital converter and shaft encoder are also presented. Also included in this chapter are aspects of the programming language Occam and its use for the experimental induction motor drive system.

Chapter 9 covers the implementation of flux vector control and direct torque control and also the experimental results which have been obtained to verify simulated results.

In chapter 10 achievements are summarised and appropriate conclusions drawn.

Chapter 2: Induction Motor Model

2.0 Review of Motor Models

The three phase induction motor can be of the synchronous or asynchronous type. This thesis, however, will only concentrate on the asynchronous motor. The asynchronous motor mainly consists of two parts: the stator, which is the stationary part, and the rotor, which is the rotating part. The stator is normally wound with a three phase distributed a.c. winding, whereas the rotor can have a cage winding or an a.c. three phase distributed winding similar to the one on the stator. The internal yoke of the stator and the rotor are generally constructed from laminations of ferro-magnetic material. The air gap between the stator and the rotor is symmetrical and normally designed to be a minimum. A picture of a stator of an induction motor and its associated windings is shown in Fig. 2.1.

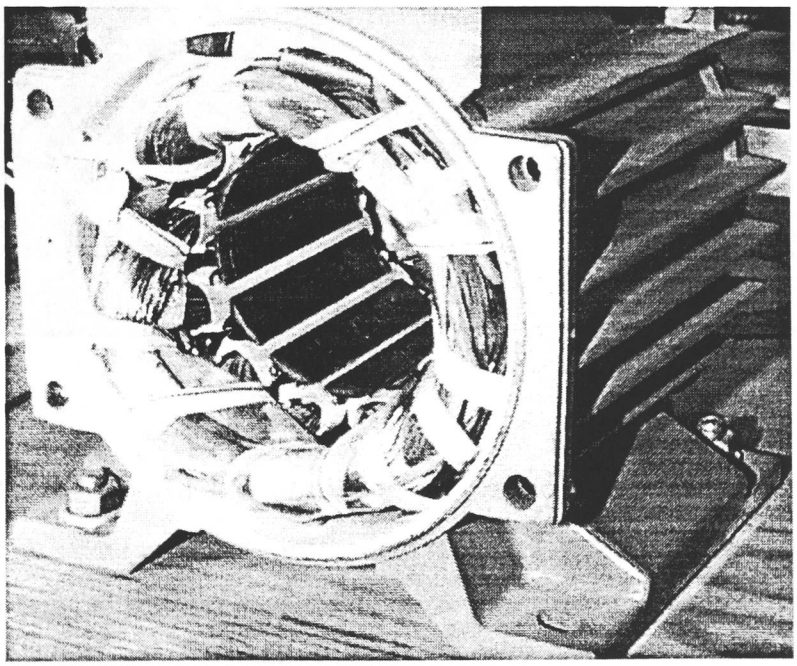

Fig. 2.1: Stator of Induction Motor

It may be seen that the stator windings are housed in slots where they are enclosed in iron laminations.

The wound rotor induction motor has a three phase symmetrical winding, which is housed in the rotor slots but insulated from the rotor. The ends of the rotor windings can be connected in a star or delta configuration and these connections are brought out from the windings to slip rings. The slip rings and associated brushes provide a means for

connecting the rotor windings to external circuit components which may be used for speed and torque control purposes.

The squirrel cage rotor induction motor, on the other hand, has a cage winding which is housed in the rotor. Such a winding consists of bars placed or cast in rotor slots and their ends short-circuited by means of end rings. The bars and shorting rings are made of copper, brass or aluminium and are not normally insulated from the rotor. This enables the casting of the rotor windings in the slots, which makes an inexpensive but reliable motor design. A typical induction motor rotor is shown in Fig. 2.2.

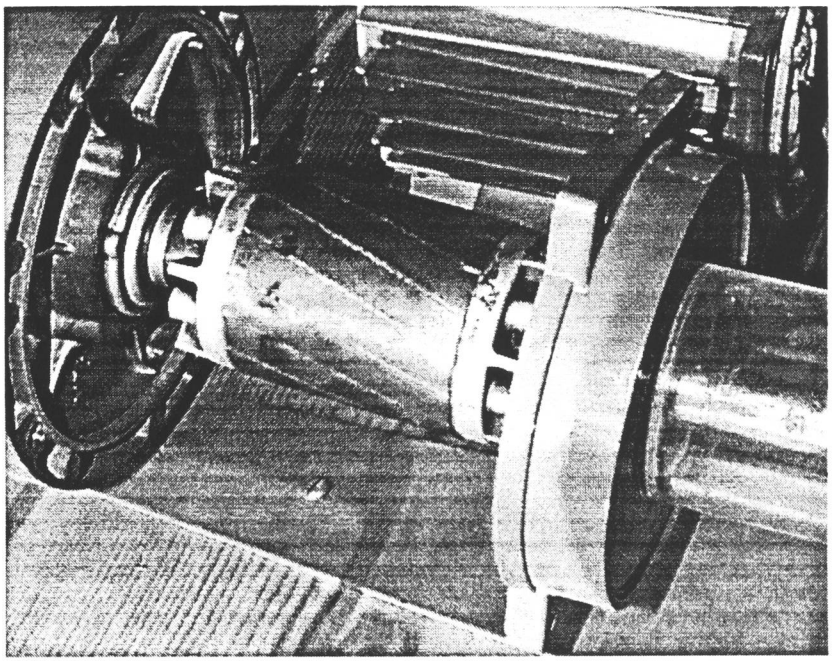

Fig. 2.2: Rotor of Induction Motor

Because of the simple and low cost cage rotor construction techniques, cage rotor induction motors have found wide application in industrial motor drive systems.

The following sections of this chapter show how a mathematical model of asynchronous motors may be derived. The mathematical transformations, required in order to simplify the analysis of these motors, are listed as follows:

1. Space vector notation allows the set of twelve voltage and flux-current equations to be reduced to four in the complex space vector form.
2. The transformation of stator and rotor quantities to a common rotating reference frame makes it possible to eliminate the dependence of the mutual inductance on the angle of rotation relative to the stator. This can be achieved because of the application of the space vector notation.

3. By referring the rotor quantities to the stator circuit, notational unification is achieved. The completed model is thereby transformed to a form which contains in its stator two fictitious windings rotating with the same angular speed.
4. The per unit system brings about notational ease and thereby simplifies the analysis of the induction motor model. All quantities are scaled to those corresponding to rated operation and therefore the results can be assessed more easily.

The resulting motor model is presented in stator fixed co-ordinates, rotor fixed co-ordinates and synchronous rotating co-ordinates in the form of equations and block diagrams. The model is also shown in the form of the unified two-axis theory of electrical machines and in the state space form.

2.1 Induction Motor Model in Natural Co-ordinates

The following simplifying assumptions are made when deriving the set of equations which describe an induction motor with three-phase windings on both the stator and the rotor.

1. The three phase induction motor is symmetrical with regard to windings and magnetic flux distribution around the air gap.
2. The higher harmonics of the spatial field distribution and of the magnetomotive force (MMF) in the air gap are disregarded.
3. The spatially distributed stator and rotor windings are replaced by a specially formed so-called concentrated coil.
4. The effects of anisotropy, magnetic saturation, iron losses and eddy currents are neglected.
5. The coil resistances and inductances are taken to be constant.

For such an idealised motor, the principle of superimposition can be applied. Fig. 2.3 shows the layout and symbols for the induction motor with concentrated windings.

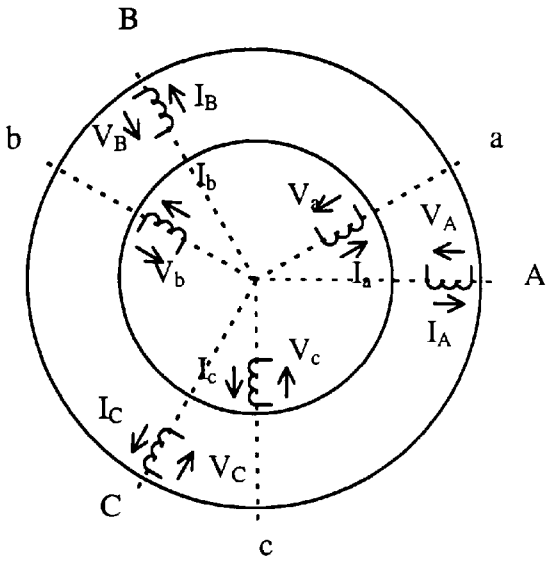

Fig. 2.3: Induction Motor Model in Natural Co-ordinates

The motor model shown in Fig. 2.3 corresponds to a motor with a single pole pair and three windings in both the stator and the rotor. Though motors with a higher number of pole pairs have more than three windings, they may be modelled by using an electrical and a mechanical base frequency in order to simplify the analysis. On the other hand, the cage rotor shown in Fig. 2.2, for example, has 16 rotor bars which is not even divisible by three. Even so, because of the current flowing in the rotor bars, a time varying, rotating magnetic field is produced in the rotor. In order to simplify the analysis, this field may be assumed to be produced by three rotor windings as shown in Fig. 2.3.

In the following, the governing equations of the induction motor model are derived.

The instantaneous stator phase voltages are given by

$$\begin{aligned} V_A &= I_A R_A + \frac{d\Psi_A}{dt} \\ V_B &= I_B R_B + \frac{d\Psi_B}{dt} \\ V_C &= I_C R_C + \frac{d\Psi_C}{dt} \end{aligned} \tag{2.1}$$

where V_A, V_B and V_C are the instantaneous stator voltage values and I_A, I_B and I_C are the instantaneous values of the stator currents. In a motor with symmetrical windings the stator resistances R_A, R_B and R_C are all equal to each other and are therefore called R_S in the following.

$$R_A = R_B = R_C = R_S \tag{2.2}$$

The flux linkages Ψ_A, Ψ_B and Ψ_C consist of the following components:

$$\begin{aligned}\Psi_A &= \Psi_{AA} + \Psi_{BA} + \Psi_{CA} + \Psi_{aA} + \Psi_{bA} + \Psi_{cA} \\ \Psi_B &= \Psi_{AB} + \Psi_{BB} + \Psi_{CB} + \Psi_{aB} + \Psi_{bB} + \Psi_{cB} \\ \Psi_C &= \Psi_{AC} + \Psi_{BC} + \Psi_{CC} + \Psi_{aC} + \Psi_{bC} + \Psi_{cC}\end{aligned} \tag{2.3}$$

where the respective components of the flux linkages with the stator phase 'A' are defined as follows:

Ψ_{AA} by the current of stator winding 'A',

Ψ_{BA} by the current of stator winding 'B',

Ψ_{CA} by the current of stator winding 'C',

Ψ_{aA} by the current of rotor winding 'a',

Ψ_{bA} by the current of rotor winding 'b',

Ψ_{cA} by the current of rotor winding 'c',

Consequently, the above components of the flux linkages are given by the equations:

$$\begin{aligned}\Psi_{AA} &= L_A I_A \quad & \Psi_{aA} &= M_{aA} I_a \\ \Psi_{BA} &= M_{BA} I_B \quad & \Psi_{bA} &= M_{bA} I_b \\ \Psi_{CA} &= M_{CA} I_C \quad & \Psi_{cA} &= M_{cA} I_c\end{aligned} \tag{2.4}$$

The self-inductance of the phase 'A' winding may be defined as:

$$L_A = n_A \frac{\Phi_{AA}}{I_A} = n_A \frac{\Phi_{MA} + \Phi_{\sigma A}}{I_A} = L_{MA} + L_{\sigma A} \tag{2.5}$$

where n_A is the number of turns of stator winding 'A' and $L_{\sigma A}$ is the leakage inductance of stator winding 'A'.

The mutual inductances are defined by:

$$M_{AB} = M_{BA} = \frac{-L_{MA}}{2} \tag{2.6}$$

where the factor *1/2* comes from the relationship

$$\Phi_{AB} = \Phi_{MA} \cos\alpha_{AB} = \Phi_{MA} \cos\frac{2\pi}{3} = \frac{-\Phi_{MA}}{2} \tag{2.7}$$

where α_{AB} is the angle between the flux linkages Ψ_A and Ψ_B. Due to the motor symmetry, it therefore follows that:

$$M_{CA} = M_{AC} = M_{AB} = M_{BA} = \frac{-L_{MA}}{2} \tag{2.8}$$

When determining the mutual inductance between the stator and the rotor windings, account must be taken of the rotating motion of the rotor. This means that the flux of the stator phase 'A' winding, induced by the current of the corresponding phase of the rotor, is a function of the angle γ_m which is the rotor position relative to the stator. Thus, the mutual inductances are given by:

$$M_{aA} = M_{Aa} = \frac{n_a \Phi_{Aa}}{I_A} = \frac{n_a \Phi_{MA} \cos\gamma_m}{I_A} = \frac{n_a}{n_A} L_{MA} \cos\gamma_m$$

$$M_{bA} = M_{Ab} = \frac{n_b \Phi_{Ab}}{I_A} = \frac{n_b \Phi_{MA} \cos\left(\gamma_m + \frac{2\pi}{3}\right)}{I_A} = \frac{n_b}{n_A} L_{MA} \cos\left(\gamma_m + \frac{2\pi}{3}\right) \qquad (2.9)$$

$$M_{cA} = M_{Ac} = \frac{n_c \Phi_{Ac}}{I_A} = \frac{n_c \Phi_{MA} \cos\left(\gamma_m + \frac{4\pi}{3}\right)}{I_A} = \frac{n_c}{n_A} L_{MA} \cos\left(\gamma_m + \frac{4\pi}{3}\right)$$

With the mutual inductances known, the stator flux linkage equations can now be expressed as follows:

$$\Psi_A = (L_{MA} + L_{\sigma A}) I_A - \frac{L_{MA}}{2}(I_B + I_C) + \frac{n_a}{n_A} L_{MA}\left(I_a \cos\gamma_m + I_b \cos\left(\gamma_m + \frac{2\pi}{3}\right) + I_c \cos\left(\gamma_m + \frac{4\pi}{3}\right)\right)$$

$$\Psi_B = (L_{MB} + L_{\sigma B}) I_B - \frac{L_{MB}}{2}(I_A + I_C) + \frac{n_b}{n_B} L_{MB}\left(I_b \cos\gamma_m + I_c \cos\left(\gamma_m + \frac{2\pi}{3}\right) + I_a \cos\left(\gamma_m + \frac{4\pi}{3}\right)\right)$$

$$\Psi_C = (L_{MC} + L_{\sigma C}) I_C - \frac{L_{MC}}{2}(I_A + I_B) + \frac{n_c}{n_C} L_{MC}\left(I_c \cos\gamma_m + I_a \cos\left(\gamma_m + \frac{2\pi}{3}\right) + I_b \cos\left(\gamma_m + \frac{4\pi}{3}\right)\right)$$

(2.10)

The equations for the rotor voltage may be defined similar to the equations (2.1) for the stator voltage. It follows that:

$$V_a = I_a R_a + \frac{d\Psi_a}{dt}$$

$$V_b = I_b R_b + \frac{d\Psi_b}{dt} \qquad (2.11)$$

$$V_c = I_c R_c + \frac{d\Psi_c}{dt}$$

where V_a, V_b and V_c are the instantaneous values of rotor voltages and I_a, I_b and I_c the instantaneous values of rotor currents, R_a, R_b and R_c are the rotor resistances of the three rotor windings, and Ψ_a, Ψ_b and Ψ_c the magnetic flux linkages with rotor phases 'a', 'b' and 'c', respectively. Similar to the stator flux linkages, the rotor flux linkages may be defined as:

$$\Psi_a = \Psi_{aa} + \Psi_{ba} + \Psi_{ca} + \Psi_{Aa} + \Psi_{Ba} + \Psi_{Ca}$$

$$\Psi_b = \Psi_{ab} + \Psi_{bb} + \Psi_{cb} + \Psi_{Ab} + \Psi_{Bb} + \Psi_{Cb} \qquad (2.12)$$

$$\Psi_c = \Psi_{ac} + \Psi_{bc} + \Psi_{cc} + \Psi_{Ac} + \Psi_{Bc} + \Psi_{Cc}$$

which can also be written in terms of currents and corresponding inductances as follows:

$$\begin{aligned}\Psi_a &= L_a I_a + M_{ba} I_b + M_{ca} I_c + M_{Aa} I_A + M_{Ba} I_B + M_{Ca} I_C \\ \Psi_b &= M_{ab} I_a + L_b I_b + M_{cb} I_c + M_{Ab} I_A + M_{Bb} I_B + M_{Cb} I_C \\ \Psi_c &= M_{ac} I_a + M_{bc} I_b + L_c I_c + M_{Ac} I_A + M_{Bc} I_B + M_{Cc} I_C\end{aligned} \tag{2.13}$$

The self-inductance of the rotor phase 'a' winding is defined by:

$$L_a = n_a \frac{\Phi_{Ma} + \Phi_{\sigma a}}{I_a} = L_{Ma} + L_{\sigma a} \tag{2.14}$$

where $L_{\sigma a}$ is the leakage inductance of rotor winding 'a'. The mutual inductances of the rotor windings are therefore given by:

$$\begin{aligned}M_{ba} = M_{ab} &= \frac{n_b \Phi_{Ma} \cos\left(\frac{2\pi}{3}\right)}{I_a} = \frac{-L_{Ma}}{2} \\ M_{ca} = M_{ac} &= \frac{n_c \Phi_{Ma} \cos\left(\frac{4\pi}{3}\right)}{I_a} = \frac{-L_{Ma}}{2}\end{aligned} \tag{2.15}$$

The mutual inductances between the stator and the rotor windings are given by the following equations:

$$\begin{aligned}M_{Aa} = M_{aA} &= \frac{n_A \Phi_{Ma} \cos\gamma_m}{I_a} = \frac{n_A}{n_a} L_{Ma} \cos\gamma_m \\ M_{Ba} = M_{aB} &= \frac{n_B \Phi_{Ma} \cos\left(\gamma_m + \frac{2\pi}{3}\right)}{I_a} = \frac{n_B}{n_a} L_{Ma} \cos\left(\gamma_m + \frac{2\pi}{3}\right) \\ M_{Ca} = M_{aC} &= \frac{n_C \Phi_{Ma} \cos\left(\gamma_m + \frac{4\pi}{3}\right)}{I_a} = \frac{n_C}{n_a} L_{MA} \cos\left(\gamma_m + \frac{4\pi}{3}\right)\end{aligned} \tag{2.16}$$

Since the stator coils have the same number of turns $n_A = n_B = n_C$ and because of the similarity of the equations (2.9) to the equations (2.16) and also because of the symmetry of the stator and the rotor windings of the motor it follows that:

$$\frac{n_a}{n_A} L_{MA} = \frac{n_A}{n_a} L_{Ma} \tag{2.17}$$

The equations resulting from the above analysis may now be rewritten in matrix form as follows:

$$\begin{bmatrix} V_A \\ V_B \\ V_C \end{bmatrix} = R_s \begin{bmatrix} I_A \\ I_B \\ I_C \end{bmatrix} + \frac{d}{dt} \begin{bmatrix} \Psi_A \\ \Psi_B \\ \Psi_C \end{bmatrix} \tag{2.18}$$

$$\begin{bmatrix} V_a \\ V_b \\ V_c \end{bmatrix} = R_r \begin{bmatrix} I_a \\ I_b \\ I_c \end{bmatrix} + \frac{d}{dt} \begin{bmatrix} \Psi_a \\ \Psi_b \\ \Psi_c \end{bmatrix} \tag{2.19}$$

$$\begin{bmatrix}\Psi_A\\ \Psi_B\\ \Psi_C\end{bmatrix} = L_{MA}\begin{bmatrix}1+\sigma_s & -\frac{1}{2} & -\frac{1}{2}\\ -\frac{1}{2} & 1+\sigma_s & -\frac{1}{2}\\ -\frac{1}{2} & -\frac{1}{2} & 1+\sigma_s\end{bmatrix}\begin{bmatrix}I_A\\ I_B\\ I_C\end{bmatrix} + \frac{n_a}{n_A}L_{MA}\begin{bmatrix}\cos\gamma_m & \cos\left(\gamma_m+\frac{2\pi}{3}\right) & \cos\left(\gamma_m+\frac{4\pi}{3}\right)\\ \cos\left(\gamma_m+\frac{4\pi}{3}\right) & \cos\gamma_m & \cos\left(\gamma_m+\frac{2\pi}{3}\right)\\ \cos\left(\gamma_m+\frac{2\pi}{3}\right) & \cos\left(\gamma_m+\frac{4\pi}{3}\right) & \cos\gamma_m\end{bmatrix}\begin{bmatrix}I_a\\ I_b\\ I_c\end{bmatrix} \quad (2.20)$$

$$\begin{bmatrix}\Psi_a\\ \Psi_b\\ \Psi_c\end{bmatrix} = L_{MA}\begin{bmatrix}1+\sigma_r & -\frac{1}{2} & -\frac{1}{2}\\ -\frac{1}{2} & 1+\sigma_r & -\frac{1}{2}\\ -\frac{1}{2} & -\frac{1}{2} & 1+\sigma_r\end{bmatrix}\begin{bmatrix}I_a\\ I_b\\ I_c\end{bmatrix} + \frac{n_a}{n_A}L_{MA}\begin{bmatrix}\cos\gamma_m & \cos\left(\gamma_m+\frac{4\pi}{3}\right) & \cos\left(\gamma_m+\frac{2\pi}{3}\right)\\ \cos\left(\gamma_m+\frac{2\pi}{3}\right) & \cos\gamma_m & \cos\left(\gamma_m+\frac{4\pi}{3}\right)\\ \cos\left(\gamma_m+\frac{4\pi}{3}\right) & \cos\left(\gamma_m+\frac{2\pi}{3}\right) & \cos\gamma_m\end{bmatrix}\begin{bmatrix}I_A\\ I_B\\ I_C\end{bmatrix} \quad (2.21)$$

The stator and rotor leakage factors σ_s and σ_r in the above equations are given by the following equations:

$$\sigma_s = \frac{L_{\sigma A}}{L_{MA}} = \frac{L_A}{L_{MA}} - 1$$
$$\sigma_r = \frac{L_{\sigma a}}{L_{Ma}} = \frac{L_a}{L_{Ma}} - 1 \quad (2.22)$$

Matrix equations (2.18-21) constitute the set of voltage and flux current equations for a three phase a.c. induction motor in natural co-ordinates. However, the mutual inductances depend on the rotor position and this leads to considerable difficulties and numerical complexity when used to model an induction motor. Space vector notation is therefore applied in the following sections, where it is shown that the number of equations is reduced and that all stator and rotor quantities can be transformed to a common reference frame.

2.2 Induction Motor Model in Space Vector Notation

Space vector notation allows the transformation of the natural instantaneous values of a three-phase system onto a complex plane located in the cross section of the motor. In this plane, the space vectors rotate with an angular speed equal to the angular frequency of the three phase supply system. The rotating magnetic field, for example, can be described by a space vector rotating with the same angular speed. Moreover, in the special case of the steady state, where the supply is sinusoidal and symmetric, the space vectors become equal to three-phase phasors, which therefore allow analysis in terms of complex algebra.

In order to transform the induction motor model, in natural co-ordinates, into its equivalent space vector form, the following factor is introduced:

$$\mathbf{a} = e^{j\frac{2\pi}{3}} = -\frac{1}{2} + j\frac{\sqrt{3}}{2} \tag{2.23}$$

The addition of equations (2.1) when multiplied by the above factor, the square of the above factor and 2/3 gives the following equation:

$$\frac{2}{3}\left(\mathbf{1}V_A + \mathbf{a}V_B + \mathbf{a}^2V_C\right) = \frac{2}{3}\left(\mathbf{1}I_A + \mathbf{a}I_B + \mathbf{a}^2I_C\right)R_S + \frac{2}{3}\frac{d}{dt}\left(\mathbf{1}\Psi_A + \mathbf{a}\Psi_B + \mathbf{a}^2\Psi_C\right) \tag{2.24}$$

The factor $\frac{2}{3}$ makes the amplitude of any space vector which represents a three phase balanced system equal to the amplitude of one phase of the three phase system. The factor $\sqrt{\frac{2}{3}}$ may also be used to define the power invariance of a three-phase system with its equivalent two-phase system. Some authors however, do not make use of the normalisation factors $\frac{2}{3}$ and $\sqrt{\frac{2}{3}}$, mainly because the normalisation factor is entirely arbitrary and depends solely on notational convenience.

The stator voltage equation may, therefore, be written in space vector form as:

$$\vec{V}_s = R_s\vec{I}_s + \frac{d\vec{\Psi}_s}{dt} \tag{2.25}$$

where $\vec{V}_s$ is the stator voltage space vector, $\vec{I}_s$ the stator current space vector and $\vec{\Psi}_s$ the stator flux linkage space vector. Similarly to the stator voltage equation, the rotor voltage equation may be written as:

$$\vec{V}_r = R_r\vec{I}_r + \frac{d\vec{\Psi}_r}{dt} \tag{2.26}$$

where $\vec{V}_r$ is the rotor voltage space vector, $\vec{I}_r$ the rotor current space vector and $\vec{\Psi}_r$ the rotor flux linkage space vector. The flux-current equations (2.20-21) may be written in the form:

$$\begin{aligned}\vec{\Psi}_s &= L_{MA}\left(\frac{3}{2} + \sigma_s\right)\vec{I}_s + \frac{3n_a}{2n_A}L_{MA}\vec{I}_r e^{j\gamma_m} \\ \vec{\Psi}_r &= L_{Ma}\left(\frac{3}{2} + \sigma_r\right)\vec{I}_r + \frac{3n_a}{2n_A}L_{Ma}\vec{I}_s e^{-j\gamma_m}\end{aligned} \tag{2.27}$$

These two equations may be further simplified by use of the following definitions:

$$
\begin{aligned}
L_s &= L_{MA}\left(\frac{3}{2}+\sigma_s\right) \\
L_r &= L_{Ma}\left(\frac{3}{2}+\sigma_r\right) \\
M &= \frac{3n_a}{2n_A}L_{MA} = \frac{3n_A}{2n_a}L_{Ma}
\end{aligned}
\tag{2.28}
$$

Thus, the complete set of space vector equations for a three phase induction motor, excluding the mechanical motion equation, can now be expressed as follows:

$$
\begin{aligned}
\vec{V}_s &= R_s\vec{I}_s + \frac{d\vec{\Psi}_s}{dt} & \vec{\Psi}_s &= L_s\vec{I}_s + Me^{j\gamma_m}\vec{I}_r \\
\vec{V}_r &= R_r\vec{I}_r + \frac{d\vec{\Psi}_r}{dt} & \vec{\Psi}_r &= L_r\vec{I}_r + Me^{-j\gamma_m}\vec{I}_s
\end{aligned}
\tag{2.29}
$$

It has, therefore, been shown that the use of space vectors reduces the number of voltage and flux-current equations from twelve in the natural co-ordinate system defined by equations (2.18-21) to four in the space vector representation defined by equations (2.29). This is equivalent to replacing the real motor having three stator phase windings and three rotor phase windings by a fictitious machine with one stator phase winding and one rotor phase winding, as shown in Fig. 2.4.

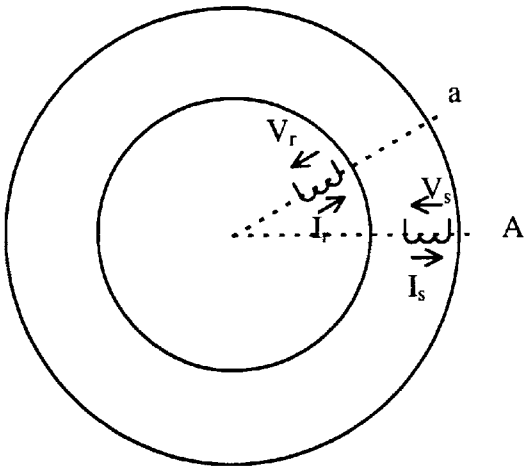

Fig. 2.4: Motor Model with one Stator and one Rotor Winding

It should be noted that the stator equations (2.29) apply to a stator fixed reference frame, while the rotor equations (2.29) apply to a rotor fixed reference frame. The presence of the factors $e^{j\gamma_m}$ and $e^{-j\gamma_m}$ indicates the dependence of mutual inductance on rotor position.

2.3 Common Rotating Co-ordinate System for Stator and Rotor

An important advantage of space vectors as a mathematical tool when applied to the analysis of induction motors is that the motor models can be represented in various systems of rectangular co-ordinates. However, this requires that the stator and rotor of the induction motor model are referred to the same co-ordinate system. This also serves to eliminate the dependence of mutual inductance on the angle γ_m, which is the angle of the rotor relative to the stator.

In order to reduce the set of equations (2.29) to a common co-ordinate system with an arbitrary angular speed Ω_k, the flux-current equations (2.29) are substituted into the voltage equations (2.29) to give:

$$\begin{aligned}\vec{V}_s &= R_s\vec{I}_s + \frac{d\left(L_s\vec{I}_s + Me^{j\gamma_m}\vec{I}_r\right)}{dt} \\ \vec{V}_r &= R_r\vec{I}_r + \frac{d\left(L_r\vec{I}_r + Me^{-j\gamma_m}\vec{I}_s\right)}{dt}\end{aligned} \tag{2.30}$$

The voltages and currents defined by equations (2.30) may now be transformed to a new co-ordinate system where the reference frame rotates with the angular speed Ω_k. This transformation is performed with the following substitutions:

$$\begin{aligned}\vec{V}_s &= \vec{V}_{sk}e^{j\gamma_k} \qquad \vec{V}_r = \vec{V}_{rk}e^{j(\gamma_k-\gamma_m)} \\ \vec{I}_s &= \vec{I}_{sk}e^{j\gamma_k} \qquad \vec{I}_r = \vec{I}_{rk}e^{j(\gamma_k-\gamma_m)}\end{aligned} \tag{2.31}$$

Equations (2.30) can then be expressed as follows:

$$\begin{aligned}\vec{V}_{sk}e^{j\gamma_k} &= R_s\vec{I}_{sk}e^{j\gamma_k} + \frac{d\left(L_s\vec{I}_{sk}e^{j\gamma_k} + M\vec{I}_{rk}e^{j\gamma_k}\right)}{dt} \\ \vec{V}_{rk}e^{j(\gamma_k-\gamma_m)} &= R_r\vec{I}_{rk}e^{j(\gamma_k-\gamma_m)} + \frac{d\left(L_r\vec{I}_{rk}e^{j(\gamma_k-\gamma_m)} + M\vec{I}_{sk}e^{j(\gamma_k-\gamma_m)}\right)}{dt}\end{aligned} \tag{2.32}$$

These two equations can be further expanded to give:

$$\vec{V}_{sk}e^{j\gamma_k} = R_s\vec{I}_{sk}e^{j\gamma_k} + L_s\left(\frac{d\vec{I}_{sk}}{dt}e^{j\gamma_k} + \vec{I}_{rk}e^{j\gamma_k}j\frac{d\gamma_k}{dt}\right) + M\left(\frac{d\vec{I}_{rk}}{dt}e^{j\gamma_k} + \vec{I}_{rk}e^{j\gamma_k}j\frac{d\gamma_k}{dt}\right) \tag{2.33}$$

$$\begin{aligned}\vec{V}_{rk}e^{j(\gamma_k-\gamma_m)} = {} & R_r\vec{I}_{rk}e^{j(\gamma_k-\gamma_m)} + L_r\left(\frac{d\vec{I}_{rk}}{dt}e^{j(\gamma_k-\gamma_m)} + \vec{I}_{rk}e^{j(\gamma_k-\gamma_m)}j\frac{d(\gamma_k-\gamma_m)}{dt}\right) \\ & + M\left(\frac{d\vec{I}_{sk}}{dt}e^{j(\gamma_k-\gamma_m)} + \vec{I}_{sk}e^{j(\gamma_k-\gamma_m)}j\frac{d(\gamma_k-\gamma_m)}{dt}\right)\end{aligned} \tag{2.34}$$

It should be noted, however, that

$$\Omega_k = \frac{d\gamma_k}{dt} \qquad p_b\Omega_m = \frac{d\gamma_m}{dt} \tag{2.35}$$

where p_b is the number of pole pairs. On substitution of equations (2.35) into equations (2.33-34) it follows that:

$$\begin{aligned}\vec{V}_{sk} &= R_s\vec{I}_{sk} + \frac{d\left(L_s\vec{I}_{sk} + M\vec{I}_{rk}\right)}{dt} + j\Omega_k\left(L_s\vec{I}_{sk} + M\vec{I}_{rk}\right)\\ \vec{V}_{rk} &= R_r\vec{I}_{rk} + \frac{d\left(L_r\vec{I}_{rk} + M\vec{I}_{sk}\right)}{dt} + j\left(\Omega_k - p_b\Omega_m\right)\left(L_r\vec{I}_{rk} + M\vec{I}_{sk}\right)\end{aligned} \tag{2.36}$$

Finally, after substituting the flux equations (2.29) into the voltage equations (2.36), the vector equations in terms of a common rotating co-ordinate system can now be expressed as follows:

$$\begin{aligned}\vec{V}_{sk} &= R_s\vec{I}_{sk} + \frac{d\vec{\Psi}_{sk}}{dt} + j\Omega_k\vec{\Psi}_{sk}\\ \vec{V}_{rk} &= R_r\vec{I}_{rk} + \frac{d\vec{\Psi}_{rk}}{dt} + j\left(\Omega_k - p_b\Omega_m\right)\vec{\Psi}_{rk}\\ \vec{\Psi}_{sk} &= L_s\vec{I}_{sk} + M\vec{I}_{rk}\\ \vec{\Psi}_{rk} &= L_r\vec{I}_{rk} + M\vec{I}_{sk}\end{aligned} \tag{2.37}$$

The index k denotes the space vectors in a co-ordinate system rotating with an arbitrary speed Ω_k. The induction motor model may thus be represented as shown in Fig. 2.5.

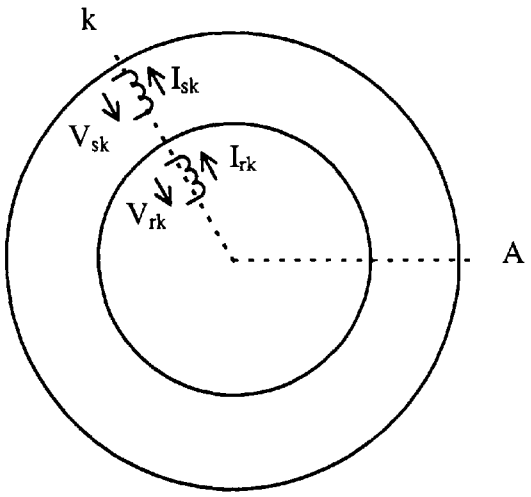

Fig. 2.5: Motor Model with Common Rotating Reference Frame

It can be seen from equations (2.37) that the mutual inductance does not depend on the rotor position, and therefore, simplification of the motor model equations (2.29) has been achieved.

2.4 Referral of Rotor Quantities to Stator

In order to have an equivalent circuit of the induction motor where stator and rotor side are not magnetically but electrically linked, the rotor quantities of equations (2.37) are referred to the stator side. On referring the rotor quantities to the stator side, the rotor current vector can be expressed as

$$\vec{I}_{rk}^{*} = \frac{n_a}{n_A}\vec{I}_{rk} \tag{2.38}$$

Substitution of equations (2.27) and equation (2.38) into equations (2.37) yields:

$$\begin{aligned}
\vec{\Psi}_{sk} &= L_{MA}\left(\frac{3}{2}+\sigma_s\right)\vec{I}_{sk} + \frac{3}{2}L_{MA}\frac{n_a}{n_A}\vec{I}_{rk} = \sigma_s L_{MA}\vec{I}_{sk} + \frac{n_A}{n_a}M\left(\vec{I}_{sk}+\vec{I}_{rk}^{*}\right) \\
\vec{\Psi}_{rk} &= L_{Ma}\left(\frac{3}{2}+\sigma_r\right)\vec{I}_{rk}^{*} + \frac{3}{2}L_{MA}\frac{n_A}{n_a}\vec{I}_{sk} = \frac{n_a}{n_A}\left(\sigma_r L_{Ma}\left(\frac{n_a}{n_A}\right)^2\vec{I}_{rk}^{*} + \frac{n_A}{n_a}M\left(\vec{I}_{sk}+\vec{I}_{rk}^{*}\right)\right)
\end{aligned} \tag{2.39}$$

In order to simplify the equations (2.39), the following definitions are used:

$L_{s\sigma} = \sigma_s L_{MA}$	stator winding leakage inductance
$L_{r\sigma} = \sigma_r L_{MA}$	rotor winding leakage inductance
$L_{r\sigma}^{*} = \left(\frac{n_A}{n_a}\right)^2 L_{r\sigma}$	rotor winding leakage inductance referred to stator
$L_M = \frac{n_A}{n_a}M = \frac{3}{2}L_{MA} = \frac{3}{2}L_{Ma}$	mutual inductance
$\vec{I}_{Mk} = \vec{I}_{sk} + \vec{I}_{rk}^{*}$	magnetising current space vector
$\vec{\Psi}_{Mk} = L_M\vec{I}_{Mk}$	mutual flux linkage vector
$\vec{\Psi}_{s\sigma k} = L_{s\sigma}\vec{I}_{sk}$	stator leakage flux linkage vector
$\vec{\Psi}_{r\sigma k}^{*} = L_{r\sigma}^{*}\vec{I}_{rk}$	rotor leakage flux linkage vector

Using the above definitions, equations (2.39) can be written as

$$\begin{aligned}
\vec{\Psi}_{sk} &= L_{s\sigma}\vec{I}_{sk} + L_M\vec{I}_{Mk} = \vec{\Psi}_{s\sigma k} + \vec{\Psi}_{Mk} \\
\vec{\Psi}_{rk} &= \frac{n_a}{n_A}\left(L_{r\sigma}^{*}\vec{I}_{rk} + L_M\vec{I}_{Mk}\right) = \frac{n_a}{n_A}\left(\vec{\Psi}_{r\sigma k} + \vec{\Psi}_{Mk}\right)
\end{aligned} \tag{2.40}$$

Substitution of the rotor flux linkage defined by equation (2.40) into the rotor voltage equation (2.37) gives the following:

$$\vec{V}_{rk} = \frac{n_A}{n_a} R_r \vec{I}^*_{rk} + \frac{n_a}{n_A}\left(\frac{d\left(\vec{\Psi}_{r\sigma k} + \vec{\Psi}_{Mk}\right)}{dt} + j\left(\Omega_k - p_b\Omega_m\right)\left(\vec{\Psi}_{r\sigma k} + \vec{\Psi}_{Mk}\right)\right) \qquad (2.41)$$

All rotor quantities may now be referred to the stator side of the induction motor model by means of the following definitions:

$$R^*_r = \left(\frac{n_A}{n_a}\right)^2 R_r \qquad \vec{V}^*_{rk} = \frac{n_A}{n_a}\vec{V}_{rk} \qquad \vec{\Psi}^*_{rk} = \frac{n_A}{n_a}\vec{\Psi}_{rk} \qquad (2.42)$$

Substitution of these terms in equation (2.41) gives the following:

$$\vec{V}^*_{rk} = R^*_r \vec{I}^*_{rk} + \left(\frac{d\left(\vec{\Psi}^*_{r\sigma k} + \vec{\Psi}_{Mk}\right)}{dt} + j\left(\Omega_k - p_b\Omega_m\right)\left(\vec{\Psi}^*_{r\sigma k} + \vec{\Psi}_{Mk}\right)\right) \qquad (2.43)$$

The flux linkage however, is made up of the mutual flux $\vec{\Psi}_{Mk}$ and the leakage flux $\vec{\Psi}^*_{r\sigma k}$

$$\vec{\Psi}^*_{rk} = \vec{\Psi}^*_{r\sigma k} + \vec{\Psi}_{Mk} = L^*_{r\sigma}\vec{I}^*_{rk} + L_M I_{Mk} \qquad (2.44)$$

Substitution of equation (2.44) in equation (2.43) gives the following rotor voltage equation:

$$\vec{V}^*_{rk} = R^*_r \vec{I}^*_{rk} + \frac{d\Psi^*_{rk}}{dt} + j\left(\Omega_k - p_b\Omega_m\right)\vec{\Psi}^*_{rk} \qquad (2.45)$$

Similarly, substitution of the magnetising current equation given by $\vec{I}_{Mk} = \vec{I}_{sk} + \vec{I}^*_{rk}$ into the flux linkage equations (2.40) gives:

$$\begin{aligned} \vec{\Psi}_{sk} &= \left(L_{s\sigma} + L_M\right)\vec{I}_{sk} + L_M\vec{I}^*_{rk} \\ \vec{\Psi}^*_{rk} &= \left(L^*_{r\sigma} + L_M\right)\vec{I}^*_{rk} + L_M\vec{I}_{sk} \end{aligned} \qquad (2.46)$$

The self-inductances, however, are the sum of the mutual and the leakage inductances:

$$\begin{aligned} L_s &= L_{s\sigma} + L_M \\ L^*_r &= L^*_{r\sigma} + L_M \end{aligned} \qquad (2.47)$$

Finally, by combining equations (2.44-47) and (2.37), the set of motor equations, where the rotor quantities have been referred to the stator side, can be expressed as follows:

$$\begin{aligned} \vec{V}_{sk} &= R_s\vec{I}_{sk} + \frac{d\vec{\Psi}_{sk}}{dt} + j\Omega_k\vec{\Psi}_{sk} \\ \vec{V}^*_{rk} &= R^*_r\vec{I}^*_{rk} + \frac{d\vec{\Psi}^*_{rk}}{dt} + j\left(\Omega_k - p_b\Omega_m\right)\vec{\Psi}^*_{rk} \\ \vec{\Psi}_{sk} &= L_s\vec{I}_{sk} + L_M\vec{I}^*_{rk} \\ \vec{\Psi}^*_{rk} &= L^*_r\vec{I}^*_{rk} + L_M\vec{I}_{sk} \end{aligned} \qquad (2.48)$$

The induction motor model given above may now be represented as shown in Fig. 2.6.

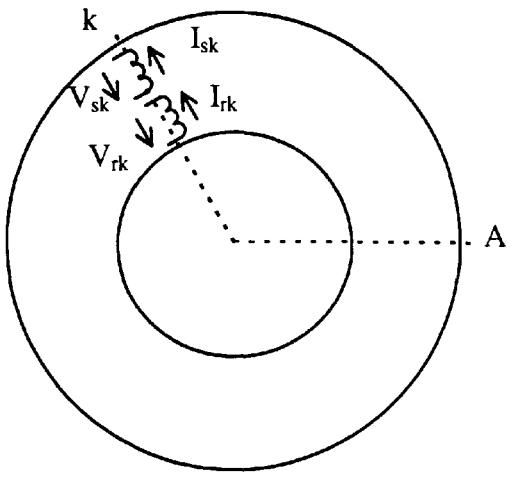

Fig. 2.6: Motor Model with two Windings in the Stator

It may be seen that the motor model now contains in its stator two fictitious windings rotating with angular speed Ω_k.

2.5 Power and Torque with Mechanical Motion Equation

This section serves to clarify the relationships of power and torque of an induction motor. The mechanical motion equation is derived and the complete set of equilibrium equations of a three-phase induction motor is presented.

The instantaneous power supplied to an electrical motor can be expressed as:

$$P(t) = \frac{3}{2}\Re\left(\vec{V}_s \vec{I}_s^*\right) \tag{2.49}$$

where $\vec{I}_s^*$ is the complex conjugate of $\vec{I}_s$. The power can also be expressed using instantaneous voltages and currents. Substitution of the space vector definition equations yields:

$$P(t) = \frac{3}{2}\Re\left(\frac{2}{3}\left(V_A + \mathbf{a}V_B + \mathbf{a}^2 V_C\right)\frac{2}{3}\left(I_A + \mathbf{a}^* I_B + \mathbf{a}^{*2} I_C\right)\right) \tag{2.50}$$

This can be simplified by using the following relations:

$$\begin{aligned} \mathbf{a}^* &= \mathbf{a}^{-1} = \mathbf{a}^2 \\ \mathbf{a}^{*2} &= \mathbf{a}^{-2} = \mathbf{a} \\ \Re(\mathbf{a}) &= \Re\left(\mathbf{a}^2\right) = -\frac{1}{2} \\ I_A + I_B + I_C &= 0 \end{aligned} \tag{2.51}$$

The expression for the instantaneous power gives:

$$P(t) = V_A I_A + V_B I_B + V_C I_C \tag{2.52}$$

For the particular case of the motor operating under steady state with a symmetrical sinusoidal supply, the space vectors can be converted directly to rotating complex phasors, as shown below.

$$\begin{aligned}\vec{V}_s &= \sqrt{2}V_{s(rms)}e^{j\varphi_u}e^{j\Omega_s t}\\ \vec{I}_s^* &= \sqrt{2}I_{s(rms)}e^{-j\varphi_i}e^{-j\Omega_s t}\end{aligned} \tag{2.53}$$

After substitution of equations (2.53) in equation (2.52) follows

$$P = 3V_{s(rms)}I_{s(rms)}\cos(\varphi_u - \varphi_i) \tag{2.54}$$

The overall electromagnetic power of an electric motor can be expressed as the sum of the power supplied to the stator (2.52) and the power in the rotor windings. This can be expressed as

$$P(t) = \frac{3}{2}\Re\left(\vec{V}_s\vec{I}_s^*\right) + \frac{3}{2}\Re\left(\vec{V}_r^s\vec{I}_r^{s*}\right) \tag{2.55}$$

The voltage vector equations (2.48) can then be substituted into equation (2.55). For a fixed reference frame $(\Omega_k = 0)$ this leads to

$$P(t) = \frac{3}{2}\left[\Re\left(R_s\vec{I}_s\vec{I}_s^* + \frac{d\vec{\Psi}_s}{dt}\vec{I}_s^*\right) + \Re\left(R_r^s\vec{I}_r^s\vec{I}_r^{s*} + \frac{d\vec{\Psi}_r^s}{dt}\vec{I}_r^{s*} - jp_b\Omega_m\vec{\Psi}_r^s\vec{I}_r^{s*}\right)\right] \tag{2.56}$$

which can be simplified to

$$P(t) = \frac{3}{2}\left(R_sI_s^2 + R_r^sI_r^{s2}\right) + \frac{3}{2}\Re\left(\frac{d\vec{\Psi}_s}{dt}\vec{I}_s^* + \frac{d\vec{\Psi}_r^s}{dt}\vec{I}_r^{s*}\right) + \frac{3}{2}p_b\Omega_m\Re\left(-j\vec{\Psi}_r^s\vec{I}_r^{s*}\right) \tag{2.57}$$

The first term in expression (2.57) represents the copper losses in the stator and rotor windings, the second term represents the power in the magnetic fields and the third term represents the electromagnetic (shaft output) power P_{out}. The instantaneous electromagnetic torque developed by an electric motor is defined as

$$T = \frac{P_{out}}{\Omega_m} \tag{2.58}$$

where P_{out} is the shaft output power and Ω_m is the mechanical angular rotor speed. The torque can then be expressed by combining equations (2.57c) and (2.58)

$$T = -\frac{3}{2}p_b\Im\left(\vec{\Psi}_r^{s*}\vec{I}_r^s\right) = -\frac{3}{2}p_bL_M\Im\left(\vec{I}_s^*\vec{I}_r^s\right) = \frac{3}{2}p_b\Im\left(\vec{\Psi}_s^*\vec{I}_s\right) \tag{2.59}$$

This torque is equal to the sum of the load torque and the acceleration torque, as shown below:

$$T = T_L + T_d \tag{2.60}$$

where T_L is the external load torque and T_d is the dynamic torque. Friction and elastic torques are neglected. If the moment of inertia is taken to be constant, the dynamic torque may be calculated as follows.

$$T_d = J\frac{d\Omega_m}{dt} \tag{2.61}$$

where J is the lumped inertia of the drive including moments of inertia of the motor, mechanical transmission, clutch and working machine. From equations (2.58) and (2.61) follows

$$\frac{d\Omega_m}{dt} = \frac{1}{J}\left(-\frac{3}{2}p_b L_M \Im\left(\vec{I}_s^{\,*}\vec{I}_r^{\,s}\right) - T_L\right) \tag{2.62}$$

The voltage equations (2.48), the flux-current equations (2.48) and the mechanical motion equation (2.62) give the complete set of electric motor equilibrium equations:

$$\begin{aligned}
\vec{V}_{sk} &= R_s\vec{I}_{sk} + \frac{d\vec{\Psi}_{sk}}{dt} + j\Omega_k\vec{\Psi}_{sk} \\
\vec{V}_{rk}^{\,s} &= R_r^s\vec{I}_{rk}^{\,s} + \frac{d\vec{\Psi}_{rk}^{\,s}}{dt} + j(\Omega_k - p_b\Omega_m)\vec{\Psi}_{rk}^{\,s} \\
\vec{\Psi}_{sk} &= L_s\vec{I}_{sk} + L_M\vec{I}_{rk}^{\,s} \\
\vec{\Psi}_{rk}^{\,s} &= L_r^s\vec{I}_{rk}^{\,s} + L_M\vec{I}_{sk} \\
\frac{d\Omega_m}{dt} &= \frac{1}{J}\left(-\frac{3}{2}p_b L_M \Im\left(\vec{I}_{sk}^{\,*}\vec{I}_{rk}^{\,s}\right) - T_L\right)
\end{aligned} \tag{2.63}$$

The set of equations (2.63) describes a machine model where stator and rotor winding rotate with an arbitrary speed Ω_k. The rotor quantities are referred to the stator side as denoted by the prime index. The relation to the instantaneous currents is as follows:

$$\begin{aligned}
\vec{I}_{sk} &= \frac{2}{3}\left(I_A + \mathbf{a}I_B + \mathbf{a}^2 I_C\right)e^{-j\Omega_k t} \\
\vec{I}_{rk}^{\,s} &= \frac{2n_a}{3n_A}\left(I_a + \mathbf{a}I_b + \mathbf{a}^2 I_c\right)e^{-j(\Omega_k t - \gamma_m)}
\end{aligned} \tag{2.64}$$

An additional advantage of using complex space vectors is that the transition to the steady state, with symmetrical sinusoidal supply, is fairly easy.

2.6 Park's Transformation

The well known Park equations can be derived from equations (2.63) for

$$\Omega_k = p_b\Omega_m \tag{2.65}$$

The complex space vectors are split into their real and imaginary components. The real part is called the direct component; denoted by index '*d*', whereas the imaginary part is

called the quadrature component; denoted by index 'q'. The stator and rotor voltage, current and flux linkage vectors are:

$$\begin{aligned} \vec{V}_{sk} &= V_{sd} + jV_{sq} & \vec{V}^s_{rk} &= V^s_{rd} + jV^s_{rq} \\ \vec{I}_{sk} &= I_{sd} + jI_{sq} & \vec{I}^s_{rk} &= I^s_{rd} + jI^s_{rq} \\ \vec{\Psi}_{sk} &= \Psi_{sd} + j\Psi_{sq} & \vec{\Psi}^s_{rk} &= \Psi^s_{rd} + j\Psi^s_{rq} \end{aligned} \tag{2.66}$$

Equations (2.63) can be split into real and imaginary part:

$$\begin{aligned} V_{sd} &= R_s I_{sd} + \frac{d\Psi_{sd}}{dt} - p_b \Omega_m \Psi_{sq} \\ V_{sq} &= R_s I_{sq} + \frac{d\Psi_{sq}}{dt} - p_b \Omega_m \Psi_{sd} \\ V^s_{rd} &= R^s_r I^s_{rd} + \frac{d\Psi^s_{rd}}{dt} \\ V^s_{rq} &= R^s_r I^s_{rq} + \frac{d\Psi^s_{rq}}{dt} \end{aligned} \tag{2.67}$$

Which are called the Park equations and describe the relations between the voltages, currents and flux linkages in rotor co-ordinates.

2.7 Relationship to Unified Theory of Electric Motors

To establish a relationship to the unified theory of electrical motors, a fixed co-ordinate system is assumed $(\Omega_k = 0)$. The complex space vectors can be written as follows:

$$\begin{aligned} \vec{V}_{sk} &= V_{s\alpha} + jV_{s\beta} & \vec{V}^s_{rk} &= V^s_{r\alpha} + jV^s_{r\beta} \\ \vec{I}_{sk} &= I_{s\alpha} + jI_{s\beta} & \vec{I}^s_{rk} &= I^s_{r\alpha} + jI^s_{r\beta} \\ \vec{\Psi}_{sk} &= \Psi_{s\alpha} + j\Psi_{s\beta} & \vec{\Psi}^s_{rk} &= \Psi^s_{r\alpha} + j\Psi^s_{r\beta} \end{aligned} \tag{2.68}$$

Thus, the voltage equations (2.63) may be spilt into real and imaginary parts, which results in the following expressions:

$$\begin{aligned} V_{s\alpha} &= R_s I_{s\alpha} + \frac{d\Psi_{s\alpha}}{dt} \\ V_{s\beta} &= R_s I_{s\beta} + \frac{d\Psi_{s\beta}}{dt} \\ V^s_{r\alpha} &= R^s_r I^s_{r\alpha} + \frac{d\Psi^s_{r\alpha}}{dt} + p_b \Omega_m \Psi^s_{r\beta} \\ V^s_{r\beta} &= R^s_r I^s_{r\beta} + \frac{d\Psi^s_{r\beta}}{dt} - p_b \Omega_m \Psi^s_{r\alpha} \end{aligned} \tag{2.69}$$

After substitution of equations (2.68) into equations (2.69) and employing matrix notation, it follows that

$$\begin{bmatrix} V_{s\alpha} \\ V_{s\beta} \\ V_{r\alpha}^{s} \\ V_{r\beta}^{s} \end{bmatrix} = \begin{bmatrix} R_s + sL_s & 0 & sL_M & 0 \\ 0 & R_s + sL_s & 0 & sL_M \\ sL_M & p_b\Omega_m L_M & R_r^s + sL_r & p_b\Omega_m L_M \\ -p_b\Omega_m L_M & sL_M & -p_b\Omega_m L_M & R_r^s + sL_r \end{bmatrix} \begin{bmatrix} I_{s\alpha} \\ I_{s\beta} \\ I_{r\alpha}^{s} \\ I_{r\beta}^{s} \end{bmatrix} \tag{2.70}$$

where $s = \frac{d}{dt}$ denotes the derivative operator. Equation (2.70) is the well known matrix form of the conventional equations of the unified two-axis theory of electric machines.

2.8 Per Unit System

Per unit systems are defined in terms of base units which mostly correspond to rated motor parameters. Commonly adopted base units are V_b, I_b and Ω_b, and from these derivative base quantities are derived. In the following, absolute physical quantities are denoted in capital letters, whereas quantities in relative units are denoted by small letters. The p.u. system for an induction motor is referred to the following base quantities:

$$\begin{aligned} V_b &= \sqrt{2}V_{s(rms)N} \\ I_b &= \sqrt{2}I_{s(rms)N} \\ \Omega_b &= 2\pi f_{sN} \end{aligned} \tag{2.71}$$

From the above base quantities, the following derivative quantities are obtained:

$$\begin{aligned} Z_b &= \frac{V_b}{I_b} \quad & L_b &= \frac{V_b}{\Omega_b I_b} \quad & \Omega_{mb} &= \frac{\Omega_b}{p_b} \\ \Psi_b &= \frac{V_b}{\Omega_b} \quad & S_b &= \frac{3}{2}V_b I_b \quad & T_b &= \frac{S_b}{\Omega_{mb}} \end{aligned} \tag{2.72}$$

The set of motor equations (2.63) is transformed into the per unit system by using the base quantities from equations (2.72).

It follows that

$$\begin{aligned} \vec{v}_{sk} &= r_s\vec{i}_{sk} + T_N\frac{d\vec{\psi}_{sk}}{dt} + j\omega_k\vec{\psi}_{sk} \\ \vec{v}_{rk} &= r_r\vec{i}_{rk} + T_N\frac{d\vec{\psi}_{rk}}{dt} + j(\omega_k - \omega_m)\vec{\psi}_{rk} \\ \vec{\psi}_{sk} &= x_s\vec{i}_{sk} + x_M\vec{i}_{rk} \\ \vec{\psi}_{rk} &= x_r\vec{i}_{rk} + x_M\vec{i}_{sk} \\ \frac{d\omega_m}{dt} &= \frac{1}{T_M}\left(\Im\left(\vec{\psi}_{sk}^{*}\vec{i}_{sk}\right) - T_L\right) \end{aligned} \tag{2.73}$$

with $T_N = \frac{1}{\Omega_b}$ and $T_M = J\frac{\Omega_{mb}}{T_b}$. The prime index for the rotor quantities referred to the stator has been dropped as the rotor quantities are referred to the same base units. The inductances in the flux-current equations have been replaced by the corresponding reactances. This does not have any effect, as the identity $l = \frac{L}{L_b} = \frac{X}{2\pi L_b} = x$ holds for the p.u. system. The developed torque T_l, expressed in p.u., attains the value of unity only when there is no reactive power input to the machine, due to the base torque definition $T_b = \frac{S_b}{\Omega_{mb}}$. If, however, the power factor is less than unity, rated operation results in a torque p.u. value less than unity.

A further advantage of the p.u. system is that the stability of the numerical solution of equations (2.73) is improved, as all state variables are scaled to unity.

2.9 Induction Motor in Stator-Fixed Co-ordinates

When the angular speed of the reference frame is set to $\omega_k = 0$, the set of induction motor vector equations (2.73) can be written as

$$\begin{aligned}
\vec{v}_s &= r_s\vec{i}_s + T_N\frac{d\vec{\psi}_s}{dt} \\
\vec{v}_r &= r_r\vec{i}_r + T_N\frac{d\vec{\psi}_r}{dt} - j\omega_m\vec{\psi}_r \\
\vec{\psi}_s &= x_s\vec{i}_s + x_M\vec{i}_r \\
\vec{\psi}_r &= x_r\vec{i}_r + x_M\vec{i}_s \\
\frac{d\omega_m}{dt} &= \frac{1}{T_M}\left(\Im\left(\vec{\psi}_s^*\vec{i}_s\right) - T_L\right)
\end{aligned} \tag{2.74}$$

The complex space vectors may then be resolved into the real and imaginary components α and β as follows:

$$\begin{aligned}
\vec{v}_s &= v_{s\alpha} + jv_{s\beta} & \vec{v}_r &= v_{r\alpha} + jv_{r\beta} \\
\vec{i}_s &= i_{s\alpha} + ji_{s\beta} & \vec{i}_r &= i_{r\alpha} + ji_{r\beta} \\
\vec{\psi}_s &= \psi_{s\alpha} + j\psi_{s\beta} & \vec{\psi}_r &= \psi_{r\alpha} + j\psi_{r\beta}
\end{aligned} \tag{2.75}$$

With equations (2.75), the set of motor equations (2.74) in stator fixed co-ordinates can then be resolved into the following components:

$$
\begin{aligned}
v_{s\alpha} &= r_s i_{s\alpha} + T_N \frac{d\psi_{s\alpha}}{dt} & \psi_{s\alpha} &= x_s i_{s\alpha} + x_M i_{r\alpha} \\
v_{s\beta} &= r_s i_{s\beta} + T_N \frac{d\psi_{s\beta}}{dt} & \psi_{s\beta} &= x_s i_{s\beta} + x_M i_{r\beta} \\
v_{r\alpha} &= r_r i_{r\alpha} + T_N \frac{d\psi_{r\alpha}}{dt} + \omega_m \psi_{r\beta} & \psi_{r\alpha} &= x_r i_{r\alpha} + x_M i_{s\alpha} \\
v_{r\beta} &= r_r i_{r\beta} + T_N \frac{d\psi_{r\beta}}{dt} - \omega_m \psi_{r\alpha} & \psi_{r\beta} &= x_r i_{r\beta} + x_M i_{s\beta} \\
\frac{d\omega_m}{dt} &= \frac{1}{T_M}\left(\psi_{s\alpha} i_{s\beta} - \psi_{s\beta} i_{s\alpha} - T_L\right)
\end{aligned}
\tag{2.76}
$$

Fig. 2.7 shows the block diagram corresponding to equations (2.76).

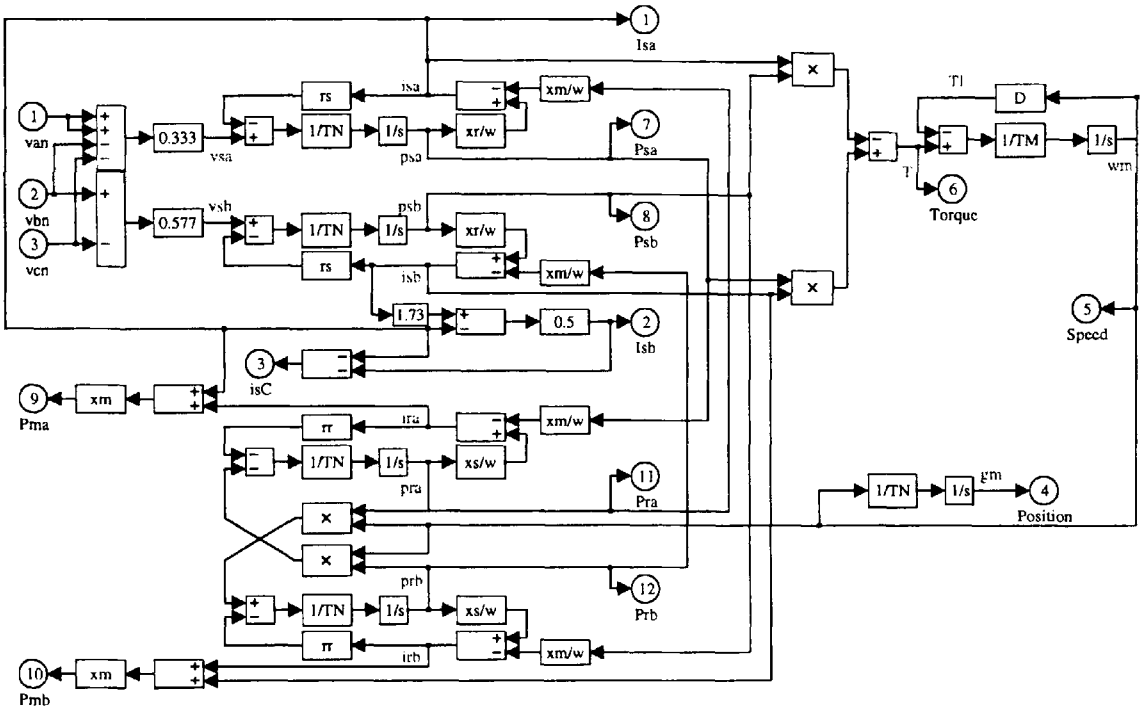

Fig. 2.7: Induction Motor Model in Stator-fixed Co-ordinates

The rotor voltage components are $v_{r\alpha} = v_{r\beta} = 0$, which is an additional condition for squirrel cage induction motors.

2.10 Induction Motor in Rotor-Fixed Co-ordinates

When the rotor state variables are subject to investigation, it is advantageous to use a co-ordinate system which is fixed to the rotor. The speed of the rotating co-ordinate system is therefore set equal to the angular speed of the rotor

$$
\omega_k = \omega_m = T_N \frac{d\gamma_m}{dt} \tag{2.77}
$$

For the set of motor equations (2.73) therefore follows:

$$\begin{aligned}
\vec{v}_s &= r_s\vec{i}_s + T_N\frac{d\vec{\psi}_s}{dt} + j\omega_m\vec{\psi}_s \\
\vec{v}_r &= r_r\vec{i}_r + T_N\frac{d\vec{\psi}_r}{dt} \\
\vec{\psi}_s &= x_s\vec{i}_s + x_M\vec{i}_r \\
\vec{\psi}_r &= x_r\vec{i}_r + x_M\vec{i}_s \\
\frac{d\omega_m}{dt} &= \frac{1}{T_M}\left(\Im\left(\vec{\psi}_s^{*}\vec{i}_s\right) - T_L\right)
\end{aligned} \tag{2.78}$$

The complex space vector equations can then be resolved in the components 'd' and 'q'.

$$\begin{aligned}
\vec{v}_s &= v_{sd} + jv_{sq} & \vec{v}_r &= v_{rd} + jv_{rq} \\
\vec{i}_s &= i_{sd} + ji_{sq} & \vec{i}_r &= i_{rd} + ji_{rq} \\
\vec{\psi}_s &= \psi_{sd} + j\psi_{sq} & \vec{\psi}_r &= \psi_{rd} + j\psi_{rq}
\end{aligned} \tag{2.79}$$

For the complex space vector equations (2.78) then follows

$$\begin{aligned}
v_{sd} &= r_s i_{sd} + T_N\frac{d\psi_{sd}}{dt} - \omega_m\psi_{sq} & \psi_{sd} &= x_s i_{sd} + x_M i_{rd} \\
v_{sq} &= r_s i_{sq} + T_N\frac{d\psi_{sq}}{dt} + \omega_m\psi_{sd} & \psi_{sq} &= x_s i_{sq} + x_M i_{rq} \\
v_{rd} &= r_r i_{rd} + T_N\frac{d\psi_{rd}}{dt} & \psi_{rd} &= x_r i_{rd} + x_M i_{sd} \\
v_{rq} &= r_r i_{rq} + T_N\frac{d\psi_{rq}}{dt} & \psi_{rq} &= x_r i_{rq} + x_M i_{sq} \\
& & \frac{d\omega_m}{dt} &= \frac{1}{T_M}\left(\psi_{sd}i_{sq} - \psi_{sq}i_{sd} - T_L\right)
\end{aligned} \tag{2.80}$$

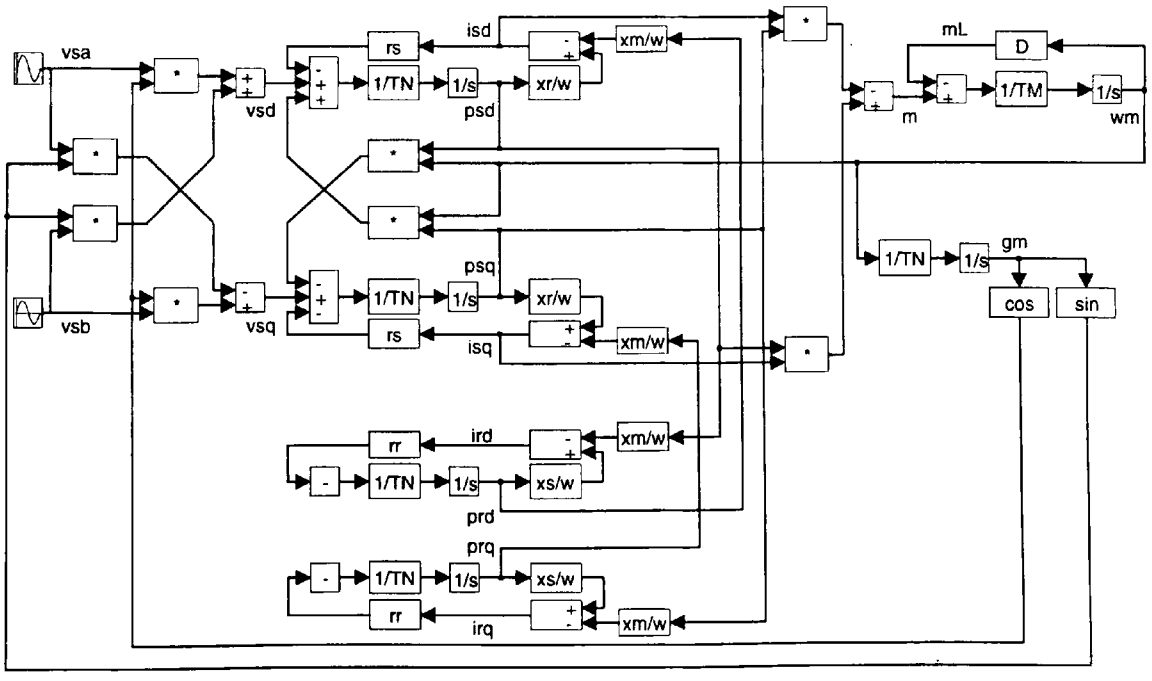

Fig. 2.8: Induction Motor Model in Rotor-fixed Co-ordinates

It is also shown in the diagram how the input voltages v_{sd} and v_{sq} can be obtained from the stator fixed voltages $v_{s\alpha}$ and $v_{s\beta}$ and the rotor position γ_m.

2.11 Induction Motor in Synchronously Rotating Co-ordinates

Vector control is based on the transformation to a co-ordinate system rotating with synchronous frequency $(\omega_k = \omega_s)$. The space vector equations (2.73) take the form

$$\begin{aligned}
\vec{v}_s &= r_s\vec{i}_s + T_N\frac{d\vec{\psi}_s}{dt} + j\omega_s\vec{\psi}_s \\
\vec{v}_r &= r_r\vec{i}_r + T_N\frac{d\vec{\psi}_r}{dt} + j(\omega_s - \omega_m)\vec{\psi}_r \\
\vec{\psi}_s &= x_s\vec{i}_s + x_M\vec{i}_r \\
\vec{\psi}_r &= x_r\vec{i}_r + x_M\vec{i}_s \\
\frac{d\omega_m}{dt} &= \frac{1}{T_M}\left(\Im(\vec{\psi}_s^*\vec{i}_s) - T_L\right)
\end{aligned} \tag{2.81}$$

These equations may be split into their real and imaginary components. However, in the transient state, the synchronous speed for the space vectors $\vec{v}_s$, $\vec{i}_s$, $\vec{\psi}_s$, $\vec{v}_r$, $\vec{i}_r$, and $\vec{\psi}_r$ is different. It is, therefore, necessary to align the co-ordinate system with one of these vectors. If the air gap flux is also taken into consideration and the rotor voltage vector is set to zero, as is the case for squirrel cage rotors, the co-ordinate system can be aligned to six different vectors. For convenience the co-ordinate system is aligned with either the stator current vector or one of the flux linkage vectors, as the torque expression (2.73) can then be simplified and the stator current can be controlled easily. In the following, the co-ordinate system is aligned with the stator flux linkage vector. For the real and imaginary components it follows

$$\begin{aligned}
\vec{v}_s &= v_{sx} + jv_{sy} & \vec{v}_r &= v_{rx} + jv_{ry} \\
\vec{i}_s &= i_{sx} + ji_{sy} & \vec{i}_r &= i_{rx} + ji_{ry} \\
\vec{\psi}_s &= \psi_{sx} & \vec{\psi}_r &= \psi_{rx} + j\psi_{ry}
\end{aligned} \tag{2.82}$$

Vector equations (2.81) can then be resolved into their components:

$$\begin{aligned}
v_{sx} &= r_s i_{sx} + T_N\frac{d\psi_{sx}}{dt} & \psi_{sx} &= x_s i_{sx} + x_M i_{rx} \\
v_{sy} &= r_s i_{sy} + \omega_s\psi_{sx} & 0 &= x_s i_{sy} + x_M i_{ry} \\
v_{rx} &= r_r i_{rx} + T_N\frac{d\psi_{rx}}{dt} - (\omega_s - \omega_m)\psi_{ry} & \psi_{rx} &= x_r i_{rx} + x_M i_{sx} \\
v_{ry} &= r_r i_{ry} + T_N\frac{d\psi_{rq}}{dt} + (\omega_s - \omega_m)\psi_{rx} & \psi_{ry} &= x_r i_{ry} + x_M i_{sy} \\
& & \frac{d\omega_m}{dt} &= \frac{1}{T_M}\left(\psi_{sx} i_{sy} - T_L\right)
\end{aligned} \tag{2.83}$$

As can be seen from torque expression (2.83), the developed torque depends only on two components. The stator flux linkage component can be kept constant, while the 'y'-component of the stator current can be used to control the torque. The torque expression is thereby transformed from a form in which four oscillating quantities appear (equations 2.76 and 2.80) to a form where one component controls the torque in a linear manner. The corresponding block diagram is shown in Fig. 2.9.

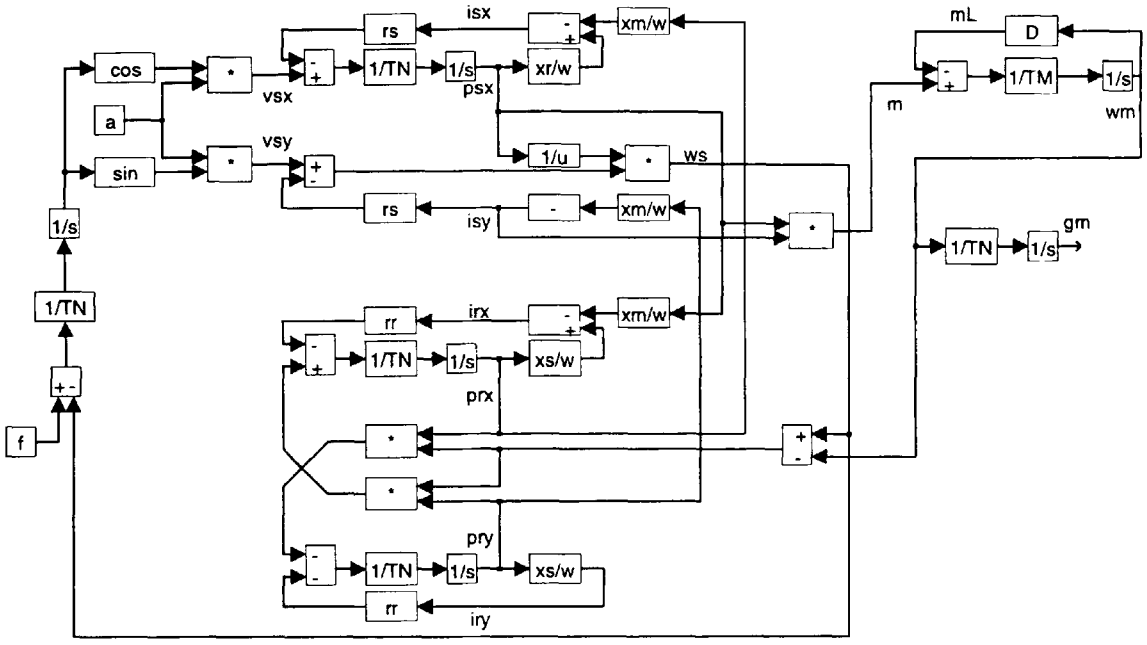

Fig. 2.9: Induction Motor Model in Stator-flux oriented Co-ordinates

The block diagram also shows that the synchronous frequency of the stator flux linkage can be obtained from equation (2.83) and is used as a feedback signal to obtain the stator voltage components in a co-ordinate system rotating with the stator flux linkage vector.

2.12 Motor Model Numerical Values used throughout Investigation

For the simulations in the following sections, a particular set of motor model parameters has been used. The induction motor under investigation has the following rated values:

$$V_{s(RMS)N} = 230V \qquad I_{s(RMS)N} = 5.2A \qquad f_s = 50Hz \tag{2.84}$$

Corresponding to equation (2.71) the per unit base quantities are:

$$V_b = 325.3V \qquad I_b = 7.35A \qquad \omega_b = 314.2\frac{rad}{s} \tag{2.85}$$

In accordance with Equ. 2.72, the derivative per unit quantities can be calculated as

$$
\begin{aligned}
Z_b &= 44.23\Omega & S_b &= 3588VA \\
\Psi_b &= 1.035Wb & \Omega_{mb} &= 157.1\frac{rad}{s} \\
L_b &= 0.1408H & T_b &= 22.84Nm
\end{aligned}
\tag{2.86}
$$

The motor parameter have been obtained from the manufacturer and are as follows:

$$
\begin{aligned}
R_s &= 3.76\Omega & L_M &= 0.268H \\
R_r &= 2.571\Omega & L_S &= 0.278H \\
p_b &= 2 & L_R &= 0.296H
\end{aligned}
\tag{2.87}
$$

The p.u. motor parameter can be calculated by dividing the absolute parameters by their corresponding base quantities. This results into the following settings:

$$
\begin{aligned}
r_s &= 0.085 & x_m &= 1.904 \\
r_r &= 0.0581 & x_s &= 1.986 \\
T_N &= 0.0032 & x_r &= 2.102 \\
T_M &= 0.1375
\end{aligned}
\tag{2.88}
$$

The load model consists of only two parameters. The moment of inertia has been chosen to give a transient response that leads to rated operation within one second for a direct on line start of the motor. The load torque has been assumed to be proportional to speed. The load torque in the p.u. system therefore gives

$$T_L = D\omega_m \tag{2.89}$$

where the parameter D has been chosen to give rated operation at rated speed. The load parameters are then given by

$$
\begin{aligned}
J &= 0.05kgm^2 \\
D &= 0.678
\end{aligned}
\tag{2.90}
$$

Chapter 3: Steady State Analysis

3.0 Introduction

This chapter deals with the conditions under which induction motors operate in the steady state, i.e. without change of rotor speed or load torque. The corresponding voltage, frequency, current and flux required for which a motor operates with a certain speed at a certain load torque are shown. The motor power conditions are examined as well as the motor efficiency and the motor power factor. The analysis is subdivided into four different categories depending on the motor supply capabilities as follows:

1. Constant voltage, constant frequency (CVCF) mode corresponds to mains supply operation. Rotor speed control cannot be carried out, as the rotor speed varies with load torque only.
2. Variable voltage, constant frequency (VVCF) operation allows the control of motor speed independently of the load torque. However, the torque-speed control area is limited by the CVCF torque speed characteristic. The poor low speed efficiency of the CVCF mode also applies for VVCF operation.
3. With constant voltage, variable frequency (CVVF) operation, much higher rotor speeds than those available with CVCF or VVCF operation can be obtained.
4. The variable voltage, variable frequency (VVVF) mode allows a much higher load torque and better efficiency at low speed operation than the above mentioned methods. A VVVF power supply is of course also capable of CVVF operation, so that the high speed mode characteristics of CVVF also apply.

When an induction motor operates in the steady state and is supplied by symmetrical and sinusoidal waveforms, the space vectors $\vec{v}_s$, $\vec{i}_s$, $\vec{i}_m$, $\vec{i}_r$, $\vec{\psi}_s$, $\vec{\psi}_m$ and $\vec{\psi}_r$ become formally identical to phasors. Therefore, no notational difference is made between the two concepts and the space vector diagrams become identical to phasor diagrams. As has been shown in section 2.11, the vector quantities in the steady state remain constant when a synchronously rotating co-ordinate system is employed. Therefore, the time related derivatives from equations 2.73 are all set to zero, as shown below.

$$
\begin{aligned}
\vec{v}_s &= r_s\vec{i}_s + j\omega_s\vec{\psi}_s \\
0 &= r_r\vec{i}_r + j(\omega_s - \omega_m)\vec{\psi}_r \\
\vec{\psi}_s &= x_s\vec{i}_s + x_m\vec{i}_r \\
\vec{\psi}_r &= x_r\vec{i}_r + x_m\vec{i}_s \\
T_l &= \Im\left(\vec{\psi}_s^{*}\vec{i}_s\right)
\end{aligned}
\tag{3.1}
$$

After substituting the flux equations (3.1c and 3.1d) into the voltage equations (3.1a and 3.1b), it follows that

$$
\begin{aligned}
\vec{v}_s &= \left(r_s + j\omega_s x_{ls}\right)\vec{i}_s + j\omega_s x_m\left(\vec{i}_s + \vec{i}_r\right) \\
0 &= \left(\frac{r_r}{s} + j\omega_s x_{lr}\right)\vec{i}_r + j\omega_s x_m\left(\vec{i}_s + \vec{i}_r\right)
\end{aligned}
\tag{3.2}
$$

where

$$
\begin{aligned}
x_{ls} &= x_s - x_m \\
x_{lr} &= x_r - x_m \\
s &= \frac{\omega_s - \omega_m}{\omega_s} = \frac{\omega_r}{\omega_s}
\end{aligned}
\tag{3.3}
$$

From equations 3.2 the well known equivalent circuit for an induction motor can be drawn, as shown in Fig. 3.1:

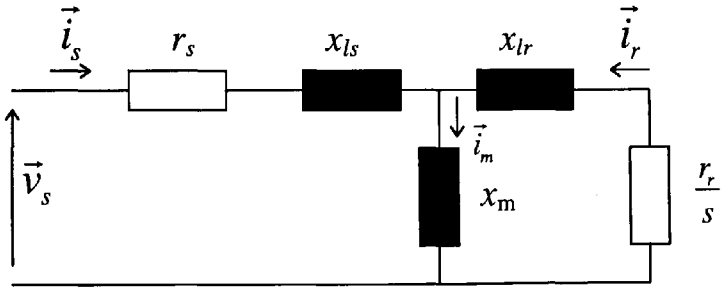

Fig. 3.1: Steady State Equivalent Circuit of Induction Motor

The impedance of the induction motor model may be calculated by substituting equations (3.3) into equations (3.2):

$$
\begin{aligned}
\vec{v}_s &= r_s\vec{i}_s + j\omega_s\left(x_s\vec{i}_s + x_m\vec{i}_r\right) \\
0 &= r_r\vec{i}_r + j(\omega_s - \omega_m)\left(x_r\vec{i}_r + x_m\vec{i}_s\right)
\end{aligned}
\tag{3.4}
$$

Equation (3.4) can then be solved for $\vec{i}_r$ to give:

$$\vec{i}_r = \frac{-jx_m(\omega_s - \omega_m)}{r_r + jx_r(\omega_s - \omega_m)}\vec{i}_s \tag{3.5}$$

This equation can be substituted into equation (3.2) and rearranged to give the following expression for the induction motor impedance:

$$\frac{\vec{v}_s}{\vec{i}_s} = \vec{z}_s = r_s + j\omega_s x_s + \frac{\omega_s^2 x_m^2}{\frac{r_r}{s} + j\omega_s x_r} \tag{3.6}$$

The following set of expressions allows calculation of current and flux for the stator and rotor of the steady state induction motor model for a known input voltage $\vec{v}_s$.

$$\begin{aligned}
\vec{i}_s &= \frac{\vec{v}_s}{\vec{z}_s} \\
\vec{\psi}_s &= \frac{\vec{v}_s - r_s\vec{i}_s}{j\omega_s} \\
\vec{i}_r &= \frac{\vec{\psi}_s - x_s\vec{i}_s}{x_m} \\
\vec{\psi}_r &= x_r\vec{i}_r + x_m\vec{i}_s
\end{aligned} \tag{3.7}$$

The corresponding phasor diagram can be seen in Fig. 3.2.

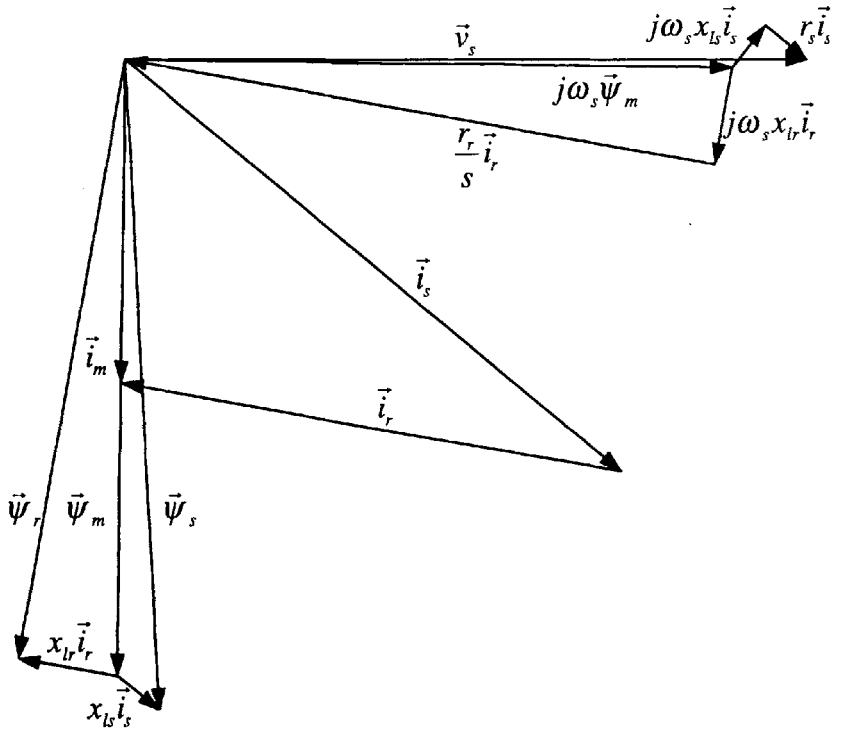

Fig. 3.2: Phasor Diagram for Rated Operation

The diagram is shown for rated operation of the motor.

3.1 Constant Voltage, Constant Frequency Operation

This section deals with the induction motor operation in the steady state when being supplied with sinusoidal voltage waveforms of constant amplitude and frequency. The motor current and flux may be calculated using equation 3.7. The developed torque may then be calculated using the torque expression from the motor model (equation 3.1). A typical torque speed characteristic is given in Fig. 3.3.

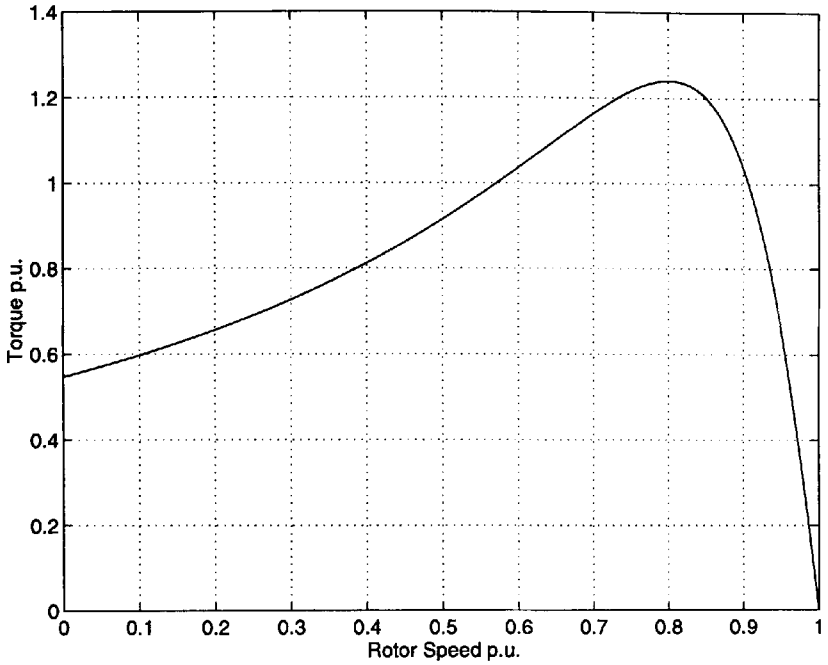

Fig. 3.3: Torque-Speed Characteristic in CVCF Operation

Only motoring action is considered in the figure. Braking action occurs for negative values of speed, whereas generator action occurs for speed values beyond unity. Fig. 3.3 shows that in the range of motor action between standstill and the speed at which the maximum torque is developed, the torque increases more than proportionally with speed. This means that within this range there is a condition of instability, in the sense that if the torque developed is greater than the resisting torque, the speed will continue to rise until the point of maximum torque has been passed. Beyond the point of maximum torque, and up to synchronism, the conditions are stable, as any increase of load torque causes the motor to slow down and, therefore, automatically to develop greater torque to meet the load requirement. Conversely, if the load torque becomes greater than the breakdown torque of the motor, a decrease in speed is accompanied by a decreased motor torque and the speed falls off to zero. It can, therefore, be said that the speed range of the motor is small in CVCF operation ($\omega_m = 0.8 - 1.0 p.u.$ in Fig. 3.3) and

that the torque directly depends on the rotor speed. Because of the increased slip frequency in high torque operation, the power conditions of the motor are acceptable in a small part of the stable operation region only. The input power P_{in}, output power P_{out}, apparent power S, reactive power Q and the power losses P_{loss} may be calculated as follows:

$$\begin{aligned} S &= |\vec{v}_s \vec{i}_s^{\,*}| \\ P_{in} &= \Re\{\vec{v}_s \vec{i}_s^{\,*}\} \\ Q &= \Im\{\vec{v}_s \vec{i}_s^{\,*}\} \\ P_{out} &= \omega_m T_l \\ P_{loss} &= P_{in} - P_{out} \end{aligned} \tag{3.8}$$

The power conditions for CVCF operation are shown in Fig. 3.4.

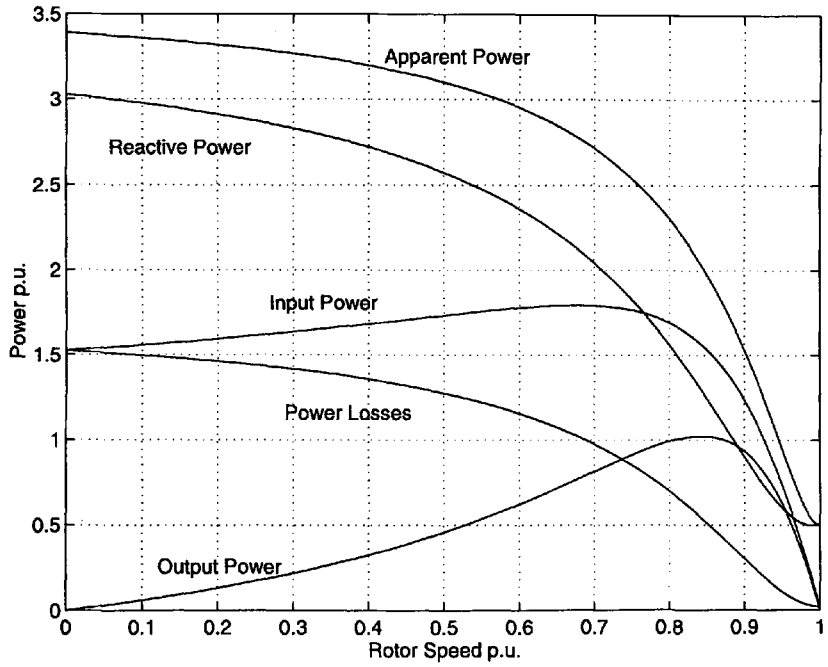

Fig. 3.4: Power Conditions in CVCF Operation

Fig. 3.4 shows how electrical and mechanical power varies with varying rotor speed. For zero speed, the apparent and reactive power are more than three times the rated apparent power. This condition may occur for a locked rotor or for a load with high inertia. The power losses are at a maximum, as the output power is zero at zero speed. For higher rotor speed, apparent power, reactive power and the power losses decrease, while the input power and the output power increase. The input power is maximised at a speed of 0.7p.u., while the output power is maximised at a rotor speed of 0.84p.u. At rated operation ($\omega_m = 0.95 p.u.$), the power losses are low and the apparent power is near unity. At synchronous operation ($\omega_m = 1 p.u.$), the input power, the output power and

the power losses become zero, while the apparent power becomes equal to the reactive power.

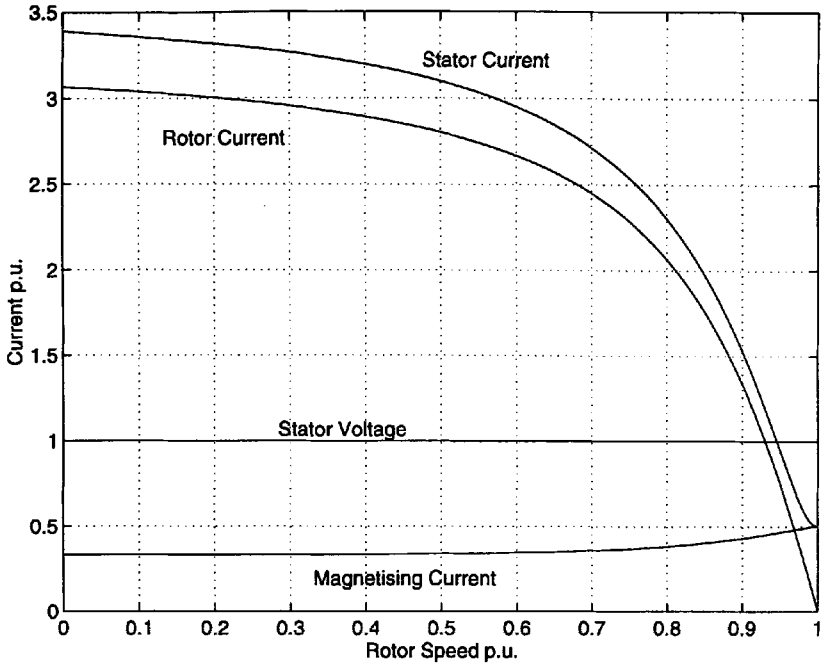

Fig. 3.5: Motor Currents in CVCF Operation

Fig. 3.5 shows the variation of the motor currents with load. It can be seen that the stator current characteristic is identical to the apparent power characteristic. This may also be seen from Equ 3.8. As the magnetising current remains low throughout the speed range, the rotor and stator current characteristics are similar. For synchronous operation however, the rotor current becomes zero and the stator current amplitude becomes equal to the magnetising current amplitude.

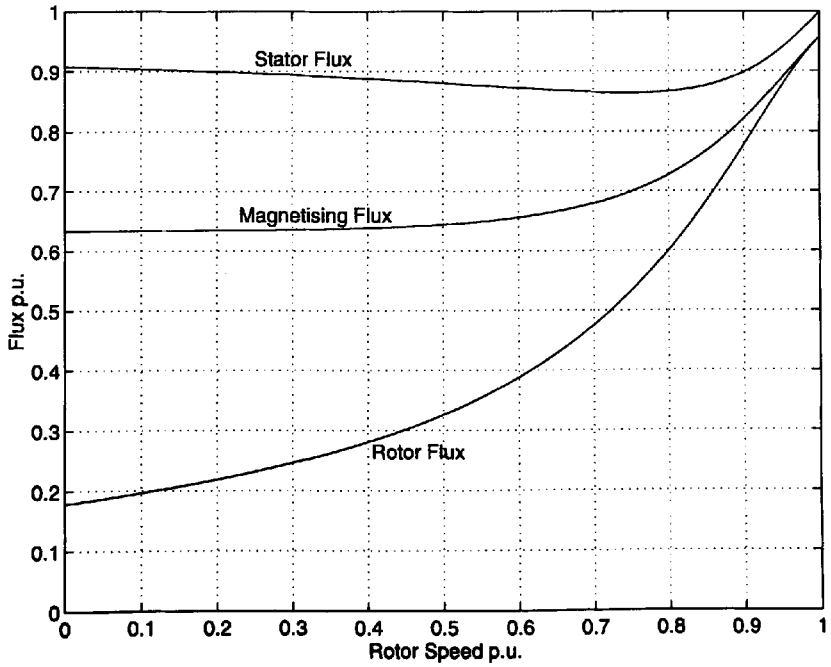

Fig. 3.6: Motor Flux in CVCF Operation

Fig. 3.6 shows the characteristics for the stator, rotor and magnetising flux. It may be seen that even at locked rotor conditions with very high currents, the rated flux levels are not exceeded. In fact, the rotor and magnetising flux are lowest for the locked rotor condition. The stator, magnetising and the rotor flux are maximised for synchronous operation ($\omega_m = \omega_s$).

The efficiency η, power factor $\cos\varphi$ and the product of efficiency and power factor $\eta\cos\varphi$ may be calculated as follows:

$$\eta = \frac{P_{out}}{P_{in}}$$
$$\cos\varphi = \frac{P_{in}}{S} \tag{3.9}$$
$$\eta\cos\varphi = \frac{P_{out}}{S}$$

The quantities are shown for CVCF operation in Fig. 3.7.

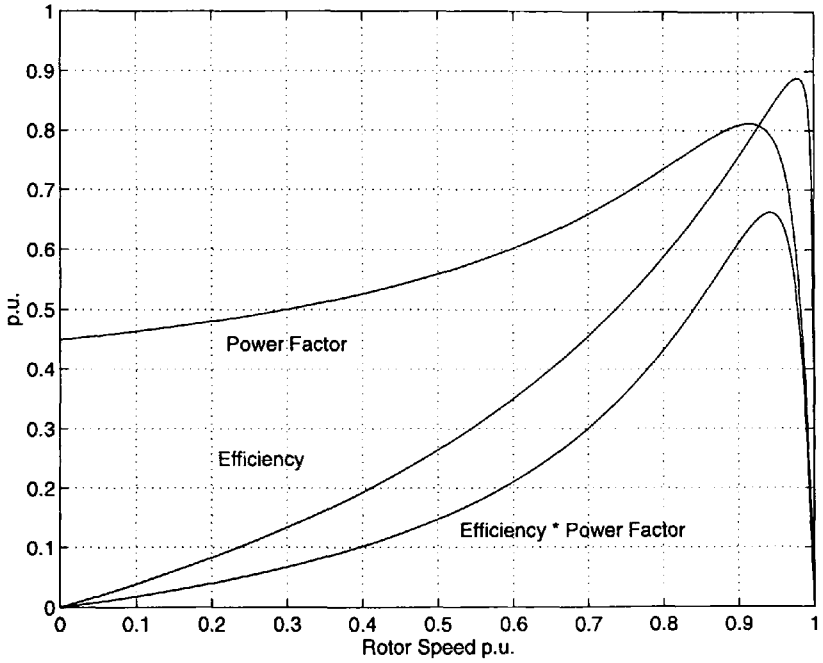

Fig. 3.7: Efficiency and Power Factor of Induction Motor (CVCF)

It can be seen from Fig. 3.7 that the power factor is maximised for a speed of $\omega_m = 0.92 p.u.$, the efficiency-power factor product at $\omega_m = 0.94 p.u.$ and the efficiency at $\omega_m = 0.98 p.u.$ Generally, the three criteria are low for low speed operation. The efficiency, for example, is below 27% for rotor speeds below half the synchronous speed ($\omega_m = 0.5 p.u.$).

The poor efficiency and power factor values can be attributed to the high slip operation at low rotor speeds. This is depicted in Fig. 3.8. It may be seen that for operation at zero

speed, the slip becomes unity. As the synchronous speed remains constant, the slip is also equal to the slip speed, which can also be seen from equation (3.9).

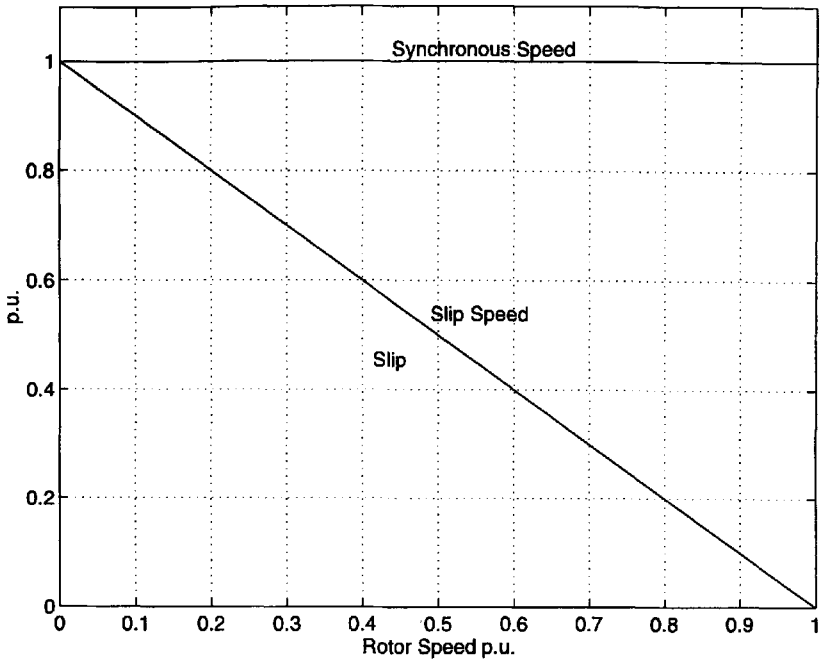

Fig. 3.8: Synchronous Speed, Slip Speed and Slip of Induction Motor (CVCF)

The CVCF operation occurs for induction motors when supplied from the mains supply. As both voltage and frequency remain constant, no control of the motor speed is possible. The speed varies with the applied load torque, which is undesirable in many applications. Since very high motor currents flow both during start-up and during fault conditions, for example a locked rotor condition, a compromise for the motor protection circuitry is required. An overcurrent relay is mostly used which provides the necessary integral action over time. However, instantaneous high current protection may not be carried out. Speed control of the driven machine may be carried out by using an electromagnetic clutch or a by-pass in pump applications. Although these methods have been used in the past, they present a most undesirable form of speed control as much of the input power to the motor is wasted. Motor speed control may be carried out by supplying the motor with either variable voltage, variable frequency or preferably with variable voltage and variable frequency, as shown below.

3.2 Variable Voltage, Constant Frequency Operation

By means of varying the voltage amplitude supplied to the motor, stable motoring operation may be obtained for all points below the torque curve for CVCF operation (Fig. 3.3). This is illustrated in Fig. 3.9, where a constant load torque between 0.1 p.u. and 1.2 p.u. has been applied.

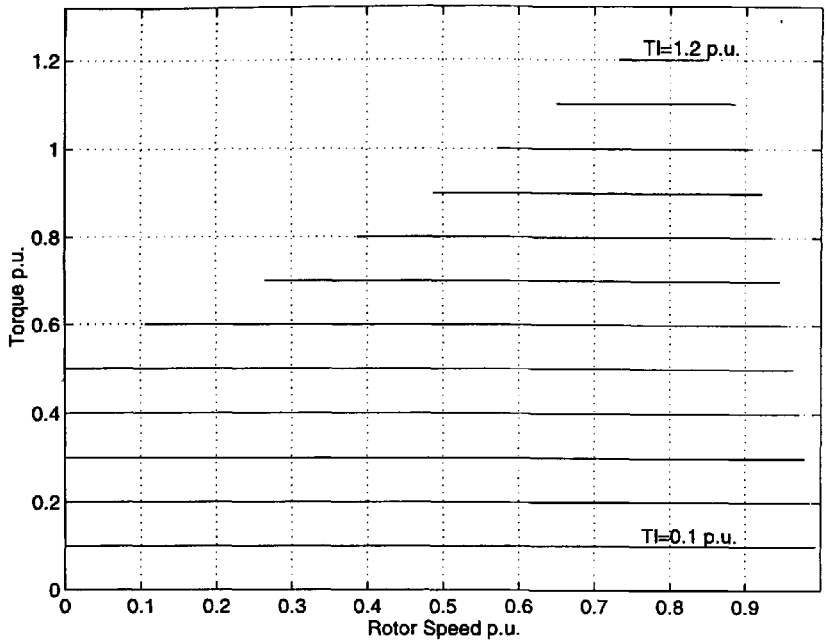

Fig. 3.9: Motor Torque in VVCF Operation

Fig. 3.10 shows the required variation of voltage amplitude with speed for constant load torque. It can be seen that between standstill and the speed at the breakdown point in CVCF operation ($\omega_m = 0.8 p.u.$), the voltage decreases with increasing speed. For higher speeds, the voltage increases with increasing speed. Therefore, for constant load torque, as is the case for cranes and lifts, the implementation of a closed loop system can be difficult as the voltage amplitude controller has to reverse its polarity at the breakdown point. However, for speed proportional loads, the voltage amplitude rises with rotor speed for the full speed range, and the implementation of a closed loop system is practical.

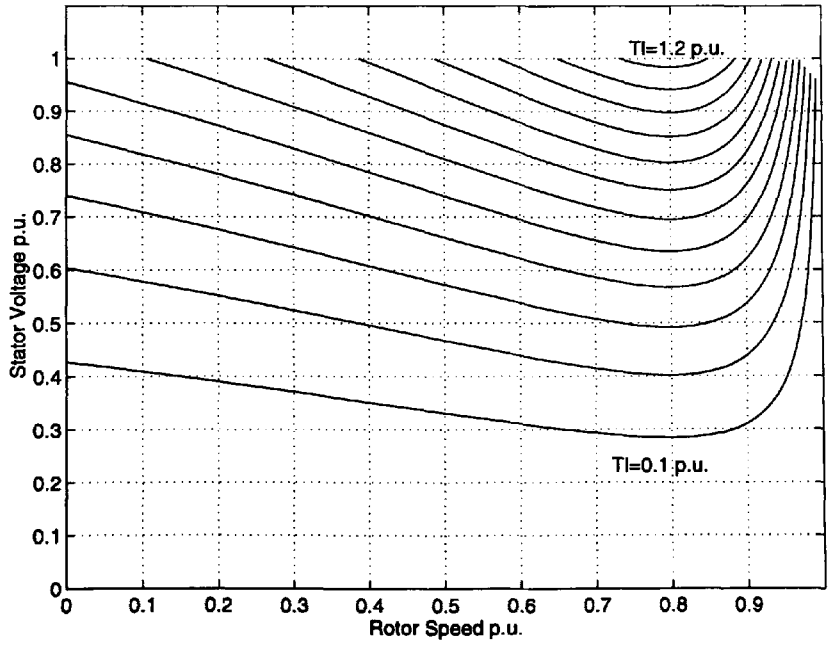

Fig. 3.10: Stator Voltage in VVCF operation

All the curves for power, current and flux (shown in Fig. 3.4 to Fig. 3.6) for CVCF operation, are the envelopes of the curves in VVCF operation (as seen for the torque and voltage curves in Fig. 3.9 and 3.10).

Because the synchronous speed is constant, the slip and slip speed characteristics for CVCF operation (Fig. 3.8) are also valid for VVCF operation. The efficiency and power factor curves (Fig. 3.7) are also the same for CVCF and VVCF operation, as the efficiency depends on speed, synchronous speed and motor parameters only.

The advantage of this type of operation when compared to CVCF operation is that speed control can be carried out independently of motor torque. Although the efficiency is as poor as in CVCF operation, the total input power can be reduced for lower torque requirements and thereby conserving energy.

3.3 Constant Voltage, Variable Frequency Operation

The CVVF operation occurs in almost all VVVF inverters in the high speed region. CVVF operation corresponds to the six-step mode when the controller 'has run out of voltage'. The CVVF mode extends the speed range of the motor drastically. While motoring operation in CVCF and VVCF mode is only possible up to synchronous speed, CVVF operation may achieve 3-4 times the rated speed of the motor. Usually the motor bearings and the motor load are the limiting factors, and not the CVVF supply. The motor torque is shown in Fig. 3.11.

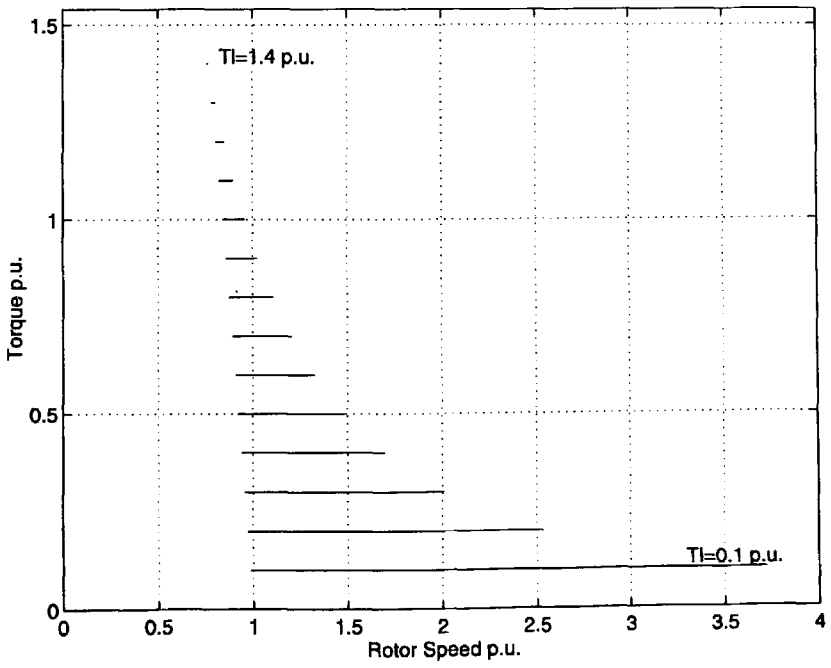

Fig. 3.11: Motor Torque in CVVF Operation

Since the stator voltage remains constant at unity, saturation may be obtained for small rotor speeds. Therefore, the curves shown in Fig. 3.11 correspond only to operating conditions where the stator flux level is at or below unity, as shown in Fig. 3.12.

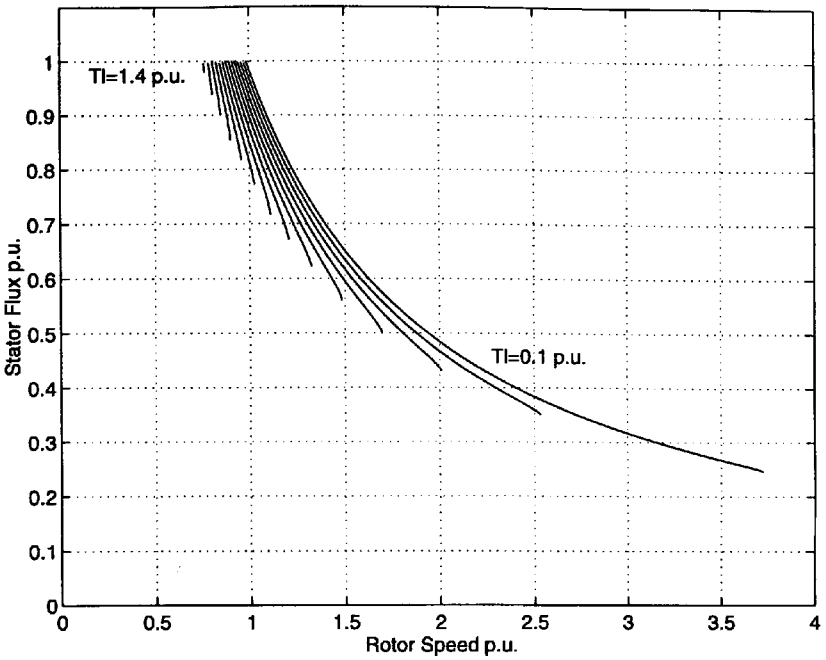

Fig. 3.12: Stator Flux in CVVF Operation

Fig. 3.12 shows the 'flux weakening range' of the rotor speed. It can be seen that for higher load torque, the flux weakening occurs for lower rotor speeds. The lower the load torque, the higher the maximum speed available. Fig. 3.13 shows that in the flux weakening range, the slip frequency increases drastically. The slip frequency increases with both, the rotor speed and the load torque.

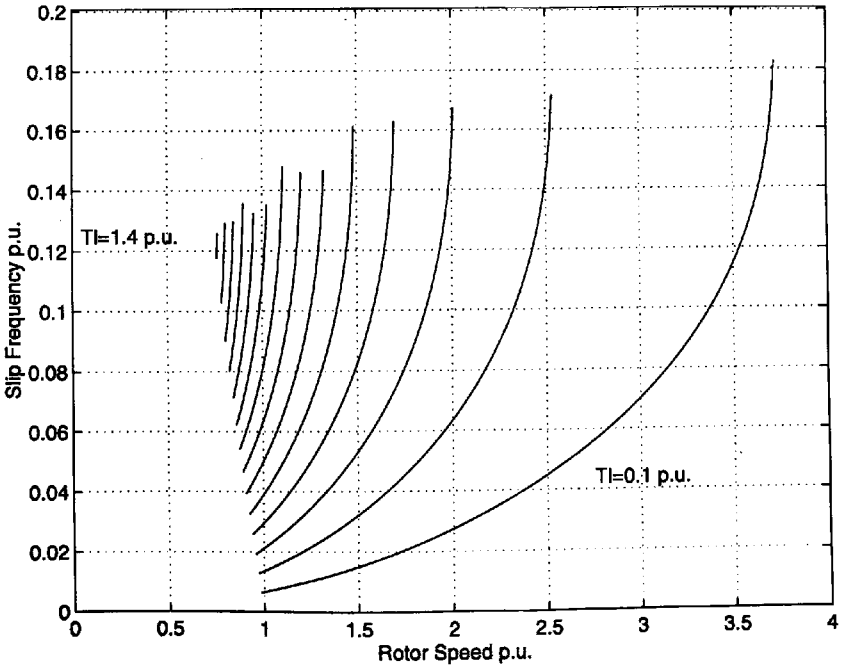

Fig. 3.13: Slip frequencies in CVVF Operation

Fig. 3.14 shows the efficiency in CVVF operation. It may be seen that the higher the load, the lower the efficiency. This, however, is true for load torques ranging from 0.4 to 1.4 p.u. only, as for lighter loads the maximum efficiency is at a higher rotor speed. The maximum efficiency for a load torque of 0.1p.u. is 95% at 225% of rated speed.

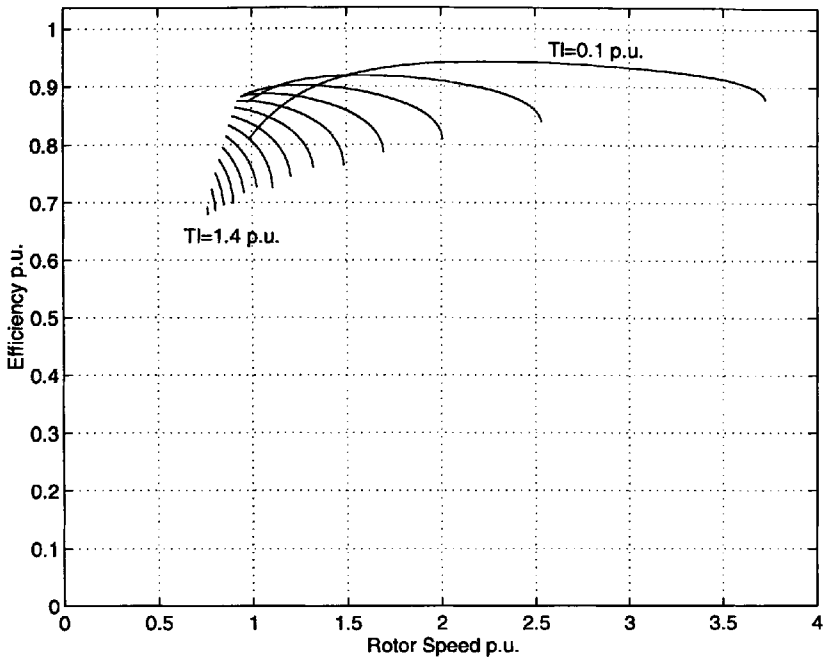

Fig. 3.14: Efficiency in CVVF Operation

The power factor has its optimum at higher speeds than the efficiency. This may be seen from Fig. 3.15. It can be seen that for light load at rated speed the power factor is very poor ($\cos\varphi = 0.23$). The maximum power factor for each load is around $\cos\varphi = 0.8$, however, at very different rotor speed.

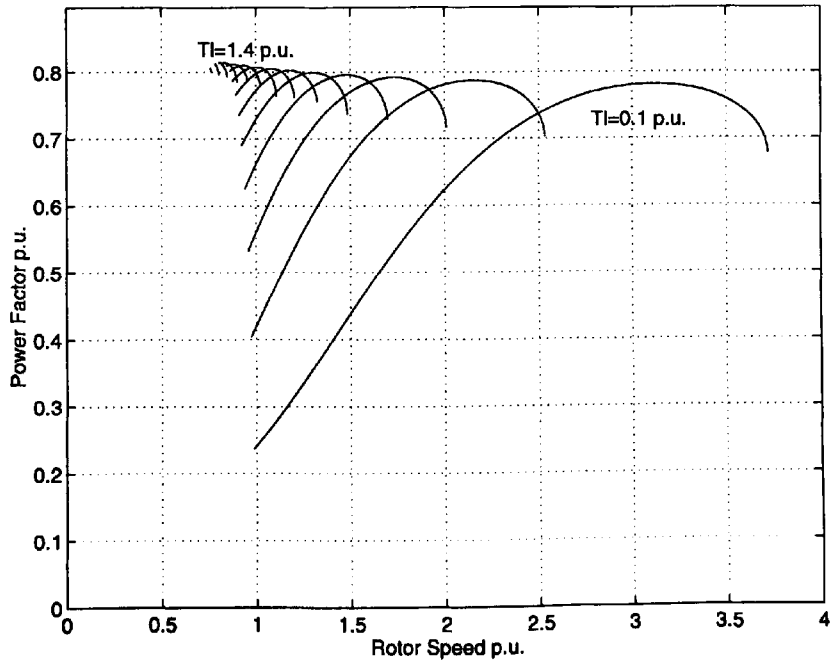

Fig. 3.15: Power Factor in CVVF Operation

The product of power factor and efficiency is shown in Fig. 3.16. It can be seen that with small load torque the efficiency-power factor product may be maximised, but only for a certain speed. For operation near rated speed, the product is at only 0.2 p.u. which means that only 20% of the apparent power is available at the motor shaft. For operation with higher torque, however, the efficiency-power factor product lies within 0.55 and 0.65 p.u. The maximum power factor-efficiency product is obtained for light loads at very high speeds.

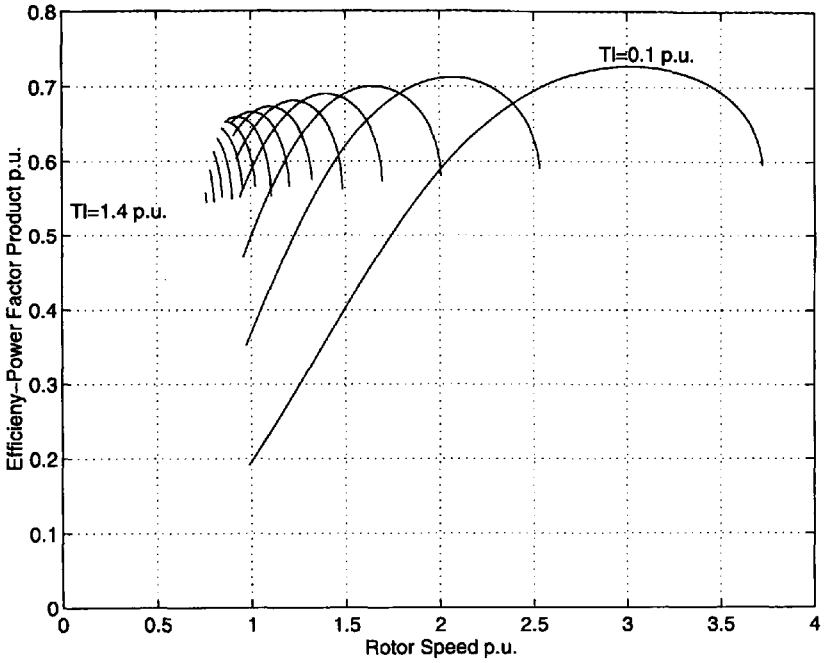

Fig. 3.16: Efficiency-Power Factor Product in CVVF Operation

The CVVF mode is used when the voltage at the inverter is at its maximum, due to mains supply limitations or maximum motor ratings, and speed control is required. The range of available speeds depends very much on the load torque and can reach 3-4 times the rated speed for light loads. For such high speeds however, the torque to overcome frictional losses can be considerable, so that the available load torque is reduced. Higher than rated load torque may be obtained for rotor speed below rated speed (Fig. 3.11). However, this is possible for limited periods only, as both the input and the output power are above their rated values and overheating of the motor can occur.

3.4 Variable Voltage, Variable Frequency Operation

It has been shown in the previous two sections that speed control of the motor is possible using VVCF or CVVF operation. However, speed control between standstill and rated speed with VVCF operation results in poor efficiency whereas speed control between standstill and rated speed with CVVF operation leads to very high currents and

saturation of the iron in the motor. In the following, the simultaneous variation of frequency and voltage is investigated.

3.4.1 Optimum Induction Motor Operation

Since both voltage and frequency are varied at the same time, a variety of voltage and frequency combinations can produce the same load torque and rotor speed conditions. Clearly, many of these combinations are not desirable as excessive stator flux or stator voltage may be required. It is shown in the following, how the governing equations for the desirable modes can be derived and how different 'optima' can be identified.

The condition for maximum efficiency requires that the input power is minimised for any given output power. The efficiency is given by

$$\eta = \frac{P_{out}}{P_{in}} = \frac{T\omega_m}{\Re\left\{\vec{v}_s\vec{i}_s^*\right\}} \tag{3.10}$$

On substitution of equation (3.1a) and (3.1e) the expression shown below follows.

$$\eta = \frac{\Im\left\{\vec{\psi}_s\vec{i}_s^*\right\}\omega_m}{\Re\left\{\left(r_s\vec{i}_s + j(\omega_m+\omega_r)\vec{\psi}_s\right)\vec{i}_s^*\right\}} \tag{3.11}$$

The stator current may be expressed by substitution of equation (3.1d) into equation 3.1b, and solving equation 3.1c for the rotor current. Rearranging results in the following expression:

$$\vec{i}_s = \vec{\psi}_s \frac{r_r + jx_r\omega_r}{x_m^2\omega_r + x_s\left(r_r + jx_r\omega_r\right)} \tag{3.12}$$

Substitution of equation 3.12 into equation 3.11 and further simplification results in the expression for the induction motor efficiency as shown below:

$$\eta = \frac{r_r\omega_m\omega_r x_m^2}{\omega_r^2\left(r_r x_m^2 + r_s x_r^2\right) + r_r\omega_m x_m^2\omega_r + r_r^2 r_s} \tag{3.13}$$

By setting the differentiation with respect to ω_r to zero, the slip frequency for which the efficiency is maximised can be found as follows:

$$\frac{\partial \eta}{\partial \omega_r} = 0$$

$$\omega_{r(\max \eta)} = r_r \sqrt{\frac{r_s}{r_s x_r^2 + r_r x_m^2}} \tag{3.14}$$

Thus, it can be seen that the maximum efficiency occurs at a constant slip frequency. Similar to the procedure shown above, slip frequencies for other 'optima' may also be found. The results are shown in Table 3.1.

Table 3.1: Solutions for optimum slip frequencies

Optimisation Criteria	Equation to be optimised	Solution
Efficiency η	$\frac{P_{out}}{P_{in}} = \frac{r_r \omega_m \omega_r x_m^2}{\omega_r^2 \left(r_r x_m^2 + r_s x_r^2\right) + r_r \omega_m x_m^2 \omega_r + r_r^2 r_s}$ $\frac{P_{out}}{P_{loss}} = \frac{r_r \omega_m \omega_r x_m^2}{\omega_r^2 \left(r_r x_m^2 + r_s x_r^2\right) + r_r^2 r_s}$	$\omega_{r(\max \eta)} = r_r \sqrt{\frac{r_s}{r_s x_r^2 + r_r x_m^2}}$
Power Factor $\cos\varphi$	$\frac{P_{in}}{P_{reac}} = \frac{r_r^2 r_s + r_r \omega_r \left(\omega_m + \omega_r\right) x_m^2 + r_s \omega_r^2 x_r^2}{\left(\omega_m + \omega_r\right)\left(r_r^2 x_s + x_r \omega_r^2 \left(x_s x_r - x_m^2\right)\right)}$	4th order polynom for $\omega_{r(\max \cos\varphi)}$, see Appendix A.1
Product of Efficiency and Power Factor $\eta \cos\varphi$	$\frac{P_{out}}{S} = \frac{\Im\left\{\vec{\psi}_s^* \vec{i}_s\right\} \omega_m}{\lvert \vec{v}_s \vec{i}_s^* \rvert} = \eta \cos\varphi$	7th order polynom for $\omega_{r(\max \eta \cos\varphi)}$, see Appendix A.2

The slip frequencies which optimise the output power also optimise the developed torque, because $P_{out} = \omega_m T_l$. Furthermore, maximum efficiency operation implies minimum loss operation. The input power to reactive power function has been chosen in favour to the input power to apparent power ($\cos\varphi$) due to mathematical convenience. However, the solution for $\omega_{r(\max \cos\varphi)}$ maximises both functions (for proof see Appendix A-1).

From the solutions given in Table 3.1, only the slip frequency maximising the efficiency is independent of the rotor speed. It is important to note that the optimum slip frequencies for all optimisation criteria are independent of the load torque. However, as will be shown in the following sections, the 'optimum' slip frequency may lead to

undesirable operating conditions for higher load torque. The following figure shows the variation of slip frequency for varying rotor speed for the different optimisation criteria.

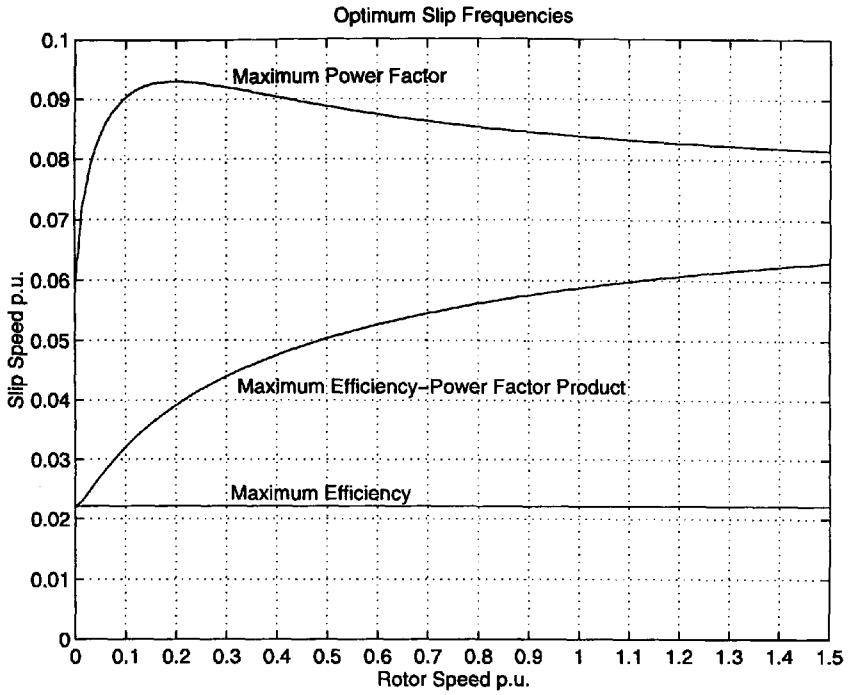

Fig. 3.17: Optimum Slip Frequencies in VVVF Operation

It can be seen from Fig. 3.17 that the optimisation for maximum efficiency results in the lowest slip frequency, whereas the optimisation for maximum power factor (input power per apparent power) yields the highest slip frequency.

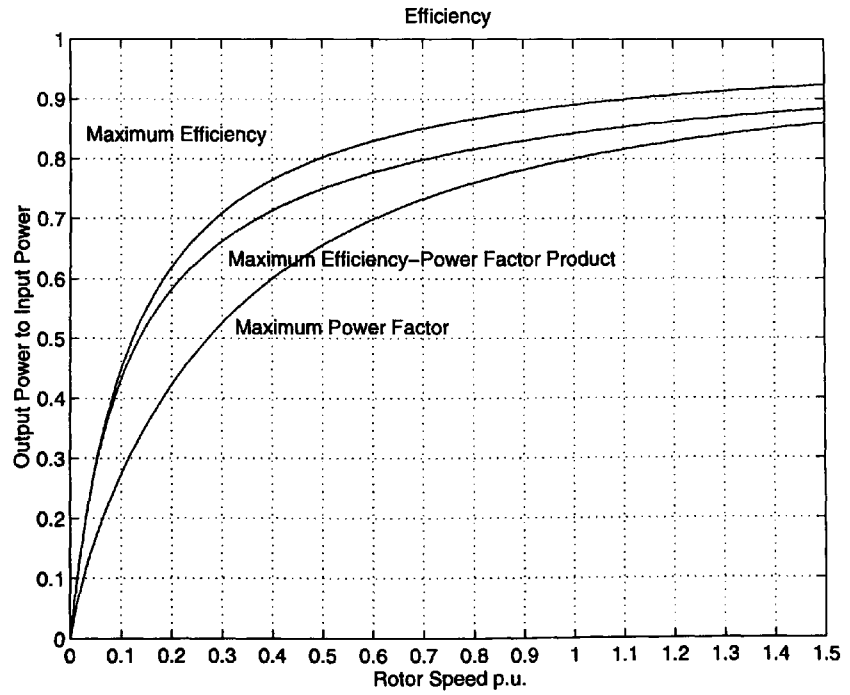

Fig. 3.18: Efficiency for different Optimisation Criteria

With each of the three different optimisation criteria, different efficiencies, power factors and efficiency-power factor products are obtained. Fig. 3.18 depicts the

efficiency for the three slip frequencies from Fig. 3.17 where it may be seen that operation with maximum power factor results in a lower efficiency operation. At half the rated speed for example, maximum power factor operation wastes 15% more power than maximum efficiency operation. Conversely, as can be seen from Fig. 3.19, maximum efficiency operation results into a power factor of $\cos\varphi = 0.61$, whereas maximum power factor operation results in a power factor of $\cos\varphi = 0.85$ for half the rated speed.

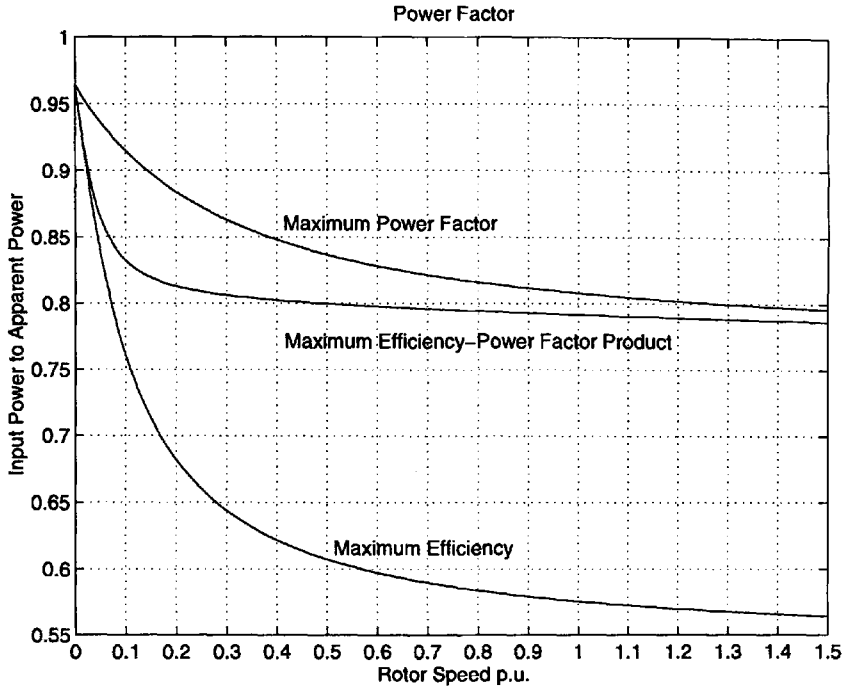

Fig. 3.19: Power Factor for different Optimisation Criteria

It may also be seen from Fig. 3.19 that for both maximum power factor operation (max $\cos\varphi$) and maximum efficiency-power factor product (max $\eta\cos\varphi$) operation the power factor is bigger than 0.707 ($\cos\varphi > 0.707$) for the full speed range. However, for speeds over 16% of rated speed, maximum efficiency operation cycles more power between supply and motor than is consumed by the motor. In Fig. 3.20 the efficiency-power factor product is shown for the three optimisation criterias. It can be seen that maximum efficiency operation is superior for rotor speeds below $\omega_m = 0.3p.u.$, whereas maximum $\cos\varphi$ operation is superior for rotor speeds above $\omega_m = 0.3p.u.$

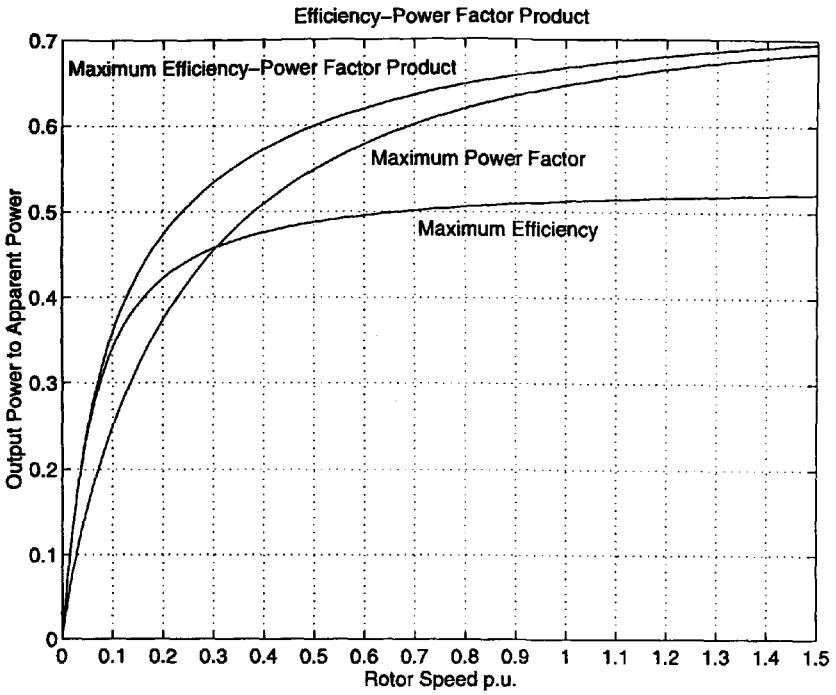

Fig. 3.20: Efficiency-Power Factor Product for different Optimisation Criteria

The power factor and efficiency graphs for VVVF operation (Fig. 3.18 and Fig. 3.19) are clearly superior to the results obtained for CVCF and VVCF (Fig. 3.7) operation. However, at higher load torque, the optimum motor operation has to be sacrificed for limited flux or limited voltage operation.

In the following, the analysis of the maximum efficiency, constant stator flux and constant voltage modes of operation are integrated. Fig. 3.21 shows the first quadrant of the torque-speed plane.

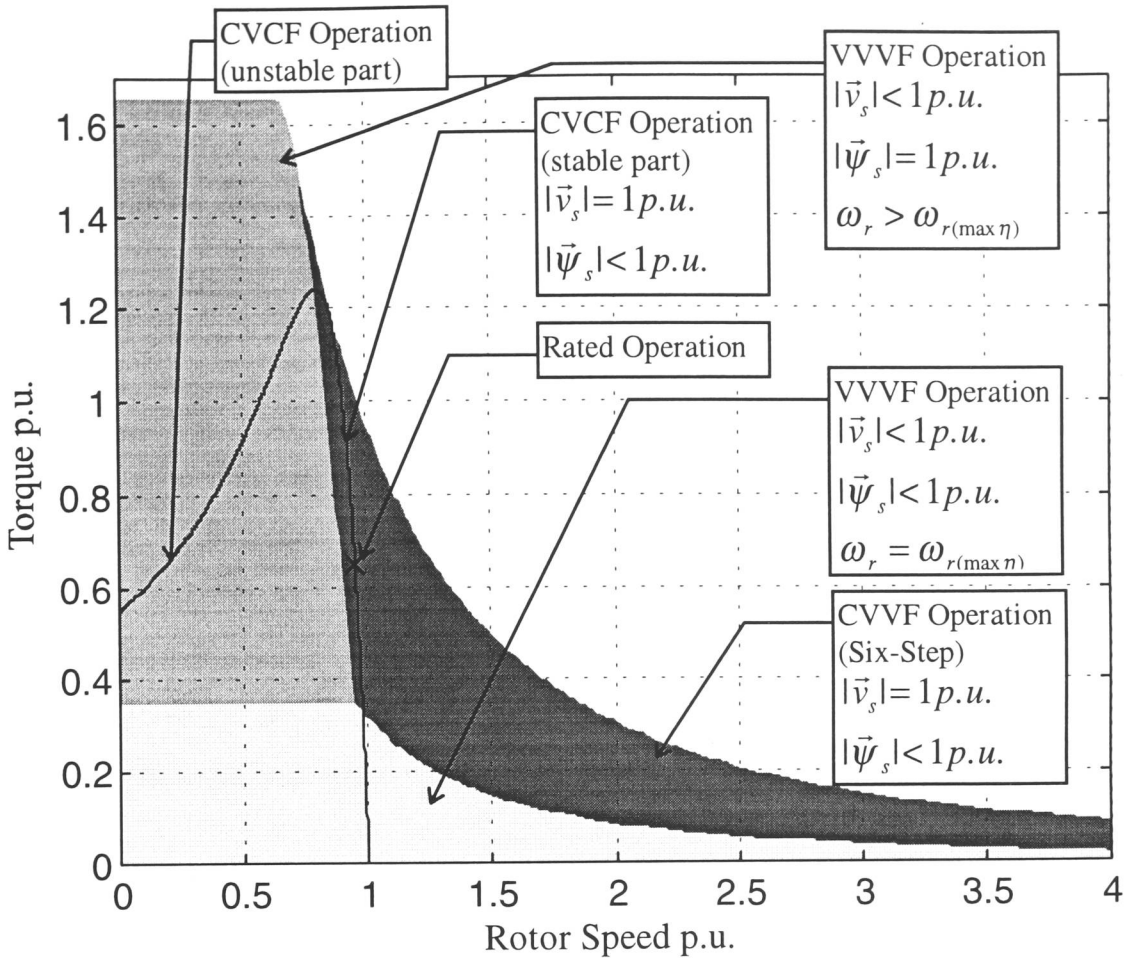

Fig. 3.21: Modes of Induction Motor Operation

The three sections in Fig. 3.21 show the possible motor torque - rotor speed combinations which allow steady state operation with variable voltage and variable frequency.

The light grey area shown in Fig. 3.21 corresponds to VVVF operation where both the stator flux level and the stator voltage level are below unity. The slip frequency is constant according to equation 3.19. This area shown marks the torque speed combinations where the efficiency has been optimised according to equations 3.13 and 3.14. It may be seen that maximum efficiency operation can only be obtained in a small portion of the full operating range. Below rated speed, maximum efficiency operation may be obtained for a load torque below 50% of rated torque. For speeds up to 1.5 times rated speed, the load torque has to decrease to only 20% of the rated torque, to still obtain maximum efficiency operation.

The medium grey area in Fig. 3.21 represents VVVF operation with constant stator flux level. The slip frequency is increased above the value from Equation 3.19 in order to limit the stator flux to unity. It may be seen that this mode of operation allows 250% of

rated torque operation from standstill to about 65% of rated speed, which is well above the breakdown torque for CVCF operation. Constant flux operation is applied for all speeds below rated speed and torque above half the rated torque. However, for higher load torque the speed below which the stator flux can be kept at 1 p.u., without increasing the supply voltage above 1 p.u., decreases.

The distinction between the light and medium grey area is made because the saturation effects are not modelled. The effect of saturation is mainly that the magnetic flux and the magnetic flux density do not increase proportionally with increase in current. However, with modelled saturation effects, the only difference would be a smoother transition from constant slip to constant stator flux level operation which has not been considered here.

The dark grey area in Fig. 3.21 corresponds to CVVF operation, where the controller has run out of voltage and only frequency variation can be carried out. Constant voltage operation has to be used when more voltage is required than is available from the mains power supply. This allows the extension of the speed range above rated speed even for higher load torque. However, due to the higher slip frequencies, this mode of operation is associated with high power losses.

Also shown is the torque speed characteristic for CVCF operation. As can clearly be seen, the operating range with VVVF and CVVF is drastically expanded when compared to CVCF or VVCF (below CVCF curve) operation.

In the following, some important quantities of the induction motor model are examined for different points of operation in the torque-speed plane. Fig. 3.22 shows the variation of the stator flux level with torque and speed. It can be seen from the figure that there are two areas where the flux is below unity and one section where the flux is unity. The three sections correspond to the three sections of Fig. 3.21. Ideally, it is this characteristic with is required for the flux reference inputs of both flux vector control and direct torque control.

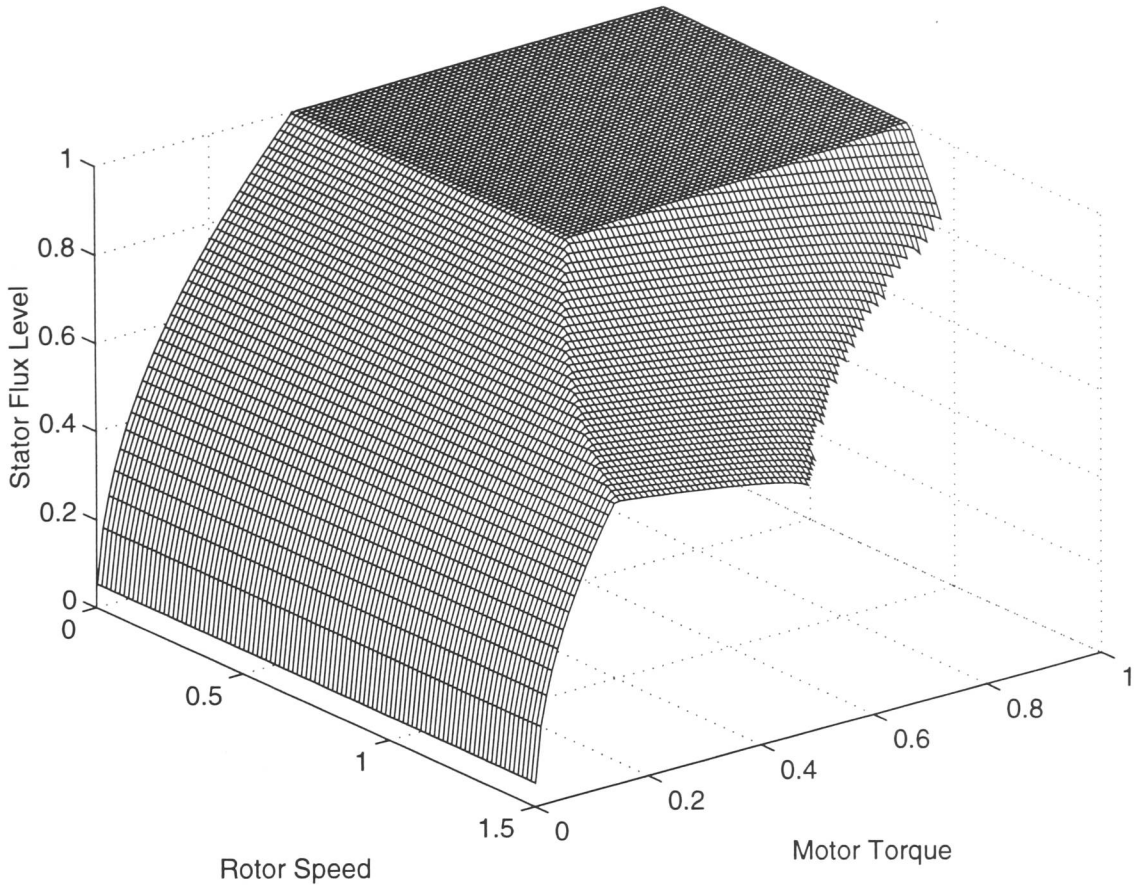

Fig. 3.22: Stator Flux Level in the Rotor Speed - Motor Torque Plane

Similarly to Fig. 3.9 and Fig. 3.11, the analysis of VVVF operation is carried out for constant load torques covering the operating range of this mode. However, CVVF operation has been included, as this mode can also be provided by a VVVF supply. Both maximum voltage and maximum stator flux operation have been taken into account for the analysis.

It is shown in Fig. 3.23 that constant load torques between 0.1 p.u. and 1.6 p.u. have been applied for the analysis of the motor operation. It may be seen that the figure corresponds to Fig. 3.21 and covers the two VVVF modes and the CVVF mode of operation.

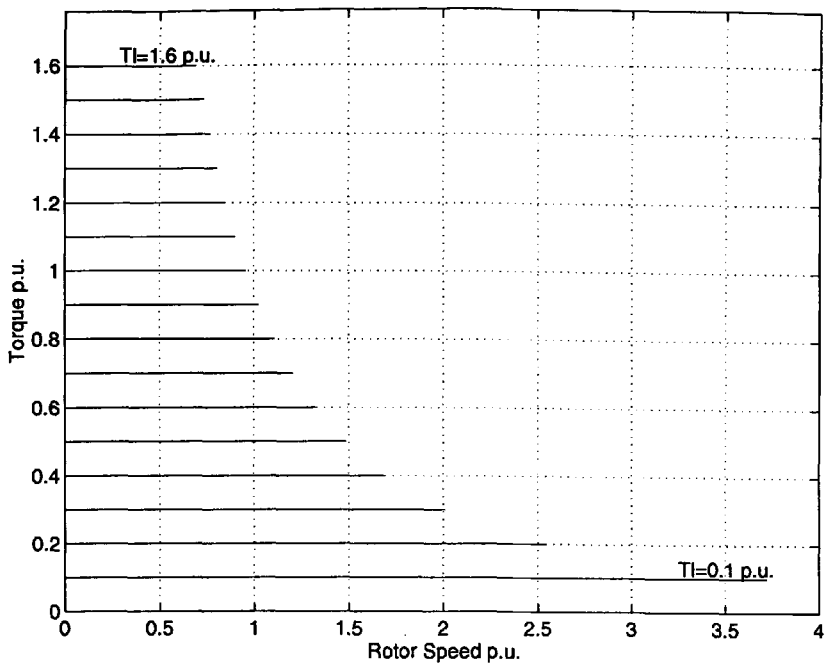

Fig. 3.23: Torque in VVVF Operation

In Fig. 3.24, the voltage variation with motor torque and rotor speed is shown. It can be seen that below maximum voltage, the voltage rises linearly with speed. However at motor speeds near zero, the voltage level is increased to compensate for the stator resistance voltage drop. It can also be seen from Fig. 3.24 that for constant stator flux operation (T_l=0.4..1.6), the gradients for different motor load are equal, whereas for light load at constant slip and reduced stator flux levels, less voltage is required.

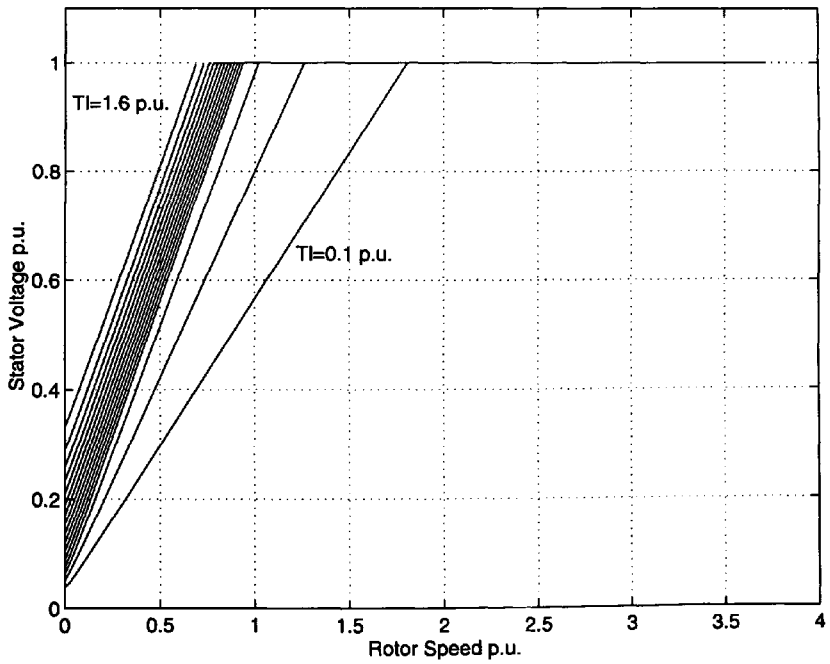

Fig. 3.24 Voltage in VVVF Operation

It may be seen from Fig. 3.25 that, essentially, the synchronous frequency rises linearly with rotor speed. As high load torque operation is associated with high slip operation, there is also an increased synchronous frequency required at larger torques. For scalar

motor control with standard P.W.M. inverter control, the characteristics shown in Fig. 3.24 and Fig. 3.25 have to be reproduced in order to take advantage of the full operating range of the motor.

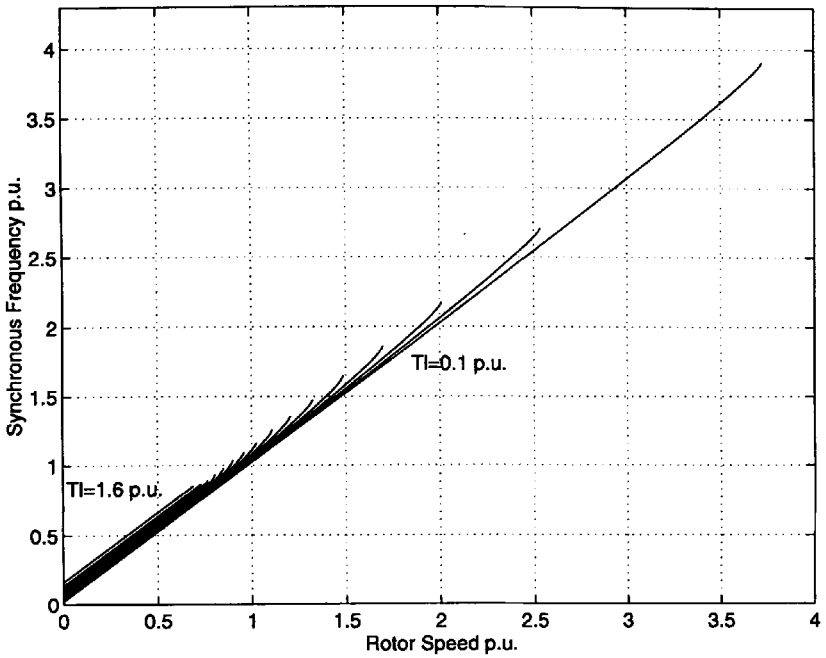

Fig. 3.25 Synchronous Frequency in VVVF Operation

The stator flux, shown in Fig. 3.26, is at unity for low speed operation and the load torque is above 0.3 p.u. However, for small values of load torque or higher rotor speeds the flux is decreased. For higher values of load torque, the flux weakening method is not applicable as only lower speed operation may be achieved.

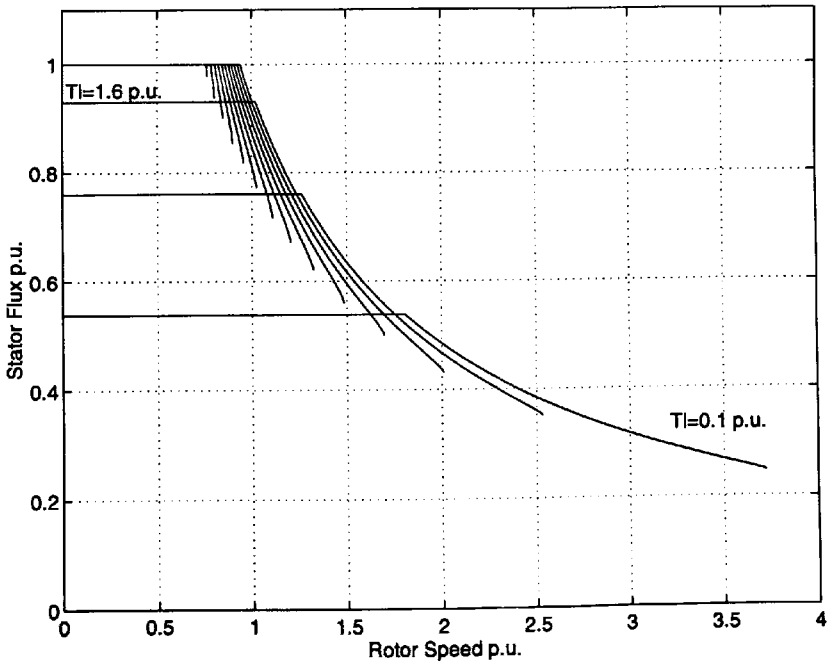

Fig. 3.26 Stator Flux in VVVF Operation

It may be seen from Fig. 3.27 that the slip frequency stays constant for low speed operation. For light load operation (T_l=0.1..0.3p.u.), the slip frequency is equal to 0.023 p.u. which corresponds to the value given by equation 3.14. For higher speed, the slip frequency rises quickly. For a scalar controller using slip frequency control, the characteristics shown are required for the steady state operation of the controller.

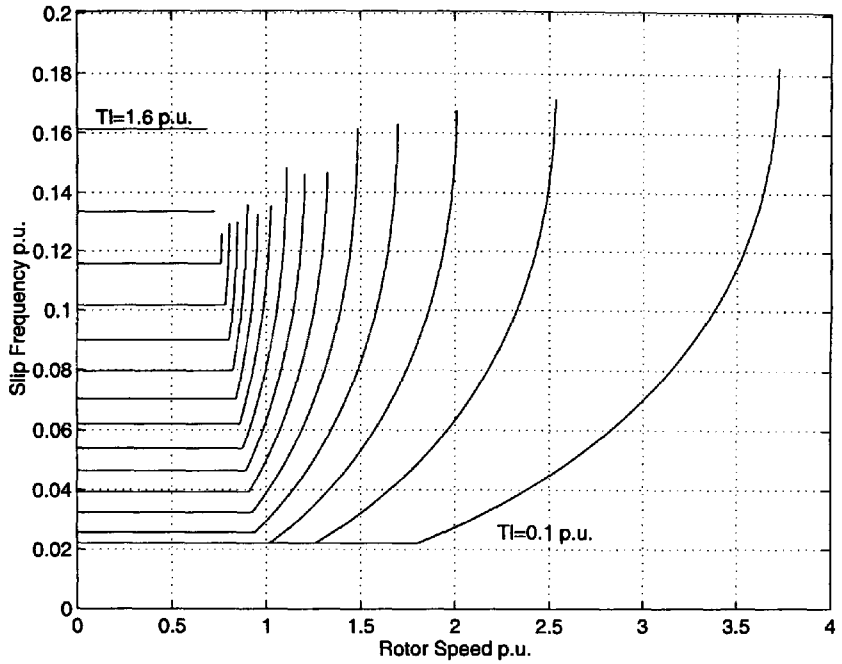

Fig. 3.27 Slip Frequency in VVVF Operation

In Fig. 3.28, the motor slip values for varying rotor speed and motor torque are shown. The slip values are unity at rotor standstill which can also be seen from equation 3.2 for $\omega_m = 0$. With increasing rotor speed, the slip values decrease. However, for CVVF operation at high speeds, the slip values rise again because of the reduced flux in the motor. The higher the load torque values, the higher the slip values. For example, for a torque value of T_l=1.6, the minimum slip value is 19% a 65% of rated speed.

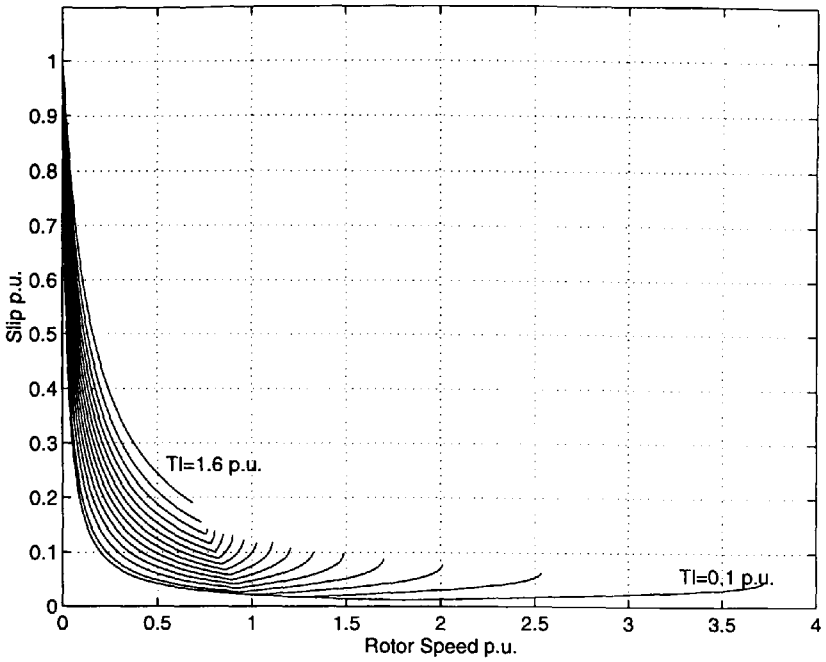

Fig. 3.28: Slip in VVVF Operation

Fig. 3.29 shows the steady state stator current values for varying rotor speed and motor torque. It can be seen by the comparison of Fig. 3.27 and Fig. 3.29 that the stator current does not depend on the rotor speed when the slip frequency is held constant. However, the stator current depends on the load torque and increases above the rated value for a load torque of T_l=0.7p.u. At a load torque of T_l=1.6p.u., for example, the stator current is at 235% of its rated value and therefore the motor can only operate at short intervals at this load to prevent overheating. For high speed operation, the motor current increases with rotor speed.

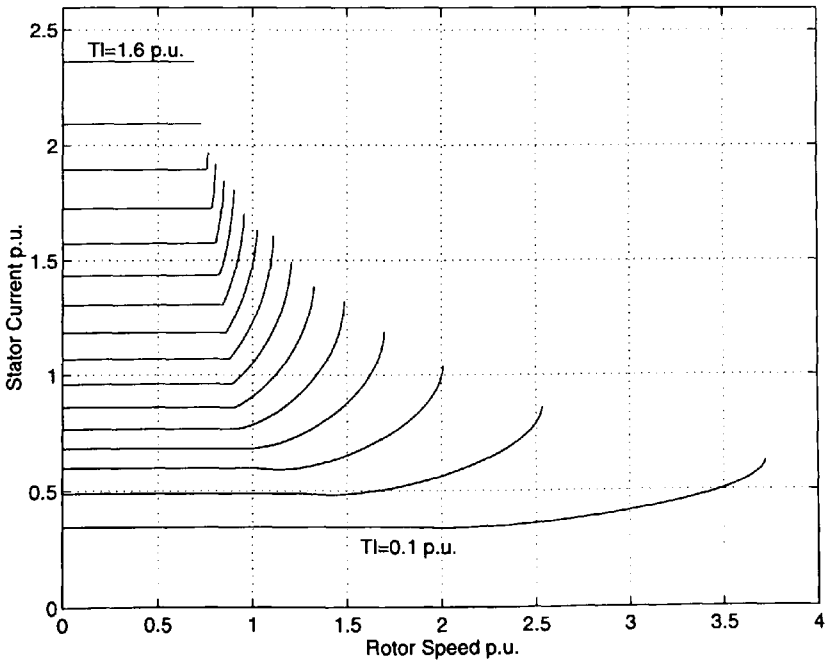

Fig. 3.29: Stator Current in VVVF Operation

The comparison of Fig. 3.30 and Fig. 3.7 shows that the induction motor efficiency in VVVF mode is much higher at low speed than in CVCF or VVCF operation. The highest efficiencies are obtained for light loads, where the stator flux is below unity. For example at half the rated speed, the efficiency in VVVF operation is at 80% for small values of load torque, whereas with CVCF or VVCF operation the efficiency is only 26%. For higher loads, the efficiency drops to about 52% for half the rated speed at maximum load. For high speed, the efficiency is identical to the CVVF operation (Fig. 3.14).

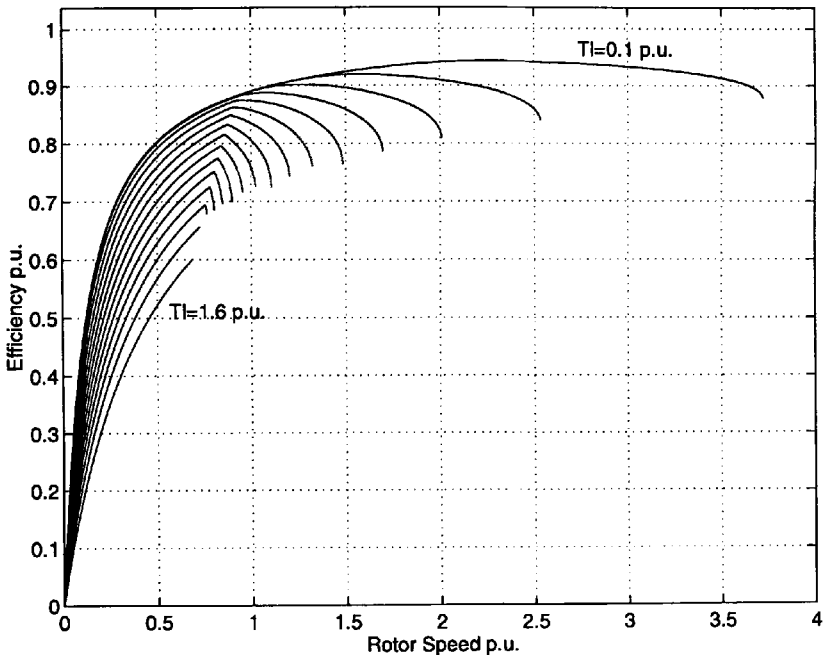

Fig. 3.30: Efficiency in VVVF Operation

It may be seen from Fig. 3.31 that the power factor in VVVF operation decreases for high operating speed of the motor. The maximum power factor of $\cos\varphi = 0.96$ is obtained at standstill. The minimum power factor of 0.56 is obtained for light load at 180% of rated speed.

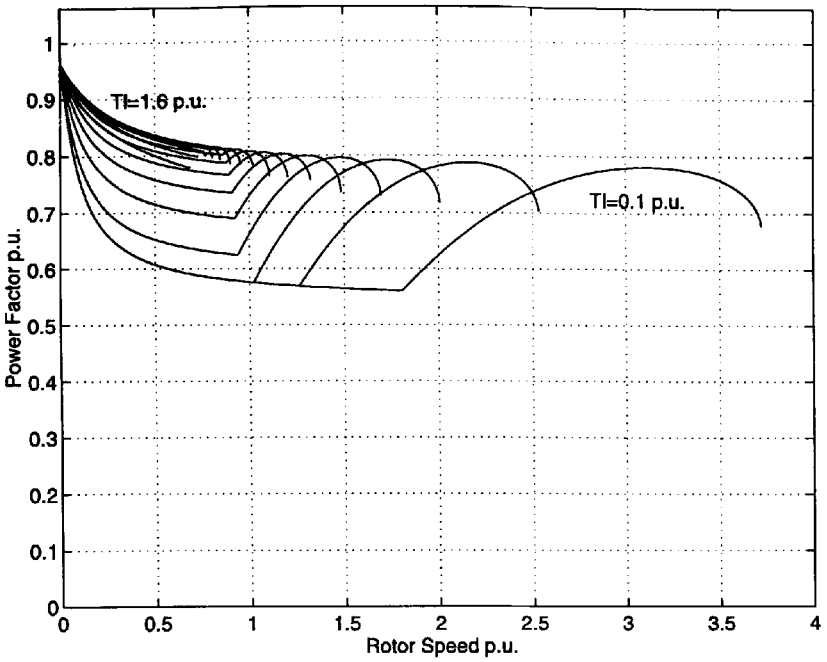

Fig. 3.31: Power Factor in VVVF Operation

It can be seen from Fig. 3.32 that the efficiency-power factor product is zero at standstill, because no output power is delivered. At low speed operation, the efficiency-power factor product is bigger for small values of load torque. However, for operation near rated speed, $\eta\cos\varphi$ is maximised for a load torque near the rated load torque. The maximum efficiency-power factor product is obtained for light load a 300% of synchronous speed, as can also be seen from Fig. 3.16.

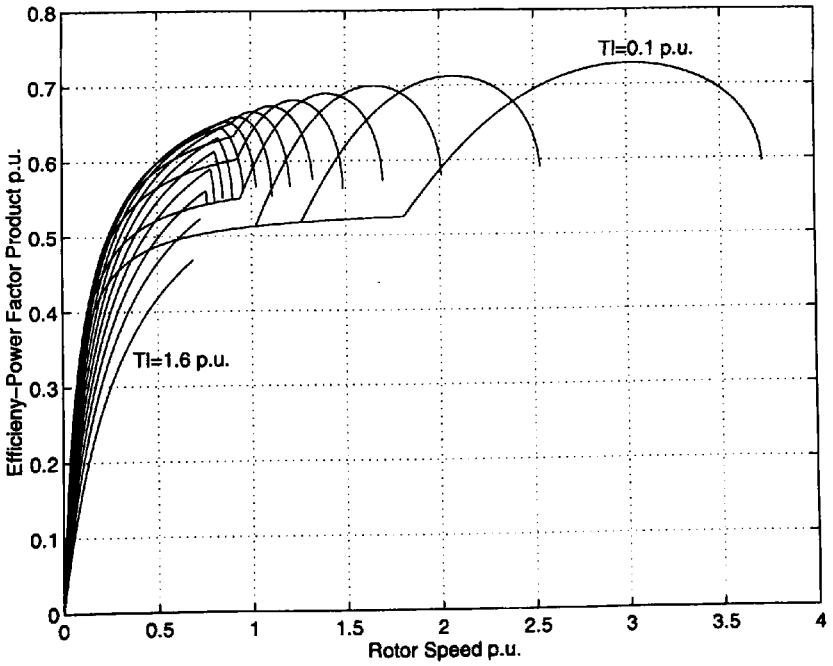

Fig. 3.32: Efficiency-Power Factor Product for VVVF Operation

3.5 Interim Conclusion

The analysis shown above has illustrated the steady state conditions required for VVVF operation of an induction motor. The CVVF operation has been included here, as this mode can automatically be provided by an VVVF inverter in the six step mode. The analysis has been carried out with respect to fundamental voltages and currents only. The additional losses due to harmonics inherent in the P.W.M. mode for VVVF operation or the six step mode in CVVF operation have not been considered. The speed torque conditions for which either P.W.M. or six step have to be applied, depend of course on the maximum voltage which can be provided by the power supply used. In fact, all curves depend on the particular set of motor parameters and on the motor model which has a varying degree of accuracy for the torque speed range. Saturation and iron losses have also not been included. Nonetheless, the procedure shown above is also valid for more accurate motor models and should not affect the general conclusions outlined below:

1. Constant slip frequency operation at reduced stator flux levels is applicable for low torque operation only.
2. Significant increase of the maximum load torque well above the breakdown torque in CVCF operation may be obtained with VVVF operation at constant stator flux. This torque is also available at standstill of the motor.
3. The highest value of efficiency are obtained at high speed, light load operation.
4. The highest power factor is obtained at standstill.
5. Maximum efficiency operation applies to light load operation only.
6. Both the VVVF and the CVVF mode of operation increase the control area in the torque speed plane (Fig. 3.21) when compared to CVCF operation and thereby allow optimum speed selection for an induction motor drive with maximum energy conservation.

Chapter 4: Six Step Operation

4.0 Review of Six Step Operation

Six step (square wave) operation is the simplest form of inverter operation. However, it allows frequency adjustment only and no voltage adjustment. The general principle of operation may be explained as follows:

Each phase of the induction motor is connected to the positive side of the d.c. link for half a cycle and to the negative side for the other half of a cycle. The three phases are shifted by 120 degrees and switching occurs every 60 degrees of a cycle. By varying the time corresponding to 360 degrees, the frequency of the fundamental can be changed. The inherent advantage of this type of operation is that it requires only two commutations (switching actions) per phase and cycle and thereby, minimum switching losses of the inverter can be achieved. However, as will be shown, undesirable low frequency components in the spectrum of the resulting voltage and current waveforms are present. A further disadvantage is that the d.c. link voltage has to be reduced by means of a separate converter for low speed operation. If this is carried out by a controlled rectifier, a low power factor of the induction motor drive presents an additional problem. Nevertheless, six step operation is inevitable in VVVF inverter operating at maximum output voltage.

4.1 Six Step Voltage Analysis

Three different voltages of an inverter system are of special interest. These are phase to neutral of d.c. supply voltages v_{ao}, v_{bo} and v_{co}, phase to phase voltages v_{ab}, v_{bc} and v_{ca} and phase to neutral of load voltages v_{an}, v_{bn} and v_{cn}, as shown in Fig. 4.1.

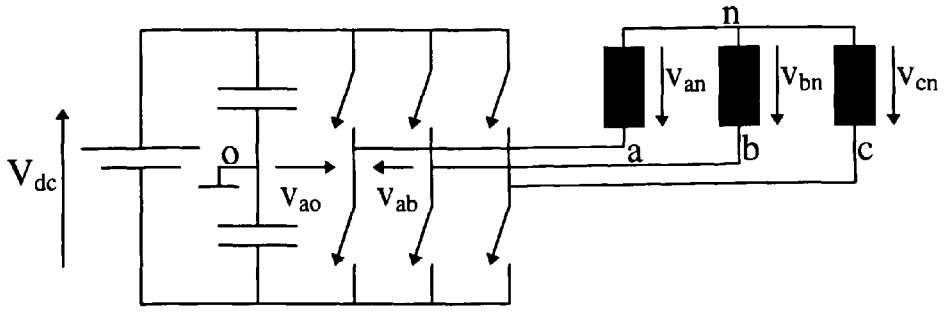

Fig. 4.1: Inverter with Star connected Motor Windings

The **phase to neutral of the d.c. supply voltages** are generated directly by the inverter control system. The resulting square wave for the motor phase 'a' is shown in Fig. 4.2.

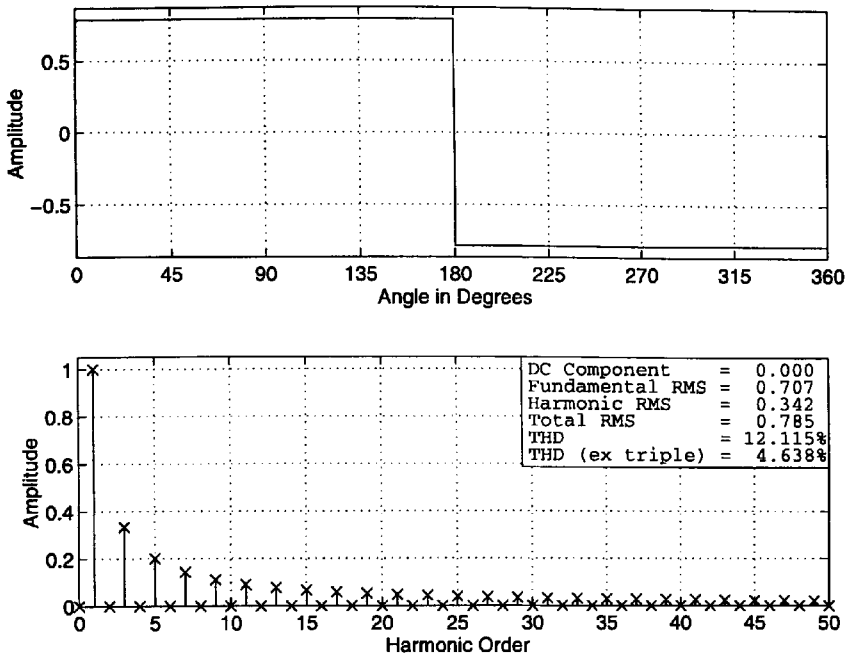

Fig. 4.2: Phase to Neutral of Supply Voltage in Six Step Mode (v_{ao})

It may be seen from Fig. 4.2 that the voltage waveform has two levels which are $+V_{dc}/2$ and $-V_{dc}/2$. The d.c. link voltage has been set to $V_{dc} = \pi/2$ to give unity amplitude of the fundamental voltage. As the voltage level between commutations is constant, the harmonic content of the waveforms can easily be obtained by Fourier analysis. Any periodic waveform may be described in the following form:

$$f_n(x) = \frac{a_0}{2} + \sum_{k=1}^{n} \left(a_k \cos(kx) + b_k \sin(kx) \right) \tag{4.1}$$

where the Fourier coefficients a_k and b_k may be calculated as follows:

$$\begin{aligned} a_k &= \frac{1}{\pi} \int_{-\pi}^{\pi} f(x)\cos(kx) \qquad k = 0,1,2... \\ b_k &= \frac{1}{\pi} \int_{-\pi}^{\pi} f(x)\sin(kx) \qquad k = 1,2,3... \end{aligned} \tag{4.2}$$

The resulting coefficients for the harmonics 1 to 13 are summarised in Table 4.1.

Table 4.1: Fourier Coefficients for Phase to Neutral of d.c. Supply Voltage

	v_{ao}	v_{ao}	v_{bo}	v_{bo}	v_{co}	v_{co}			
k	a_k	b_k	a_k	b_k	a_k	b_k	amp	RMS	Seq.
1	$\frac{\sqrt{3}}{2}$	$\frac{1}{2}$	$-\frac{\sqrt{3}}{2}$	$\frac{1}{2}$	0	-1	1	$\frac{1}{\sqrt{2}}$	+
2	0	0	0	0	0	0	0	0	0
3	0	$-\frac{1}{3}$	0	$-\frac{1}{3}$	0	$-\frac{1}{3}$	$\frac{1}{3}$	$\frac{1}{3\sqrt{2}}$	0
4	0	0	0	0	0	0	0	0	0
5	$-\frac{\sqrt{3}}{10}$	$\frac{1}{10}$	$\frac{\sqrt{3}}{10}$	$\frac{1}{10}$	0	$-\frac{1}{5}$	$\frac{1}{5}$	$\frac{1}{5\sqrt{2}}$	-
6	0	0	0	0	0	0	0	0	
7	$\frac{\sqrt{3}}{14}$	$\frac{1}{14}$	$-\frac{\sqrt{3}}{14}$	$\frac{1}{14}$	0	$-\frac{1}{7}$	$\frac{1}{7}$	$\frac{1}{7\sqrt{2}}$	+
8	0	0	0	0	0	0	0	0	0
9	0	$-\frac{1}{9}$	0	$-\frac{1}{9}$	0	$-\frac{1}{9}$	$\frac{1}{9}$	$\frac{1}{9\sqrt{2}}$	0
10	0	0	0	0	0	0	0	0	0
11	$-\frac{\sqrt{3}}{22}$	$\frac{1}{22}$	$\frac{\sqrt{3}}{22}$	$\frac{1}{22}$	0	$-\frac{1}{11}$	$\frac{1}{11}$	$\frac{1}{11\sqrt{2}}$	-
12	0	0	0	0	0	0	0	0	0
13	$\frac{\sqrt{3}}{26}$	$\frac{1}{26}$	$-\frac{\sqrt{3}}{26}$	$\frac{1}{26}$	0	$-\frac{1}{13}$	$\frac{1}{13}$	$\frac{1}{13\sqrt{2}}$	+

The following conclusions can be drawn from Table 4.1:

- Since the RMS value of the fundamental is $V_{1(RMS)} = 1/\sqrt{2}$ and the d.c. link voltage is $V_{dc} = \pi/2$, it follows that $V_{1(RMS)} / V_{dc} = \sqrt{2}/\pi = 0.45$. This means that only 45% of the d.c. link voltage is converted to a three phase supply with arbitrary frequency. This value could be increased for one phase only, whereby the voltage of the other two phases would be decreased making the three phase voltage system unbalanced and causing undesirable effects. Therefore, 45% of the d.c. link voltage is the maximum voltage which can be achieved with six step operation and in fact is also the maximum voltage of any modulation scheme with d.c. link. This value is, therefore, used as a reference for comparison of different modulation schemes.

- Due to the symmetry of the waveform, the spectrum contains only odd integer harmonics.
- The harmonics k = 3, 9, 15, ... have the same Fourier coefficients for the phases 'a', 'b' and 'c'. The harmonics in the three phases are therefore of zero sequence.
- The harmonics k = 1, 7, 13, ... have a positive phase sequence.
- The harmonics k = 5, 11, 17, ... have a negative phase sequence.
- The amplitudes and RMS values of the harmonics decrease with 1/k. This is an additional advantage as the impedance of the induction motor increases with k anyway (when the real part of the impedance is neglected). Therefore, the current amplitudes decrease with $1/k^2$, making the current waveforms more sinusoidal.
- The amplitudes of the harmonics are equal for the three phases. This shows that the set of voltages is balanced.

The **phase to phase** voltages may be calculated from the phase to neutral of load voltages as follows.

$$\begin{aligned} v_{ab} &= v_{ao} - v_{bo} \\ v_{bc} &= v_{bo} - v_{co} \\ v_{ca} &= v_{co} - v_{ao} \end{aligned} \tag{4.3}$$

The voltage waveform for the voltage v_{ab} is shown in Fig. 4.3.

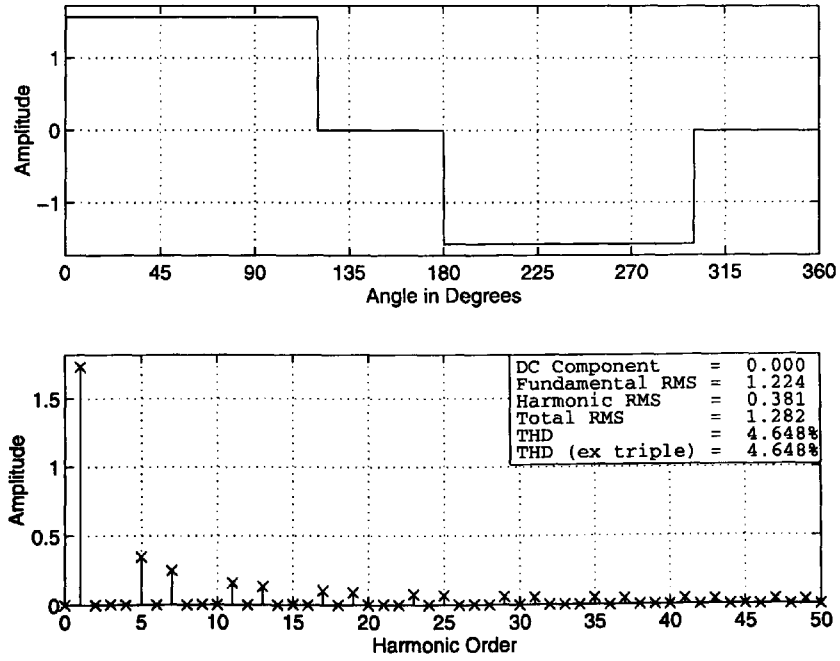

Fig. 4.3: Phase to Phase Voltage in Six Step Mode (v_{ab})

It may be seen from Fig. 4.3, that the phase to phase voltage has three levels and that the maximum voltage values are doubled compared to the phase to neutral of supply voltages. The Fourier coefficients for the phase to phase voltages are summarised in Table 4.2.

Table 4.2: Fourier Coefficients for Phase to Phase Voltages

	v_{ab}	v_{ab}	v_{bc}	v_{bc}	v_{ca}	v_{ca}			
k	a_k	b_k	a_k	b_k	a_k	b_k	amp	RMS	Seq.
1	$\sqrt{3}$	0	$-\frac{\sqrt{3}}{2}$	$\frac{3}{2}$	$-\frac{\sqrt{3}}{2}$	$-\frac{3}{2}$	$\sqrt{3}$	$\frac{\sqrt{3}}{\sqrt{2}}$	+
2	0	0	0	0	0	0	0	0	0
3	0	0	0	0	0	0	0	0	0
4	0	0	0	0	0	0	0	0	0
5	$-\frac{\sqrt{3}}{5}$	0	$\frac{\sqrt{3}}{10}$	$\frac{3}{10}$	$\frac{\sqrt{3}}{10}$	$-\frac{3}{10}$	$\frac{\sqrt{3}}{5}$	$\frac{\sqrt{3}}{5\sqrt{2}}$	-
6	0	0	0	0	0	0	0	0	
7	$\frac{\sqrt{3}}{7}$	0	$-\frac{\sqrt{3}}{14}$	$\frac{3}{14}$	$-\frac{\sqrt{3}}{14}$	$-\frac{3}{14}$	$\frac{\sqrt{3}}{7}$	$\frac{\sqrt{3}}{7\sqrt{2}}$	+
8	0	0	0	0	0	0	0	0	0
9	0	0	0	0	0	0	0	0	0
10	0	0	0	0	0	0	0	0	0
11	$-\frac{\sqrt{3}}{11}$	0	$\frac{\sqrt{3}}{22}$	$\frac{3}{22}$	$\frac{\sqrt{3}}{22}$	$-\frac{3}{22}$	$\frac{\sqrt{3}}{11}$	$\frac{\sqrt{3}}{11\sqrt{2}}$	-
12	0	0	0	0	0	0	0	0	0
13	$\frac{\sqrt{3}}{13}$	0	$-\frac{\sqrt{3}}{26}$	$\frac{3}{26}$	$-\frac{\sqrt{3}}{26}$	$-\frac{3}{26}$	$\frac{\sqrt{3}}{13}$	$\frac{\sqrt{3}}{13\sqrt{2}}$	+

The comparison of Table 4.1 and Table 4.2 shows that the amplitudes in Table 4.2 have increased by a factor of $\sqrt{3}$. The phase sequence of the harmonics 1, 5, 7, 11, 13,... is identical to the phases sequences for the phase to neutral of supply voltages.

The harmonics for k = 3, 9, 15, 21, ... have disappeared as a direct result of equation 3.3.

The **phase to neutral of load** voltages v_{an}, v_{bn} and v_{cn} may be calculated with respect to v_{ao}, v_{bo} and v_{co} as follows:

The **line to neutral of the d.c. supply voltages** may be expressed as

$$\begin{aligned} v_{ao} &= v_{an} + v_{no} \\ v_{bo} &= v_{bn} + v_{no} \\ v_{co} &= v_{cn} + v_{no} \end{aligned} \tag{4.4}$$

Adding these equations together results in

$$v_{ao} + v_{bo} + v_{co} = v_{an} + v_{bn} + v_{cn} + 3v_{no} \tag{4.5}$$

As the star point of the motor is not connected to the power supply, the voltage at point 'n' is not equal to the voltage at point 'o'. It follows that the sum of the three phase currents is zero.

$$i_{sa} + i_{sb} + i_{sc} = 0 \tag{4.6}$$

As the equivalent circuits for each phase are identical, the phase currents may be expressed by the voltage across each motor winding and its impedance Z.

$$\frac{v_{an}}{Z} + \frac{v_{bn}}{Z} + \frac{v_{cn}}{Z} = 0 \tag{4.7}$$

Cancelling the motor impedances from equation (4.7) proves that the sum of the three voltages across the motor windings is zero.

$$v_{an} + v_{bn} + v_{cn} = 0 \tag{4.8}$$

The following relationship can be drawn for the star point to the neutral of the d.c. supply voltage from equations 4.5 and 4.8.

$$v_{no} = \frac{v_{ao} + v_{bo} + v_{co}}{3} \tag{4.9}$$

This result can be substituted into equation 4.4, which gives the following expressions for the line to neutral voltages of the motor.

$$\begin{aligned} v_{an} &= \frac{2v_{ao} - v_{bo} - v_{co}}{3} \\ v_{bn} &= \frac{2v_{bo} - v_{ao} - v_{co}}{3} \\ v_{cn} &= \frac{2v_{co} - v_{ao} - v_{bo}}{3} \end{aligned} \tag{4.10}$$

The voltage waveform for the voltage across the motor winding 'a' is given in Fig. 4.4.

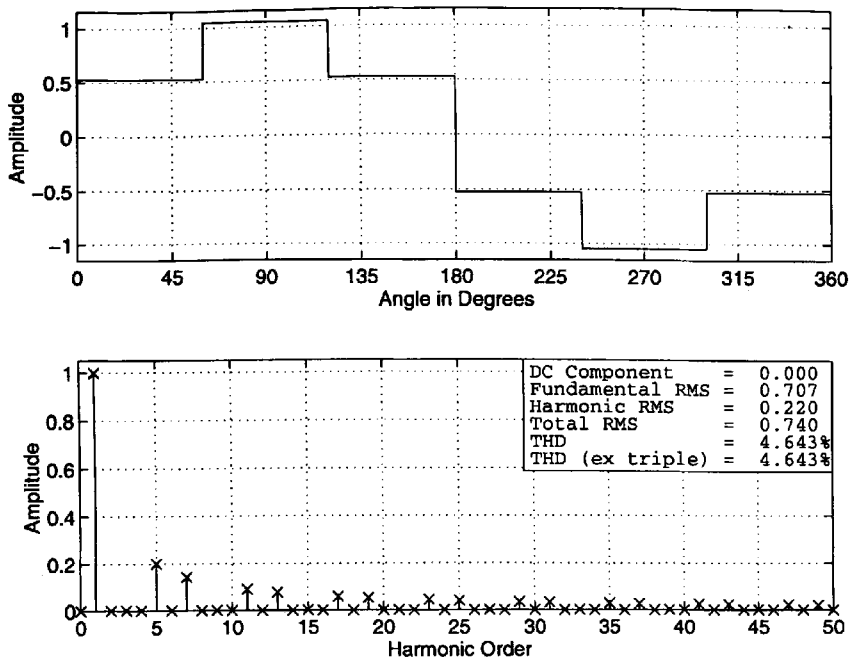

Fig. 4.4: Phase to Neutral of Load Voltage in Six Step Mode (V_{an})

It may be seen from Fig. 4.4 that this voltage has four levels (zero vectors are not selected) which are $+2/3\ V_{dc}$, $+1/3\ V_{dc}$, $-1/3\ V_{dc}$, and $-2/3\ V_{dc}$. Comparison to Fig. 4.2 shows that the voltages are in phase with the phase to neutral of the d.c. supply voltages. The Fourier coefficients of the voltage waveforms, calculated according to equation 4.2, are tabulated in Table 4.3.

Table 4.3: Fourier Coefficients for Phase to Neutral of Load Voltage

	v_{ao}	v_{ao}	v_{bo}	v_{bo}	v_{co}	v_{co}			
k	a_k	b_k	a_k	b_k	a_k	b_k	amp	RMS	Seq.
1	$\frac{\sqrt{3}}{2}$	$\frac{1}{2}$	$-\frac{\sqrt{3}}{2}$	$\frac{1}{2}$	0	-1	1	$\frac{1}{\sqrt{2}}$	+
2	0	0	0	0	0	0	0	0	0
3	0	0	0	0	0	0	0	0	0
4	0	0	0	0	0	0	0	0	0
5	$-\frac{\sqrt{3}}{10}$	$\frac{1}{10}$	$\frac{\sqrt{3}}{10}$	$\frac{1}{10}$	0	$-\frac{1}{5}$	$\frac{1}{5}$	$\frac{1}{5\sqrt{2}}$	-
6	0	0	0	0	0	0	0	0	
7	$\frac{\sqrt{3}}{14}$	$\frac{1}{14}$	$-\frac{\sqrt{3}}{14}$	$\frac{1}{14}$	0	$-\frac{1}{7}$	$\frac{1}{7}$	$\frac{1}{7\sqrt{2}}$	+
8	0	0	0	0	0	0	0	0	0

9	0	0	0	0	0	0	0	0	0
10	0	0	0	0	0	0	0	0	0
11	$-\frac{\sqrt{3}}{22}$	$\frac{1}{22}$	$\frac{\sqrt{3}}{22}$	$\frac{1}{22}$	0	$-\frac{1}{11}$	$\frac{1}{11}$	$\frac{1}{11\sqrt{2}}$	-
12	0	0	0	0	0	0	0	0	0
13	$\frac{\sqrt{3}}{26}$	$\frac{1}{26}$	$-\frac{\sqrt{3}}{26}$	$\frac{1}{26}$	0	$-\frac{1}{13}$	$\frac{1}{13}$	$\frac{1}{13\sqrt{2}}$	+

The only difference to Table 4.1 is that the harmonics for k = 3, 9, 15, 21, ... have cancelled. This can be seen directly from equation 4.10.

4.2 Six Step Current Analysis

The analysis of the motor currents in six step mode may be carried out conveniently by using the dynamic induction motor model. Although the steady state model may also be used, the use of the dynamic model has the following advantages:

- Due to torque variations in six step mode, there are also small speed variations which can be analysed with the dynamic model.
- Positive and negative sequences for the higher order slip frequencies (k=5, 7, 11, 13,...) have to be taken into account with the steady state model.

Fig. 4.5 shows the model employed for the simulations of the motor variables in six step mode.

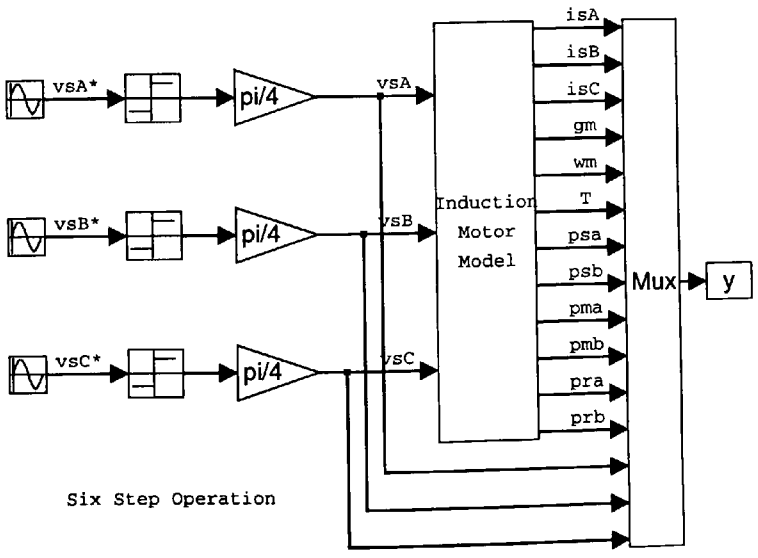

Fig. 4.5: Model for Six Step Waveform Analysis

The resulting stator current waveform is shown in Fig. 4.6. It may be seen from the figure that the dominant harmonics in the spectrum are the 5th, 7th, 11th and 13th harmonic. This is in accordance with Table 4.3, which shows the harmonic components for the voltages across the motor windings. Comparison with the voltage spectrum of Fig. 4.4 shows that the harmonic amplitudes decrease more rapidly with increasing harmonic order for the current than for the voltage. The current waveform is divided into six sections which corresponds to the six sections seen in Fig. 4.4. There is a phase lag between the current waveform and the voltage waveform from Fig. 4.4 of approximately 52 degrees, which corresponds to the phasor diagram for steady state operation (Fig. 3.2).

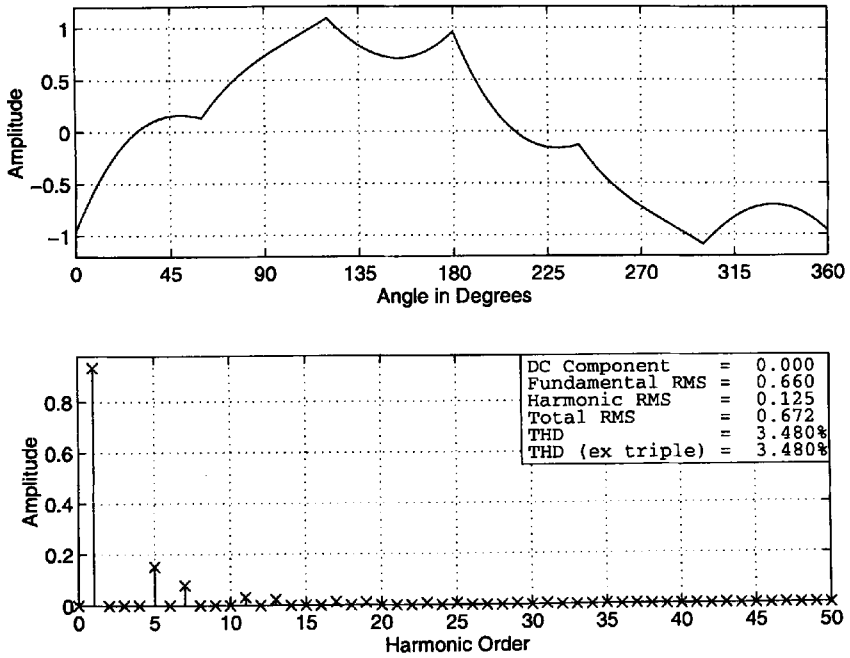

Fig. 4.6: Stator Current in Six Step Mode (i_{sa})

The magnetising current waveform is depicted in Fig. 4.7. The waveform is smoother than the stator current waveform, because of the main inductance through which this current flows. The dominant harmonic is the 5th harmonic.

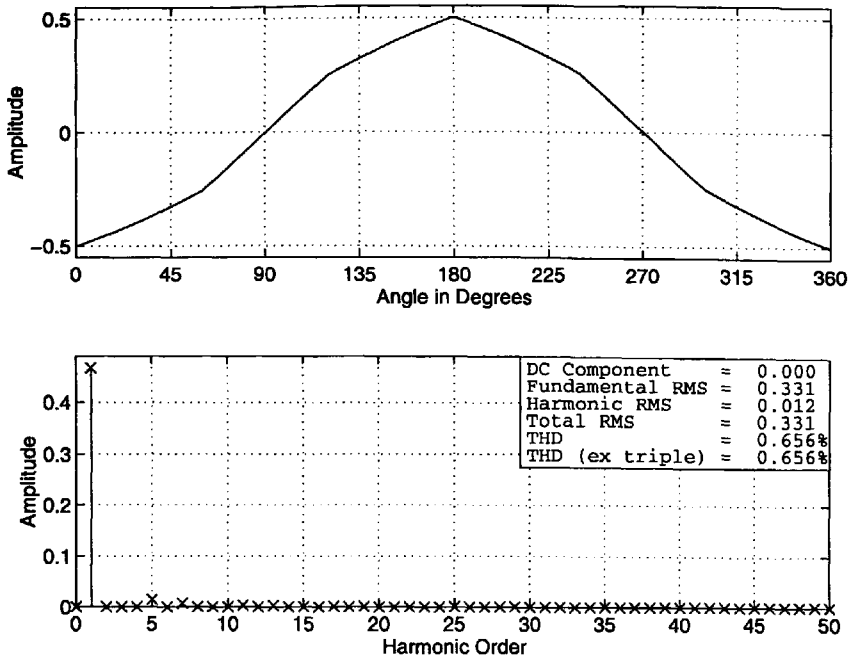

Fig. 4.7: Magnetising Current in Six Step Mode (i_{ma})

Fig. 4.8 shows the rotor current waveform in six step mode. It shows a higher harmonic distortion than the stator current waveform because of the low slip operation at rated speed which results in a more resistive rotor current path. The dominant harmonics are the same as for the stator and magnetising currents.

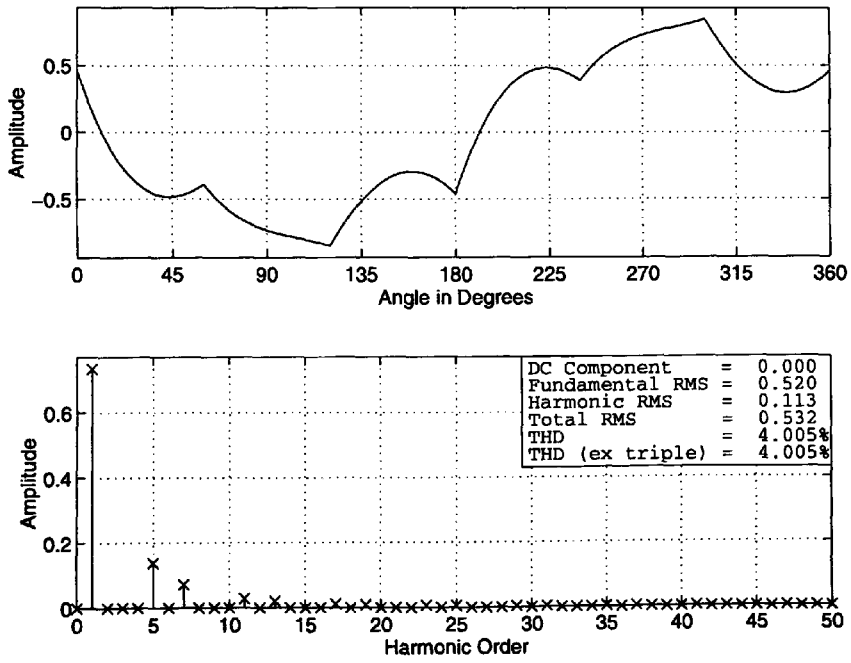

Fig. 4.8: Rotor Current in Six Step Mode (i_{ra})

4.3 Six Step Flux Analysis

It may be seen from Fig. 4.9, that the stator flux waveform lags the voltage waveform (Fig. 4.4) by 90 degrees.

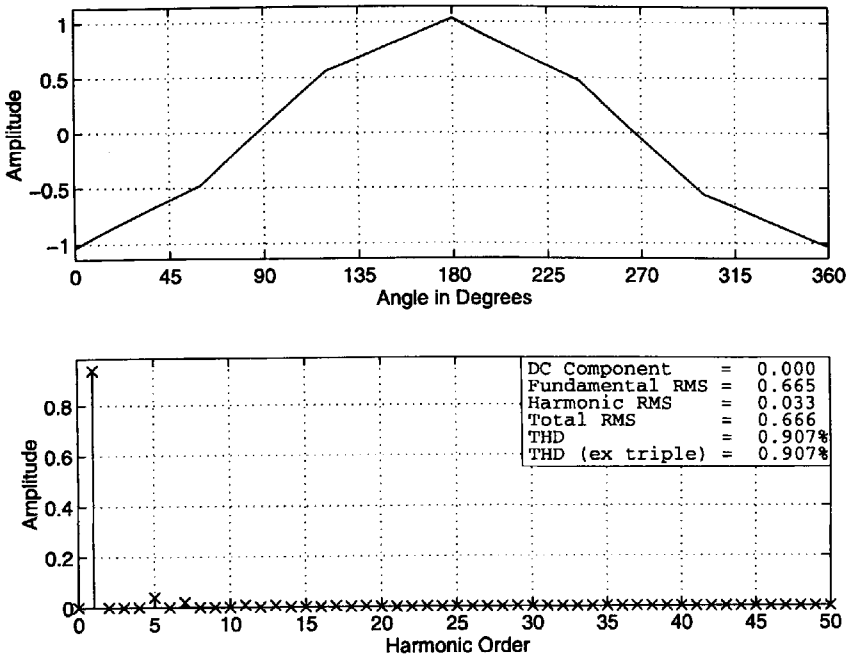

Fig. 4.9: Stator Flux in Six Step Mode (ψ_{sa})

Fig. 4.10 shows the magnetising flux waveform in six step mode, which is smoother than the stator flux waveform, and therefore has a slightly reduced harmonic content which mainly consists of the 5th harmonic.

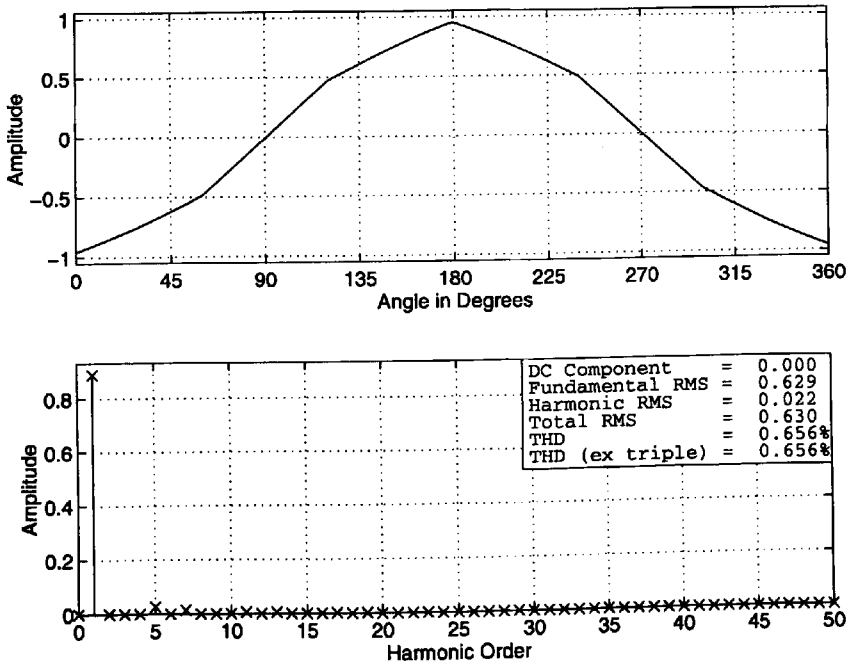

Fig. 4.10: Magnetising Flux in Six Step Mode (ψ_{ma})

The rotor flux waveform, shown in Fig. 4.11, is an almost perfect sine wave, with very low total harmonic distortion. It also has the biggest phase lag to the voltage waveform.

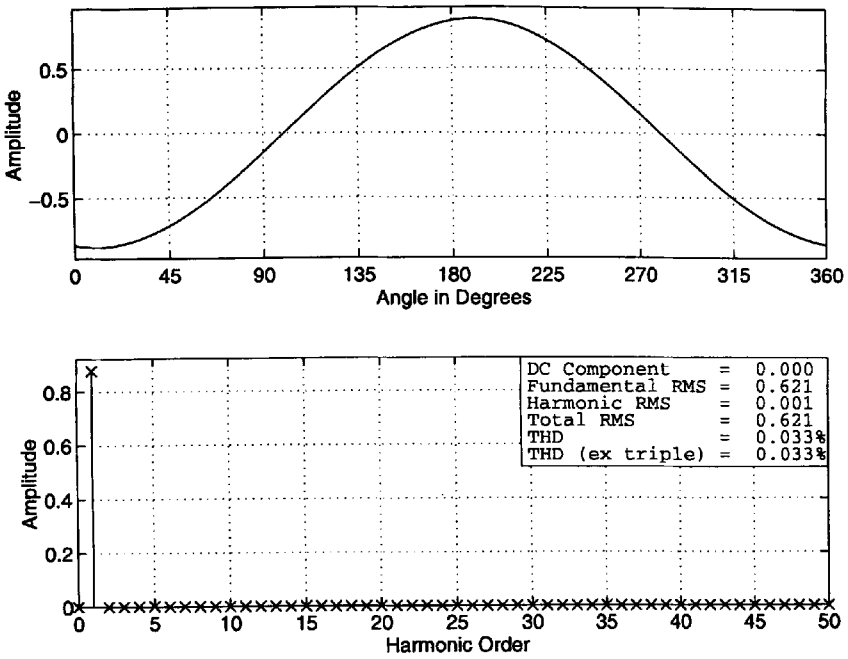

Fig. 4.11: Rotor Flux in Six Step Mode (ψ_{ra})

4.4 Six Step Power, Torque and Speed Analysis

Whereas the six step voltage, current and flux waveforms have a fundamental component and dominant harmonics of order 5, 7, 11, 13, ..., the waveforms of input power, output power, the motor torque and the rotor speed all have a d.c. component and harmonics of order 6, 12, 18, 24, ... in their harmonic spectra.

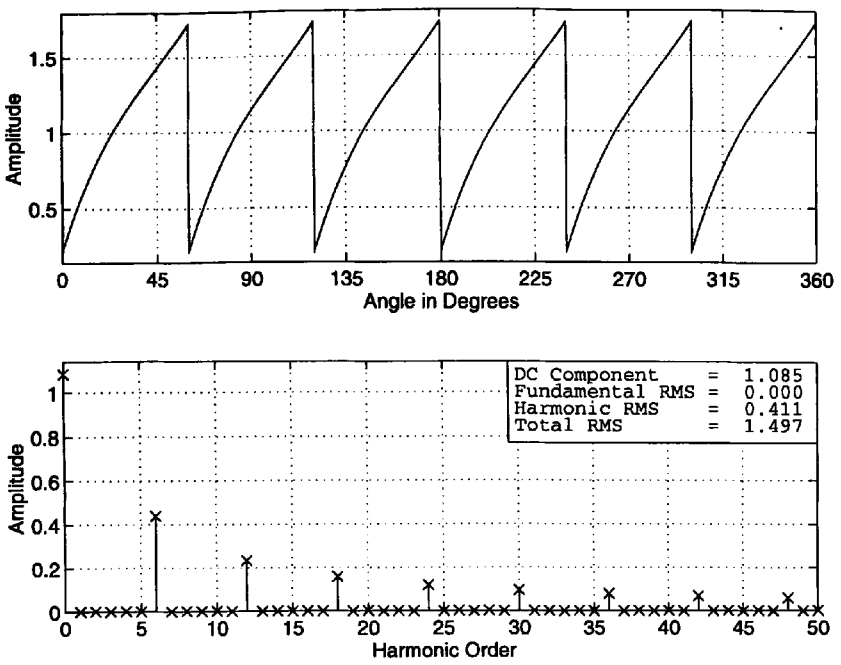

Fig. 4.12: Input Power in Six Step Mode (P_{in})

It may be seen from the input power waveform in Fig. 4.12 that the power has a sawtooth waveform. The instantaneous input power is lowest just after a commutation and is highest just before a commutation of the inverter.

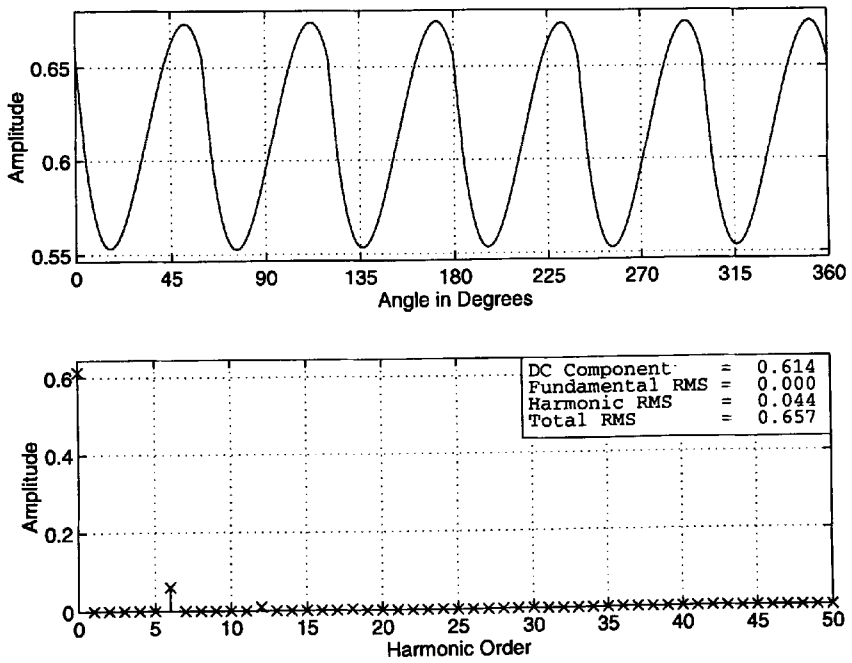

Fig. 4.13: Output Power in Six Step Mode (P_{out})

On the other hand, the output power waveform in six step mode (Fig. 4.13) is smooth and oscillates around an average value ($P_{out} = 0.614$).

Fig. 4.14 shows the waveform and spectrum of the developed motor torque. The waveform of the motor torque is almost identical to the waveform of the output power

(Fig. 4.13), as the motor speed is constant. As can be seen from the spectrum in Fig. 4.14, the torque variations are mainly due to the 6th harmonic.

The motor speed waveform is shown in Fig. 4.15. It can be seen that the speed variations are minute and therefore harmonic components are not shown in the spectrum of Fig. 4.15. However, the speed variations depend on the inertia present in the drive system and can be larger for drives with a low inertia.

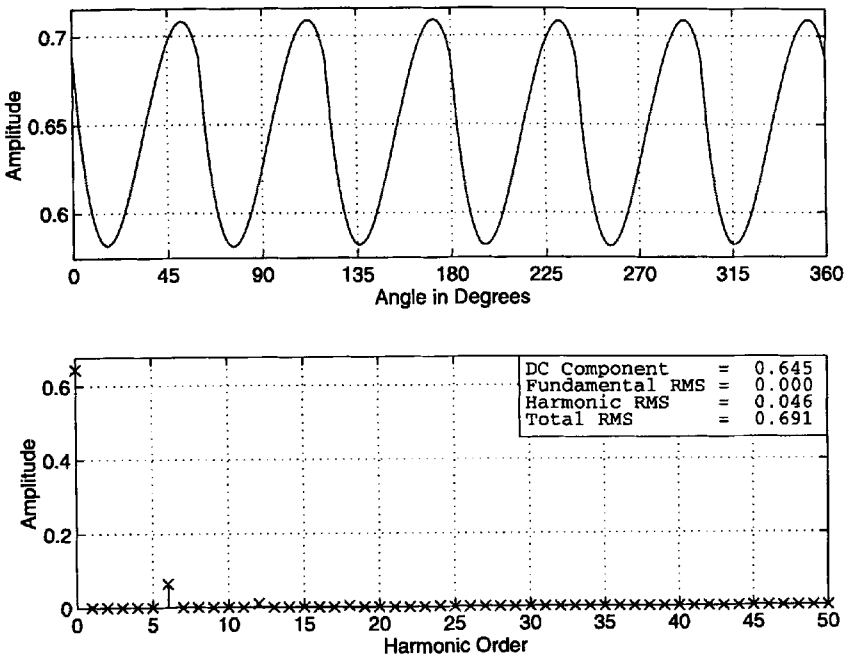

Fig. 4.14: Developed Torque in Six Step Mode (T)

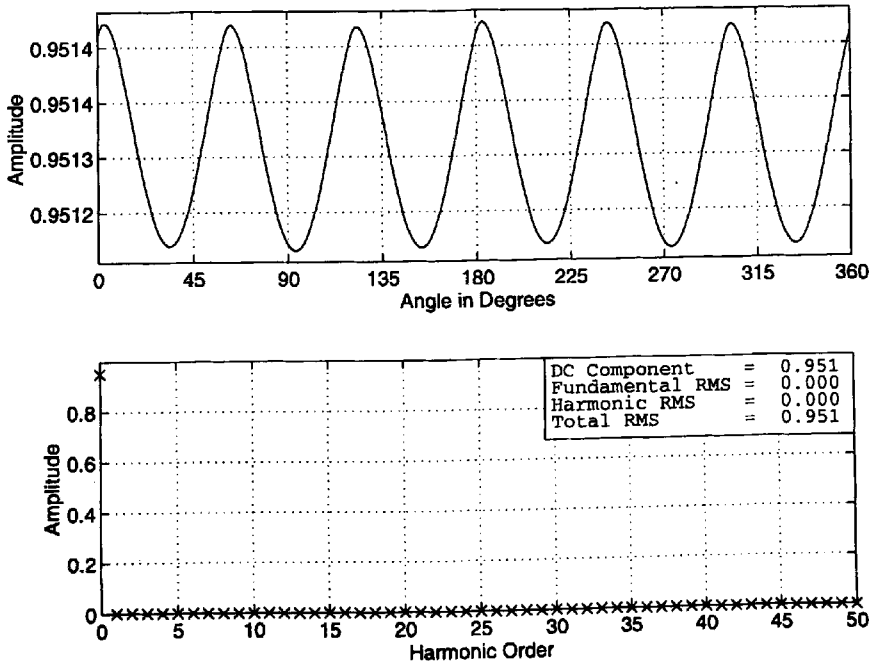

4.15: Rotor Speed in Six Step Mode (ω_m)

4.5 Interim Conclusion

The waveforms and the harmonic content for six step mode have been investigated and the rated operating condition has been examined. It has been found that the harmonics of concern for the voltage, current and flux are the 5th, 7th, 11th, 13th,... harmonics, which are odd non triple harmonics. The harmonics concerning the input power, output power, torque and speed are the 6th, 12th, 18th, 24th,... harmonics, which are the even triple harmonics.

The six step mode is not an inverter operation mode which looses relevance in modern inverters, but is used in VVVF converters for high speed operation where maximum voltage is required. It may be seen from Fig. 3.21, that a large area in the torque-speed plane exists where the six step mode (CVVF) applies.

Torque pulsations may be reduced by the use of filters connected in line with the motor phases. This on the other hand, introduces extra cost for components and space and also extra losses.

Depending on the motor operating condition, there is a certain amount of power at harmonic frequencies supplied to the motor. This power can be regarded as a waste of energy as it does not contribute to the production of extra average torque. One way of minimising this power is to use a higher d.c. link voltage, so that the p.w.m. mode is used for a larger operating area in the torque speed plane (Fig. 3.21). This, of course, depends on the availability of suitable mains supply voltage. The six step mode can then be used for higher speeds, corresponding to higher supply frequencies. This also reduces the harmonic content of the current, flux, power, torque and speed waveforms.

Chapter 5: Pulse Width Modulation

5.0 Pulse Width Modulation Strategies

An inverter operating in six-step (square wave) operation allows frequency control only. The control of the voltage magnitude usually has to be carried out in a separate converter supplying the d.c. link which feeds the inverter. However, it is desirable to integrate the voltage and frequency control into the inverter in order to save components and costs. The simultaneous but independent control of frequency and voltage may be achieved with an inverter operating in the p.w.m. mode. The frequency adjustment is carried out in a similar manner to the six step operation, whereas the voltage adjustment is realised by introducing small notches within the six step waveform during which the output phase is connected to the negative polarity of the constant voltage d.c. link. This then decreases the amplitude of the fundamental component of the resulting waveform. An increase in the amplitude of the fundamental component amplitude above that for six step operation cannot be obtained.

There are only two switching actions per phase and cycle in six step operation. The introduction of further pulses per cycle inevitably increases the switching losses. However, a higher number of switching actions can decrease the total harmonic distortion (THD) and, therefore, decrease the motor copper and iron power losses due to harmonics. With the advent of resonant switching techniques in the d.c. link in small to medium power drives, the problem of high switching losses may be overcome and harmonic motor losses (iron and copper) and even audible noise may be reduced to a minimum by means of high frequency switching. For large power drives, however, the switching frequency is restricted to a few hundred Hertz and hence low pulse numbers need to be considered. In the following, a number of different p.w.m. strategies, including triangular carrier based modulation, space vector modulation and the harmonic elimination technique are considered. Firstly, however, the minimum requirements for voltage regulation are established.

5.1 P.w.m. Waveforms with Minimum Number of Switching Actions

A minimum of six switching actions per phase and cycle are required for simultaneous frequency and voltage adjustment of inverter output waveforms having half- and quarter wave symmetry. Lower numbers of switching actions are not considered here as they

generally include even harmonics. Six switching actions per phase and cycle allow a single pulse to be placed centrally at 90 and 270 degrees within the six step waveform as shown in Fig. 5.1. It may be seen that a single pulse of approximately 28 degrees has been introduced to achieve a fundamental output voltage magnitude of 50% of the six step output. The same may be achieved by shortening the main pulse from 180 degrees to approximately 97 degrees, as shown in Fig. 5.2.

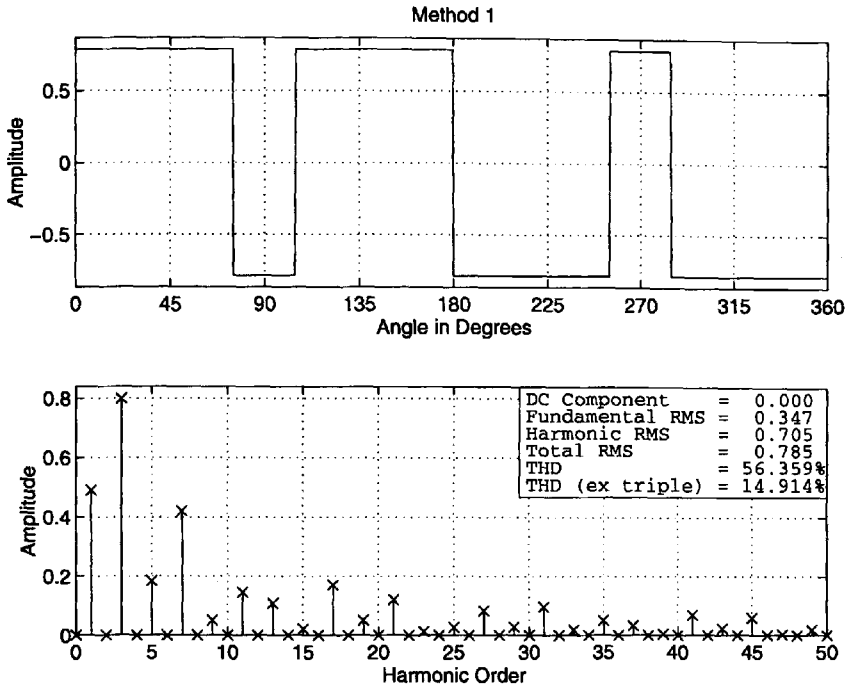

Fig. 5.1: Voltage adjustment with minimum amount of switching actions (Method 1)

Comparison of the two frequency spectra in Fig. 5.1 and Fig. 5.2 shows that the harmonic content of the waveforms are quite different. For example, the fifth harmonic is smaller with method 1 but the seventh harmonics is smaller with method 2. The relationship between pulse width and amplitude of fundamental and the dominant harmonics is shown in Fig. 5.3 for method 1 and Fig. 5.4 for method 2.

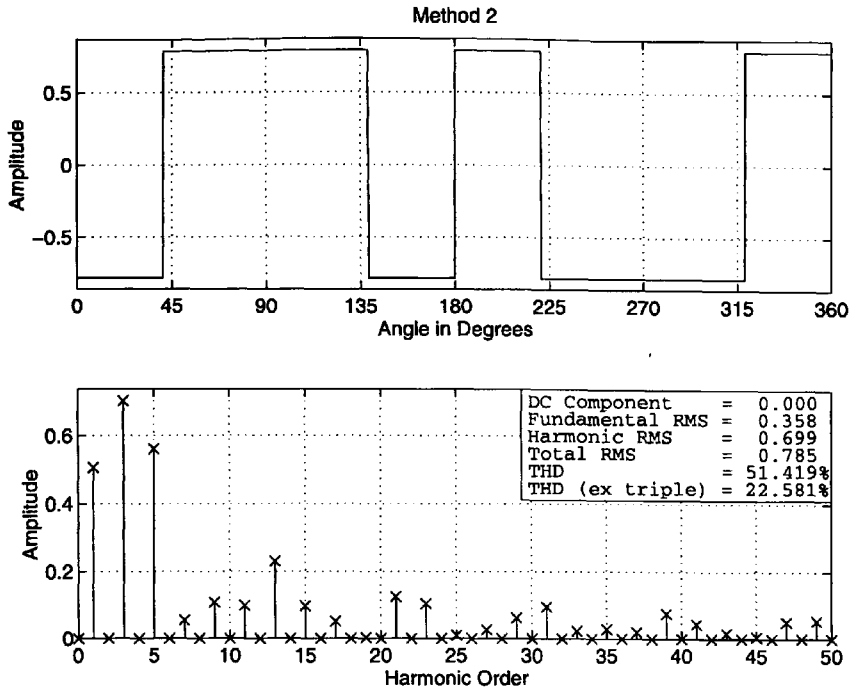

Fig. 5.2: Voltage adjustment with minimum amount of switching actions (Method 2)

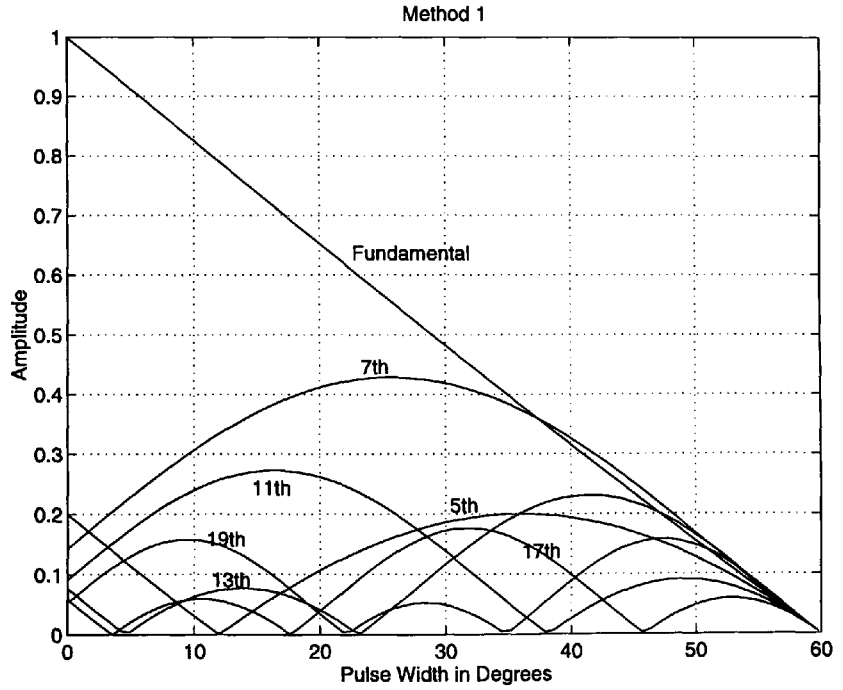

Fig. 5.3: Amplitudes of the Fundamental and Harmonics (Method 1)

It may be seen from Fig. 5.3 that the relation between the pulse width and the amplitude of the fundamental is almost linear. For zero pulse width, the results correspond to six step operation with the dominant harmonics 5, 7, 11, 13, 17, and 19 in sequence. A slight increase in pulse width reduces the harmonics 5, 13, and 17 but increases the harmonics 7, 11 and 19. Further increase of the pulse width varies the harmonic content

considerably. For a pulse width of 25 degrees, the 7th harmonic has a maximum higher than any other harmonic for any pulse width. At a pulse width of 60 degrees, all non-triple harmonics and the fundamental become zero. The resulting square wave waveform consists then of triple harmonics only, which all cancel for a three phase system.

Fig. 5.4 shows the amplitudes of the fundamental and the harmonics against the pulse width for method 2. A pulse width of 60 degrees corresponds to triple frequency square wave operation with zero fundamental and triple harmonics only. Operation at 180 degrees corresponds to six step operation. Slight decrease of the pulse width in six step operation decreases all harmonics. The maximum harmonic is the 5th harmonic, with a maximum at a pulse width of 107 degrees.

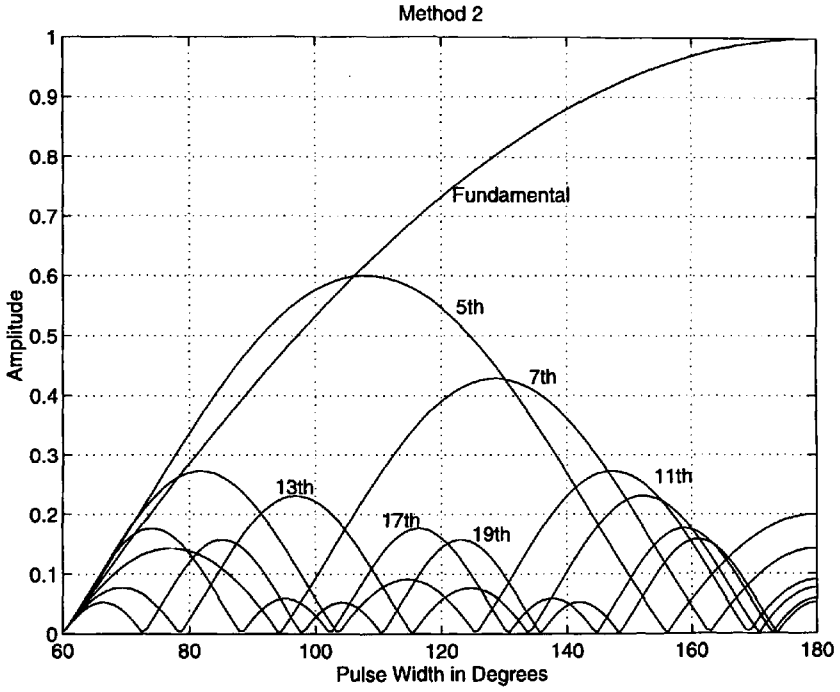

Fig. 5.4: Amplitudes of the Fundamental and Harmonics (Method 2)

The assessment of the methods is simplified when the total harmonic distortion (THD) is used as a figure of merit. The triple harmonics are thereby excluded as they cancel for three phase operation. A comparison of the two methods is shown in Fig. 5.5.

Method 1 gives less total harmonic distortion for most of the output voltage range, whereas method 2 is superior for fundamental amplitudes between 93.85% and 100% of the amplitude for six step operation. The THD shown may be viewed as a benchmark for p.w.m. schemes with additional switching actions. However, for voltages near 100%, the THD for p.w.m. schemes converge to the THD for six step operation which is

equal to 4.64%. Many p.w.m. schemes thereby use over-modulation whereby pulses are dropped to increase the fundamental output voltage to six step level.

The resulting waveforms for p.w.m. with only six switching actions per phase and cycle have a large total harmonic distortion but also have the minimum number of switching actions per cycle. Two different solutions can be found with which it is possible to adjust the fundamental voltage amplitude from 0% to 100%. With the first method, a notch is placed centrally at 90 and 270 degrees of the six step waveform, whereas with the second method the main pulse of the six step operation is shortened symmetrically. The first method gives less THD for most of the output voltage range, whereas the second method is superior for fundamental amplitudes just below the maximum amplitude in six step mode.

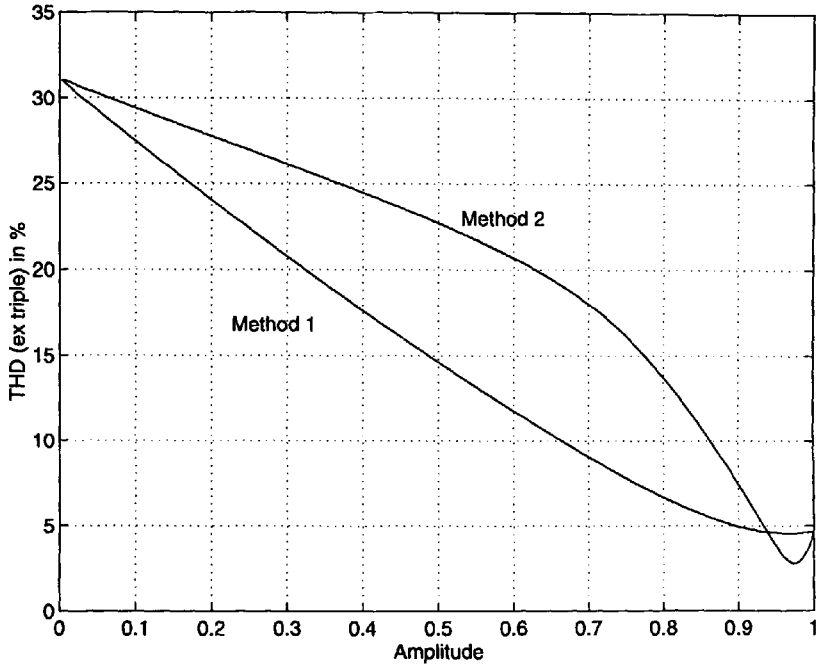

Fig. 5.5 Comparison of Method 1 and Method 2

5.2 Natural Sampling

In natural sampling a sinusoidal reference waveform is compared with a triangular carrier signal. The point of intersection of the two signals determines the switching instants of the inverter. A block diagram of the system configuration is shown in Fig. 5.6. The modulation strategy may be implemented by means of analogue electronics using comparators and integrators for the triangular reference signal, or by digital electronics and micro-processors. When the ratio R between the carrier frequency f_c and the frequency of the modulated sine wave f_m becomes an integer number, frequency components are obtained at multiples of the fundamental only. This not only reduces the

content of undesirable frequency components in the signal but also simplifies the analysis of the p.w.m. waveforms. Fig. 5.7 shows the sampling process for natural sampling in detail.

The switching points for the p.w.m. waveform are given by the intersection of the rising and falling edges of the triangular carrier signal and the reference sine wave. The following result for the switching angles can be obtained.

$$\alpha_i = \frac{\pi}{2R}\left(2i - 1 + (-1)^i M \sin\alpha_i\right) \tag{5.1}$$

As the equation is non-linear with respect to the switching angles α_i , a Newton-Raphson algorithm may be employed to find the solutions for α_i within a few iterations as follows:

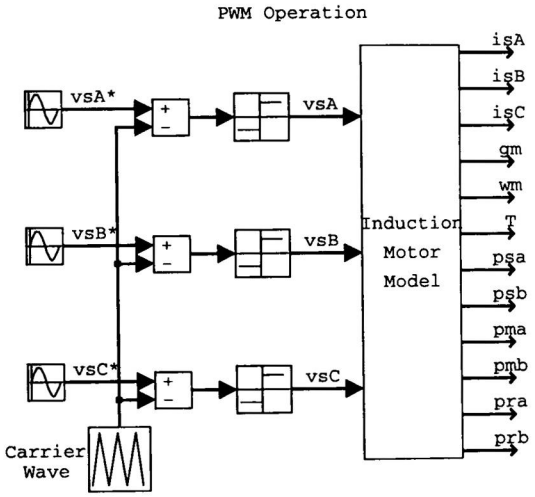

Fig. 5.6: Model for p.w.m. Waveform Analysis

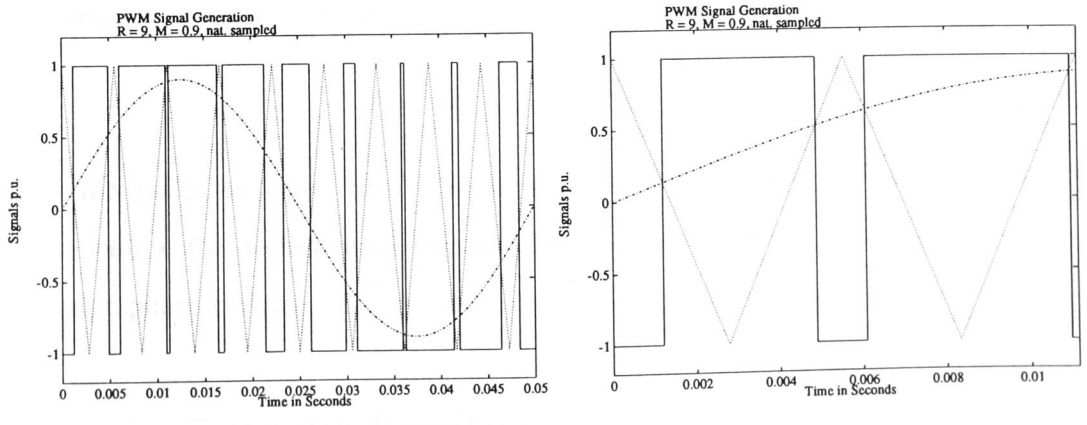

Fig. 5.7: Sampling Process of Natural Sampling

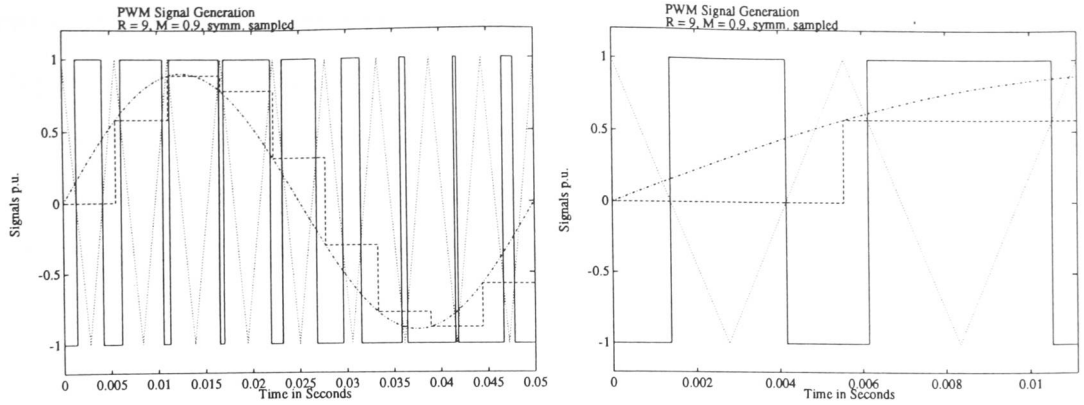

Fig. 5.8: Sampling Process of Regular Symmetric Sampling

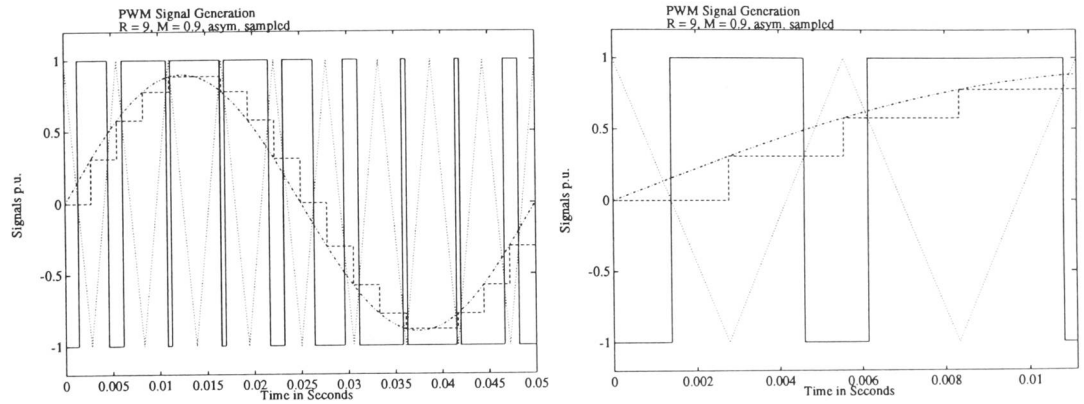

Fig. 5.9 : Sampling Process of Regular Asymmetric Sampling

$$\alpha_{i\ \ improved} = \alpha_i - \frac{\frac{\pi}{2R}\left(2i-1+(-1)^i M\sin\alpha_i\right)-\alpha_i}{\frac{\pi}{2R}(-1)^i M\cos\alpha_i - 1} \tag{5.2}$$

The starting value for α_i is set to the centre of each edge which is given by

$$\alpha_{i\ \ start} = \frac{\pi}{R}\left(i-\frac{1}{2}\right) \tag{5.3}$$

When the ratio between carrier frequency and modulated frequency assumes triple integer values, the dominant harmonics also occur at triple integer values which cancel for a three phase system.

5.3 Regular Symmetric Sampling

In this type of sinusoidal sampling a reference sine wave is sampled once in a triangular carrier signal cycle and this sampled signal is then compared with the triangular carrier

signal. Fig. 5.8 shows the triangular carrier wave, the sinusoidal reference signal, the sampled reference signal and the resulting p.w.m. pulses.

The switching points for the p.w.m. waveform are given by the intersection of the rising or falling edge of the triangular carrier signal and the sampled reference sine wave.

The switching angles may be calculated as follows:

$$\alpha_i = \frac{\pi}{2R}\left(2i-1+(-1)^i M \sin\left(\frac{2\pi}{R} Int\frac{i-1}{2}\right)\right) \tag{5.4}$$

5.4 Regular Asymmetric Sampling

In this type of sinusoidal sampling a reference sine wave is sampled twice in a triangular carrier signal cycle and this sampled signal is compared with the triangular carrier signal. Fig. 5.9 shows the triangular carrier wave, the sinusoidal reference signal, the sampled reference signal and the resulting p.w.m. pulses.

The switching angles for the p.w.m. waveform are given by the intersection of the rising or falling edge of the triangular carrier signal and the sampled reference sine wave and may be calculated as follows:

$$\alpha_i = \frac{\pi}{2R}\left(2i-1+(-1)^i M \sin\left((i-1)\frac{\pi}{R}\right)\right) \tag{5.5}$$

In Fig. 5.10 a typical waveform in asymmetric sampling for R=9 and M=0.5 may be seen. The dominant harmonic is equal to the pulse number R. Furthermore, the 7th and 11th harmonic are also present in the frequency spectrum.

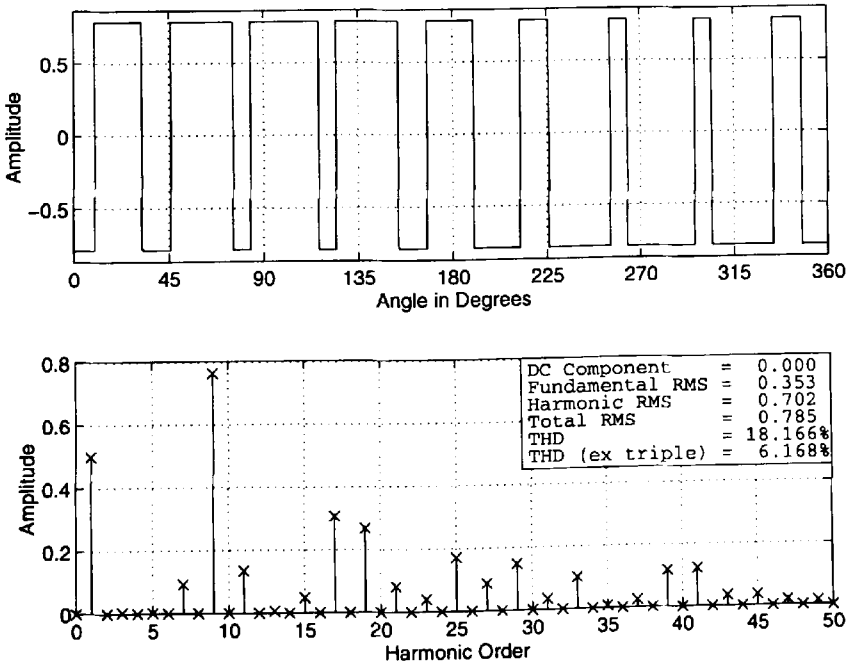

Fig. 5.10 Waveform and Spectrum of Regular Asymmetric Sampling

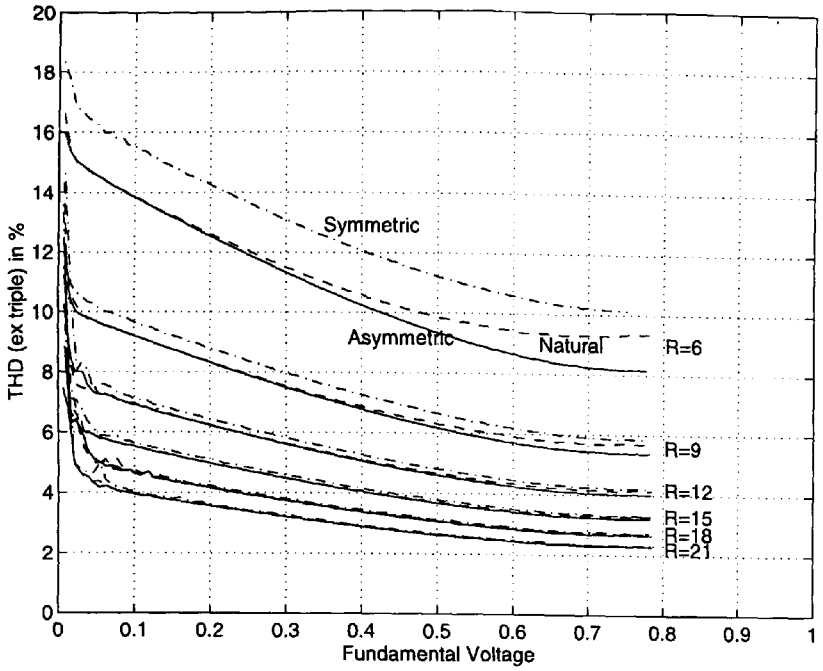

Fig. 5.11: Comparison of Regular Symmetric,
Regular Asymmetric and Natural Sampling p.w.m.

Fig. 5.11 shows a comparison between regular symmetric, regular asymmetric and natural sampling. The THD for natural and asymmetric sampling is equal for low fundamentals, whereas for high fundamental voltages it may be seen that asymmetric sampling is superior to natural sampling. Symmetric sampling gives higher THD for the full modulation range when compared to asymmetric and natural sampling. For higher pulse numbers, all strategies converge and there is virtually no difference with respect to the THD at pulse numbers higher than R=18.

5.5 Synchronous Sigma Delta Modulation

Synchronous Sigma-Delta modulation may be used when the switching instants have to be synchronised to an external clock signal. This is necessary, for example, in a resonant DC link inverter where switching is possible at regular intervals only, i.e. when the voltage across the switching devices is zero. The performance of this strategy is poor at low pulse numbers, however, the aim of the resonant link inverter is to increase the switching frequency. At high switching frequencies, the performance of different modulation strategies is generally very good and hence sigma delta modulation may be used with advantage. The block diagram shown in Fig. 5.12 shows that the difference between the voltage command V_{ref} and the modulator output V_{out} is integrated and fed to a comparator. The comparator is sampled at the clock frequency $f_c = 1/T_c$ and the

output is stored for the next clock period. The output signal is used as a switch command to directly control the switching state of the respective inverter leg. Three independent modulators can be used to control a three phase inverter (Mertens 1992).

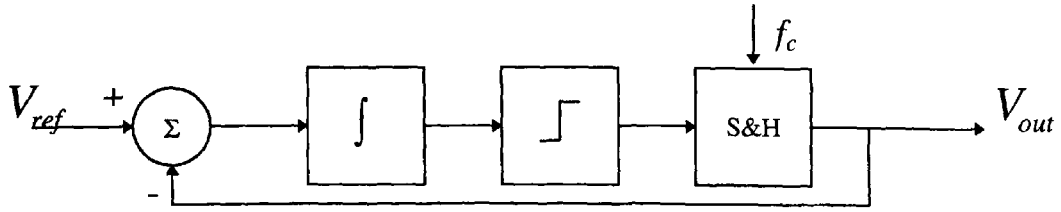

Fig. 5.12: Block Diagram of Sigma Delta Modulation

It has been found that synchronous sigma delta modulation can be superior to p.w.m. only for high modulation indices and only if the sigma delta clock frequency f_c can be chosen at above eight times the switching frequency of p.w.m. (Mertens 1992).

5.6 Space Vector Modulation

The space vector modulation technique uses voltage space vectors to generate the p.w.m. patterns for all three phases of the drive system simultaneously. The voltage-time area of a reference voltage space vector and the sampling time is made equal to the voltage time areas using the two adjacent switching state vectors, as shown in the following expression.

$$T\vec{V}_{ref} = T_a\vec{V}_a + T_b\vec{V}_b \tag{5.6}$$

The durations for the application of voltage vector $\vec{V}_a$ and $\vec{V}_b$ are T_a and T_b, respectively which can be calculated by splitting equation (5.6) in real and imaginary parts. The remainder of the sampling period is filled with one of the two zero vectors. The relationship (5.6) may also be expressed in terms of switching angles as follows.

$$\frac{\pi}{R}\vec{V}_{ref} = \alpha_a\vec{V}_a + \alpha_b\vec{V}_b \tag{5.7}$$

$$\frac{\pi}{R} = \alpha_a + \alpha_b + \alpha_0 \tag{5.8}$$

The angles α_a and α_a correspond to the duration of the application of voltage vectors $\vec{V}_a$ and $\vec{V}_b$, respectively. The zero voltage vectors $\vec{V}_0$ and $\vec{V}_7$ are selected for α_0. The voltage vectors $\vec{V}_a$ and $\vec{V}_b$ are the two adjacent switching state vectors which can be realised with a three phase inverter to the reference voltage vector $\vec{V}_{ref}$, as illustrated for the first sextant of the complex voltage vector plane shown in Fig. 5.13.

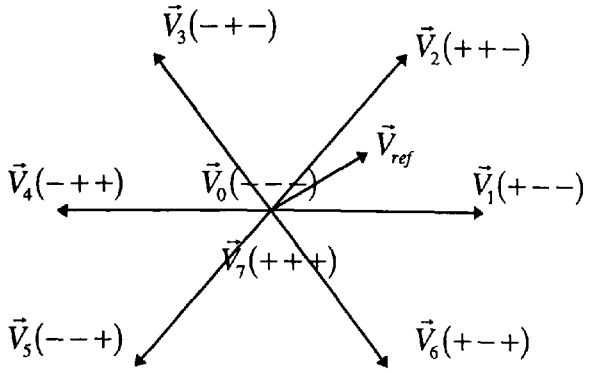

Fig. 5.13: Space Vector Modulation

For the case shown, $\vec{V}_a = \vec{V}_1$ and $\vec{V}_b = \vec{V}_2$. The switching angles α_a, α_b and α_0 may be calculated by splitting equation (5.7) into real and imaginary part as follows:

$$\begin{aligned} \alpha_a &= \frac{M}{R}\left(3\cos\alpha - \sqrt{3}\sin\alpha\right) \\ \alpha_b &= \frac{M}{R} 2\sqrt{3}\sin\alpha \\ \alpha_0 &= \frac{\pi}{R} - \alpha_a - \alpha_b \end{aligned} \tag{5.9}$$

where M is the modulation index and R is the number of α_a, α_b and α_0 triplets per half cycle of the fundamental waveform. The angle α is the angle between $\vec{V}_{ref}$ and $\vec{V}_a$. A typical sequence of the application of the voltage vectors is shown below:

first sextant second sextant third sextant

$$\vec{V}_1 - \vec{V}_2 - \vec{V}_7 - \vec{V}_2 - \vec{V}_1 - \vec{V}_0 - \vec{V}_1 \ldots V_2 - \vec{V}_3 - \vec{V}_0 - \vec{V}_3 - \vec{V}_2 - \vec{V}_7 - \vec{V}_2 \ldots \vec{V}_3 - \vec{V}_4 - \vec{V}_7 - \vec{V}_4 - \vec{V}_3 - \vec{V}_0 - \vec{V}_3 \ldots$$

The zero voltage vector $\vec{V}_7$ is thereby selected after voltage vectors with an even index number ($\vec{V}_2, \vec{V}_4, \vec{V}_6$), whereas zero voltage vector $\vec{V}_0$ is selected after non zero voltage vectors with an odd index number ($\vec{V}_1, \vec{V}_3, \vec{V}_5$), which minimises the number of switching actions. A space vector modulated waveform for a modulation index of M=0.5 and R=9 may be seen with its associated spectrum in Fig. 5.14.

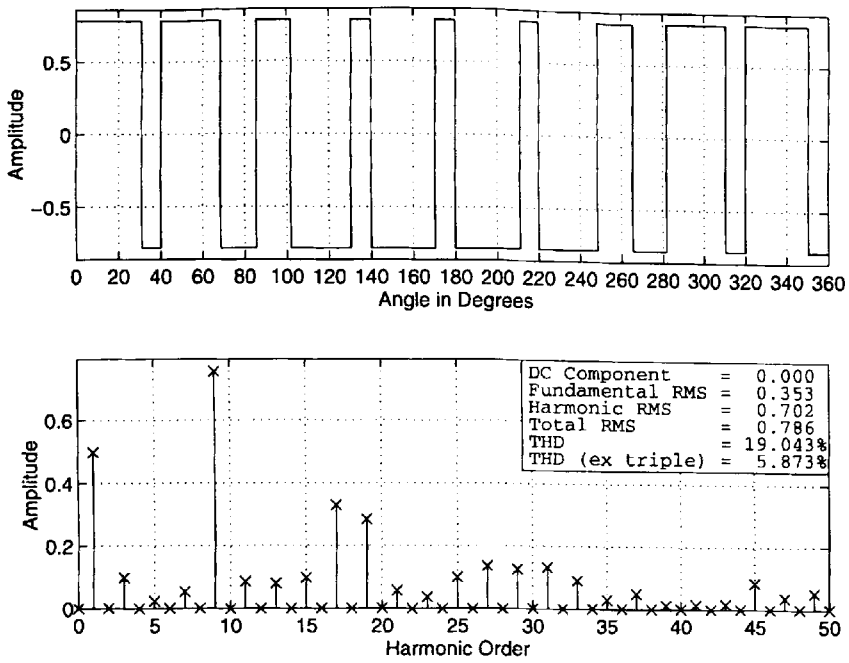

Fig. 5.14: Waveform and Spectrum of Space Vector Modulation (M=0.5, R=9)

The 20 degrees intervals shown in the waveform of Fig. 5.14, correspond to the application of $\vec{V}_a$, $\vec{V}_b$ and one of the zero voltage vectors. The resulting total harmonic distortion of the spectrum shown in Fig. 5.14 is lower than for regular asymmetric sampling. Fig. 5.15 shows the THD for triple pulse numbers R.

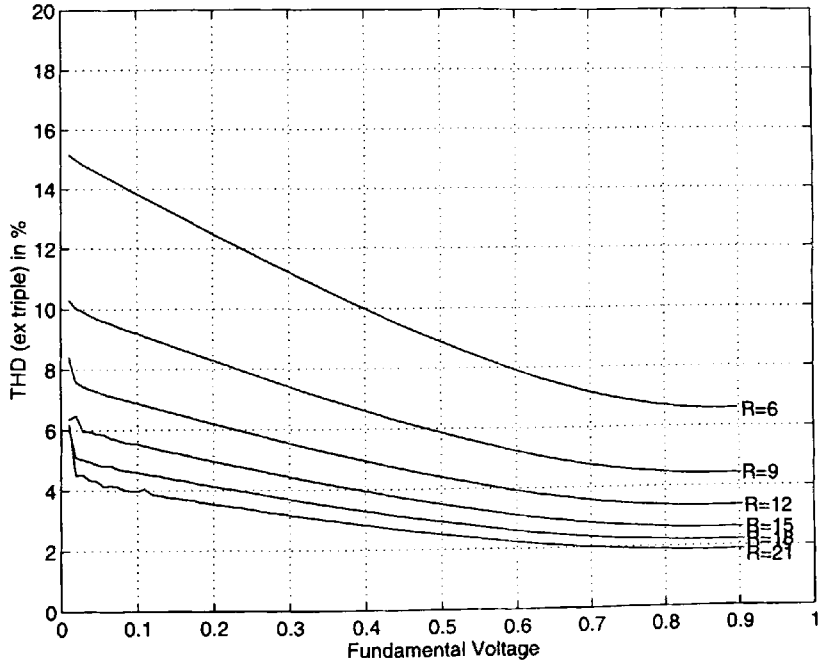

Fig. 5.15: THD of Space Vector Modulation

It may be seen from Fig. 5.15 that the modulation range is extended to 91% of the six-step voltage, whereas with natural sampling, regular symmetric and regular asymmetric

sampling only 78% of the six step voltage (Fig. 5.11) can be achieved when sinusoidal reference waves.

5.7 Hysteresis Current Control

This mode of p.w.m. waveform generation can work with closed loop control only. Current reference signals are compared to measured motor phase currents and the error controls the switching actions for the individual motor phases. When the measured current is higher than the reference current, the phase is connected to the negative side of the DC link in order to reduce the current in that particular motor phase, whereas when the measured current is lower than the reference current, the phase is connected to the positive side of the DC link to increase the current in that particular phase.

Fig. 5.16 shows a hysteresis current controller with an simplified steady state induction motor model.

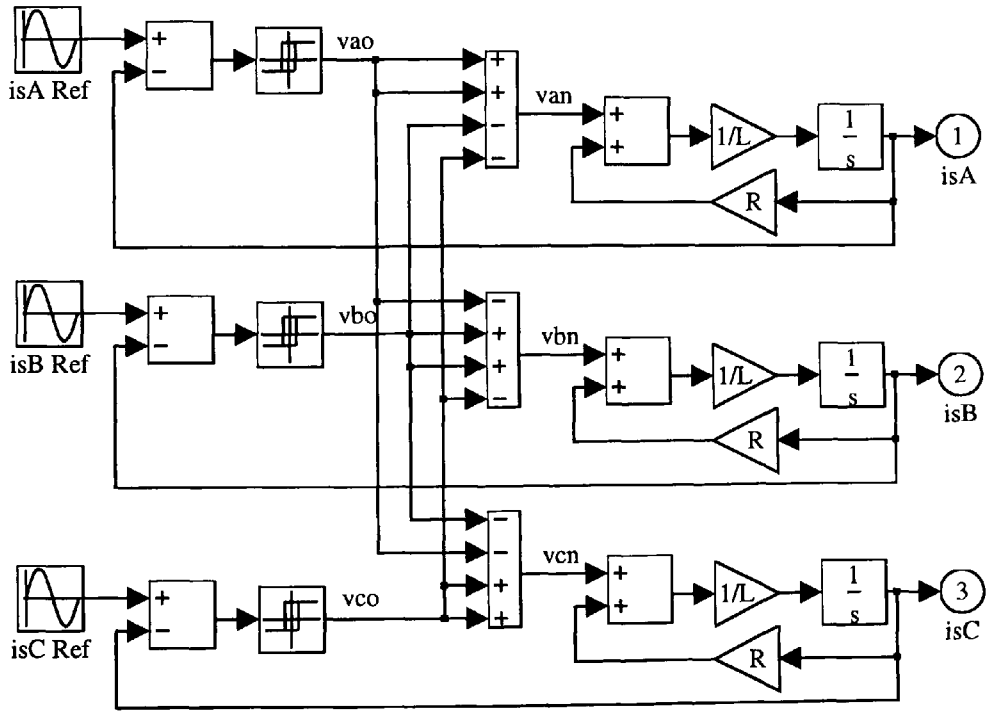

Fig. 5.16: Hysteresis Current Controller

The resistance values 'R' and inductance values 'L' in Fig. 5.16 are the lumped equivalent circuit parameters for a particular motor slip calculated from the steady state equivalent circuit (Fig. 3.1). The voltages 'vao', 'vbo' and 'vco' are phase to neutral of the d.c. link voltages, whereas the voltages 'van', 'vbn' and 'vcn' are the phase to neutral of the load voltages, corresponding to an inverter with star connected motor windings (Fig. 4.1). The three integrators in Fig. 5.16 are denoted '1/s', where 's'

corresponds to the complex Laplace operator. The currents signals 'isa Ref', 'isb Ref' and 'isc Ref' form a balanced three phase system and are the reference currents for the simulation model (Fig. 5.16).

The simulated current waveforms for rated slip (s=4.91%) and a hysteresis setting of 0.03 p.u. are shown in Fig. 5.17. It can be seen that the stator current waveforms ('isa', isb' and 'isc' in Fig. 5.16) follow the reference current waveforms closely.

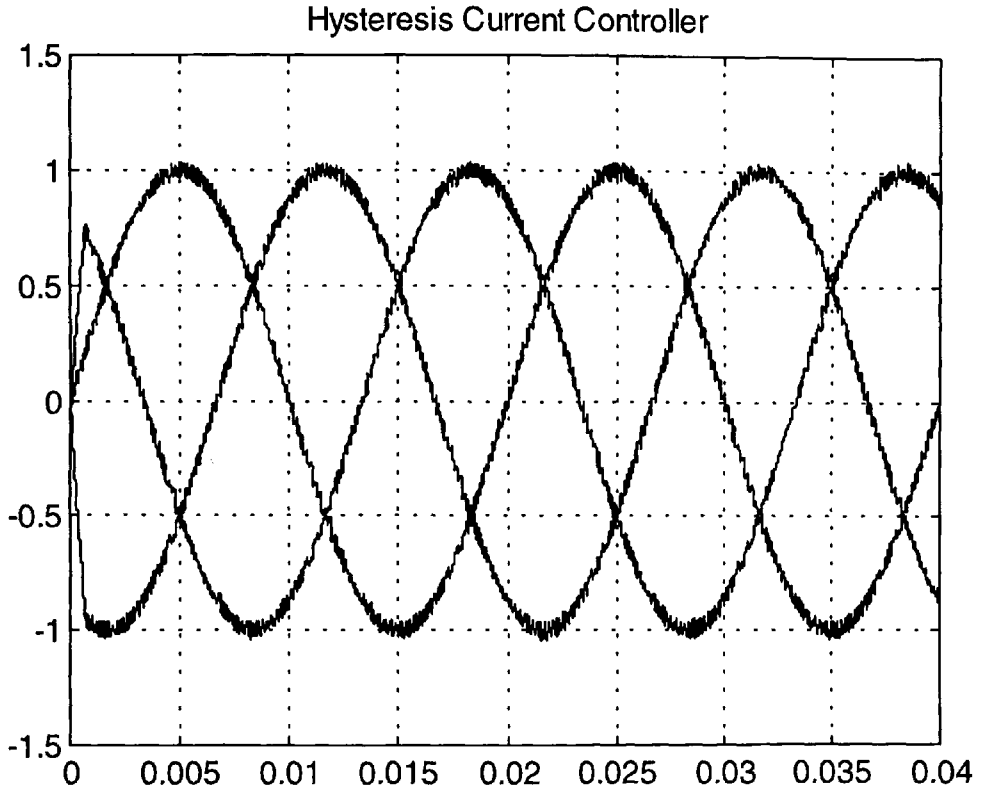

Fig. 5.17: Current Waveforms of Hysteresis Current Control

The average switching frequency may be varied be varying the hysteresis setting of the relay circuit in Fig. 5.16. The dynamic performance of this modulation scheme is excellent, because there is no subcycle switching when there is a large difference of reference current and actual current for a particular motor phase. Thus, no inverter switching is carried out during such a period and the current in that phase can reach the reference current with minimum delay. However there are a number of drawbacks (Holtz, 1994):

1. There is no intercommunication between the individual hysteresis controllers of the three phases and hence no strategy to generate zero voltage vectors.

2. There is a tendency at lower speed to lock into limit cycles which comprise only non-zero voltage vectors.
3. The current error is not strictly limited. The signal will leave the hysteresis band whenever the zero vector is turned on while the back EMF vector has a component that opposes the previous switching state vector. The maximum overshoot is twice the hysteresis band width.
4. As the switching frequency is variable, undesirable sub-harmonics of the current spectrum are introduced.

The drawbacks of this modulation scheme may be overcome by using a carrier based modulation scheme as part of a current control loop (Holtz 1994).

5.8 Harmonic Elimination Technique

The harmonic elimination technique allows one to determine pulse width modulated signals where certain harmonics are zero. Preferably, the low order harmonics near the fundamental are cancelled. When the waveforms have half and quarter wave symmetry, only odd harmonics are contained in the spectrum. Triple harmonics cancel for a three phase system, because they are of zero sequence. Therefore, the harmonics of concern for the harmonic elimination technique are the 5th, 7th, 11th, 13th, 17th, 19th, ..., which are the odd non-triple integer harmonics. For N switching actions per quarter wave ($4N+2$ for full wave), $N-1$ harmonics may be eliminated from the voltage spectrum using this technique (Bowes 1990). The technique involves the solution of a non-linear set of N equations with N unknown switching angles. For the solution of such a set of equations, appropriate numerical methods have to be employed. With the advent of numerical software packages such as Matlab, these algorithms are readily available. However, due to the numerical complexity, the online solution during the operation of the motor is possible only for certain linearisations, which do not produce exact cancellation of the harmonics of concern (Bowes 1990). Therefore, in most cases, the switching angles are pre computed and stored in a table accessed by a micro controller.

One difficulty of this technique is that due to the periodicity of the trigonometric functions involved, a large number of solutions to the non-linear set of equations exists. This is particularly true for a large N. The individual solutions all cancel the harmonics of concern, but have quite different properties with respect to the total harmonic distortion because the remaining harmonics can have very different amplitudes. Furthermore, the maximum modulation index may be different for the solutions.

The N non-linear equations to be solved result directly from the Fourier analysis for the amplitudes of the harmonics.

$$V_k = \frac{1}{4}\left|\int_0^{\alpha_1} e^{-jkx}dx - \int_{\alpha_1}^{\alpha_2} e^{-jkx}dx + \int_{\alpha_2}^{\alpha_3} e^{-jkx}dx \ldots \int_{2\pi-\alpha_1}^{2\pi} e^{-jkx}dx\right| \tag{5.10}$$

The solution for the individual harmonics may be found as follows:

$$V_k = \left|1 + 2\sum_{i=1}^{N}(-1)^i \cos(k\alpha_i)\right| \tag{5.11}$$

for N=4, for example, the set of non-linear equations is given by

$$\begin{aligned} V_1 &= |1 - 2\cos\alpha_1 + 2\cos\alpha_2 - 2\cos\alpha_3 + 2\cos\alpha_4| \\ 0 &= 1 - 2\cos(5\alpha_1) + 2\cos(5\alpha_2) - 2\cos(5\alpha_3) + 2\cos(5\alpha_4) \\ 0 &= 1 - 2\cos(7\alpha_1) + 2\cos(7\alpha_2) - 2\cos(7\alpha_3) + 2\cos(7\alpha_4) \\ 0 &= 1 - 2\cos(11\alpha_1) + 2\cos(11\alpha_2) - 2\cos(11\alpha_3) + 2\cos(11\alpha_4) \end{aligned} \tag{5.12}$$

Due to the periodicity of the cosine functions in equation 5.12 and because the fundamental V_1 may be solved for positive and negative values, four different sets of solutions for the switching angles $\alpha_1 \ldots \alpha_4$ may be found, which are shown in Fig. 5.18.

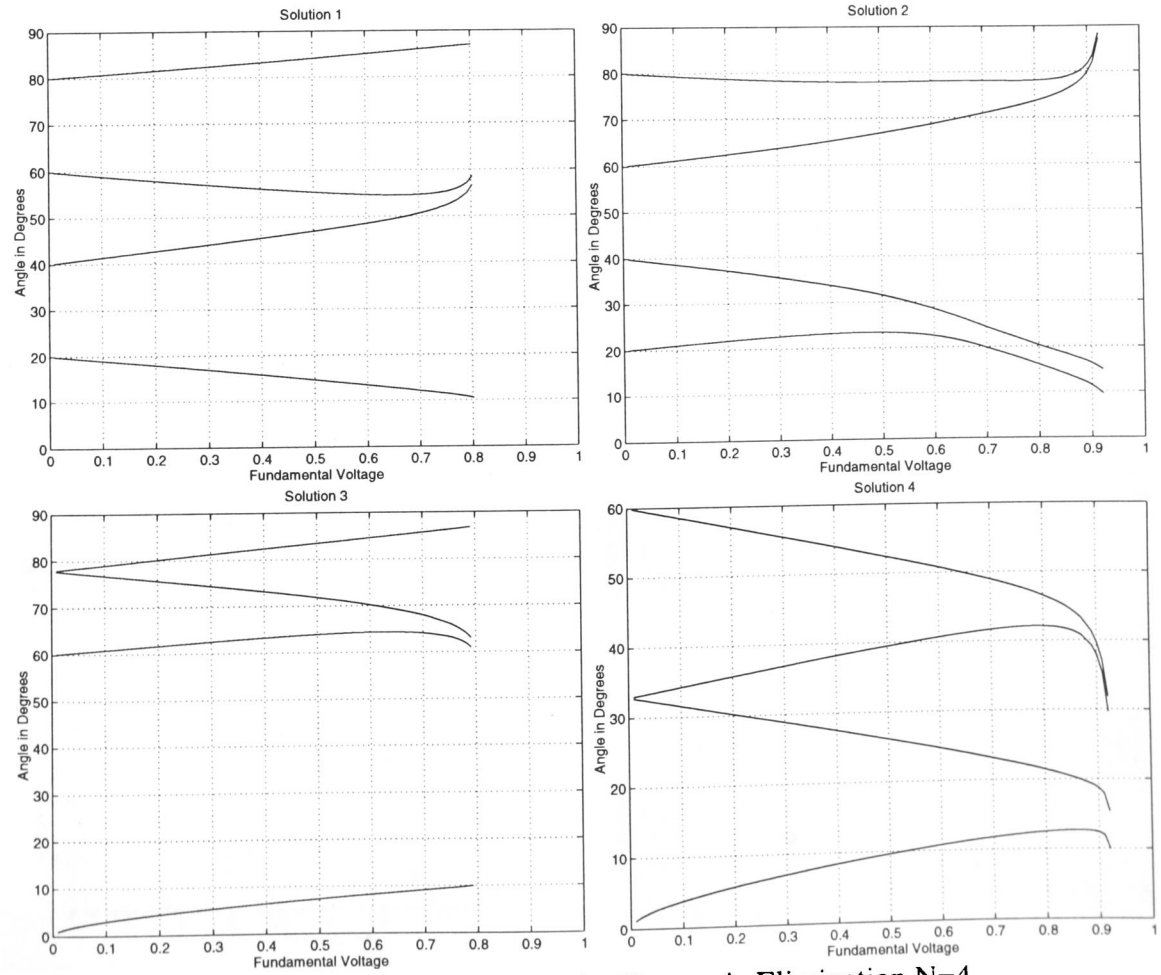

Fig. 5.18: Switching angles for Harmonic Elimination N=4

Fig. 5.18 shows the required variation of the switching angles $\alpha_1 \ldots \alpha_4$ for fundamental voltages ranging from 0 p.u. to 0.8 p.u. .for solutions 1 and 3 and from 0 p.u. to 0.92 p.u. for solutions 2 and 4.

With solution 4 the angles are within 0-60 degrees, whereas with solutions 1-3 the angles cover 0-90 degrees. For a fundamental amplitude near zero, solutions 1 and 2 converge to square wave operation with triple frequencies because switching occurs every 20 degrees of a cycle of the output waveform. Furthermore, it may be seen that due to numerical problems with the non-linear equation solver, not all solutions could be found up to the maximum modulation index as seen in solution 1 and solution 2 diagrams of Fig 5.18, because the equation solver returns the switching angles for solutions 2 and 4 in these cases.

The waveforms and spectra for a fundamental amplitude of V_1 =0.5 p.u. for the solutions 1-4 are shown in Fig. 5.19.

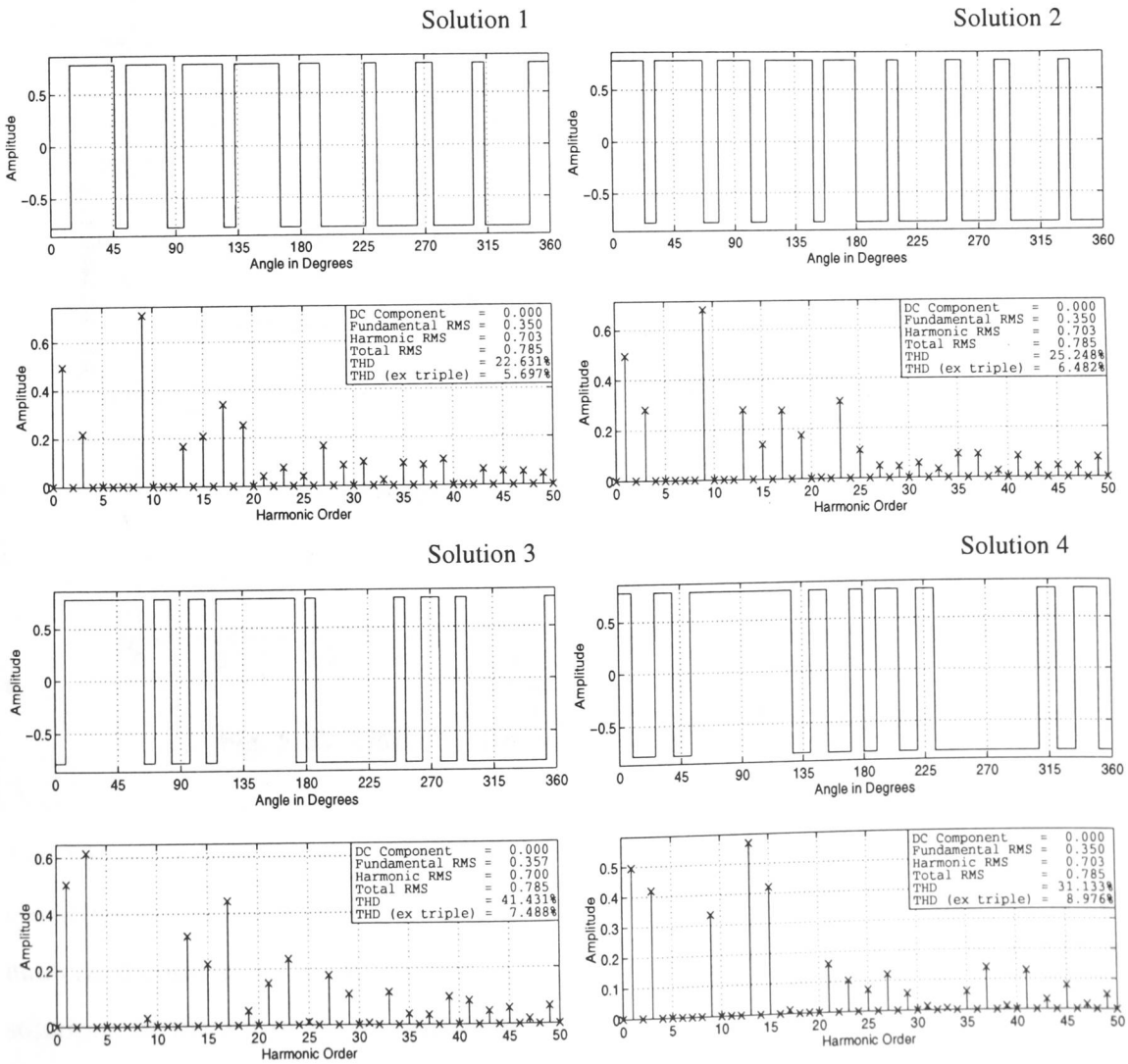

Fig. 5.19 Waveforms and Spectra for Harmonic Elimination p.w.m. (N=4)

It may be seen that the harmonics 5, 7 and 11 have cancelled in all cases. However, the THD is quite different for solutions 1-4. This is mainly due to the difference of the 13th harmonic, which is largest for solution 4, which has also the maximum THD. Solution 1 has minimum THD and also the lowest 13th harmonic. A comparison of the THD for the four solutions may be seen in Fig. 5.20. The figure shows that solutions 1 and 2 result in almost identical low THD's for fundamental output voltages between 0 to 20% of the six step voltage. Solutions 3 and 4 however, have much larger harmonic distortions, but are also improved for higher fundamental voltages. Solution 1 has the minimum THD for its entire modulation range from 0% to 80% of the six step voltage. For higher modulation indices, solution 4 has lowest THD up to 88% of the six step voltage. For the range between 88% and 92% of the six step voltage, solution 2 results in minimum THD operation.

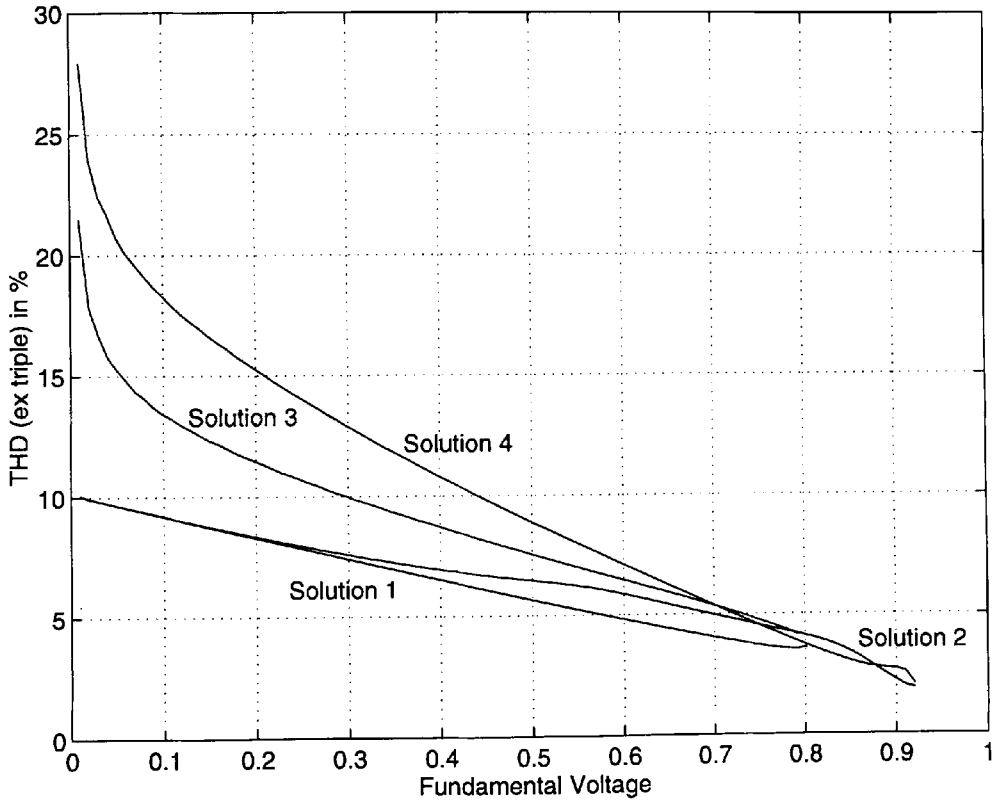

Fig. 5.20: THD of Harmonic elimination p.w.m. (N=4)

The harmonic elimination method can effectively cancel certain harmonics from the spectrum of p.w.m. waveforms. The online computation is not practical, due to the numerical complexity involved. Even the off-line computation can prove difficult if all solutions of the set of non-linear equations are to be found, in order to optimise, for example, the THD.

5.9 Minimum Total Harmonic Distortion

p.w.m. waveforms may be optimised with respect to different optimisation criteria. Normally, these techniques require extensive off-line computations. For minimum copper losses, the harmonics of the motor current may be minimised. The r.m.s value of the harmonic current is given by:

$$I_{Har} = \sqrt{\sum_{k=2}^{\infty} I_k^2} \tag{5.13}$$

Under the assumption that the harmonic current depends mainly on the magnetising inductance 'L' of the motor, the harmonic current may be expressed in terms of the applied voltage as follows:

$$I_k = \frac{V_k}{2\pi f_k L} \tag{5.14}$$

The THD can be expressed in terms of the voltage harmonics as shown below:

$$THD = \sqrt{\sum_{k=2}^{\infty} \left(\frac{V_k}{k}\right)^2} \tag{5.15}$$

The factor $2\pi f_1 L$ of Equ. 5.15 does not need to be considered for the minimisation. For N=4, simulations have been carried out and the resulting THD can be seen in Fig. 5.21.

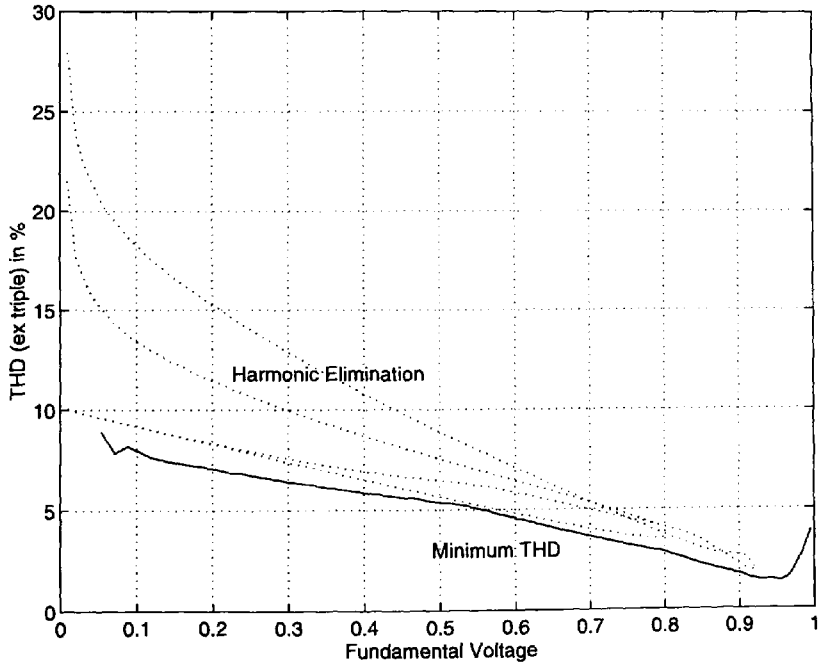

Fig. 5.21: Minimum THD Operation

The resulting THD is shown in comparison to the THD for harmonic elimination, which has been carried out for the same number of switching actions. As can be seen, the THD

is higher for the harmonic elimination technique. Optimum THD operation also provides a smooth transition to six step operation, whereas with the harmonic elimination technique the maximum fundamental achievable is 92% of the six step fundamental. In fact, it is the range between 92% and 100% where the optimum THD technique achieves the overall minimum THD. For output fundamentals around 55% of the six step voltage, the harmonic elimination technique achieves THD's very close to the optimum THD's.

The required variation of the switching angles $\alpha_1 ... \alpha_4$ for minimum THD operation with fundamental output voltage may be seen in Fig. 5.22.

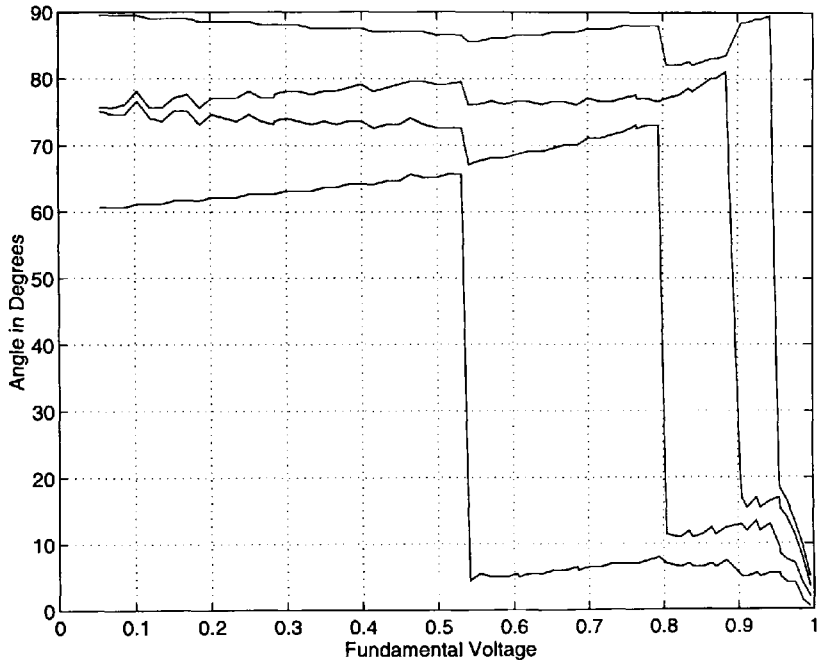

Fig. 5.22: Variation of switching angles for minimum THD operation (N=4)

It can be seen from Fig. 5.22 that discontinuous variation of the switching angles $\alpha_1 ... \alpha_4$ is required in order to achieve minimum THD operation for the full range of fundamental output voltage amplitudes. For example, for fundamental amplitudes up to 52% of the six step voltage all switching angles are between 60 and 90 degrees. Thus, switching occurs towards the centre of each half wave cycle, as shown in Fig. 5.23. However, for output voltages at 85% of the six step voltage, for example, two switching actions occur near 10 degrees and two near 80 degrees (Fig. 5.22).

An on-line implementation of the switching angle calculation does not seem practical. Instead, the switching angles need to be calculated off-line and then stored in a table for

access from a micro controller. The waveform and the harmonic spectrum for a fundamental of 50% is shown in Fig. 5.23.

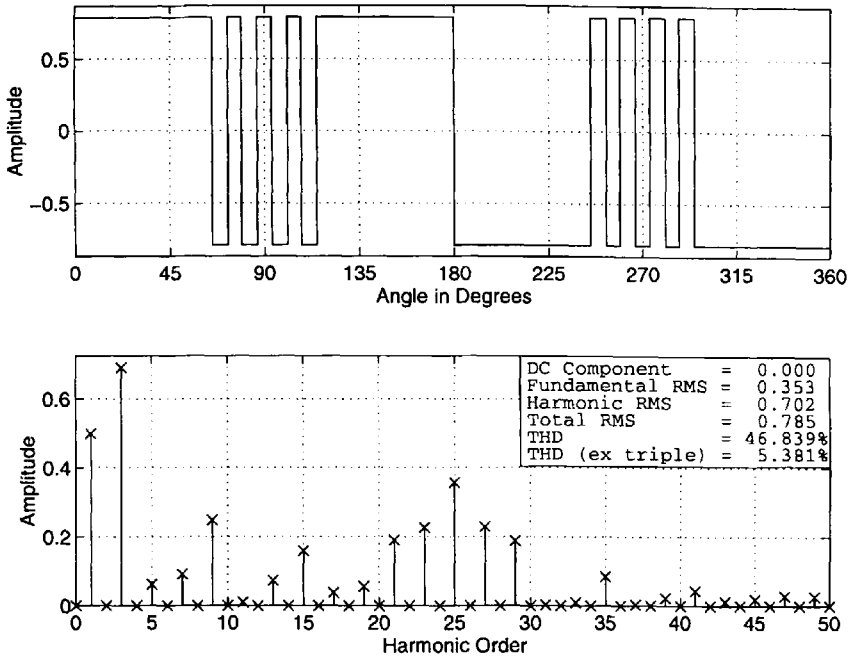

Fig. 5.23: Minimum THD operation for N=4

It can be seen from the spectrum in Fig. 5.23, that the 5th, 7th and 11th harmonics are present in the frequency spectrum. However, these harmonics and the 13th are relatively small, so that the overall THD is lower than the THD for the harmonic elimination technique where the 5th, 7th and 11th harmonics have cancelled but the 13th harmonic is considerably bigger (Fig. 5.19).

5.10 Interim Conclusion

In the previous sections, different modulation schemes have been considered. Each of these schemes has some merits and drawbacks, and the choice for a particular modulation scheme depends on a number of factors. When a resonant DC link is used, the sigma delta modulation technique can give good results at high enough switching frequencies. As is shown in chapter 6, the closed loop current modulator is a good choice for current controlled flux vector control. Closed loop current control may also be carried out in field co-ordinates, whereby a rectangular current error boundary may be used (Holtz 1994). A major portion of the unavoidable current harmonics is thereby transferred to the rotor field axis where they have no direct influence on the motor torque. Open loop voltage modulators may be used for low as well as high switching

frequency operation. By synchronisation of switching frequency and output frequency, sub-harmonics may be avoided. For the synchronised case, a comparison between six different modulation schemes is made below.

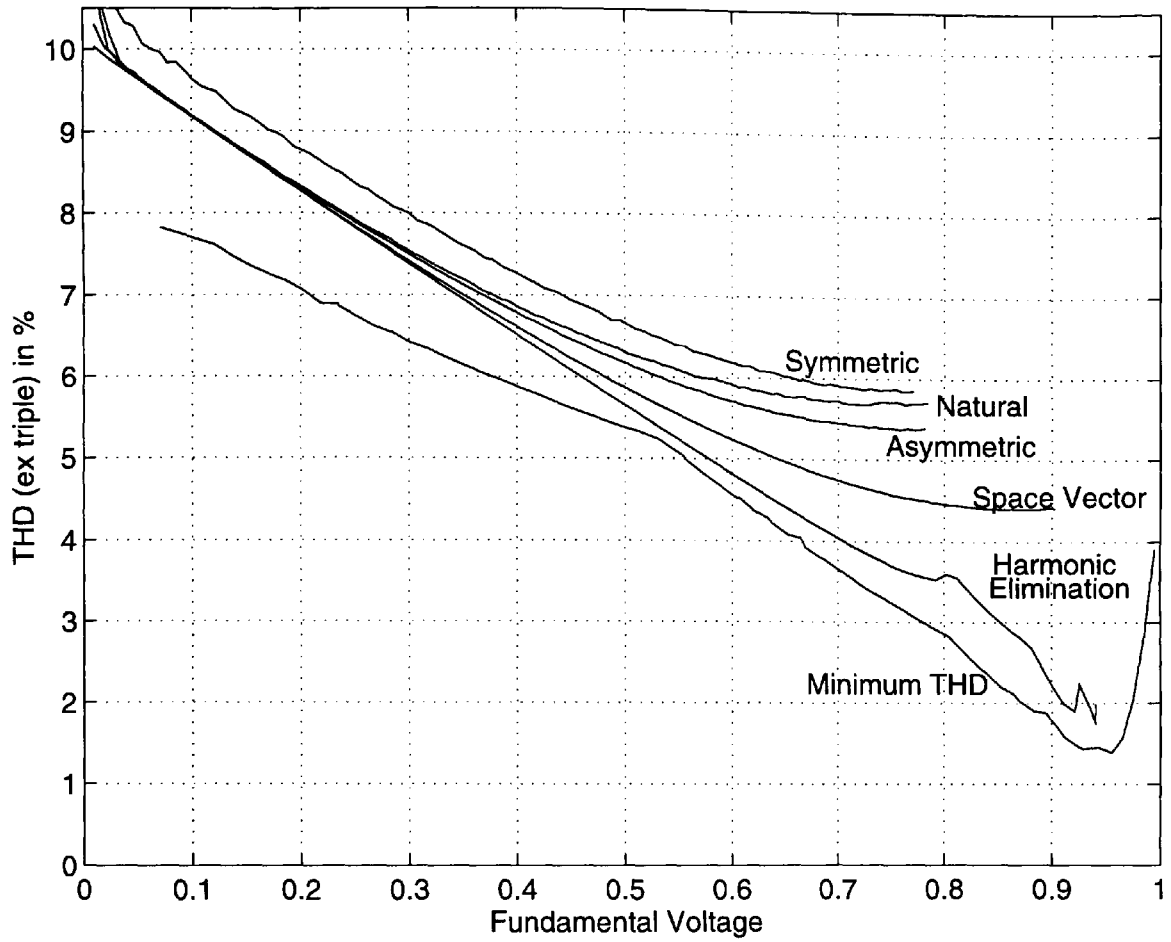

Fig. 5.24: Comparison of Synchronised p.w.m. Strategies for 18 Switching Actions (R=9, N=4)

Again, the THD distortion is used as a figure of merit. The number of switching actions per phase and cycle for all schemes is 18. Regular symmetric sampling gives the highest THD of all modulators investigated. The natural sampling, regular asymmetric sampling, space vector and the harmonic elimination technique result in the same THD for low fundamental output voltages. For higher output voltage, symmetric, natural and asymmetric sampling have a maximum modulation index of $\pi/4 = 0.785$, space vector modulation of $\pi\sqrt{3}/6 = 0.907$ and the harmonic elimination technique of 0.93. For higher output voltages, over-modulation has to be used, which is not shown in the figure. Minimum THD operation can achieve operation up to the six step mode. Similarly to the minimum THD technique, the angle variation for the harmonic elimination technique is also discontinuous because three of the four solutions have

been used for different parts of the output voltage range. For continuous variation, solution 2 may be used which has a higher THD.

In summary, when neither pre-processing nor discontinuous switching angle variation is desired, space vector modulation is the best choice of the considered modulation schemes. Solution 2 of the harmonic elimination technique may be used when the switching angles can be stored in memory for access by a micro-processor system, but continuous angle variation is required. Harmonic elimination may also be used when certain resonant frequencies of the drive are to be avoided. For a micro controller implementation with emphasis on steady state performance, the minimum THD may be used to minimise the harmonic r.m.s current of the motor.

Chapter 6: Flux Vector Control

6.0 Review of Flux Vector Control Systems

Flux vector control of squirrel cage rotor induction motors enables the independent control of motor torque and motor flux for both, steady states and transient states. Hence it is possible to achieve precise speed, torque and position control with good dynamic response.

The independent control of motor flux and torque is desirable for any type of electric motor. For separately exited d.c. motors, for example, this type of control has been carried out for a long time because of the ease of access to armature and field winding. For the squirrel cage rotor induction motor, however, the separation of motor flux and motor torque is more difficult because both are dependent on amplitude and frequency of the three phase voltage system applied to the stator windings of the induction motor.

However, in 1969, a method proposed by Blaschke allowed the stator current space vector to be expressed in terms of a flux producing component and a torque producing component. This was achieved by using a co-ordinate system for the stator current components which rotates with the applied frequency of the three phase system and is aligned with the motor flux space vector. Much of the pioneering work into this new method was also carried out by Leonhard.

With the advances made in micro electronics, digital implementations of flux vector control have been available on the a.c. electric variable speed drives market for a number of years. Flux vector control is normally classified into so-called 'true flux vector control' and 'sensor-less flux vector control'.

The 'true flux vector control systems' require a shaft encoder for feedback of the rotor position. Shaft encoders are generally quite expensive and mounting them to the shaft of an induction motor increases the maintenance requirements of the installation. However, because of the very accurate motor position feedback, a high control accuracy and a fast dynamic response to load variations and set point variations can be achieved. Flux vector control with shaft encoder is normally used in applications such as paper production where high accuracy speed control, torque control, synchronisation control and position control may be required.

With sensor-less flux vector control systems, a dynamic response inferior to vector control systems with sensor, but superior to V/f control systems can be achieved. These

systems give the benefits of vector control without the inconvenience of fitting an encoder to the motor shaft. Sensor-less flux vector control can also be used for simple applications such as fan and pump control where good dynamic response is normally not required. However, it is possible to automatically optimise the motor flux level so that energy savings can be achieved. These savings are of course in addition to the savings of having a variable speed drive fitted in the first place.

Flux vector control methods may also be divided into direct and indirect flux vector control systems. In both cases, the stator current space vector is co-ordinate transformed and fed to a modulator, which produces signals for the inverter bridge. For low inverter switching frequencies, voltage modulators are more suited than current modulators. For such systems, the current reference signal has to be converted to a voltage reference signal by using the stator voltage equation from the motor model.

The motor flux control may be carried out with respect to stator flux, magnetising flux or rotor flux, which combined with: direct vector control, indirect vector control, voltage modulation and current modulation results in twelve basic vector control configurations. Further variation is introduced by using sensor-less, measured speed or measured position control configuration.

6.1 Indirect Flux Vector Control

The indirect flux vector control method uses motor flux and motor torque reference signals which are converted directly into their respective stator current components. There is no feedback of motor flux or motor torque. A co-ordinate transformation is carried out using an angle of the motor flux space vector which depends on reference quantities only. The system is open loop with respect to the motor flux and the motor torque. As mentioned above, the stator current is resolved into a flux producing and into a torque producing component. This is achieved by using a co-ordinate transform. The motor model equations are shown in Equ. 6.1.

$$\begin{aligned}
\vec{v}_s &= r_s\vec{i}_s + T_N s\vec{\psi}_s + j(\omega_m + \omega_r)\vec{\psi}_s \\
0 &= r_r\vec{i}_r + T_N s\vec{\psi}_r + j\omega_r\vec{\psi}_r \\
\vec{\psi}_s &= x_s\vec{i}_s + x_M\vec{i}_r \\
\vec{\psi}_r &= x_r\vec{i}_r + x_M\vec{i}_s \\
s\omega_m &= \frac{1}{T_M}\left(\Im\left(\frac{x_M}{x_r}\vec{\psi}_r^{*}\vec{i}_s\right) - T_l\right)
\end{aligned} \tag{6.1}$$

The model equations (Equ. 6.1) may be expressed in terms of co-ordinates rotating with either the rotor flux vector, the magnetising flux vector or the stator flux vector as shown in the following sections.

6.1.1 Rotor Flux Orientation

When the co-ordinate system is aligned with the x-component of the rotor flux vector, the y-component of the rotor flux vector becomes zero. The real and imaginary components for the other vector quantities may be substituted into the model equations (6.1) using the expressions shown below.

$$\begin{aligned} \vec{v}_s &= v_{sx} + jv_{sy} & \vec{i}_r &= i_{rx} + ji_{ry} \\ \vec{i}_s &= i_{sx} + ji_{sy} & \vec{\psi}_r &= \psi_{rx} \\ \vec{\psi}_s &= \psi_{sx} + j\psi_{sy} \end{aligned} \tag{6.2}$$

On substitution of equations 6.2 into 6.1, the motor model may be expressed in terms of vector components in field co-ordinates as follows.

$$\begin{aligned} v_{sx} &= r_s i_{sx} + T_N s\psi_{sx} & \psi_{sx} &= x_s i_{sx} + x_M i_{rx} \\ v_{sy} &= r_s i_{sy} + (\omega_m + \omega_r)\psi_{sx} & \psi_{sy} &= x_s i_{sy} + x_M i_{ry} \\ 0 &= r_r i_{rx} + T_N s\psi_{rx} & \psi_{rx} &= x_r i_{rx} + x_M i_{sx} \\ 0 &= r_r i_{ry} + \omega_r \psi_{rx} & 0 &= x_r i_{ry} + x_M i_{sy} \\ s\omega_m &= \frac{1}{T_M}\left(\frac{x_M}{x_r}\psi_{rx} i_{sy} - T_l\right) \end{aligned} \tag{6.3}$$

Hence, the stator current components may be expressed as follows:

$$i_{sx} = \frac{\psi_{rx}}{x_M}\left(1 + s\frac{T_N x_r}{r_r}\right) \qquad i_{sy} = \frac{Tx_r}{\psi_{rx} x_M} \tag{6.4}$$

It may be seen that the x-component of the stator current depends on rotor flux level and motor parameters only. With constant rotor flux, the motor torque may be regulated with the y-component of the stator current. However, for this to work, the stator current components need to be transformed to a co-ordinate system which is fixed to the stator axis. Thus, the angle between rotor flux vector and the fixed stator axis is required. This angle can be calculated from rotor position and slip angle as follows:

$$\gamma_s = \gamma_m + \frac{Tr_r}{sT_N\psi_{rx}^2} \tag{6.5}$$

It can be seen from Equ. 6.5 that the slip angle depends on torque, flux and the rotor resistance. Hence, modelling errors of rotor resistance affect the accuracy of the decoupling of flux and torque, especially because of the integration where errors are accumulated.

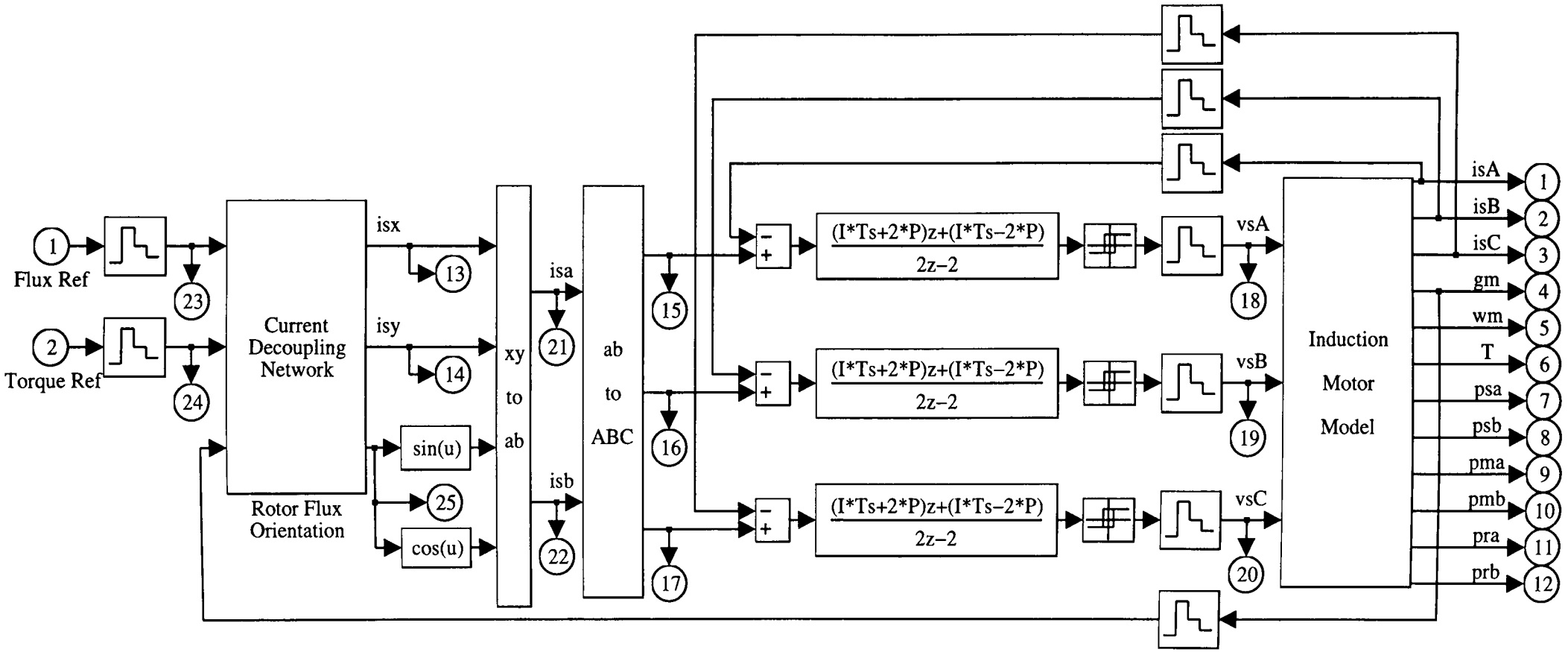

Fig. 6.1: Current Controlled, Indirect Flux Vector Control

A simple configuration of an indirect flux vector control system is shown in Fig. 6.1. The input signals of the simulation model in Fig. 6.1 are the reference rotor flux level and the reference motor torque. Thus, the system represents torque control. A speed control loop may be added to the system using speed feedback or a speed estimator. The inputs of the current decoupling network are the sampled rotor flux level and motor torque reference values and the measured rotor position (angle 'gm' = γ_m). The current decoupling network implements equations 6.4 and 6.5 and may be represented in Simulink form as shown in Fig. 6.2.

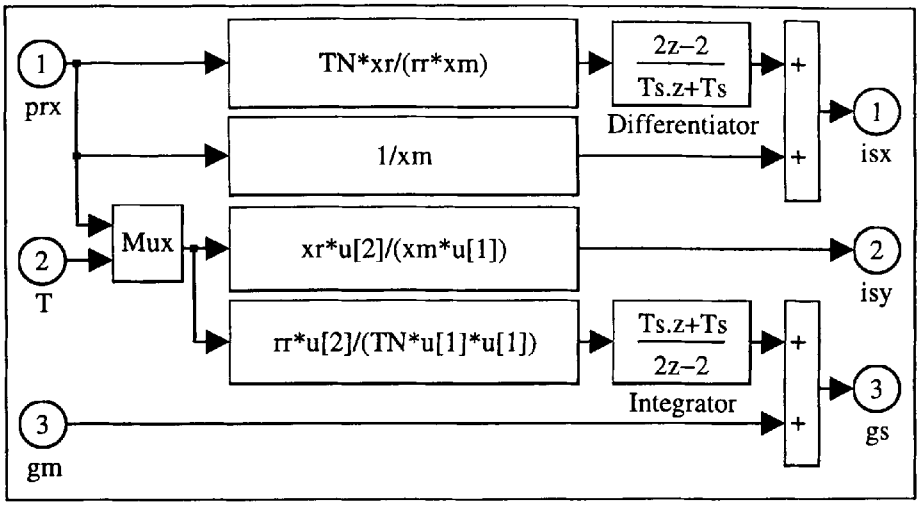

Fig. 6.2: Current Decoupling Network for Rotor Flux Orientation

The outputs of the simulation model of Fig. 6.2 are the reference 'x'-component of the stator current the reference y-component of the stator current and the angle of the stator current vector for transformation from field co-ordinates to stator oriented co-ordinates. This transformation can be carried out using the sine and cosine signals of the stator current angle as shown in Fig. 6.3.

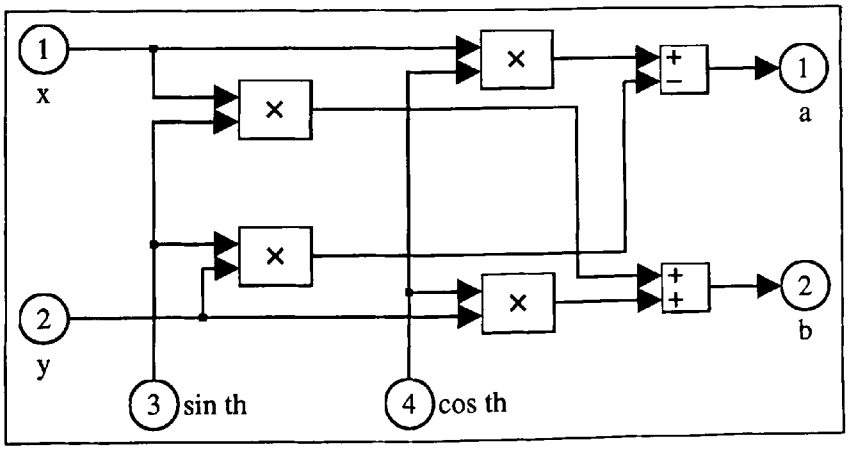

Fig. 6.3: Co-ordinate Transformation of the Reference Stator Current Vector

The calculations correspond to Equ. 2.70 in chapter 2. The outputs of the simulation model shown in Fig. 6.3 are the real and imaginary components of the reference stator current space vector in stator oriented co-ordinates. As shown in Fig. 6.1, these components are transformed to the three phase system using the simulation model shown in Fig. 6.4.

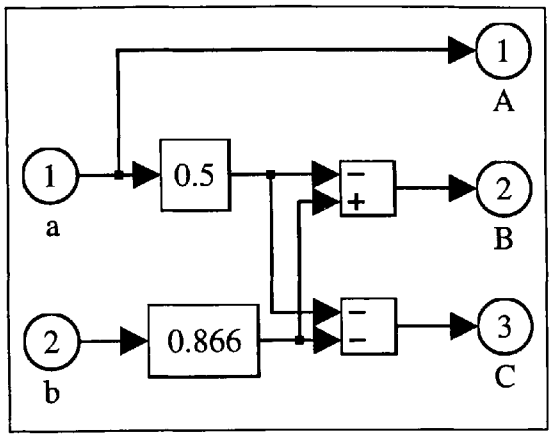

Fig. 6.4: Two Axis to Three Axis Transformation

The calculations correspond to Equ. 2.50 in chapter 2. The outputs of the simulation model shown in Fig. 6.4 are the three reference phase currents which are fed into the current modulator as shown in Fig. 6.1. The reference currents are compared to the measured motor currents and the error current signals are fed into a PI controller. The PI controller prevents any long term drifts of the error current signal. The output of the PI controller is fed to a relay simulation block, thereby introducing hysteresis to the modulator. The 'P' and 'I' components have been optimised to give the least variation of the error current signal and the least long term drift. The outputs of the current modulator shown in Fig. 6.1 are the p.w.m. input voltage waveforms which are fed to the induction motor model. A Simulink model of a three phase cage rotor induction motor is shown in Fig. 6.5.

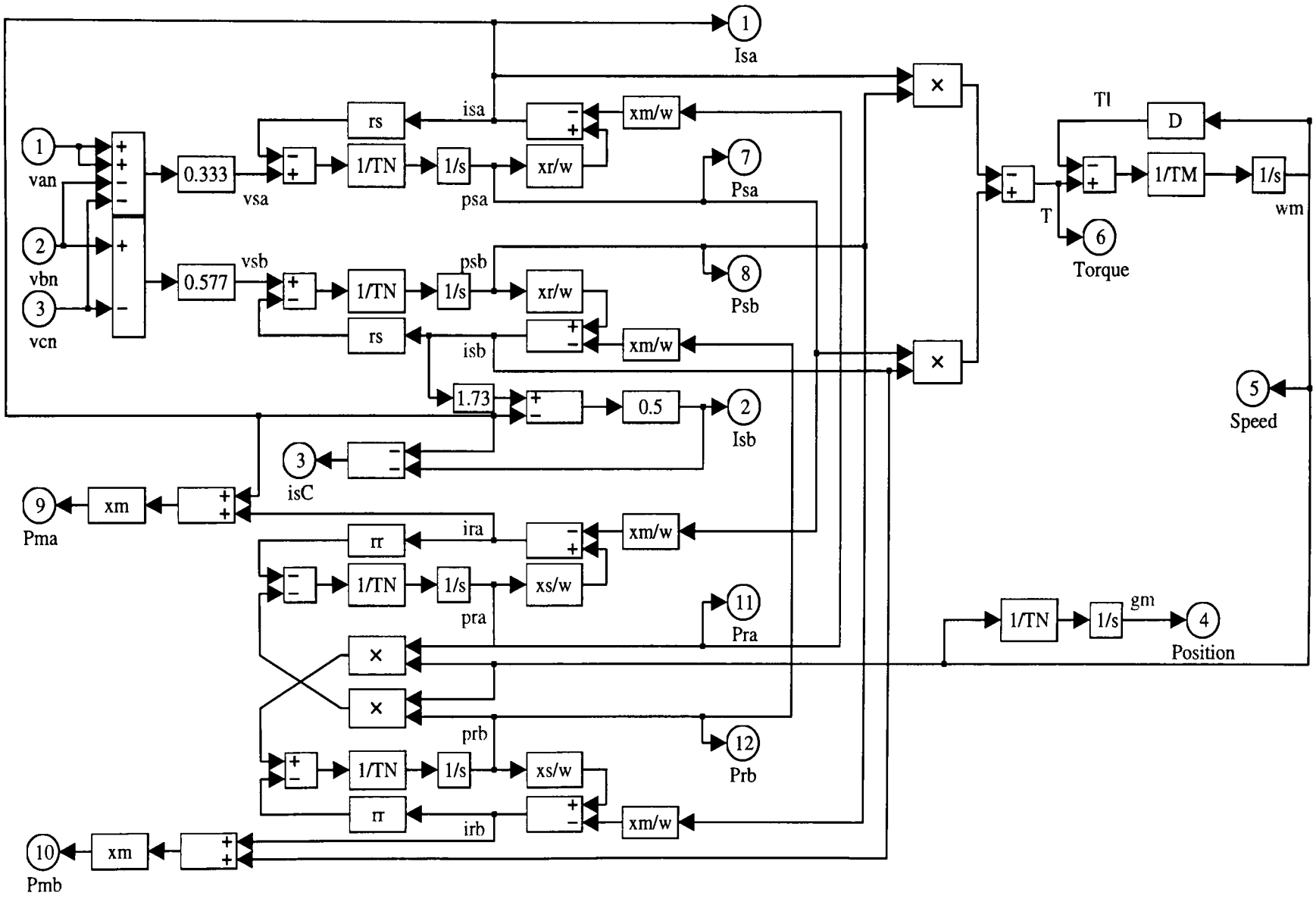

Fig. 6.5: Induction Motor Model

The outputs of the induction motor simulation model are the three phase currents, the rotor angle, the rotor speed, the motor torque, and the real and imaginary components of the stator flux vector, the magnetising flux vector and the rotor flux vector in stator oriented co-ordinates. The Simulink simulation model shown in Fig. 6.5 corresponds to Equ. 2.76 in chapter 2.

Simulation results of the system described above are shown in Fig. 6.6 to Fig. 6.9. In Fig. 6.6 the rotor flux level and the developed motor torque are shown. As the rotor flux angle calculation relies on reference quantities of flux and torque, it is vital that these reference quantities correspond to the actual rotor flux and motor torque. Otherwise decoupling is lost. Hence, the rotor flux reference value has been varied slowly and smoothly, for the actual rotor flux to follow accordingly. Similarly, for the motor torque reference signal, only gradual changes, though with a much shorter time constant, are allowed so that reference torque and actual torque always correspond. In case PI-controller are used to generate the motor flux and the motor torque reference signals, slowly varying values may be achieved by means of a rate limiter.

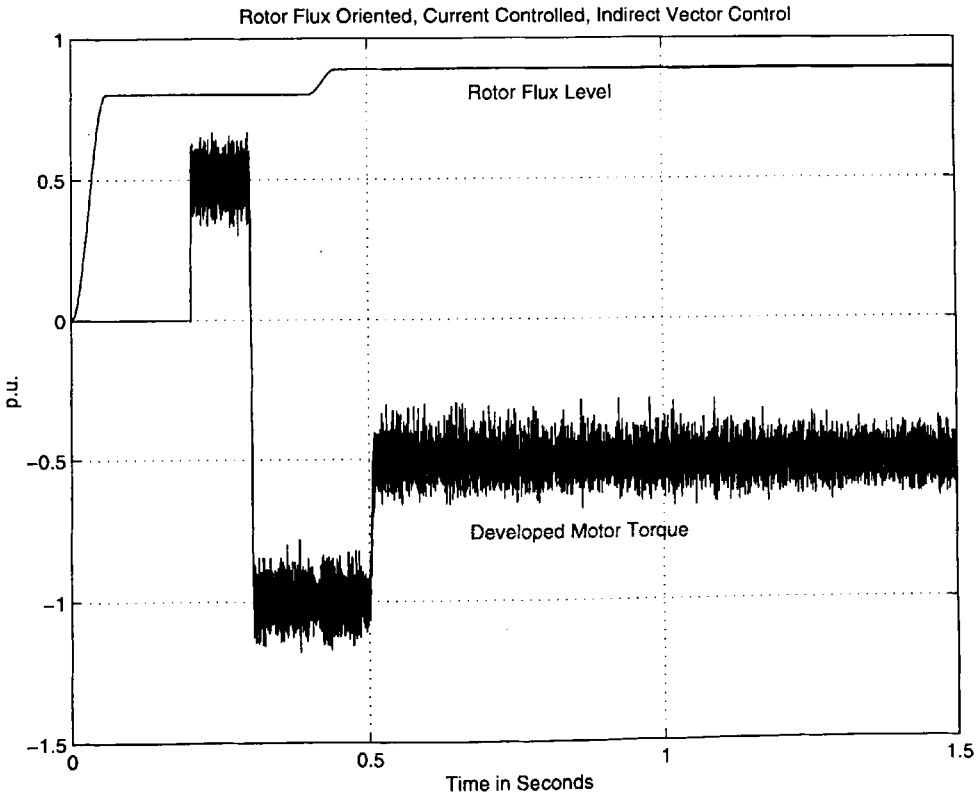

Fig. 6.6: Rotor Flux Level and Motor Torque in
Rotor Flux Oriented, Current Controlled, Indirect Vector Control

It can be seen from Fig. 6.6 that the rotor flux level does not vary when the developed motor torque changes, and the torque does not vary when the rotor flux level changes. Thus the two variables are decoupled from each other. The large torque variations are due to the relatively large sampling time ($T_s = 150\mu s$) chosen for the current modulator in Fig. 6.1. In most commercial inverters, however, the current modulator and the vector control algorithm run at different sampling rates. Typically, the vector control algorithm would be evaluated every $100\mu s$, whereas the modulator could operate at switching frequencies between 2kHz and 14kHz. The actual switching instances are thereby not necessarily synchronised.

In Fig. 6.7 the variation of the stator current, expressed in field co-ordinates, is shown. It can be seen that the initial rise of the rotor flux level requires a peak current of 150% of the rated motor current. Because the reference signals of rotor flux level and motor torque have been varied as 's'-shapes, the current variations in field co-ordinates are smooth. It may also be seen that during rotor flux level variations, the y-component of the stator current must vary so that the developed motor torque is not affected. This can also be seen from Equ. 6.4b.

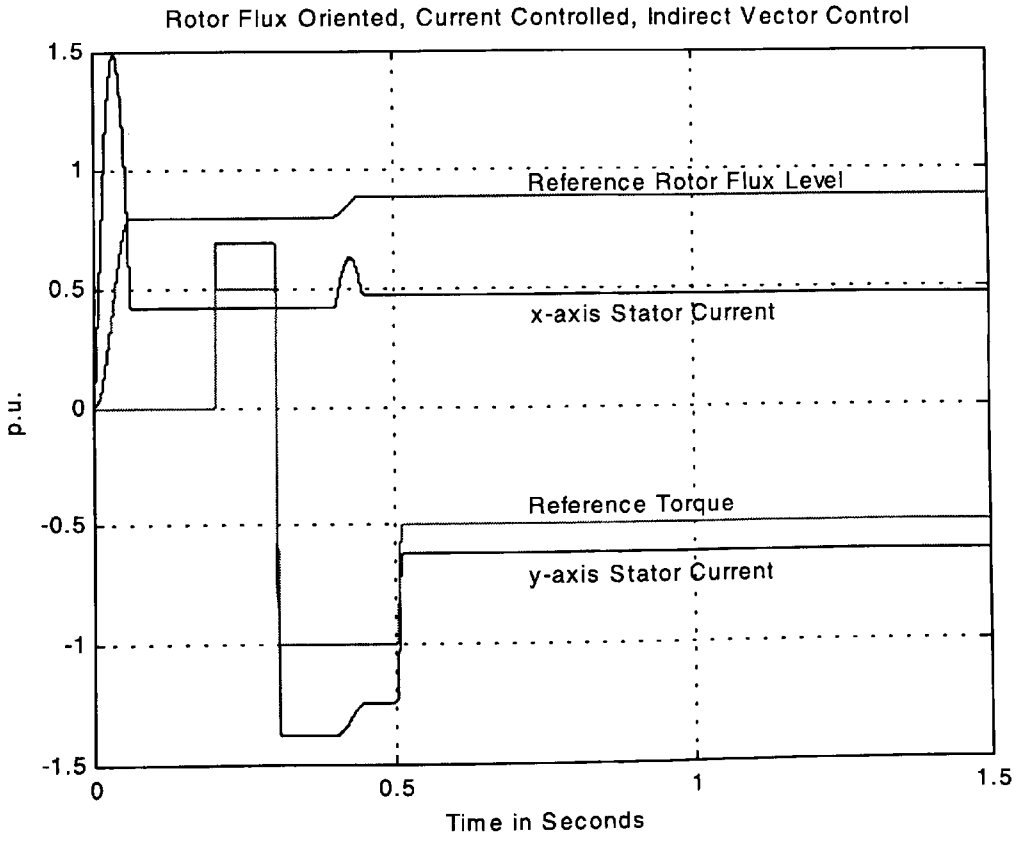

Fig. 6.7: Stator Current Variations in Field Co-ordinates in Rotor Flux Oriented, Current Controlled, Indirect Vector Control

Transformation of the stator current components expressed in field co-ordinates into stator fixed co-ordinates results in the variation of the stator current components as shown in Fig. 6.8. It can be seen that amplitude, frequency and phase variation of the stator current is required to obtain rotor flux level and motor torque variations which follow their respective reference quantities as shown in Fig. 6.6 and Fig. 6.7.

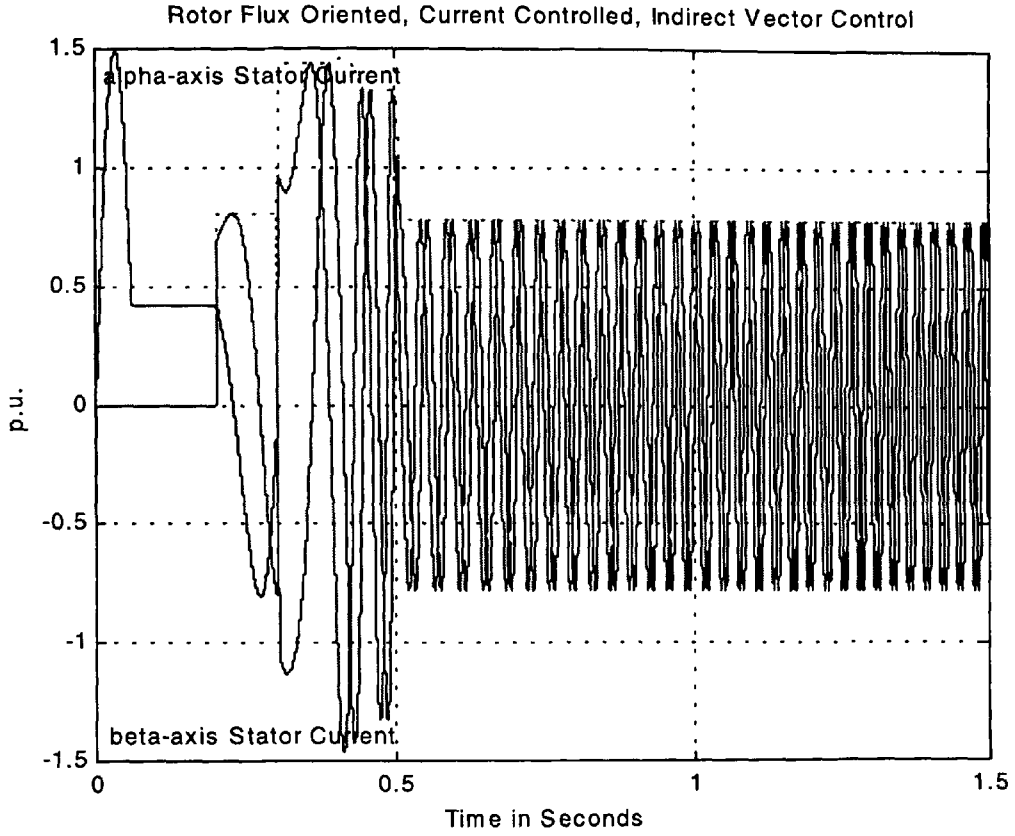

Fig. 6.8: Stator Current Variations in Stator Fixed Co-ordinates in Rotor Flux Oriented, Current Controlled, Indirect Vector Control

Transformation from the two-axis system to the three-axis system results in the time variation of the reference motor phase currents as shown in Fig. 6.9.

Clearly, the amplitude, frequency and phase variation of the three motor phase currents would be very difficult to generate with scalar control methods. Because of the co-ordinate transform used by vector control, precise control of motor flux and motor torque can be achieved, as shown in Fig. 6.6.

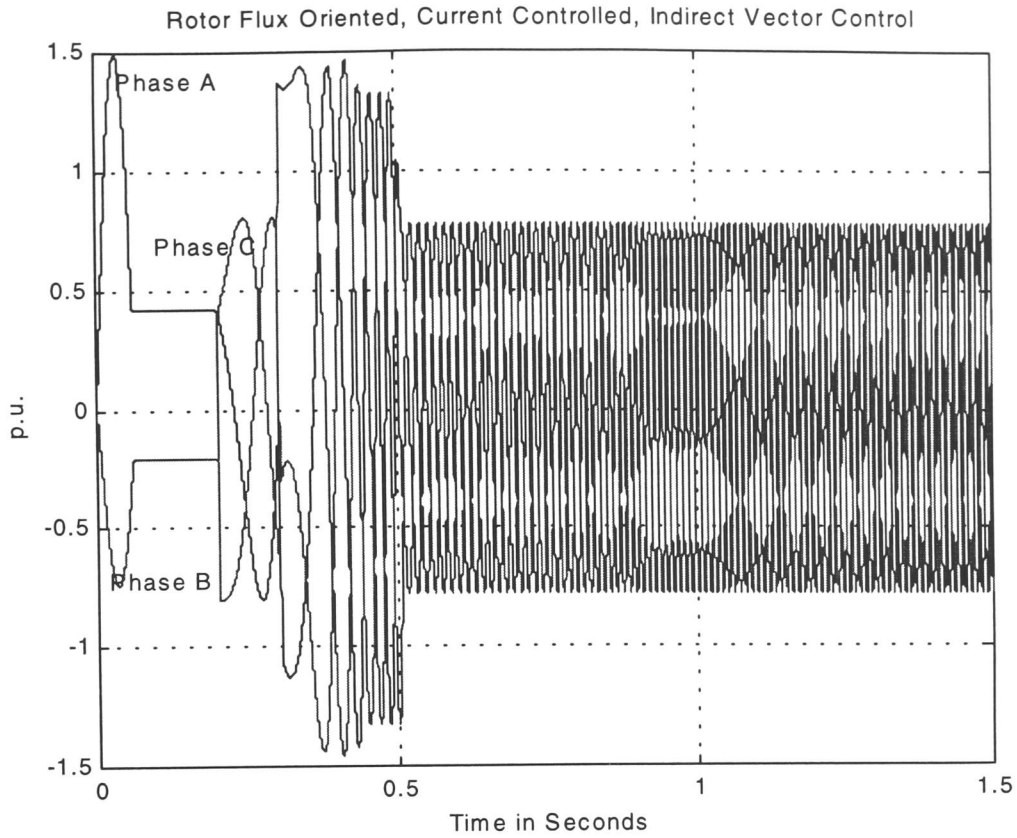

Fig. 6.9: Reference Stator Current Variations of Phases A, B and C in Rotor Flux Oriented, Current Controlled, Indirect Vector Control

Fig. 6.10 shows the time variation of the stator flux level, the magnetising flux level and the rotor flux level. Because the rotor flux level is controlled, the stator flux level and the magnetising flux level are not decoupled from variations of motor torque. Thus, as can be seen from Fig. 6.10, the magnetising and stator flux change when the motor torque changes. Furthermore, there is also a considerable overshoot of the magnetising and stator flux level for fast changes of the rotor flux level. Overshoot beyond unity causes saturation of the stator and magnetising flux and the simulation results for flux levels > 1.0 p.u. are invalid as saturation effects are not included in the motor model. Saturation may be avoided by controlling the stator flux level instead of the rotor flux level.

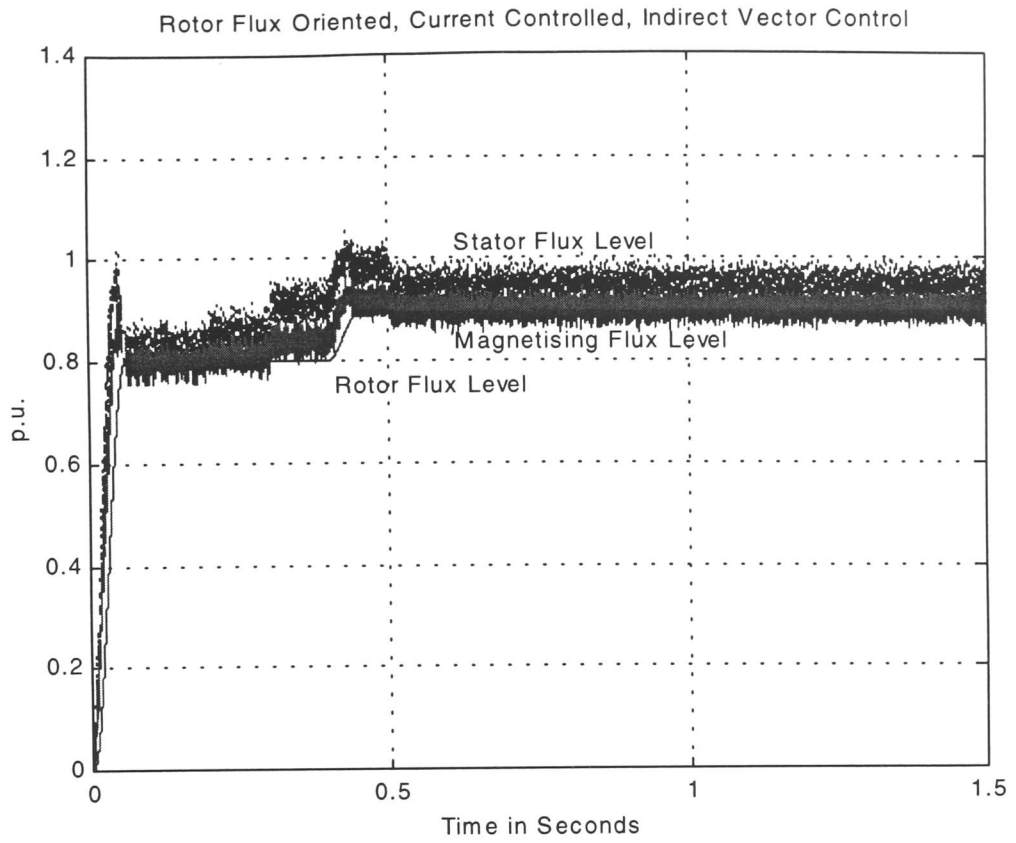

Fig. 6.10: Stator, Magnetising and Rotor Flux Level in
Rotor Flux Oriented, Current Controlled, Indirect Vector Control

The advantage of rotor flux orientation is that the current decoupling network is very simple. However, a disadvantage is that the stator flux level and the magnetising flux level may saturate when the rotor flux level or the motor torque varies.

6.1.2 Stator Flux Orientation

When the co-ordinate system for the description of the stator current components is aligned with the instantaneous stator flux space vector, the stator flux level may be controlled. Similarly to the derivation of the current decouling equations for rotor flux orientation, the equations for stator flux orientation may be derived as follows:

The complex space vector quantities of Equ. 6.1 may be substituted by their real and imaginary parts. As the co-ordinate system is aligned with the stator flux vector, the imaginary component of the stator flux space vector becomes zero. This is shown in the following expressions:

$$\begin{aligned} \vec{v}_s &= v_{sx} + jv_{sy} & \vec{i}_r &= i_{rx} + ji_{ry} \\ \vec{i}_s &= i_{sx} + ji_{sy} & \vec{\psi}_r &= \psi_{rx} + j\psi_{ty} \\ \vec{\psi}_s &= \psi_{sx} \end{aligned} \qquad (6.6)$$

On substitution of Equ. 6.6 into Equ. 6.1 the following set of expressions are obtained:

$$\begin{aligned} v_{sx} &= r_s i_{sx} + T_N s\psi_{sx} & \psi_{sx} &= x_s i_{sx} + x_M i_{rx} \\ v_{sy} &= r_s i_{sy} + (\omega_m + \omega_r)\psi_{sx} & 0 &= x_s i_{sy} + x_M i_{ry} \\ 0 &= r_r i_{rx} + T_N s\psi_{rx} - \psi_{ry}\omega_r & \psi_{rx} &= x_r i_{rx} + x_M i_{sx} \\ 0 &= r_r i_{ry} + \omega_r \psi_{rx} + T_N s\psi_{ry} & \psi_{ry} &= x_r i_{ry} + x_M i_{sy} \\ s\omega_m &= \frac{1}{T_M}(\psi_{sx} i_{sy} - T_l) \end{aligned} \tag{6.7}$$

The equations for the current decoupling network may be derived from equations (6.7) as follows:

$$\begin{aligned} i_{sx} &= \frac{\psi_{sx}(r_r + sT_N x_r) + i_{sy}\omega_r(x_s x_r - x_m^2)}{r_r x_s + sT_N(x_s x_r - x_m^2)} \\ i_{sy} &= \frac{T}{\psi_{sx}} \\ \omega_r &= \frac{i_{sy}(r_r x_s + sT_N(x_s x_r - x_m^2))}{\psi_{sx} x_r - i_{sx}(x_s x_r - x_m^2)} \end{aligned} \tag{6.8}$$

The equations may be represented in a Simulink model as shown in Fig. 6.11. As can be seen by comparison with the decoupling network for rotor flux orientation (Fig. 6.2), the decoupling network for stator flux orientation is considerably more complex. The equations (6.8) have been converted to discrete time using the following approximation for the Laplace variable 's':

$$s = \frac{2(z-1)}{T_s(z+1)} \tag{6.9}$$

In equation 6.9, 'T_s' represents the sampling time and 'z' the discrete time operator.

Simulation results for stator flux orientation are shown in Fig. 6.12 to Fig. 6.15.

It can be seen from Fig. 6.12 that the stator flux level and the developed motor torque are decoupled from each other. The stator flux level exhibits much higher ripples around its reference value because of the much shorter time constant, when compared to the rotor flux level (Fig. 6.6).

Fig. 6.13 shows the variation over time of the stator current components in field co-ordinates for the desired stator flux and motor torque variations. The waveform of the x-axis stator current component is considerably more complex than its counterpart for rotor flux oriented vector control. This can also be seen from the increased complexity of the decoupling equations (6.8).

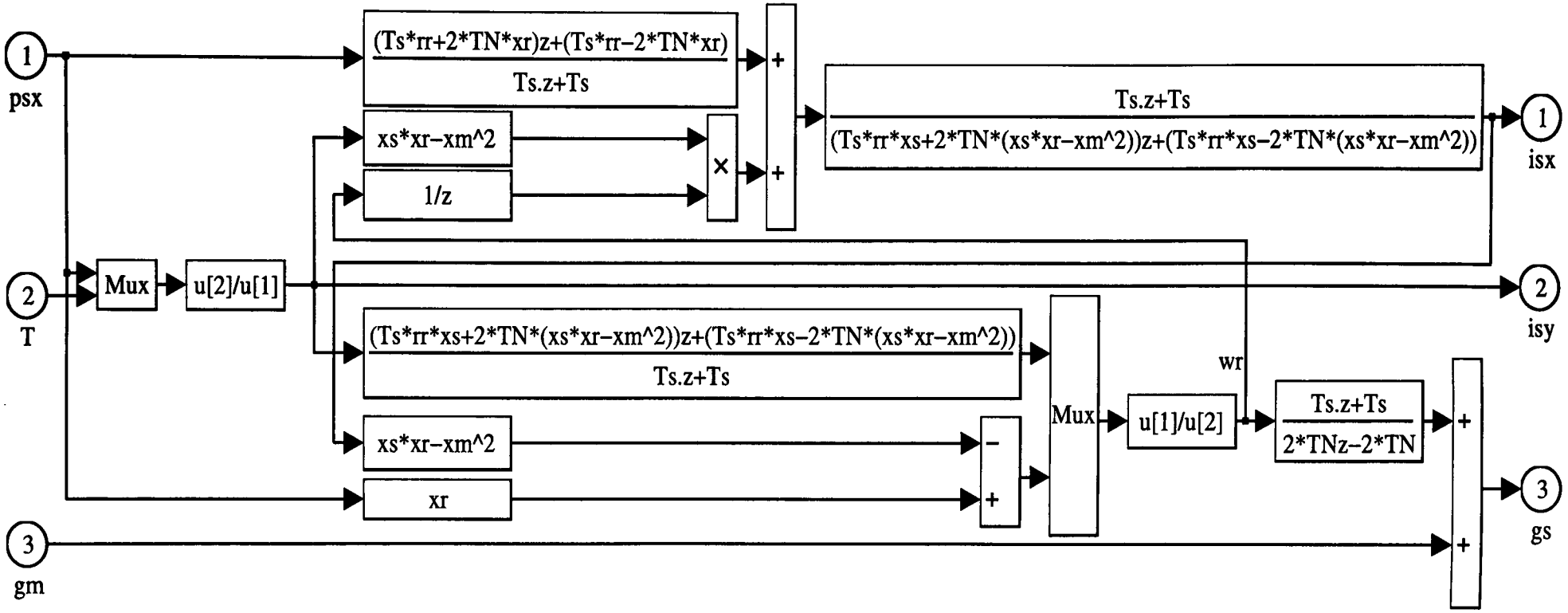

Fig. 6.11: Current Decoupling Network for Stator Flux Orientation

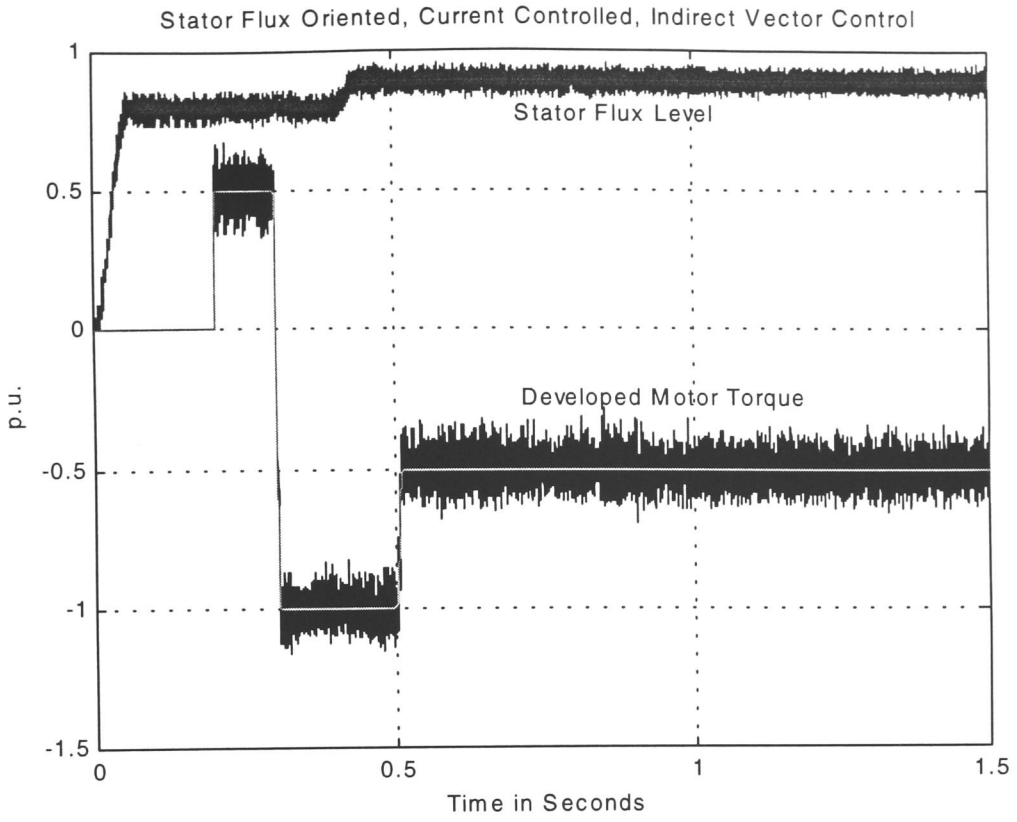

Fig. 6.12: Stator Flux Level and Motor Torque in
Stator Flux Oriented, Current Controlled, Indirect Vector Control

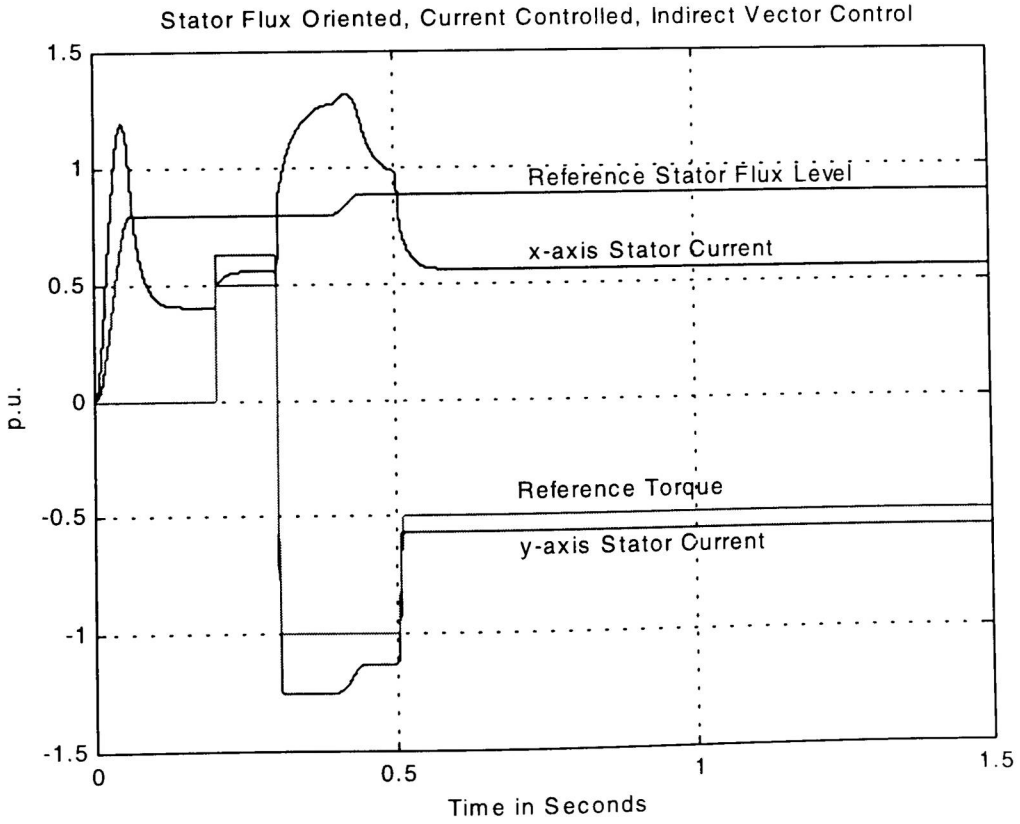

Fig. 6.13: Stator Current Variations in Field Co-ordinates in
Stator Flux Oriented, Current Controlled, Indirect Vector Control

Transformation of the stator current components, using the integrated slip frequency calculated in Equ. 6.8c, yields the variation in time of the α and β stator current components shown in Fig. 6.14. The more complex amplitude variation when compared to rotor flux orientation (Fig. 6.8) can clearly be seen.

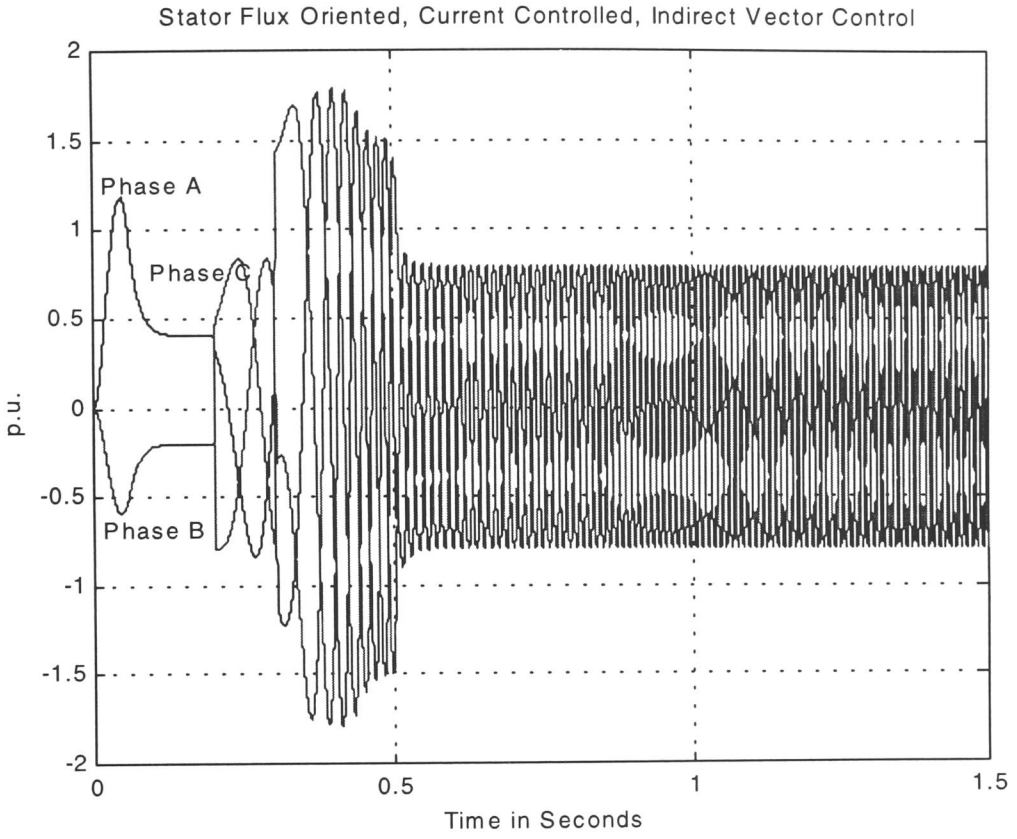

Fig. 6.14: Stator Current Variations in Stator Fixed Co-ordinates in Stator Flux Oriented, Current Controlled, Indirect Vector Control

Fig. 6.15 shows the variation with time of the stator flux level, the magnetising flux level and the rotor flux level during stator flux level control. It is evident from Fig. 6.15 that the rotor flux level varies considerably during both transients of the stator flux level and torque transients.

Due to stator flux control, an overshoot of the stator flux level as with rotor flux control (Fig. 6.10) is avoided.

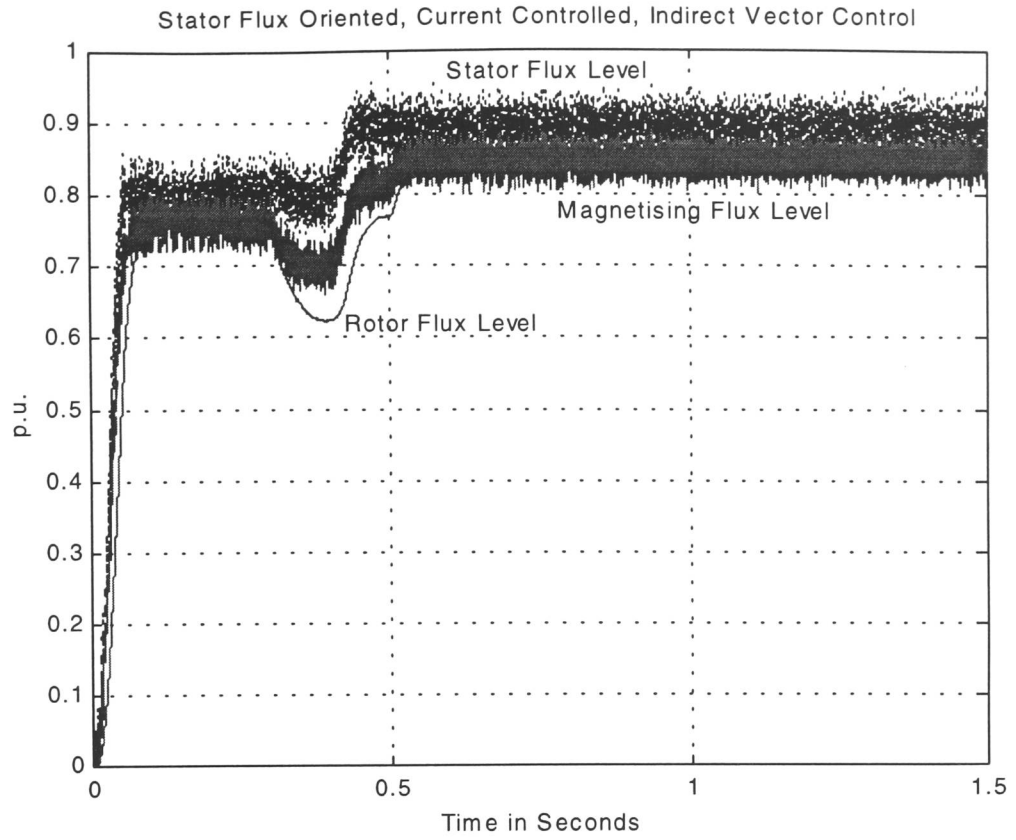

Fig. 6.15: Stator, Magnetising and Rotor Flux Level in
Stator Flux Oriented, Current Controlled, Indirect Vector Control

6.1.3 Magnetising Flux Orientation

When the co-ordinate system for the description of the stator current components is aligned with the instantaneous magnetising flux space vector, the magnetising flux level may be controlled. Similarly to the derivation of the current decouling equations for rotor flux orientation, the equations for magnetising flux orientation may be derived as follows.

The complex space vector quantities of Equ. 6.1 may be substituted by their real and imaginary parts. As the co-ordinate system is aligned with the magnetising flux vector, the imaginary component of the magnetising flux space vector becomes zero. This is shown in the following expressions:

$$\begin{aligned} \vec{v}_s &= v_{sx} + jv_{sy} & \vec{i}_r &= i_{rx} + ji_{ry} \\ \vec{i}_s &= i_{sx} + ji_{sy} & \vec{\psi}_r &= \psi_{rx} + j\psi_{ry} \\ \vec{\psi}_s &= \psi_{sx} + j\psi_{sy} & \vec{\psi}_m &= \psi_{mx} \end{aligned} \tag{6.10}$$

On substitution of Equ. 6.10 into Equ. 6.1 follows the following set of expressions:

$$
\begin{aligned}
v_{sx} &= r_s i_{sx} + T_N s\psi_{sx} & \psi_{sx} &= x_s i_{sx} + x_M i_{rx} \\
v_{sy} &= r_s i_{sy} + (\omega_m + \omega_r)\psi_{sx} & \psi_{sy} &= x_s i_{sy} + x_M i_{ry} \\
0 &= r_r i_{rx} + T_N s\psi_{rx} - \psi_{ry}\omega_r & \psi_{rx} &= x_r i_{rx} + x_M i_{sx} \\
0 &= r_r i_{ry} + \omega_r \psi_{rx} + T_N s\psi_{ry} & \psi_{ry} &= x_r i_{ry} + x_M i_{sy} \\
s\omega_m &= \frac{1}{T_M}\left(\psi_{mx} i_{sy} - T_l\right) & \psi_{mx} &= x_m(i_{sx} + i_{rx}) \\
& & 0 &= x_m(i_{sy} + i_{ry})
\end{aligned}
\qquad (6.11)
$$

The equations for the current decoupling network may be derived from Equ. 6.11 as follows:

$$
\begin{aligned}
i_{sx} &= \frac{\psi_{mx}\left(r_r + sT_N x_r\right) + i_{sy}\omega_r x_m\left(x_r - x_m\right)}{x_m\left(r_r + sT_N\left(x_r - x_m\right)\right)} \\
i_{sy} &= \frac{T}{\psi_{mx}} \\
\omega_r &= \frac{i_{sy} x_m\left(r_r + sT_N\left(x_r - x_m\right)\right)}{\psi_{mx} x_r - i_{sx} x_m\left(x_r - x_m\right)}
\end{aligned}
\qquad (6.12)
$$

The equations may be represented in a Simulink model as shown in Fig. 6.17.

The angle between the synchronously rotating magnetising flux space vector is obtained by adding the measured rotor position and the integrated slip frequency ω_r.

Alternatively, the motor speed may be measured or estimated (in case of sensor-less flux vector control) and the sum of motor speed and slip frequency integrated.

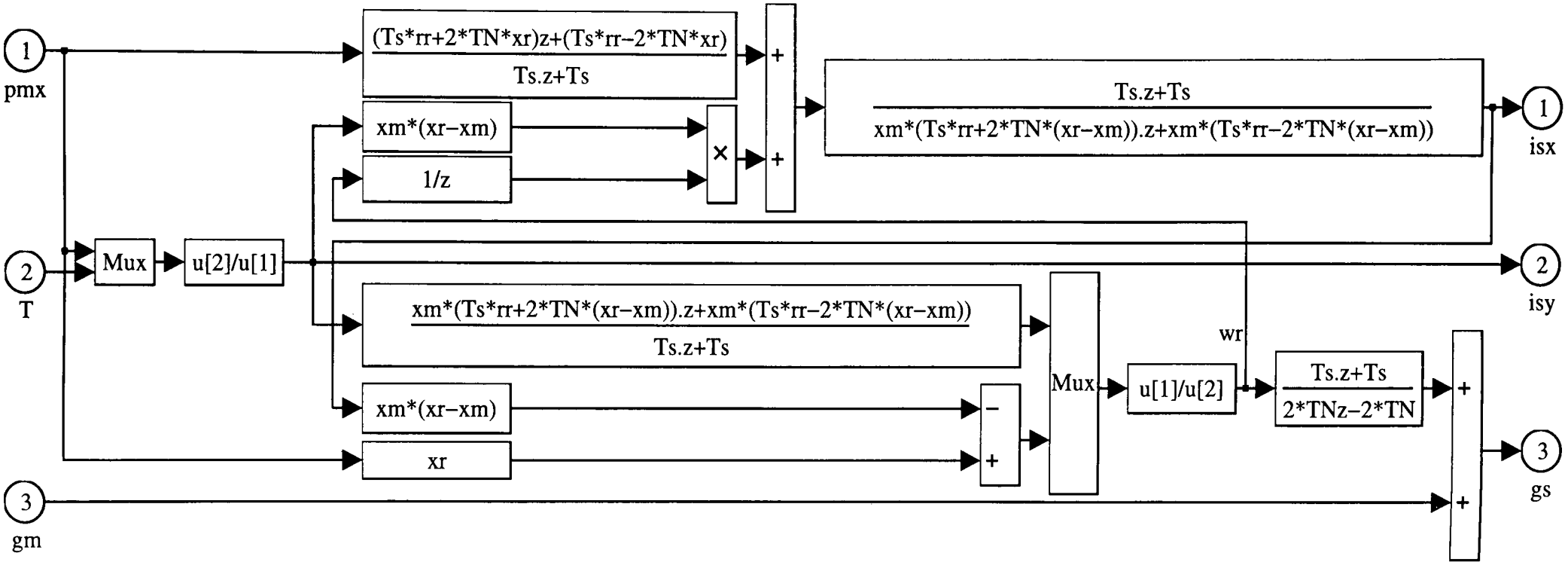

Fig. 6.16: Current Decoupling Network for Magnetising Flux Orientation

Simulation results for the case of magnetising flux control are shown in Fig. 6.17-6.20. Fig 6.17 shows the magnetising flux level and the developed motor torque. It can be seen that both are controlled accurately and without influencing each other (decoupling has been achieved).

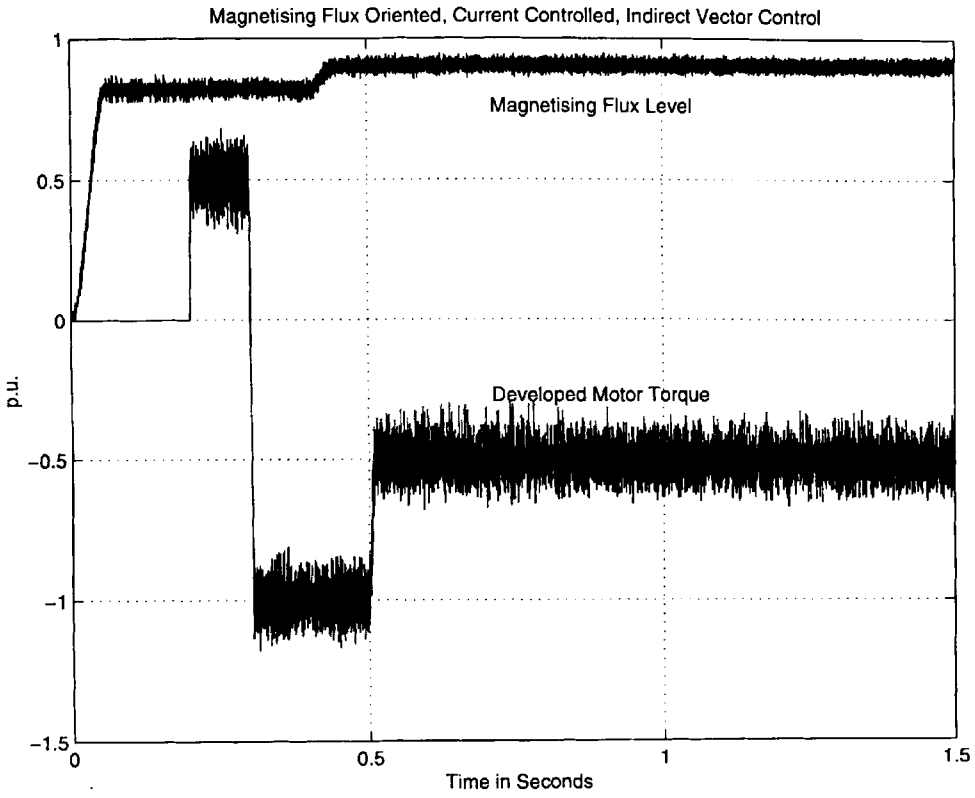

Fig. 6.17: Magnetising Flux Level and Motor Torque in Magnetising Flux Oriented, Current Controlled, Indirect Vector Control

The variation in time of the stator current components in field co-ordinates is shown in Fig. 6.18. Similarly to stator flux oriented control, complex variations of the x-axis component are necessary to achieve the desired variation of the magnetising flux level and the developed torque as shown in Fig. 6.17.

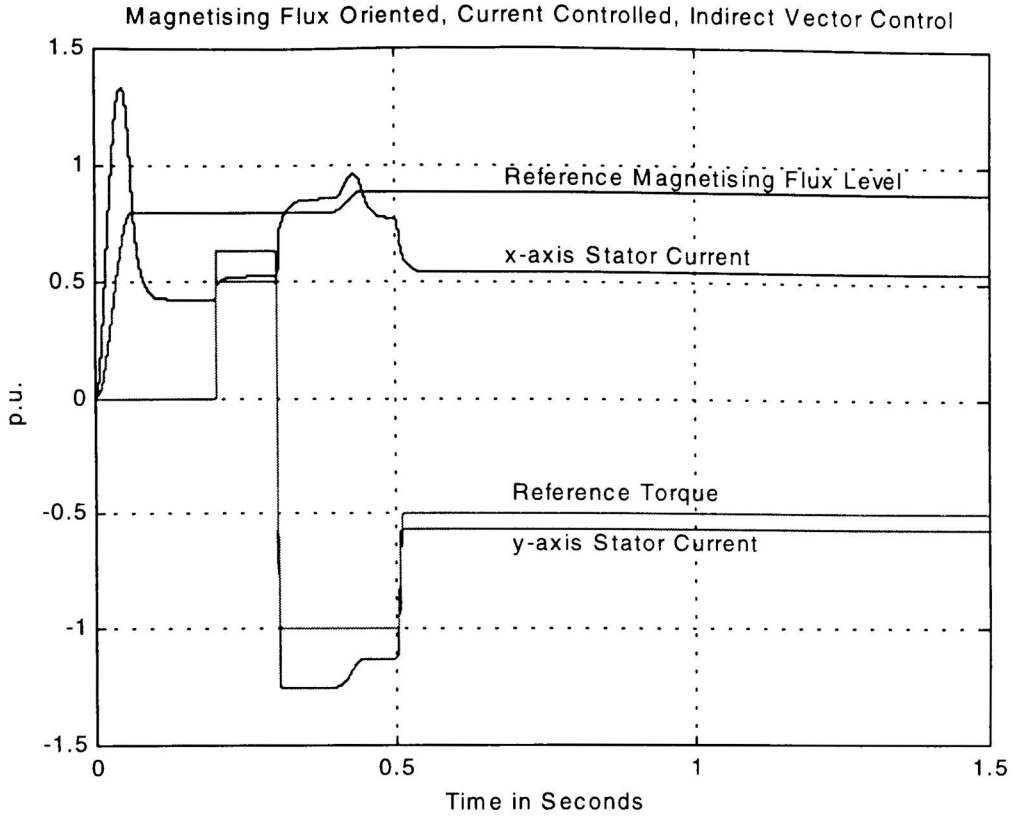

Fig. 6.18: Stator Current Variations in Field Co-ordinates in Magnetising Flux Oriented, Current Controlled, Indirect Vector Control

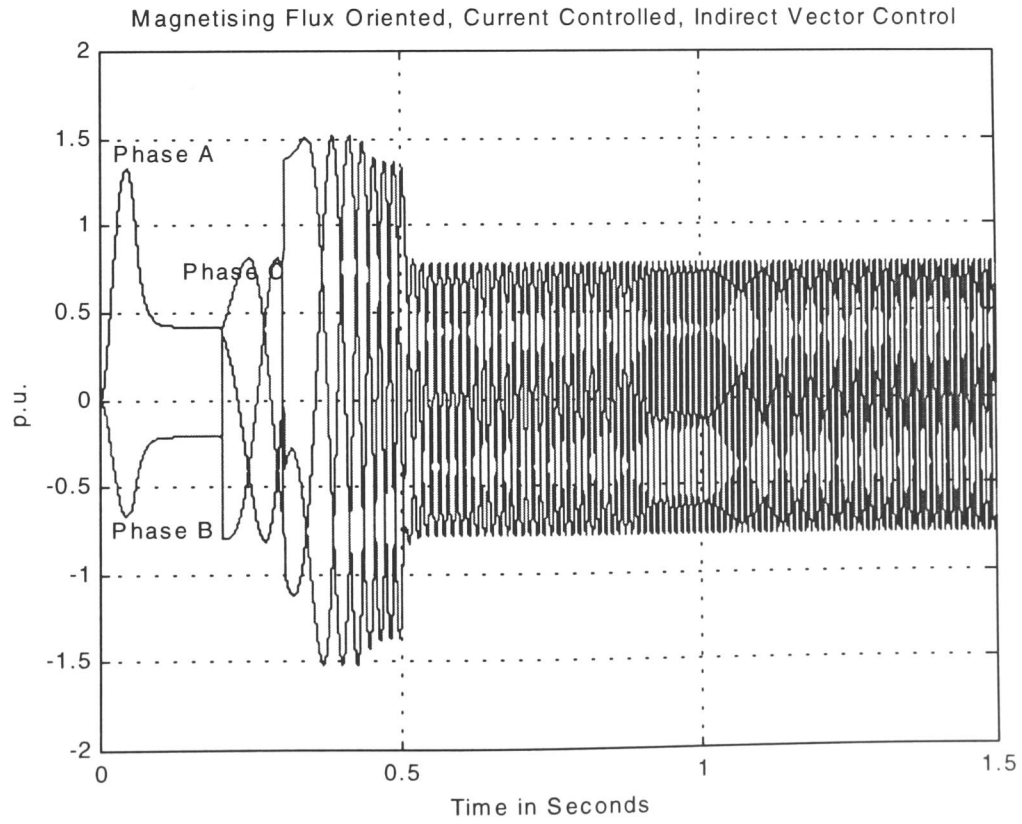

Fig. 6.19: Reference Stator Current Variations of Phases A, B and C in Magnetising Flux Oriented, Current Controlled, Indirect Vector Control

The reference motor phase current components for magnetising flux control are depicted in Fig. 6.19. Similarly to the case of stator flux oriented control, complex variations of frequency, phase and amplitude of the three phase current system are required to obtain the desired variation of magnetising flux level and developed motor torque.

In Fig. 6.20, the stator flux level, magnetising flux level and the rotor flux level are shown. It can be seen that both the stator flux level and the rotor flux level are not decoupled from variations in magnetising flux level and motor torque. However, it can also be seen that the total variation is small when compared to stator flux and rotor flux level control.

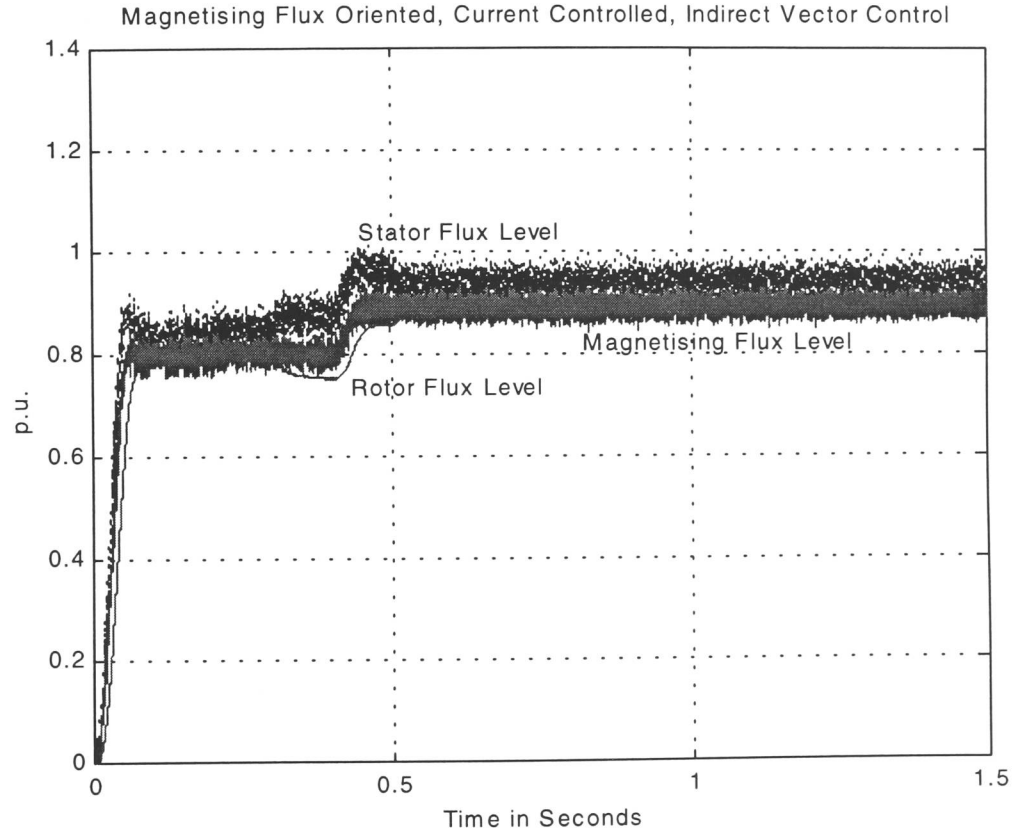

Fig. 6.20: Stator, Magnetising and Rotor Flux Level in
Magnetising Flux Oriented, Current Controlled, Indirect Vector Control

6.2 Direct Flux Vector Control

The direct flux vector control method uses an estimated (Kalman filter, observer) or measured (search coils) motor flux space vector as a feedback signal. The motor flux may be estimated from a combination of measured quantities such as the motor phase currents, the d.c. link current, phase to phase voltages, d.c. link voltage, rotor speed and

rotor position. The estimated or measured amplitude of the motor flux space vector is compared to the amplitude of a reference motor flux space vector. The resulting error signal is fed to a motor flux controller. Similarly, the developed motor torque may be measured (torque transducer) or estimated and compared to a reference torque signal. The two controller output signals are converted into their respective stator current components by means of a current decoupling network. The angle of the motor flux space vector with respect to stationary co-ordinates is used for the co-ordinate transform of the stator current. The system is a closed loop with respect to the motor flux and motor torque.

A simulation model of a system using measured rotor flux components and measured motor torque is shown in Fig. 6.21. In practice, however, it is very difficult to measure the rotor flux components (and the motor torque) directly. Nontheless the system described serves to illustrate the operation under direct vector control.

When the direct flux vector control system shown in Fig. 6.21 is compared to the indirect flux vector control system of Fig. 6.1, it can be seen that a current decoupling network has not been included. This is because the PI-controller for motor flux and motor torque adjust the x and y components of the stator current space vector automatically, in order to minimise the error between measured and reference quantities.

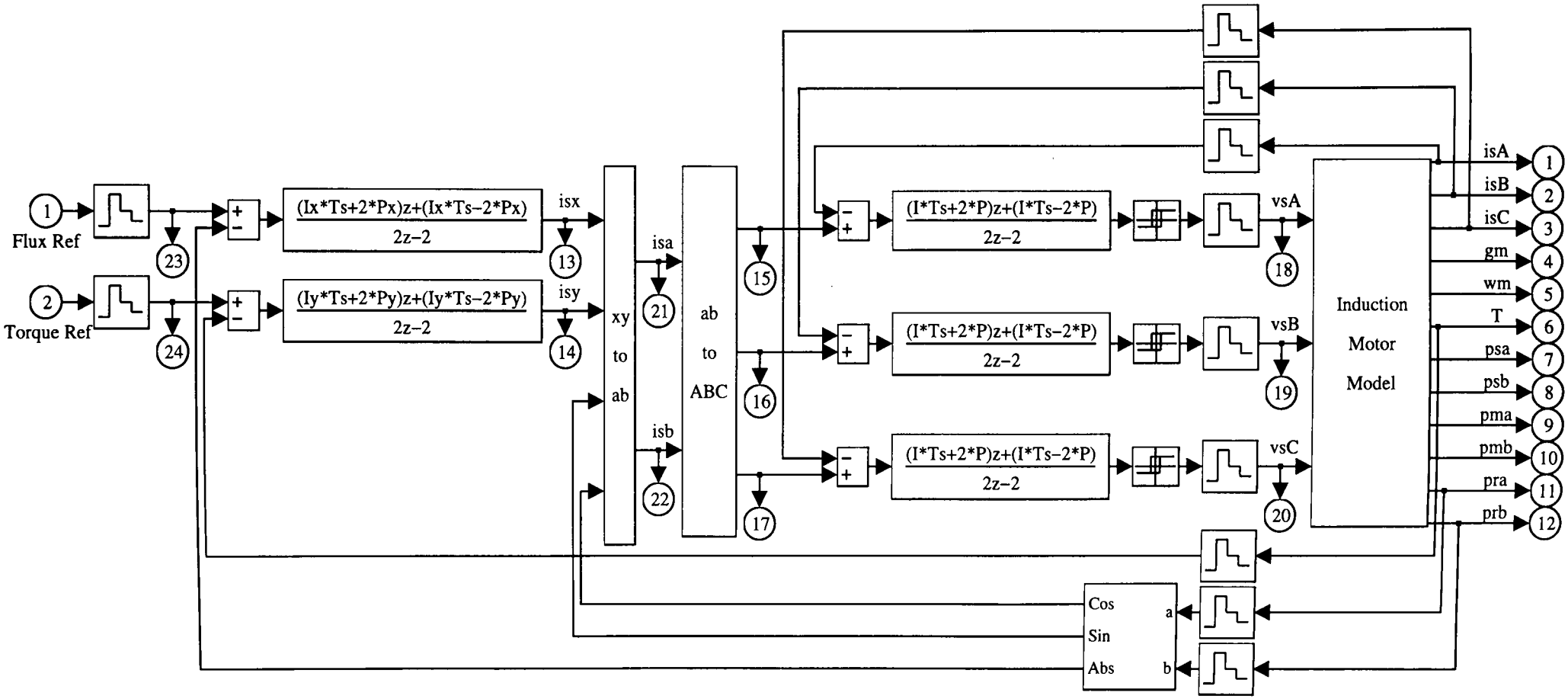

Fig. 6.21: Current Controlled, Rotor Flux Oriented, Direct Vector Control

The resulting variation of rotor flux level and motor torque is shown in Fig. 6.22. It can be seen that transient variations of the developed motor torque do not affect the rotor flux level and vice versa.

The variation of the stator current components to achieve the desired variation of rotor flux level and motor torque is shown in Fig. 6.23. Comparison to open loop control (Fig. 6.7) shows that the x and y components of the reference stator current exhibit some ripples. This is due to the feedback action of the torque measurement and could be reduced by increasing the time constants of the PI controller or adding a separate filter to the torque measurement. However, this can adversely affect the response time of the vector control system. It should be noted that ripples in reference quantities generally also increase the ripples in the controlled output quantities.

This is further illustrated in Fig. 6.24, where the phase components of the stator currents are shown.

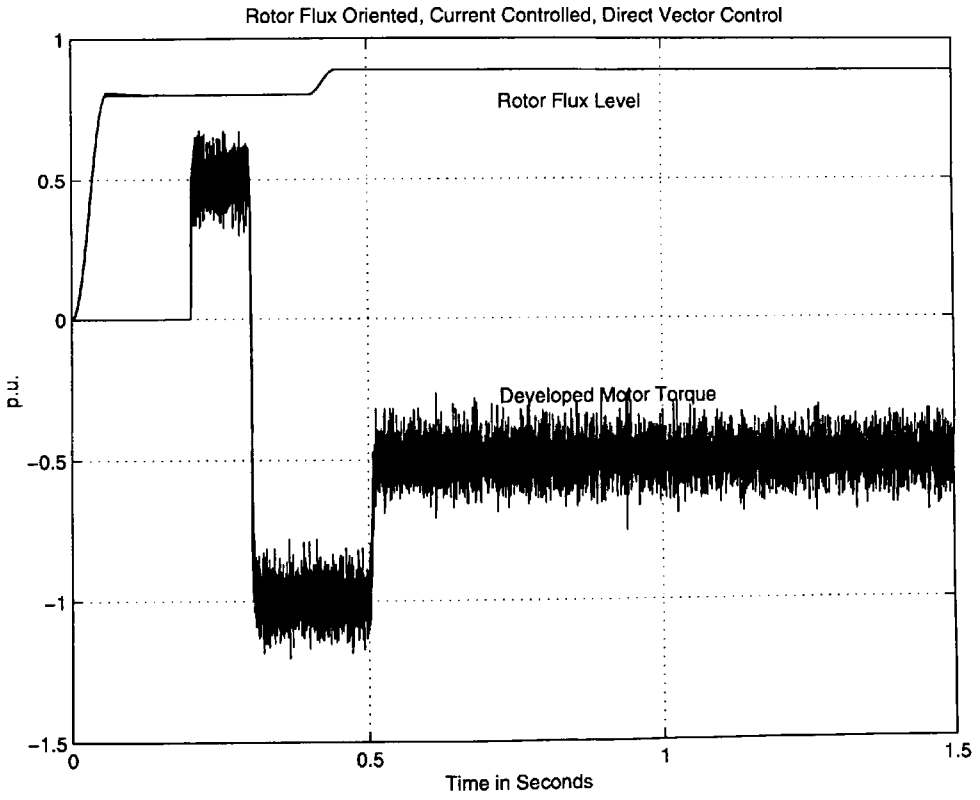

Fig. 6.22: Rotor Flux Level and Motor Torque in
Rotor Flux Oriented, Current Controlled, Direct Vector Control

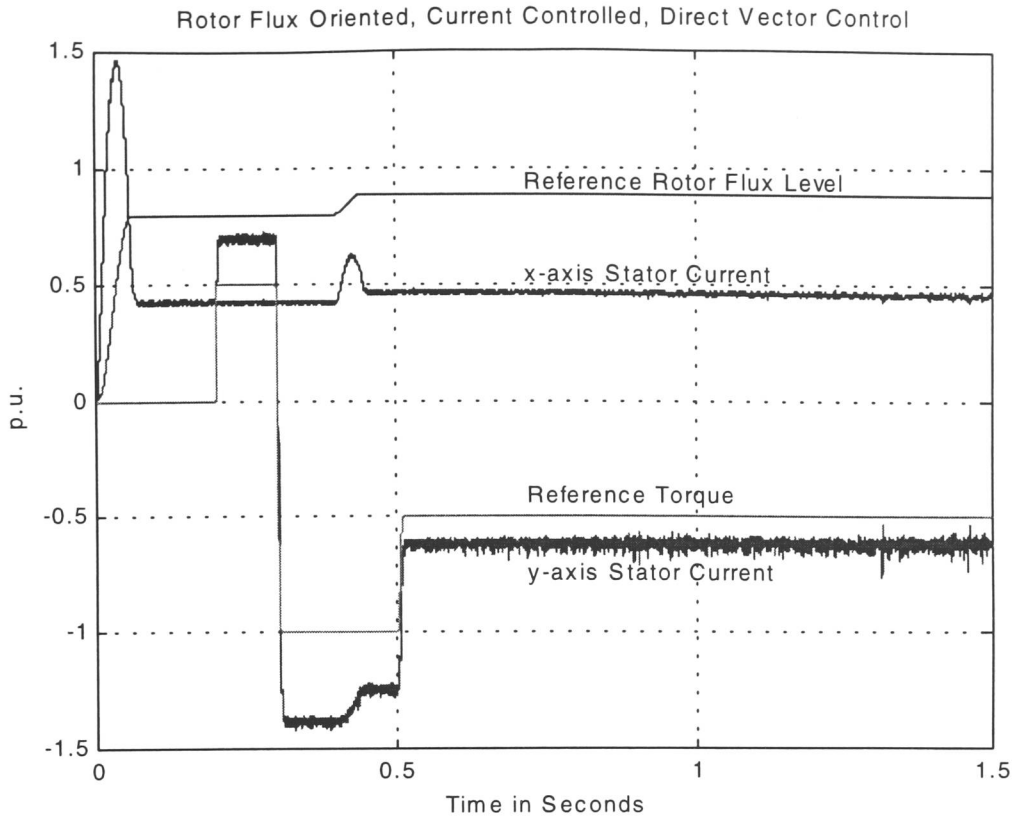

Fig. 6.23: Stator Current Variations in Field Co-ordinates in Rotor Flux Oriented, Current Controlled, Direct Vector Control

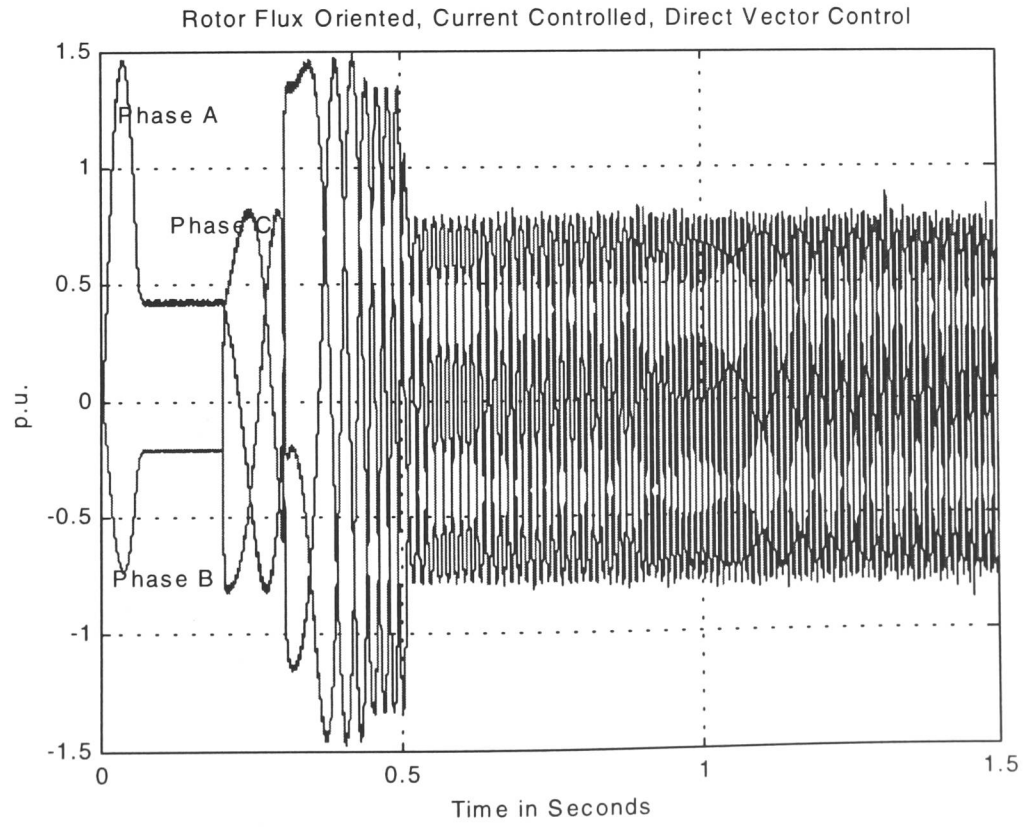

Fig. 6.24: Reference Stator Current Variations of Phases A, B and C in Rotor Flux Oriented, Current Controlled, Direct Vector Control

Fig. 6.25 shows the variation of the stator, rotor and magnetising flux vector for rotor flux oriented direct vector control. Similarly to the indirect vector control case (Fig. 6.10) overshoots of the stator flux level at transients of the rotor flux level may be seen.

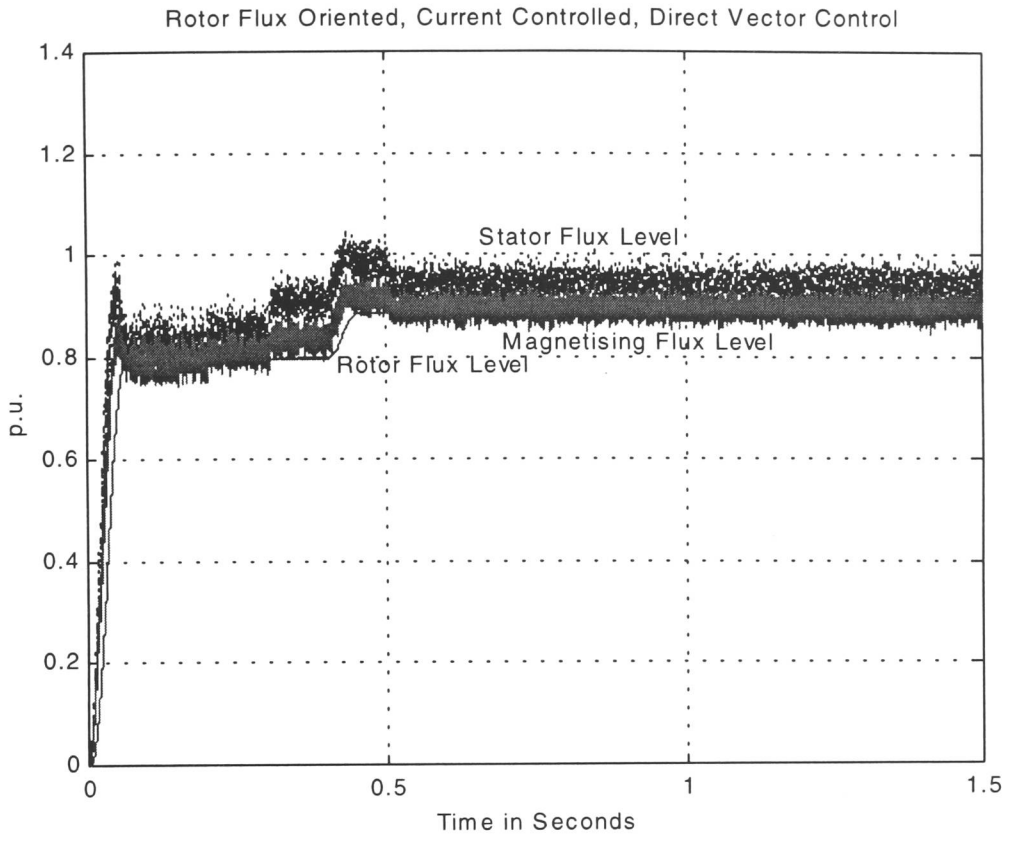

Fig. 6.25: Stator, Magnetising and Rotor Flux Level in
Rotor Flux Oriented, Current Controlled, Direct Vector Control

The system described above (Fig. 6.20) uses direct feedback of the developed motor torque and the rotor flux components. Unless a torque transducer and search coils are fitted to the installation, these signals are not normally available. Thus, a flux and torque estimator is required. One simple rotor flux and torque estimator can be derived as follows.

From the motor model given by equations (6.1), the rotor voltage equation, the rotor and stator flux linkage equation and the developed motor torque may be expressed in synchronously rotating co-ordinates as shown in Equ. 6.13.

$$\begin{aligned} 0 &= T_N s\vec{\psi}_r + \vec{i}_r r_r + j\vec{\psi}_r \omega_r \\ \vec{\psi}_r &= x_r \vec{i}_r + x_m \vec{i}_s \\ \vec{\psi}_s &= x_s \vec{i}_s + x_m \vec{i}_r \\ T &= \Im\{\vec{\psi}_s^* \vec{i}_s\} \end{aligned} \tag{6.13}$$

These expressions may be solved for the rotor flux component, the motor slip frequency and the motor torque. The results are shown in Equ. 6.14.

$$\psi_{rx} = \frac{i_{sx} r_r x_m}{T_N s x_r + r_r}$$
$$\omega_r = \frac{i_{sy} r_r x_m}{\psi_{rx} x_r} \tag{6.14}$$
$$T = \frac{x_m}{x_r} i_{sy} \psi_{rx}$$

The sum of the slip frequency and the measured motor speed may be integrated to give the angle of the rotor flux vector referred to the stationary stator axis, as shown in expression 6.15.

$$\gamma_s = \frac{\omega_m + \omega_r}{T_N s} \tag{6.15}$$

This angle can be used for the decoupling of the 'x' and 'y' components of the stator current. A simulation model of a rotor flux oriented, current controlled, direct flux vector control system is shown in Fig. 6.26.

In this system, the measured quantities are two motor phase currents and the motor speed. The speed measurement could also be eliminated be using a speed estimator.

Fig. 6.27 shows the variation or rotor flux level and the developed motor torque for the direct vector control system with rotor flux level and motor torque estimation described in Fig. 6.26. Similarly to the other flux vector control systems described above, the main objective of vector control, i.e. the decoupled control of motor flux level and motor torque has been achieved.

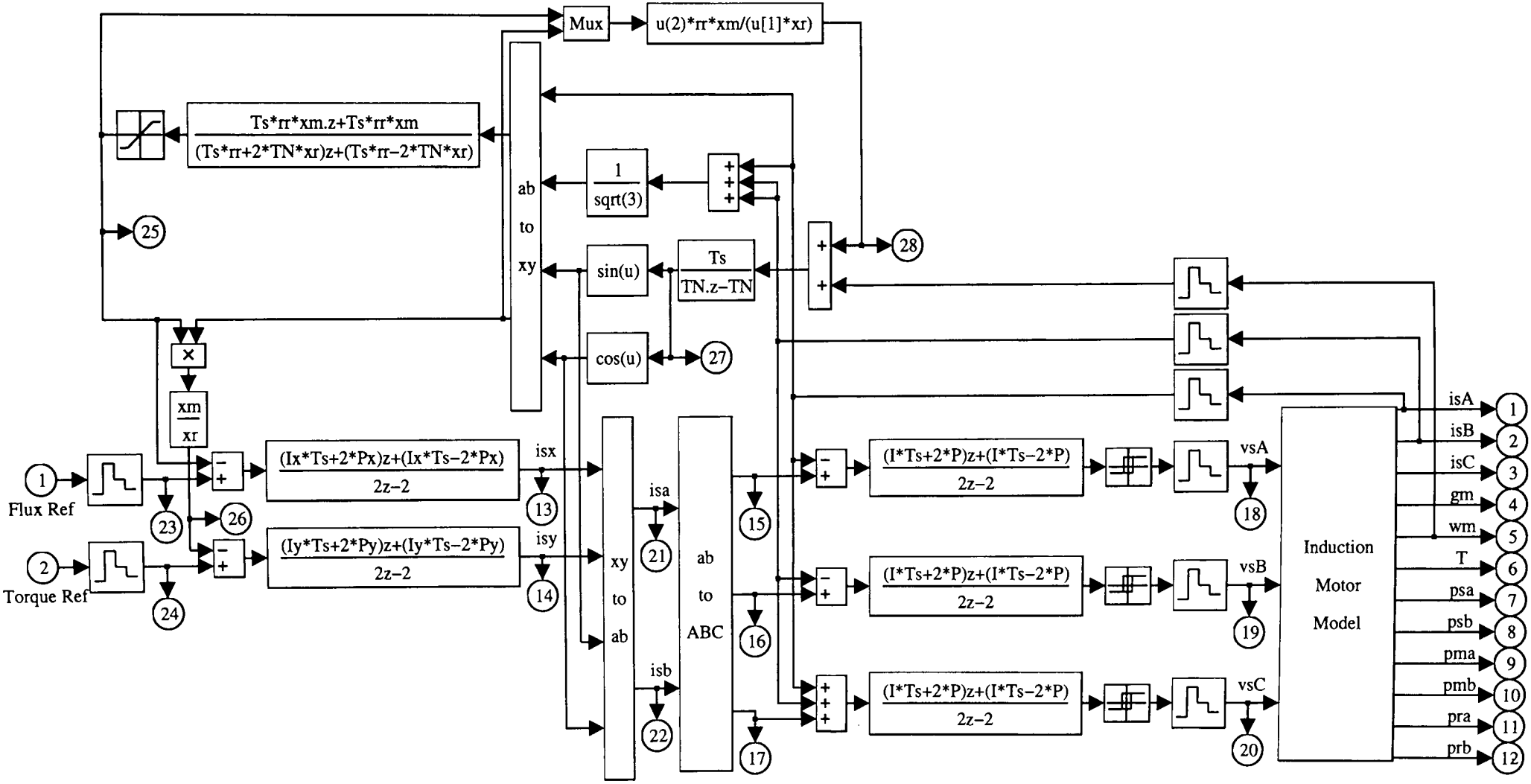

Fig. 6.26: Current Controlled, Rotor Flux Oriented, Direct Vector Control with Rotor Flux and Motor Torque Estimation

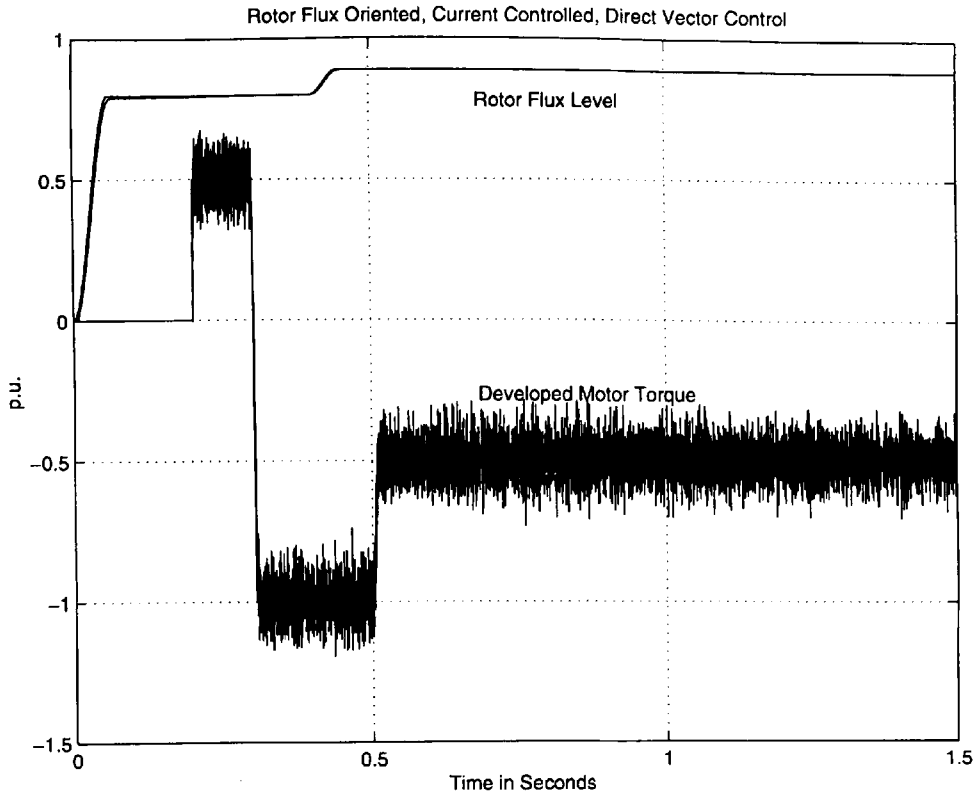

Fig. 6.27: Rotor Flux Level and Motor Torque in
Rotor Flux Oriented, Current Controlled, Direct Vector Control
with Rotor Flux and Motor Torque Estimation

The variation of the 'x' and 'y' components of the reference stator current space vector is shown in Fig. 6.28. Similarly to direct vector control with flux and torque measurements, there is a ripple on the stator current components. The general shape, however, corresponds to the indirect vector control case, as shown in Fig. 6.7.

The reference phase currents are depicted in Fig. 6.29. As can be seen, the ripple on the 'x' and 'y' stator current components in field co-ordinates causes some deviation in amplitude, however, the general shape corresponds to the indirect vector control case shown in Fig. 6.9.

The stator, magnetising and rotor flux levels for direct vector control with flux and torque estimation are shown in Fig. 6.30. Again, some overshoot of the stator current flux level is apparent.

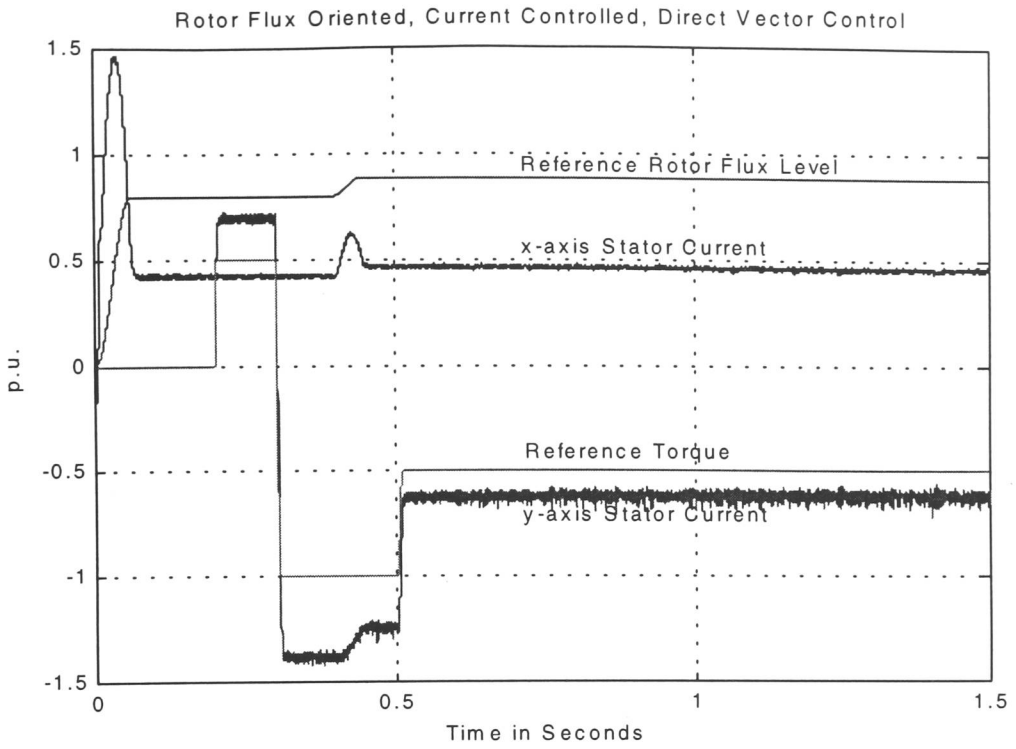

Fig. 6.28: Stator Current Variations in Field Co-ordinates in Rotor Flux Oriented, Current Controlled, Direct Vector Control with Rotor Flux and Motor Torque Estimation

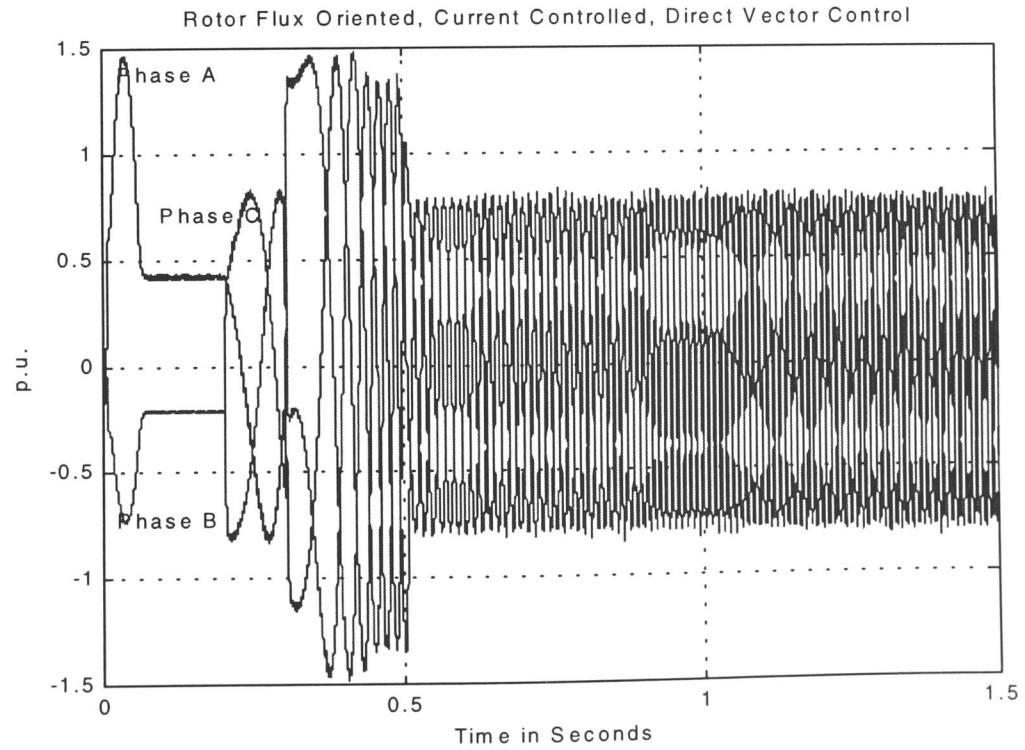

Fig. 6.29: Reference Stator Current Variations of Phases A, B and C in Rotor Flux Oriented, Current Controlled, Direct Vector Control with Rotor Flux and Motor Torque Estimation

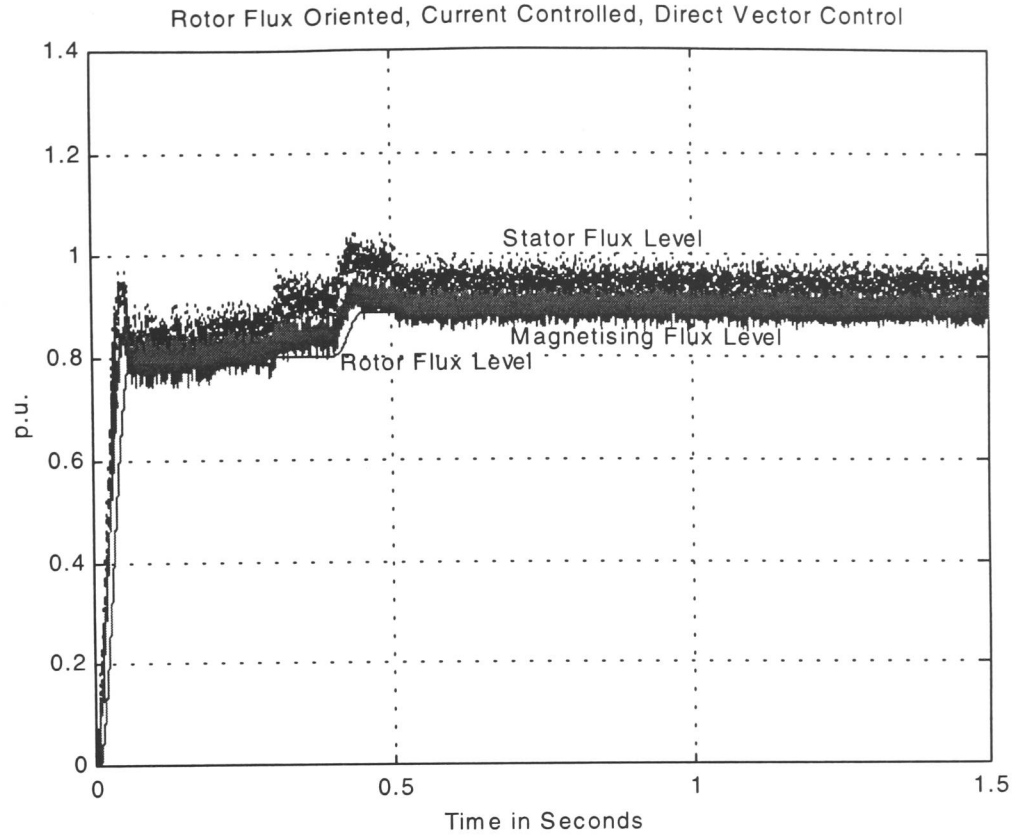

Fig. 6.30: Stator, Magnetising and Rotor Flux Level in
Rotor Flux Oriented, Current Controlled, Direct Vector Control
with Rotor Flux and Motor Torque Estimation

6.3 Parameter Detuning Consequences

It has been shown in the sections above that vector control makes possible the decoupled control of motor flux and motor torque. However, for these simulations, it has been assumed that the exact values of the motor parameters are known. This is not the case in practice. A difference between the 'true' motor parameters and the motor parameters used by the flux vector controller is inevitable because of the following reasons:

1. The motor parameters can vary with temperature.
2. The motor parameters are not constant for all motor operating conditions such as high torque, low speed operation or high speed and low torque operation.
3. The motor parameters can vary during the lifetime of the motor.

The adverse effect on the control behaviour when the motor model parameters are different from those used by the controller is shown in the following.

For the simulations, the model shown in Fig. 6.26 has been used. The motor parameters which are used by the controller are the rotor resistance, the magnetising inductance and the rotor leakage inductance. Fig. 6.35 shows the variations with time of the rotor flux level and the developed torque. Both the reference quantities and the actual quantities are shown. The simulation has been carried out for the case that the estimated rotor resistance is only 90% of the actual rotor resistance. It can be seen from the figure that the developed rotor flux level is higher than the reference flux level. Furthermore, there are transient changes of the rotor flux level when the developed motor torque changes. This means that decoupling is not fully achieved.

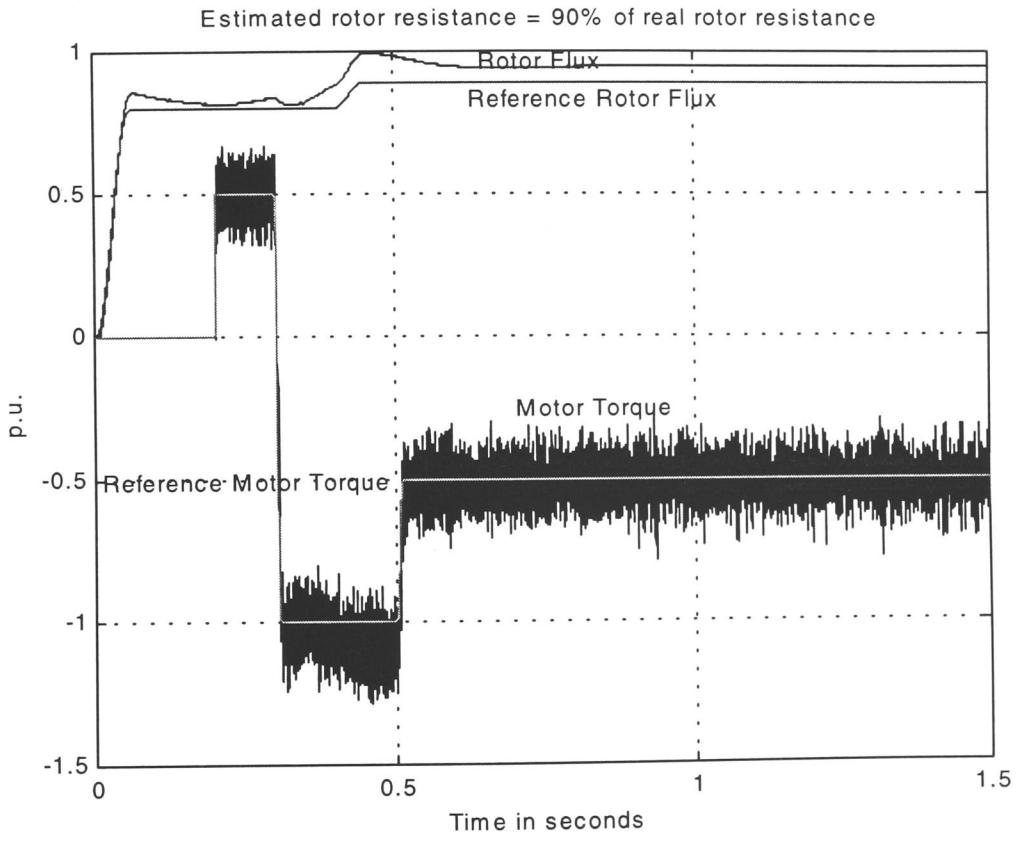

Fig. 6.31: Vector control with detuned parameters: $r_{rc} = 0.9r_r$

Similarly to the rotor flux level, the developed motor torque shows some transient variation and a small steady state error. However, the absolute effect of the rotor resistance modelling error is larger for the rotor flux level than for the developed motor torque.

Fig. 6.32 shows the effect on the rotor flux level and on the developed torque in the case where the rotor resistance value used by the controller is 110% of its actual value. In this

case, the developed motor torque level is smaller than its reference value. There are transients and steady state errors in both rotor flux level and motor torque.

The effect of modelling errors of the magnetising inductance is shown in Fig. 6.33. It has been assumed for the simulation, that the magnetising inductance used by the controller is only 90% of its correct value. Similarly to the erroneous rotor resistance case, the actual rotor flux level is higher than its reference value, but both the transient variation and steady state variation is smaller for the modelling errors in magnetising inductance than for the modelling errors in rotor resistance.

Fig. 6.34 depicts the case where the magnetising inductance is 110% of the actual value. Again, steady state errors and transient errors of both rotor flux level and motor torque are apparent.

The influence of modelling errors in rotor leakage inductance are shown in Fig. 6.35 and 6.36. The figures show that there are only marginal steady state and transient variations of rotor flux level and developed motor torque with respect to modelling errors of rotor leakage inductance.

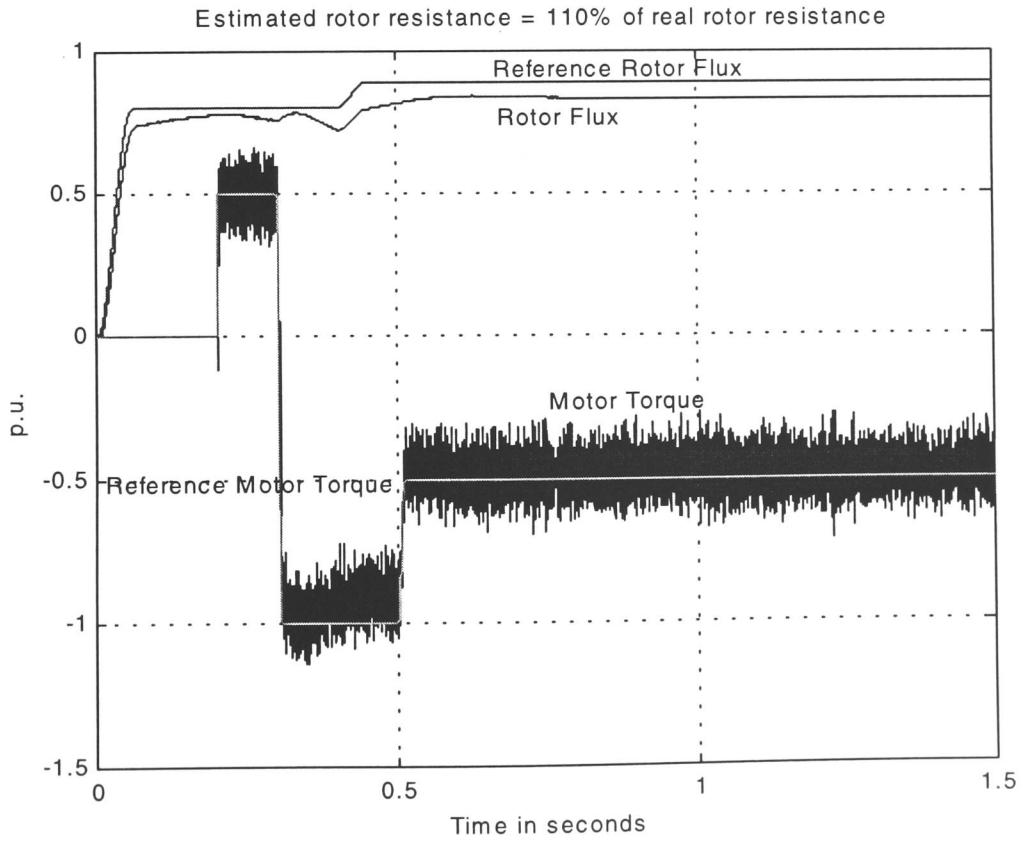

Fig. 6.32: Vector control with detuned parameters: $r_{rc} = 1.1 r_r$

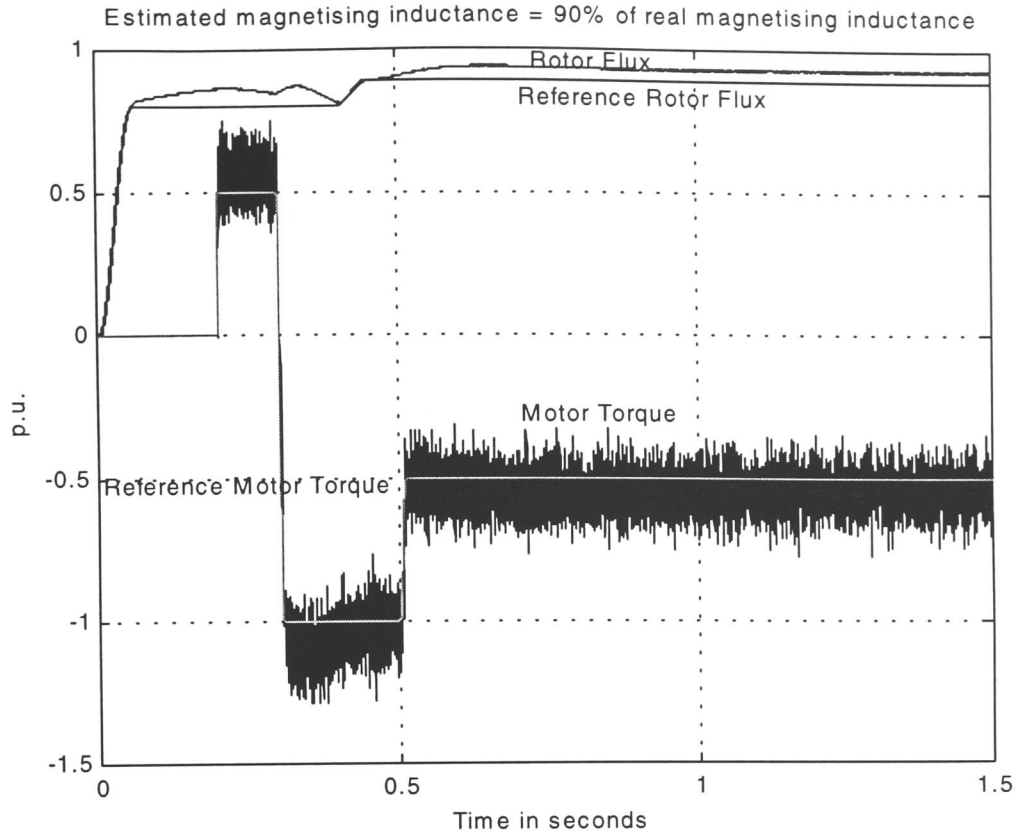

Fig. 6.33: Vector control with detuned parameters: $x_{Mc} = 0.9x_M$

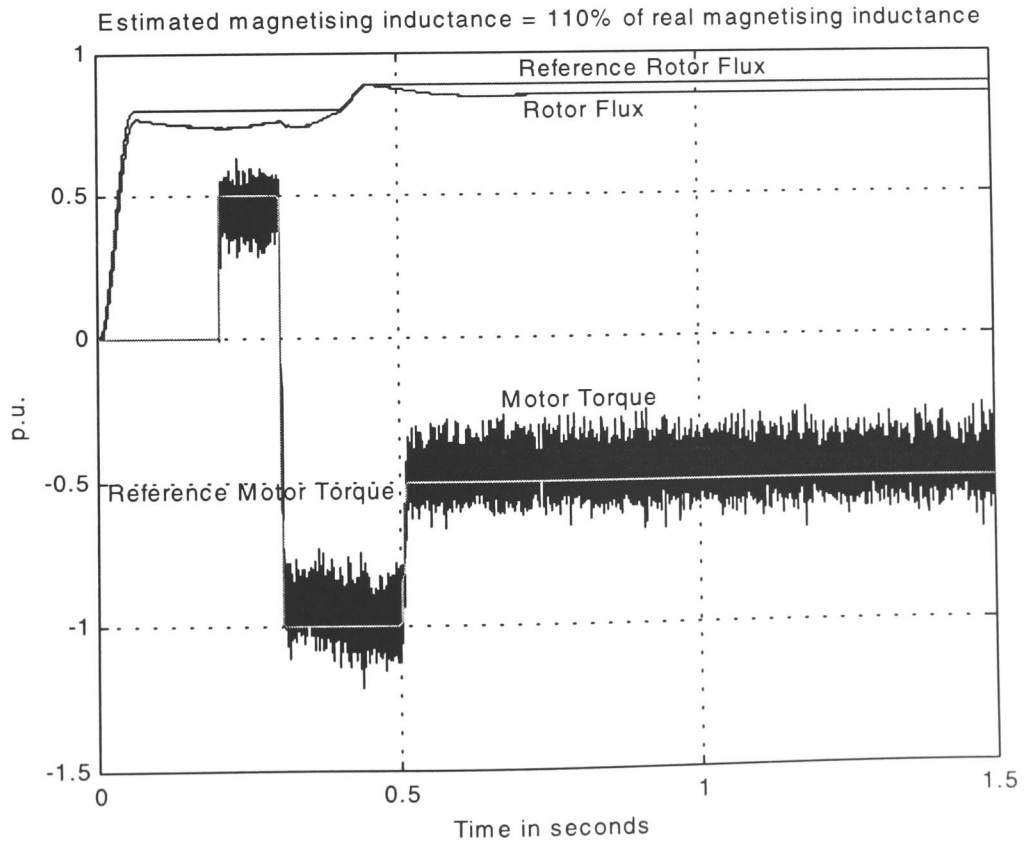

Fig. 6.34: Vector control with detuned parameters: $x_{Mc} = 1.1x_M$

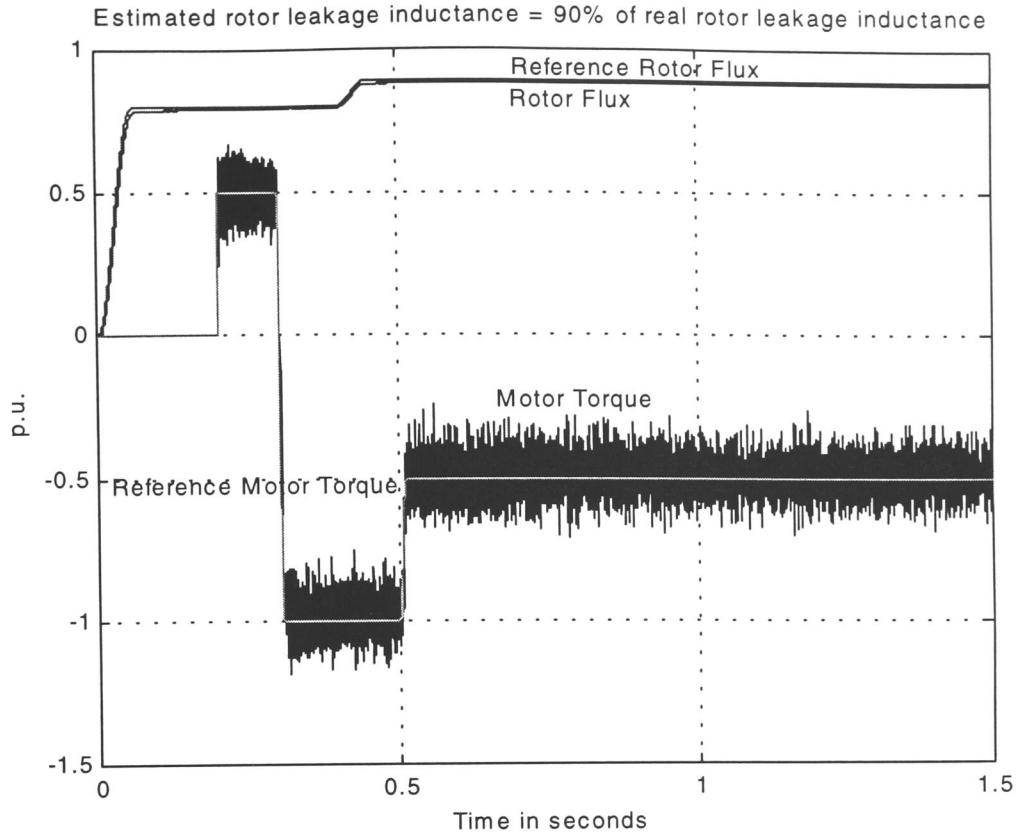

Fig. 6.35: Vector control with detuned parameters: $x_{lrc} = 0.9x_{lr}$

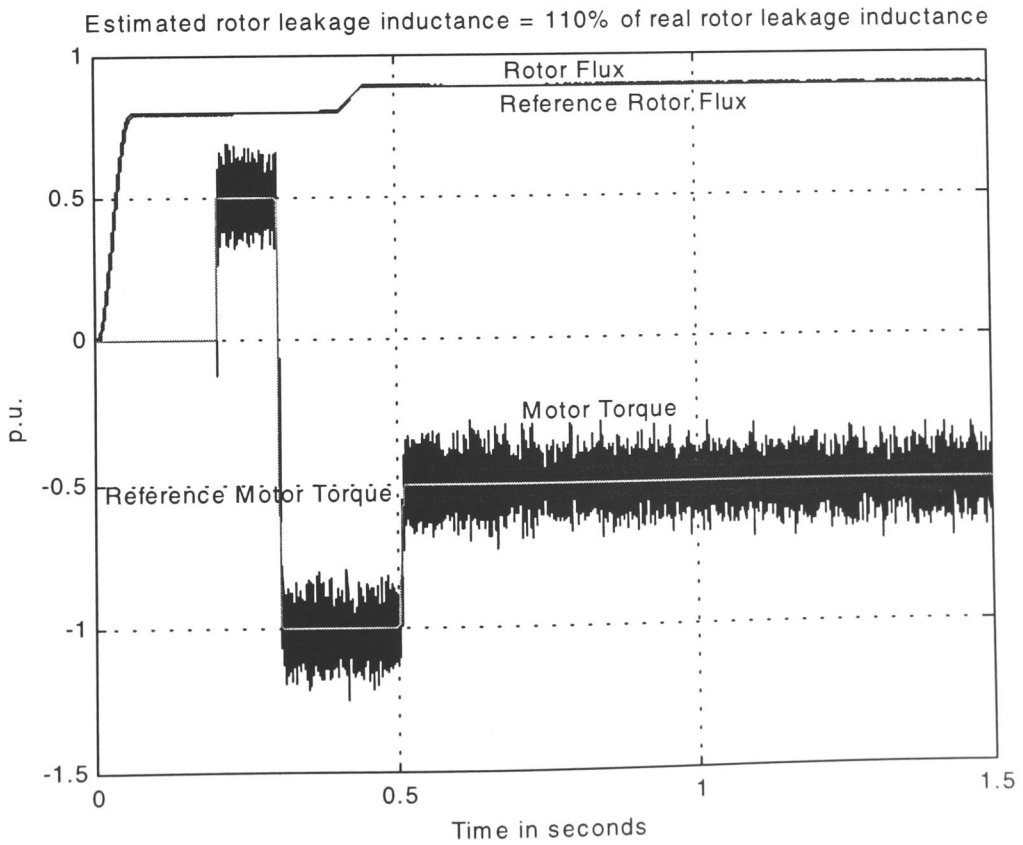

Fig. 6.36: Vector control with detuned parameters: $x_{lrc} = 1.1x_{lr}$

6.4 Interim Conclusion on Flux Vector Control

It has been shown in this chapter that by means of the flux vector control method, it is possible to control both the motor flux and the motor torque of a squirrel cage rotor induction motor independently. Therefore, control characteristics similarly to those of the separately exited d.c. motor may be obtained. This allows the inexpensive induction motor to be controlled with high dynamic accuracy, making it suitable for high performance applications.

It has also been shown that the performance of the flux vector control system is sensitive mainly to modelling errors in rotor resistance and magnetising inductance. The sensitivity to modelling errors in the rotor leakage inductance is negligible for the simulation case shown.

The effect of modelling errors in stator resistance and stator leakage inductance values, when current controlled modulators are used, has very little influence because the induction motor model stator equation is not required for the flux vector control system.

The sensitivity to motor parameter modelling errors is reduced for direct flux vector control when compared to indirect flux vector control, because of the feedback action.

Furthermore, it has been shown that considerable complexity is inherent in the controller of a flux vector control system. It is shown in the following chapter that the decoupled control of motor flux and motor torque may also be achieved without the use of a co-ordinate transformation.

Chapter 7: Direct Torque Control

7.0 Review of Direct Torque Control Systems

Decoupling of motor flux and motor torque may be achieved without the use of a co-ordinate transform algorithm in the control system of the induction motor drive system. This was first realised in 1985 by both Takahashi (1985) and Depenbrock (1985). With direct torque control, a look-up table is used which directly selects inverter power switch settings. These settings are applied to the inverter for fixed time intervals. Three different signals are used as inputs for the look-up table, as shown below:

1. **Stator flux level error:** This value is calculated from the difference between reference stator flux level and estimated stator flux level. The difference is converted into an integer number which can have only two different values by means of a two level hysteresis comparator. The values indicate that the estimated stator flux is either too small or too large.
2. **Developed torque error:** This value is calculated from the difference between reference torque and estimated torque. This difference is converted into an integer number by means of a three level comparator which can have only three different values. The values indicate that the estimated developed torque is either too small, too large or within a given error limit.
3. **Location of the stator flux space vector:** The estimated angle of the stator flux space vector with reference to the fixed stator axis is converted into an integer number which can have only six different values. These values correspond to six, sixty degrees sections of the complex plane as illustrated in the following sections.

Hysteresis comparators are used for the generation of the look-up table inputs in order to control the generation of zero voltage vectors. This, in turn, gives control over the average switching frequency of the inverter.

The switching states of the inverter are applied for a fixed time interval. In each interval, the estimation of developed torque and stator flux space vector is updated and the look-up table inputs are re-calculated, which in turn selects one out of eight different inverter state combinations for the following time interval.

7.1 Takahashi's Direct Torque Control

A Simulink representation of a direct torque control system can be seen in Fig. 7.1

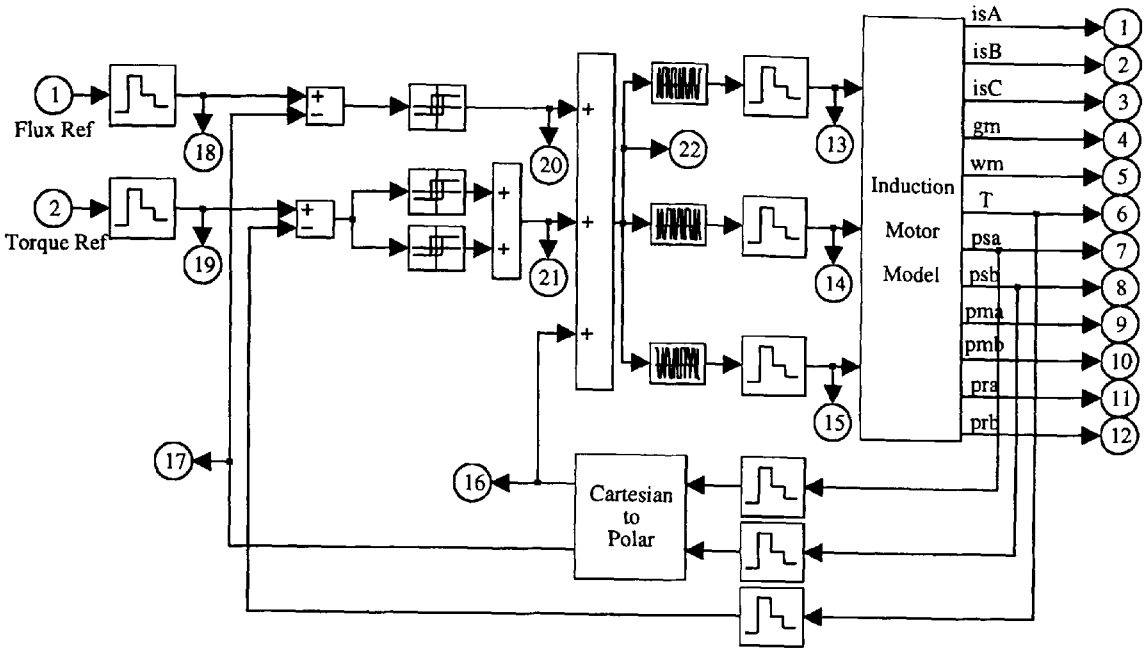

Fig. 7.1: Direct Torque Control System

It may be seen from Fig. 7.1 that the system requires feedback of the motor torque signal and the stator flux space vector components. These signals are not normally available and thus have to be estimated from measured quantities such as the motor currents. However, the system serves to illustrate a basic direct torque control system. The contents of the switching table shown in Fig. 7.1 are illustrated in Table 7.1.

Table 7.1: Direct Torque Control Voltage Vector Selection Table

ψ_{err}	T_{err}	γ_{s1}	γ_{s2}	γ_{s3}	γ_{s4}	γ_{s5}	γ_{s6}
1	2	$\vec{v}_2$	$\vec{v}_3$	$\vec{v}_4$	$\vec{v}_5$	$\vec{v}_6$	$\vec{v}_1$
1	1	$\vec{v}_0$	$\vec{v}_7$	$\vec{v}_0$	$\vec{v}_7$	$\vec{v}_0$	$\vec{v}_7$
1	0	$\vec{v}_6$	$\vec{v}_1$	$\vec{v}_2$	$\vec{v}_3$	$\vec{v}_4$	$\vec{v}_5$
0	2	$\vec{v}_3$	$\vec{v}_4$	$\vec{v}_5$	$\vec{v}_6$	$\vec{v}_1$	$\vec{v}_2$
0	1	$\vec{v}_7$	$\vec{v}_0$	$\vec{v}_7$	$\vec{v}_0$	$\vec{v}_7$	$\vec{v}_0$
0	0	$\vec{v}_5$	$\vec{v}_6$	$\vec{v}_1$	$\vec{v}_2$	$\vec{v}_3$	$\vec{v}_4$

The error signals ψ_{err} and T_{err} shown in Table 1 are calculated by means of hysteresis comparators as follows:

$$\psi_{err} = 1 \text{ for } \psi_{ref} - \psi_{est} > \psi_H$$

$$\psi_{err} = 0 \text{ for } \psi_{ref} - \psi_{est} < -\psi_H$$

$$T_{err} = 2 \text{ for } T_{ref} - T_{est} > T_H$$

$$T_{err} = 1 \text{ for } (T_{err} = 0)\&(T_{ref} - T_{est} > 0)\&(T_{ref} - T_{est} < T_H) \tag{7.1}$$

$$T_{err} = 1 \text{ for } (T_{err} = 2)\&(T_{ref} - T_{est} < 0)\&(T_{ref} - T_{est} > -T_H)$$

$$T_{err} = 0 \text{ for } T_{ref} - T_{est} < -T_H$$

In the equations above, ψ_{ref} represents the stator flux reference level, T_{ref} is the reference torque signal, ψ_{est} is the estimated motor flux level and T_{est} is the estimated motor torque. The hysteresis levels for the flux comparator and the torque comparator are represented by ψ_H and T_H, respectively.

The locations of the stator flux space vector ($\gamma_{s1},\ldots,\gamma_{s6}$) are shown in the complex plane of Fig. 7.2.

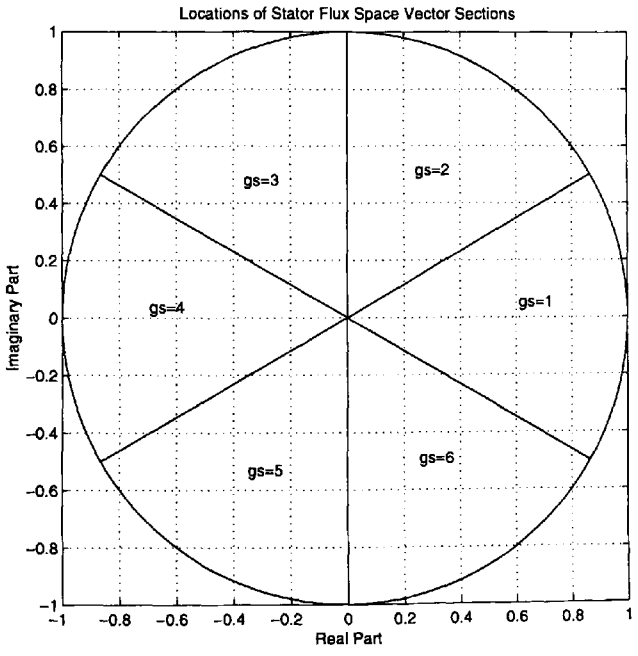

Fig. 7.2: Locations of the Stator Flux Space Vector

The voltage vectors $\vec{v}_0$ to $\vec{v}_7$ are defined in Fig. 5.13. It should be noted that the system shown in Fig. 7.1 does not contain any motor parameters and PI-controllers. The only adjustable variables are the hysteresis width of the comparators for the stator flux error

and the motor torque error. The simulated performance of the direct torque control system is shown in Fig. 7.3 to Fig. 7.5.

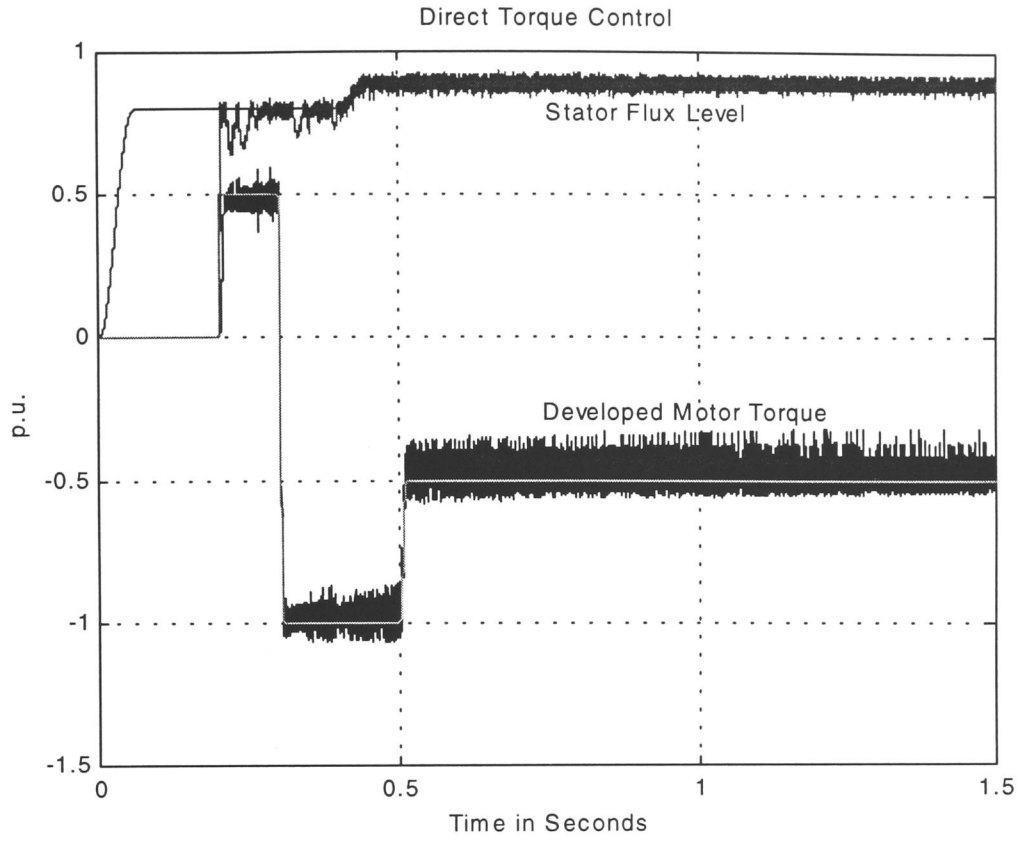

Fig. 7.3: Stator Flux level and Motor Torque in Direct Torque Control

Fig. 7.3 shows that initially, the stator flux generated is zero although the stator flux reference level rises to 0.8p.u. However, stator flux is developed when the torque reference signal is non-zero. This effect may be explained as follows:

It may be seen from expressions Equ. 7.1 that the torque error signal is $T_{err} = 1$ for the case that there is a torque error smaller than the hysteresis band width. According to Table 7.1, this condition always selects a zero voltage vector. When motor flux at zero torque demand is required, a 'dither torque signal' may be introduced (Takahashi, 1988) or a different switching table may be used (see next section).

However, apart from the zero torque condition, it may be seen from Fig. 7.3 that the stator flux and the motor torque are decoupled from each other. It should be noted that this has been achieved without the use of a co-ordinate transform algorithms.

It may be seen from Fig. 7.4 that there is an initial inrush current due to the sudden flux and torque built-up when the reference motor torque signal leaves the torque hysteresis band. At high speed operation, the waveforms are comparable to those for the flux vector control case.

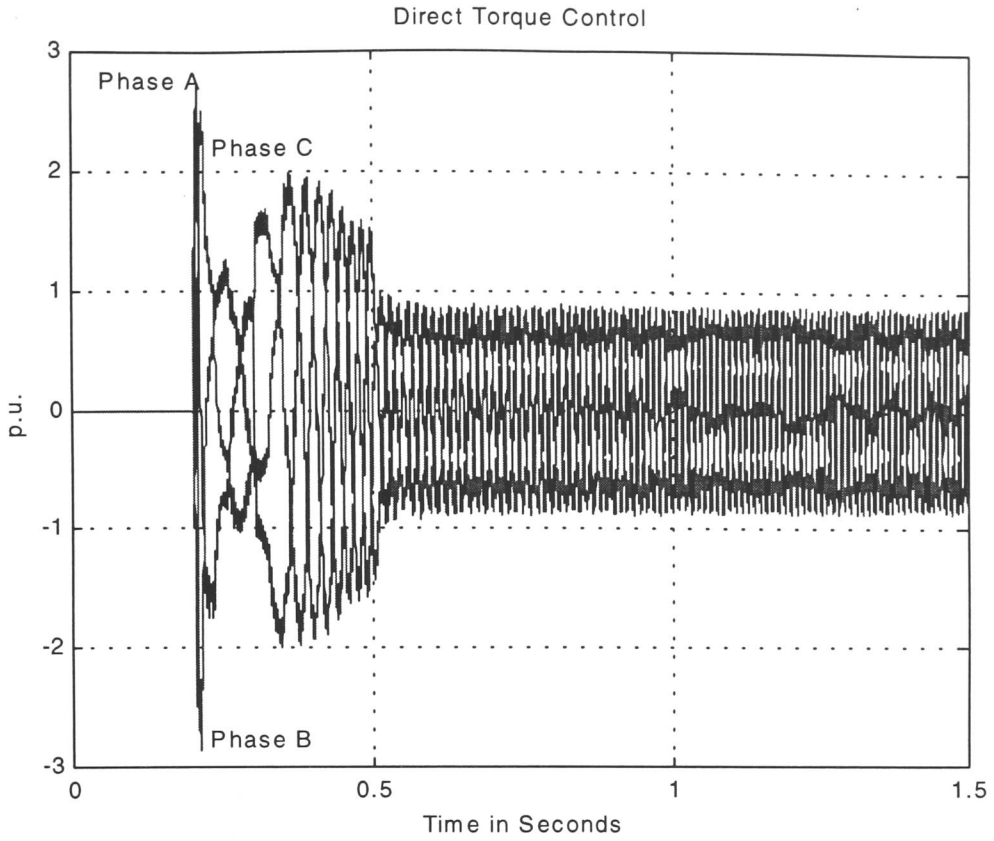

Fig. 7.4: Stator Current Variations in Direct Torque Control

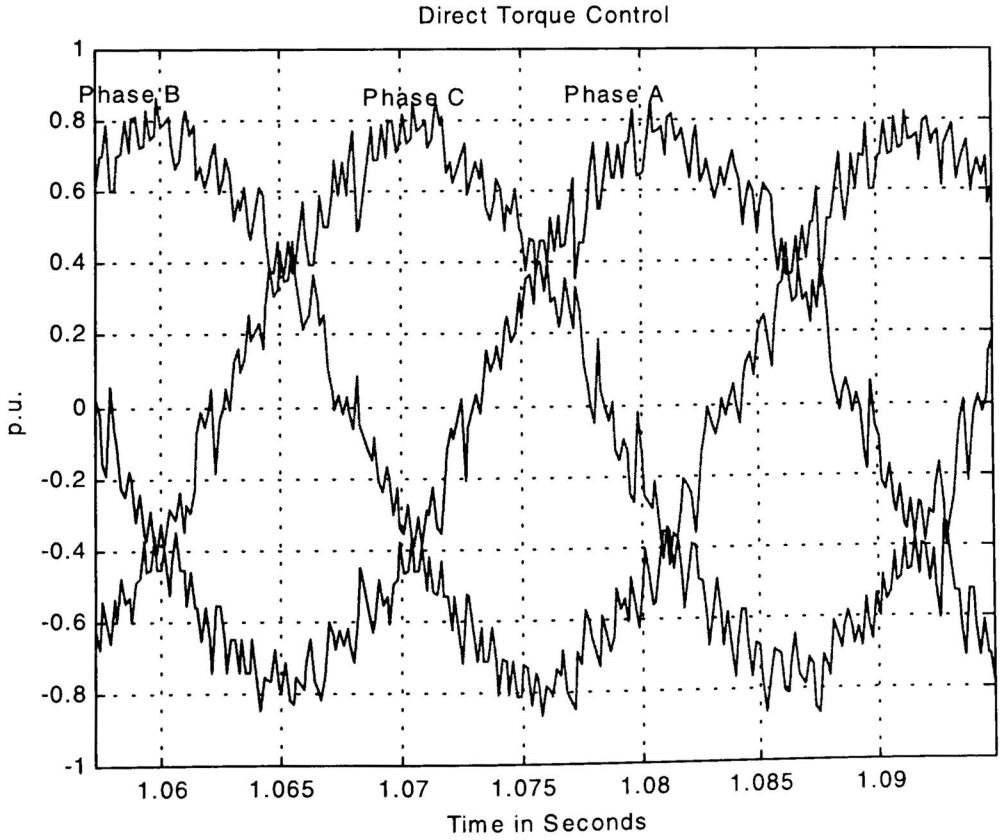

Fig. 7.5: Stator Current Variations in Direct Torque Control

A voltage or current modulator with sinusoidal reference waveforms has not been used for the generation of the stator current waveforms, yet the current waveforms approach those of sine waves, as may be seen from Fig. 7.5, which shows a close-up of the stator current waveforms.

Fig. 7.6 shows the stator flux level, the magnetising flux level and the rotor flux level waveforms in direct torque control. Due to the flux build-up during torque build-up, some transients occur in the motor flux waveforms. It can also be seen that at t=0.5s, the magnetising flux level and the rotor flux level attain new values, because of the motor torque change (see Fig. 7.3). Therefore, magnetising flux and rotor flux are not decoupled from the torque transients since the stator flux level is controlled. This corresponds to the stator flux oriented, flux vector control case (Fig. 6.15).

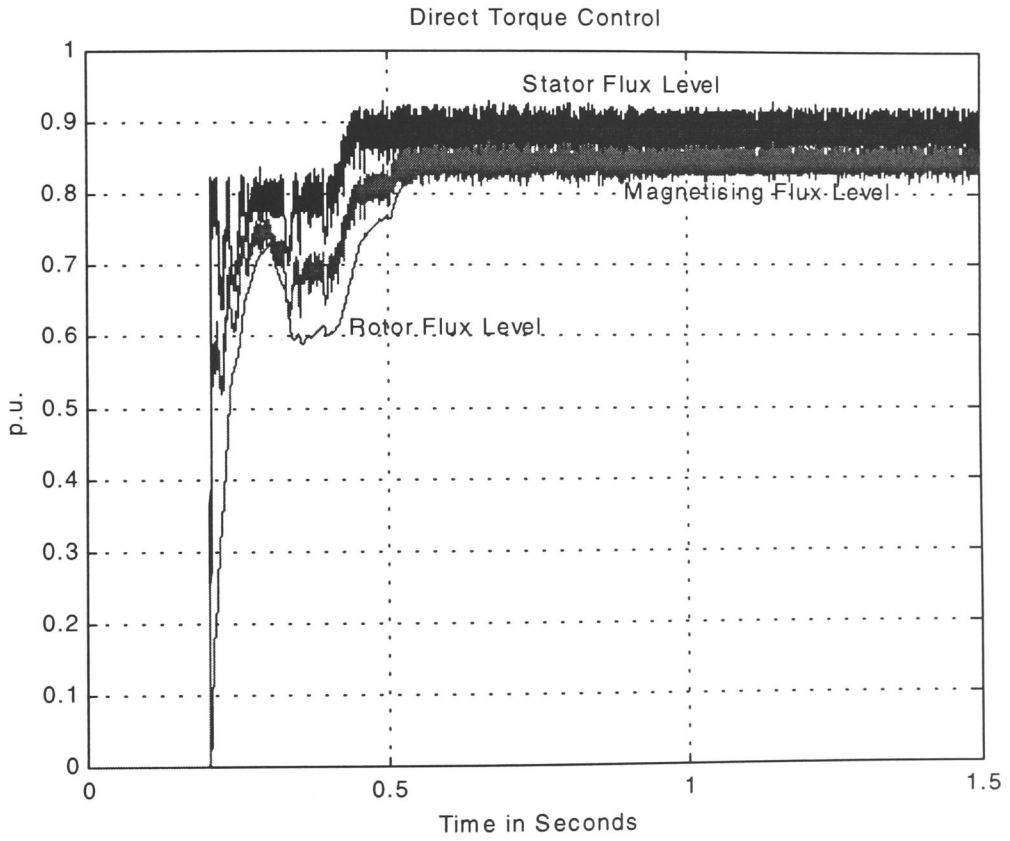

Fig. 7.6: Stator Flux level, Magnetising Flux Level
and Rotor Flux Level in Direct Torque Control

As mentioned above, when flux build-up at zero torque is required, then a modified switching table may be used. This is shown in the following section.

7.2 Direct Torque Control with Modified Switching Table

A weakness of the direct torque control system shown in the previous section is that the stator flux level can not be controlled at zero developed torque. In order to expand the switching table (Table 7.1) a further state of the stator flux level error signal ψ_{err} is introduced as shown in Table 7.2.

Table 7.2: Modified Direct Torque Voltage Vector Selection Table

ψ_{err}	T_{err}	γ_{s1}	γ_{s2}	γ_{s3}	γ_{s4}	γ_{s5}	γ_{s6}
2	2	$\vec{v}_2$	$\vec{v}_3$	$\vec{v}_4$	$\vec{v}_5$	$\vec{v}_6$	$\vec{v}_1$
2	1	$\vec{v}_1$	$\vec{v}_2$	$\vec{v}_3$	$\vec{v}_4$	$\vec{v}_5$	$\vec{v}_6$
2	0	$\vec{v}_6$	$\vec{v}_1$	$\vec{v}_2$	$\vec{v}_3$	$\vec{v}_4$	$\vec{v}_5$
1	2	$\vec{v}_7$	$\vec{v}_0$	$\vec{v}_7$	$\vec{v}_0$	$\vec{v}_7$	$\vec{v}_0$
1	1	$\vec{v}_0$	$\vec{v}_7$	$\vec{v}_0$	$\vec{v}_7$	$\vec{v}_0$	$\vec{v}_7$
1	0	$\vec{v}_7$	$\vec{v}_0$	$\vec{v}_7$	$\vec{v}_0$	$\vec{v}_7$	$\vec{v}_0$
0	2	$\vec{v}_3$	$\vec{v}_4$	$\vec{v}_5$	$\vec{v}_6$	$\vec{v}_1$	$\vec{v}_2$
0	1	$\vec{v}_7$	$\vec{v}_0$	$\vec{v}_7$	$\vec{v}_0$	$\vec{v}_7$	$\vec{v}_0$
0	0	$\vec{v}_5$	$\vec{v}_6$	$\vec{v}_1$	$\vec{v}_2$	$\vec{v}_3$	$\vec{v}_4$

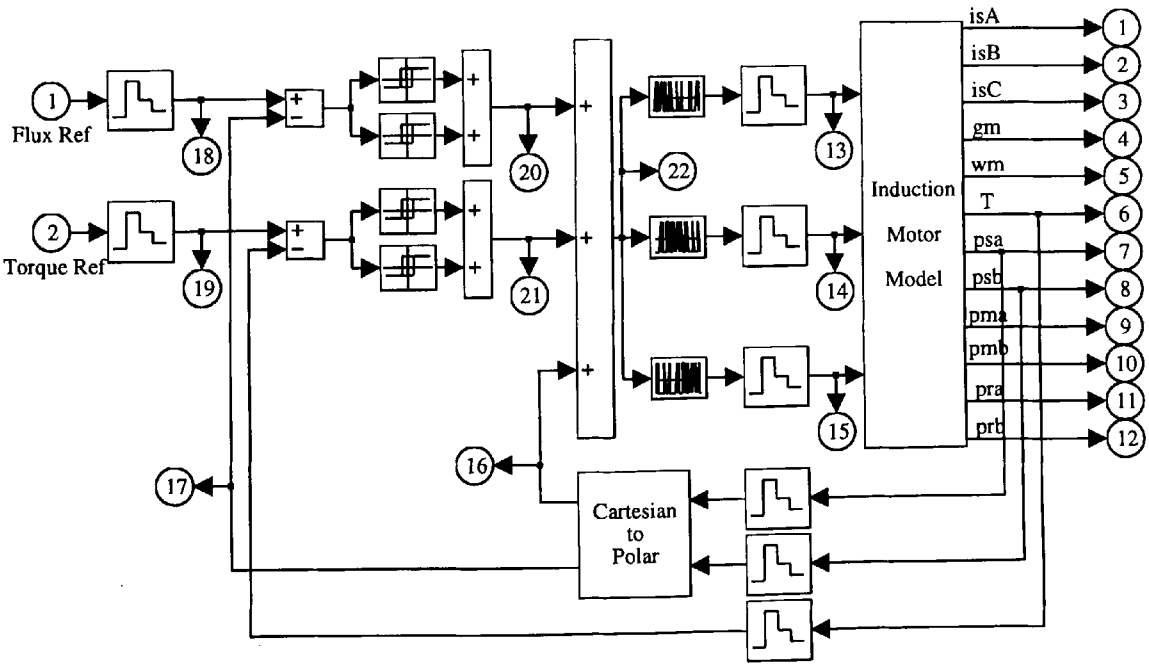

Fig. 7.7 Direct Torque Control System with modified Switching Table

A direct torque control system based on the switching table (Table 7.2) is shown in Fig. 7.7. It can be seen from the figure that there is a two level hysteresis comparator for both the stator flux and the stator torque.

Simulation results of the system shown in Fig. 7.7 are depicted in Fig. 7.8 to Fig. 7.10. It can be seen from Fig. 7.8 that the stator flux level follows the reference flux level signal even when there is no torque demand. It can clearly be seen that for all stator flux level changes there are no transients in motor torque and vice versa. Both variables are decoupled from each other.

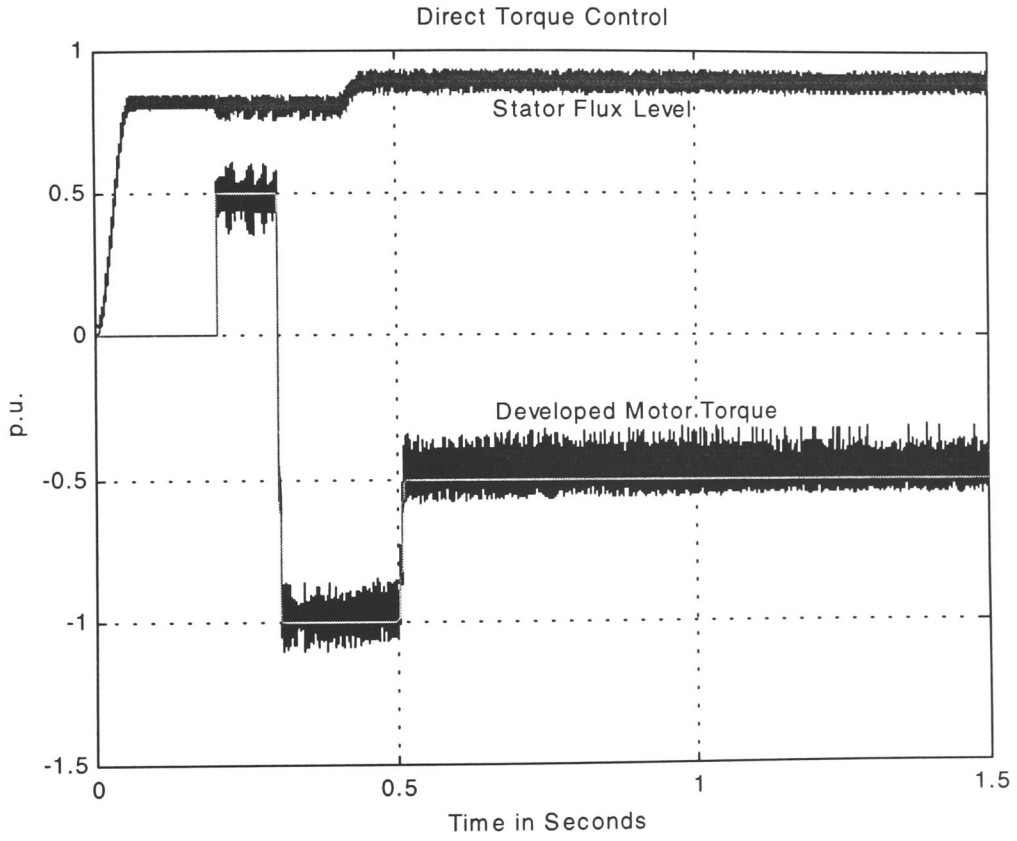

Fig. 7.8: Stator Flux level and Motor Torque in
Direct Torque Control with modified Switching Table

Fig. 7.9 shows the variations in time of the three stator current phases with the direct torque control system shown in Fig. 7.7. It may be seen that the current waveforms vary smoothly and there is only a small initial transient current when compared to Fig. 7.4.

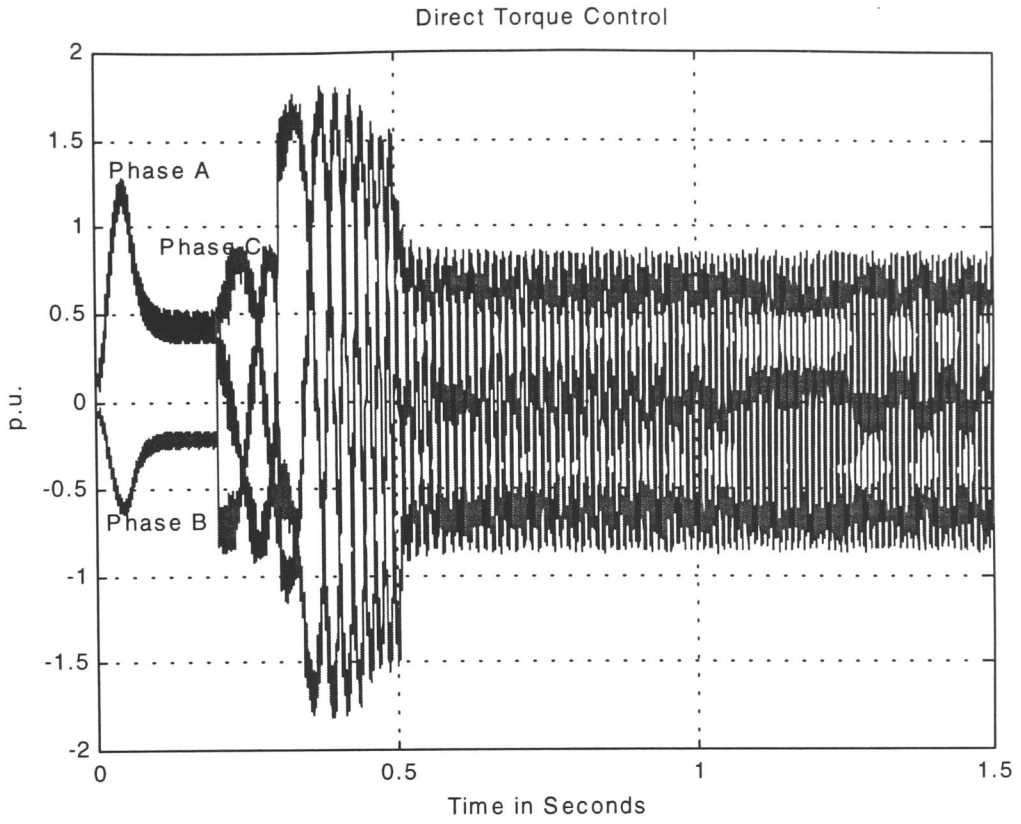

Fig. 7.9: Stator Current Variations in

Direct Torque Control with modified Switching Table

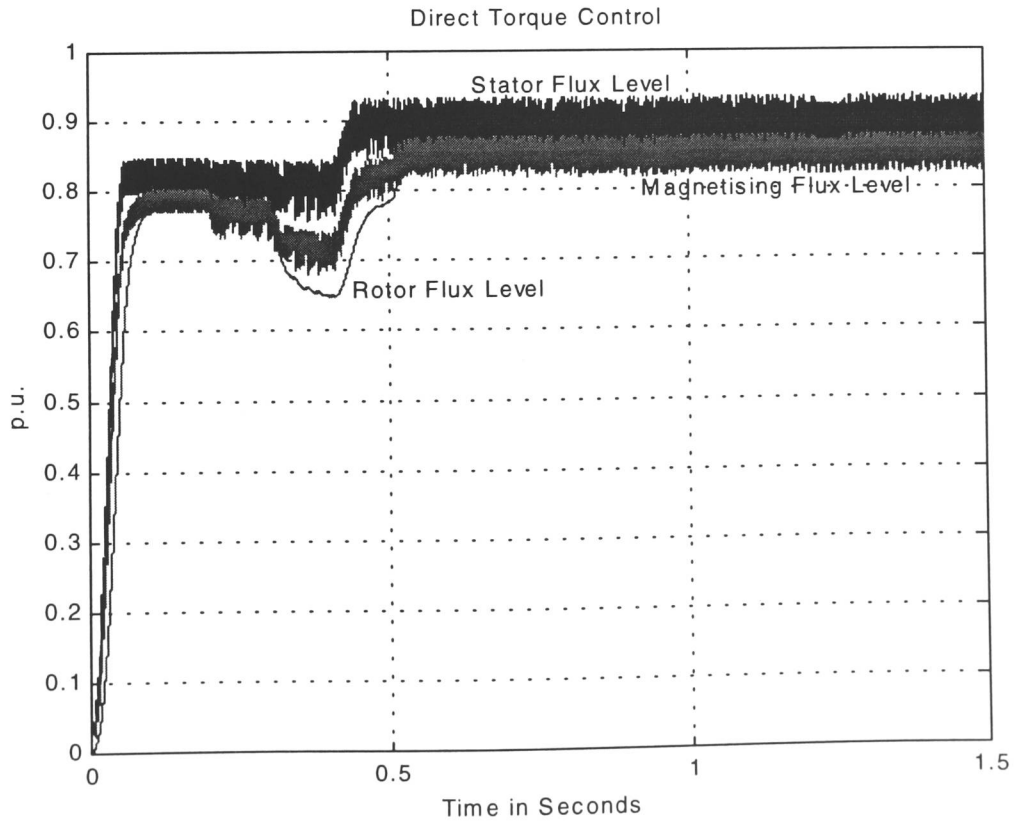

Fig. 7.10: Stator Flux level, Magnetising Flux Level

and Rotor Flux Level in Direct Torque Control with modified Switching Table

Fig. 7.10 shows the variations in time of the stator flux level, the magnetising flux level and the rotor flux level. As expected, the magnetising flux level and the rotor flux level are not decoupled from variations in developed motor torque, because stator flux level control is employed with direct torque control.

7.3 Direct Torque Control with Flux and Torque Estimation

The estimation of the stator flux space vector in stator oriented co-ordinates may be carried out in a number of different ways. The estimators can be categorised by their required input signals, which are the signals to be measured. In the following, three different estimators are described.

7.3.1 Direct Torque Control with $i_{sA} - i_{sB} - \gamma_m$ Estimator

The stator flux space vector may be estimated by measuring two motor currents and the rotor position signal γ_m. The stator flux vector may be calculated in a co-ordinate system fixed to the rotor of the induction motor as follows:

The motor model equations in rotor oriented co-ordinates are given by the set of equations Equ. 2.78. Successive substitutions of the rotor voltage equation (Equ. 2.78b) and the rotor flux linkage equation (Equ 2.78d) into the stator flux linkage equation (Equ. 2.78c) results in the following expression:

$$\vec{\psi}_s = \vec{i}_s \frac{r_r x_s + T_N s\left(x_s x_r - x_M\right)}{r_r + T_N s x_r} \tag{7.2}$$

It should be noted, however, that the expression (Equ. 7.2) for the stator flux vector is valid in rotor oriented co-ordinates only. Therefore the measured stator currents have to be converted into rotor oriented co-ordinates before Equ. 7.2 is applied. Similarly, the result of Equ. 7.2 has to be converted back to stator oriented co-ordinates in order to determine the sector of the stator flux space vector in stator oriented co-ordinates according to Fig. 7.2.

The motor torque may be estimated by the cross product expression of the stator flux vector and the stator current vector, which is valid in any co-ordinate system:

$$T_{est} = i_{s\beta}\psi_{s\alpha} - i_{s\alpha}\psi_{s\beta} \tag{7.3}$$

A direct torque control system based upon the estimator described is shown in Fig. 7.11.

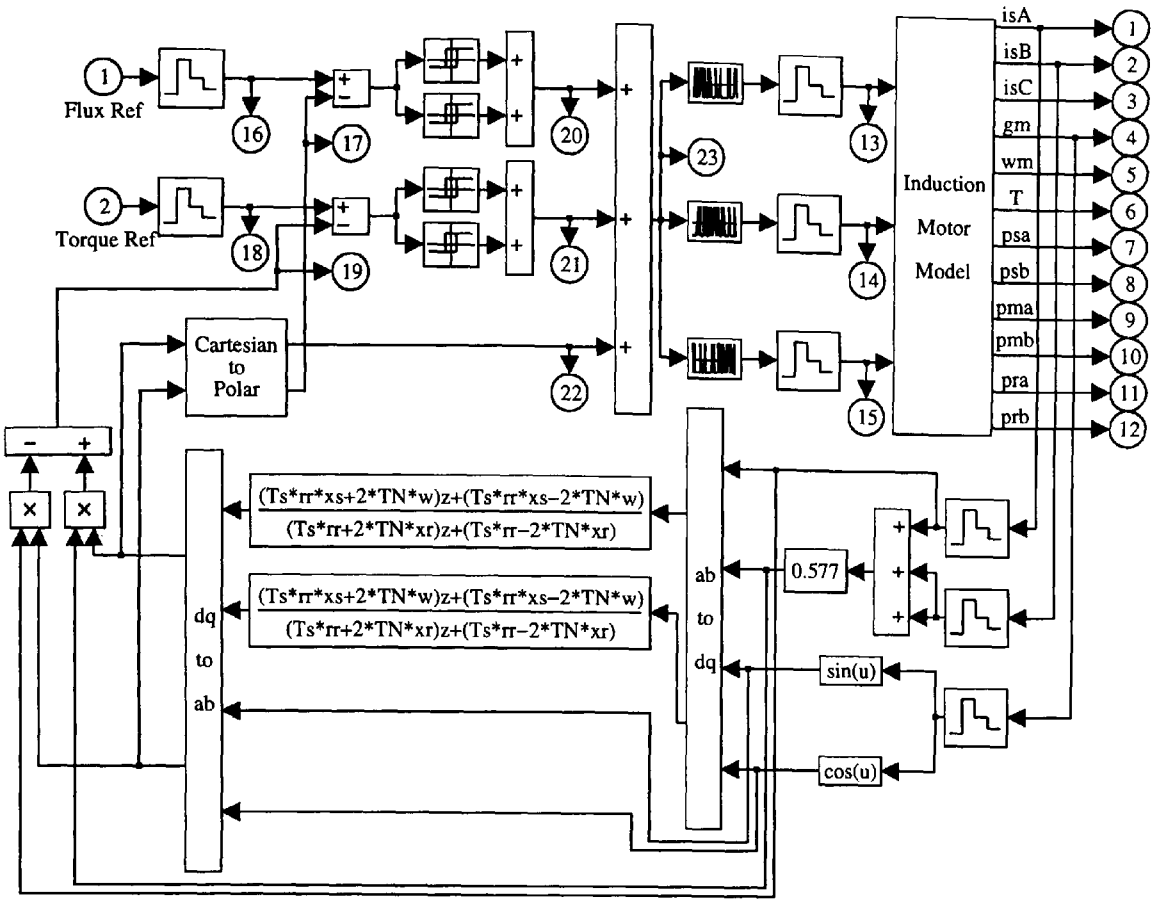

Fig. 7.11: Direct Torque Control System with $i_{sA} - i_{sB} - \gamma_m$ Estimator

The individual stages of the torque and stator flux space vector estimation may be identified from Fig. 7.11 as follows:

The input variables of the estimator are two motor phase currents and the rotor position measured by a shaft encoder. The motor phase currents are converted from the 'A'-'B'-'C' co-ordinate system to the stator oriented $\alpha - \beta$ system. The co-ordinate system is then changed to rotor orientation using the sine and cosine signals of the measured rotor position γ_m. The discrete form of Equ. 7.2 is applied to the stator current components using the discrete Tustin approximation (Equ. 6.9). This results in the stator flux components expressed in rotor oriented co-ordinates. The sine and cosine signals of the measured rotor position are then applied to convert the stator flux components into stator oriented co-ordinates. For the feedback to the direct torque control system both the amplitude of the stator flux vector and the phase sector according to Fig. 7.2 are required. In addition, it may be seen from Fig. 7.11 that the developed motor torque is computed according to Equ. 7.3.

Simulation results of the direct torque control system shown in Fig. 7.11 are shown in Fig. 7.12 to Fig. 7.14.

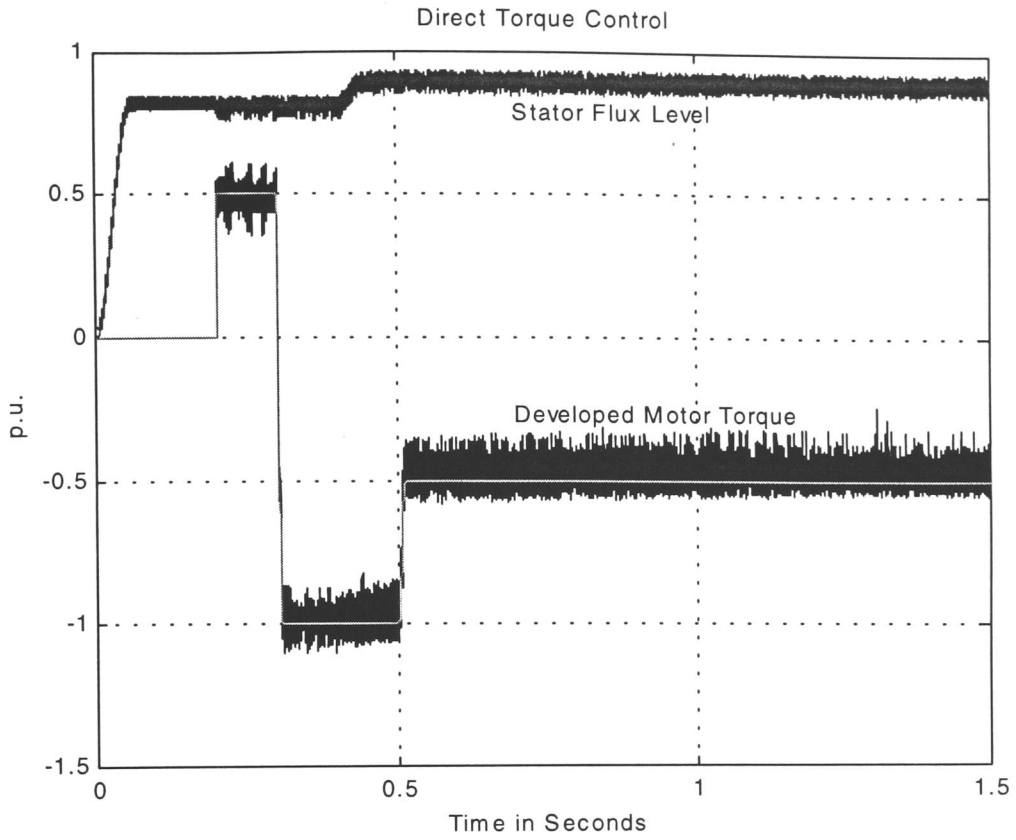

Fig. 7.12: Stator Flux Level and Motor Torque in
Direct Torque Control with $i_{sA} - i_{sB} - \gamma_m$ Estimator

It may be seen that the ideal case, shown in Fig. 7.8 to Fig. 7.10, where the stator flux space vector components and the developed motor torque are accurately measured, is closely resembled by Fig. 7.12 to Fig. 7.14. However, as shown in section 7.5, there is a difference in the performance of the two control systems when the motor parameters used by the estimator depart from the true motor model parameters.

It can be argued that the main advantage of direct torque control - the absence of a co-ordinate transform - is offset by the requirement of a co-ordinate transform for the flux estimation. However, the particular co-ordinate transform used, requires the rotor position angle γ_m, which can be measured with a shaft encoder, whereas in rotor flux oriented flux vector control, the angle of the rotor flux space vector is required which can not be measured directly. Instead, this angle needs to be calculated from the rotor position angle and the slip angle, which can result in considerable errors as shown in section 6.4.

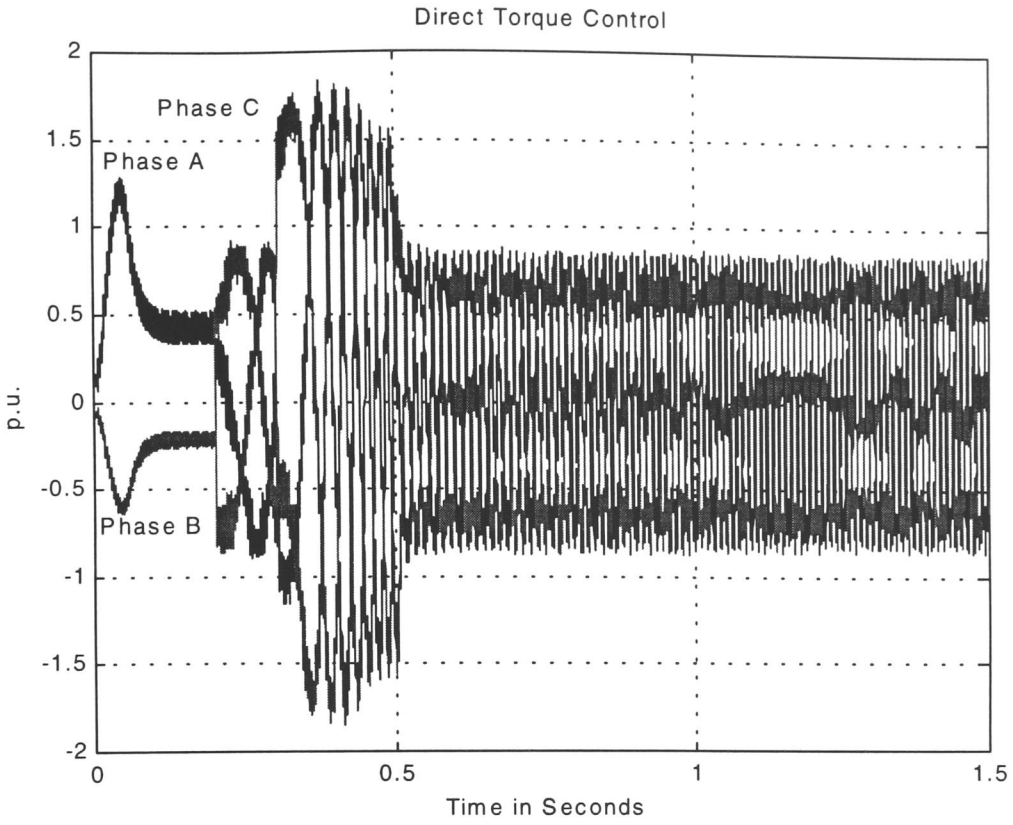

Fig. 7.13: Stator Current Variations in

Direct Torque Control with $i_{sA} - i_{sB} - \gamma_m$ Estimator

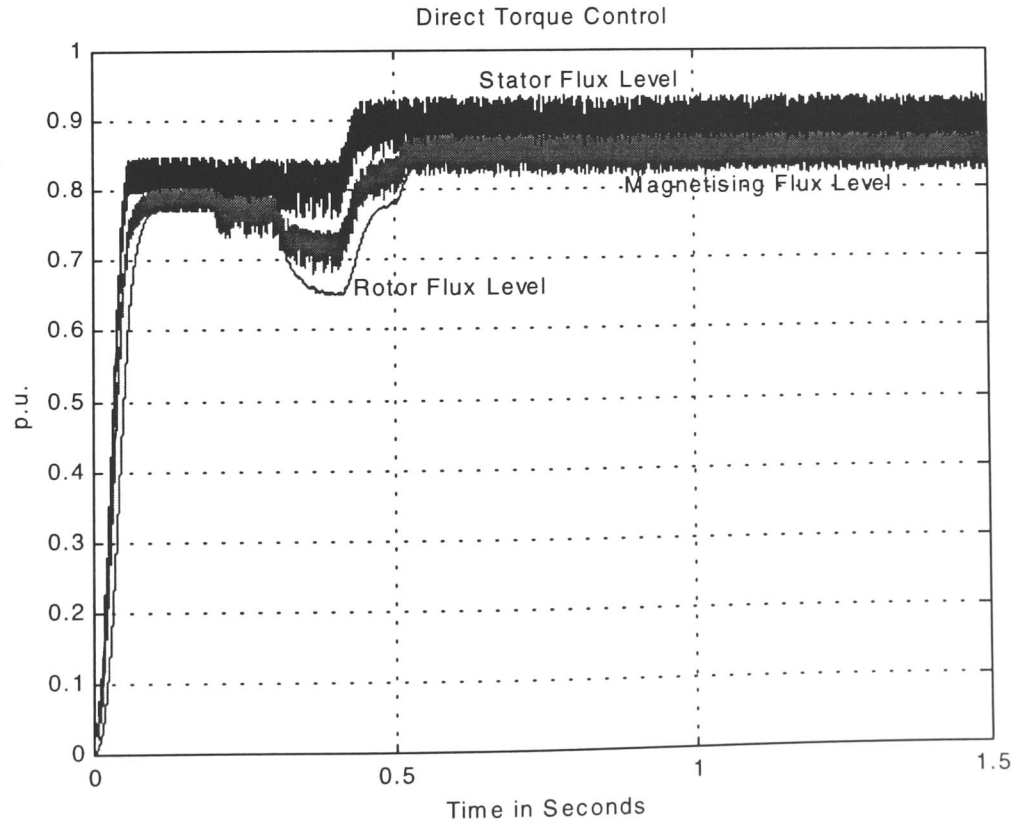

Fig. 7.14: Stator Flux level, Magnetising Flux Level

and Rotor Flux Level in Direct Torque Control with $i_{sA} - i_{sB} - \gamma_m$ Estimator

7.3.2 Direct Torque Control with $i_{sA} - i_{sB} - V_{DC}$ Estimator

In case sensor-less direct torque control is desired, a measured rotor speed or rotor position signal is not available. In order to obtain an estimation of the stator flux space vector, two possible methods may be applied:

1. An estimator which does not require speed or position signals may be used, or
2. The motor speed may be estimated and fed into a flux estimator which relies on speed information.

A stator flux and torque estimation based on the stator voltage equation does not require speed or position information when stationary co-ordinates are applied. In this case, the stator flux space vector may be calculated as follows:

$$\vec{\psi}_s = \frac{\vec{v}_s - r_s \vec{i}_s}{T_N s} \tag{7.4}$$

A direct torque control system with stator flux estimation based on Equ. 7.4 is shown in Fig. 7.15.

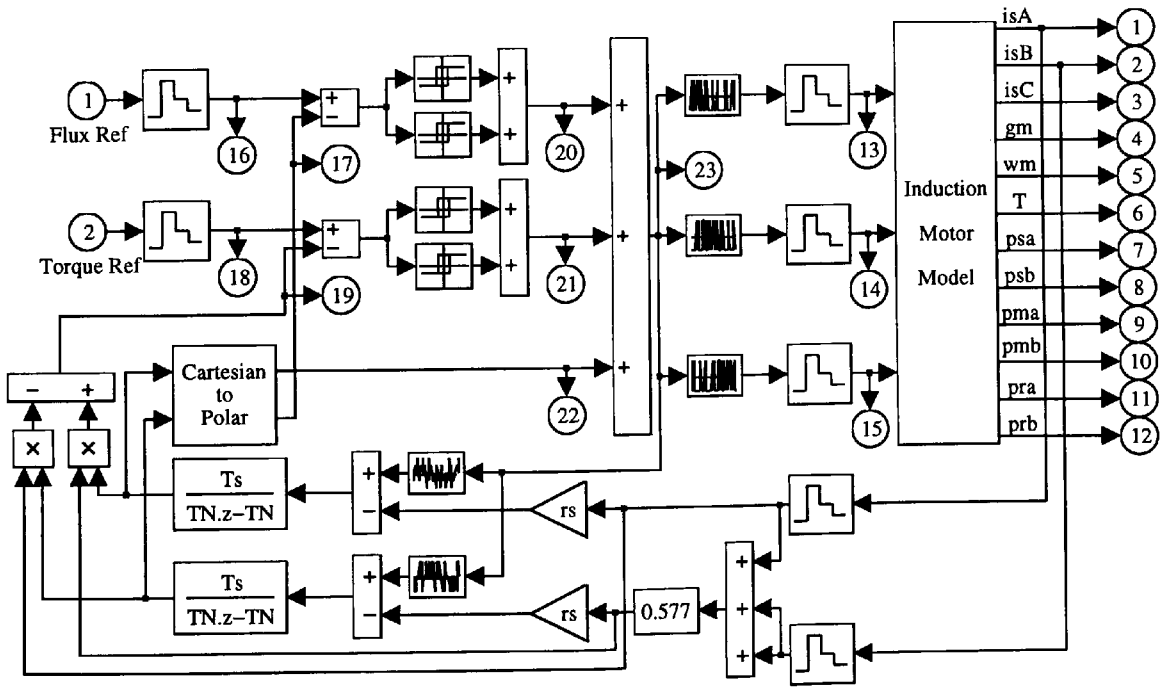

Fig. 7.15: Direct Torque Control System with $i_{sA} - i_{sB} - V_{DC}$ Estimator

It may be see from the system shown in Fig. 7.15, that the stator voltage space vector components are derived from the inverter internal switch settings. This avoids the measurement of the fast varying stator voltages. In practice, the D.C. link voltage is measured from which the α and β components of the stator voltage space vector can be derived.

It should be noted that a co-ordinate transform is not required for the estimator shown in Fig. 7.15. Furthermore, the calculations according to Equ. 7.4 are very simple and can be implemented without imposing high computational demands on the micro processor used for the control of the inverter. However, the accuracy of the estimation is limited because of the open loop integration which can lead to large flux estimation errors (Kazmierkowski 1994).

For the ideal case simulated, however, it can be seen from Fig. 7.16 to Fig. 7.18 that there is virtually no difference to the case where the stator flux space vector and the developed motor torque have been measured (Fig. 7.8 to Fig. 7.10).

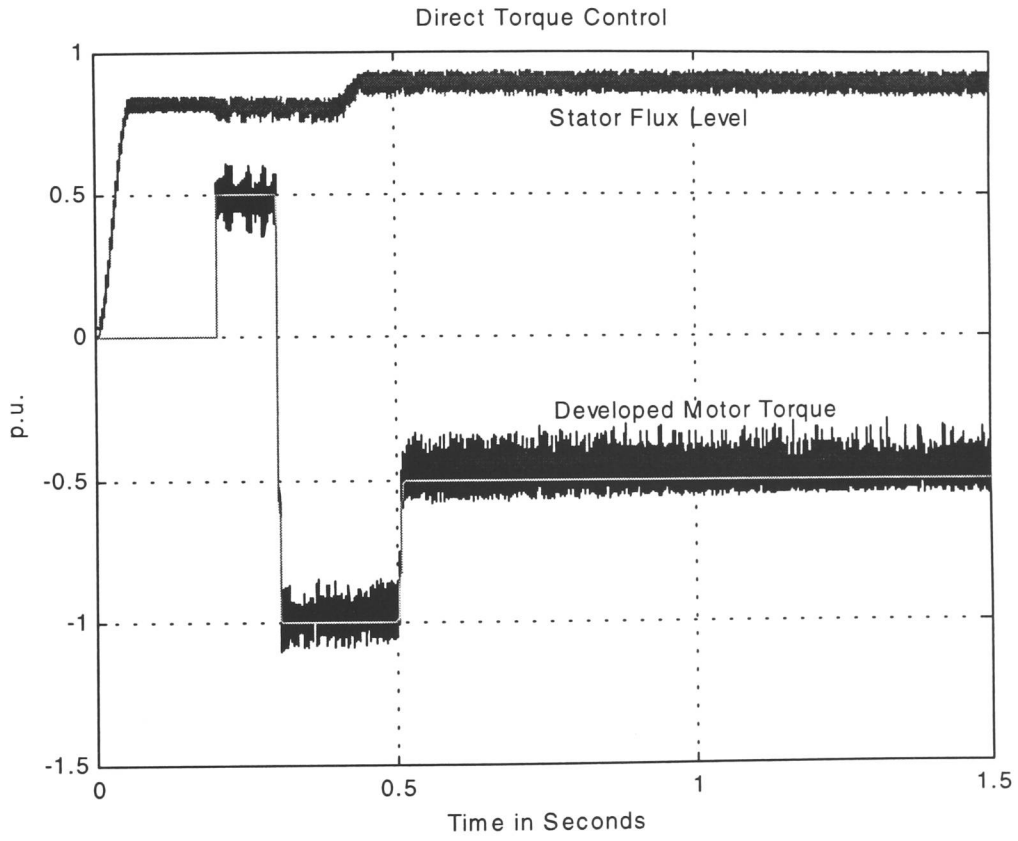

Fig. 7.16: Stator Flux Level and Motor Torque in Direct Torque Control with $i_{sA} - i_{sB} - V_{DC}$ Estimator

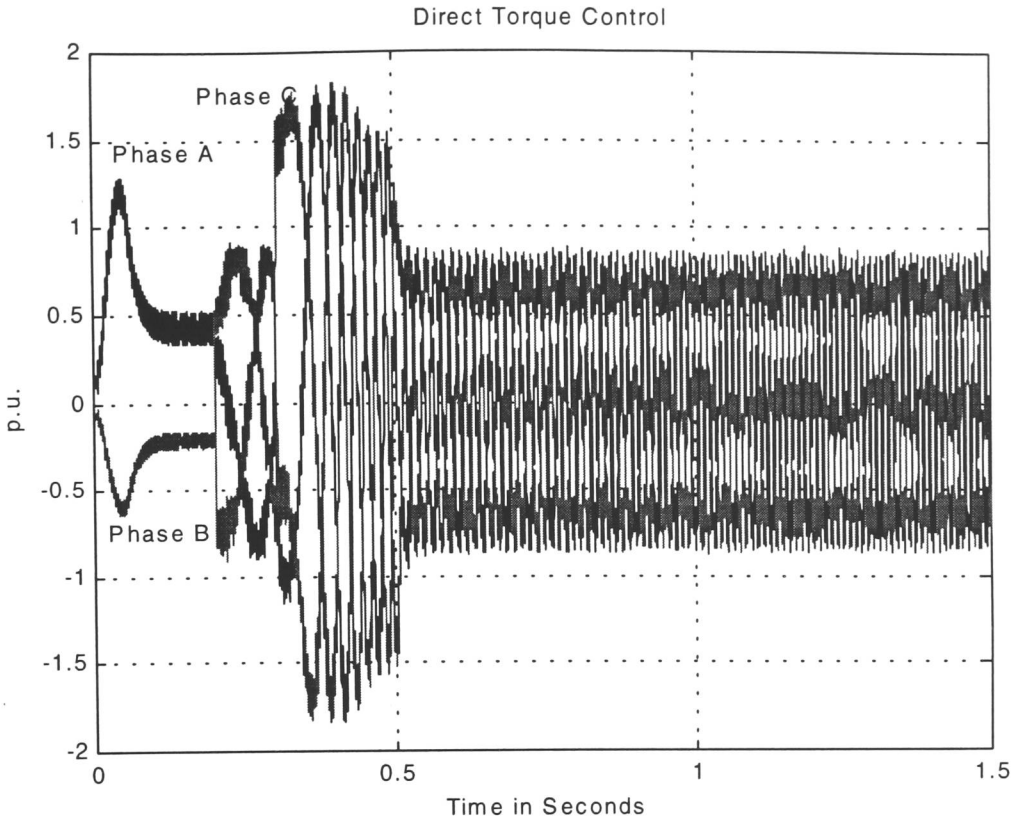

Fig. 7.17: Stator Current Variations in

Direct Torque Control with $i_{sA} - i_{sB} - V_{DC}$ Estimator

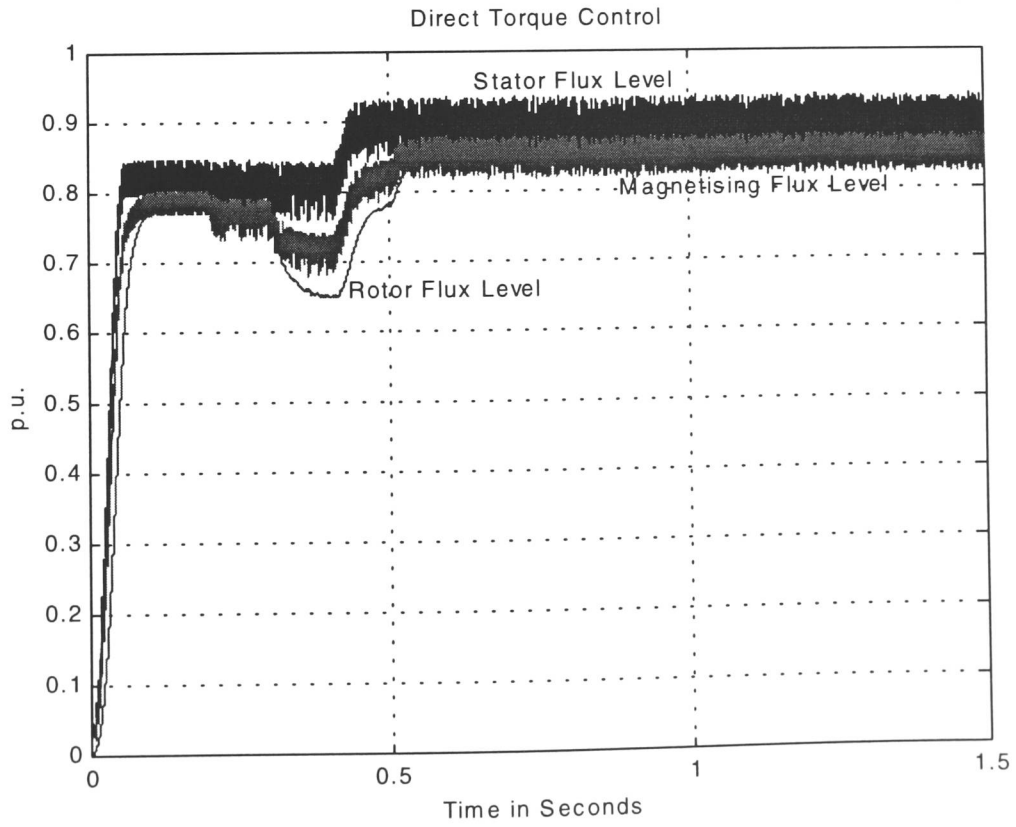

Fig. 7.18: Stator Flux level, Magnetising Flux Level

and Rotor Flux Level in Direct Torque Control with $i_{sA} - i_{sB} - V_{DC}$ Estimator

7.3.3 Direct Torque Control with $i_{sA} - i_{sB} - \omega_m$ Estimator

Another variation of stator flux space vector estimation which does not require a co-ordinate transform may be obtained as follows: The motor model equations in stator fixed co-ordinates are given by Equ. 2.74. The rotor voltage equation (Equ. 2.74b) may be rearranged to give the rotor current space vector. This result may be substituted into the rotor flux linkage equation (Equ. 2.74d). On rearranging the result for the rotor flux space vector, the following expression may be obtained:

$$\vec{\psi}_r = \vec{i}_s \frac{r_r x_m}{r_r - j\omega_m x_r + T_N s x_r} \tag{7.5}$$

The stator flux space vector may be obtained from the rotor flux space vector and the stator current space vector on substitution of Equ. 2.74d into Equ. 2.74c.

$$\vec{\psi}_s = \frac{x_s x_r - x_M^2}{x_r} \vec{i}_s + \frac{x_M}{x_r} \vec{\psi}_r \tag{7.6}$$

A direct torque control system using the estimator described by Equ. 7.5 and Equ. 7.6 is shown in Fig. 7.19.

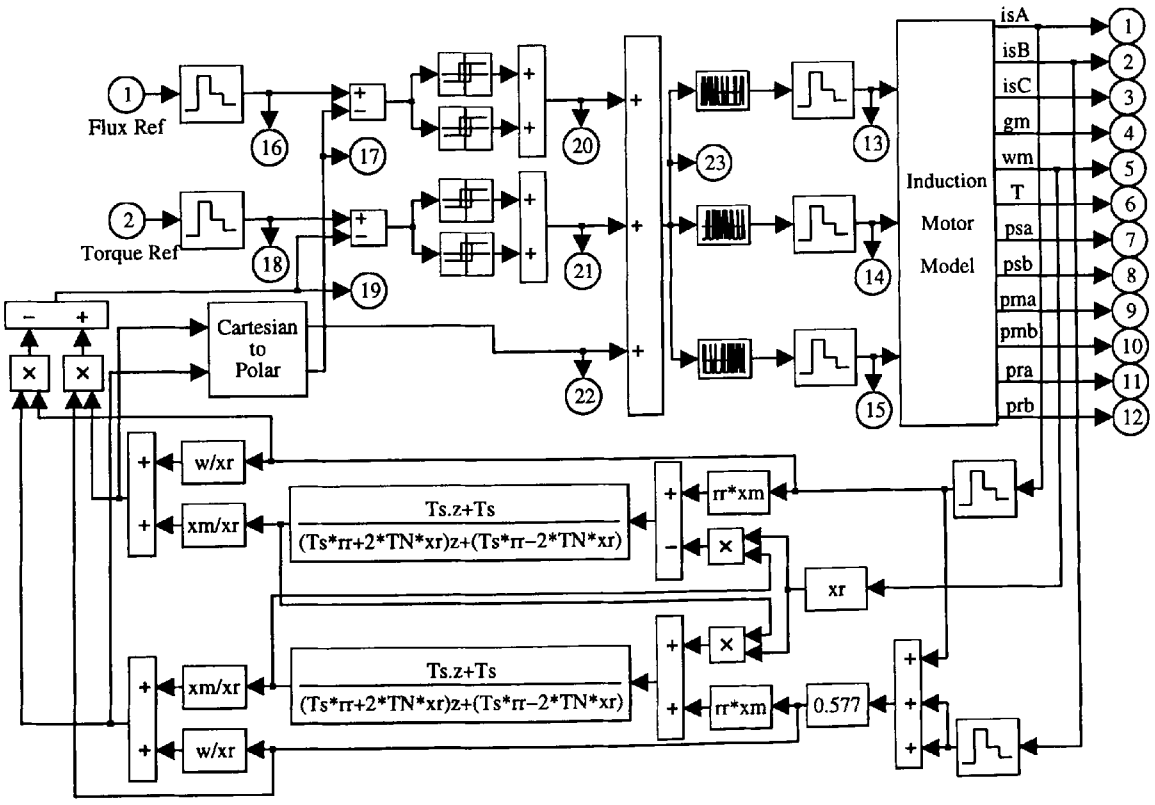

Fig. 7.19: Direct Torque Control System with $i_{sA} - i_{sB} - \omega_m$ Estimator

Simulation results of the system shown in Fig. 7.19 are shown in Fig. 7.20 to Fig. 7.22.

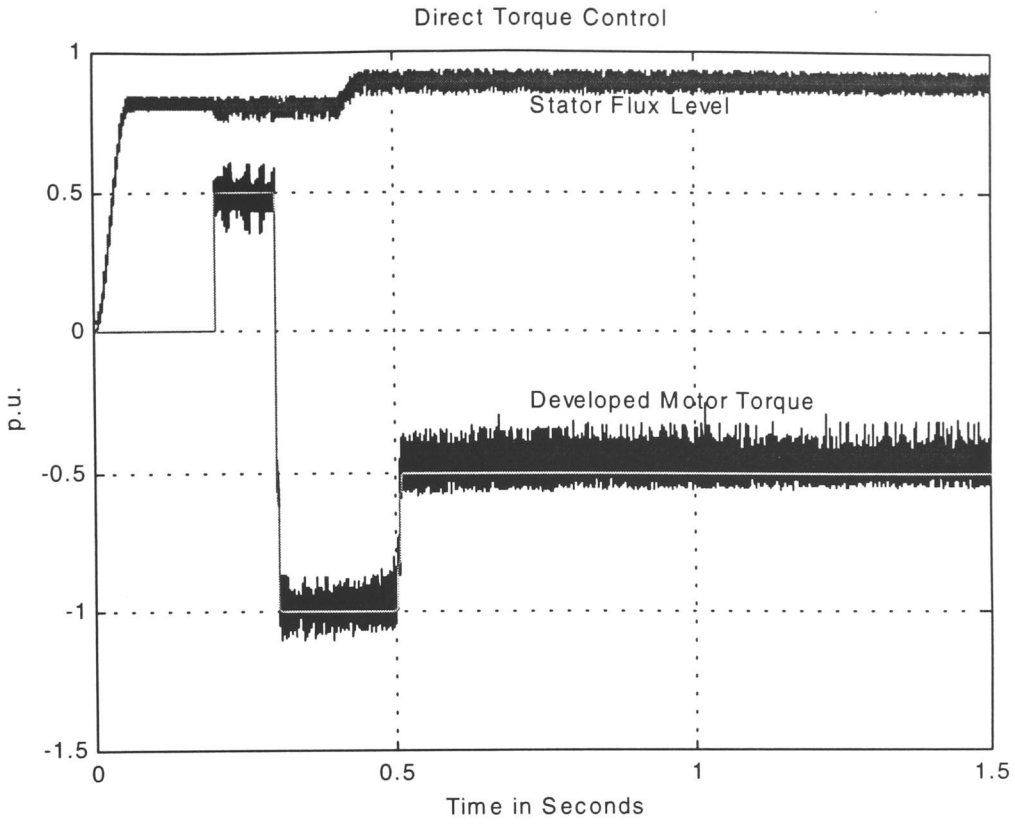

Fig. 7.20: Stator Flux Level and Motor Torque in Direct Torque Control with $i_{sA} - i_{sB} - \omega_m$ Estimator

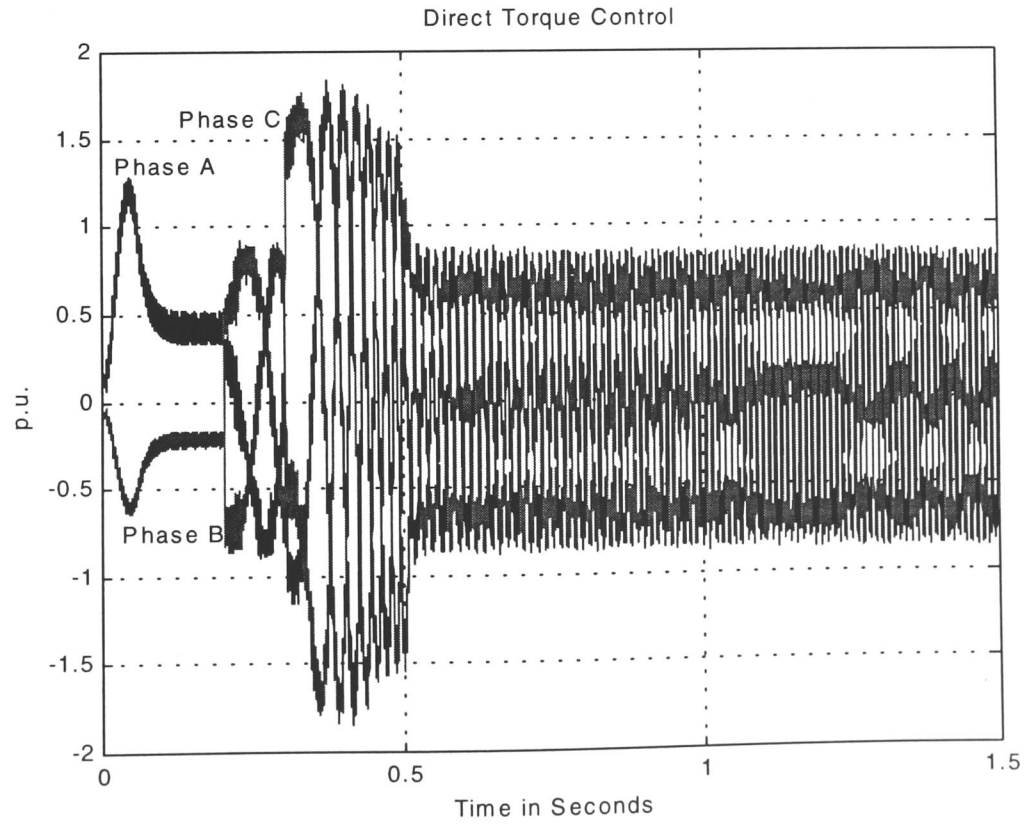

Fig. 7.21: Stator Current Variations in Direct Torque Control with $i_{sA} - i_{sB} - \omega_m$ Estimator

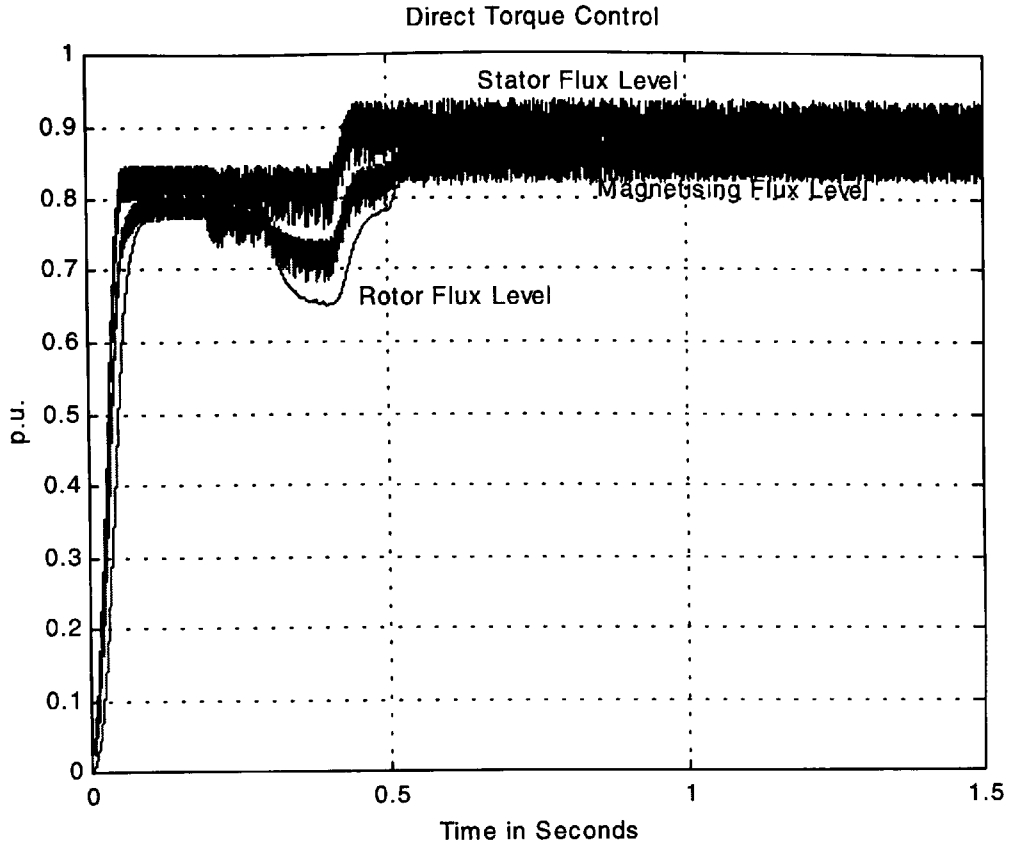

Fig. 7.22: Stator Flux level, Magnetising Flux Level
and Rotor Flux Level in Direct Torque Control with $i_{sA} - i_{sB} - \omega_m$ Estimator

The Fig. 7.20 to Fig. 7.21 shown that there is virtually no difference to the ideal case depicted in Fig. 7.8 to Fig. 7.10.

7.4 Parameter Detuning Effects

The direct torque control systems shown in Fig. 7.11, Fig. 7.15 and Fig. 7.19 all depart from their ideal behaviour when the motor model parameters used are different from the true motor model parameters. The stator flux estimation with the $i_{sA} - i_{sB} - \gamma_m$ estimator and the $i_{sA} - i_{sB} - \omega_m$ estimator have similar characteristics, which are described below. However, the direct torque control system with the stator flux estimation according to the $i_{sA} - i_{sB} - V_{DC}$ estimator, performed very poorly, thus this system is not considered here. The control characteristics of stator flux and motor torque, for the direct torque control systems shown in Fig. 7.11 and Fig. 7.19, when the rotor resistance, the magnetising inductance, the stator leakage inductance and the rotor leakage inductance divert from the true model parameters, are shown in Fig. 7.23 to 7.30.

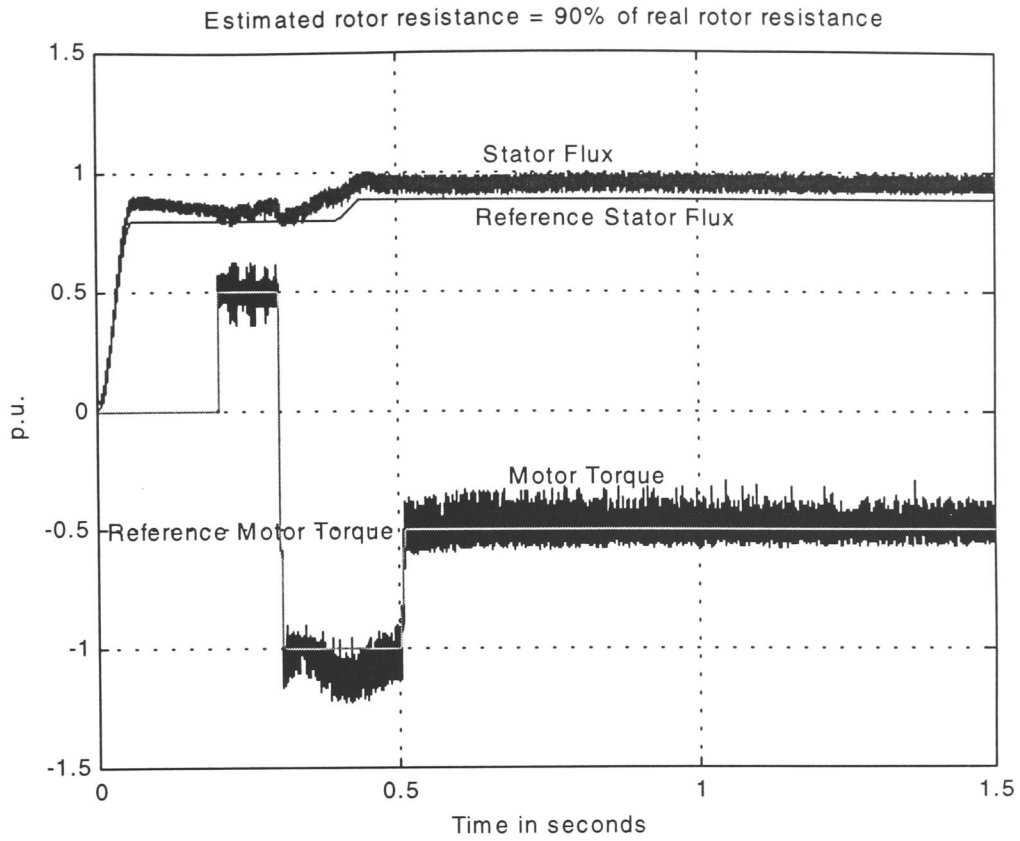

Fig. 7.23: Direct Torque Control with detuned parameters: $r_{rc} = 0.9r_r$

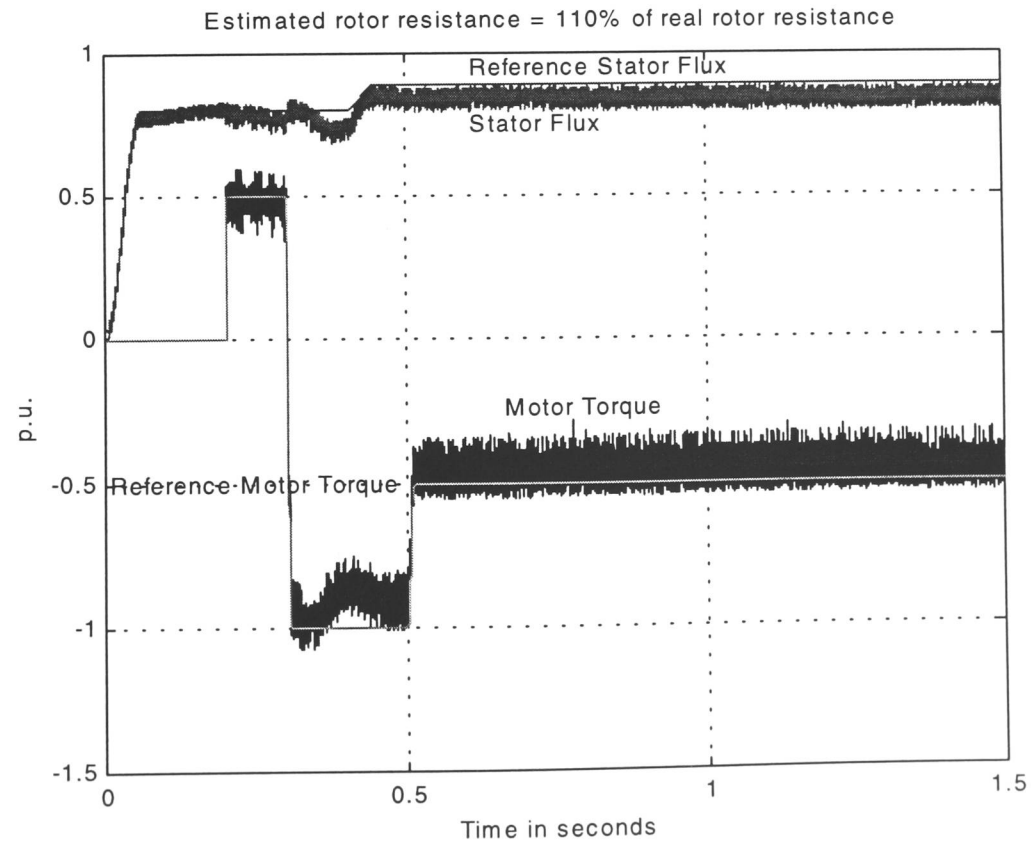

Fig. 7.24: Direct Torque Control with detuned parameters: $r_{rc} = 1.1r_r$

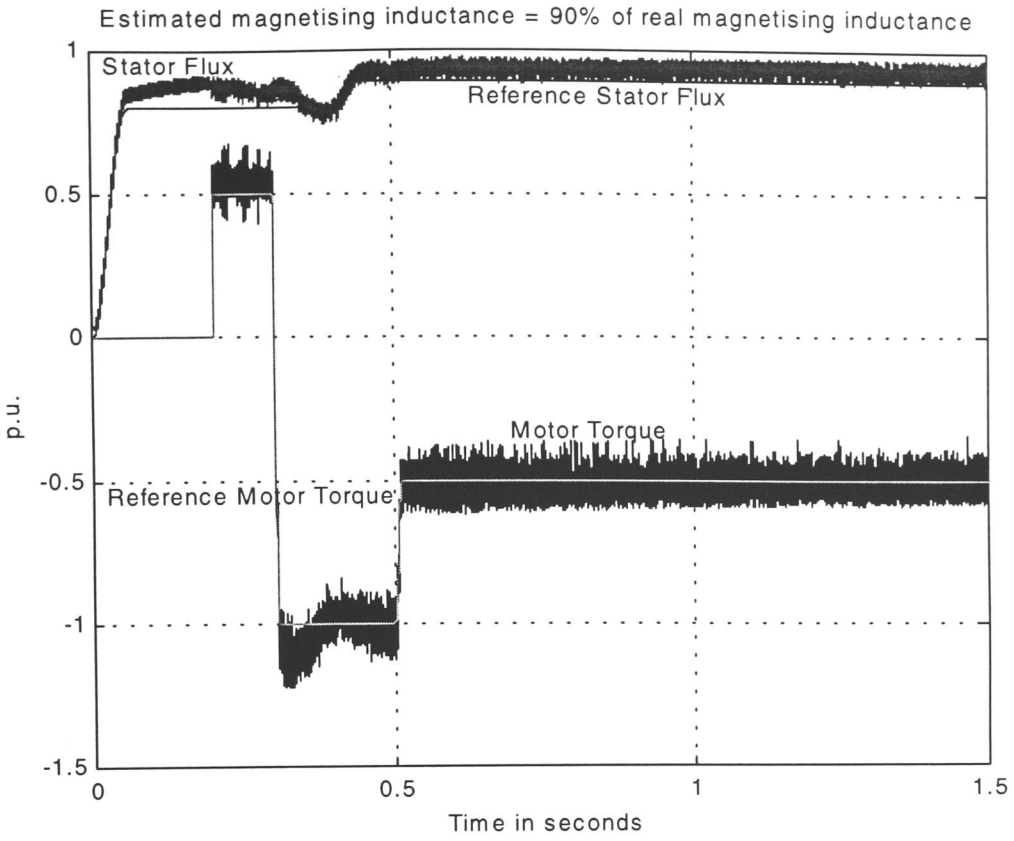

Fig. 7.25: Direct Torque Control with detuned parameters: $x_{Mc} = 0.9x_M$

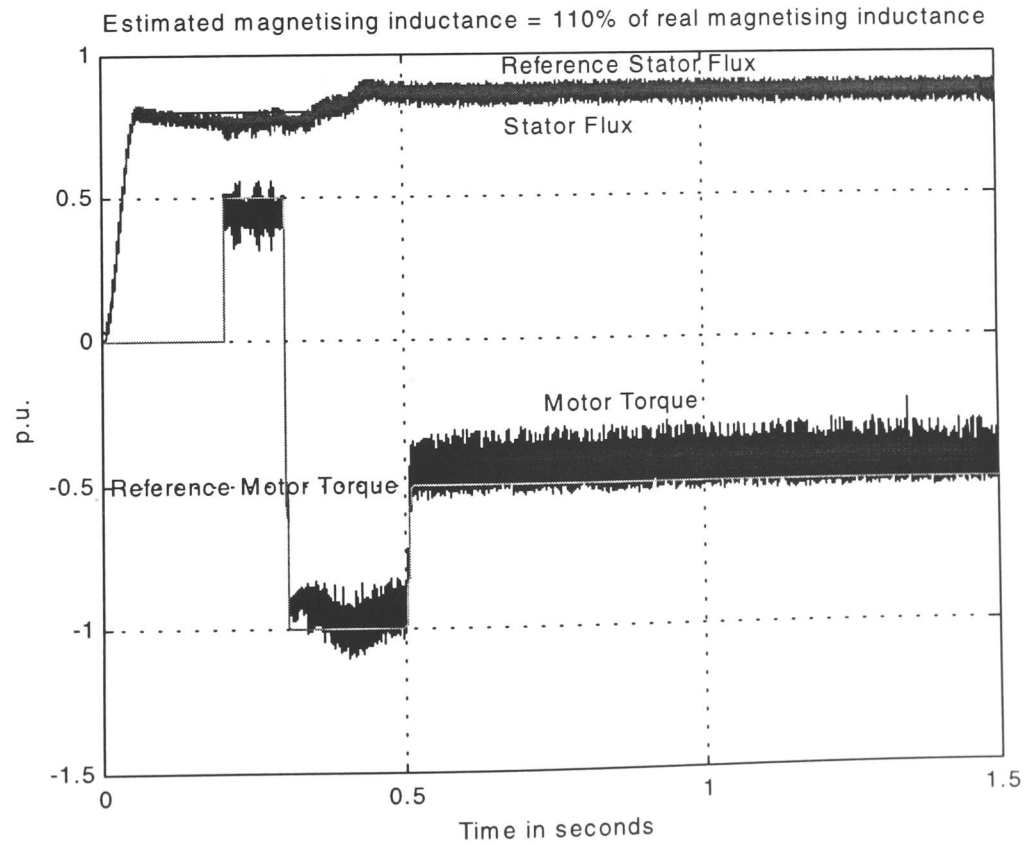

Fig. 7.26: Direct Torque Control with detuned parameters: $x_{Mc} = 1.1x_M$

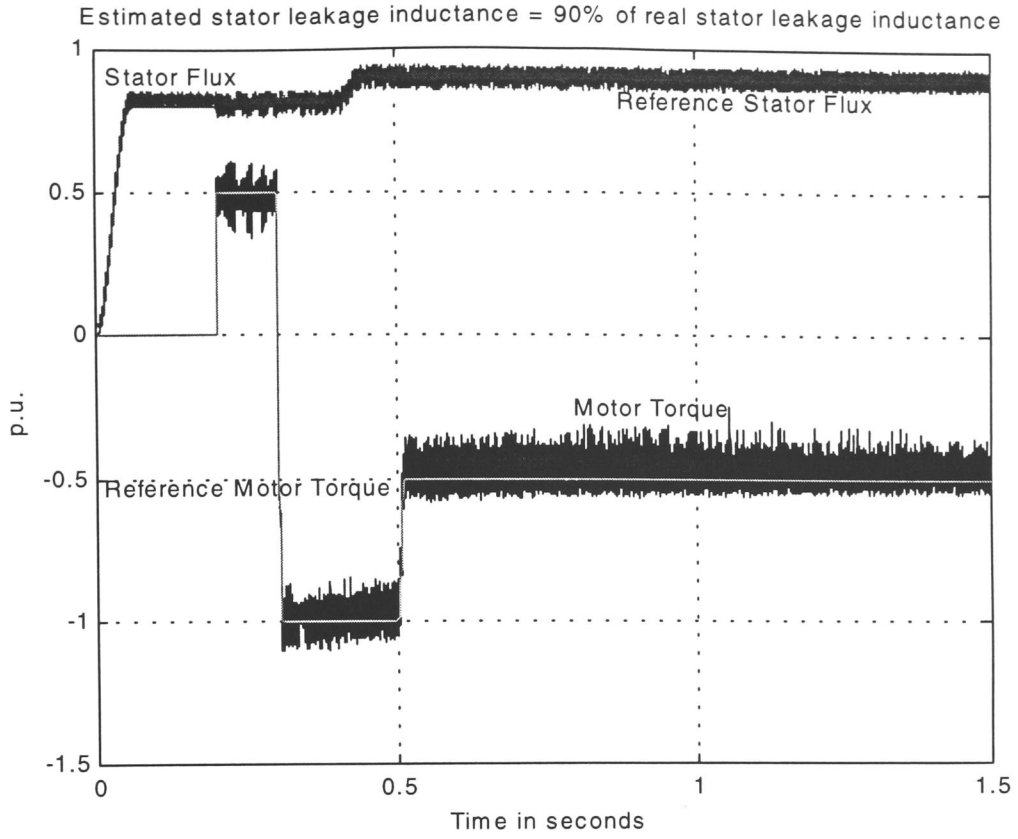

Fig. 7.27: Direct Torque Control with detuned parameters: $x_{lsc} = 0.9x_{ls}$

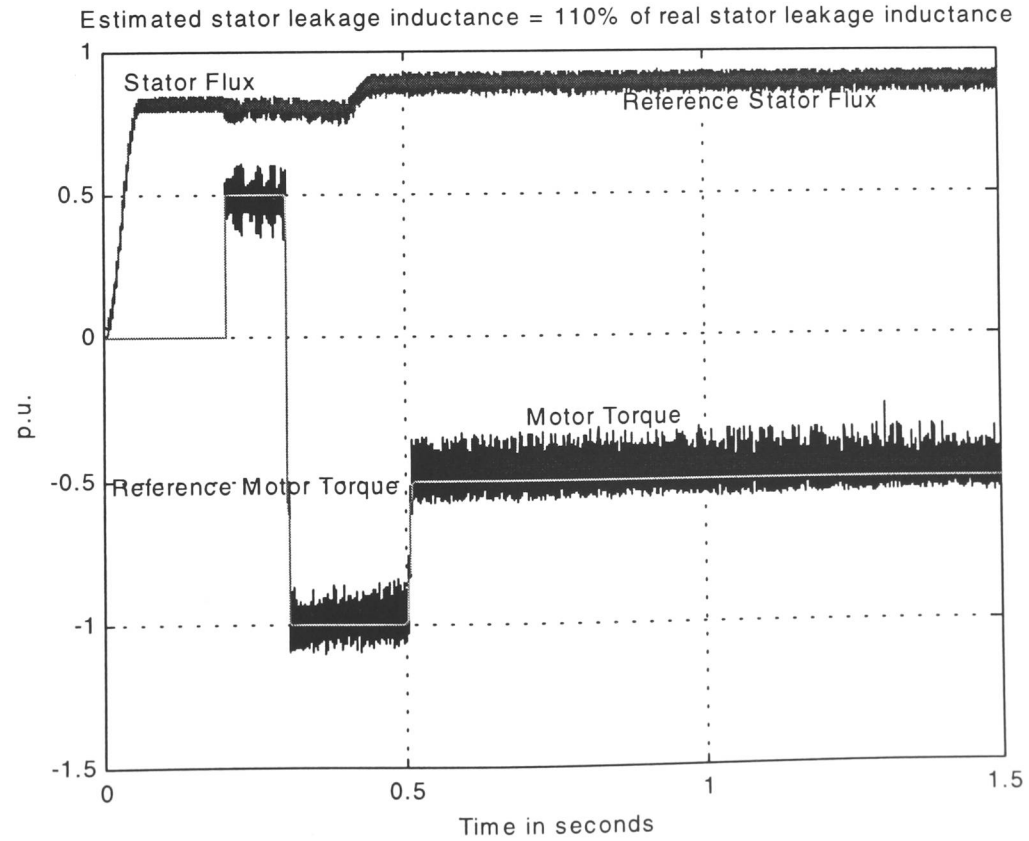

Fig. 7.28: Direct Torque Control with detuned parameters: $x_{lsc} = 1.1x_{ls}$

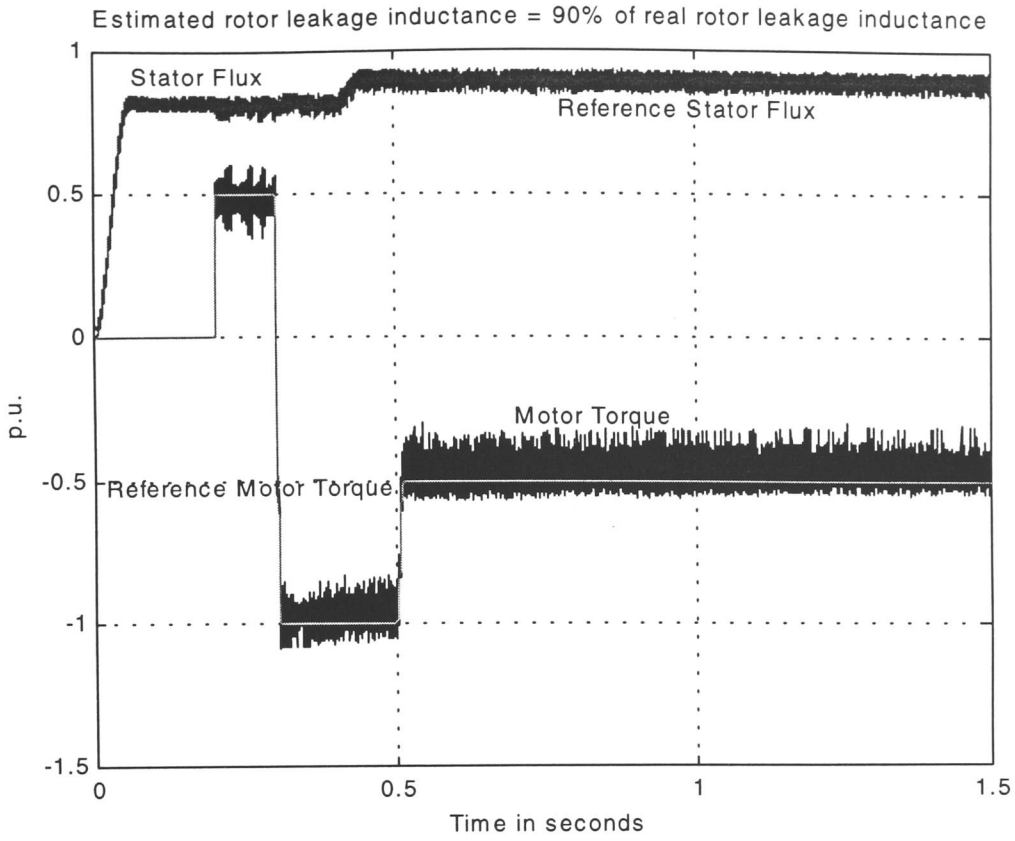

Fig. 7.29: Direct Torque Control with detuned parameters: $x_{lrc} = 0.9x_{lr}$

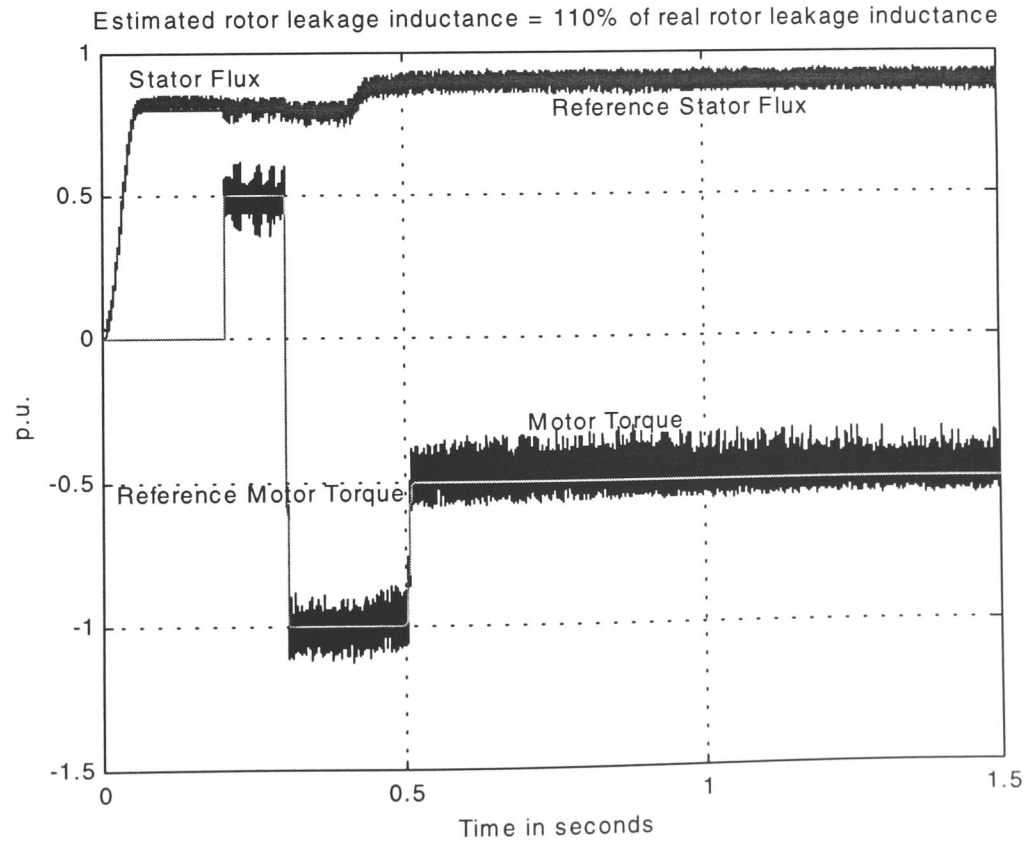

Fig. 7.30: Direct Torque Control with detuned parameters: $x_{lrc} = 1.1x_{lr}$

In Fig. 7.23 and Fig. 7.24, the effect on the control characteristic of stator flux level and motor torque is shown for a variation of the rotor resistance from the true rotor resistance by 10%. It can be seen that both transient and steady state variations from the reference values occur. The comparison to the simulation results for flux vector control shown in Fig. 6.31 and Fig. 6.32 shows similar characteristics in both cases.

The effect of the variation of magnetising inductance on the control characteristics of stator flux level and motor torque is shown in Fig. 7.25 and Fig. 7.26. Similarly to the variation of rotor resistance, steady state and transient state variations of the stator flux level and the developed motor torque occur. In comparison to the flux vector control case in Fig. 6.33 and 6.34 the variations are very similar.

The variation in control behaviour when the stator leakage inductance or the rotor leakage inductance departs from its true motor model value, shown in Fig. 7.27 to Fig. 7.30, are virtually not noticeable.

7.5 Effect of the Application of a Voltage Vector on the Flux and Torque of a Cage Rotor Induction Motor

The main difference between conventional operation of p.w.m. inverters and direct torque control (DTC) operation is that in the DTC speed control system the output voltages from the inverter are always applied to the motor at instants corresponding to multiples of the sampling time T_s. This difference is illustrated in Fig. 7.31.

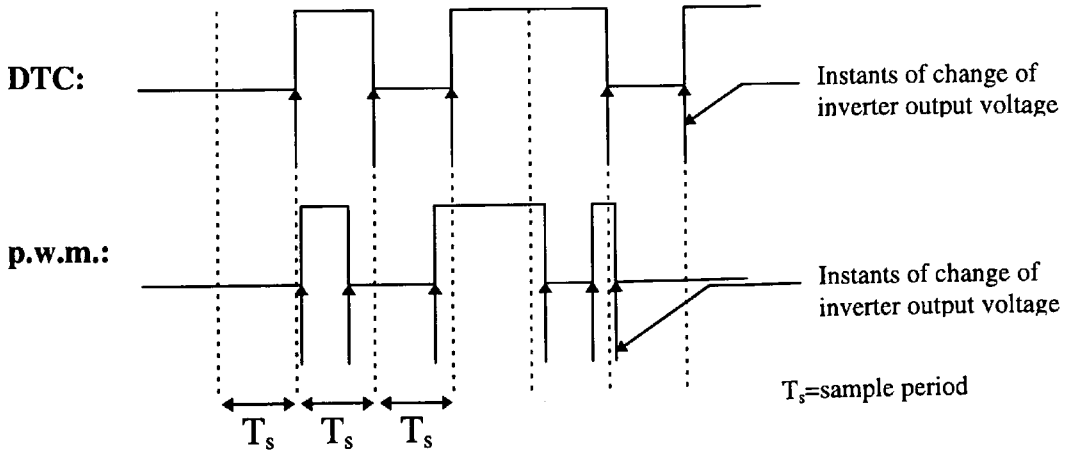

Fig. 7.31: Comparison of Switching Instants for DTC and p.w.m.

Thus, for the application of a three phase set of inverter output voltages to the motor for a duration T_s when the motor is in a known state, the calculated effects in terms of change of motor flux and motor torque are shown in Fig. 7.32. This initial motor state has been

determined from the steady state model of the induction motor, where constraints such as maximum efficiency under light load operation, maximum stator flux operation and maximum stator voltage operation have been taken into account. It may be seen from Fig. 7.32 that the voltage vectors $\vec{v}_1$ to $\vec{v}_6$ can all have the same effect on stator flux level and motor torque depending on the stator flux angle. However, normally an independent variation of both stator flux level and motor torque is required at the same time in order to provide the decoupling between flux and torque. It may be seen from Fig. 7.32 that, for example, at a stator flux angle of 30 degrees only voltage vector $\vec{v}_1$ will provide a 4% increase in stator flux level and a 8% decrease of motor torque.

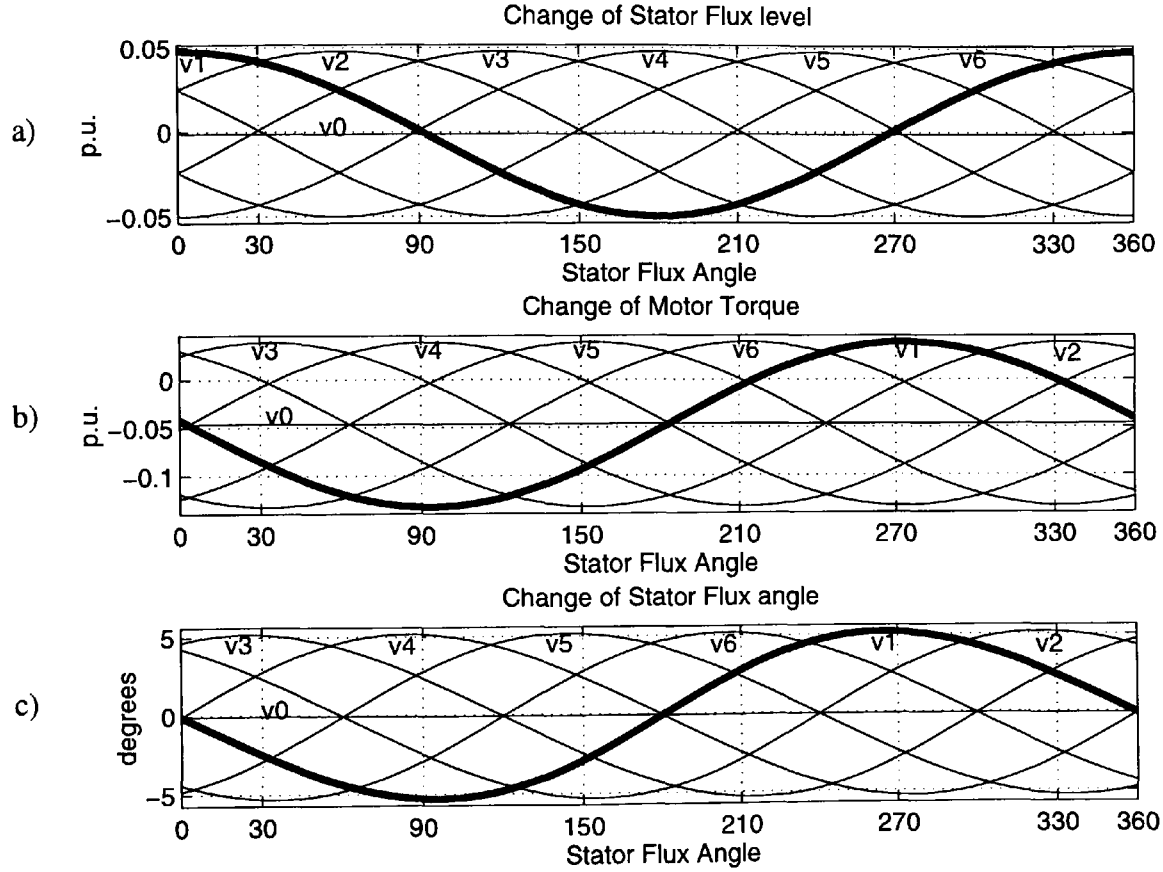

Fig. 7.32:The effect of the application of voltage vectors $\vec{v}_0$ to $\vec{v}_6$ for a sampling time of T_s=150μs for varying stator flux angles in terms of a) Stator flux level, b) Motor torque and c) Stator flux angle. Initial motor state: T_l=0.1p.u., ω_m=1p.u.

However, for the ideal case of steady state operation, neither variation of stator flux or motor torque is required. It may also be seen from Fig. 7.32 that the variation of stator flux level and motor torque caused by the application of each voltage vector passes through zero for two different angles for each voltage vector. For example, voltage vector $\vec{v}_1$ (shown in bold in Fig. 7.32) passes through the zero crossing points at 90 and 270 degrees for the stator flux level variation and at 215 and 330 degrees for the motor torque

variation. However, though the application of voltage vector $\vec{v}_1$ for a stator flux angle of 90 degrees keeps the stator flux level constant, the corresponding torque change will be a reduction in torque by 0.17p.u. and therefore voltage vector $\vec{v}_1$ is not appropriate for this particular steady state case. However, it can be appreciated that ripples in both stator flux level and motor torque are inevitable and that a selection procedure is desirable which keeps these variations to a minimum. Selection of the voltage vector $\vec{v}_0$ keeps the stator flux level almost constant but reduces the motor torque by about 0.05 p.u. regardless of stator flux angle.

The effect of the application of the voltage vectors on stator flux level, motor torque and stator flux angle is of course dependent upon the operation conditions of the motor. This is illustrated in Fig. 7.33, where a high torque-zero speed motor state has been considered.

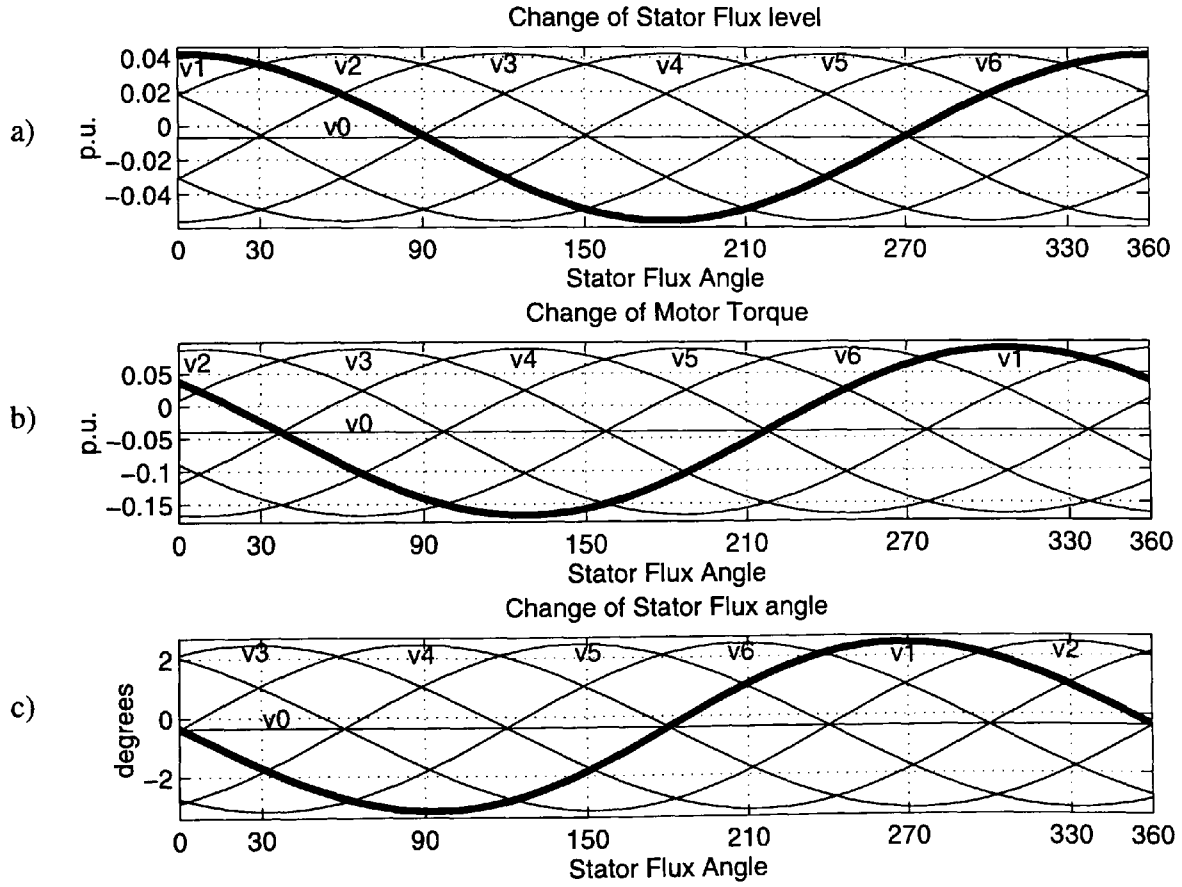

Fig. 7.33:The effect of the application of voltage vectors $\vec{v}_0$ to $\vec{v}_6$ for a sampling time of T_s=150μs for varying stator flux angles in terms of a) Stator flux level, b) Motor torque and c) Stator flux angle. Initial motor state: T_L=1.6p.u., ω_m=0p.u.

The comparison of figures 7.32 and 7.33 shows a number of differences. The application of voltage vector $\vec{v}_0$ causes a larger decrease of the stator flux level but a smaller

decrease of the motor torque. The maximum changes of motor torque have increased and also the stator flux angles for which maximum torque changes are caused by the application of the voltage vectors $\vec{v}_1$ to $\vec{v}_6$, have increased by approximately 35 degrees. It may similarly be seen that the corresponding change of the stator flux angle has changed to approximately half the value in Fig. 7.33.

Fig. 7.34 illustrates the effect of motor operating conditions on the maximum positive and maximum negative changes of stator flux level due to the application of voltage vectors $\vec{v}_1$ to $\vec{v}_6$. The variation of the stator flux level due to the application of voltage vector $\vec{v}_0$ is also shown. As can be seen, there is only a marginal dependence on rotor speed (curves are essentially parallel to the x-axis) and a small dependence on the motor torque. For small values of load torque it can be seen from curves (a) in Fig. 7.34 that the achievable stator flux change becomes larger. Similarly, from the curves corresponding to (b) in Fig. 7.34 it can be seen that the changes in stator flux level become less for small values of load torque. Also, from curves (c) it can be seen that the smaller the value of load torque, the smaller the achievable reduction in stator flux.

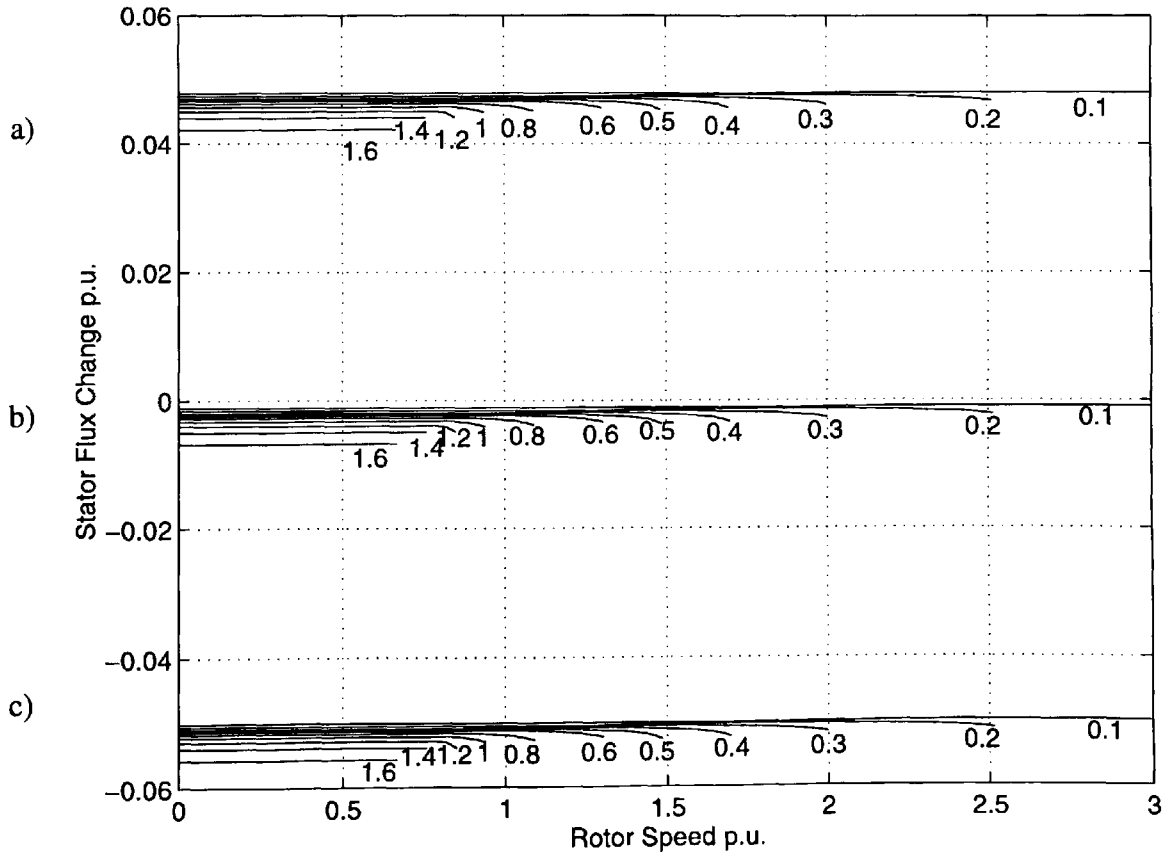

Fig. 7.34:The effect of initial rotor speed and motor torque on the stator flux level change due to the application of voltage vectors $\vec{v}_0$ to $\vec{v}_6$ for a sampling time of T_s=150μs. Parameter: Motor torque p.u. a) maximum positive change b) change due to selection of $\vec{v}_0$ c) maximum negative change

In Fig. 7.35 the stator flux angles are shown for which the maximum reduction of the stator flux level is achieved. It may be seen that the overall angle variation with motor torque and stator flux is very low (< 0.32 degrees) and the influence can therefore be neglected.

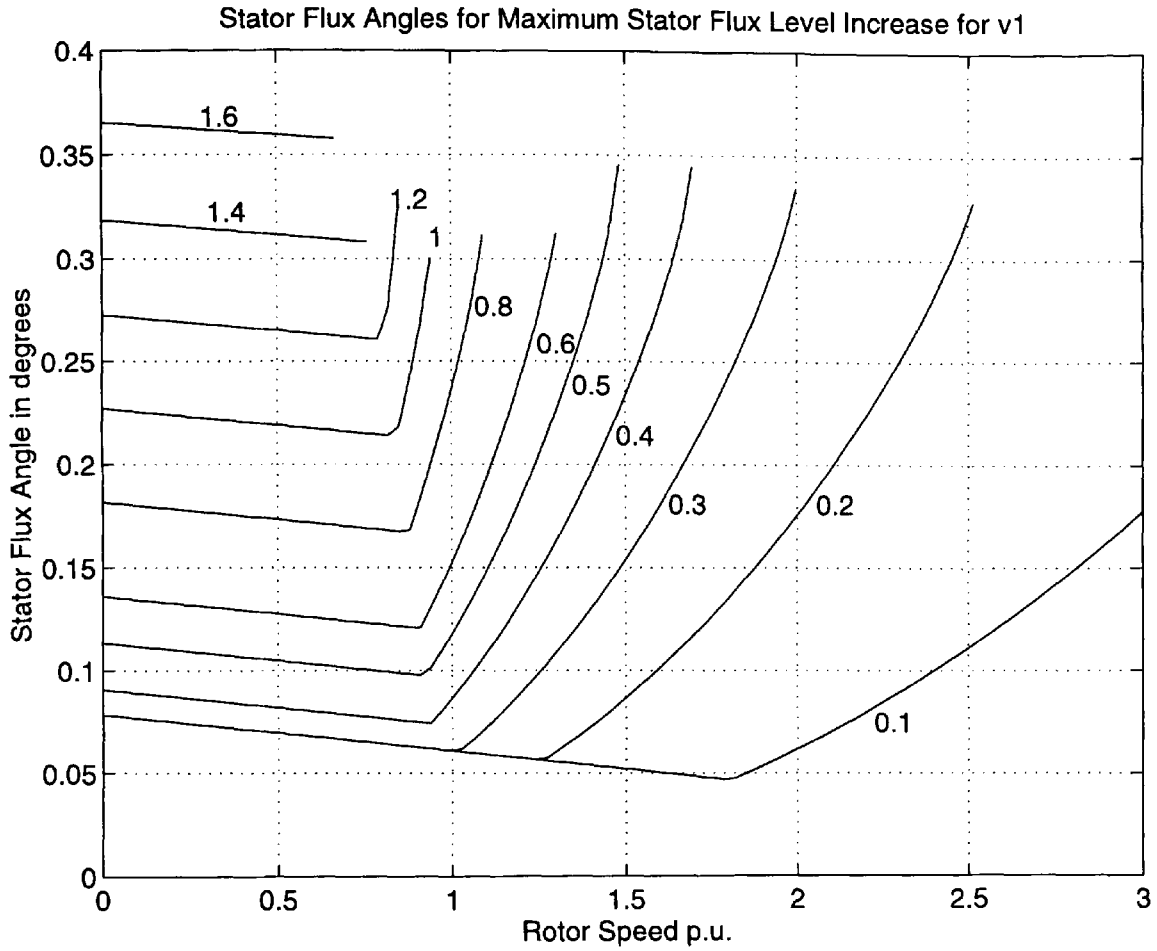

Fig. 7.35:The effect of initial rotor speed and motor torque on the stator flux angle for which a maximum stator flux level reduction is obtained when voltage vector $\vec{v}_1$ is selected. Sampling time T_s=150μs. Parameter: Motor torque p.u.

The same plot is obtained for the stator flux angles at which selection of voltage vector $\vec{v}_1$ causes a maximum increase in stator flux level. The angle variation is thereby the same, but all angles are increased by 180 degrees.

It can therefore be said that the influence of the motor operating condition on stator flux variation is minimal and can be neglected.

However, as has be seen on Fig. 7.32 and 7.33, the influence of the motor conditions on the motor torque changes is substantially bigger than those for the stator flux level change. The maximum torque increase and decrease levels are shown in Fig. 7.36.

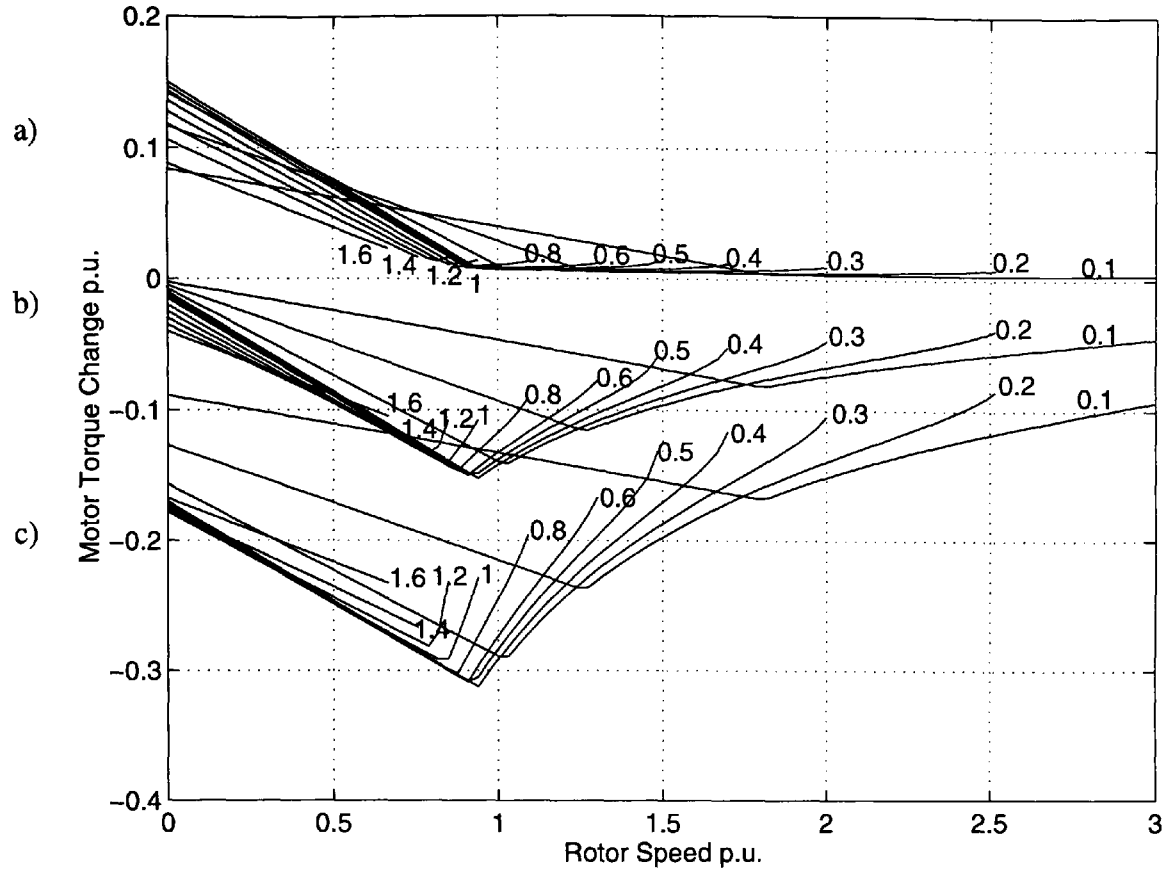

Fig. 7.36:The effect of initial rotor speed and motor torque on the motor torque change due to the application of voltage vectors $\vec{v}_0$ to $\vec{v}_6$ for a sampling time of T_s=150μs. Parameter: Motor torque p.u. a) maximum positive change b) change due to selection of $\vec{v}_0$ c) maximum negative change

It can clearly be seen that there is a big influence of both the motor torque and the rotor speed on the motor torque changes due to the application of a voltage vector for the sampling time T_s. The maximum positive torque change is obtained at zero speed for medium loads (stator flux level =1p.u.). The maximum negative torque change is obtained near rated speed for medium loads (ω_m=0.95p.u., T_l=0.4p.u.). The minimum torque reduction is obtained for light loads at low speed by selecting voltage vector $\vec{v}_0$, whereas the minimum torque increase is obtained for light load at high speed. There is also a region where the maximum torque decrease with one of the decelerating vectors can be less than with voltage vector $\vec{v}_0$, depending on the load conditions (ω_m=0.95 p.u. ΔT_l=-0.14p.u.). The maximum torque increase for high speed operation is always very much less than the maximum torque reduction or the reduction obtained for voltage vector $\vec{v}_0$.

It is not only the effect of the application of voltage vectors which varies with motor load conditions (Fig. 7.36), but also the stator flux angle at which maximum and minimum changes occur, as shown in Fig. 7.37.

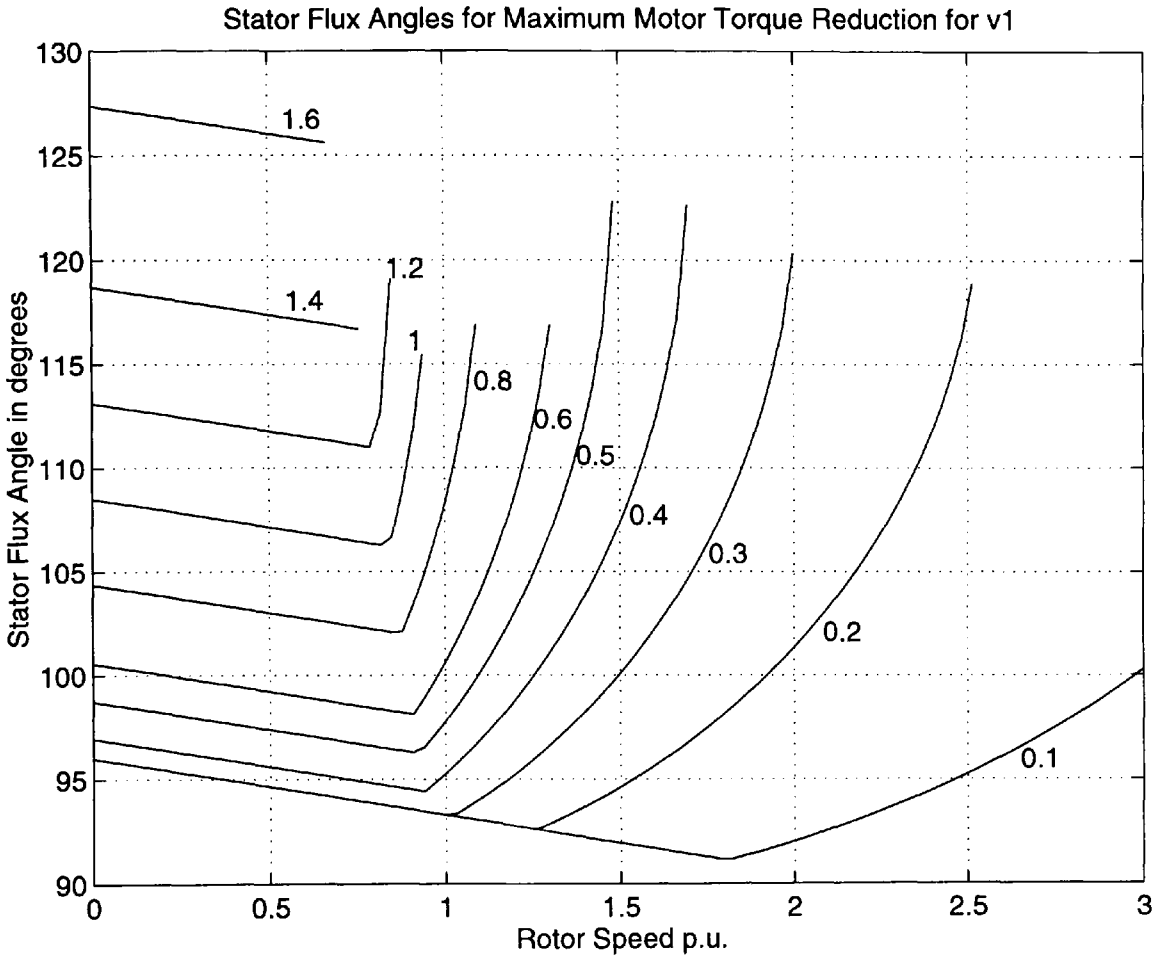

Fig. 7.37:The effect of initial rotor speed and motor torque on the stator flux angle for which maximum motor torque reduction is obtained when voltage vector $\vec{v}_1$ is selected. Sampling time T_s=150μs. Parameter: Motor torque p.u.

The general characteristic of the curves shown in Fig. 7.37 corresponds to Fig. 7.35 where the angles which cause maximum increase and decrease of the stator flux level are shown. It also corresponds to the general VVVF slip frequency characteristic shown in Fig. 3.20. For the motor torque and rotor speeds shown, the stator flux angle varies by 36.2 degrees, which does have an considerable effect on the performance of direct torque control. The angles are equal for constant slip frequency operation (T_l=0.1...0.3p.u. and generally decrease with rotor speed for VVVF operation. When the inverter has run out of voltage and the CVVF mode is used, the stator flux angles rise sharply. The same graph is obtained for the stator flux angles at which a maximum motor torque reduction is obtained, with 180 degrees added to the angles shown.

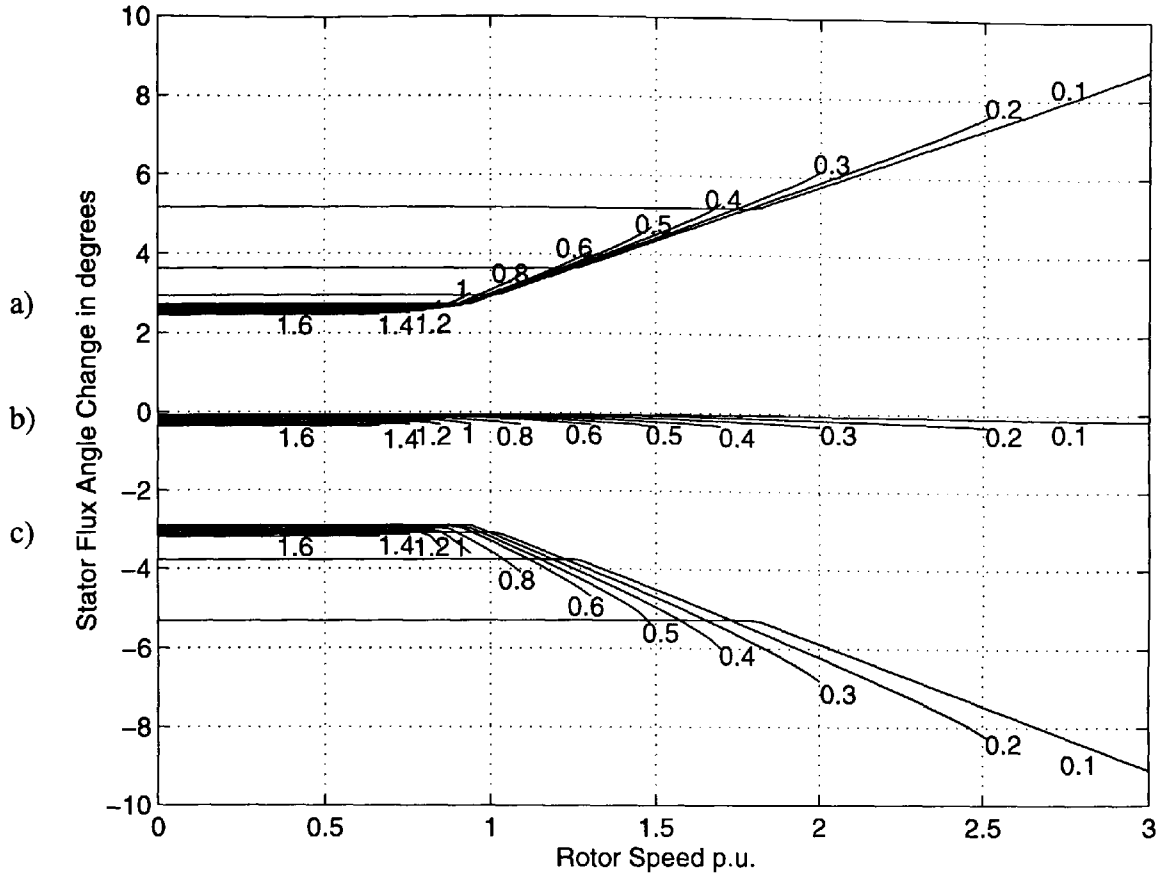

Fig. 7.38:The effect of initial rotor speed and motor torque on the stator flux angle change due to the application of voltage vectors $\vec{v}_0$ to $\vec{v}_0$ for a sampling time of T_s=150µs. Parameter: Motor torque p.u. a) maximum positive change b) change due to selection of $\vec{v}_0$ c) maximum negative change

Fig. 7.38 shows the change of the stator flux angle which occurs due to the application of voltage vectors $\vec{v}_0$ to $\vec{v}_0$ for different motor states. It can be seen that the selection of voltage vector $\vec{v}_0$ keeps the angle of the stator flux vector virtually constant regardless of rotor speed and motor torque. The maximum angle increase is constant for VVVF operation and rises linearly with rotor speed in CVVF operation. For maximum efficiency operation (T_l=0.1..0.3p.u.), the change of stator flux angle is bigger than for constant flux operation (T_l=0.4..1.6p.u.).

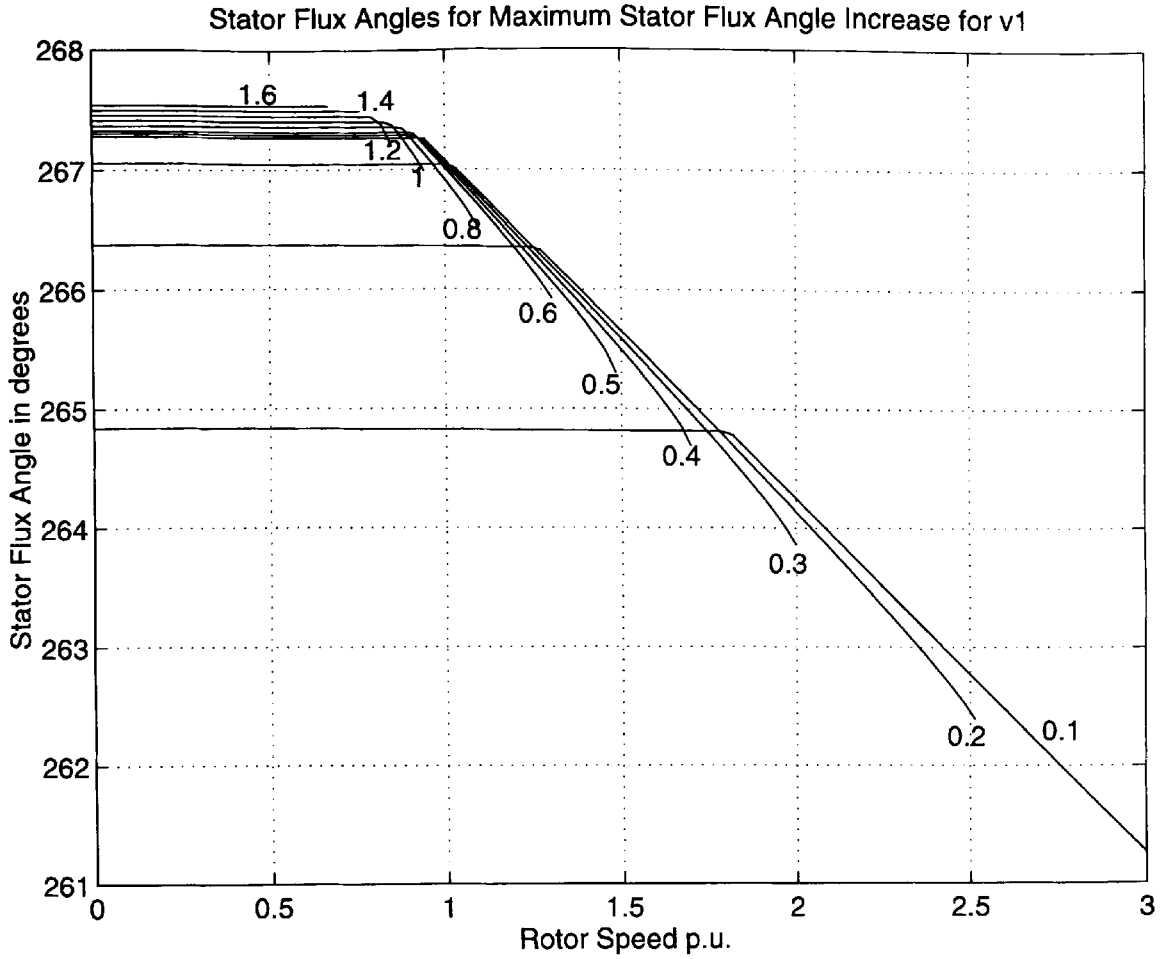

Fig. 7.39:The effect of initial rotor speed and motor torque on the stator flux angle for which maximum stator flux angle increase is obtained when voltage vector $\vec{v}_1$ is selected. Sampling time T_s=150μs. Parameter: Motor torque p.u.

It can be seen from Fig. 7.39 that the angle for which maximum stator flux angle changes are obtained varies by about 6.2 degrees. There is a speed dependence on this angle in the field weakening zone (CVVF operation), whereas in VVVF operation the angle depends on load torque only. Fig 7.33 shows that the stator flux angle variation is a distorted sine wave. This can also be seen by comparison of Fig. 7.39 and Fig. 7.40. I can be seen that the initial angle difference is approximately 172 degrees for VVVF operation and decreases to 162 degrees for light load high speed operation. Therefore, there is no simple means of prediction the resulting stator flux angle change accurately, which in turn makes a selection procedure difficult.

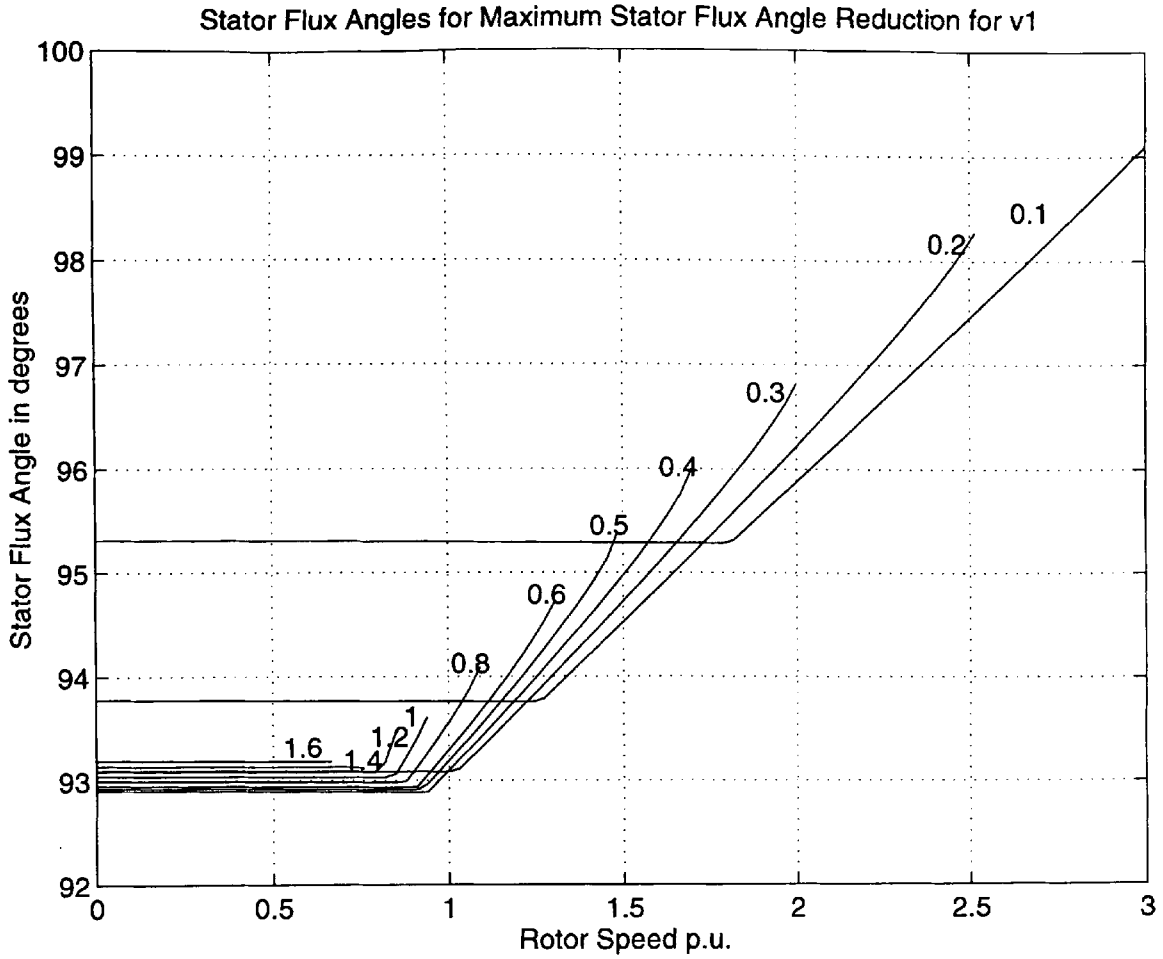

Fig. 7.40: The effect of initial rotor speed and motor torque on the stator flux angle for which maximum stator flux angle decrease is obtained when voltage vector $\vec{v}_1$ is selected. Sampling time T_s=150μs. Parameter: Motor torque p.u.

7.6 Optimum Performance

An optimum performance of motor flux and motor torque operation is a matter of definition. For example, it is possible to define a cost function which measures the variation from the actual motor flux level and the actual developed motor torque from their respective reference values as follows:

$$C = \left(T_{ref} - T_{est}\right)^2 + \left(\psi_{ref} - \psi_{est}\right)^2 \tag{7.7}$$

It is also possible to introduce weights into Equ. 7.7 to emphasise variations in torque, for example. As far as simulation is concerned, all seven different voltage vectors can be 'tried' for each sample interval T_s during a simulation and the one which minimises the cost function given by Equ. 7.7 after each sampling interval can be selected. Such an approach is possible with strategies such as direct torque control, because the duration of

the application for each voltage vector is constant. Simulation results of this procedure are shown in Fig. 7.41 to Fig. 7.43.

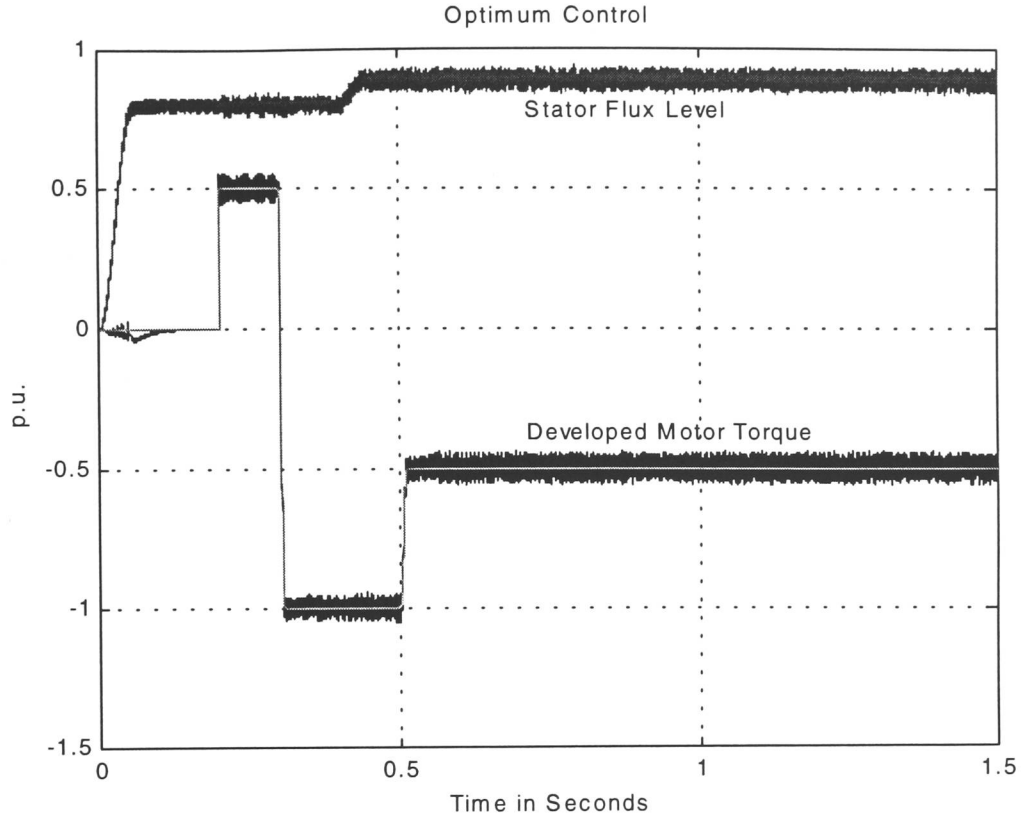

Fig. 7.41: Stator Flux Level and Motor Torque in Optimum Control

It may be seen from Fig. 7.41 that the total variation of the motor torque ripples is lower with optimum control than with direct torque control (Fig. 7.4) or flux vector control (Fig. 6.17). The mean value of the error signal $T_{ref} - T_{est}$ is zero. However, there are small torque variations during zero torque operation even in optimum control.

Fig. 7.42 shows the variation in time of the three stator currents during optimum control. It may be seen that the variations are not all that different from direct torque control and flux vector control.

In Fig. 7.43, the variations in time of the stator flux level, the magnetising flux level and the rotor flux level during optimum control are shown. Similarly to the curves shown previously for direct torque control and flux vector control, the magnetising flux level and the rotor flux level are not decoupled from variations in motor torque, because only the stator flux level is controlled.

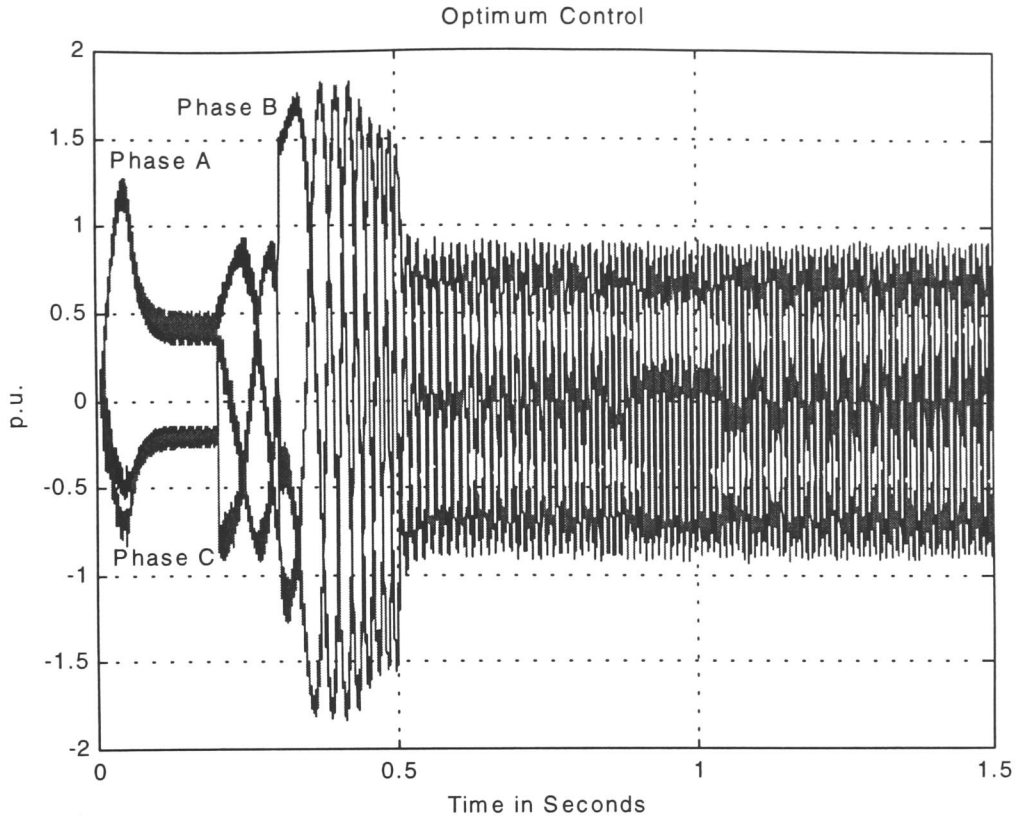

Fig. 7.42: Stator Currents in Optimum Control

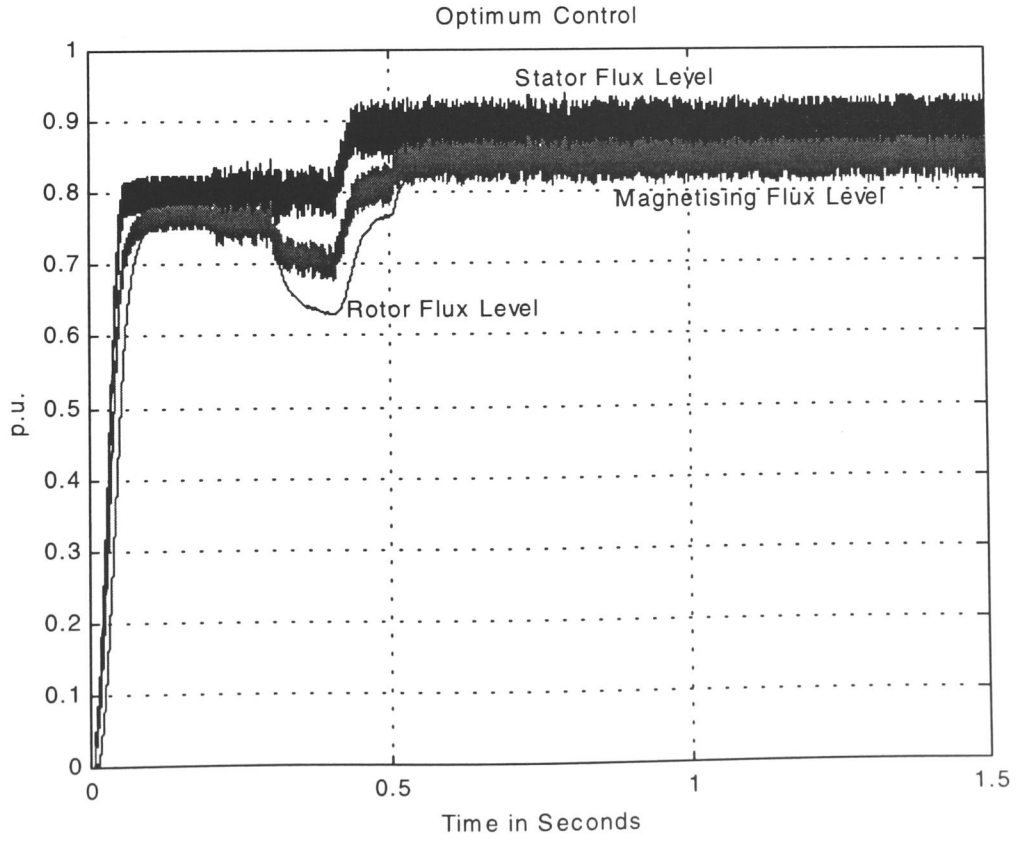

Fig. 7.43: Stator Flux, Magnetising Flux and Rotor Flux in Optimum Control

7.7 Interim Conclusion on Direct Torque Control

It has been shown in this chapter that the method of direct torque control allows the independent and decoupled control of motor torque and motor flux. The strategy is based on stator flux control and does not work with magnetising flux control or rotor flux control.

Clearly, the strategy is simpler to implement than flux vector control as voltage or current modulators and co-ordinate transformations are not required. The main characteristic of direct torque control is that the application time of each voltage vector is constant.

As far as sensitivity to motor parameters is concerned, the direct torque control strategy itself does not require any motor parameters. However, for the stator flux estimation motor parameters are required and in both direct torque control and flux vector control observer or Kalman filter techniques may be employed to reduce the sensitivity to parameter detuning. For the systems investigated, direct torque control performed at least as good as flux vector control. The most notable differences are that with direct torque control the average torque is not exactly equal to the reference torque, but the torque variations were smaller with direct torque control that with flux vector control. However, this concerns mainly the current modulator in flux vector control and may not be the case for other modulators.

The DTC techniques described in this chapter are all based on the assumption that the selection of a particular voltage vector and its application for a known sampling time has a pre-determined effect on stator flux level and motor torque in terms of their increase or decrease. However, this is not always true because of the following reasons:

1. When the inverter is operating near its voltage limits, the stator flux angle for which an increase of stator flux may be achieved, is limited to a small section within each sixty degree segment.
2. The alignment of the six sixty degrees sections is not always perfect. It can vary by as much as twenty degrees for different motor operation conditions. For example, for an alignment error of plus twenty degrees section '1' should cover the stator flux vector angles between -10 and +50 degrees, as opposed to -30 and + 30 degrees for ideal conditions.

3. The same alignment problem as for the stator flux applies equally to the developed motor torque. Furthermore, there is a variation between stator flux section alignment and torque section alignment.
4. The actual amount of increase or decrease for either flux or torque varies for different motor conditions. For example, at high speed operation, only a small increase in motor torque may be achieved with the application of a certain voltage vector during the sampling time interval. However, a much bigger torque change may be achieved for breaking action.
5. The average values of flux and torque are not always equal to the reference values as positive ripples may be different from negative ripples.
6. With DTC, the stator flux level is not kept constant when zero torque is required. However, this can be overcome by either a modified switching table (section 7.5) or a dither torque signal which is added to the reference torque signal (Takahashi, 1988).
7. 'True' p.w.m. is not possible with DTC as the switching times are forced into a sampling time grid. Thus, the THD with DTC is higher than with vector control employing an 'optimum' p.w.m. strategy (chapter 3). However, as is shown in chapter 3, the differences between different switching strategies can be neglected at higher switching frequencies.
8. Similarly to hysteresis current control, the given hysteresis band may be exceeded for the quantity to be controlled. In the worst case, this can be twice the hysteresis band width.
9. The selection of inverter states made by the look-up table is based on the fact that the application of a certain voltage vector has a known effect with regard to stator flux level and motor torque level in terms of increase or decrease. Because the stator flux space vector location is quantised into six sections, this does not always work equally well. There are certain angles where a supposedly increase in stator flux actually results in a flux decrease which in turn results in a wider stator flux ripple band. However, this is not to say that there is always a different voltage vector which would increase the stator flux and provide a torque increase or decrease as required. This is particularly true for operation near the voltage limit of the inverter.

The advantages of direct torque control compared to flux vector control may be listed as follows:

1. The controller is simpler and less computations are required.
2. 'Pulse dropping' of short pulses which are generated by p.w.m. schemes is not necessary with DTC as each pulse has at least a duration of one sampling interval.
3. The DTC controller does not add further dynamics to the system because of the bang-bang action of the look-up table selection of inverter states. This gives a quick and tight control of stator flux and motor torque.
4. Similarly to space vector p.w.m., a specific strategy for the selection of zero vectors is given with DTC. This reduces torque and flux ripples and conserves energy as no power is taken from the D.C. link during the periods when zero vectors are selected. It should be noted that p.w.m. strategies which use a separate modulation process for each phase do not have a specific zero vector selection strategy.
5. Similarly to space vector p.w.m., voltage vectors are selected with regard to the overall effect of an inverter switch application for a given time interval. For space vector p.w.m. the voltage-time integral is controlled, whereas for DTC stator flux level and motor torque are controlled.
6. The switching frequency of DTC is not fixed. This gives an effect called 'spread spectrum switching' which may also be achieved by p.w.m. strategies with random sampling in FVC. It has the advantage that audible noise is reduced. The average switching frequency depends on the sampling rate of the controller and the hysteresis bandwidth of the stator flux and torque quantiser.

Chapter 8:
Design of Experimental Induction Motor Drive System

This chapter describes in detail the design of the experimental three phase induction motor drive system used in this project. It has been used for the evaluation of p.w.m., flux vector control and direct torque control strategies. Fig. 8.1 shows a photograph of the experimental induction motor drive system.

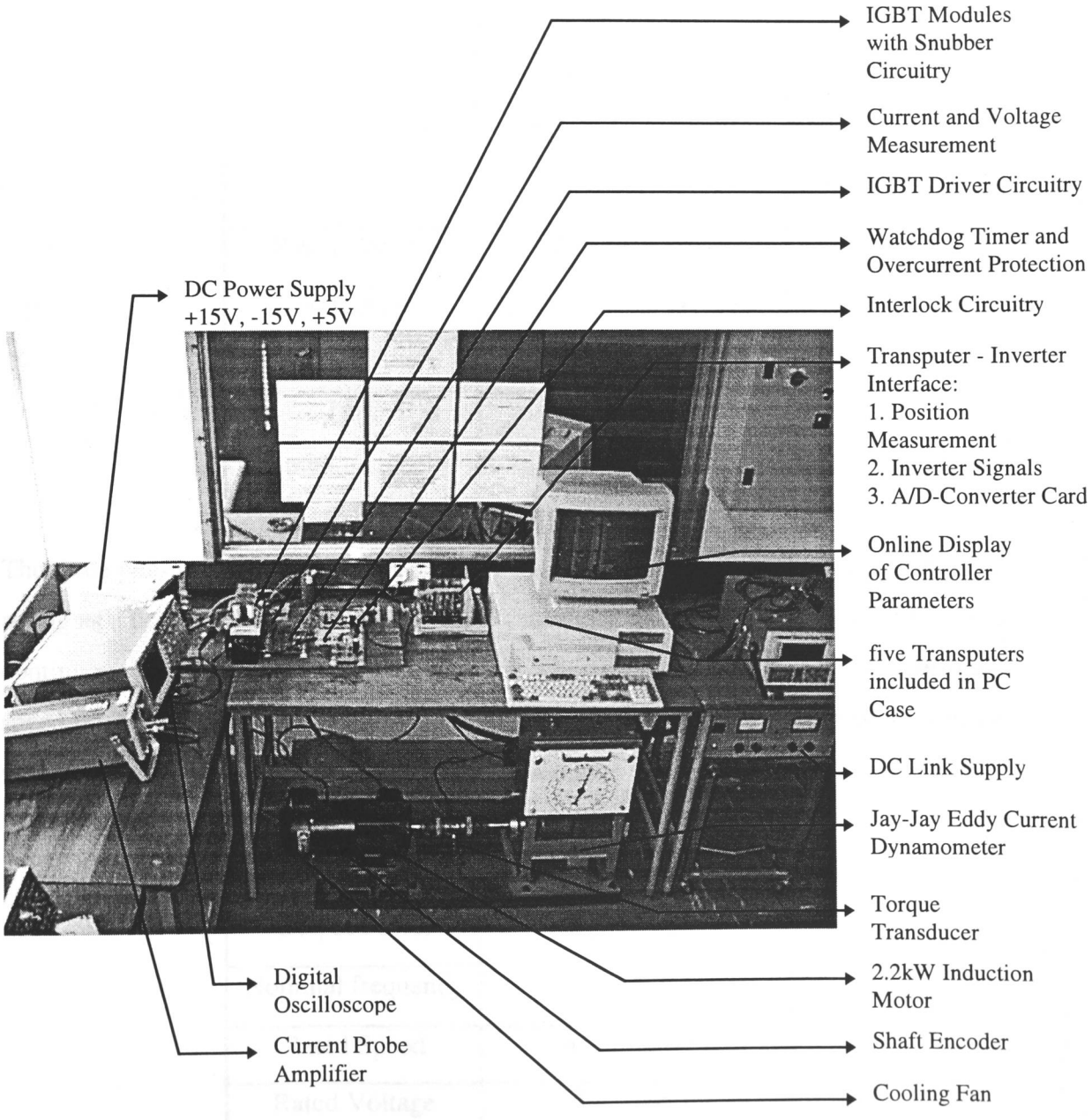

Fig. 8.1: Experimental Induction Motor Drive System

8.0 Induction Motor Drive System

The drive system consists of a 2.2 kW three phase cage rotor induction motor, shaft encoder, cooling fan, torque transducer and a Jay-Jay eddy current dynamometer. Table 8.1 shows the relevant motor specifications.

Table 8.1: Nameplate Data of motor used for Experiments

Output Power	$P_{out} = 2.2kW$
Nominal frequency	$f_s = 50Hz$
Power factor	$\cos\varphi = 0.88$
Rated Speed	$n = 1420rpm$
Rated Voltage	$V_N = 220V / 380V$ $V_N = 240V / 415V$
Rated Current	$I_N = 9A / 5.2A$
Protection	Class B, IP55, WB2182
Manufacturer	Leroy Somer
Type	LS100L1
Serial Number	334181

The three phase induction motor is force cooled by a small single phase induction motor acting as a cooling fan. This is necessary because self cooling would not be sufficient at continuous low speed - high torque operation. The cooling fan however, which turns at a speed of 2905 rpm, produces more audible noise than the three phase induction motor with converter. The cooling fan data is summarised in Table 8.2.

Table 8.2: Nameplate Data of Cooling Fan Motor

Output Power	$P_{out} = 110W$
Nominal frequency	$f_s = 50Hz$
Rated Speed	$n = 2905rpm$
Rated Voltage	$V_N = 240V$
Rated Current	$I_N = 0.45A$
Manufacturer	Leroy Somer

The load attached to the induction motor in the experimental set-up is a Jay-Jay eddy current dynamometer. The load torque can be adjusted by a rheostat between 0-58 Nm. One limitation of the dynamometer is that it cannot produce a load torque at zero speed. The relevant data is summarised in Table 8.3.

Table 8.3: Nameplate Data of Jay-Jay Eddy Current Dynamometer

Torque	$0-58Nm$
Serial Number	230181
Type	DM3/50
Manufacturer	Educational Measurements Limited, Warsash, Southampton

A torque transducer has been fitted between motor and load in order to monitor the generated torque. The transducer works by means of strain gauges in bridge configuration which are glued to the shaft between motor and load. The maximum supply voltage to the bridge is 20V. The data is shown in Table 8.4.

Table 8.4: Nameplate Data of Torque Transducer

Torque Range	0-25 lb ft
Sensitivity	2.208mV/V
Maximum Torque	50 lb ft
Maximum Voltage	20V
Type	2400/AX
Serial Number	S2-E-6084
Manufacturer	EEL Limited, Holyhead

A shaft encoder has been fitted to obtain accurate information on the position of the rotor shaft. The output signals from the encoder are two square wave signals and one marker pulse. The number of pulses delivered by the encoder is 1024 per revolution. The shaft encoder data is shown in Table 8.5.

Table 8.5: Data of Shaft Encoder

Pulses/rev	1024
quadrature signals	2
marker pulse	1
Supply voltage	5V
Type	500
Manufacturer	Servodynamic Ltd., Wolverhampton

8.1 Control Electronics

The control electronics of the experimental electrical drive system consists of the following parts:

1. A three phase IGBT bridge circuit with snubbers.
2. Driver boards for the IGBT's including interlock circuitry.
3. A board containing the over-current, watchdog and manual switch-off protection circuitry.
4. Isolated voltage supplies for the gate drivers.
5. Three Transputer interfaces for A/D conversion, gate driver signals and shaft encoder.

Furthermore, additional circuitry for the measurement of d.c. link voltage, two phase currents, motor torque, rotor speed and rotor position has also been built and made part of the test rig. The rotor position is interfaced to Transputers by means of a serial communication link directly, whereas the filtered analogue signals are connected to an analogue to digital converter card with Transputer-serial link interface.

The circuitry for the complete experimental electrical drive system can be represented in block diagram form as shown in Fig. 8.2. The control electronics is connected to Transputers T1, T2 and T3 via serial link interfaces. These three Transputers are connected to Transputer T0 and a Master Transputer, which in turn is connected to a PC, as shown in Fig. 8.2. The software for all five Transputers can be down-loaded from the PC to perform the following main functions:

1. Control of the induction motor.
2. Data acquisition of measured quantities and controller variables.
3. Execution of PC keyboard commands in real time.

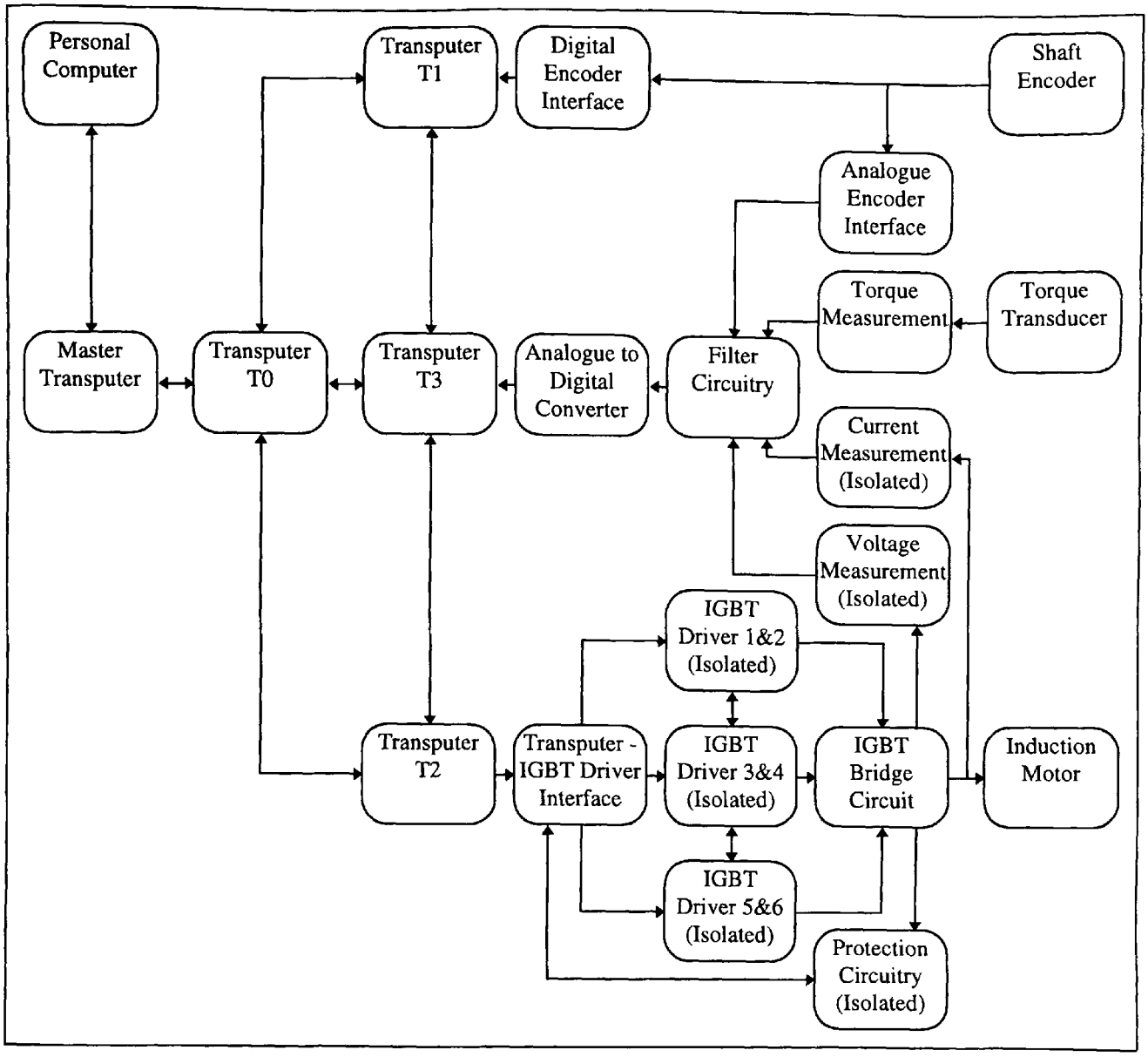

Fig. 8.2: Block Diagram of Experimental Drive System

In the following, the individual circuits are described in detail.

8.1.1 IGBT Bridge Circuit

The IGBT bridge circuit is shown in Fig. 8.3. Because of the intended use as an experimental drive system, high power rated IGBT modules have been used. The higher initial costs are offset by improved overload capability. Power diodes in parallel with each IGBT are also included in the modules. The DC link consists of a mains rectifier and a DC link filter. Initial switch-on current transients due to capacitor

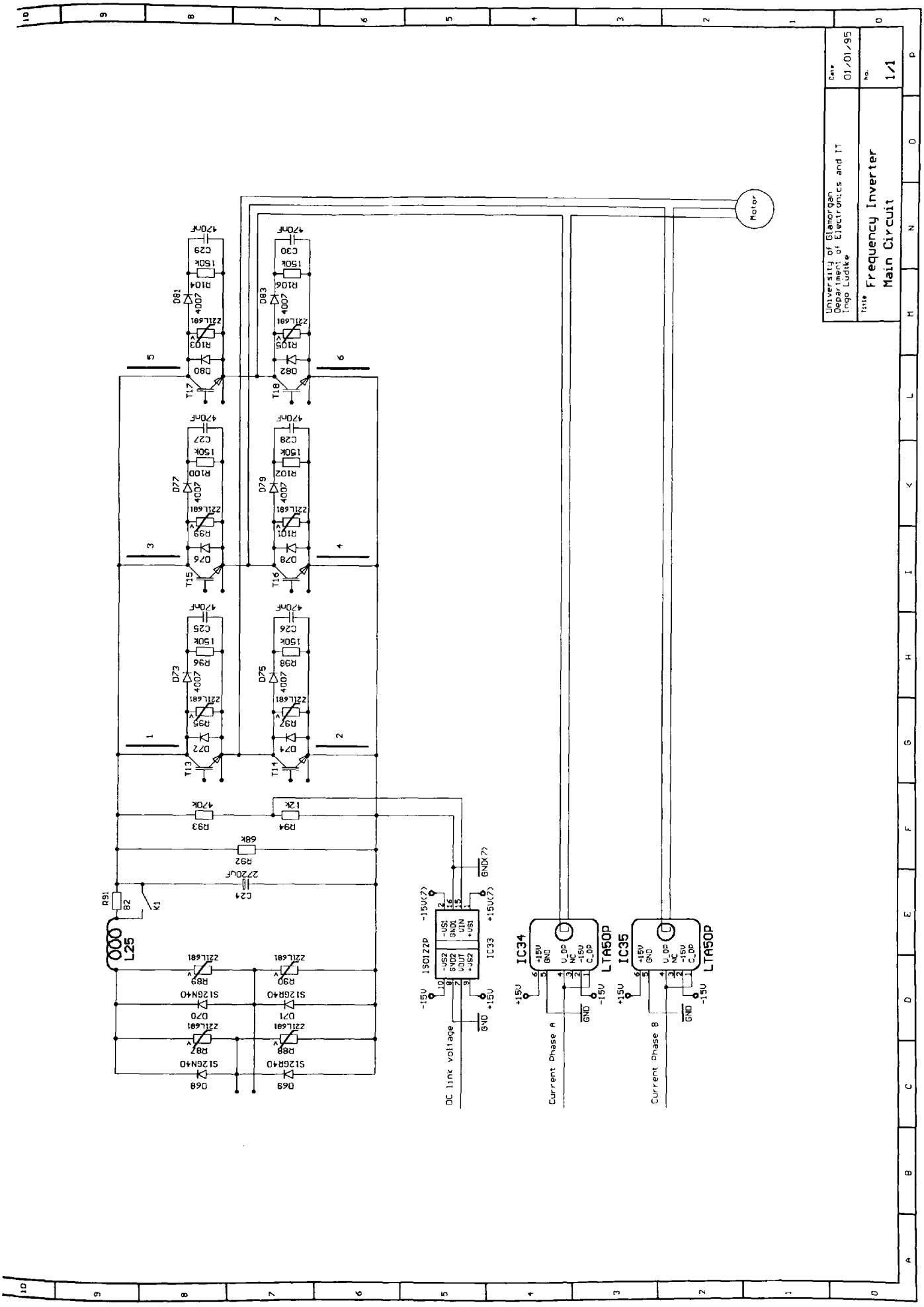

Fig. 8.3: Schematic diagram of the IGBT bridge circuit

charging are reduced by means of a resistor connected in series with the DC link which can be short-circuited by a relay contact K1 for normal operation. The resistor R92 is used for capacitor discharge after the inverter has been switched off. The voltage divider consisting of R93 and R94 is used for the measurement of the DC link voltage. The DC link voltage and two phase currents are interfaced to the Transputers using an isolation amplifier and two current transducers.

The isolation amplifier requires an isolated voltage supply which is taken from the switched mode power supplies described in section 8.2.4.

The current transducers allow instantaneous measurement of a.c. and d.c. currents in total isolation from the power circuit. The current signal obtained is filtered and connected to the A/D converter card. The sensitivity has been adjusted by passing the current carrying conductor through the transducer core five times.

The power diodes and IGBT's are protected by means of varistors, which can short-circuit any high voltage spikes generated by the mains supply or by the inverter itself. In each inverter leg, the positive and negative supply is fed through a toroidal ferrite ring which has approximately eighty windings on the secondary side. This allows disablement of the driver signals by detection of fast current changes, which occur under short-circuit conditions. A snubber circuit is connected across each IGBT in order to minimise switching losses and peak voltages.

8.1.2 IGBT Driver Circuit

A circuit diagram of the driver circuits for the six IGBT's may be seen in Fig. 8.4, 8.5 and 8.6. The circuits consist of a 5V to 15V interface and the interlock circuitry preventing simultaneous switch-on by introducing a delay of $2.8\mu s$ between the upper and lower IGBT's in the same inverter leg. For the signal isolation, magnetic coupling has been used instead of photo-coupling, in order to increase the reliability and to reduce the coupling capacitance between high and low voltage parts of the circuit. However, this has resulted in increased complexity of the circuit as a signal pulse recovery circuit is necessary when magnetic coupling is used. Each of the six IGBT drivers has an own +15V voltage supply, which allows control over the IGBT gates even when there are no changes of the input signal over longer periods of time. This is important for control strategies like Direct Torque Control, where a minimum switching frequency can not be guaranteed. Each IGBT gate driver also has a supply

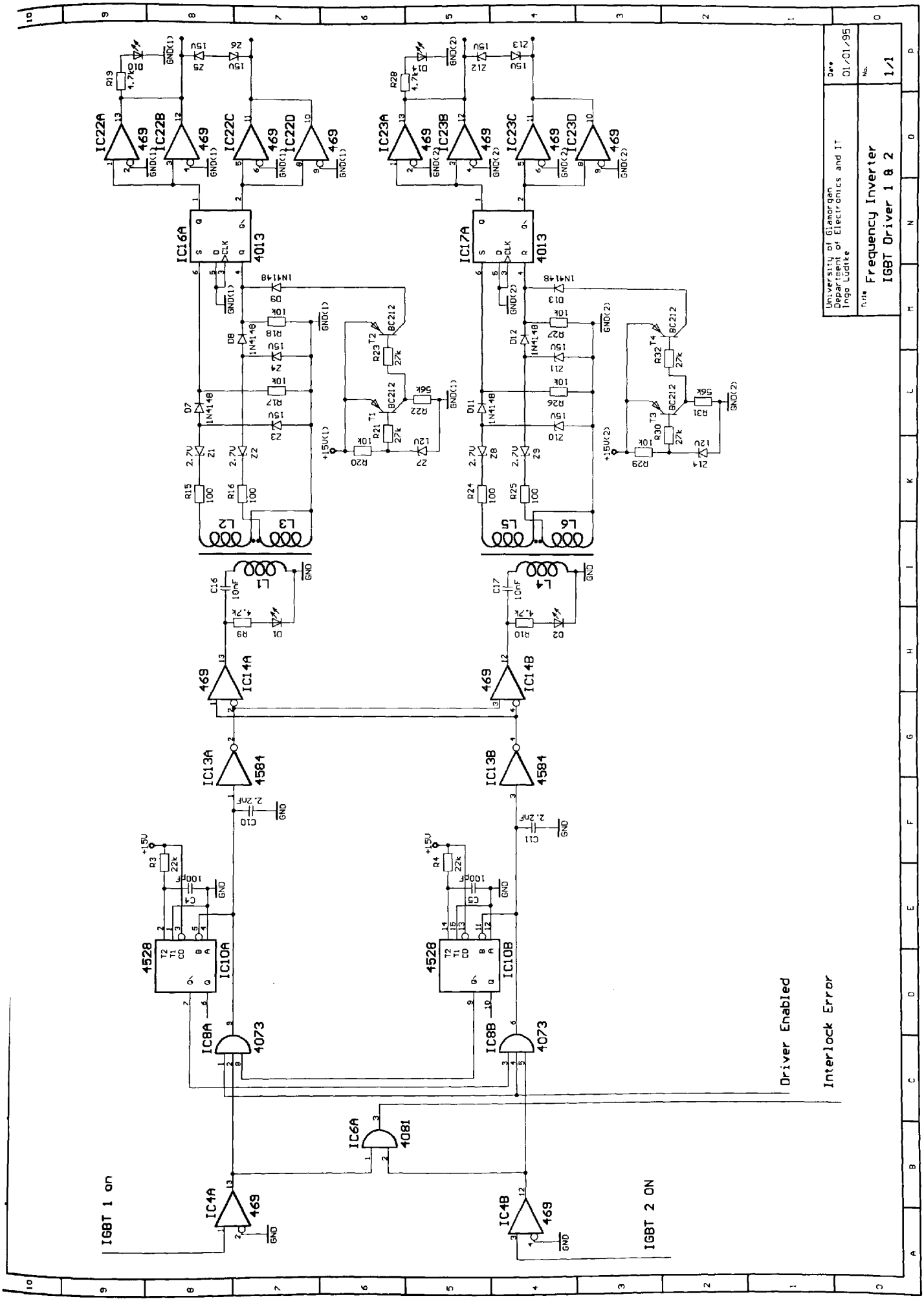

Fig. 8.4: Schematic diagram of IGBT driver circuits 1 & 2

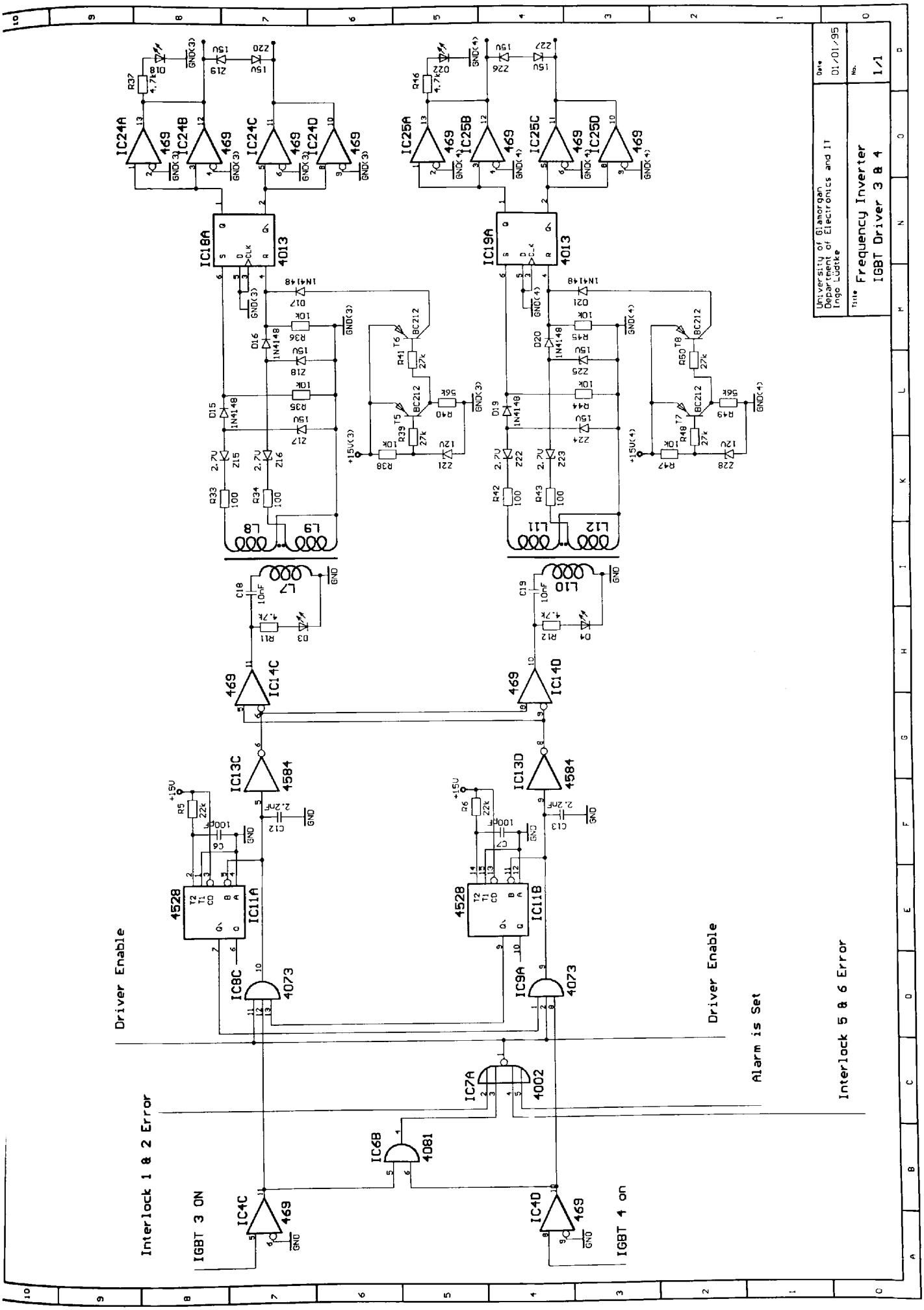

Fig. 8.5: Schematic diagram of IGBT driver circuits 3 & 4

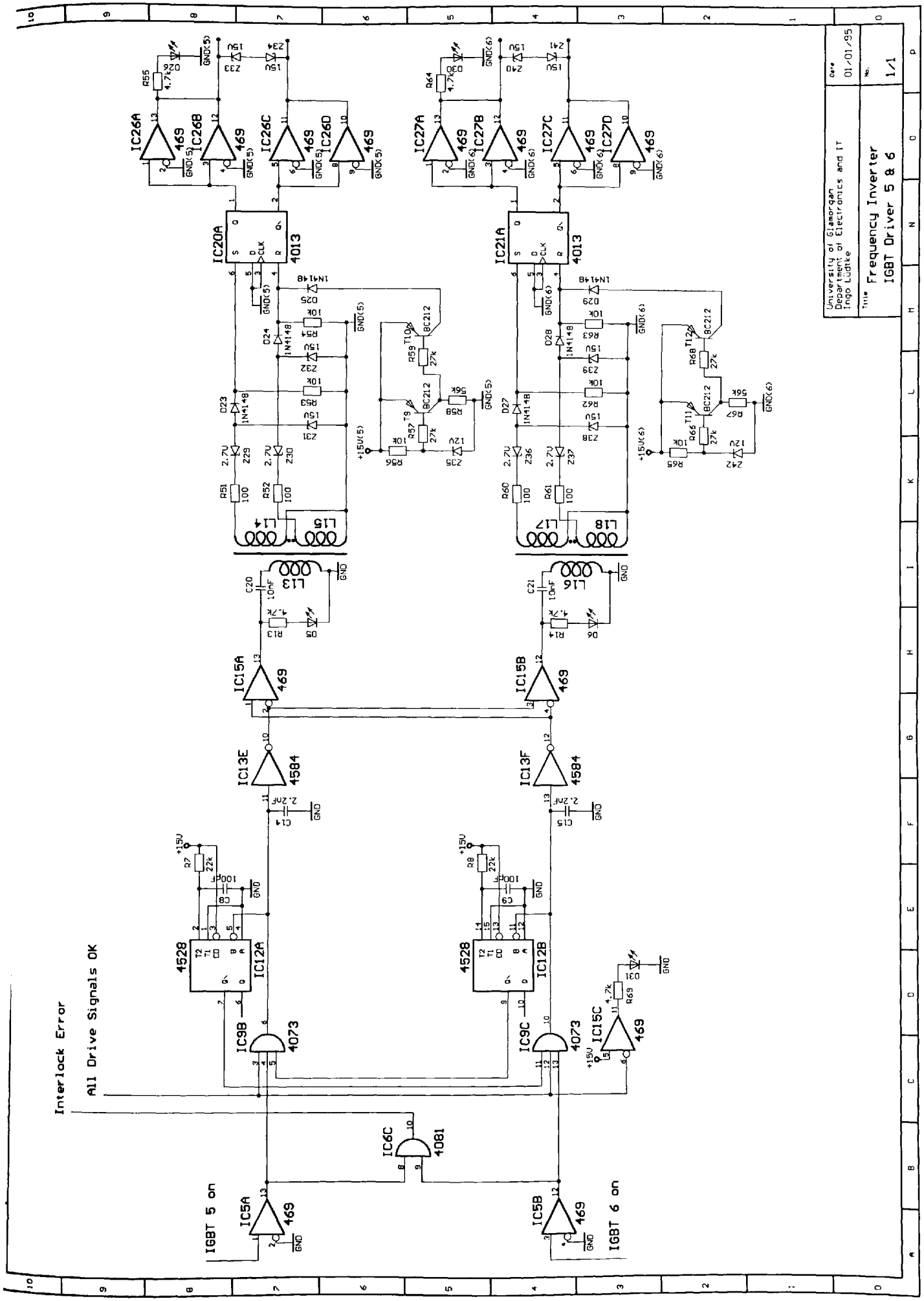

Fig. 8.6: Schematic diagram of IGBT driver circuits 5 & 6

under voltage protection. This part of the circuit ensures a reset signal at the D-flip-flops when the supply voltage is below +12V. This protects the inverter also at the initial switch-on when correct control signals may not be established yet. In order to prevent high voltages at the IGBT gates, two zener diodes are connected back to back at each gate input. The gate drive circuit provides +15V for switch-on and -15V for switch-off across the IGBT gates without the use of a bipolar supply.

A schematic diagram of the Transputer interface circuitry for the gate driver is shown in Fig. 8.7.

8.1.3 Protection Circuitry

The protection circuitry, shown in Fig. 8.8, is used to detect fast current changes in the inverter legs, and detect whether the software program running on the Transputers outputs a watchdog signal. A manual switch-off is also provided. The error signal may be reset manually, or automatically with another signal from the Transputer interface. The over-current limit may be adjusted by means of the potentiometer R78. The protection circuitry has been built on a PCB, which is shown in Fig. 8.9.

8.1.4 Isolated Power Supplies

A switched mode power supply with seven +15V outputs and a single -15V output has been designed for the provision of floating voltage supplies. Although, in principle, only a single supply for the three lower IGBTs is required, three separate supplies have been used because of the high power requirement of the IGBT gates at higher switching frequency. It is also believed that the circuit symmetry resulting from using six supplies for the six IGBT reduces mutual interference problems. Two more supplies are required for the DC link voltage measurement as may be seen from the circuit diagram in Fig. 8.10. A 555 timer circuit provides a frequency signal of approximately 250kHz. This signal is used to drive fast D-type flip-flops. Both outputs are connected to two high current drivers in parallel, thereby providing an output voltage swing of 30V with a 15V supply at twice the current rating of a single driver. The driver outputs are connected to a capacitor and the primary side of the toroid transformer in series. Two secondary sides are connected to each primary side. The voltages on the secondary side is full wave rectified and feeds a 15V voltage regulator. Decoupling capacitors are used to provide a smooth voltage supply.

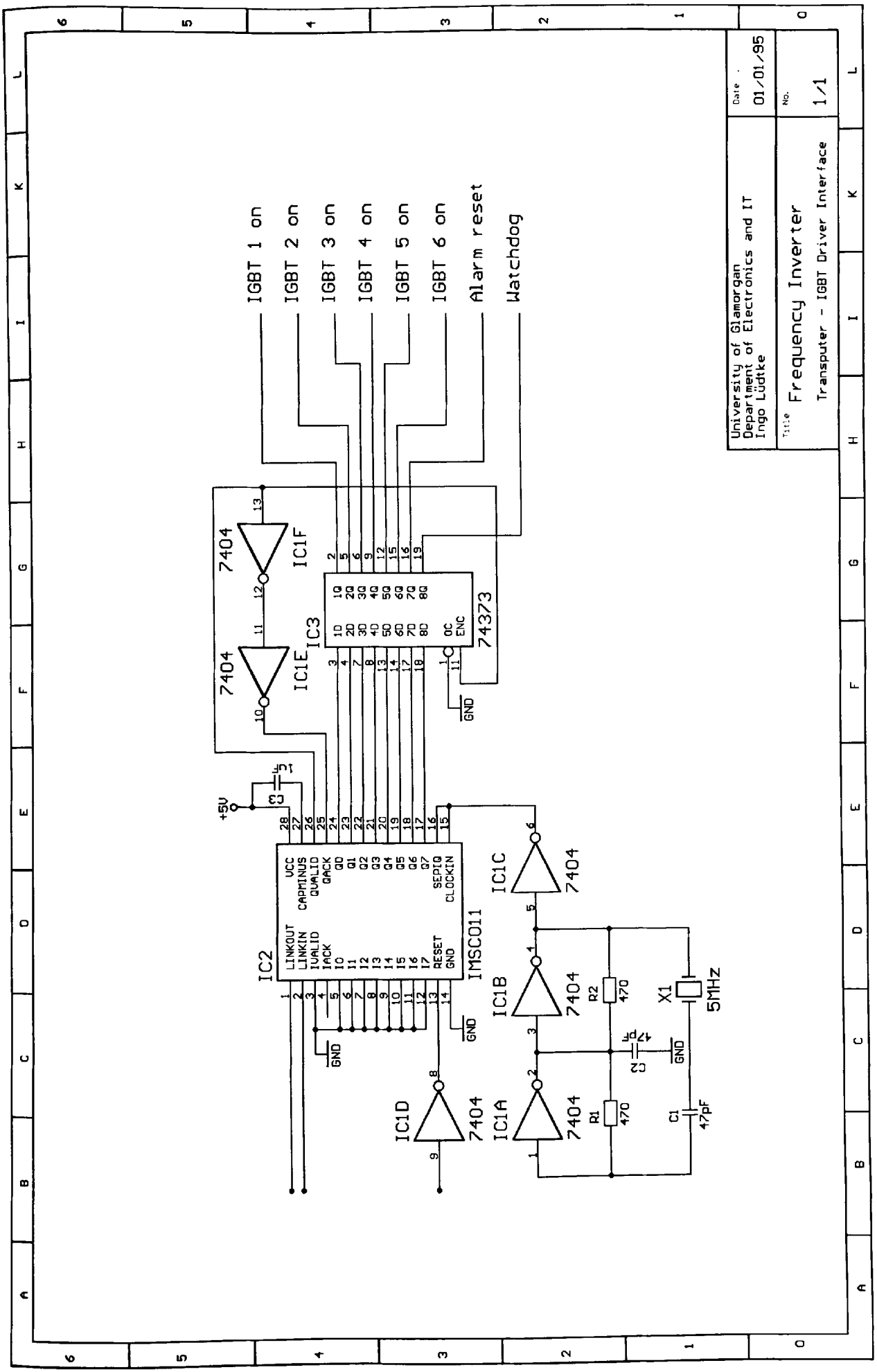

Fig. 8.7: Schematic diagram of the gate driver Transputer interface

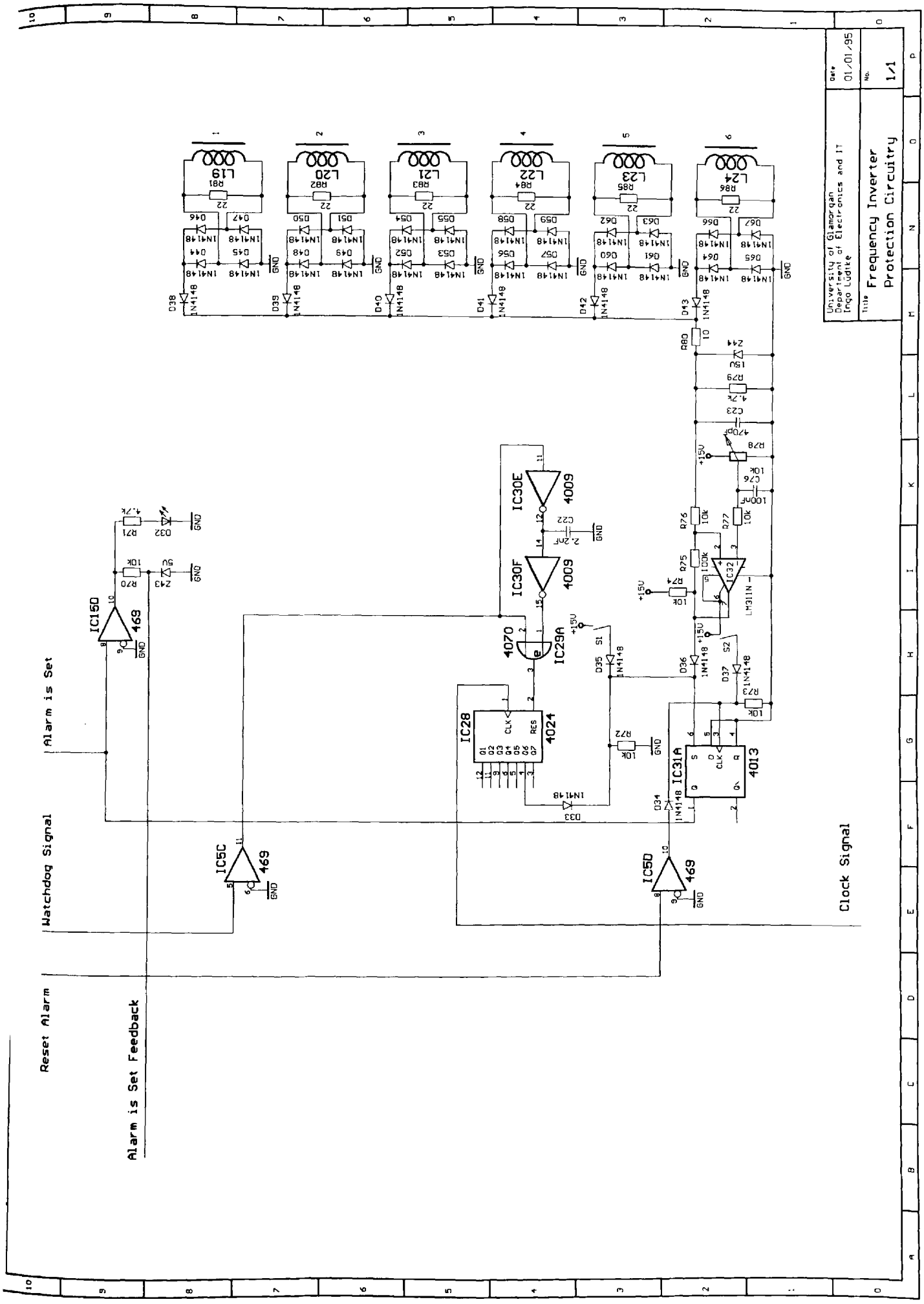

Fig. 8.8: Schematic diagram of the inverter protection circuitry

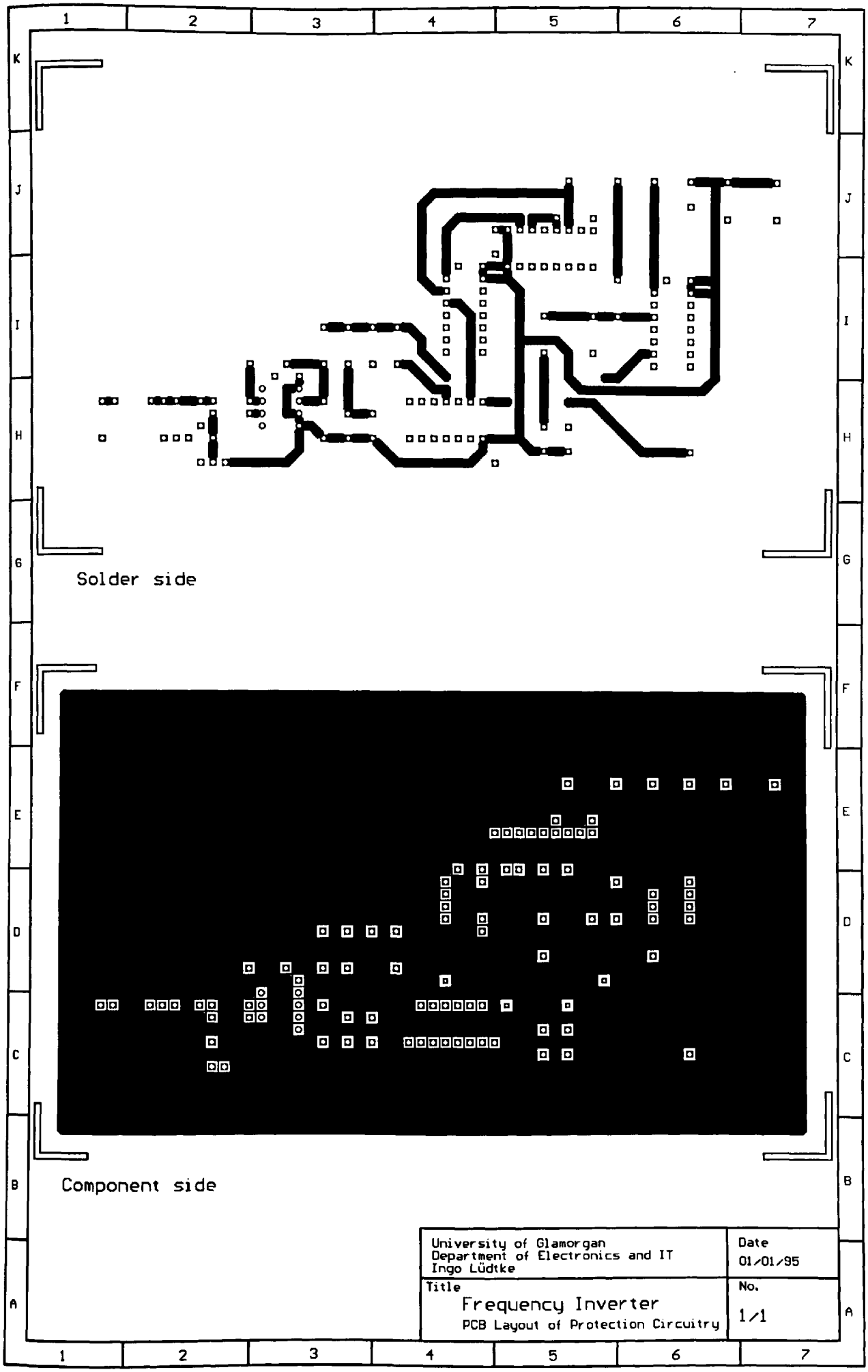

Fig. 8.9: PCB layout of the IGBT protection circuit

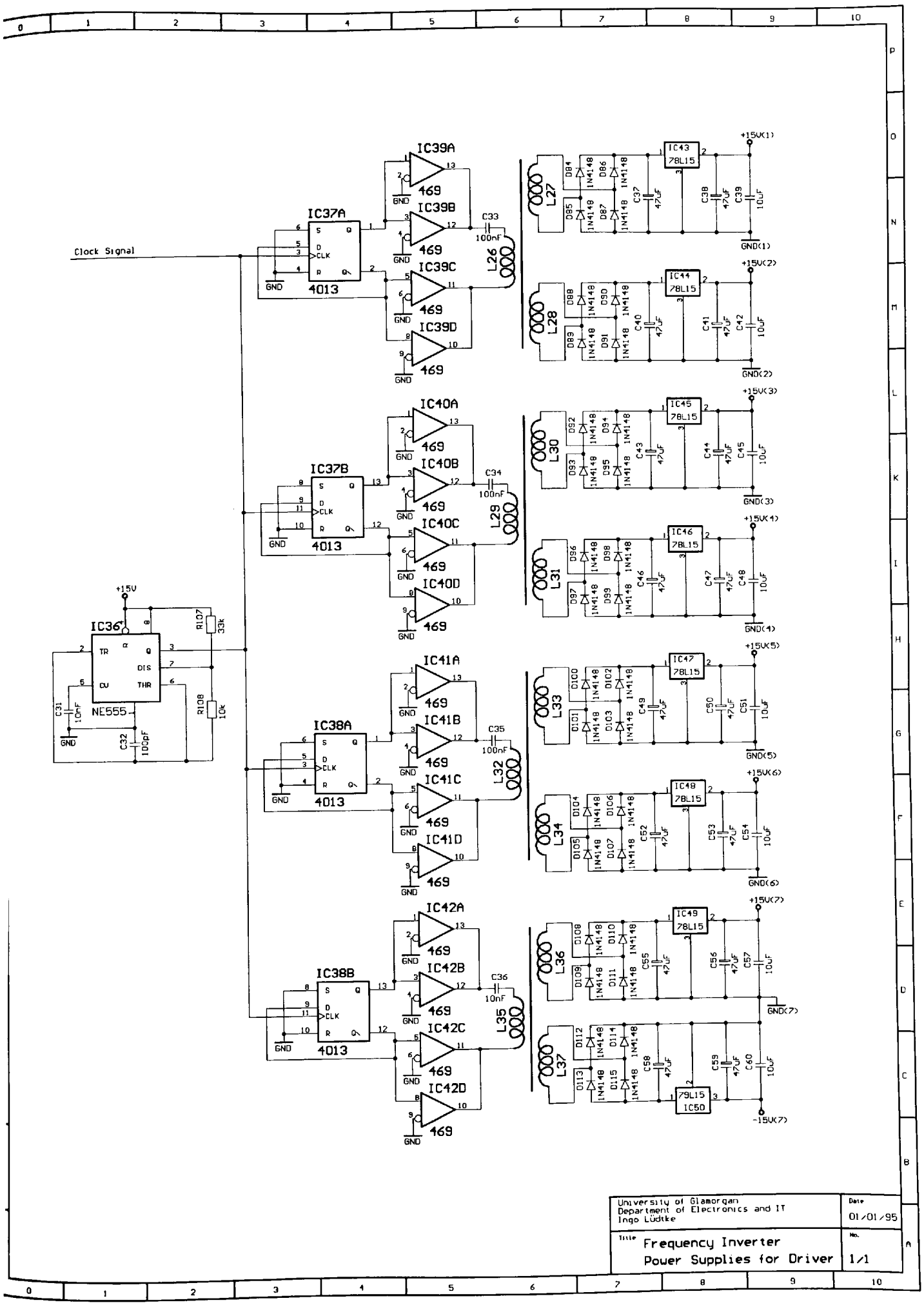

Fig. 8.10: Schematic diagram of the isolated power supply circuit

8.1.5 A/D-Converter

An analogue to digital converter card has been utilised to interface the analogue measurements to the Transputers. As $16\mu s$ are required for a single measurement and transfer to the Transputer, the A/D card is the main bottleneck of the system. A reduction in overall cycle time may be achieved by using a memory mapped solution and avoiding the serial link interface. The relevant data for the converter card is summarised in Table 8.6.

Table 8.6: A/D Converter Data

Voltage Range	+10/-10V
Resolution	12 bit
Sample rate	$16\mu s$
Transputer Interface	IMSC011 link adapter with 5 MHz Clock
No. of Channels	8
Type	IDB534/1
Manufacturer	University of Bangor

8.1.6 Torque Measurement

A voltage signal proportional to the developed motor torque is obtained from the torque transducer. As the strain gauge bridge is supplied with 20V and the sensitivity is 2.203mV/V, only 44mV are obtained at the highest load torque of 25 lbft (33.9 Nm). Since many of the experiments have been carried out at a reduced voltage, typical motor torques obtained in higher speed operation are only a tenth of the highest transducer load torque. Hence voltages of around 5mV are obtained from the torque transducer, which are amplified by means of an instrumentation amplifier and filtered as described in the filter circuit section. Fig. 8.11 illustrates the circuit of the instrumentation amplifier. The instrumentation amplifier allows the gain to be selected by means of a single resistor value, which is also shown in Fig. 8.11. The layout of the PCB designed for this circuit is shown in Fig. 8.12.

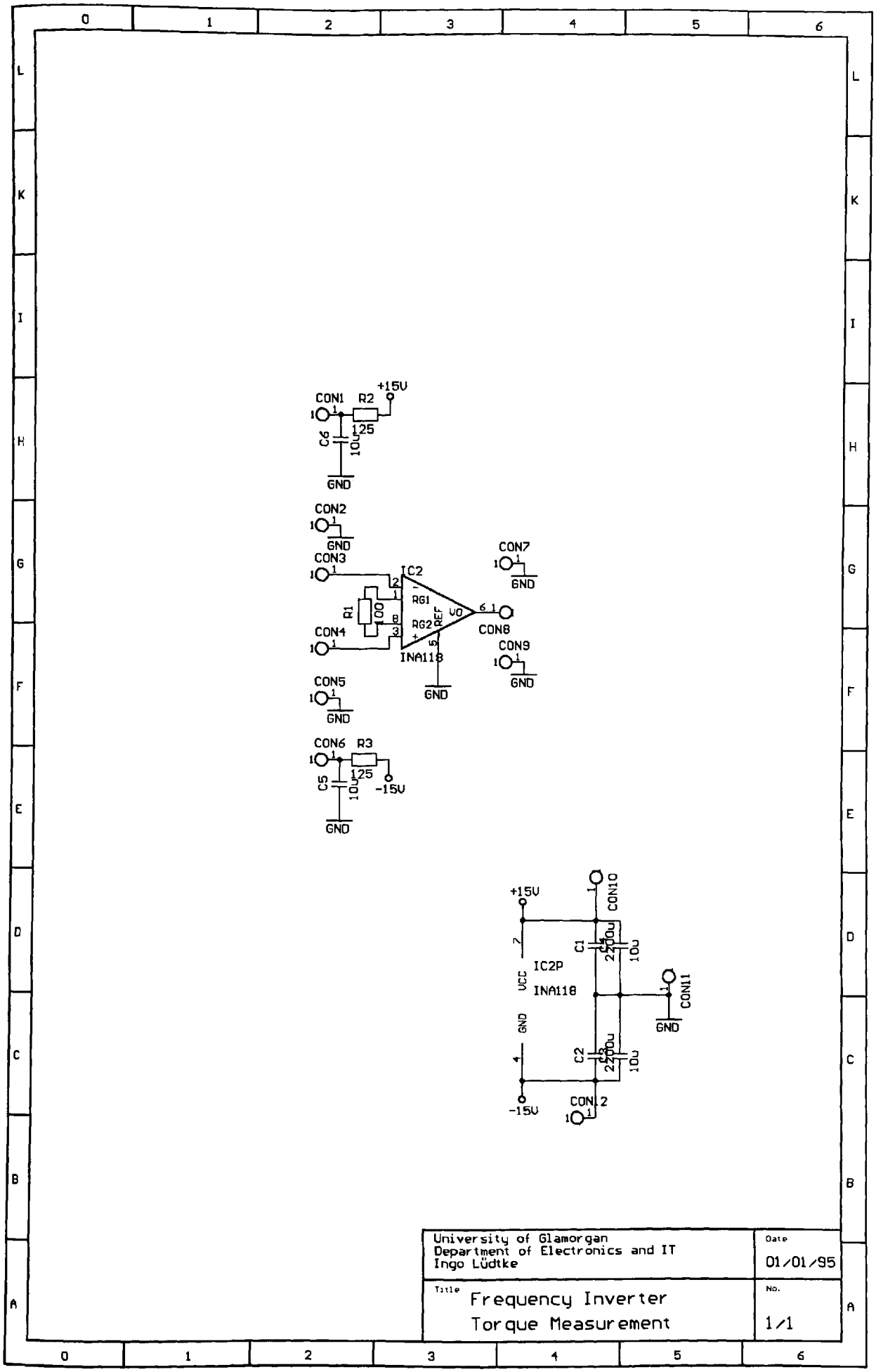

Fig. 8.11: Schematic diagram of the torque measurement circuit

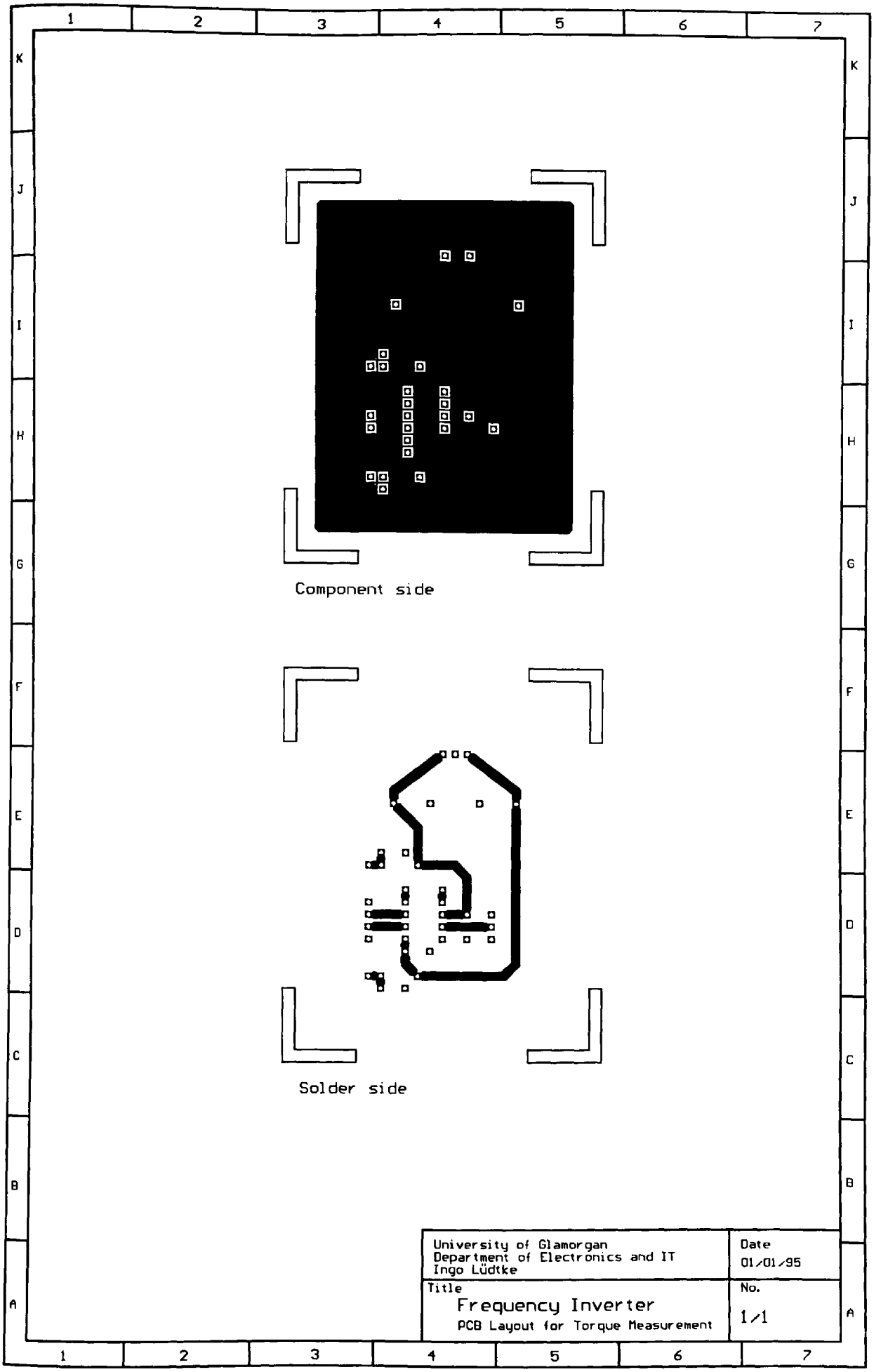

Fig. 8.12: PCB layout of the torque measurement circuit

8.1.7 Speed Measurement

Speed measurement has been carried out by using a frequency to voltage conversion of the shaft encoder signals. A schematic diagram of the circuit is shown in Fig. 8.13. The direction of rotation is detected by means of IC6-8, and an arbitrary inversion of the output signal may be carried out by means of Mosfet Q1. This achieves a bipolar analogue voltage output for clockwise and anti-clockwise rotation of the rotor. The number of pulses is doubled by means of the "Exclusive OR" IC3. This achieves a reduction of the voltage ripple in the analogue output voltage. The frequency to voltage conversion is carried out by a standard frequency to voltage converter (LM2917, IC4). The PCB layout for the speed measurement circuit may be seen in Fig. 8.14.

8.1.8 Filter Circuitry

The filter circuits are used to ensure that the analogue signals contain frequency components below the Nyquist frequency only. The sampling rate for vector and direct torque control is $1/150\mu s = 6.67kHz$, hence all frequency components above $3.33kHz$ have to be damped to a voltage smaller than the A/D converter resolution (4.9mV). This may be achieved by using an 8th order Butterworth lowpass filter. For maximum accuracy, a standard filter chip has been chosen where only resistors are required for the selection of the corner frequency. A schematic diagram of the circuit is shown in Fig. 8.15 and the PCB layout for the filter circuit is shown in Fig. 8.16 and Fig. 8.17

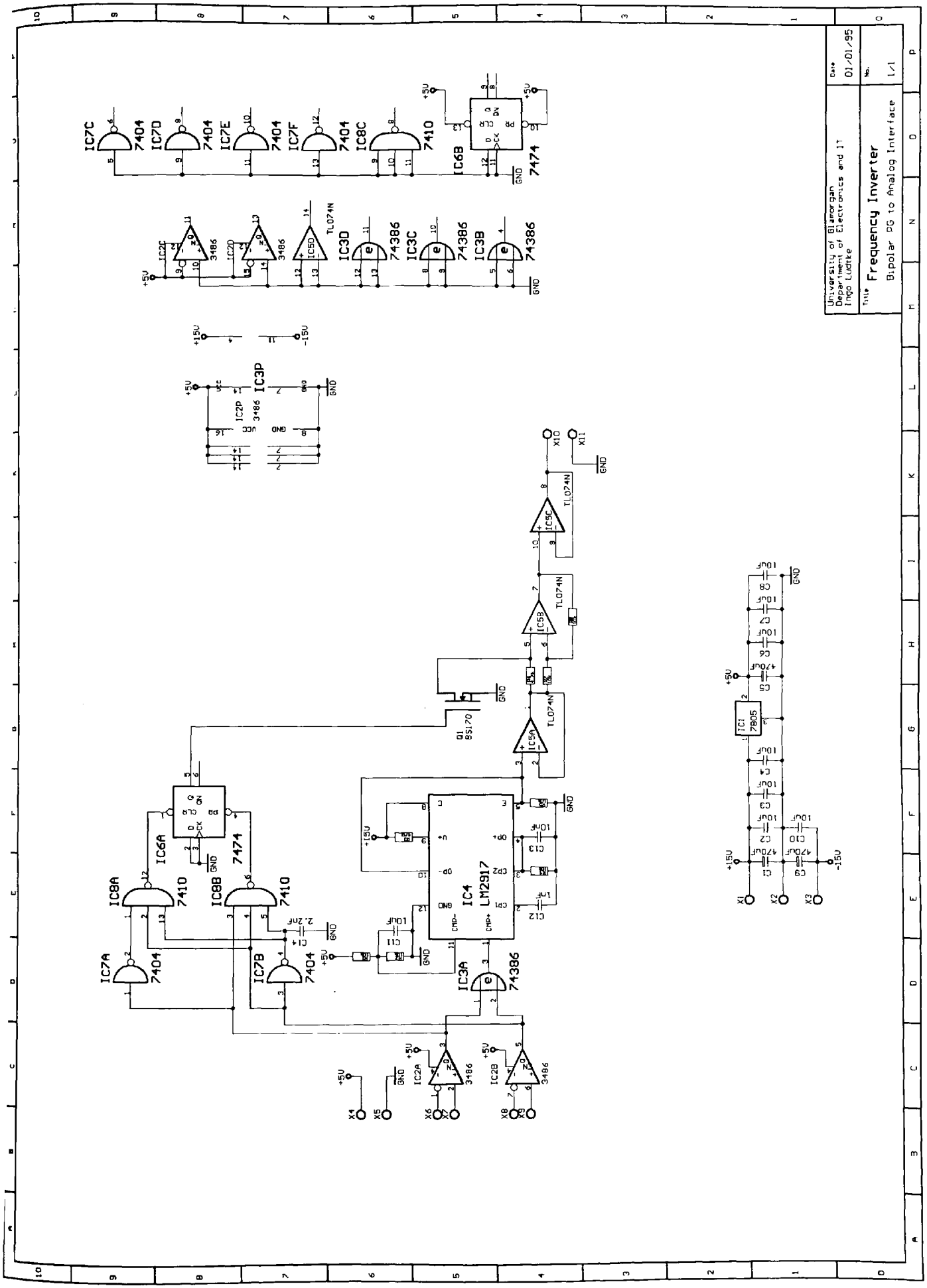

Fig. 8.13: Schematic diagram of the speed measurement circuit

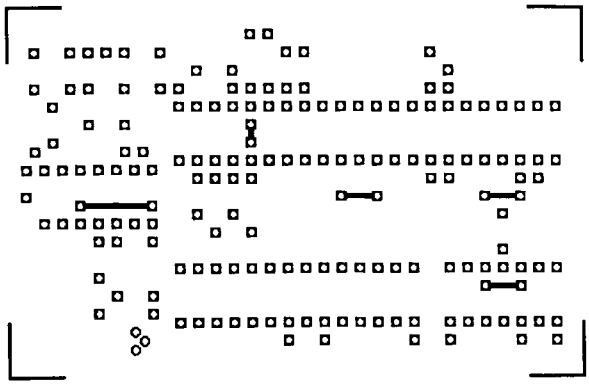

Component side

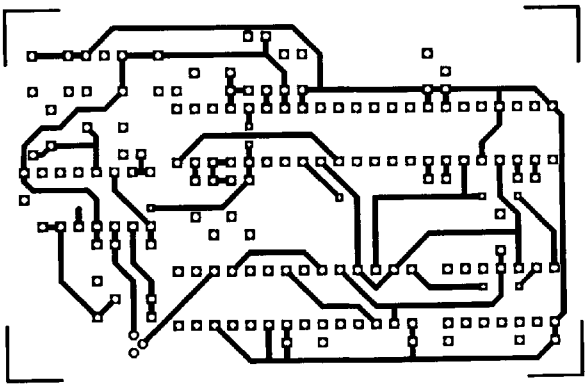

Solder side

University of Glamorgan Department of Electronics and IT Ingo Lüdtke	Date 01/01/95
Title Frequency Inverter PCB Layout of Speed Measurement	No. 1/1

Fig. 8.14: PCB layout of the speed measurement circuit

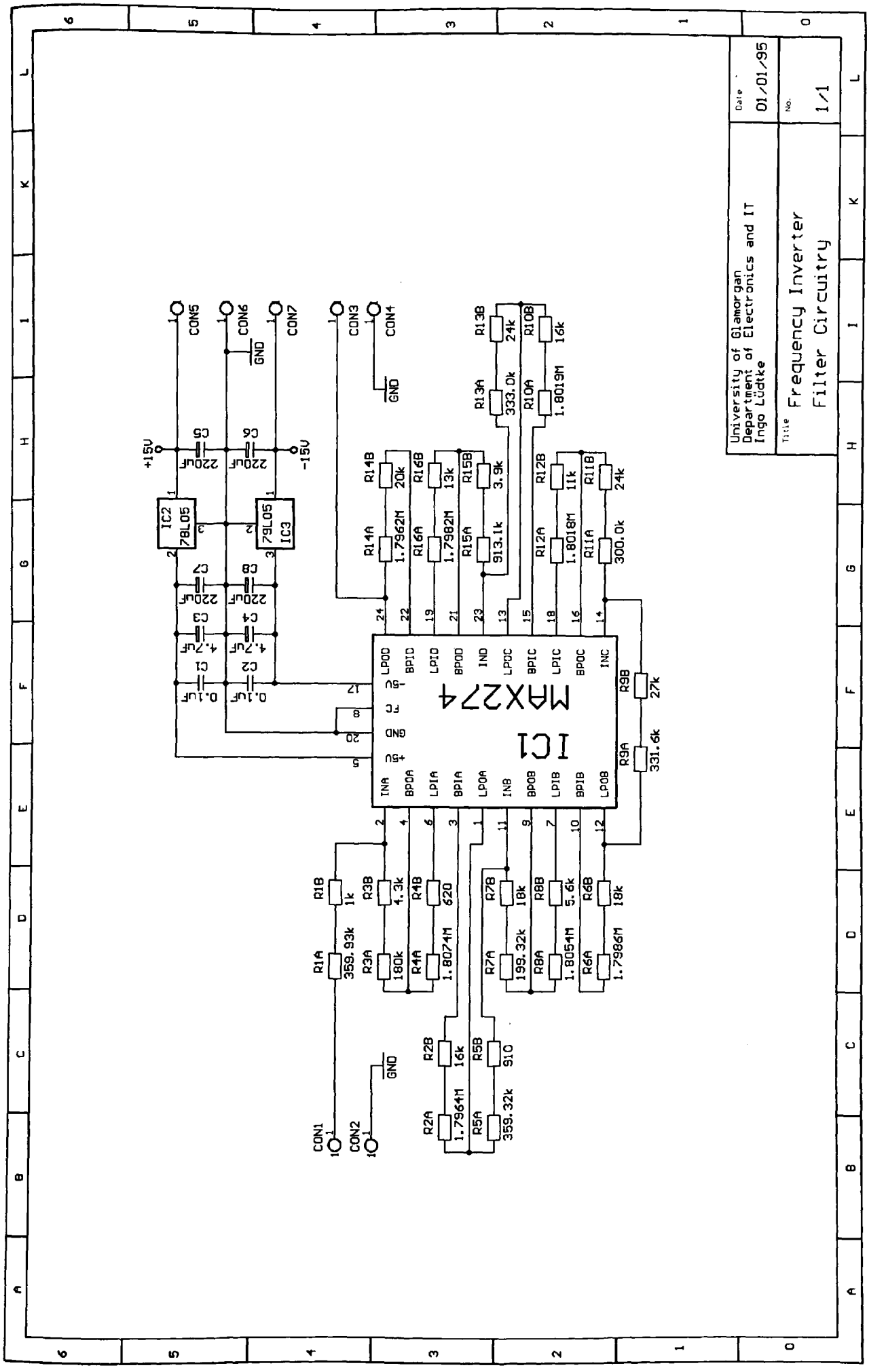

Fig. 8.15: Schematic diagram of the filter circuitry

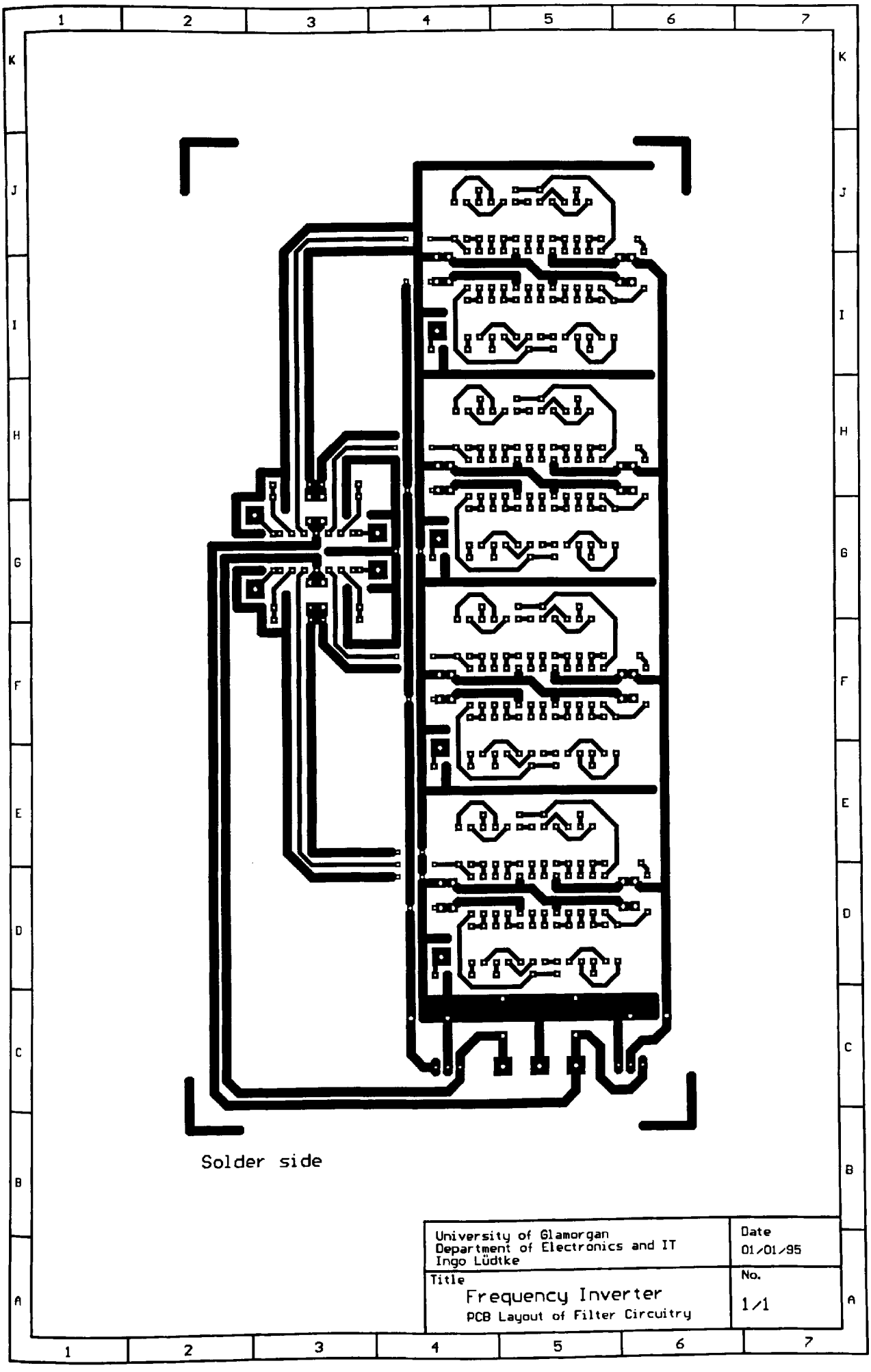

Fig. 8.16: Solder side PCB layout of the filter circuitry

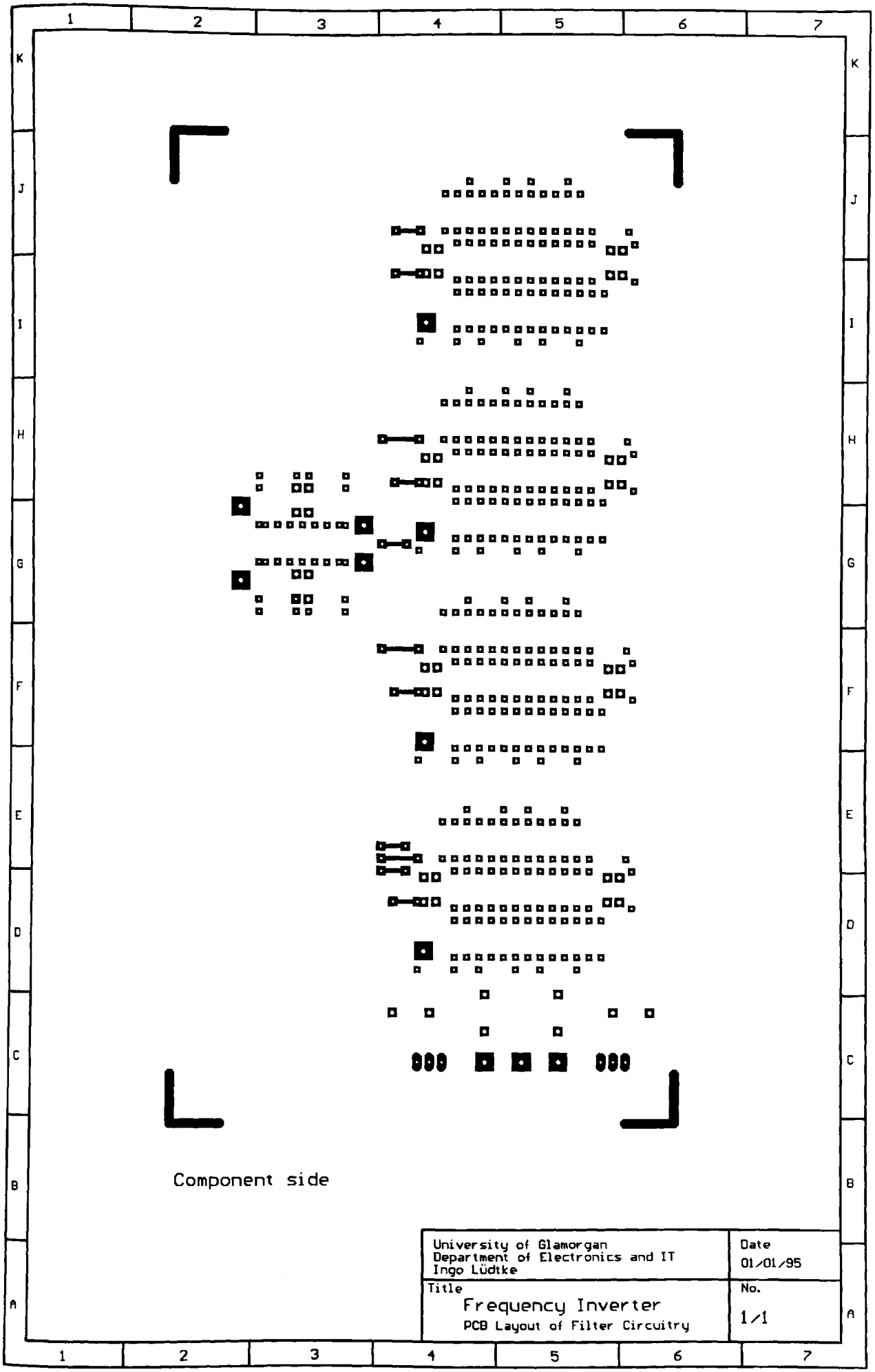

Fig. 8.17: Component side PCB layout of the filter measurement circuit

8.1.9 Position Measurement

The circuit used for position measurement and the corresponding Transputer interface is shown in Fig. 8.19. This circuit has proven to be quite complex, as the control of the unsynchronised Transputer readout and counter increments requires a considerable amount of control logic. Its implementation is event-driven, i.e. the high-low and low-high transitions of certain control signals define the state of other control signals. The link adapter chip IC19 transfers the eight bits at the inputs I0-7 to the Transputer when the software running on the Transputers initiates a channel read (QValid=1) and the data at the input is valid (IValid =1). On transfer of the data to the Transputer, the transmission is acknowledged (IAck=1). As twelve bits have to be read from the synchronous up/down counters (IC12-14), a second byte is presented at the inputs of the link adapter (IC19) via the multiplexer chips IC17 and IC18. Again, successful transmission is acknowledged by setting IAck=1. The two latches (IC15-16) transfer the data from the counters to the multiplexers at the initial data request from the Transputer software. The data then remains constant for two subsequent read cycles. The detailed function of the control circuit (IC1-7) is shown in form of a flowchart diagram in Fig. 8.20.

The control circuit has been designed using P-Spice. A resulting timing diagram of the control signals is shown in Fig. 8.18.

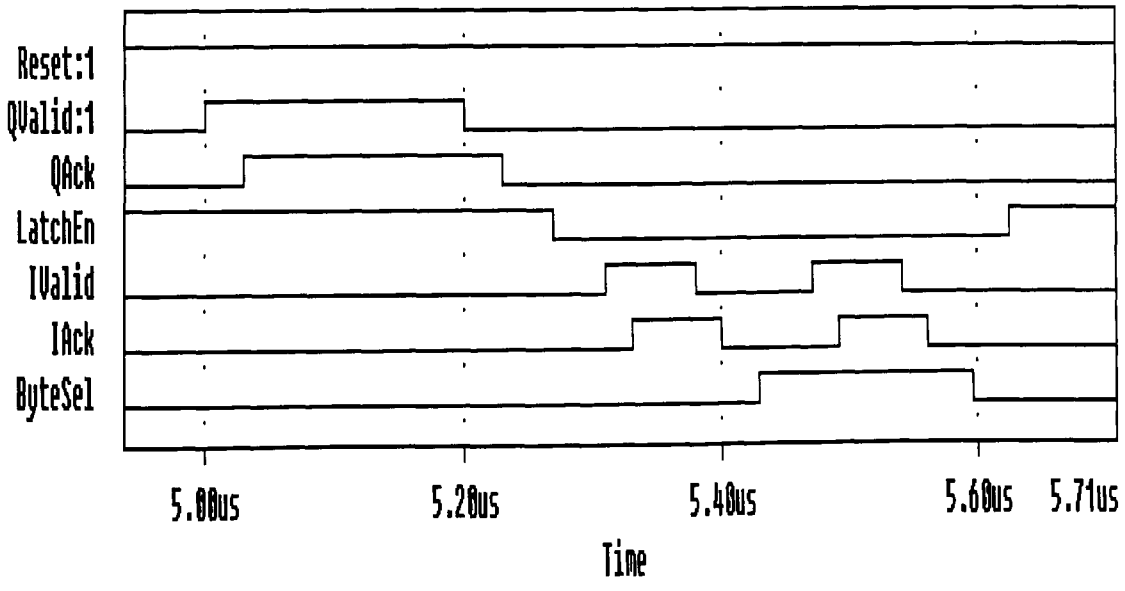

Fig. 8.18: P-Spice timing diagram simulation of position measurement control signals

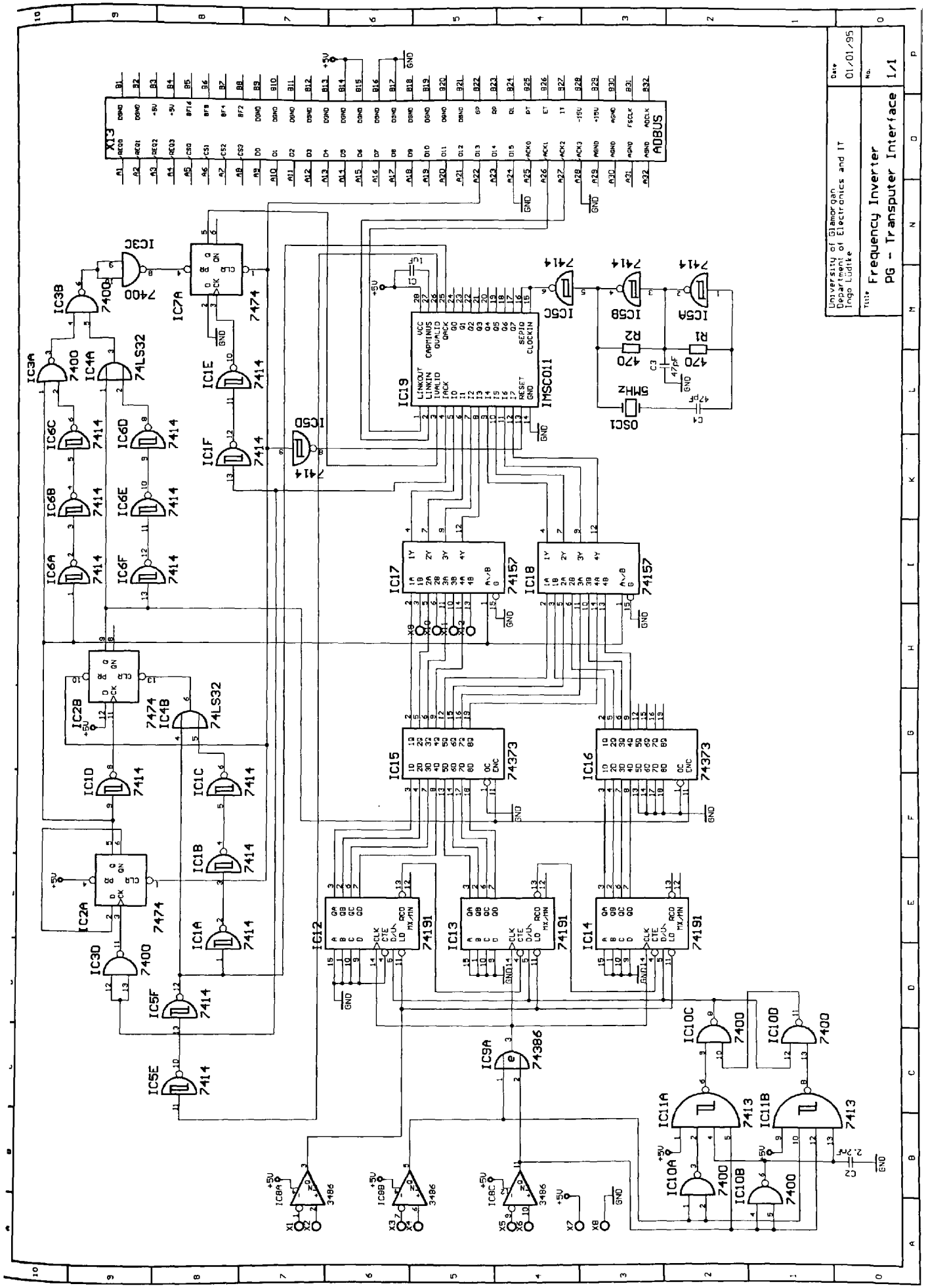

Fig. 8.19: Schematic diagram of the position measurement circuit

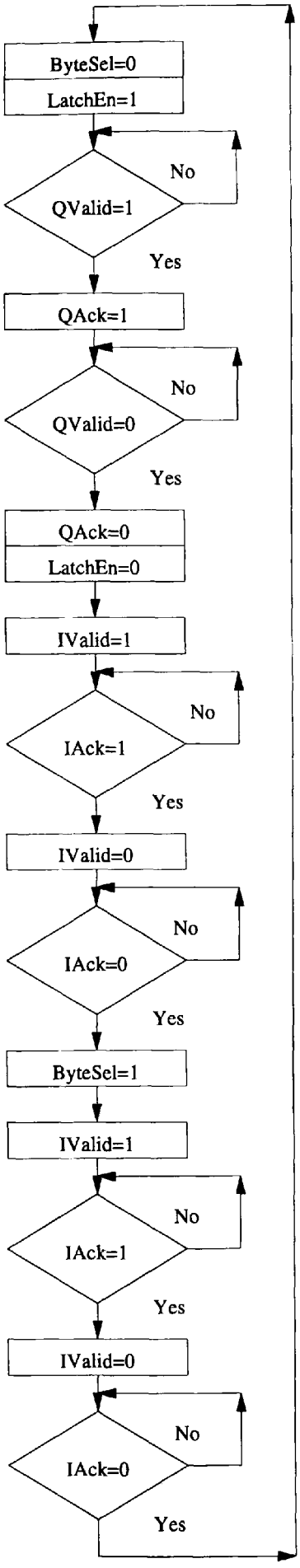

Fig. 8.20: Flowchart of position measurement control logic

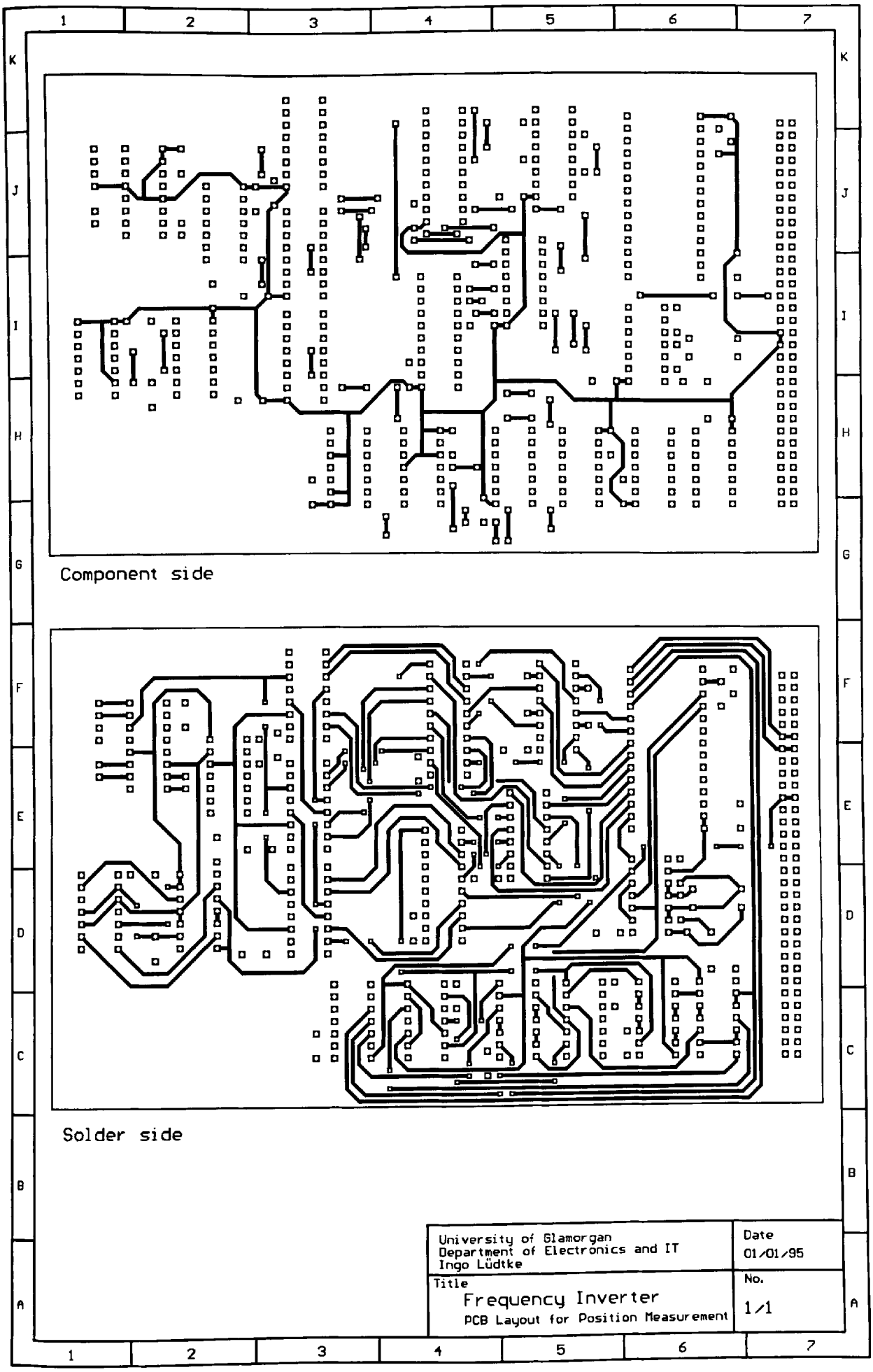

Fig. 8.21: PCB layout of the position measurement circuit

8.1.10 Transputer Board

The micro processors used for this project are Transputers. The inherent advantage of this type of processor is that it allows interconnection of several processors via serial links and therefore the total processing power of a system may be easily increased. The associated programming language Occam allows one to deal with several parallel processors efficiently. Even on a single Transputer, several processes may be formulated as parallel tasks, which are then automatically sequentialised according to priorities, time slicing and current process status (idle or running).

For the control of induction motors however, the efficient use of the processor has proven to be difficult. The algorithms required are generally short and depend on all input quantities at all stages in the algorithm. As the communication between several processors is comparatively slow, the time saved for running parts of the program on different processors is more than lost by the extra communication required between the processors. Another disadvantage is that Transputers are a dying species and that the availability of Transputers is poor. The latest Transputer model (T9000) has not proven to be a success, the manufacturer is no longer existing, and the key personnel working on the development of the Transputers have recognised the failure of their product. Due to the poor utilisation of the increased processing power made available by using several Transputers, the increased system cost is hardly justified. Many single processors on the market are faster and cheaper than Transputers, and do not require one to deal with the problems associated with the communication between several processors.

Nonetheless, for the implementation of an experimental induction motor drive system, the multi-Transputer system has proven useful for tasks like online display of controller parameters and data acquisition without increasing the cycle time by more than $30\mu s$. The Transputer is also a fast processor in its own right and performs 32 and 64 bit floating point arithmetic operations efficiently.

The Transputers used are TRAM modules housed on a B008 motherboard which plugs into a standard PC slot. The specification of the configured card is summarised in Table 8.7.

Table 8.7: Data of Transputer Card

Type	IMS B008
No of TRAMS	5
Transputer Type	5 x T800c
Memory	5 x 2MB
Clock Speed	20MHz
Manufacturer	Inmos Ltd.

By means of link connections on the B008 motherboard, the five Transputers may be interconnected as shown in Fig. 8.22.

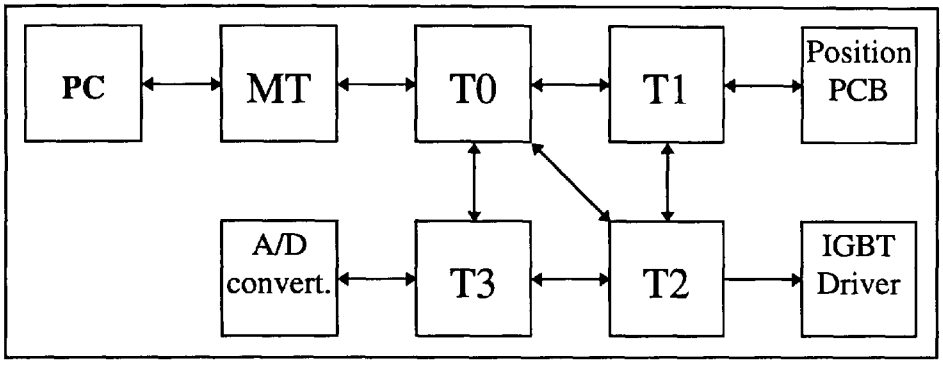

Fig. 8.22: Transputer Network with Inverter Interface

The PC is connected to the Master Transputer (MT). The Master Transputer connects to the Transputer network (T0-T4). Transputer 1 is connected to the position measurement PCB, Transputer 2 is connected to the IGBT driver PCB and Transputer 3 is connected to the analogue to digital converter. This configuration allows the measurements and the inverter output to be carried out in parallel to reduce the overall cycle time.

8.2 Occam Software

The software for the five Transputers has been developed with the 'Occam Development System', Version 1.2, 1988 from Inmos Ltd. The Occam programme listings for vector control and direct torque control are given in Appendix A-2. However, the general approach with some key examples is described below.

The software running on Transputer T1 reads in the rotor position and estimates the rotor speed. It then passes the results to Transputer T2 where the main control

algorithm is running. The software on Transputer T3 reads in the A/D converted currents for two motor phases and performs some scaling and range checking. The results are then also passed to Transputer T2. Transputer T0 is used to pass reference and control data from the Master Transputer to Transputer T2. It also transfers internal controller data from T2 to the Master Transputer. When the user wishes to stop the motor, all processes on T1-T3 are terminated by T0. The Master Transputer runs the 'Occam Development System' and controls the user input and output via the PC keyboard and screen. A terminal program runs on the PC to interface between Master Transputer and PC.

8.2.1 Software on Master Transputer

The software on the Master Transputer allows the user to change reference values, display measured and controller variables on screen and change from the step response mode to the slowly varying reference speed mode. It further starts the acquisition mode upon which the 5000 last samples of 23 internal controller variables are sent from Transputer T2 via T0 to the Master Transputer and converted to a Matlab file and stored on the hard disk of the PC for subsequent evaluation. Values may be read from the PC keyboard with a channel read instruction as follows:

```
keyboard ? int
```

Data may be displayed on the PC screen as shown below.

```
T0.to.host ? real32
goto.xy (screen, 20, i+1)
write.real32 (screen, real32, 5, 4)
```

where *"real32"* is a 32 bit floating point number and *"i"* is an index corresponding to the variables used.

8.2.2 Software on Transputer T0

The software on Transputer T0 controls the communication between the Master Transputer and the Transputer T2. The Occam "ALT" construct is used to serve either the Master or the Transputer T2, as shown below:

```
ALT
  host.to.T0 ? int
    ...serve the host request
  T2.to.T0 ? I
    ...serve the T2 request
```

It may be seen that the "ALT" construct allows the two channels to be watched continuously, without using polling or interrupts.

8.2.3 Software on Transputer T1

The position signal is obtained with two simple channel read and channel write instructions, as shown below:

```
T1.to.Edge0 ! TRUE
Edge0.to.T1 ? position
```

The first instruction initiates the transfer of the counter status to the link adapter, whereas the second instruction reads in the two bytes from the link adapter. The position information is also used for speed estimation. In its simplest form, the speed signal may be calculated as follows.

$$\omega_{mk} = \frac{\gamma_k - \gamma_{k-1}}{T}$$

However, due to the differentiation of the quantised position signal, the speed signal may be very noisy, especially at low motor speed, where the change of position during one sampling interval is small. Hence a lowpass filter is required to obtain the average speed over a number of samples. The time constant of the lowpass filter however, limits the performance of the outer speed control loop. In order to reduce the time constant a modified differentiation algorithm has been used. Samples for the speed estimation are only taken when the position signal has changed and the differentiation is carried out over five different position readings. The differentiation interval T is adjusted accordingly. The resulting speed signal is then filtered with a 4th order digital lowpass filter.

8.2.4 Software on Transputer T2

Transputer T2 is used for the calculation of the direct torque control and flux vector control algorithms. However, the communications with the other Transputers and the inverter is identical. After initialisations and set-up of tables for the sine and cosine functions, the program is synchronised to the internal clock of the Transputer. This is necessary because the program has different cycle times depending on the program branches executed. Since sample time dependent algorithms such as the flux estimator, filter and controller are implemented, it is vital that the sampling time stays

constant. The speed, position and the two phase currents are transferred from the Transputers T1 and T3 as shown below.

```
timer ? AFTER time PLUS 148
timer ? time
PAR
  T1.to.T2 ? gam; omega
  T3.to.T2 ? isa; isb
```

The read instructions from T1 and T3 run in parallel, as indicated by the PAR construct. The cycle time is set to 150μs which consists of 148μs for the program and 2μs for the Timer instruction itself.

8.2.5 Software on Transputer T3

The software on Transputer T3 reads the analogue to digital converted data from the link adapter on the ADC card, scales the data, and passes it to Transputer T2. The data may be obtained as follows:

```
T3.to.Edge2 ! 5 (BYTE)
Edge2.to.T3 ? d1
T3.to.Edge2 ! 3 (BYTE)
Edge2.to.T3 ? d2
isa := (REAL32 ROUND ((INT d1) - 2049)) * 6.59E-4 (REAL32)
isb := (REAL32 ROUND ((INT d2) - 2044)) * 6.59E-4 (REAL32)
```

The first instruction selects the analogue channel number 5 and initiates the analogue to digital conversion for that channel. The second instruction reads the two bytes directly into a 16 bit integer variable. The data is scaled and converted into a 32 bit floating point number using the instructions shown above.
The data is transferred to the Transputer T2 using the following instruction

```
T3.to.T2 ! isa; isb
```

8.3 Interim Conclusion

This chapter has summarised the development of the equipment used for the experimental three phase induction motor drive. A successful implementation of vector control and direct torque control has been obtained.

Chapter 9: Implementation of Flux Vector Control and Direct Torque Control with Practical Results

9.0 Integration of Software into Experimental Induction Motor Drive Systems

In this chapter, the implementation of flux vector control and direct torque control using the experimental frequency inverter system described in Chapter 8, is shown. Furthermore, practical results of the systems are shown and it is seen that motor flux and motor torque have been successfully decoupled with both the flux vector control system and the direct torque control system.

The network of five Transputers and its interaction to the components of the experimental drive system is shown in Fig. 8.2. The tasks for the individual Transputers have been described in section 8.2.

In both the direct torque control system and the flux vector control system, the control algorithm has been implemented on Transputer T2 (see Fig. 8.2). The more general tasks of this Transputer, such as sample time synchronisation, data acquisition and user interaction can be seen from the source code given in Appendix B.

9.1 Implementation of Flux Vector Control

In this section, the implementation of the rotor flux oriented, current controlled, direct flux vector control system with rotor flux space vector and motor torque estimation, as shown in Fig. 6.26, is described.

After data declaration and initialisation, and the synchronisation with Transputers T1 and T3, the algorithm starts by reading the rotor position signal and the rotor speed signal from Transputer T1. In parallel with this, the measured motor phase currents are transferred from Transputer T3 to Transputer T2. This may be expressed in the Occam programming language by the following statement:

```
PAR
  T1.to.T2 ? gam; omega
  T3.to.T2 ? isa; isb
```

where 'gam' represents the rotor position γ_m and 'omega' represents the rotor speed ω_m. The motor phase currents 'isa' and 'isb' are converted to the stationary two axis $\alpha-\beta$ system using Equ. 2.24 and Equ 2.25 and solving the complex stator current space vector for its real and imaginary parts as shown in Equ. 9.1.

$$\begin{aligned} a &= e^{j\frac{2\pi}{3}} = -\frac{1}{2} + j\frac{\sqrt{3}}{2} \\ \vec{i}_s &= \frac{2}{3}\left(i_{sA} + a i_{sB} + a^2 i_{sC}\right) = \frac{2i_{sA} - i_{sB} - i_{sC}}{3} + j\frac{i_{sB} - i_{sC}}{\sqrt{3}} \end{aligned} \tag{9.1}$$

Furthermore, because the sum of the three motor currents is zero, the expression for the real part of the complex stator current space vector may be simplified as shown in Equ. 9.2.

$$\vec{i}_s = i_{s\alpha} + j i_{s\beta} = i_{sA} + j\frac{i_{sA} + 2i_{sB}}{\sqrt{3}} \tag{9.2}$$

As the stator current of phase 'A' is equal to the real part of the stator current space vector $\vec{i}_s$, only the imaginary part needs to be converted as shown below in Occam format.

```
isbeta := (isa + (isb + isb)) * 0.5773502692 (REAL32)
```

The transformation of the stator current space vector from stationary co-ordinates to a co-ordinate system which is rotating with the rotor flux space vector, may be carried out using Equ. 2.31, where the angle $\gamma_k = -\gamma_s$ may be used. The conversion from vector notation to real and imaginary components is shown in Equ. 9.3.

$$\left(i_{s\alpha} + j i_{s\beta}\right)e^{-i\gamma_s} = i_{s\alpha}\cos\gamma_s + i_{s\beta}\sin\gamma_s + j\left(i_{s\beta}\cos\gamma_s - i_{sa}\sin\gamma_s\right) \tag{9.3}$$

The Occam version of Equ. 9.3 is shown below.

```
isx := (isa * cosTa[gam.s]) + (isbeta * sinTa[gam.s])
isy := (isbeta * cosTa[gam.s]) - (isa * sinTa[gam.s])
```

The estimated rotor flux level may be calculated from Equ. 6.14a and by converting it into its discrete equivalent and using the values given in Equ. 2.88 the following equation, shown in Occam format, may be obtained.

```
pr := (pr * 0.99869753(REAL32))+(0.0024792799(REAL32) * isx)
```

Because of the integration necessary to obtain the rotor flux level from the stator current, the result of the integration is prevented from over- and under-flow as shown below.

```
IF
  pr > 2.0 (REAL32)
    pr := 2.0 (REAL32)
  pr < 1.0E-2 (REAL32)
    pr := 1.0E-2 (REAL32)
  TRUE
    SKIP
```

The slip frequency may be obtained from the torque component of the stator current and the rotor flux level as shown in the following Occam statement.

```
omega.sl := 0.05264624652865 (REAL32) * (isy / pr)
```

Again, the numerical values of the motor parameters given in Equ. 2.88 have been used to simplify the calculations. The slip frequency may be integrated over time and scaled to the same format as that of the measured rotor position by using the following set of Occam expressions.

```
gam.sl := gam.sl + (7.68(REAL32)*(omega.sl + omega.sl.old))
omega.sl.old := omega.sl
IF
  gam.sl > 2047.0 (REAL32)
    gam.sl := gam.sl - 2048.0 (REAL32)
  gam.sl < 0.0 (REAL32)
    gam.sl := gam.sl + 2048.0 (REAL32)
  TRUE
    SKIP
```

The angle of the rotor flux space vector, referred to the stator axis, which is used for the transformation of the stator current components (Equ. 9.3) may be obtained as follows:

```
gam.s := gam + (INT ROUND gam.sl)
IF
  gam.s > 2047
    gam.s := gam.s - 2048
  gam.s < 0
    gam.s := gam.s + 2048
```

```
    TRUE
      SKIP
```

The torque reference signal is generated by using a PID speed controller. In order to prevent over- or under flow of the signal, a numerical limiter is employed, as shown below:

```
omega.err := omega.ref - omega
tor.ref := ((Kp1 * omega.err) + (Kd1 * omega.err.old)) +
           (Ki1 * tor.ref)
omega.err.old := omega.err
IF
  tor.ref > 2.0 (REAL32)
    tor.ref := 2.0 (REAL32)
  tor.ref < (-2.0 (REAL32))
    tor.ref := -2.0 (REAL32)
  TRUE
    SKIP
```

Similarly, the reference value of the field component of the stator current reference space vector is generated by a PID rotor flux controller as is shown in the following set of Occam statements.

```
pr.err := pr.ref - pr
isx.ref := ((Kp2 * pr.err) + (Kd2 * pr.err.old)) +
           (Ki2 * isx.ref)
pr.err.old := pr.err
IF
  isx.ref > 2.0 (REAL32)
    isx.ref := 2.0 (REAL32)
  isx.ref < (-2.0 (REAL32))
    isx.ref := -2.0 (REAL32)
  TRUE
    SKIP
```

The developed motor torque may be estimated using Equ. 6.14c, as shown below.

```
tor := 0.905711388 (REAL32) * (pr * isy)
```

The torque component of the stator current reference space vector is generated using a PID torque controller. The output of this controller is limited to avoid over- or under flow of the output variable.

```
tor.err := tor.ref - tor
isy.ref := ((Kp3 * tor.err) + (Kd3 * tor.err.old)) +
           (Ki3 * isy.ref)
tor.err.old := tor.err
IF
  isy.ref > 2.0 (REAL32)
    isy.ref := 2.0 (REAL32)
  isy.ref < (-2.0 (REAL32))
    isy.ref := -2.0 (REAL32)
  TRUE
    SKIP
```

By using Equ. 9.4, the stator current reference space vector may be converted to stationary co-ordinates in the two-axis system by using the angle of the rotor flux space vector γ_s, which is referred to stationary co-ordinates.

$$i_{s\alpha} + ji_{s\beta} = \left(i_{sx} + ji_{sy}\right)e^{i\gamma_s} = i_{sx}\cos\gamma_s - i_{sy}\sin\gamma_s + j\left(i_{sx}\sin\gamma_s + i_{sy}\cos\gamma_s\right) \quad (9.4)$$

This may be expressed in Occam as follows:

```
isa.ref := (isx.ref * cosTa[gam.s])-(isy.ref * sinTa[gam.s])
isbeta.ref :=(isx.ref * sinTa[gam.s])+(isy.ref*cosTa[gam.s])
```

The reference stator current components may be converted to the three phase 'A', 'B', 'C' reference system as follows:

```
isB.ref:=(0.866025(REAL32)*isbeta.ref)-(0.5(REAL32)*isa.ref)
isC.ref:=-((0.866(REAL32)*isbeta.ref)+(0.5(REAL32)*isa.ref))
```

The inverter power switch settings can be obtained from the comparison of the measured stator currents and their reference values as shown below.

```
IF
  isa > isa.ref
    out := A.neg              %phase 'A' to minus of d.c. link
  TRUE
    out := A.pos              %phase 'A' to plus of d.c. link
IF
  isb > isB.ref
    out := out + B.neg        %phase 'B' to minus of d.c. link
  TRUE
    out := out + B.pos        %phase 'B' to plus of d.c. link
```

```
IF
  (-(isa+isb)) > isC.ref
    out := out + C.neg        %phase 'C' to minus of d.c. link
  TRUE
    out := out + C.pos        %phase 'C' to plus of d.c. link
```

At the end of each program cycle, the inverter power switch settings are transmitted to the IGBT driver circuitry using the following Occam statements.

```
k := k >< watchdog
T2.to.Edge1 ! BYTE (out + k)
```

A watchdog signal, which is basically a square wave signal with a pulse width of one sampling interval (150μs) is output at the same time.

9.2 Practical Results of Flux Vector Control

In the following, practical results obtained from the flux vector control system described above, are shown. The first set of curves (Fig. 9.1 to Fig. 9.3) shows steady state operation at $\omega_m = -0.1 p.u.$ and $T_l = 0.085 p.u.$

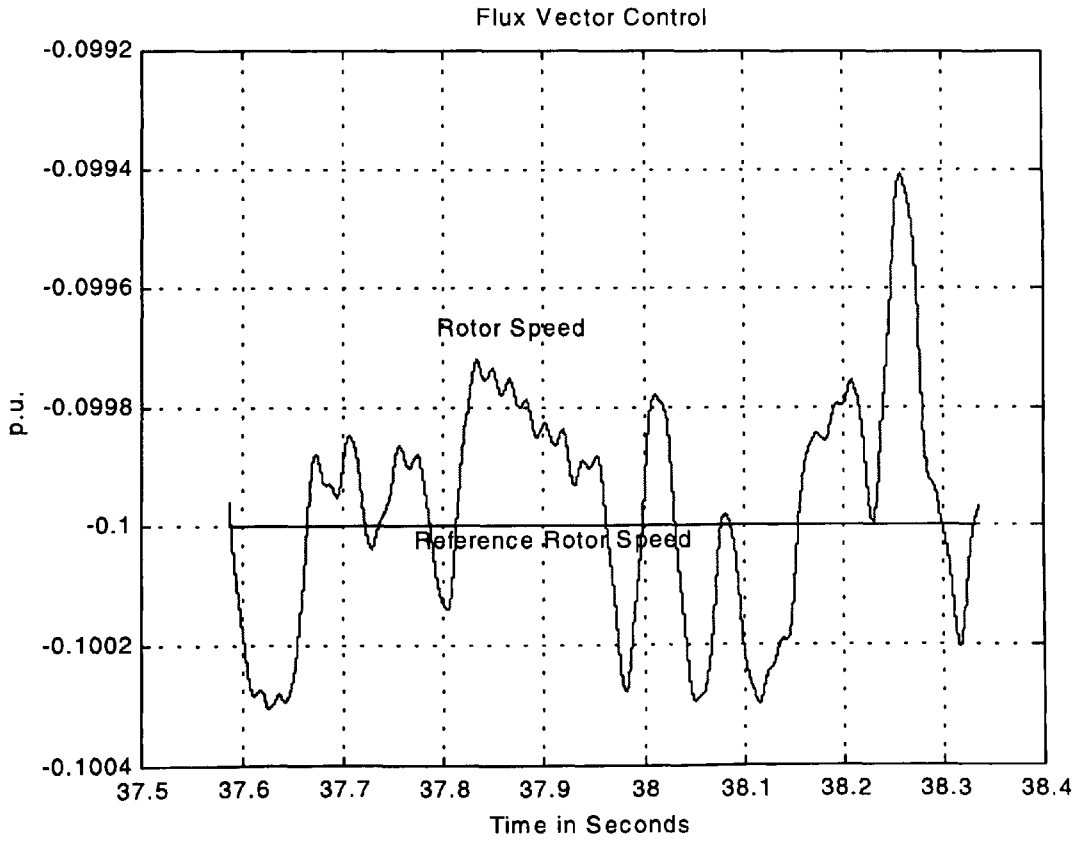

Fig. 9.1: Motor speed variations with time using Flux Vector control

It may be seen from Fig. 9.1 that the actual rotor speed waveform has small oscillations above and below the speed reference signal. The maximum value of the oscillation above the reference signal may be calculated as shown in Equ. 9.5:

$$\frac{(-0.0994)-(-0.1)}{-0.1}100\% = -0.6\% \tag{9.5}$$

As may be seen from Equ. 9.5, the maximum speed deviation from the reference speed value shown in Fig. 9.1, is 0.6%.

In Fig. 9.2, the rotor flux level and the motor torque are shown. It may be seen that the reference values match the estimated values well, and no steady state error may be seen. However it should be noted that good control over the estimated variables does not necessarily imply that there is also good control over the actual motor variables.

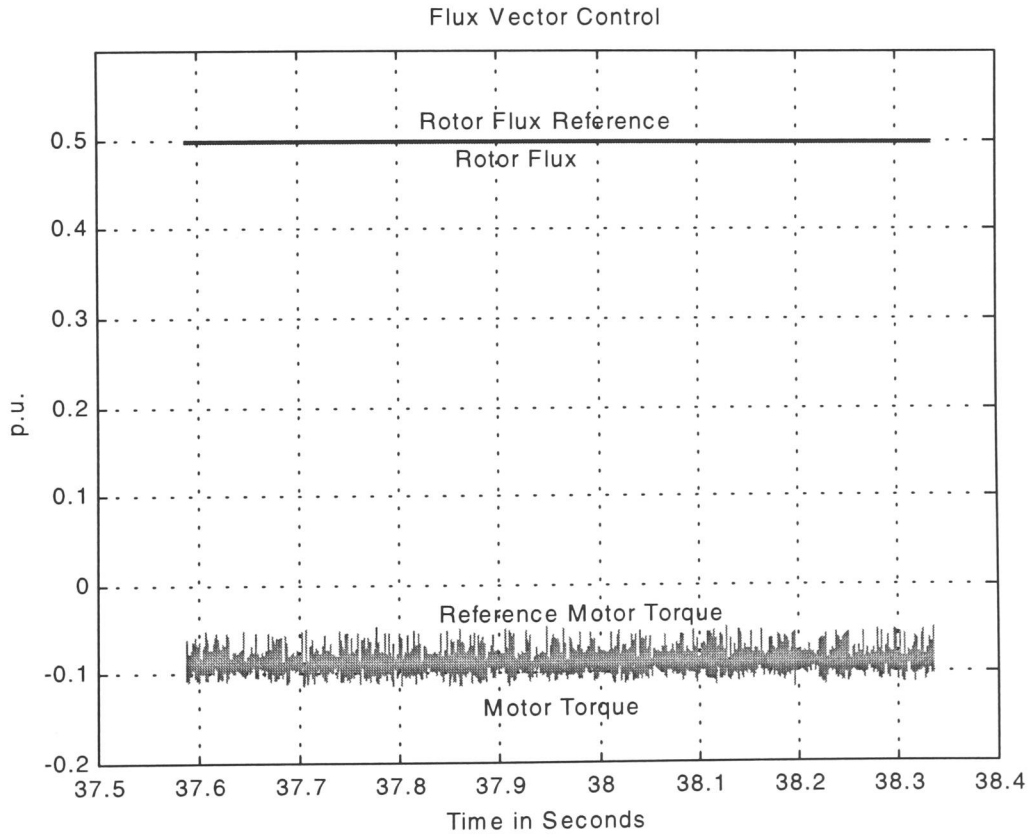

Fig. 9.2: Rotor Flux and Motor Torque variations with time using Flux Vector Control

The actual waveforms of the measured stator currents is shown in Fig. 9.3. It may be seen that the waveforms approximate those of sine waves.

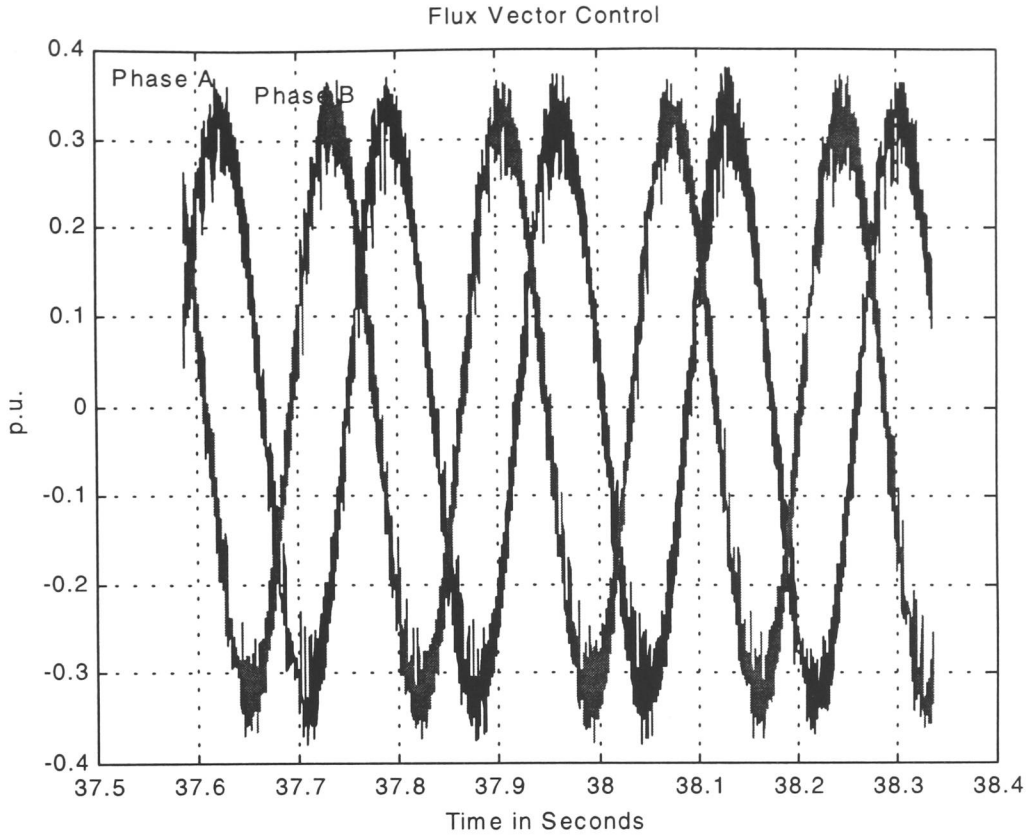

Fig. 9.3: Stator currents variations with time using Flux Vector Control

The following set of wave forms (Fig. 9.4 to Fig. 9.6) show the behaviour of the flux vector control system during transient operation. As can be seen from Fig. 9.4, the rotor speed reference signal has been changed from $\omega_m = +0.1 p.u.$ to $\omega_m = -0.1 p.u.$ at $t = 83.4$ seconds. It may be seen that the actual motor speed decelerates within 150ms to standstill and then accelerates again with reverse sense of rotation. There is a speed transient at $t = 83.45$ seconds which probably caused by the backlash in the eddy current dynamometer, which is used to load the induction motor.

If may be seen from Fig. 9.5 that there is a torque transient, associated with the step change of the speed reference signal, varying from $T_l = 0.085 p.u.$ to $T_l = -0.15 p.u.$. As can be seen, the rotor flux level does not vary during this transient. Therefore, decoupling of rotor flux and motor torque has been achieved. It may also be seen from Fig. 9.4 and Fig. 9.5 that the absolute value of the developed motor torque reduces after the torque transient due to the PI-action of the speed controller. The speed controller may be improved by using the PI-action for small variation from the reference value only, otherwise a fixed reference torque may be applied (torque control).

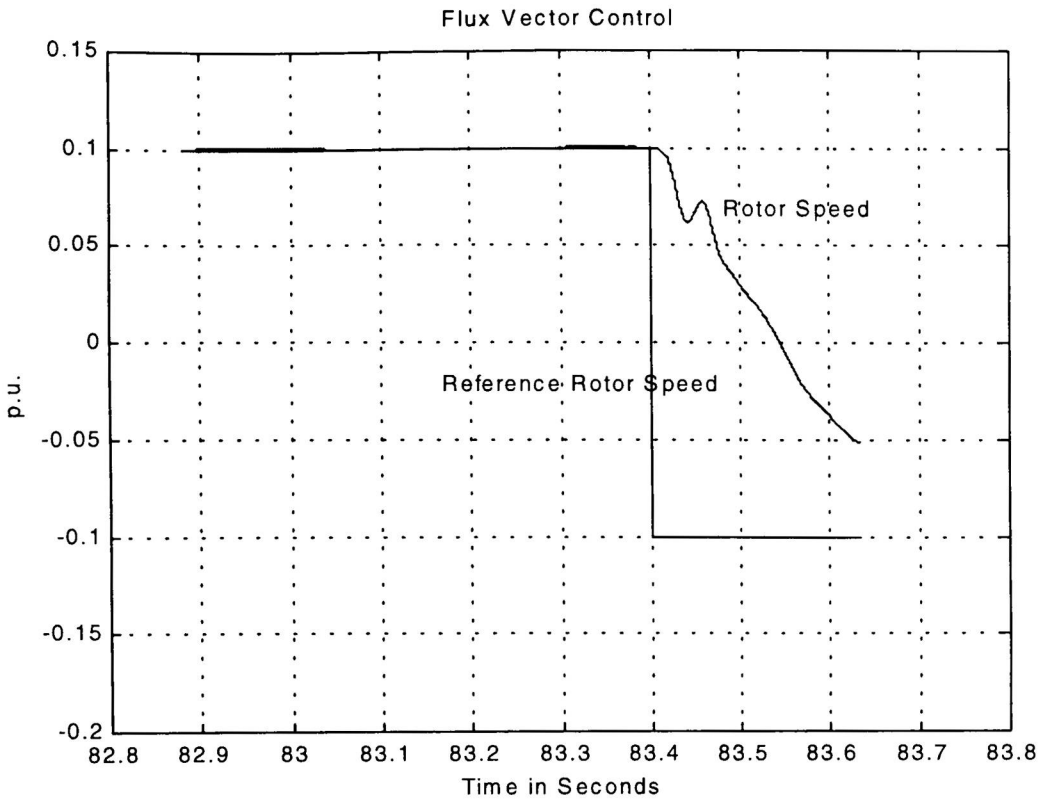

Fig. 9.4: Rotor Speed variations with time using during Transient Operation using Flux Vector Control

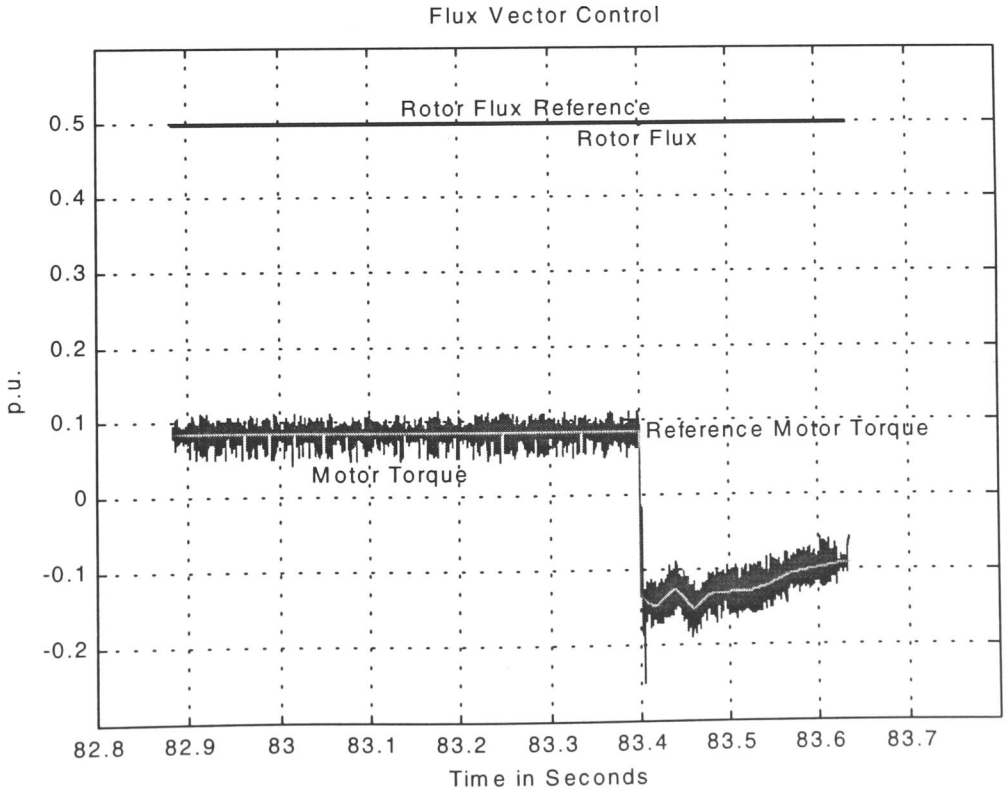

Fig. 9.5: Rotor Flux and Motor Torque variations with time using during Transient Operation using Flux Vector Control

The variation of the stator current in phase 'A' and phase 'B' are shown in Fig. 9.6. It may be seen that the output frequency changes considerably after the step in the speed reference signal has been applied. This is mainly due to the negative slip frequency which is generated to brake the motor.

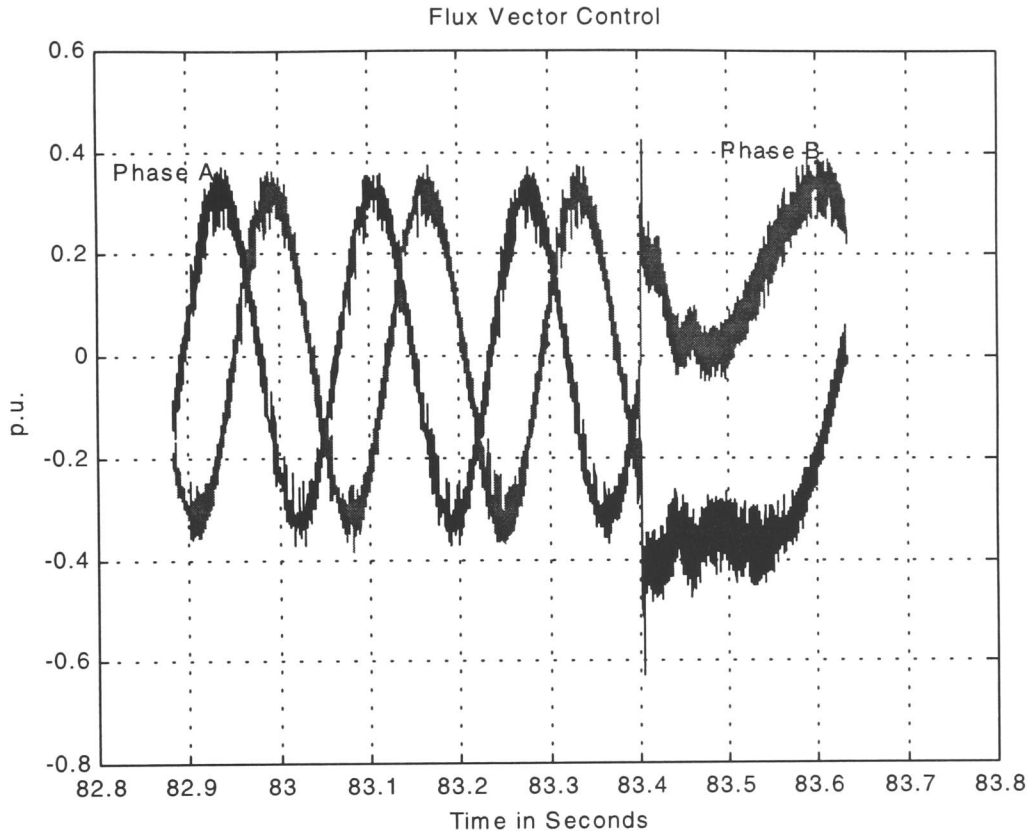

Fig. 9.6: Stator Currents variations with time during Transient Operation using Flux Vector Control

The steady state and transient state curves shown, demonstrate that the decoupling of the rotor flux and the motor torque has been achieved.

9.3 Implementation of Direct Torque Control

In this section, the implementation of the direct torque control with stator flux and motor torque estimation, being as shown in the control system of Fig. 7.11, is described. After data declaration and data initialisation, synchronisation with Transputers T1 and T3 is carried out. The direct torque control algorithm starts by reading the rotor position signal and the rotor speed signal from Transputer T1. In parallel with this, the measured

motor phase currents are transferred from Transputer T3 to Transputer T2. This may be expressed in the Occam programming language by the following statement:

```
PAR
  T1.to.T2 ? gam; omega
  T3.to.T2 ? isa; isb
```

Similarly to the case of flux vector control, the β-component of the stator current space vector may be calculated by means of Equ. 9.2, which is expressed in the Occam programming language in the following form:

```
isbeta := (isa + (isb + isb)) * 0.5773502692 (REAL32)
```

For the stator flux estimation, a co-ordinate transform to rotor oriented co-ordinates is necessary for the system shown in Fig. 7.11. This may by achieved by using Equ. 9.3. However, the rotor position angle must be used instead of the angle of the rotor flux vector. In Occam format, this may be expressed as follows:

```
isd := (isa * cosTa[gam]) + (isbeta * sinTa[gam])
isq := (isbeta * cosTa[gam]) - (isa * sinTa[gam])
```

The components of the rotor flux space vector may be calculated by means of Equ. 7.2, or alternatively split into two parts using the rotor flux linkage equation as shown below.

```
prd := (prd*0.99869753701(REAL32))+(0.002479279(REAL32)*isd)
prq := (prq*0.99869753701(REAL32))+(0.002479279(REAL32)*isq)
psd := (prd*0.9057113889(REAL32))+(0.2622282037(REAL32)*isd)
psq := (prq*0.9057113889(REAL32))+(0.2622282037(REAL32)*isq)
```

The numerical values have been obtained using the parameters given by Equ. 2.88. The stator flux components, given in rotor oriented co-ordinates, may be transformed to a co-ordinate system fixed to the stationary stator axis using Equ. 9.4. However, the rotor position angle γ_m must be used instead of the rotor flux space vector angle γ_s. The stator flux space vector components are numerically confined to reasonable values in order to prevent erroneous numerical over- and under flow. This may be expressed in the Occam programming language as shown below:

```
ps.al := (psd * cosTa[gam]) - (psq * sinTa[gam])
ps.be := (psd * sinTa[gam]) + (psq * cosTa[gam])
IF
  ps.al > 2.0 (REAL32)
    ps.al := 2.0 (REAL32)
  ps.al < (-2.0 (REAL32))
    ps.al := -2.0 (REAL32)
  TRUE
    SKIP
IF
  ps.be > 2.0 (REAL32)
    ps.be := 2.0 (REAL32)
  ps.be < (-2.0 (REAL32))
    ps.be := -2.0 (REAL32)
  TRUE
    SKIP
```

The stator flux level may be calculated from the stator flux space vector components according to the following expression:

```
ps:=sqrtTa[INT ROUND(1024.0(REAL32)*
    ((ps.al*ps.al)+(ps.be*ps.be)))]
```

Scaling has been used in order to use a look-up table for the square root function. The torque reference signal is generated by using a PID speed controller. In order to prevent over- or under flow of the signal, a numerical limiter is employed, as shown below:

```
omega.err := omega.ref - omega
tor.ref := tor.ref + ((n0 * omega.err) + (n1 * omega.err.1))
omega.err.1 := omega.err
IF
  tor.ref > 2.0 (REAL32)
    tor.ref := 2.0 (REAL32)
  tor.ref < (-2.0 (REAL32))
    tor.ref := -2.0 (REAL32)
  TRUE
    SKIP
```

The developed motor torque may be calculated according to Equ. 7.3 using the stator current space vector components and the stator flux space vector components, as shown in the following Occam statement.

```
tor := (psd * isq) - (psq * isd)
```

The torque error signal T_{err} may be calculated using Equ. 7.1 as follows:

```
IF
  tor < (tor.ref - TauHyst)
    Tau := 2
  tor > (tor.ref + TauHyst)
    Tau := 0
  (Tau = 2) AND (tor.ref < tor)
    Tau := 1
  (Tau = 0) AND (tor.ref > tor)
    Tau := 1
  TRUE
    SKIP
```

Similarly, the flux level error signal ψ_{err} may also be calculated using Equ. 7.1.

```
IF
  ps < (ps.ref + PhiHyst)
    Phi := 1
  ps > (ps.ref - PhiHyst)
    Phi := 0
  TRUE
    SKIP
```

The location of the stator flux space vector may be obtained using a look-up table. The inputs to the look-up table are the stator flux vector components. Using appropriate comparisons inputs for the look-up table may be generated as shown in the following Occam statement.

```
Theta :=
ThetaTa[INT(ps.al>z)][INT(ps.be>z)][INT((w3*ABS(ps.be))>ABS(ps.al))]
```

The direct torque control table may be accessed using the stator flux level error, the torque error and the stator flux space vector location being given as follows:

```
out := vvTa[Phi][Tau][Theta]
```

At the end of each program cycle, the inverter power switch settings, including a watchdog signal, are transmitted to the IGBT driver circuitry using the following Occam statements.

```
k := k >< watchdog
T2.to.Edge1 ! BYTE (out + k)
```

9.4 Practical results of Direct Torque Control

In the following, the practical results obtained with the flux vector control system described above (Fig. 7.11), are shown. Fig. 9.7 and Fig. 9.8 show slowly varying speed operation from $\omega_m = 0.135 p.u.$ to $\omega_m = -0.015 p.u.$

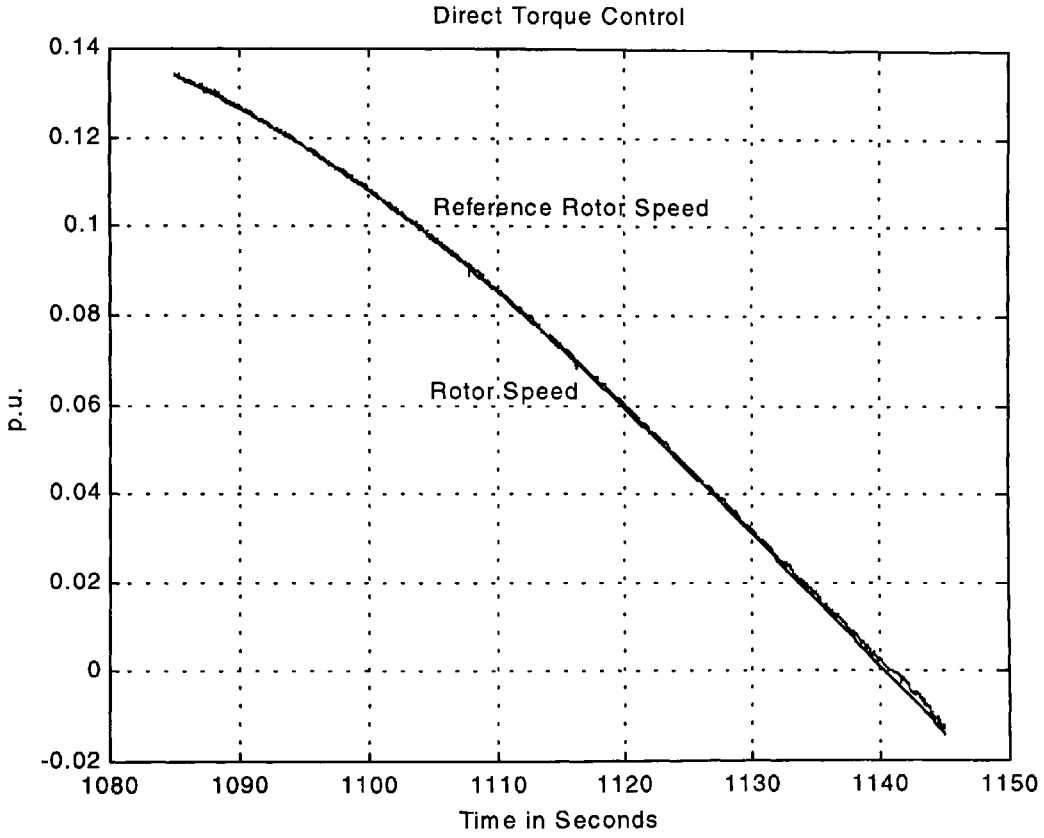

Fig. 9.7: Rotor speed variations with time using
Slowly Varying Operation of Direct Torque Control

Fig. 9.7 shows a sinusoidal varying speed reference signal with the estimated speed signal obtained from the shaft encoder. The data captured in the figure corresponds to 60 seconds of operation. It can be seen that the estimated speed follows the reference speed closely. At $t = 1140$ seconds the rotor is at standstill. The rotor then accelerates slowly to 1.5% of its nominal speed in the reverse direction.

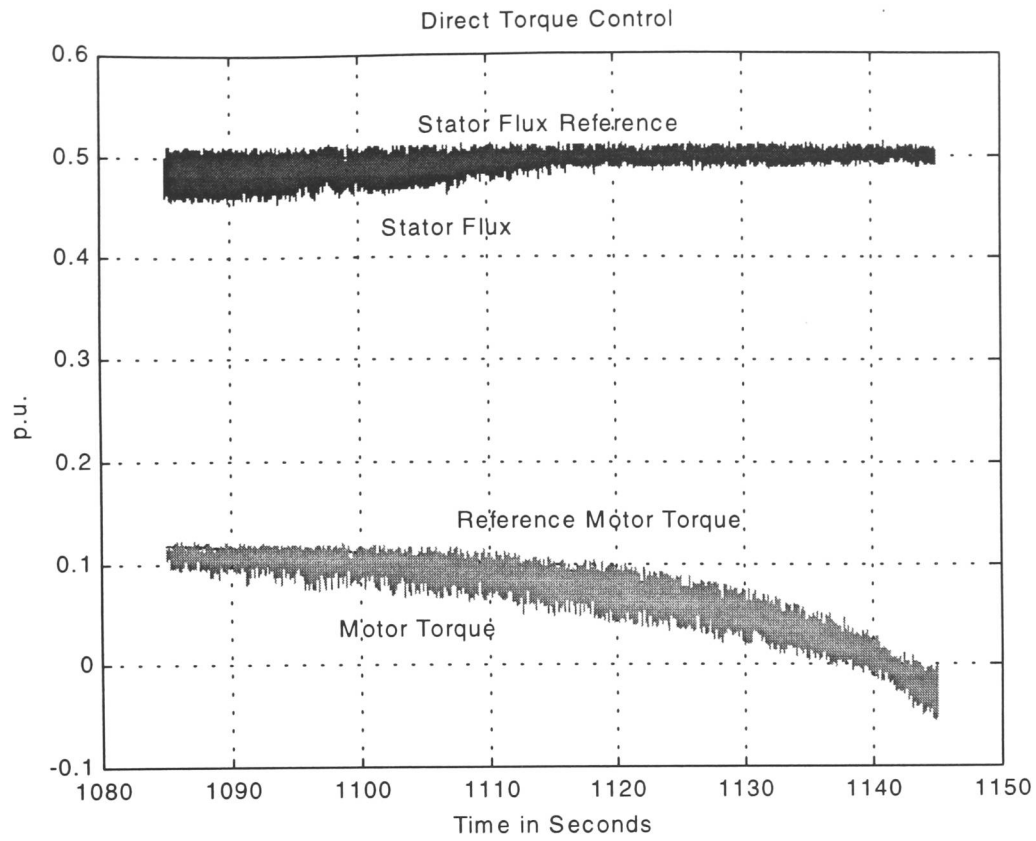

Fig. 9.8: Stator Flux and Motor Torque variations with time during slowly varying Operation using Direct Torque Control

The stator flux level and the estimated motor torque may be seen in Fig. 9.8. It is evident from the figure that the stator flux and the motor torque follow their reference values closely. It may also be seen that the stator flux variations depend on the operational conditions of the motor.

Fig. 9.8 also shows that there is zero developed torque at zero speed. This is because the load, being an eddy current dynamometer, can not generate torque at zero speed.

The set of curves shown in Fig. 9.9 to Fig. 9.11 illustrate slowly varying speed operation with an initial step on the speed reference signal from $\omega_m = -0.1 p.u.$ to $\omega_m = 0 p.u.$

It may be seen from Fig. 9.9 that the estimated speed signal follows the reference speed signal closely, though there is a marginal error around zero speed.

Fig. 9.10 shows that the stator flux level and the motor torque both follow their reference signals closely. There is a peak of developed motor torque at $t = 150.5ms$ which is essential to decelerate the motor to standstill. As can be seen, the stator flux level is not affected by this variation in motor torque, thus decoupling of stator flux and motor torque has been achieved.

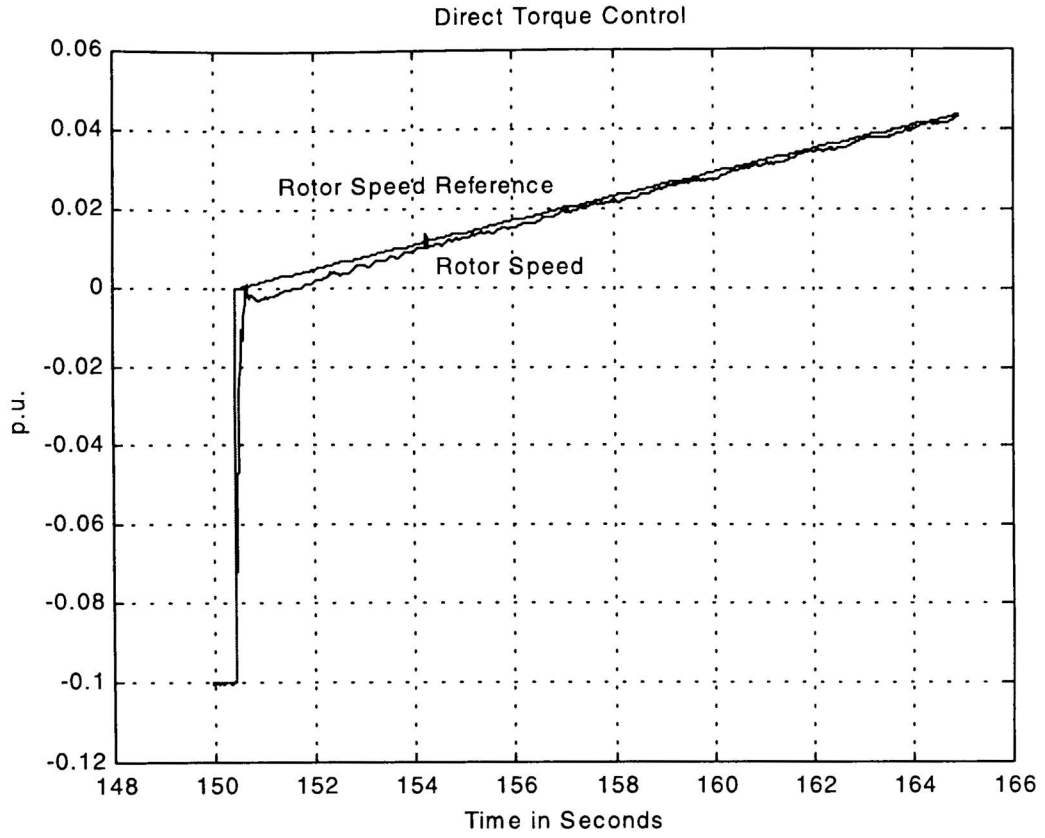

Fig. 9.9: Motor Speed variations with time using Direct Torque Control

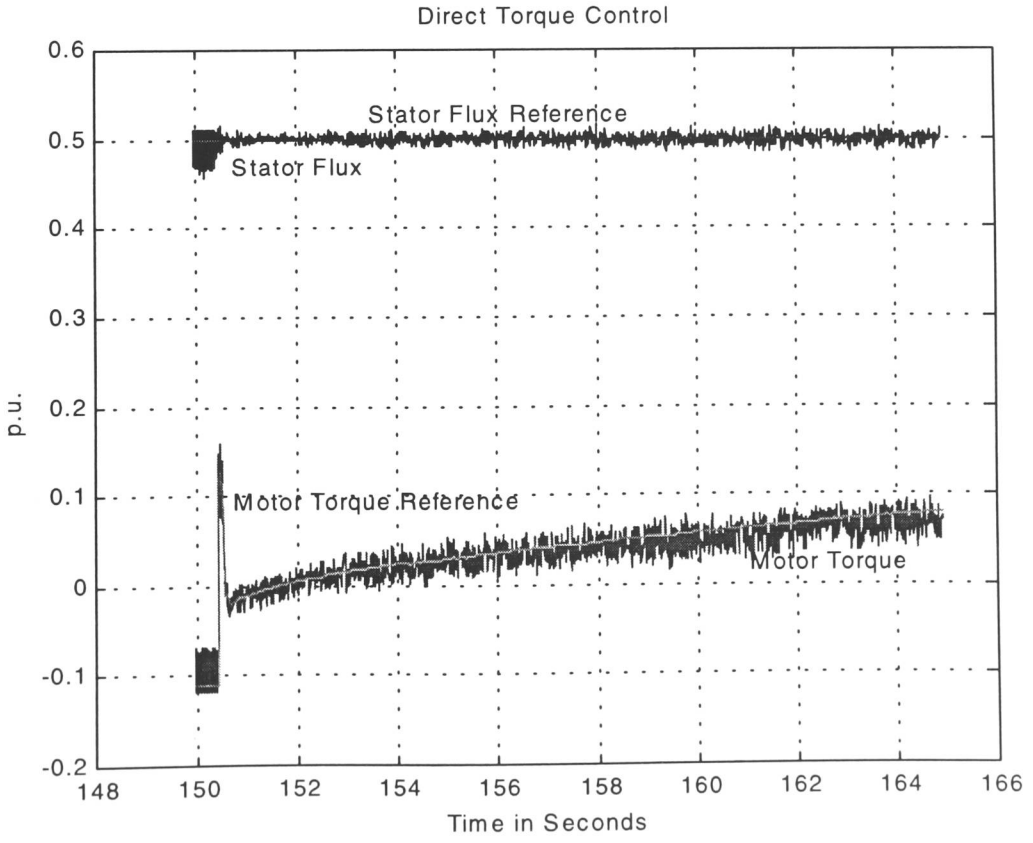

Fig. 9.10: Stator Flux and Torque variations with time using Direct Torque Control

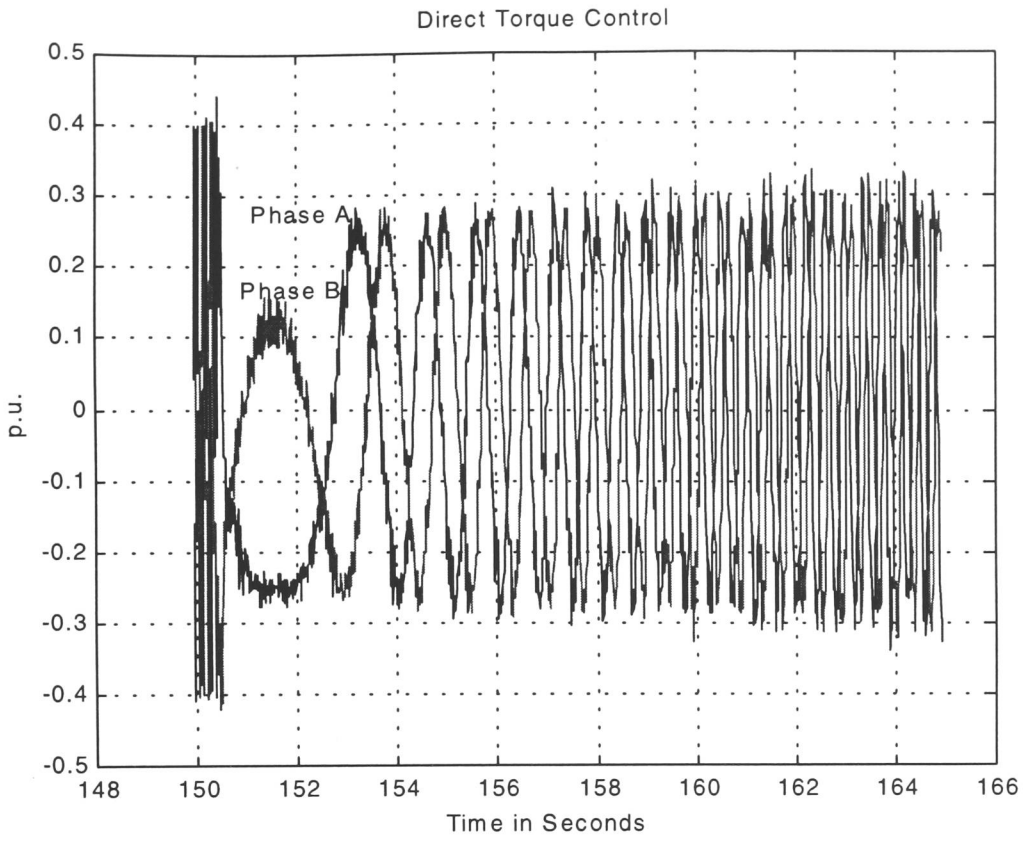

Fig. 9.11: Stator Currents variations with time using Direct Torque Control

Fig. 9.11 shown the variation of the stator phase currents. It may be seen that the frequency of the current wave forms increases smoothly.

Fig. 9.12 shows the stator flux level, the motor torque and the rotor speed both as estimated and reference wave forms for a step change of the rotor speed from $\omega_m = +0.05 p.u.$ to $\omega_m = -0.05 p.u.$ There is no transient of the stator flux level, during the transient change of the motor torque.

In Fig. 9.13, the stator flux level, the motor torque and the rotor speed signals are shown both as reference and estimated quantities. In this case, the rotor speed has been varied according to a sine wave with a period of 30 seconds. It may be seen that the stator flux ripple vary according to the operating condition. The controlled variables shown in the figure follow their reference quantities closely.

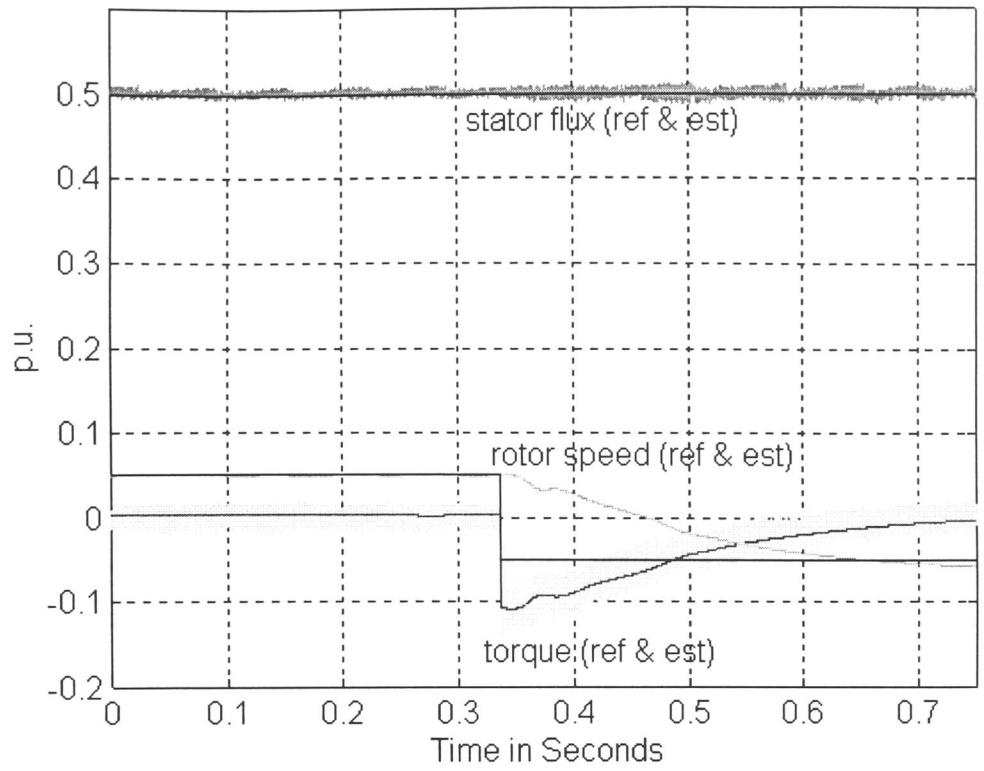

Fig. 9.12: Stator Flux, Motor Torque and Rotor Speed during Step Operation using Direct Torque Control

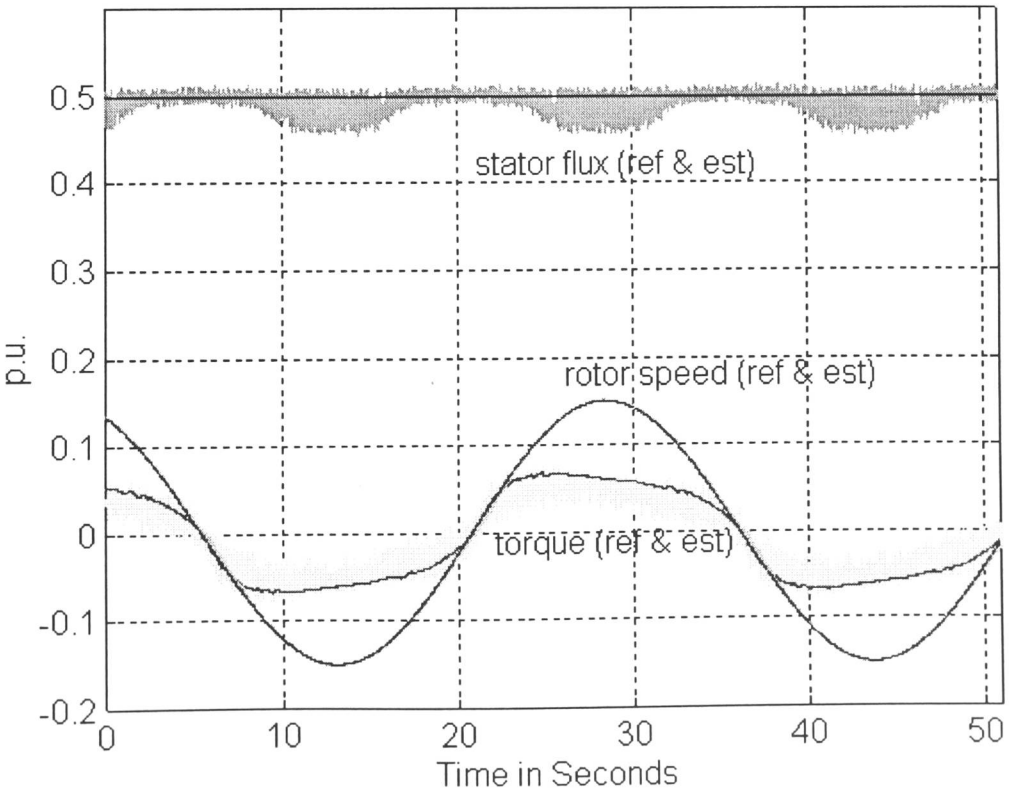

Fig. 9.13: Stator Flux, Motor Torque and Rotor Speed during slowly variable Operation using Direct Torque Control

9.5 Interim Conclusion

In this chapter, the implementation of two high performance control strategies for three phase cage rotor induction motors has been described. The first being the rotor flux oriented, current controlled direct flux vector control with rotor flux and torque estimation and the second being the direct torque control system with stator flux and torque estimation.

The software implementation of the algorithms for the two control strategies has been described in detail.

It has been found that although the direct torque control algorithm appears less complex, very similar computational requirements on the micro controller have resulted for the two systems. This is due to the fact that the flux estimation is usually seen to be separate from the basic direct torque control algorithm. However, in a practical system it is also required, thus increasing the total amount of computations to approximately the level required for the flux vector control algorithm. In any case, the amount of computations required for the user interface, data acquisition and synchronisation of the individual processors far outweighs the amount of software required for the induction motor control algorithm.

Both systems have been found to accurately control the rotor speed of the induction motor. The motor torque and the motor flux have been shown to be decoupled for both systems.

Chapter 10: Conclusion and Further Work

10.0 Conclusions

The steady state induction motor analysis reported in chapter 3 of this thesis has given further insight into the operational areas of VVVF operation. It has been shown how motor variables such as voltage, flux and current vary during operation of the motor at different rotor speeds and at different load torques. It has also been shown that the operational area in the rotor speed - motor torque plane, where the motor efficiency may be optimised, is limited to light motor torque operation only and corresponds to constant slip operation. The other operating areas, of course, being the constant voltage and constant flux ones. The product of efficiency and power factor has been newly identified as a desirable optimisation criteria as it represents a good compromise between maximum efficiency and maximum power factor operation.

The waveforms and the harmonic content for the six step mode of operation have been investigated and the rated operating condition has been examined. It has been found that the undesirable harmonics in the voltage, current and flux waveforms are the 5th, 7th, 11th, 13th,...6N±1 (N=1,2,3,...) harmonics, as only the fundamental voltage, current and flux waveforms are beneficial for the production of constant motor torque. It has also been shown that these harmonics produce input power, output power, torque and speed waveforms containing the 6th, 12th, 18th, 24th,...6N (N=1,2,3) harmonics, which are the even triple harmonics.

The six step mode of operation is still particularly relevant to modern day inverters, because it is used in VVVF converters for high speed operation where maximum voltage is required. It has been shown, that there exists a large operational area in the motor torque-rotor speed plane which corresponds to the six step mode (CVVF) of operation.

The undesirable effects of six step operation, which are mainly torque pulsations and motor heating due to the high harmonic content in the supply voltage, have been analysed. It has been shown that motor operating conditions may be improved by using a higher d.c. link voltage, so that the p.w.m. mode is used for a larger operating area in the torque-speed plane. The six step mode then being used for higher speeds,

corresponding to higher motor supply frequencies which further reduces the harmonic content of the current, flux, power, torque and speed waveforms.

A study of different p.w.m. strategies has been made and it has been shown that for the synchronised mode of operation at low switching frequencies, the regular symmetric sampling method has the highest total harmonic distortion of the six different p.w.m. methods considered. It has also been shown that the space vector modulation scheme is superior to natural sampling and asymmetric regular sampling in terms of both the total harmonic distortion and the maximum achievable output voltage. Similarly, it is shown that the known methods of harmonic elimination and minimum total harmonic distortion technique, both described in chapter 5 of this thesis, have the lowest total harmonic distortion of the six systems considered. However, the relationship between the switching angle variation and the required output voltage magnitude is discontinuous, which can produce current transients during the voltage variation from one side of the switching angle discontinuity to the other. This effect can be of particular concern when closed loop speed control is desired.

Numerous methods used for high frequency p.w.m. generation were also investigated. It was found that the hysteresis current control method gives good steady state performance and excellent dynamic response. 'Limit cycles', which may present a problem with dedicated hardware solutions are shown to be automatically eliminated when micro processor control is used.

The results of the investigation have also shown that the sigma-delta modulation technique can give good results at high switching frequencies when the current feedback signals required for hysteresis current control, are not available.

Different flux vector control schemes have also been considered in this thesis. A comparison of simulated systems for different motor flux orientations has been carried out. In particular, the rotor flux vector orientation, the stator flux vector orientation and the magnetising flux vector orientation have been considered. It has been shown that each of these systems have the capability to decouple the motor flux and the motor torque. It has also been shown that the performance of the flux vector control systems is sensitive to modelling errors in both rotor resistance and magnetising inductance. It is similarly shown that the sensitivity of the flux vector control systems to modelling errors in the rotor leakage inductance is negligible for the simulation cases shown. The

effect of modelling errors in stator resistance and stator leakage inductance values, when current controlled modulators are used, is shown to have very little influence on the control performance of the system because the induction motor model stator equation is not required for the flux vector control system. It is also evident from the work done that the sensitivity to motor parameter modelling errors is shown to be reduced for direct flux vector control when compared to indirect flux vector control, because of the inherent feedback action in the system. Furthermore, it has been shown that considerable complexity exists in the controller of a flux vector control system.

It is also demonstrated in this thesis that the method of direct torque control also allows the independent and decoupled control of motor torque and motor flux. However, this method only works with stator flux control and it does not work with magnetising flux control or rotor flux control.

It is also apparent from the investigation reported, that the direct torque control strategy is simpler to implement than the flux vector control method because voltage modulators, current modulators and co-ordinate transformations are not required.

As far as sensitivity to motor parameters is concerned, the direct torque control strategy itself does not require any motor parameters. However, for the estimation of the stator flux the motor parameters are required. In both direct torque control and flux vector control observer or Kalman filter techniques may be employed to reduce the sensitivity to parameter detuning. From the results of the systems investigated, is was again apparent that the direct torque control method performed as well as the flux vector control system. The most notable differences are that with direct torque control the average torque is not exactly equal to the reference torque, but the torque variations were smaller for the direct torque control technique than for the flux vector control system. It is suggested that torque variations in the flux vector control system could possibly be reduced by using other modulation schemes.

The direct torque control technique is based on the assumption that the selection of a particular voltage vector and its application for a known sampling time has a pre-determined effect on stator flux level and motor torque with regards to their relative increase or decrease during the application time. However, the results of the investigation reported in this thesis has shown, that the actual effect of the application of a voltage vector for a fixed amount of time on the motor torque and the motor flux,

depends strongly on the steady state rotor speed and motor torque of the induction motor at that time. The reasons for this, which have not previously been reported, may be summarised as follows:

1. When the inverter is operating near its voltage limits, the stator flux angle for which an increase of stator flux may be achieved, is limited to a small section within each sixty degree segment.
2. The alignment of the six, sixty degree sections, is not always perfect. This alignment can vary by as much as twenty degrees for different motor operational conditions. For example, for an alignment error of plus twenty degrees, the first sixty degrees section should cover the stator flux vector angles between -10 and +50 degrees, say, as opposed to -30 and +30 degrees for the ideal conditions.
3. The same alignment problem as for the stator flux applies equally to the developed motor torque. Furthermore, there is a variation between stator flux section alignment and torque section alignment.
4. The actual amount of increase or decrease of either flux or torque varies for different motor conditions. For example, at high speed operation, only a small increase in motor torque may be achieved with the application of a certain voltage vector during the sampling time interval. However, a much bigger torque change may be achieved for breaking action.
5. The average values of flux and torque are not always equal to the reference values because the ripple content above and below the reference value may be different.
6. With the original direct torque control system described in chapter 7, the stator flux level is not kept constant when zero torque is required. However, it is shown that this can be overcome by either a modified switching table (section 7.5) or a 'dither torque signal' which is added to the reference torque signal.
7. Conventional sinusoidal asymmetric or symmetric sampled p.w.m. is not possible with direct torque control as the switching times are forced into a sampling time grid. Thus, the total harmonic distortion with direct torque control is higher than with vector control employing an 'optimum' p.w.m. strategy (chapter 5). However, as is shown in chapter 5, the differences between different switching strategies can be neglected at higher switching frequencies.
8. Similarly to hysteresis current control, the specified hysteresis band may be exceeded for the quantity to be controlled.

9. Because the stator flux space vector location is quantised into only six sections, there are certain angles where a supposedly demanded increase in stator flux actually results in an unwanted flux decrease which in turn results in an unwanted wider stator flux ripple band. However, this is not to say that there is always a different voltage vector which would increase the stator flux and provide a torque increase or decrease as required. This is particularly true for operation near the voltage limit of the inverter.

It is also apparent from the investigation reported, that the advantages of direct torque control compared to flux vector control may be summarised as follows:

1. The control algorithm is less complex and requires a reduced computational capability.
2. 'Pulse dropping' of short pulses which are generated by p.w.m. schemes is not necessary with direct torque control as each pulse has at least a duration of one sampling interval.
3. The direct torque control method does not increase the order of the complete system, the system remaining 5th order (or 6th order when the rotor position is included) throughout. The bang-bang action of the look-up table selection of inverter states gives a quick and tight control of stator flux and motor torque.
4. Similarly to space vector p.w.m., a specific strategy for the selection of zero vectors is given with direct torque control. This reduces torque and flux ripples and conserves energy as no power is taken from the d.c. link during the periods when zero vectors are selected. It should be noted that p.w.m. strategies which use a separate modulation process for each phase do not have a specific zero vector selection strategy.
5. Similarly to space vector p.w.m., voltage vectors are selected with regard to the overall effect of an inverter switch application for a given time interval. For space vector p.w.m. the voltage-time integral is controlled, whereas for direct torque control stator flux level and motor torque are controlled.
6. The switching frequency of direct torque control is not fixed. This gives an effect called 'spread spectrum switching' which may also be achieved by p.w.m. strategies with random sampling in flux vector control. It has the advantage that audible noise is reduced. The average switching frequency depends on the sampling rate of the controller and the hysteresis bandwidth of the stator flux and torque error quantiser.

A 3kW three phase induction motor drive test facility was designed and constructed in order to test and verify the simulation results of the systems reported. The three phase test system was then interfaced with a system controller which was based on a parallel system architecture in order to keep the overall cycle time at a minimum. The control algorithms in the process controller mainly consisted of

1. rotor flux orientation,
2. current controlled modulation,
3. rotor flux estimation, and
4. torque estimation

for the direct flux vector control system. However, in the case of the direct torque control systems only

1. stator flux estimation and
2. torque estimation

are required. It is important to note that the control system algorithm for the flux vector control system and the direct torque control system proved particularly satisfactorily for the decoupling of motor flux and motor torque, as is apparent from the experimental results illustrated in chapter 9.

It became evident from the experimental results that although the direct torque control algorithm appears less complex, in practice very similar computational requirements of the micro controllers are required for the two systems. This is due to the fact that the flux estimation process is usually seen to be separate from the basic direct torque control system, whereas, in the practical system, it is also required. Therefore, this leads to an increase in the total number of computations almost equal to the number required for the flux vector control algorithm. In reality, the number of computations required in the interface system, and for the data acquisition and synchronisation of individual processors in the multi-processor system far outweighs the amount of processing power required for either the flux vector control or the direct torque control strategy.

Finally, it may be concluded that the investigation reported in this thesis has led to many novel system architectures and direct torque control strategies which has significantly improved the overall controllability of induction motor drive systems. It is thought that the results of this thesis should be of great interest to the present day electrical drives industry.

10.1 Further Work

Further work into direct torque control is required in order to establish a relationship for the width settings of the hysteresis comparators and the motor operating conditions. This should also include the dependence of optimum width settings on motor parameters. An 'optimum' switching strategy, such as defined by Equ. 7.7 in the body of this thesis, may thereby be used as a benchmark for new control strategies.

The stator flux estimation techniques using feedback from two current sensors and measured values of the d.c link voltage can be further improved by using observer and Kalman filter techniques. In the past, such techniques as harmonic injection have also been applied to flux vector control systems in order to obtain information on motor parameters. An equivalent of the approach for direct torque control systems has yet to be found.

One possible approach to finding suitable hysteresis width settings is the use of on-line optimisation techniques. The actual effect of the application of a voltage vector may thereby be monitored during operation of the motor and the hysteresis width settings adjusted accordingly. A variation of this approach would be to include the voltage vector selection scheme in the strategy. Similarly to the approach used for optimum control, the total variation of motor flux and torque may be evaluated based on the implementation of Equ. 7.7 by means of an on-line technique, with continuously updated torque and stator flux changes in terms of stator flux angle location and voltage vector applied.

The application of resonant d.c. link techniques applied to direct torque control systems has recently commenced investigation. It is believed that this area will continue to grow in order to raise the inverter switching frequency of the systems.

References

Baader, U; Depenbrock, M; Gierse, G: 'Direct Self Control (DSC) of Inverter-Fed Induction Machine: A Basis for Speed Control Without Speed Measurement', IEEE Transactions on Industry Applications, Vol. 28, No. 3, pp. 581-588, 6 1992

Baader, U; Depenbrock, M; Gierse, G: 'Direct Self Control of Inverter-Fed Induction Machine, A Basis for Speed Control without Speed - Measurement', IEEE, pp. 486-492, 1989

Blaschke, F.: 'The principle of field orientation as applied to the new TRANSVEKTOR closed loop control system for rotating field machines', Siemens Review, 1972

Boldea, I; Nasar, S A: 'Torque Vector Control (TVC) - A Class of Fast and Robust Torque - Speed and Position Digital Controllers for Ele.Drives', Electric Machines and Power Systems, Vol. 15, pp. 135-148, 1988

Boldea, I; Nasar, S A; Fu, Z X: 'Torque Transient Capabilities of Vector Controlled AC Motors with Identical Stators', pp. 627-631

Boldea, I; Trica, A L: 'Torque Vector Controlled (TVC) Voltage-Fed Induction Motor-Drives-Very Low Speed Performance Via Sliding Mode Control', ICEM Proceedings, Vol. 3, pp. 1212-1217, 1990

Bose, B K: 'Evaluation of Modern Power Semiconductor Devices and Future Trends of Converters', IEEE Transactions on Industry Applications, Vol. 28, No. 2, pp. 403-413, 3/4 1992

Bose, B K: 'Power Electronics - An Emerging Technology', IEEE Transactions on Industrial Electronics, Vol. 36, No. 3, pp. 403-412, 8 1989

Bowes, S R; Clark P R: 'Tranputer-Based Optimal PWM Control of Inverter Drives', IEEE Transactions on Industry Applications, Vol. 28, No. 1, pp. 81-88, 1/2 1992

Bowes, S R; Clark P R: 'Transputer-Based Harmonic-Elimination PWM Control of Inverter Drives', IEEE Transactions on Industry Applications, Vol. 28, No. 1, pp. 72-80, 1/2 1992

De Doncker, R W A A: 'Field-Oriented Controllers with Rotor Deep Bar Compensation Circuits', IEEE Transactions on Industry Applications, Vol. 28, No. 5, pp. 1062-1071, 9/10 1992

Depenbrock, M: 'Direkte Selbstregelung (DSR) für hochdynamische Drehfeldantriebe mit Stromrichterspeisung', ETZ Archiv, Vol. 7, Part 7, pp. 211-218, 1988

Depenbrock, M; Klaes, N R: 'Determination of the Induction Motor Machine Parameters and their Dependencies on Saturation', IEEE, pp. 17-22, 1989

Divan, D M: 'The Resonant DC Link Converter-A New Concept in Static Power Conversation', IEEE Transactions on Industry Applications, Vol. 25, No. 2, pp. 317-325, 3/4 1989

Enjeti, P N; Ziogas, P D, Ehsani, M: 'Unbalanced PWM Converter Analysis and Corrective Measures', IEEE, pp. 861-870, 1989

Enjeti, P N; Ziogas, P D; Lindsay, J F; Rashid, M H: 'A New Current Control Scheme for ac Motor Drives', IEEE Transactions on Industry applications, Vol. 28, No. 4, pp. 842-849, 7/8 1992

Green, T C; Dunnigan, M W; Holliday, D; Wade, S; Williams, B W: 'Measurement and On-line Estimation Approaches to Parameter Variation in Vector Controllers', 1993

Habetler, T G; Divan, D M: 'Control Strategies For Direct Torque Control Using Discrete Pulse Modulation', IEEE, pp. 514-522, 1989

Handley, P G; Boys, J T: 'Practical real-time PWM madulators: an assessment', IEE Proceedings-B, Vol. 139, No. 2, pp. 96-102, 3 1992

Hasse, K: 'Drehzahlregelverfahren fü schnelle Umkehrantriebe mit Stromrichter-gespeistem Asynchron-Kurzschlussläufermotoren', Regelungs- Prozessdaten-verarbeitung, 2, 60-71, 1972

Ho, E; Sen, P C: 'Control Dynamics of Speed Drive Systems Using Sliding Mode Controllers with Integral Compensation', IEEE, pp. 639-655, 1989

Holtz, J: 'Pulsewidth Modulation - A Survey', IEEE Transactions on Industrial Electronics, Vol. 39, No. 5, pp. 410-420, 12 1992

Holtz, J; Lammert, P; Lotzkat, W: 'High-Speed Drive System with Ultrasonic MOSFET PWM Inverter and Single-Chip Microprocessor Control', IEEE Transactions on Industry Applications, Vol. IA-23, No. 6, pp. 1010-1015, 11/12 1897

Holtz, J; Thimm, T: 'Identification of the Machine Parameters in a Vector Controlled Induction Motor Drive', IEEE, pp. 601-606, 1989

Honderd, G; Tuijp, W F J; Jongkind, W van den Bosch, P P J: 'Control at low speed of an Induction Motor', pp. 344-348, 1993

Jayne, M G; Murray-Shelley, R; Luk, P; Schaper, D; Sicaroudi, S: 'Implementation of PWM Control Strategies for Inverter Drives using Microelectronic Techniques' 1990

Kazmierkowski, M. P.: 'Automatic control of converter-fed drives', Elsevier, 1994

Leonhard, W: 'Field-Orientation for Controlling AC-Machines - Principle and Application', pp. 277-282, 1970

Lipo, T A; Turnbull, F G: 'Analysis and Comparison of Two Types of Square-Wave Inverter Drives', IEEE Transactions on Industry Applications, Vol. IA-11, No. 2, pp. 137-147, 3/4 1975

Lorenz, R D; Lawson, D B: 'A Simplified Approach to Continuous On-Line Tuning of Field-Oriented Induction Machine Drives', IEEE Transactions on Industry Applications, Vol. 26, No. 3, pp. 420-424, 5/6 1990

Lorenz, R D; Yang S M: 'ac Induction Servo Sizing for Motion Control Applications via Loss Minimizing Real-Time Flux Control', IEEE Transactions on Industry Applications, Vol. 28, No. 3, pp. 589-593, 5/6 1992

Lorenz, R D; Yang S M: 'Efficiency-Optimized Flux Trajectories for Closed-Cycle Operation of Field-Orientation Machine Drives', IEEE Transactions on Industry Applications, Vol. 28, No. 3, pp. 574-580, 5/6 1992

Luk, C K P; Jayne, M G; Rees, D; Schaper, D W: 'A Digital Model for a Three Phase Induction Motor Drive using a Personal Computer (PC) Software Package', 1991

Mertens, A: 'Harmonic Distortion in Three Phase Inverters Controlled by Synchronous Sigma-Delta-Modulation', Eur. Trans. Elect. Power Eng. (Germany), Vol. 2, Part 6, pp. 351-358, 11/12 1992

Ohtani, T; Takada, N; Tanaka K: 'Vector Control of Induction Motor without Shaft Encoder', IEEE Transactions on Industry Applications, Vol. 28, No. 1, pp. 157-164, 1/2 1992

Schauder, C: 'Adaptive Speed Identification For Vector Control of Induction Motors Without Rotational Transducers', IEEE, pp. 493-499, 1989

Schauder, C: 'Adaptive Speed Identification for Vector Control of Induction Motors without Rotational Transducers', IEEE Transactions on Industry Applications, Vol. 28, No. 5, pp. 1054-1061, 9/10 1992

Sukegawa, T; Kamiyama, K; Takahashi, J; Ikimi, T; Matsutake, M: 'A Multiple PWM GTO Line-Side Converter for Unity Power Factor and Reduced Harmonics', IEEE Transactions on Industry Applications, Vol. 28, No. 6, pp. 1302, 12 1992

Takahashi, I; Asakawa, S: 'Ultra-Wide Seed Control of an Induction Motor Covered 10 ^6 Range', 22ND Annual Meeting IEEE, pp. 227-232, 1987

Takahashi, I; Ide, Y: 'Decoupling Control of Trust and Attractive Force of a LIM Using a Space Vector Control Inverter', IEEE Transactions on Industry Applications, Vol. 29, No. 1, pp. 161-167, 1/2 1993

Takahashi, I; Iwata, M: 'High Resolution Position Control under 1 sec. of an Induction Motor with full digitized methods', IEEE, pp. 632-638, 1989

Takahashi, I; Mochikawa, H: 'A New Control of PWM Inverter Waveform for Minimum Loss Operation of an Induction Motor Drive', IEEE Transactions on Industry Applications, Vol. IA-21, No. 4, pp. 580-587, 5/6 1985

Takahashi, I; Noguchi, T: 'A New Quick Response and High-Efficiency Control Strategy of an Induction Motor', IEEE Transactions on Industry Applications, Vol. IA-22, No. 5, pp. 820-827, 9/10 1986

Takahashi, I; Ohmori, Y: 'High-Performance Direct Torque Control of an Induction Motor', IEEE Transactions on Industry Applications, Vol. 25, No. 2, pp. 257-264, 3/4 1989

Appendix A: Steady State Optimisation

A.1 Optimisation for Maximum Power Factor

The power factor may be calculated as the ratio of motor input power divided by the apparent power as follows:

$$\cos\varphi = \frac{P_{in}}{S} \tag{A.1}$$

However, because of the algebraic complexity involved in subsequent calculations when using Equ. A.1 for finding an optimum motor slip frequency ω_r, the following expression will be used to maximise the power factor $\cos\varphi$:

$$\cot\varphi = \frac{P_{in}}{P_{reac}} = \frac{\Re\left\{\vec{v}_s \vec{i}_s^{\,*}\right\}}{\Im\left\{\vec{v}_s \vec{i}_s^{\,*}\right\}} \tag{A.2}$$

Similarly to Equ. 3.11 and Equ. 3.12, the result for equation A.2, depending only on rotor speed, slip frequency and motor parameters, may be found as shown in Equ. A.3.

$$\cot\varphi = \frac{P_{in}}{P_{reac}} = \frac{r_r^2 r_s + r_r\omega_r(\omega_m+\omega_r)x_m^2 + r_s\omega_r^2 x_r^2}{(\omega_m+\omega_r)\left(r_r^2 x_s + x_r\omega_r^2\left(x_s x_r - x_m^2\right)\right)} \tag{A.3}$$

On differentiation of Equ. A.3 with respect to the motor slip ω_r, the following polynom may be obtained. The solutions of the polynom may be found by numerical methods.

$$\begin{aligned}
&\omega_r^4 + \omega_r^3 k_3 + \omega_r^2 k_2 + \omega_r k_1 + k_0 = 0 \\
&k_3 = \frac{2r_r\omega_m x_m^2}{r_r x_m^2 + r_s x_r^2} \\
&k_2 = \frac{r_r\left(r_r^2 x_m^2 x_s + r_r r_s x_r\left(3x_m^2 - 2x_s x_r\right) + \omega_m^2 x_m^2 x_r\left(x_m^2 - x_r x_s\right)\right)}{x_r\left(x_m^2 - x_r x_s\right)\left(r_r x_m^2 + r_s x_r^2\right)} \\
&k_1 = \frac{2r_r^2\omega_m x_m^2\left(r_r x_s + r_s x_r\right)}{x_r\left(x_m^2 - x_r x_s\right)\left(r_r x_m^2 + r_s x_r^2\right)} \\
&k_0 = \frac{r_r^3 x_s\left(r_r r_s - \omega_m^2 x_m^2\right)}{x_r\left(x_r x_s - x_m^2\right)\left(r_r x_m^2 + r_s x_r^2\right)}
\end{aligned} \tag{A.4}$$

A.2 Optimisation for Maximum Efficiency-Power Factor Product

The efficiency-power factor product may be calculated as shown in Equ. A.5.

$$\eta\cos\varphi = \frac{P_{out}}{P_{in}}\frac{P_{in}}{S} = \frac{P_{out}}{S} = \frac{\Im\left\{\vec{\psi}_s^{\,*}\vec{i}_s\right\}\omega_m}{\left|\vec{v}_s\vec{i}_s^{\,*}\right|} \tag{A.5}$$

Similarly to Equ. 3.11 and Equ. 3.12, the result for equation A.5, depending only on rotor speed, slip frequency and motor parameters, may be found as shown in Equ. A.6.

$$\eta\cos\varphi = \frac{r_r\omega_m\omega_r x_m^2}{\sqrt{\left(r_r^2+\omega_r^2x_r^2\right)\left(r_r^2\left(r_s^2+x_s^2(\omega_m+\omega_r)^2\right)+2r_rr_s\omega_r x_m^2(\omega_m+\omega_r)+\omega_r^2\left(r_s^2x_r^2+(\omega_m+\omega_r)^2\left(x_sx_r-x_m^2\right)^2\right)\right)}} \tag{A.6}$$

On differentiation of Equ. A.6 with respect to the motor slip ω_r, the following polynom may be obtained. The solutions of the polynom may be found by numerical methods.

$$\omega_r^7+\omega_r^6k_6+\omega_r^5k_5+\omega_r^4k_4+\omega_r^2k_2+\omega_rk_1=0$$

$$k_6 = \frac{3\omega_m}{2}$$

$$k_5 = \frac{r_r^2\left(x_m^4-2x_m^2x_rx_s+2x_r^2x_s^2\right)+2r_rr_sx_m^2x_r^2+x_r^2\left(r_s^2x_r+\omega_m^2\left(x_m^4-2x_m^2x_rx_s+2x_r^2x_s^2\right)\right)}{2x_r^2\left(x_m^4-2x_m^2x_rx_s+x_r^2x_s^2\right)}$$

$$k_4 = \frac{r_r\omega_m\left(r_r\left(x_m^4-2x_m^2x_rx_s+2x_r^2x_s^2\right)+r_sx_m^2x_r^2\right)}{2x_r^2\left(x_m^4-2x_m^2x_rx_s+x_r^2x_s^2\right)} \tag{A.7}$$

$$k_2 = -\frac{r_r^3\omega_m\left(r_rx_s^2+r_sx_m^2\right)}{2x_r^2\left(x_m^4-2x_m^2x_rx_s+x_r^2x_s^2\right)}$$

$$k_1 = \frac{r_r^4\left(r_s^2+\omega_m^2x_s^2\right)}{2x_r^2\left(x_m^4-2x_m^2x_rx_s+x_r^2x_s^2\right)}$$

The polynom coefficients k_0 and k_3 are zero.

Appendix B: Occam Source Code Listings

B.1 Implementation of Flux Vector Control

The following Occam source code listing is the complete program code of the implementation of flux vector control as described in chapter 8 and chapter 9. The software runs on five Transputers as shown in the configuration part of the listing below.

```
**Listed On  29-5-97 8:13  **
**List of Fold**       "New Transputer Configuration"
**List of File**       "positi00.tsr"
**File Last Modified    31-10-96 9:22
**List all lines  with Fold Headers
**Excluding : NO LIST folds
--{{{  link definitions
VAL link0out IS 0:
VAL link0in  IS 4:
VAL link1out IS 1:
VAL link1in  IS 5:
VAL link2out IS 2:
VAL link2in  IS 6:
VAL link3out IS 3:
VAL link3in  IS 7:
--}}}
--{{{  include libaries
#USE userio
#USE krnlhdr
#USE msdos
#USE filerhdr
--}}}
--{{{  keyboard definitions
VAL esc IS 223:
VAL left IS 203:
VAL right IS 204:
VAL up IS 201:
VAL down IS 202:
VAL space IS 32:
VAL pgup IS 222:
VAL pgdown IS 220:
VAL F1 IS 229:
--}}}

[23][5000]REAL64 dat:
PRI PAR
  VAL start IS 77:
  VAL end IS 99:
  CHAN OF ANY host.to.T0:
  CHAN OF ANY T0.to.host:
  PLACE host.to.T0 AT link2out:
  PLACE T0.to.host AT link2in:
  INT i, int:
  REAL32 real32:
  BOOL continue:
  SEQ
    goto.xy (screen, 10, 1)
    write.full.string (screen, "isa                    p.u.")
    goto.xy (screen, 10, 2)
    write.full.string (screen, "isb                    p.u.")
    goto.xy (screen, 10, 3)
    write.full.string (screen, "gam                    / 2048")
    goto.xy (screen, 10, 4)
    write.full.string (screen, "gam.s                  / 2048")
    goto.xy (screen, 10, 5)
    write.full.string (screen, "gam.sl                 / 2048")
    goto.xy (screen, 10, 6)
    write.full.string (screen, "omega.ref              p.u.")
    goto.xy (screen, 10, 7)
    write.full.string (screen, "omega                  p.u.")
```

```
    goto.xy (screen, 10, 8)
    write.full.string (screen, "omega.sl                p.u.")
    goto.xy (screen, 10, 9)
    write.full.string (screen, "isbeta                  p.u.")
    goto.xy (screen, 10, 10)
    write.full.string (screen, "isx                     p.u.")
    goto.xy (screen, 10, 11)
    write.full.string (screen, "isy                     p.u.")
    goto.xy (screen, 10, 12)
    write.full.string (screen, "pr.ref                  p.u.")
    goto.xy (screen, 10, 13)
    write.full.string (screen, "pr                      p.u.")
    goto.xy (screen, 10, 14)
    write.full.string (screen, "tor.ref                 p.u.")
    goto.xy (screen, 10, 15)
    write.full.string (screen, "tor                     p.u.")
    goto.xy (screen, 10, 16)
    write.full.string (screen, "isx.ref                 p.u.")
    goto.xy (screen, 10, 17)
    write.full.string (screen, "isy.ref                 p.u.")
    goto.xy (screen, 10, 18)
    write.full.string (screen, "isalpha.ref             p.u.")
    goto.xy (screen, 10, 19)
    write.full.string (screen, "isbeta.ref              p.u.")
    goto.xy (screen, 10, 20)
    write.full.string (screen, "isA.ref                 p.u.")
    goto.xy (screen, 10, 21)
    write.full.string (screen, "isB.ref                 p.u.")
    goto.xy (screen, 10, 22)
    write.full.string (screen, "T                       us")
    goto.xy (screen, 10, 23)
    write.full.string (screen, "time                    s")
    host.to.T0 ! start
    continue := TRUE
    WHILE continue
      ALT
        T0.to.host ? i
          IF
            i = 77
              SEQ
                write.full.string (screen, "sampled data")
                T0.to.host ? dat
                continue := FALSE
            TRUE
              SEQ
                T0.to.host ? real32
                goto.xy (screen, 20, i+1)
                write.real32 (screen, real32, 5, 4)
        keyboard ? int
          host.to.T0 ! end
    [1840][500]BYTE dat.byte RETYPES dat:
    VAL matlab IS [0,5000,23,0,4]:
    VAL [20]BYTE matlab.byte RETYPES matlab:
    VAL var.dat IS ['d','a','t', 0 (BYTE)]:
    INT result, length:
    [abs.id.size]BYTE name:
    SEQ
      length := 11
      [name FROM 0 FOR length] := "g:\data.mat"
      open.tkf.file (from.filer, to.filer, tkf.open.block.write,
                     length, name, result)
      write.tkf.block (from.filer, to.filer, 20, matlab.byte, result)
      write.tkf.block (from.filer, to.filer, 4, var.dat, result)
      SEQ i = 0 FOR 1840
        write.tkf.block (from.filer, to.filer, 500, dat.byte[i], result)
      close.tkf.file (from.filer, to.filer, result)
      goto.xy (screen, 50, 22)
      write.full.string(screen, "data saved ok")
  SKIP


**Listed On  29-5-97 8:13  **
**List of Fold**       "New Transputer Configuration"
**List of File**       "PWMout07.tsr"
**File Last Modified    12-11-96 11:33
```

```
**List all lines  with Fold Headers
**Excluding : NO LIST folds
--{{{  link definitions
VAL link0out IS 0:
VAL link0in  IS 4:
VAL link1out IS 1:
VAL link1in  IS 5:
VAL link2out IS 2:
VAL link2in  IS 6:
VAL link3out IS 3:
VAL link3in  IS 7:
--}}}
--{{{  protocol definitions ver 5
PROTOCOL message
  CASE
    terminate.tag
    vdc.now; REAL32
    isd.now; REAL32
    isq.now; REAL32
    torque.now; REAL32
    Tx.now; INT
    out.now; INT
    Speed.now; REAL32
    Flux.now; REAL32
    psd.now; REAL32
    psq.now; REAL32
    TorqueRef.now; REAL32
    Phi.now; INT
    Tau.now; INT
    Theta.now; INT
    dat.now; [14][2048]REAL32
    adc; INT
:

PROTOCOL control
  CASE
    vdc.req
    isd.req
    isq.req
    torque.req
    Tx.req
    out.req
    Speed.req
    Flux.req
    psd.req
    psq.req
    TorqueRef.req
    Phi.req
    Tau.req
    Theta.req
    dat.req

    term.tag
    configure.tag
    FluxRef.now;REAL32
    SpeedRef.now;REAL32
    T.now; INT
    aquisition.tag
    Observer.now;[16][100]REAL32;[16][100]REAL32
:
--}}}

--{{{  SC T0P
--:::A  3 10
--{{{F T0P
--:::F manage09.tsr
PROC T0P (CHAN OF ANY host.to.T0, T0.to.host, T0.to.T2, T2.to.T0,
                      T0.to.T1, T1.to.T0, T0.to.T3, T3.to.T0)
  VAL end IS 99:
  INT i, int:
  REAL32 real32:
  BOOL continue:
  [23][5000]REAL32 dat:
  [23][5000]REAL64 dat64:
  SEQ
```

```
    continue := TRUE
    WHILE continue
      ALT
        host.to.T0 ? int
          T0.to.T2 ! int
        T2.to.T0 ? i
          IF
            i = 77
              SEQ
                T2.to.T0 ? dat
                SEQ k = 0 FOR 23
                  SEQ l = 0 FOR 5000
                    dat64[k][l] := REAL64 ROUND dat[k][l]
                T0.to.host ! i; dat64
                continue := FALSE
            TRUE
              SEQ
                T2.to.T0 ? real32
                T0.to.host ! i; real32
:
--}}}F
--...F code
--:::A  1 2
--:::F manage09.dcd
--...F descriptor
--:::A  1 4
--:::F manage09.dds
--...F debug
--:::A  1 5
--:::F manage09.ddb
--...F CODE SC T0P
--:::A  2 10
--:::F manage09.csc
--}}}
--{{{  SC T1P
--:::A  3 10
--{{{F T1P
--:::F signal12.tsr
PROC T1P (CHAN OF ANY T0.to.T1, T1.to.T0, T1.to.T2,
                      T2.to.T1, T1.to.Edge0, Edge0.to.T1)
  PRI PAR
    TIMER timer:
    INT16 position:
    BOOL continue:
    REAL64 x, x1, x2, x3, x4, y, y1, y2, y3, y4, xx1,
           n0, n1, n2, n3, n4, d1, d2, d3, d4, angle, omega:
    INT pos, pos1, pos2, pos3, pos4, pos5, diff, int, pos.pu,
        time, time1, time2, time3, time4, time5, calctime:
    SEQ
      x := 0.0 (REAL64)
      xx1 := 0.0 (REAL64)
      x1 := 0.0 (REAL64)
      x2 := 0.0 (REAL64)
      x3 := 0.0 (REAL64)
      x4 := 0.0 (REAL64)
      y := 0.0 (REAL64)
      y1 := 0.0 (REAL64)
      y2 := 0.0 (REAL64)
      y3 := 0.0 (REAL64)
      y4 := 0.0 (REAL64)

      n0 := 0.07699098913960E-7 (REAL64)
      n1 := 0.30796394767663E-7 (REAL64)
      n2 := 0.46194595704208E-7 (REAL64)
      n3 := 0.30796393435395E-7 (REAL64)
      n4 := 0.07699099580094E-7 (REAL64)

      d1 := -3.95074409047721 (REAL64)
      d2 :=  5.85344171948210 (REAL64)
      d3 := -3.85463384437136 (REAL64)
      d4 :=  0.95193633855205 (REAL64)

      diff := 0
      position := 0 (INT16)
      continue := TRUE
```

```
      T2.to.T1 ? int
      T1.to.Edge0 ! TRUE
      Edge0.to.T1 ? position
      pos := ((INT position) /\ 255) \/ (((INT position) /\ 28672) >> 4)
      pos1 := pos
      pos2 := pos
      pos3 := pos
      pos4 := pos
      pos5 := pos
      timer ? time5
      timer ? time4
      timer ? time3
      timer ? time2
      timer ? time1
      WHILE continue
        SEQ
          timer ? time
          T1.to.Edge0 ! TRUE
          Edge0.to.T1 ? position
          pos := ((INT position) /\ 255) \/ (((INT position) /\ 28672) >> 4)
          IF
            pos = pos1
              x := xx1
            TRUE
              SEQ
                diff := pos - pos5
                IF
                  diff < (-1000)
                    diff := diff + 2048
                  diff > 1000
                    diff := diff - 2048
                  TRUE
                    SKIP
                x := (REAL64 ROUND diff) / (REAL64 ROUND (time MINUS time5))
                pos5 := pos4
                pos4 := pos3
                pos3 := pos2
                pos2 := pos1
                pos1 := pos
                time5 := time4
                time4 := time3
                time3 := time2
                time2 := time1
                time1 := time
                xx1 := x
           y := ((((n0 * x ) + (n1 * x1)) + ((n2 * x2) + (n3 * x3))) + (n4 *
x4))-
                (((d1 * y1) + (d2 * y2)) + ((d3 * y3) + (d4 * y4)))
          x4 := x3
          x3 := x2
          x2 := x1
          x1 := x
          y4 := y3
          y3 := y2
          y2 := y1
          y1 := y
          pos.pu := pos + pos
          IF
            pos.pu > 2047
              pos.pu := pos.pu - 2048
            TRUE
              SKIP
          T1.to.T2 ! pos.pu; 19.53125 (REAL32) * (REAL32 ROUND y)
          ALT
            T2.to.T1 ? int
              continue := FALSE
            TRUE & SKIP
              SKIP
    SKIP
:
--})})F
--...F code
--:::A  1 2
--:::F signal12.dcd
--...F descriptor
```

```
--:::A  1 4
--:::F signal12.dds
--...F debug
--:::A  1 5
--:::F signal12.ddb
--...F CODE SC T1P
--:::A  2 10
--:::F signal12.csc
--}}}
--{{{  SC T2P
--:::A  3 10
--{{{F T2P
--:::F AAANAI11.tsr
PROC T2P (CHAN OF ANY T0.to.T2, T2.to.T0, T1.to.T2, T2.to.T1,
                      T2.to.T3, T3.to.T2, T2.to.Edge1, Edge1.to.T2)
  #USE mathvals
  #USE snglmath
  PRI PAR
    --{{{  output definitions
    VAL nothing IS 0:
    VAL reset IS 64:
    VAL watchdog IS 128:
    VAL A.neg IS 32:
    VAL A.pos IS 16:
    VAL B.neg IS  8:
    VAL B.pos IS  4:
    VAL C.neg IS  2:
    VAL C.pos IS  1:

    VAL v0 IS A.neg + (B.neg + C.neg): --42
    VAL v1 IS A.pos + (B.neg + C.neg): --26
    VAL v2 IS A.pos + (B.pos + C.neg): --22
    VAL v3 IS A.neg + (B.pos + C.neg): --38
    VAL v4 IS A.neg + (B.pos + C.pos): --37
    VAL v5 IS A.neg + (B.neg + C.pos): --41
    VAL v6 IS A.pos + (B.neg + C.pos): --25
    VAL v7 IS A.pos + (B.pos + C.pos): --21

    VAL [8]INT v IS [v0,v1,v2,v3,v4,v5,v6,v7]:
    --}}}
    VAL Kp1 IS 1.10033 (REAL32):
    VAL Ki1 IS 1.0 (REAL32):
    VAL Kd1 IS -1.09967 (REAL32):
    VAL Kp2 IS 165.9 (REAL32):
    VAL Ki2 IS -0.6522 (REAL32):
    VAL Kd2 IS -6.3333 (REAL32):
    VAL Kp3 IS 0.51757 (REAL32):
    VAL Ki3 IS 1.0 (REAL32):
    VAL Kd3 IS 0.018609 (REAL32):
    VAL t IS 1000.0 (REAL32):
    VAL end IS 99:
    TIMER timer:
    [23][5000]REAL32 dat:
    INT time, time2, int, n, j, i, k, gam, gam.s, out, xx, tt, tt.old,
        step.time, step.time.old, calc.time, si, start:
    BOOL continue:
    REAL32 isa, isb, isbeta, omega, isx, isy, pr, omega.sl, omega.sl.old,
           omega.err, omega.err.old, omega.ref, tor.ref, isx.ref, isy.ref,
           tor.err, tor.err.old, pr.err, pr.err.old, pr.ref, isa.ref,
           isbeta.ref, isB.ref, isC.ref, gam.sl, tor:
    [2048]REAL32 sinTa, cosTa:
    REAL32 Fc:
    SEQ
      SEQ i = 0 FOR 2048
        SEQ
          sinTa[i] := SIN (3.067961576E-3(REAL32) * (REAL32 ROUND i))
          cosTa[i] := COS (3.067961576E-3(REAL32) * (REAL32 ROUND i))
      continue := TRUE
      k := 0
      tt.old := 0
      tt := 0
      xx := 0
      si := 0
      Fc := -50.0 (REAL32)
      i := 1
```

```
j := 1
isa := 0.0 (REAL32)
isb := 0.0 (REAL32)
isbeta := 0.0 (REAL32)
gam := 0
omega := 0.0 (REAL32)
gam.s := 0
pr := 0.0 (REAL32)
isx := 0.0 (REAL32)
isy := 0.0 (REAL32)
omega.sl := 0.0 (REAL32)
omega.sl.old := 0.0 (REAL32)
gam.sl := 0.0 (REAL32)
gam.s := 0
omega.ref := -0.1 (REAL32)
omega.err := 0.0 (REAL32)
omega.err.old := 0.0 (REAL32)
tor.ref := 0.0 (REAL32)
pr.ref := 0.5 (REAL32)
pr.err := 0.0 (REAL32)
pr.err.old := 0.0 (REAL32)
isx.ref := 0.0 (REAL32)
tor.err := 0.0 (REAL32)
tor.err.old := 0.0 (REAL32)
isy.ref := 0.0 (REAL32)
step.time := 0
step.time.old := 0

T0.to.T2 ? int
T2.to.T1 ! int
T2.to.T3 ! int
T2.to.T0 ! 0;77
T2.to.Edge1 ! BYTE nothing
T2.to.Edge1 ! BYTE (nothing + watchdog)
T2.to.Edge1 ! BYTE (nothing + reset)
timer ? start
timer ? time
WHILE continue
  SEQ
    timer ? time2
    calc.time := time2 MINUS time
    timer ? AFTER time PLUS 148
    timer ? time
    PAR
      T1.to.T2 ? gam; omega
      T3.to.T2 ? isa; isb
    isbeta := (isa + (isb + isb)) * 0.5773502692 (REAL32)
    isx := (isa * cosTa[gam.s]) + (isbeta * sinTa[gam.s])
    isy := (isbeta * cosTa[gam.s]) - (isa * sinTa[gam.s])
    pr := (pr * 0.99869753 (REAL32)) + (0.0024792799(REAL32) * isx)
    IF
      pr > 2.0 (REAL32)
        pr := 2.0 (REAL32)
      pr < 1.0E-2 (REAL32)
        pr := 1.0E-2 (REAL32)
      TRUE
        SKIP
    omega.sl := 0.05264624652865 (REAL32) * (isy / pr)
    gam.sl := gam.sl + (7.68 (REAL32) * (omega.sl + omega.sl.old))
    omega.sl.old := omega.sl
    IF
      gam.sl > 2047.0 (REAL32)
        gam.sl := gam.sl - 2048.0 (REAL32)
      gam.sl < 0.0 (REAL32)
        gam.sl := gam.sl + 2048.0 (REAL32)
      TRUE
        SKIP
    gam.s := gam + (INT ROUND gam.sl)
    IF
      gam.s > 2047
        gam.s := gam.s - 2048
      gam.s < 0
        gam.s := gam.s + 2048
      TRUE
        SKIP
```

```
            omega.err := omega.ref - omega
            tor.ref := ((Kp1 * omega.err) + (Kd1 * omega.err.old)) +
                       (Ki1 * tor.ref)
            omega.err.old := omega.err
            IF
              tor.ref > 2.0 (REAL32)
                tor.ref := 2.0 (REAL32)
              tor.ref < (-2.0 (REAL32))
                tor.ref := -2.0 (REAL32)
              TRUE
                SKIP
            pr.err := pr.ref - pr
            isx.ref := ((Kp2 * pr.err) + (Kd2 * pr.err.old)) +
                       (Ki2 * isx.ref)
            pr.err.old := pr.err
            IF
              isx.ref > 2.0 (REAL32)
                isx.ref := 2.0 (REAL32)
              isx.ref < (-2.0 (REAL32))
                isx.ref := -2.0 (REAL32)
              TRUE
                SKIP
            tor := 0.905711388 (REAL32) * (pr * isy)
            tor.err := tor.ref - tor
            isy.ref := ((Kp3 * tor.err) + (Kd3 * tor.err.old)) +
                       (Ki3 * isy.ref)
            tor.err.old := tor.err
            IF
              isy.ref > 2.0 (REAL32)
                isy.ref := 2.0 (REAL32)
              isy.ref < (-2.0 (REAL32))
                isy.ref := -2.0 (REAL32)
              TRUE
                SKIP
            isa.ref := (isx.ref * cosTa[gam.s]) - (isy.ref * sinTa[gam.s])
            isbeta.ref := (isx.ref * sinTa[gam.s]) + (isy.ref * cosTa[gam.s])
            isB.ref := (0.8660254038(REAL32)*isbeta.ref)-(0.5(REAL32)*isa.ref)
                                                          isC.ref      :=
((0.8660254038(REAL32)*isbeta.ref)+(0.5(REAL32)*isa.ref))
            IF
              isa > isa.ref
                out := A.neg
              TRUE
                out := A.pos
            IF
              isb > isB.ref
                out := out + B.neg
              TRUE
                out := out + B.pos
            IF
              (-(isa+isb)) > isC.ref
                out := out + C.neg
              TRUE
                out := out + C.pos
            k := k >< watchdog
            T2.to.Edge1 ! BYTE (out + k)
            step.time := time /\ 8388608
            IF
              step.time <> step.time.old
                SEQ
                  step.time.old := step.time
                  omega.ref := -omega.ref
              TRUE
                SKIP
            dat[0][si] := isa
            dat[1][si] := isb
            dat[2][si] := REAL32 ROUND gam
            dat[3][si] := REAL32 ROUND gam.s
            dat[4][si] := gam.sl
            dat[5][si] := omega.ref
            dat[6][si] := omega
            dat[7][si] := omega.sl
            dat[8][si] := isbeta
            dat[9][si] := isx
            dat[10][si] := isy
```

```
            dat[11][si] := pr.ref
            dat[12][si] := pr
            dat[13][si] := tor.ref
            dat[14][si] := tor
            dat[15][si] := isx.ref
            dat[16][si] := isy.ref
            dat[17][si] := isa.ref
            dat[18][si] := isbeta.ref
            dat[19][si] := isa.ref
            dat[20][si] := isB.ref
            dat[21][si] := REAL32 ROUND calc.time
            dat[22][si] := (REAL32 ROUND (time MINUS start)) * 1.0E-6(REAL32)
            ALT
              T0.to.T2 ? int
                continue := FALSE
              TRUE & SKIP
                SEQ
                  tt := time /\ 16384
                  IF
                    tt <> tt.old
                      SEQ
                        tt.old := tt
                        T2.to.T0 ! xx; dat[xx][si]
                        IF
                          xx = 22
                            xx := 0
                          TRUE
                            xx := xx + 1
                    TRUE
                      SKIP
            IF
              si = 4999
                si := 0
              TRUE
                si := si + 1
        T2.to.Edge1 ! BYTE nothing
        T2.to.T0 ! 77;dat
        ALT
          T1.to.T2 ? gam; omega
            T2.to.T1 ! end
          T3.to.T2 ? isa; isb
            T2.to.T3 ! end
          TRUE & SKIP
            SKIP
        ALT
          T1.to.T2 ? gam; omega
            T2.to.T1 ! end
          T3.to.T2 ? isa; isb
            T2.to.T3 ! end
          TRUE & SKIP
            SKIP
      SKIP
:
--}}}F
--...F code
--:::A  1 2
--:::F AAANAI11.dcd
--...F descriptor
--:::A  1 4
--:::F AAANAI11.dds
--...F link
--:::A  1 9
--:::F AAANAI11.dlk
--...F debug
--:::A  1 5
--:::F AAANAI11.ddb
--...F CODE SC T2P
--:::A  2 10
--:::F AAANAI11.csc
--}}}
--{{{  SC T3P
--:::A  3 10
--{{{F T3P
--:::F trans215.tsr
PROC T3P (CHAN OF ANY T0.to.T3, T3.to.T0, T3.to.T2,
```

```
                    T2.to.T3, T3.to.Edge2, Edge2.to.T3)
  PRI PAR
    INT int:
    INT16 d1, d2:
    BOOL continue:
    REAL32 isa, isb:
    SEQ
      d1 := 2051 (INT16)
      d2 := 2044 (INT16)
      continue := TRUE
      T2.to.T3 ? int
      WHILE continue
        SEQ
          T3.to.Edge2 ! 5 (BYTE)
          Edge2.to.T3 ? d1
          T3.to.Edge2 ! 3 (BYTE)
          Edge2.to.T3 ? d2
          isa := (REAL32 ROUND ((INT d1) - 2049)) * 6.59E-4 (REAL32)
          isb := (REAL32 ROUND ((INT d2) - 2044)) * 6.59E-4 (REAL32)
          IF
            isa > 2.0 (REAL32)
              isa := 2.0 (REAL32)
            isa < (-2.0 (REAL32))
              isa := -2.0 (REAL32)
            TRUE
              SKIP
          IF
            isb > 2.0 (REAL32)
              isb := 2.0 (REAL32)
            isb < (-2.0 (REAL32))
              isb := -2.0 (REAL32)
            TRUE
              SKIP
          T3.to.T2 ! isa; isb
          --T3.to.T2 ! 0.0(REAL32); 0.0(REAL32)
          ALT
            T2.to.T3 ? int
              continue := FALSE
            TRUE & SKIP
              SKIP
    SKIP
:
--}}}F
--...F code
--:::A  1 2
--:::F trans215.dcd
--...F descriptor
--:::A  1 4
--:::F trans215.dds
--...F debug
--:::A  1 5
--:::F trans215.ddb
--...F CODE SC T3P
--:::A  2 10
--:::F trans215.csc
--}}}
CHAN OF ANY host.to.T0, T0.to.host,
            T0.to.T1, T1.to.T0,
            T0.to.T2, T2.to.T0,
            T0.to.T3, T3.to.T0,
            T1.to.T2, T2.to.T1,
            T2.to.T3, T3.to.T2,
            T1.to.Edge0, Edge0.to.T1,
            T2.to.Edge1, Edge1.to.T2,
            T3.to.Edge2, Edge2.to.T3:
PLACED PAR
  PROCESSOR 0 T8
    PLACE host.to.T0 AT link1in:
    PLACE T0.to.host AT link1out:
    PLACE T0.to.T2 AT link0out:
    PLACE T2.to.T0 AT link0in:
    PLACE T0.to.T1 AT link2out:
    PLACE T1.to.T0 AT link2in:
    PLACE T0.to.T3 AT link3out:
    PLACE T3.to.T0 AT link3in:
```

```
  T0P (host.to.T0, T0.to.host, T0.to.T2, T2.to.T0,
       T0.to.T1, T1.to.T0, T0.to.T3, T3.to.T0)
PROCESSOR 1 T8
  PLACE T0.to.T1 AT link1in:
  PLACE T1.to.T0 AT link1out:
  PLACE T1.to.T2 AT link2out:
  PLACE T2.to.T1 AT link2in:
  PLACE T1.to.Edge0 AT link0out:
  PLACE Edge0.to.T1 AT link0in:
  T1P (T0.to.T1, T1.to.T0, T1.to.T2, T2.to.T1, T1.to.Edge0, Edge0.to.T1)
PROCESSOR 2 T8
  PLACE T0.to.T2 AT link3in:
  PLACE T2.to.T0 AT link3out:
  PLACE T1.to.T2 AT link1in:
  PLACE T2.to.T1 AT link1out:
  PLACE T2.to.T3 AT link2out:
  PLACE T3.to.T2 AT link2in:
  PLACE T2.to.Edge1 AT link0out:
  PLACE Edge1.to.T2 AT link0in:
  T2P (T0.to.T2, T2.to.T0, T1.to.T2, T2.to.T1,
      T2.to.T3, T3.to.T2, T2.to.Edge1, Edge1.to.T2)
PROCESSOR 3 T8
  PLACE T0.to.T3 AT link0in:
  PLACE T3.to.T0 AT link0out:
  PLACE T3.to.T2 AT link1out:
  PLACE T2.to.T3 AT link1in:
  PLACE T3.to.Edge2 AT link3out:
  PLACE Edge2.to.T3 AT link3in:
  T3P (T0.to.T3, T3.to.T0, T3.to.T2, T2.to.T3, T3.to.Edge2, Edge2.to.T3)
```

B.2 Implementation of Direct Torque Control

The following Occam source code listing is the complete program code of the implementation of direct torque control as described in chapter 8 and chapter 9. The software runs on five Transputers as shown in the configuration part of the listing below.

```
**Listed On  29-5-97 8:12  **
**List of Fold**       "New Transputer Configuration"
**List of File**       "positi01.tsr"
**File Last Modified    10-11-96 12:40
**List all lines  with Fold Headers
**Excluding : NO LIST folds
--{{{  link definitions
VAL link0out IS 0:
VAL link0in  IS 4:
VAL link1out IS 1:
VAL link1in  IS 5:
VAL link2out IS 2:
VAL link2in  IS 6:
VAL link3out IS 3:
VAL link3in  IS 7:
--}}}
--{{{  include libaries
#USE userio
#USE krnlhdr
#USE msdos
#USE filerhdr
--}}}
--{{{  keyboard definitions
VAL esc IS 223:
VAL left IS 203:
VAL right IS 204:
VAL up IS 201:
VAL down IS 202:
VAL space IS 32:
VAL pgup IS 222:
VAL pgdown IS 220:
VAL F1 IS 229:
VAL F2 IS 228:
--}}}

[23][5000]REAL64 dat:
PRI PAR
  VAL start IS 77:
  VAL end IS 99:
  CHAN OF ANY host.to.T0:
  CHAN OF ANY T0.to.host:
  PLACE host.to.T0 AT link2out:
  PLACE T0.to.host AT link2in:
  INT i, int:
  REAL32 real32:
  BOOL continue:
  SEQ
    goto.xy (screen, 10, 1)
    write.full.string (screen, "isa                    p.u.")
    goto.xy (screen, 10, 2)
    write.full.string (screen, "isb                    p.u.")
    goto.xy (screen, 10, 3)
    write.full.string (screen, "gam                    / 2048")
    goto.xy (screen, 10, 4)
    write.full.string (screen, "is.beta                p.u.")
    goto.xy (screen, 10, 5)
    write.full.string (screen, "isd                    p.u.")
    goto.xy (screen, 10, 6)
    write.full.string (screen, "isq                    p.u.")
    goto.xy (screen, 10, 7)
    write.full.string (screen, "prd                    p.u.")
    goto.xy (screen, 10, 8)
    write.full.string (screen, "prq                    p.u.")
    goto.xy (screen, 10, 9)
```

```
write.full.string (screen, "psd                    p.u.")
goto.xy (screen, 10, 10)
write.full.string (screen, "psq                    p.u.")
goto.xy (screen, 10, 11)
write.full.string (screen, "ps.al                  p.u.")
goto.xy (screen, 10, 12)
write.full.string (screen, "ps.be                  p.u.")
goto.xy (screen, 10, 13)
write.full.string (screen, "ps.ref                 p.u.")
goto.xy (screen, 10, 14)
write.full.string (screen, "ps                     p.u.")
goto.xy (screen, 10, 15)
write.full.string (screen, "omega.ref              p.u.")
goto.xy (screen, 10, 16)
write.full.string (screen, "omega                  p.u.")
goto.xy (screen, 10, 17)
write.full.string (screen, "tor.ref                p.u.")
goto.xy (screen, 10, 18)
write.full.string (screen, "tor                    p.u.")
goto.xy (screen, 10, 19)
write.full.string (screen, "Tau                    (torque error)")
goto.xy (screen, 10, 20)
write.full.string (screen, "Phi                    (flux error)")
goto.xy (screen, 10, 21)
write.full.string (screen, "Theta                  (flux location)")
goto.xy (screen, 10, 22)
write.full.string (screen, "T                      us")
goto.xy (screen, 10, 23)
write.full.string (screen, "time                   s")
host.to.T0 ! start
continue := TRUE
WHILE continue
  ALT
    T0.to.host ? i
      IF
        i = 77
          SEQ
            goto.xy (screen, 55, 10)
            write.full.string (screen, "converting data...  ")
            T0.to.host ? dat
            continue := FALSE
        TRUE
          SEQ
            T0.to.host ? real32
            goto.xy (screen, 20, i+1)
            write.real32 (screen, real32, 5, 4)
    keyboard ? int
      SEQ
        goto.xy (screen, 55, 10)
        IF
          int = esc
            SEQ
              host.to.T0 ! end
              write.full.string (screen, "program finish    ")
          int = F1
            SEQ
              host.to.T0 ! 1
              write.full.string (screen, "variable omega ref")
          int = F2
            SEQ
              host.to.T0 ! 2
              write.full.string (screen, "step responses    ")
          TRUE
            SKIP
[1840][500]BYTE dat.byte RETYPES dat:
VAL matlab IS [0,5000,23,0,4]:
VAL [20]BYTE matlab.byte RETYPES matlab:
VAL var.dat IS ['d','a','t', 0 (BYTE)]:
INT result, length:
[abs.id.size]BYTE name:
SEQ
  length := 11
  [name FROM 0 FOR length] := "g:\data.mat"
  open.tkf.file (from.filer, to.filer, tkf.open.block.write,
                 length, name, result)
```

```
      write.tkf.block (from.filer, to.filer, 20, matlab.byte, result)
      write.tkf.block (from.filer, to.filer, 4, var.dat, result)
      SEQ i = 0 FOR 1840
        write.tkf.block (from.filer, to.filer, 500, dat.byte[i], result)
      close.tkf.file (from.filer, to.filer, result)
      goto.xy (screen, 50, 22)
      write.full.string(screen, "data saved ok")
  SKIP



**Listed On  29-5-97 8:12  **
**List of Fold**       "New Transputer Configuration"
**List of File**       "PWMout09.tsr"
**File Last Modified    12-11-96 9:12
**List all lines  with Fold Headers
**Excluding : NO LIST folds
--{{{  link definitions
VAL link0out IS 0:
VAL link0in  IS 4:
VAL link1out IS 1:
VAL link1in  IS 5:
VAL link2out IS 2:
VAL link2in  IS 6:
VAL link3out IS 3:
VAL link3in  IS 7:
--}}}
--{{{  protocol definitions ver 5
PROTOCOL message
  CASE
    terminate.tag
    vdc.now; REAL32
    isd.now; REAL32
    isq.now; REAL32
    torque.now; REAL32
    Tx.now; INT
    out.now; INT
    Speed.now; REAL32
    Flux.now; REAL32
    psd.now; REAL32
    psq.now; REAL32
    TorqueRef.now; REAL32
    Phi.now; INT
    Tau.now; INT
    Theta.now; INT
    dat.now; [14][2048]REAL32
    adc; INT
:

PROTOCOL control
  CASE
    vdc.req
    isd.req
    isq.req
    torque.req
    Tx.req
    out.req
    Speed.req
    Flux.req
    psd.req
    psq.req
    TorqueRef.req
    Phi.req
    Tau.req
    Theta.req
    dat.req

    term.tag
    configure.tag
    FluxRef.now;REAL32
    SpeedRef.now;REAL32
    T.now; INT
    aquisition.tag
    Observer.now;[16][100]REAL32;[16][100]REAL32
:
```

```
--}}}

--{{{  SC T0P
--:::A  3 10
--{{{F T0P
--:::F manage11.tsr
PROC T0P (CHAN OF ANY host.to.T0, T0.to.host, T0.to.T2, T2.to.T0,
                      T0.to.T1, T1.to.T0, T0.to.T3, T3.to.T0)
  VAL end IS 99:
  INT i, int:
  REAL32 real32:
  BOOL continue:
  [23][5000]REAL32 dat:
  [23][5000]REAL64 dat64:
  SEQ
    continue := TRUE
    WHILE continue
      ALT
        host.to.T0 ? int
          T0.to.T2 ! int
        T2.to.T0 ? i
          IF
            i = 77
              SEQ
                T2.to.T0 ? dat
                SEQ k = 0 FOR 23
                  SEQ l = 0 FOR 5000
                    dat64[k][l] := REAL64 ROUND dat[k][l]
                T0.to.host ! i; dat64
                continue := FALSE
            TRUE
              SEQ
                T2.to.T0 ? real32
                T0.to.host ! i; real32
:
--}}}F
--...F code
--:::A  1 2
--:::F manage11.dcd
--...F descriptor
--:::A  1 4
--:::F manage11.dds
--...F debug
--:::A  1 5
--:::F manage11.ddb
--...F CODE SC T0P
--:::A  2 10
--:::F manage11.csc
--}}}
--{{{  SC T1P
--:::A  3 10
--{{{F T1P
--:::F signal14.tsr
PROC T1P (CHAN OF ANY T0.to.T1, T1.to.T0, T1.to.T2,
                      T2.to.T1, T1.to.Edge0, Edge0.to.T1)
  PRI PAR
    TIMER timer:
    INT16 position:
    BOOL continue:
    REAL64 x, x1, x2, x3, x4, y, y1, y2, y3, y4, xx1,
           n0, n1, n2, n3, n4, d1, d2, d3, d4, angle, omega:
    INT pos, pos1, pos2, pos3, pos4, pos5, diff, int, pos.pu,
        time, time1, time2, time3, time4, time5, calctime:
    SEQ
      x := 0.0 (REAL64)
      xx1 := 0.0 (REAL64)
      x1 := 0.0 (REAL64)
      x2 := 0.0 (REAL64)
      x3 := 0.0 (REAL64)
      x4 := 0.0 (REAL64)
      y := 0.0 (REAL64)
      y1 := 0.0 (REAL64)
      y2 := 0.0 (REAL64)
      y3 := 0.0 (REAL64)
      y4 := 0.0 (REAL64)
```

```
n0 := 0.07699098913960E-7 (REAL64)
n1 := 0.30796394767663E-7 (REAL64)
n2 := 0.46194595704208E-7 (REAL64)
n3 := 0.30796393435395E-7 (REAL64)
n4 := 0.07699099580094E-7 (REAL64)

d1 := -3.95074409047721 (REAL64)
d2 :=  5.85344171948210 (REAL64)
d3 := -3.85463384437136 (REAL64)
d4 :=  0.95193633855205 (REAL64)

diff := 0
position := 0 (INT16)
continue := TRUE
T2.to.T1 ? int
T1.to.Edge0 ! TRUE
Edge0.to.T1 ? position
pos := ((INT position) /\ 255) \/ (((INT position) /\ 28672) >> 4)
pos1 := pos
pos2 := pos
pos3 := pos
pos4 := pos
pos5 := pos
timer ? time5
timer ? time4
timer ? time3
timer ? time2
timer ? time1
WHILE continue
  SEQ
    timer ? time
    T1.to.Edge0 ! TRUE
    Edge0.to.T1 ? position
    pos := ((INT position) /\ 255) \/ (((INT position) /\ 28672) >> 4)
    IF
      pos = pos1
        x := xx1
      TRUE
        SEQ
          diff := pos - pos5
          IF
            diff < (-1000)
              diff := diff + 2048
            diff > 1000
              diff := diff - 2048
            TRUE
              SKIP
          x := (REAL64 ROUND diff) / (REAL64 ROUND (time MINUS time5))
          pos5 := pos4
          pos4 := pos3
          pos3 := pos2
          pos2 := pos1
          pos1 := pos
          time5 := time4
          time4 := time3
          time3 := time2
          time2 := time1
          time1 := time
          xx1 := x
    y := ((((n0 * x ) + (n1 * x1)) + ((n2 * x2) + (n3 * x3))) + (n4 *
x4))-
         (((d1 * y1) + (d2 * y2)) + ((d3 * y3) + (d4 * y4)))
    x4 := x3
    x3 := x2
    x2 := x1
    x1 := x
    y4 := y3
    y3 := y2
    y2 := y1
    y1 := y
    pos.pu := pos + pos
    IF
      pos.pu > 2047
        pos.pu := pos.pu - 2048
```

```
            TRUE
              SKIP
          T1.to.T2 ! pos.pu; 19.53125 (REAL32) * (REAL32 ROUND y)
          ALT
            T2.to.T1 ? int
              continue := FALSE
            TRUE & SKIP
              SKIP
    SKIP
:
--}}}F
--...F code
--:::A  1 2
--:::F signal14.dcd
--...F descriptor
--:::A  1 4
--:::F signal14.dds
--...F debug
--:::A  1 5
--:::F signal14.ddb
--...F CODE SC T1P
--:::A  2 10
--:::F signal14.csc
--}}}
--{{{  SC T2P
--:::A  3 10
--{{{F T2P
--:::F AAANAI13.tsr
PROC T2P (CHAN OF ANY T0.to.T2, T2.to.T0, T1.to.T2, T2.to.T1,
                      T2.to.T3, T3.to.T2, T2.to.Edge1, Edge1.to.T2)
  #USE mathvals
  #USE snglmath
  PRI PAR
    --{{{  output definitions
    VAL nothing IS 0:
    VAL reset IS 64:
    VAL watchdog IS 128:
    VAL A.neg IS 32:
    VAL A.pos IS 16:
    VAL B.neg IS  8:
    VAL B.pos IS  4:
    VAL C.neg IS  2:
    VAL C.pos IS  1:

    VAL v0 IS A.neg + (B.neg + C.neg): --42
    VAL v1 IS A.pos + (B.neg + C.neg): --26
    VAL v2 IS A.pos + (B.pos + C.neg): --22
    VAL v3 IS A.neg + (B.pos + C.neg): --38
    VAL v4 IS A.neg + (B.pos + C.pos): --37
    VAL v5 IS A.neg + (B.neg + C.pos): --41
    VAL v6 IS A.pos + (B.neg + C.pos): --25
    VAL v7 IS A.pos + (B.pos + C.pos): --21

    VAL [8]INT v IS [v0,v1,v2,v3,v4,v5,v6,v7]:
    --}}}
    VAL [2][2][2]INT ThetaTa IS [[[3,4],[3,2]],[[0,5],[0,1]]]:
    VAL [2][3][6]INT vvTa IS [[[v5,v6,v1,v2,v3,v4],
                               [v7,v0,v7,v0,v7,v0],
                               [v3,v4,v5,v6,v1,v2]],
                              [[v6,v1,v2,v3,v4,v5],
                               [v0,v7,v0,v7,v0,v7],
                               [v2,v3,v4,v5,v6,v1]]]:
    VAL T IS 0.00015 (REAL32):
    VAL Tn IS 0.25 (REAL32):
    VAL Kp IS 1.1 (REAL32):
    VAL n0 IS Kp * ((T / (Tn + Tn)) + 1.0 (REAL32)):
    VAL n1 IS Kp * ((T / (Tn + Tn)) - 1.0 (REAL32)):
    VAL end IS 99:
    VAL z IS 0.0 (REAL32):
    VAL w3 IS 1.732050808 (REAL32):
    TIMER timer:
    [23][5000]REAL32 dat:
    INT time, time2, int, n, j, i, k, gam, out, xx, tt, tt.old, si.xx,
        step.time, step.time.old, calc.time, si, start, Tau, Phi, Theta,
        n.th.sample:
```

```
    BOOL continue, down, slow:
    REAL32 isa, isb, isbeta, omega, isd, isq, prd, prq, ps.al, ps.be, ps,
           omega.err, omega.err.1, omega.ref, tor.ref, psd, psq,
           tor.err, ps.err, ps.ref, tor, TauHyst, PhiHyst,ttt:
    [2048]REAL32 sinTa, cosTa, sqrtTa:
    SEQ
      ps.ref := 0.5 (REAL32)
      omega.ref := 0.1 (REAL32)
      SEQ i = 0 FOR 2048
        SEQ
          sinTa[i] := SIN (3.067961576E-3 (REAL32) * (REAL32 ROUND i))
          cosTa[i] := COS (3.067961576E-3 (REAL32) * (REAL32 ROUND i))
          sqrtTa[i] := SQRT (9.765625E-4 (REAL32) * (REAL32 ROUND i))
      continue := TRUE
      k := 0
      tt.old := 0
      tt := 0
      xx := 0
      si := 0
      si.xx := 0
      prd := 0.0 (REAL32)
      prq := 0.0 (REAL32)
      isbeta := 0.0 (REAL32)
      ttt := 0.0 (REAL32)
      gam := 0
      down := FALSE
      slow := FALSE
      n.th.sample := 0
      omega := 0.0 (REAL32)
      ps := 0.0 (REAL32)
      isd := 0.0 (REAL32)
      isq := 0.0 (REAL32)
      TauHyst := 0.005 (REAL32)
      PhiHyst := 0.003 (REAL32)
      omega.err := 0.0 (REAL32)
      omega.err.1 := 0.0 (REAL32)
      tor.ref := 0.0 (REAL32)
      ps.err := 0.0 (REAL32)
      tor.err := 0.0 (REAL32)
      step.time := 0
      step.time.old := 0
      Tau := 0
      Phi := 0

      T0.to.T2 ? int
      T2.to.T1 ! int
      T2.to.T3 ! int
      T2.to.T0 ! 0;77
      T2.to.Edge1 ! BYTE nothing
      T2.to.Edge1 ! BYTE (nothing + watchdog)
      T2.to.Edge1 ! BYTE (nothing + reset)
      timer ? start
      timer ? time
      WHILE continue
        SEQ
          timer ? time2
          calc.time := time2 MINUS time
          timer ? AFTER time PLUS 148
          timer ? time
          PAR
            T1.to.T2 ? gam; omega
            T3.to.T2 ? isa; isb
          isbeta := (isa + (isb + isb)) * 0.5773502692 (REAL32)
          isd := (isa * cosTa[gam]) + (isbeta * sinTa[gam])
          isq := (isbeta * cosTa[gam]) - (isa * sinTa[gam])
                                                              prd       :=
(prd*0.99869753701243(REAL32))+(0.00247927991350(REAL32)*isd)
                                                              prq       :=
(prq*0.99869753701243(REAL32))+(0.00247927991350(REAL32)*isq)
                                                              psd       :=
(prd*0.90571138898276(REAL32))+(0.26222820378685(REAL32)*isd)
                                                              psq       :=
(prq*0.90571138898276(REAL32))+(0.26222820378685(REAL32)*isq)
          ps.al := (psd * cosTa[gam]) - (psq * sinTa[gam])
          ps.be := (psd * sinTa[gam]) + (psq * cosTa[gam])
```

```
            IF
              ps.al > 2.0 (REAL32)
                ps.al := 2.0 (REAL32)
              ps.al < (-2.0 (REAL32))
                ps.al := -2.0 (REAL32)
              TRUE
                SKIP
            IF
              ps.be > 2.0 (REAL32)
                ps.be := 2.0 (REAL32)
              ps.be < (-2.0 (REAL32))
                ps.be := -2.0 (REAL32)
              TRUE
                SKIP
            ps := sqrtTa[INT ROUND(1024.0(REAL32)*
                        ((ps.al * ps.al) + (ps.be * ps.be)))]
            omega.err := omega.ref - omega
            tor.ref := tor.ref + ((n0 * omega.err) + (n1 * omega.err.1))
            omega.err.1 := omega.err
            IF
              tor.ref > 2.0 (REAL32)
                tor.ref := 2.0 (REAL32)
              tor.ref < (-2.0 (REAL32))
                tor.ref := -2.0 (REAL32)
              TRUE
                SKIP
            tor := (psd * isq) - (psq * isd)
            IF
              tor < (tor.ref - TauHyst)
                Tau := 2
              tor > (tor.ref + TauHyst)
                Tau := 0
              (Tau = 2) AND (tor.ref < tor)
                Tau := 1
              (Tau = 0) AND (tor.ref > tor)
                Tau := 1
              TRUE
                SKIP
            IF
              ps < (ps.ref + PhiHyst)
                Phi := 1
              ps > (ps.ref - PhiHyst)
                Phi := 0
              TRUE
                SKIP
                                                                  Theta       :=
ThetaTa[INT(ps.al>z)][INT(ps.be>z)][INT((w3*ABS(ps.be))>ABS(ps.al))]
            out := vvTa[Phi][Tau][Theta]
            k := k >< watchdog
            T2.to.Edge1 ! BYTE (out + k)
            IF
              slow
                SEQ
                  ttt := ttt + 0.001 (REAL32)
                  IF
                    ttt > 2047.0 (REAL32)
                      ttt := ttt - 2047.0 (REAL32)
                    TRUE
                      SKIP
                  omega.ref := 0.15 (REAL32) * sinTa[INT ROUND ttt]
              TRUE
                SEQ
                  step.time := time /\ (8388608)
                  IF
                    step.time <> step.time.old
                      SEQ
                        step.time.old := step.time
                        omega.ref := -omega.ref
                    TRUE
                      SKIP
            dat[0][si] := isa
            dat[1][si] := isb
            dat[2][si] := REAL32 ROUND gam
            dat[3][si] := isbeta
            dat[4][si] := isd
```

```
        dat[5][si] := isq
        dat[6][si] := prd
        dat[7][si] := prq
        dat[8][si] := psd
        dat[9][si] := psq
        dat[10][si] := ps.al
        dat[11][si] := ps.be
        dat[12][si] := ps.ref
        dat[13][si] := ps
        dat[14][si] := omega.ref
        dat[15][si] := omega
        dat[16][si] := tor.ref
        dat[17][si] := tor
        dat[18][si] := REAL32 ROUND Tau
        dat[19][si] := REAL32 ROUND Phi
        dat[20][si] := REAL32 ROUND Theta
        dat[21][si] := REAL32 ROUND calc.time
        dat[22][si] := (REAL32 ROUND (time MINUS start)) * 1.0E-6(REAL32)
        ALT
          T0.to.T2 ? int
            IF
              int = 1
                SEQ
                  slow := TRUE
                  n.th.sample := 79
              int = 2
                SEQ
                  slow := FALSE
                  n.th.sample := 0
              TRUE
                continue := FALSE
          TRUE & SKIP
            SEQ
              tt := time /\ 8192
              IF
                tt <> tt.old
                  SEQ
                    tt.old := tt
                    T2.to.T0 ! xx; dat[xx][si]
                    IF
                      xx = 22
                        xx := 0
                      TRUE
                        xx := xx + 1
                TRUE
                  SKIP
        IF
          si.xx = n.th.sample
            SEQ
              si.xx := 0
              IF
                si = 4999
                  si := 0
                TRUE
                  si := si + 1
          TRUE
            si.xx := si.xx + 1
      T2.to.Edge1 ! BYTE nothing
      T2.to.T0 ! 77;dat
      ALT
        T1.to.T2 ? gam; omega
          T2.to.T1 ! end
        T3.to.T2 ? isa; isb
          T2.to.T3 ! end
        TRUE & SKIP
          SKIP
      ALT
        T1.to.T2 ? gam; omega
          T2.to.T1 ! end
        T3.to.T2 ? isa; isb
          T2.to.T3 ! end
        TRUE & SKIP
          SKIP
    SKIP
:
```

```
--}}}F
--...F code
--:::A  1 2
--:::F AAANAI13.dcd
--...F descriptor
--:::A  1 4
--:::F AAANAI13.dds
--...F link
--:::A  1 9
--:::F AAANAI13.dlk
--...F debug
--:::A  1 5
--:::F AAANAI13.ddb
--...F CODE SC T2P
--:::A  2 10
--:::F AAANAI13.csc
--}}}
--{{{  SC T3P
--:::A  3 10
--{{{F T3P
--:::F trans216.tsr
PROC T3P (CHAN OF ANY T0.to.T3, T3.to.T0, T3.to.T2,
                      T2.to.T3, T3.to.Edge2, Edge2.to.T3)
  PRI PAR
    INT int:
    INT16 d1, d2:
    BOOL continue:
    REAL32 isa, isb:
    SEQ
      d1 := 2051 (INT16)
      d2 := 2044 (INT16)
      continue := TRUE
      T2.to.T3 ? int
      WHILE continue
        SEQ
          T3.to.Edge2 ! 5 (BYTE)
          Edge2.to.T3 ? d1
          T3.to.Edge2 ! 3 (BYTE)
          Edge2.to.T3 ? d2
          isa := (REAL32 ROUND ((INT d1) - 2049)) * 6.59E-4 (REAL32)
          isb := (REAL32 ROUND ((INT d2) - 2044)) * 6.59E-4 (REAL32)
          IF
            isa > 2.0 (REAL32)
              isa := 2.0 (REAL32)
            isa < (-2.0 (REAL32))
              isa := -2.0 (REAL32)
            TRUE
              SKIP
          IF
            isb > 2.0 (REAL32)
              isb := 2.0 (REAL32)
            isb < (-2.0 (REAL32))
              isb := -2.0 (REAL32)
            TRUE
              SKIP
          T3.to.T2 ! isa; isb
          --T3.to.T2 ! 0.0(REAL32); 0.0(REAL32)
          ALT
            T2.to.T3 ? int
              continue := FALSE
            TRUE & SKIP
              SKIP
    SKIP
:
--}}}F
--...F code
--:::A  1 2
--:::F trans216.dcd
--...F descriptor
--:::A  1 4
--:::F trans216.dds
--...F debug
--:::A  1 5
--:::F trans216.ddb
--...F CODE SC T3P
```

```
--:::A  2 10
--:::F trans216.csc
--}}}
CHAN OF ANY host.to.T0, T0.to.host,
            T0.to.T1, T1.to.T0,
            T0.to.T2, T2.to.T0,
            T0.to.T3, T3.to.T0,
            T1.to.T2, T2.to.T1,
            T2.to.T3, T3.to.T2,
            T1.to.Edge0, Edge0.to.T1,
            T2.to.Edge1, Edge1.to.T2,
            T3.to.Edge2, Edge2.to.T3:
PLACED PAR
  PROCESSOR 0 T8
    PLACE host.to.T0 AT link1in:
    PLACE T0.to.host AT link1out:
    PLACE T0.to.T2 AT link0out:
    PLACE T2.to.T0 AT link0in:
    PLACE T0.to.T1 AT link2out:
    PLACE T1.to.T0 AT link2in:
    PLACE T0.to.T3 AT link3out:
    PLACE T3.to.T0 AT link3in:
    T0P (host.to.T0, T0.to.host, T0.to.T2, T2.to.T0,
            T0.to.T1, T1.to.T0, T0.to.T3, T3.to.T0)
  PROCESSOR 1 T8
    PLACE T0.to.T1 AT link1in:
    PLACE T1.to.T0 AT link1out:
    PLACE T1.to.T2 AT link2out:
    PLACE T2.to.T1 AT link2in:
    PLACE T1.to.Edge0 AT link0out:
    PLACE Edge0.to.T1 AT link0in:
    T1P (T0.to.T1, T1.to.T0, T1.to.T2, T2.to.T1, T1.to.Edge0, Edge0.to.T1)
  PROCESSOR 2 T8
    PLACE T0.to.T2 AT link3in:
    PLACE T2.to.T0 AT link3out:
    PLACE T1.to.T2 AT link1in:
    PLACE T2.to.T1 AT link1out:
    PLACE T2.to.T3 AT link2out:
    PLACE T3.to.T2 AT link2in:
    PLACE T2.to.Edge1 AT link0out:
    PLACE Edge1.to.T2 AT link0in:
    T2P (T0.to.T2, T2.to.T0, T1.to.T2, T2.to.T1,
        T2.to.T3, T3.to.T2, T2.to.Edge1, Edge1.to.T2)
  PROCESSOR 3 T8
    PLACE T0.to.T3 AT link0in:
    PLACE T3.to.T0 AT link0out:
    PLACE T3.to.T2 AT link1out:
    PLACE T2.to.T3 AT link1in:
    PLACE T3.to.Edge2 AT link3out:
    PLACE Edge2.to.T3 AT link3in:
    T3P (T0.to.T3, T3.to.T0, T3.to.T2, T2.to.T3, T3.to.Edge2, Edge2.to.T3)
```

Appendix C : Published Papers Relating to this Thesis

Paper 1: A comparative study of high performance speed control strategies for voltage sourced p.w.m. inverter fed incution motor drives, IEE Seventh international conference on Electrical Machines and Drives, University of Durham, UK, 11-13 September 1995

Paper 2: The Simulation of PWM Drives using Matlab, 28th Uiniversities Power Engineering Conference, Vol. 2 pp. 724-727, 1993

A COMPARATIVE STUDY OF HIGH PERFORMANCE SPEED CONTROL STRATEGIES FOR VOLTAGE-SOURCED PWM INVERTER-FED INDUCTION MOTOR DRIVES

I Lüdtke, M G Jayne

University of Glamorgan, UK

The present paper investigates the performance of different three-phase cage rotor induction motor control systems.
Firstly, the field oriented methods, namely direct and indirect vector control, are investigated in both the voltage and current controlled forms. Furthermore, the possibility of field orientation aligned with the stator, airgap (main) and rotor flux vector is considered.
Secondly, direct torque control methods are examined. It is found that direct torque control is less complex and gives better control characteristics than the vector control methods.
Thirdly, a new control strategy based on direct torque control is considered in detail. It has been found that the performance of direct torque control can be improved further by using a more complex switching table with a mapping algorithm.

INTRODUCTION

The technological improvements in power semiconductor and microprocessor technology have made possible rapid application of advanced control techniques for ac motor drive systems (1). The cage rotor induction motor is of particular interest as it is robust, reliable and maintenance free (2). Induction motors can work in dirty and explosive environments and compared to commutator motors they have lower cost, weight and inertia (3). However, the relative simplicity of the induction motor mechanical design is contrasted by a complex dynamic structure (multivariable, nonlinear, important quantities not observable) (4). The equations governing the behaviour of the squirrel cage rotor induction motor may be expressed in the per unit system as follows (Kazmierkowski and Tunia (5)):

$$\vec{v}_s = r_s\vec{i}_s + j\omega\vec{\psi}_s + T_n p\vec{\psi}_s \tag{1}$$

$$0 = r_r\vec{i}_r + j(\omega-\omega_m)\vec{\psi}_r + T_n p\vec{\psi}_r \tag{2}$$

$$\vec{\psi}_s = x_s\vec{i}_s + x_m\vec{i}_r \tag{3}$$

$$\vec{\psi}_r = x_r\vec{i}_r + x_m\vec{i}_s \tag{4}$$

$$p\omega_m = \frac{1}{T_m}\left(\Im\{\vec{\psi}_s\vec{i}_s\} - m_L\right) \tag{5}$$

where the stator voltage, the stator current and the stator flux linkage space phasors are denoted by $\vec{v}_s$, $\vec{i}_s$ and $\vec{\psi}_s$, respectively. The rotor current and rotor flux linkage space phasors are denoted by $\vec{i}_r$ and $\vec{\psi}_r$. The mechanical speed is denoted by ω_m, m_L denotes the load torque, p denotes the derivative operator and ω denotes the speed of the reference coordinate system. The motor parameters r_s, r_r, x_s, x_r, x_m, T_n and T_m are given in the appendix. It is shown in the following how these equations may be applied to construct different control strategies for an induction motor.

FIELD ORIENTED CONTROL

Field-oriented control has since its introduction in 1969 by Hasse (6), and Blaschke (7) been constantly developed and improved. The present paper investigates the principles of direct field-oriented control and indirect field-oriented control for stator flux, rotor flux and airgap flux orientation of the coordinate system. The parameter sensitivity of the complex coordinate transform is a well known weakness of field oriented control systems. Much research has been carried out in order to reduce the sensitivity to motor parameters (8-10). The stator and rotor resistance varies slowly with temperature and can be adapted with appropriate algorithms. However, resistance change due to the skin effect can vary rapidly and is therefore difficult to adapt. As the true motor parameters depart from the estimated parameters, a degradation in performance is apparent. Despite these problems, field oriented control is superior to other control strategies such as constant V/f control, slip control or torque angle control.

Principle of Vector Control

The expression for the electromagnetic torque from equation (5) may also be expressed as follows:

$$m = \Im\{\vec{\psi}_s\vec{i}_s\} = |\vec{\psi}_s||\vec{i}_s|\sin\delta \tag{6}$$

where δ is the angle between the stator current space phasor and the stator flux space phasor. It may be seen that for constant stator flux, the current component $|\vec{i}_s|\sin\delta$ can be used to control the torque. The stator current space phasor has therefore to be resolved into a component i_{sx} in line with the flux space phasor and a component i_{sy} orthogonal to the flux space phasor. Therefore, a coordinate transform of the stator current becomes necessary. The stator current space phasor has

to be turned by the angle of the flux space phasor relative to the stator axis of the motor. The flux space phasor then becomes a stationary reference frame and the stator current space phasor moves relative to it. The stator current component i_{sx} is used to control the flux and the component i_{sy} is used to control the torque.

Current decoupling Network

With the aid of a current decoupling network, appropriate values for the reference stator current components i_{sx}^* and i_{sy}^* may be calculated from reference values for torque and flux. When the stator flux is chosen as the controlled variable, equation (4) may be substituted into equation (2), and equation (3) solved for $\vec{i}_r$ may then be substituted into the resulting equation. It then follows that

$$\vec{i}_s = \frac{\vec{\psi}_s(x_r(T_n p + j(\omega_s - \omega_m)) + r_r)}{(x_s x_r - x_m^2)(T_n p + j(\omega_s - \omega_m)) + r_r x_s} \qquad (7)$$

The speed of the coordinate system ω from equation (2) has now become the reference speed of the stator flux phasor. Resolving equation (7) into real and imaginary parts and solving equation (6) for the torque producing component of the stator current space phasor yields:

$$i_{sy} = \frac{m}{p_{sx}} \qquad (8)$$

$$\omega_s = \omega_m + \frac{i_{sy}(r_r x_s + T_n p(x_s x_r - x_m^2))}{\psi_{sx} x_r - i_{sx}(x_s x_r - x_m^2)} \qquad (9)$$

$$i_{sx} = \frac{i_{sy}(\omega_s - \omega_m)(x_s x_r - x_m^2) + \psi_{sx}(r_r + x_r T_n p)}{r_r x_s + T_n p(x_s x_r - x_m^2)} \qquad (10)$$

Equations (8-10) represent the current decoupling network for stator flux oriented vector control. Similar expressions may be obtained for airgap and rotor flux oriented vector control. Although the equations simplify for rotor flux orientation, there are still the magnetizing inductance, the rotor self inductance, and the rotor resistance present in the equations.

The stator current components i_{sx} and i_{sy} from equations (8) and (10) can then be transformed to stator oriented coordinates and by means of current feedback, current control may be achieved.

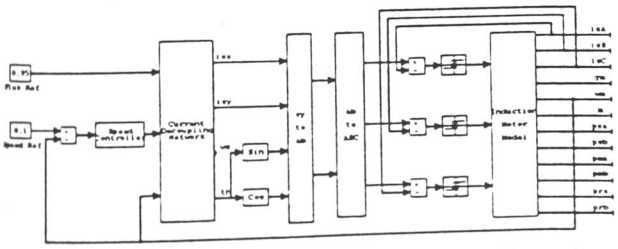

Fig.1: Current Controlled, Indirect Vector Control

Indirect vector control in a current controlled configuration is shown in Fig. 1. The angle for the coordinate transform is obtained by integration of the reference angular frequency of the stator flux phasor (equation 9). The current control method used consists of instantaneous current control loops with three independent hysteresis controllers. Alternatively, two hysteresis controllers or space vector based controllers in field coordinates may be used. Other options include sigma-delta modulation, triangular carrier based schemes related to conventional PWM methods or space vector based intelligent predictive current controllers.

Voltage decoupling Network

The voltage control method is preferred to the current control method when the induction motor drive is intended for high power applications. For such applications, the switching frequency is low and therefore the current contains more harmonics. Direct comparison of a highly distorted current and the reference current makes the correct determination of the switching instants difficult and therefore the open loop voltage control method is more practical. Similarly to the current decoupling networks, the voltage decoupling can be achieved for stator, airgap and rotor flux vector orientation.

For stator flux orientation, the stator voltage equation (1) can be used directly for the voltage decoupling. Separation of equation (1) into real and imaginary parts yields:

$$v_{sx} = r_s i_{sx} + T_n p \psi_{sx} \qquad (11)$$

$$v_{sy} = r_s i_{sy} + \omega_s \psi_{sx} \qquad (12)$$

An indirect vector control scheme with voltage control is shown in Fig. 2.

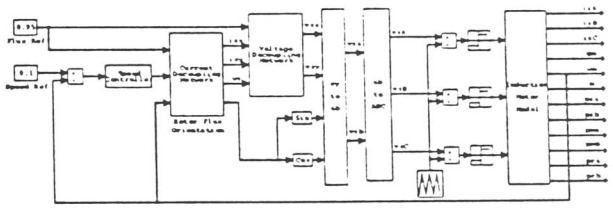

Fig. 2: Voltage Controlled, Indirect Vector Control

The voltage modulation in Fig. 2 is achieved by means of a triangular carrier waveform. Depending on the sampling of the reference voltage waveform, regular symmetric, regular asymmetric or natural sampling may be obtained. Other methods of feedforward voltage modulation include the space vector modulation and the sigma delta modulation. Clearly, the overall performance of the vector control system depends also on the choice of the modulation scheme.

Direct Vector Control

In direct vector control the flux vector is either measured or estimated, and the angle obtained is used for the

coordinate transform of the stator current space phasor. With the flux vector available, the torque can be calculated according to equation (6) and in addition to the speed controller from Fig. 1 and 2, a flux and a torque controller can be included in the system as shown in Fig. 3.

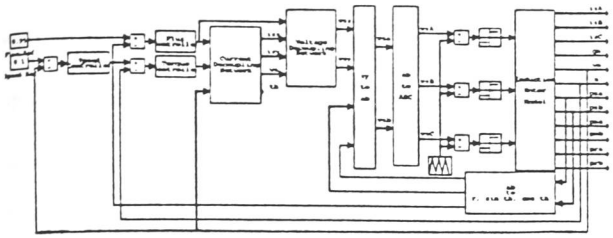

Fig. 3: Voltage Controlled, Direct Vector Control

It can be seen from Fig. 3 that the system inherits a considerable complexity and the control system depends on all motor parameters.

DIRECT TORQUE CONTROL

When, in the mid 1980s, it appeared that the induction motor speed control systems would be standardized on the basis of the field oriented control philosophy, direct flux and torque control (torque vector control, direct self control) was introduced by Depenbrock (11) and Takahashi (12). Torque vector controlled drives are capable of controlling the stator flux and the torque more accurately in comparison to vector control, while the controller complexity is reduced considerably. The current trend in induction motor controller design is therefore towards direct torque control (Boldea and Nasar, 13). The first commercial torque vector controlled induction motor drive is announced for 1995 (14).

Principle of Direct Torque Control

Controllers based on direct torque control do not require a complex coordinate transform. The decoupling of the nonlinear ac motor structure is obtained by the use of on-off control, which can be related to the on-off operation of the inverter power switches. Similarly to direct vector control, the flux and the torque are either measured or estimated and used as feedback signals for the controller. However, as opposed to vector control, the states of the power switches are determined directly by the measured and the reference torque and flux signals. This is achieved by means of a switching table, the inputs of which are the torque error, the stator flux error and the stator flux angle quantized into six sections. The outputs of the switching table are the settings for the switching devices of the inverter. The error signal of the stator flux is quantized into two levels by means of a hysteresis comparator. The error signal of the torque signal is quantized into three levels by means of a three stage hysteresis comparator (Fig. 4).

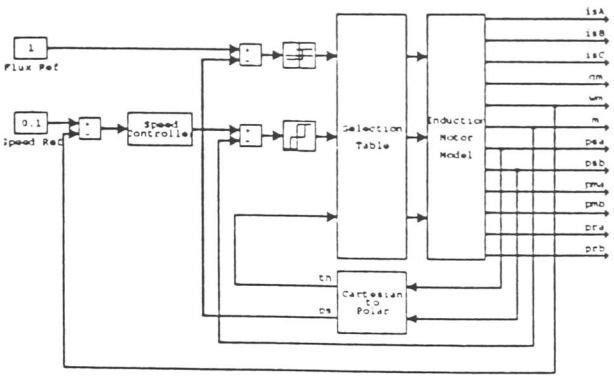

Fig. 4 Direct Torque Control

The equation (6) for the developed torque may be also be expressed in terms of rotor flux and stator flux. This is obtained by solving equation (3) for the rotor current and substitution of the resulting expression into equation (4). The expression may then be solved for the stator current and substituted into equation (5) which results in:

$$m = \frac{x_m}{x_s x_r - x_m^2} |\vec{\psi}_s| |\vec{\psi}_r| \sin\delta_\psi \qquad (12)$$

where δ_ψ is the angle between the stator and the rotor flux linkage space phasors. For constant stator and rotor flux linkage, the angle δ_ψ may be used to control the torque of the motor. From equation (1) in may be obtained that, for a stator fixed reference frame ($\omega = 0$) and $r_s = 0$,

$$\psi_s = \frac{1}{T_n}\int_0^t \vec{v}_s dt \qquad (13)$$

The stator voltage space phasor $\vec{v}_s$ may assume only six different nonzero states and two zero states as shown in Fig. 5 for a dc link voltage of 2 p.u.

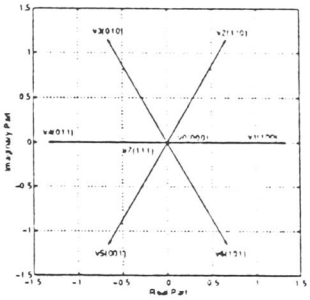

Fig. 5: Voltage Vectors of Three-Phase PWM Inverter

The change of the stator flux vector per switching instant is therefore determined by equation (13) and Fig. 5. The zero vectors v_0 and v_7 halt the rotation of the stator flux vector and decrease its magnitude slightly. The rotor flux vector however, continues to rotate with almost synchronous frequency, and thus the angle δ_ψ changes and the torque changes accordingly (equation 12). The complex stator flux plane may be divided into six sections and a suitable set of switching vectors identified as shown in Table 1:

Table 1: Switching Table for Direct Torque Control

		θ = 1	θ = 2	θ = 3	θ = 4	θ = 5	θ = 6
Φ = 1	τ = 1	v_2	v_3	v_4	v_5	v_6	v_1
	τ = 0	v_0	v_7	v_0	v_7	v_0	v_7
	τ = −1	v_6	v_1	v_2	v_3	v_4	v_5
Φ = 0	τ = 1	v_3	v_4	v_5	v_6	v_1	v_2
	τ = 0	v_7	v_0	v_7	v_0	v_7	v_0
	τ = −1	v_5	v_6	v_1	v_2	v_3	v_4

The inputs Φ, τ and θ of Table 1 correspond to the stator flux error, torque error and stator flux location signals, respectively (Fig. 4).

NEW CONTROL STRATEGY

A new control strategy has been developed, whereby voltage vectors are selected to minimize the error in the stator flux-torque plane. It has been found, when compared to direct torque control, that the torque ripples can be reduced, while the dynamic performance is improved. Similarly to direct flux and torque control, the parameter sensitivity is reduced when compared to field oriented control, as no coordinate transform is involved. The strategy makes use of tables containing the sections in the stator flux-torque plane for which a certain voltage vector applies. By means of a mapping algorithm a voltage vector is then selected.

Principle of New Switching Strategy

As opposed to direct torque control, where the errors of stator flux and torque are quantized to only two or three levels (Φ and τ) and the location of the stator flux vector to six levels (θ), the actual values of flux and torque error and the stator flux angle are used in the proposed scheme. For each motor state, a stator flux error - torque error plane similar to Fig. 6 may be obtained.

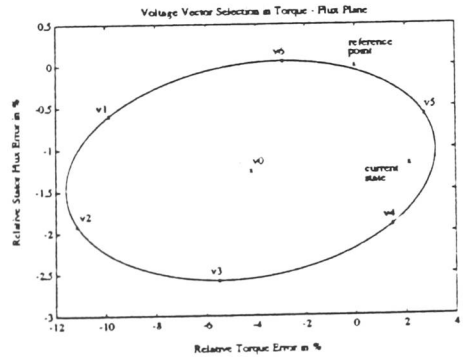

Fig. 6: Voltage Vector Selection

Fig. 6 shows the initial state (current state) of the motor and the reference state, which is the origin of the stator flux error - torque error plane. The stator flux and torque errors are also shown for the next sampling interval, when the voltage vectors v_0 to v_6 are applied. It can be seen that the possible choices are distributed on a ellipse. The centre of that ellipse marks the state which would result if v_0 were chosen. The resulting states move on that ellipse when the stator flux angle changes. Their position in Fig. 6 is shown for a stator flux angle of zero degrees. The errors for stator flux and torque appear as distances from the origin to the points marked by v_0 to v_6. The voltage vector leading to a state which is closest to the reference point is then chosen by the switching strategy. The resulting total error for assumed motor states in the stator flux-torque error plane is shown in Fig. 7.

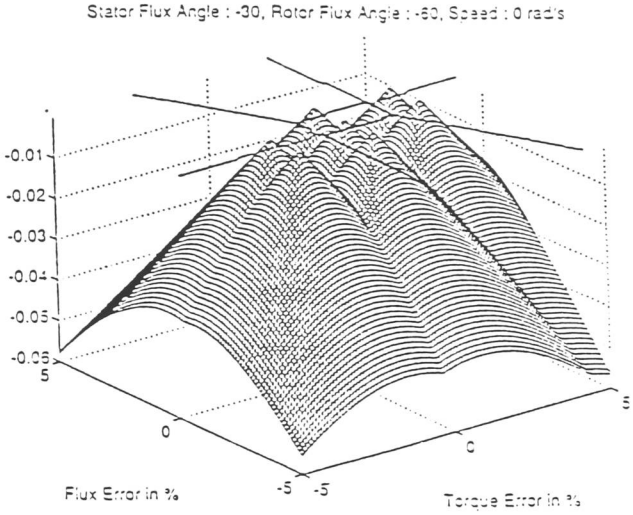

Fig. 7: Voltage Vector Selection

The selection for the voltage vector giving the least total error is already made. The resulting error is shown negative to give peaks in the figure instead of valleys. Seven peaks may be identified. They correspond to motor states which, after the next switching instant, lead to a total error of zero. The contour plot of the graph is also shown in Fig. 7. It may be seen that the seven sections indicated by lines, separate the areas in which a certain voltage vector should be chosen. Fig. 8 shows an example of the contour plots which have been produced for different motor states and reference values.

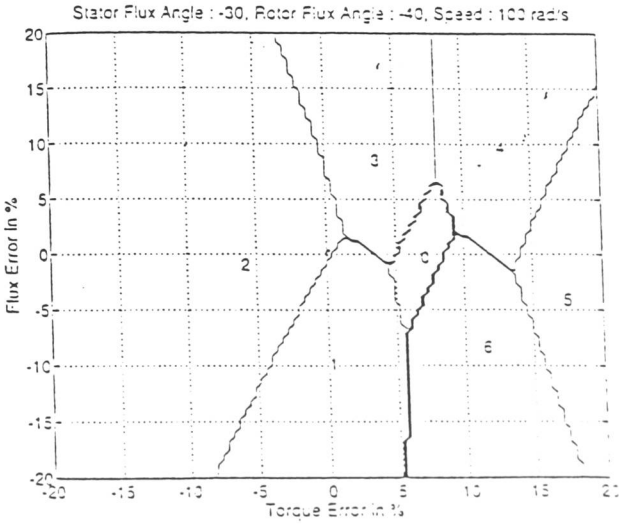

Fig. 8: Voltage Vector Selection

ie strategy has been implemented by saving the section ordinates in a table and selecting the voltage vectors by eans of a mapping algorithm.

IMULATION RESULTS

The different combinations of stator, airgap and rotor flux riented, direct and indirect, current and voltage controlled vector control configurations have been compared to direct torque control and the new switching strategy. It has been found that the direct vector control schemes are generally superior to the indirect vector control schemes. The three configurations with the fastest response to reference torque changes are stator flux oriented current control, airgap flux oriented voltage control and rotor flux oriented current control. These have been compared to direct torque control and the new strategy in Fig. 9 and 10.

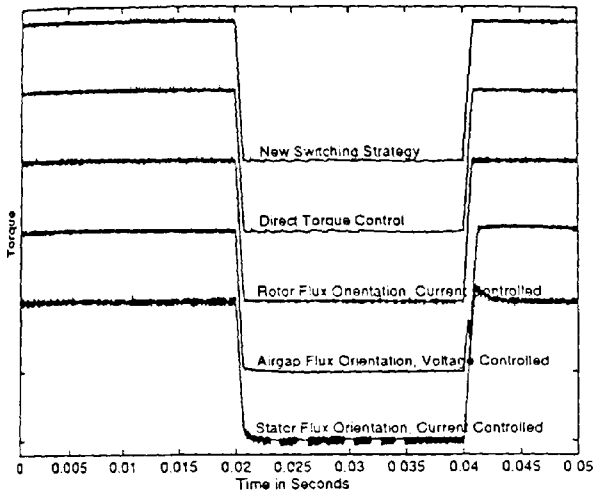

Fig. 9: Voltage Vector Selection

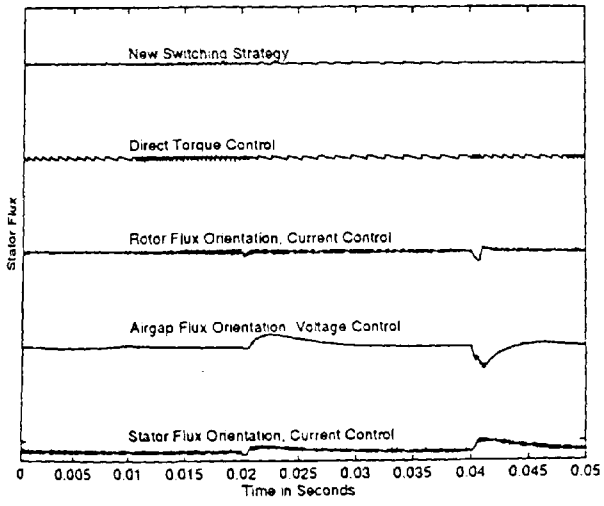

Fig. 10: Voltage Vector Selection

It may be seen that all schemes follow the reference torque signal closely. However, the stator flux in the vector control schemes is not completely decoupled from the torque. The amplitude of the stator flux in direct torque control and in the new scheme is not influenced by torque transients. It has also been found that stator flux and torque ripples are reduced with the new switching strategy.

CONCLUSION

Different types of vector control, direct torque control and a new control strategy based on direct torque control have been considered in this paper.

It has been found that the field oriented methods generally have a higher parameter sensitivity than the direct torque control methods. Moreover, the higher complexity of these methods may be seen as a disadvantage compared to direct torque control methods.

The characteristics of the direct torque control schemes can be summarized as follows:

1) a coordinate transform is not required.
2) a voltage or current modulator is not required.
3) a voltage or current decoupling network is not required.
4) the torque response time is faster than for vector control.
5) the torque and flux ripples are reduced.
6) the variation of the stator current for constant torque operation is reduced.

It has also been found that the full potential of speed control by means of an inverter is not fully utilized by direct torque control. The new strategy described improves the performance of direct torque control further. However, the new strategy makes the selection of switching states complex, since precalculated values have to be loaded into the control system. The strategy may be applied in induction motor drive systems where highest performance and smooth torque are of paramount importance.

APPENDIX: MOTOR PARAMETERS

$P_m = 2.2\ kW$	$x_m = 1.9035$ p.u.
$n = 1426\ l/min$	$x_s = 1.9863$ p.u.
$p = 4$	$x_r = 2.1017$ p.u.
$r_s = 0.085$ p.u.	$T_n = 0.0032$ p.u.
$r_r = 0.0581$ p.u.	$T_m = 0.1375$ p.u.

REFERENCES

[1] Enjeti, P.N., Ziogas, P.D, Lindsay, J.F. and Rashid, M.H.: "A New Current Control Scheme for ac Motor Drives" IEEE Trans. Industry Applications, Vol. 28, pp. 842-849, August 1992.

[2] Takahashi, I. and Nogushi, T. : "A New Quick-Response and High-Efficiency Control Strategy of an Induction Motor" IEEE Trans. Industry Applications, Vol. IA-22, pp. 820-827, October 1986.

[3] Bose, B.K. : "Adjustable Speed AC Drive Systems" IEEE Press selected reprint series, 1980.

[4] Slemon, G.R. : "Electric Machines and Drives" Addison-Wesley Publishing Company Inc., 1992.

[5] Kazmierkowski, M.P. and Tunia, H : "Automatic Control of Convertor-Fed Drives", Elsevier, 1994

[6] Hasse, K: 'Drehzahlregelvervahren für schnelle Umkehrantriebe mit stromrichtergespeisten Asynchron-Kurzschlußläufermotoren', Regelungs-Prozeßdatenverarbeitung, 2, pp. 60-71, 1972

[7] Blaschke, F 'The principle of field orientation as applied to the new TRANSVECTOR closed loop control system for rotating machines', Siemens Review, pp 217-226, 1972

[8] Bortsov, Y A: 'Adaptive Control of Electric Drives', SOV. ELECT. ENG (USA), Vol. 63, No. 3, pp. 30-36, 1992

[9] Chan, C C; Wang, H: 'An Effective Method for Rotor Resistance Identification for High-Performance Induction Motor Vector Control', IEEE Transactions on Industrial Electronics, Vol. 37, No. 6, pp. 447-482, 12 1990

[10] Fetz, J: 'Parameter Adaptation for a Field oriented Induction Machine fed by a PWM Inverter and Determination of the fundamental currents in the range of overmodulation', EPE Florence 1991, 2, pp. 138-144, 1991

[11] Depenbrock, M: 'Direkte Selbstregelung (DSR) für hochdynamische Drehfeldantriebe mit Stromrichterspeisung', ETZ Archiv, Vol. 7, Part 7, pp. 211-218, 1988

[12] Takahashi, I; Noguchi, T: 'A New Quick Response and High-Efficiency Control Strategy of an Induction Motor', IEEE Transactions on Industry Applications, Vol. IA-22, No. 5, pp. 820-827, 9/10 1986

[13] Boldea, I. and Nasar, S.A. : "Vector Control of AC Drives" CRC Press Inc., 1992.

[14] Sacks, T : "ABB heralds a new aera in motor control" Electrical Review, Dec-Jan 1995

THE SIMULATION OF PWM DRIVES USING MATLAB

I. Lüdtke M. G. Jayne C. Cabral

University of Glamorgan, UK University of the Algarve, Portugal

The paper contains an in-depth analysis of the performance of three-phase, cage rotor induction motor drives when supplied with a range of pulse-width-modulated, PWM, waveforms. It is shown that by using the software package, MATLAB, a complete simulation of the drive system can be made in both the transient and steady states. The effects of supplying the motor with a range of PWM waveform strategies, on the motor current, input power, output power, torque and speed are presented in detail. It is shown that the incorrect choice of voltage waveform strategy can have very undesirable effects on the output parameters of the motor. The paper also describes how MATLAB is particularly useful for the simulation of drive systems employing vector control and other control strategies.

1 INTRODUCTION

The technological improvements in power semiconductor and microprocessor technology have made possible rapid application of advanced control techniques for ac motor drive systems [1]. The cage rotor induction motor is of particular interest as it is robust, reliable and maintenance free [2]. Induction motors can work in dirty and explosive environments and compared to commutator motors they have lower cost, weight and inertia [3]. However, the relative simplicity of the induction motor mechanical design is contrasted by a complex dynamic structure (multivariable, nonlinear, important quantities not observable) [4]. As this dynamic structure leads to differential equations which limit a closed solution to very special cases, evaluation of these equations can only be done by numerical computation [5]. The software package MATLAB allows, due to its flexibility and expandability, the development of a set of functions for a detailed analysis of the induction motor drive.

2 STEADY STATE INDUCTION MOTOR MODEL

The steady state model of an induction motor is used for the harmonic analysis of current, power and developed torque, when the motor is supplied by a voltage source PWM inverter. The investigation is carried out at standstill and rated speed. The PWM waveforms supplied to the motor are regular asymmetric, symmetric and natural sampled. This is done for carrier- to modulation frequency ratios of triple even, triple odd, non triple even and non triple odd integer values. Two different ways of generating the PWM input voltages are investigated. The PWM signals are generated with either three reference sinewaves or with just one reference sinewave where the other two PWM signals are phase shifted by 120 or 240 degrees. All quantities have been calculated in both the time and the frequency domain.

2.1 Equivalent Circuit

If the induction motor is operating in the steady state, a simple equivalent circuit can be used to calculate the values of current, power and torque. In the literature RMS values are used in these calculations. It will be shown that inverse Fourier analysis can be used to obtain values in the time domain. The results of this analysis give the instantaneous values of current, power and torque, which may similarly be transformed back to the frequency domain, to determine the magnitudes and orders of the harmonics. The advantage of this method is that the time consuming calculations necessary when using the dynamic model are avoided. The results obtained from the dynamic model coincide with those from the steady state model. The commonly used steady state equivalent circuit is shown in Fig. 1.

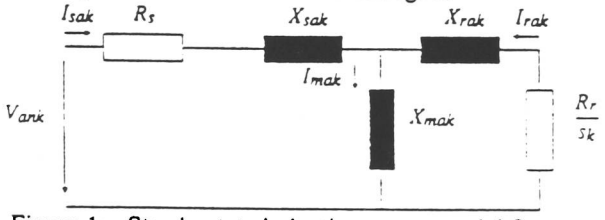

Figure 1: Steady state induction motor model for phase A

By use of the index k, the equivalent circuit can be used for each harmonic calculation, provided the reactances are calculated according to the following

$$X_{sk} = k2\pi f_s L_{ls}$$
$$X_{mk} = k2\pi f_s L_m$$
$$X_{rk} = k2\pi f_s L_{lr} \quad (1)$$

where f_s represents the fundamental supply frequency. For positive sequence harmonics of the applied voltage waveform the slip can be written as

$$s_k = \frac{(k-1)+s_1}{k} \quad (2)$$

and for the negative sequence harmonics the slip may be written as

$$s_k = \frac{(k+1)-s_1}{k} \quad (3)$$

where s_1 represents the slip at fundamental frequency. R_s is the stator resistance per phase and $R_s + jX_s$ is termed the stator leakage impedance. Similarly, for the rotor, R_r is the equivalent rotor resistance per phase and X_r is the equivalent rotor leakage reactance. X_m is the reactance of the path of the magnetizing current. All quantities are referred to the stator side of the motor for convenience of analysis. The following effects of a real induction motor are not included in this model:

- variation of ohmic resistance with temperature
- iron losses

- tooth saturation which alters the eddy current coefficient and consequently the effective resistance
- tooth and core saturation which affects the leakage flux per unit current and therefore the effective inductive reactance
- magnetizing reactance dependence of magnetic saturation
- slight variations in speed steaming from torque variations
- non uniform magnetic field in the air gap
- skin effect

When the equivalent circuit is used for an analysis at higher frequencies it may be further simplified. It is important to note that when the modulated waveforms applied to each phase of the equivalent circuit are not identical in every respect, then each phase has to be analysed individually. However, when the input voltage waveforms are identical, such as occurs when a 120 and 240 degrees phase shift is introduced to the modulated waveforms, then it is only necessary to analyse one phase.

2.2 Calculations with Equivalent Circuit

Fig. 2 shows a simplified model of an induction motor supplied by an ideal inverter.

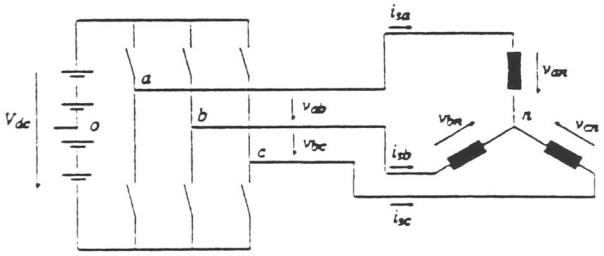

Figure 2: Star connected motor supplied by an ideal inverter

It may be shown that the input voltages for the equivalent induction motor circuits can be calculated as follows:

$$v_{an} = \frac{1}{3}(2v_{ao} - v_{bo} - v_{co})$$

$$v_{bn} = \frac{1}{3}(2v_{bo} - v_{ao} - v_{co})$$

$$v_{cn} = \frac{1}{3}(2v_{co} - v_{ao} - v_{bo}) \qquad (4)$$

where the PWM generator voltages v_{ao}, v_{bo} and v_{co} are calculated according to the PWM strategy. Figure 3 shows a resulting input voltage waveform for asymmetric sampling.

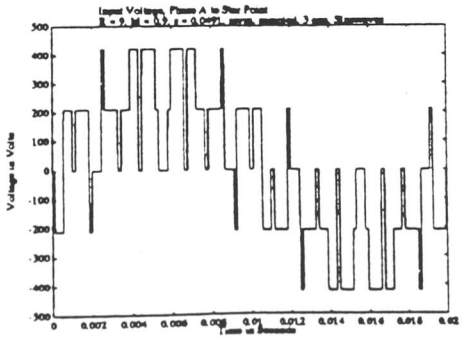

Figure 3: Phase A to motor star point voltage

These voltages are then Fourier transformed and used to calculate the stator, rotor and magnetizing currents for each Harmonic. Figure 4 shows the resulting spectrum for the voltage waveform in figure 3.

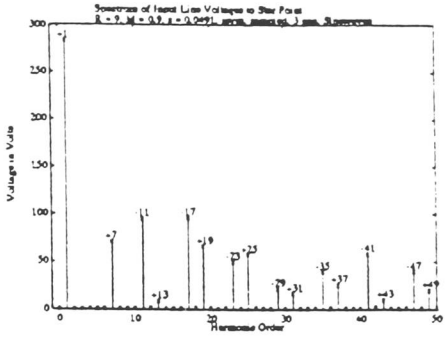

Figure 4: Harmonics of phase A to motor star point voltage

With these transformed input voltages the spectrum of the currents can be calculated according to the equivalent circuit. The resulting spectrum for the stator line current is shown in figure 5.

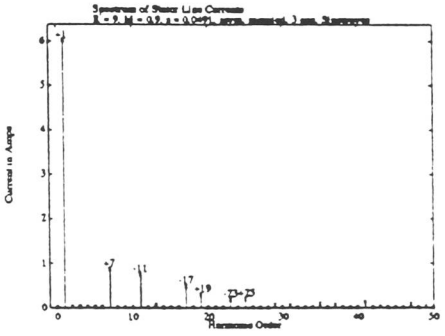

Figure 5: Harmonics of phase A stator current

It may be shown that by use of the inverse Fourier transform the currents i_{sa}, i_{ma}, and i_{ra} are determined in the time domain, shown in figure 6. These instantaneous values of current can be used to calculate the instantaneous values of power and torque for the induction motor.

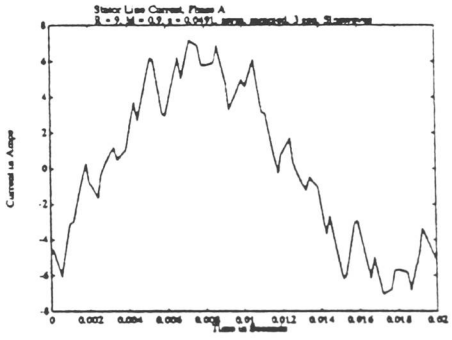

Figure 6: Phase A stator current

The motor input power is given by

$$p_e = v_{ao}i_{sa} + v_{bo}i_{sb} + v_{co}i_{sc} \qquad (5)$$

The spectrum of the motor input power can be calculated by means of a Fourier transform. This is relevant for the supply side of the induction motor drive, these harmonics do appear as disturbances in the DC-link supply of the inverter.

The developed torque cannot be calculated with reference to only one equivalent circuit using instantaneous variables, all three equivalent circuits have to be taken into account. This is because torque is only produced by the interaction of one stator phase with two other rotor phases. If a rotor phase and a stator phase form a positive sequence (a-b, b-c and c-a) the developed torque has to be taken positive, in case of negative sequence (a-c, c-b and b-a) the developed torque has to be taken negative. The resulting instantaneous torque is of course dependent on the signs of the instantaneous currents. The instantaneous developed torque can be described as

$$T_e = \frac{L_m p}{2\sqrt{3}}(i_{ra}i_{sb} - i_{ra}i_{sc} + i_{rb}i_{sc} - i_{rb}i_{sa} + i_{rc}i_{sa} - i_{rc}i_{sb}) \quad (6)$$

As the sum of rotor currents and the sum of stator currents are zero, the previous equation can be simplified to

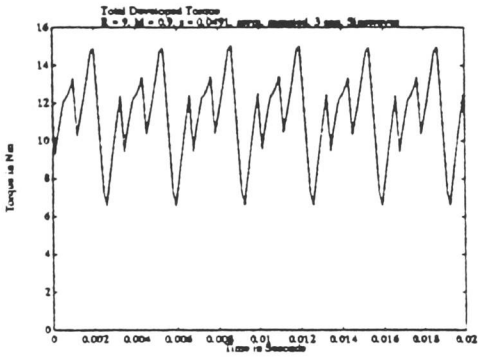

Figure 7: Developed torque of induction motor

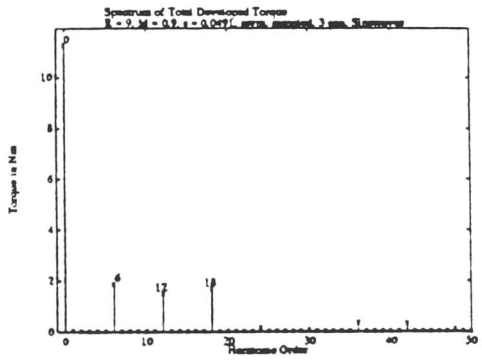

Figure 8: Harmonics of developed torque

$$T_e = \frac{\sqrt{3}}{2} L_m p(i_{ra}i_{sb} - i_{rb}i_{sa}) \quad (7)$$

The resulting output power is given by

$$p_m = T_e \omega_{mech} \quad (8)$$

3 DYNAMIC INDUCTION MOTOR MODEL

A transient induction motor model has been used for the analysis of the dynamic behaviour of an induction motor. The varied parameters are the motor load, input voltage (sinusoidal and PWM), and the inertia. This model has also been used for an on-line estimation of the rotor flux vector, which is essential for vector control. Furthermore, the speed, torque and current controller together with a hysteresis current controlled voltage fed PWM inverter have been included in the model. The dynamic equivalent circuit is shown in Figure 9.

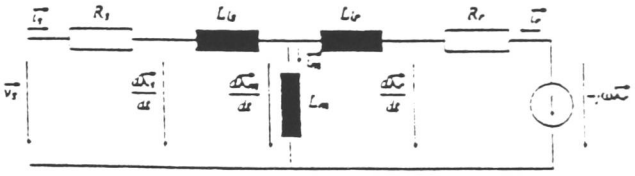

Figure 9: Dynamic induction motor model

This induction motor model includes all three phases, as the voltage, flux and current variables are in space vector notation. The resulting fifth order differential equation system is solved with a Runge-Kutta algorithm. The speed of the motor during a direct on-line start is shown in figure 10.

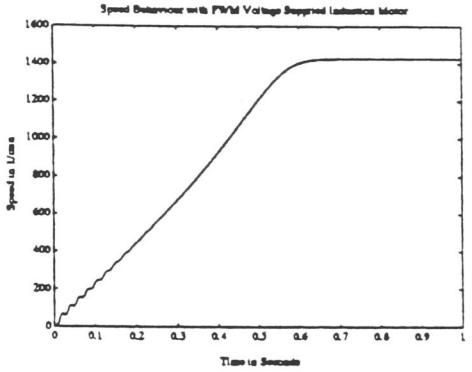

Figure 10: Speed of induction motor at direct on-line start

The relation between steady state and dynamic torque over speed behaviour is shown in figure 11.

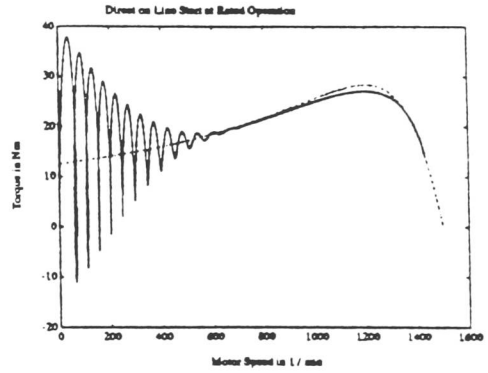

Figure 11: Torque / Speed plot of direct on line start with sinusoidal voltage supply

It can be seen that the torque transient of the dynamic motor model is oscillating around the steady state level. If the motor is supplied with a PWM voltage which has the same RMS value of the fundamental frequency, then no difference in the speed behaviour during startup can be seen. However, the developed torque shows large ripples which match to those obtained by the steady state model. The torque over speed curve is shown in figure 12.

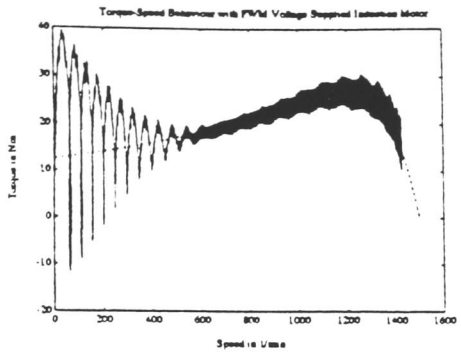

Figure 12: Torque / Speed plot of direct on line start with PWM voltage supply

4 CONCLUSION

The simulation package MATLAB has been used for a steady state and transient analysis of a PWM supplied induction motor. It is found that this easy to use software package permits a very short program development time. The results obtained in the simulation of the induction motor drive can be summarized as follows:

1) PWM signal generation strategy with one reference sinewave has got some advantages in the behaviour of output torque, but input power and stator and rotor current have got a high harmonic content. Especially the dominant harmonic of order R is not cancelled. These harmonics do produce a large amount of losses and hot spots in the stator windings which could destroy the insulation. If R is a triple integer then there is no difference between these two modes.

2) Symmetric regular sampling produces an increased harmonic content in voltage, current, power and torque compared with asymmetric or natural sampling. The differences between asymmetric and natural sampling are not that high. The only difference is that natural sampling produces a harmonic content with symmetric sidelobe amplitudes. Natural sampling is not very convenient for real time digital computation because an approximation algorithm has to be solved. So regular asymmetric sampling seems to be most advantageous.

3) During starting, when the slip is near 1 and the motor behaviour is more inductive, the current, output power and torque curves are quite smooth. This means that the problems with harmonics in the output torque appear mainly at rated speed.

4) With an increased R the instantaneous current and torque behaviour becomes more smooth, but there are limits determined by the inverter. For power MOSFETs switching losses and switching time allow carrier frequencies only upto a given limit.

5) The dynamic model analysis shows that there is no difference in speed behaviour, when the motor is fed with PWM voltages. This assumes that the fundamental of the PWM voltage has the same RMS value as the reference sinusoidal supply. The torque simulation results show that after the first inrush period a high harmonic content is apparent. This has also been found in the steady state model.

6) With reduced supply frequency the voltage has to be reduced as well, otherwise the stator currents would be too high. This reduction can be done proportional to frequency for higher speeds, but for low speed additional voltage has to be fed into machine because of the stator resistance.

7) Inertia is a parameter which determines the speed of the transient behaviour only, it has no other influences. A speed proportional load determines the speed of the transient behaviour and the slip of the motor. If the load increases above the rated value, the current increases and the motor is overloaded.

Appendix : Motor Data

P_m	= 2.2 kW	L_m	= 268 mH
n	= 1426 $1/min$	L_{l_s}	= 11.65 mH
p	= 4	L_{l_r}	= 27.9 mH
R_s	= 3.76 Ω	V_{an}	= 230 V
R_r	= 2.571 Ω	s	= 4.91 %

References

[1] Enjeti, P.N., Ziogas, P.D, Lindsay, J.F. and Rashid, M.H. : "A New Current Control Scheme for ac Motor Drives" IEEE Trans. Industry Applications, Vol. 28, pp. 842-849, August 1992.

[2] Takahashi, I. and Nogushi, T. : "A New Quick-Response and High-Efficiency Control Strategy of an Induction Motor" IEEE Trans. Industry Applications, Vol. IA-22, pp. 820-827, October 1986.

[3] Bose, B.K. : "Adjustable Speed AC Drive Systems" IEEE Press selected reprint series, 1980.

[4] Gabriel, R. and Leonhard, W. : "Field-Oriented Control of a Standard AC Motor Using Microprocessors" IEEE Trans. Industry Applications, Vol. IA-16, pp. 186-192, March/April 1980.

[5] Slemon, G.R. : "Electric Machines and Drives" Addison-Wesley Publishing Company Inc., 1992.

[6] Boldea, I. and Nasar, S.A. : "Vector Control of AC Drives" CRC Press Inc., 1992.

[7] Boldea, I. and Nasar, S.A. : "Electric Machine Dynamics" Macmillan Publishing Company, 1986.

[8] Bowes, S.R. and Clements, R.R. : "Digital computer simulation of variable-speed PWM inverter-machine drives" IEE Proc., Vol 130, Pt. B, No. 3, May 1983.

[9] Terman, F.E. : "The Fourier Transform and its Applications" Electrical and Electronic Engineering Series, Mc Graw-Hill, 1965.

[10] Murphy, J.M.D. and Turnbull, F.G. : "Power Electronic Control of AC Motors" Pergamon Press, 1988.

Addresses of Authors

I. Lüdtke, Department of Electronics and Information Technology, University of Glamorgan, Pontypridd, Mid Glamorgan CF37 1DL, United Kingdom

Dr. M. G. Jayne, Department of Electronics and Information Technology, University of Glamorgan, Pontypridd, Mid Glamorgan CF37 1DL, United Kingdom

Prof. C. Cabral, University of the Algarve, Faro, Portugal